School of Civil Engineering

THE EFFECTIVE SHEAR STRENGTH OF ARTIFICIALLY FISSURED OVERCONSOLIDATED CLAYS

Ali Sabzalisenejani

"This thesis is presented as part of the requirements for
the award of the Degree of Doctor of Philosophy
of the
Curtin University of Technology"

March 1998

ABSTRACT

The effective shear strength of artificially overconsolidated clays with continuous fissures, or with discontinuous or partial fissuring, has been discussed from both the experimental and numerical points of view.

Direct shear and triaxial tests have been conducted on a range of unfissured, partially and fully fissured specimens of artificially overconsolidated clay samples in the laboratory. Specimens subjected to direct shear tests have been prepared in three different preconsolidation pressures and two or three different Overconsolidation ratios (OCR) for unfissured, partially and fully fissured specimens. Specimens subjected to triaxial tests also were prepared for three different preconsolidation pressures and overconsolidation ratios. In order to investigate the effect of orientation of fissures, artificially overconsolidated fissured triaxial specimens were prepared in three different orientations at 30°, 45° and 60° to the direction of minimum principal stress (σ_3).

For both direct shear and triaxial tests, special tools and devices were designed and constructed to prepare unfissured, partially and fully fissured specimens.

Taking into account the number of parameters which influence the effective shear strength of overconsolidated clays, and the time which is needed to artificially prepare the overconsolidated specimens and to run drained tests, as well as the impossibility or impracticality of the laboratory simulations for some specific cases,

numerical methods were used to complement the experimental component of the investigation.

Numerical modelling of direct shear and triaxial specimens utilised the FLAC (Fast Lagrangian Analysis of Continua, Itasca, 1993) program for two dimensional simulation of the direct shear tests and the ANSYS (1996) program for three dimensional simulation of triaxial tests. The experimental results have been used to calibrate the coefficients of the numerical models and to verify the results obtained from numerical models.

Strain softening behaviour was simulated numerically for unfissured and fully fissured specimens subjected to direct shear tests. Using the obtained experimental and numerical results of the study of direct shear tests with respect to the effects of different parameters on the effective shear strength of the spacing subjected to direct shear tests and also FLAC programming, FLACish (FISH), a model was written designated as the Homogenised Strain Softening Model (HSSM). In this model the effects of different parameters discussed in this thesis, are applied to the Mohr Coulomb parameters (c'_u and ϕ'_u) of unfissured specimens. This model was used to predict the effective shear strength of cases in which laboratory simulation was impractical or not feasible.

The advantage of this model (HSSM) is that it relates the effective shear strength of the fissured mass to the corresponding Coulomb parameters (c'_u and ϕ'_u) of the intact or unfissured overconsolidated clay specimen with reduction functions relating to the parameters discussed in this thesis.

The numerical models developed by ANSYS were calibrated and verified by the experimental results, and then used to predict or estimate the effects of confining pressure, orientation of fissures on the three dimensional modelling of the partially and fully fissured overconsolidated triaxial specimens.

In this thesis the effects of the type of clay, preconsolidation (P'_c) pressure, Overconsolidation ratio (OCR), size of sample, rate of shearing and fissure parameters, such as spacing, width and orientation of fissure were discussed and identified or quantified to estimate the effective shear strength of the artificially overconsolidated fissured samples. These results are applicable for the estimation of

the effective shear strength of the naturally overconsolidated fissured mass by homogenising the effects of the parameters on the Mohr Coulomb parameters (c'_u and ϕ'_u) of the intact or unfissured clay mass.

LIST OF PUBLICATIONS

Some of the results of the experimental and numerical studies carried out in this thesis have been reported in four papers: These are:

Sabzalisenejani, Ali; Nikraz, H. (1997). Laboratory simulation of parameters which are effective on the effective shear strength of naturally overconsolidated fissured clays. Fourth International Conference on Civil Engineering, Tehran, Iran.

Sabzalisenejani, Ali; Nikraz, H. (1997). Computer modelling of the overconsolidated unfissured, partially and fully fissured clay samples in direct shear test by using FLAC. Third Asian Young Geotechnical Engineers Conference 1997, Singapore.

Sabzalisenejani, Ali; Nikraz, H. (1998). A numerical approach for the prediction of the effective shear strength of stiff fissured clay samples based on direct shear test and FLAC modelling. 2nd International Symposium on the Geomechanics of HARD SOILS SOFT ROCKS, Napoli, Italy.

Sabzalisenejani, Ali; Nikraz, H. (1998). Computer modelling of triaxial samples for fully, partially and unfissured overconsolidated clay samples by using ANSYS. Thirteenth Southeast Asian Geotechnical Conference, Taipei, Taiwan.

ACKNOWLEDGMENTS

This investigation was carried out in the School of Civil Engineering of Curtin University of Technology under the supervision of Dr. Nikraz. The author wishes to express his deepest sense of gratitude to Dr. Hamid Nikraz for his constant support, valuable supervision, and encouragement.

The author also appreciates the help that received from the other academic staff of the School of Civil Engineering, especially Mr. Martin Press and Professor B.V Rangan.

The author is grateful to many people and organisations for providing support facilities. Particular thanks are extended to Department of Mine, Western Australia, for providing support facilities for running the FLAC models and School of Civil Engineering of University of Western Australia for giving some facility for running the large direct shear tests.

I would like to thank the Technical Staff in the School of Civil Engineering of Curtin University of Technology. Thanks to Mr. R.C. Lewis, Mr. R.G. Cutter, Mr. F. Andronis, Mr. M. Ellis, and Mr. D.S. Edwards.

The Author wishes to acknowledge the support of a scholarship provided by the Ministry of Culture and Higher Education of Islamic Republic of Iran.

Finally I wish to thank my family, especially my wife, and daughters for their help, patience, encouragement through my study.

TABLE OF CONTENTS

CHAPTER 2

LITERATURE REVIEW

LIST OF FIGURES

LIST OF TABLES

LIST OF NOTATIONS

a	constant of Equation (7.28), or effective area of the Bellofram in Equation (6.1)and parameter
A_0	initial area of the triaxial specimen
A	area of the axial specimen in Equation (6.1)
b	constant of Equation (7.28), and a parameter
c	constant of Equation (7.28), and a parameter
c_u or C_u	undrained shear strength
C_c	compression index
C_v	coefficient of consolidation
c'_p or C'_P	effective peak cohesion
c'_r or C'_r	effective residual cohesion
c'_{fs} or C'_{fs}	effective cohesion of a fully fissured specimen
c'_{pf} or C'_{pf}	effective cohesion of a partially fissured specimen
c'_u or C'_U	effective cohesion of an unfissured specimen
D	diameter of the triaxial specimen
$e_{p'_c}$	final void ratio for the preconsolidation pressure of p'_c
E	modulus of elasticity (Young's modulus)
E_A	apparent Young's modulus
E_i	intact Young's modulus
G	shear modulus
G_s	specific gravity
H	Height of the triaxial specimen
h_0	initial height of a direct shear box specimen
h_f	final height of a direct shear box specimen after consolidation
i	inclination angle of fissures
K	permeability
K_N or k_n	normal stiffness
K_t, K_S	shear stiffness
K_v	bulk modulus
K_0	coefficient of earth pressure at test
l	length of the specimen

n	number of fissures with width of w
p_6, p_7, p_8, and p_9	pressures from pore pressure, cell pressure, back pressure and low chamber controllers respectively
P'_c	preconsolidation pressure
OCR	overconsolidation ratio
R_6	stress ratio
s_1, s_2, s_3	total axial, effective axial and effective radial stresses respectively
t_{100}	time required for 100% consolidation of the specimen
t_f	time required for the failure of the specimen
v_7, v_8, v_9	volume changes from cell pressure, back pressure, and lower chamber controllers respectively.
w	width of fissure
α	crack propagation in Equation (2.2)
$\alpha_{1,2}$	coefficients in Equations (5.37) and (5.38)
α_f	percentage of fissure surface
β	angle between the axis of crack and direction of uniaxial compressive stress (Equation 2.2)
$\beta_{1,2}$	coefficients in Equations (5.37) and (5.38)
γ	density of material
$\gamma_{1,2}$	coefficients in Equations (5.37) and (5.38)
ϕ'	effective friction angle
ϕ'_p	effective peak friction angle
ϕ'_r	effective residual friction angle
ϕ'_u	effective peak friction angle of an unfissured specimen
ϕ'_F	effective peak friction angle of a fully fissured specimen
ϕ'_{PF}	effective peak friction angle of a partially fissured specimen
ϕ'_{FS}	effective fully softened friction angle
μ	coefficient of friction
ν	Poisson's ratio
$\theta_{1,2}$	coefficients in Equations (5.37) and (5.38)
σ_3	confining pressure
σ_c	uniaxial compressive stress
σ_N	normal stress
σ_r	redial stress
σ_t	tangential stress
σ_{XX}	normal stress in x direction
σ_{YY}	normal stress in y direction
σ'_1	effective axial stress (effective maximum principal stress)
σ'_3	effective confining pressure (effective minimum principal stress)
τ_u	undrained shear strength
τ_{xy}	shear stress in xy direction
$\tau_{r\theta}$	radial shear stress
τ'_p	effective peak shear strength
τ'_r	effective residual shear strength

τ'_u	effective shear strength of an unfissured specimen
τ'_f	effective shear strength of a fully fissured specimen
τ'_{PF}	effective shear strength of a partially fissured specimen
λ	constant in Equation (6.7)
$\psi_{1,2}$	coefficients in Equations (5.37) and (5.38)
ω	water content

CHAPTER 1

INTRODUCTION

1.1 BACKGROUND OF THE THESIS AND DEFINITION OF THE PROBLEM

The importance of fissures in soils, as well as joints in rocks, is widely accepted in Geology, Geomechanics, Rock Mechanics, and Contaminant Migration. Fissures in clays can affect the physical and mechanical behaviour of clay substances and will generally increase the hydraulic conductivity of clays (Garga, 1970 and 1988; Apted, 1977). Elastic parameters, such as Poisson's ratio and modulus of elasticity, will also be affected. Poisson's ratio increases as the intensity of fissures in a sample increases, but modulus of elasticity will decrease (Costa - Filho, 1980).

Fissures can influence the overall shear strength of clay mass and control the path of failure surfaces through the mass in the naturally fissured slopes (Skempton, 1977, Vallejo, 1985-89).

For assessing the long-term stability of natural slopes made of stiff fissured clays and shales, a knowledge of the drained shear strength of these materials is required. If a landslip already exists, or there are pre-existing shear surfaces, the strength of the slide surface will be at residual. If there has been no previous failure, the possibility

of a "first time slide" should be considered and the field strength or overall effective strength of the fissured mass for the first failure corresponds to the "fully softened" effective strength of the intact substance (Skempton, 1964). Fully softened strength happens when there is no further volume change at a constant shearing stress.

In a review of the slope stability of a cutting in Brown London clay, Skempton (1977) reported that the fully softened angle of friction was the same as the effective peak strength of the clay substance. Chandler and Skempton (1974) obtained the cohesion intercept by back analysing the failed slopes and argued that although the field cohesion at the time of the first failure was small , it could not be zero. Moon (1984) suggested a value for c' about equal to the residual effective cohesion determined by laboratory tests. Therefore , the effective shear strength parameters they suggest for the analysis of the first time slides are, the fully softened angle of friction ϕ', assumed to be equal to the peak angle of friction determined by laboratory test, and the fully softened cohesion c' is assumed to be equal to the cohesion obtained in residual tests.

However other researchers have investigated this feature and to a certain extent, proved by back analysing failed slopes in natural fissured mass, that the overall effective strength or effective strength of the fissured mass is different from fully softened strength of the clay substance suggested by Skempton. MacGregor, et al., (1990) and Thorne (1984) believe that the fully softened strength suggested by Skempton (1977) and Chandler (1984) is not applicable for cases fissure surfaces are slickensided and polished.

1.2 OBJECTIVES OF THE STUDY

Taking into account these different points of view, this thesis sets out to determine generalised procedures for assessing the effective shear strength of fissured clays.

It is of interest to relate the effective shear strength of a partially fissured clay specimen to the effective shear strength of the unfissured and fully fissured specimens of that clay mass, as well as to the fissure parameters which are understandable and measurable parameters.

The first objective was to establish and simulate experimentally the parameters which control the effective shear strength of an overconsolidated fissured clay mass and quantify their effect by using artificially overconsolidated clay specimens in the laboratory.

From the study of laboratory tests on the artificially overconsolidated unfissured, partially and fully fissured specimens, relationships of c'_f and ϕ'_f (effective peak Mohr Coulomb parameters of fissured specimens) with c'_u and ϕ'_u (effective peak Mohr Coulomb parameters of unfissured specimens), were determined individually for each of the parameters discussed in this thesis.

The second objective was to develop numerical techniques to simulate strain softening behaviour for unfissured and fully fissured overconsolidated clay specimens subjected to direct shear tests and then to apply the effects of the parameters discussed in this thesis on the effective shear strength of unfissured specimens and to develop a numerical model by utilising FLAC programming, FLACish (FISH). The model was used to evaluate the Mohr Coulomb effective shear strength parameters of a fissured specimen (c'_f and ϕ'_f) for any assumed initial condition. That model also was used to estimate c'_f and ϕ'_f for cases where simulations were impractical or impossible in the laboratory.

The final objective was to simulate numerically the triaxial specimens by utilising ANSYS (1996) and study the effects of the orientation of fissures for fully fissured and partially fissured overconsolidated clay specimens and also the effects of confining pressure on the behaviour of the specimens.

1.3 METHODOLOGY FOR EXPERIMENTAL AND NUMERICAL STUDIES

1.3.1 Experimental Studies

Two experimental methods to investigate the problem are as follows:

(a) The first is, taking large samples of a fissured clay mass and testing them in the laboratory or in the field. The samples must be representative of the soil for laboratory tests. For this method of investigation , the effects of sampling

disturbance, sample size, potential limitations of the representativeness of the results for the site which is being investigated, as well as the cost of investigation, are problems.

(b) The second method is, to consider separately the effects of the parameters that control the effective strength of the fissured mass and to combine these effects to determine the overall mass strength. This can be done using naturally fissured or artificially fissured clays.

Considerable research has been carried out on the impact of fissures in naturally fissured clays as indicated in previous sections. Many researchers have studied the drained and undrained shear strength of naturally fissured specimens taken from different materials with different stress histories , and different sample sizes. The results, because of the lack of sufficient details of the fissures, are too variable to be comparable to allow the prediction of the behaviour of fissured clays. There are naturally fissured clays in places like Newcastle, Botany Bay in Australia, but because of a lack of control of fissures in the naturally fissured specimens , to investigate the effects of fissures on the overall effective shear strength of the specimens or to predict the overall effective shear strength of the fissured mass, would be difficult.

The experimental section of this study has been based on the second method of investigation. For the most important of parameters influencing mass strength of the fissured mass, such as type of mineral, preconsolidation pressure, overconsolidation ratio, disturbance of specimens, rate of shearing, and fissure parameters like spacing, width, and orientation, a large number of laboratory tests was carried out on artificially fissured clays. After experimental results for each simplified case, had been obtained they were applied to more complicated cases using numerical modeling and programming.

1.3.2 Numerical Studies

Taking into account the number of tests required to study the effects of the parameters, the time was needed to mix the powder of the two different types of pure clays and make and cure the paste, the time needed to prepare artificially

overconsolidated clay specimens, the very slow rate of loading or shearing to satisfy the drained condition of tests, numerical modeling was used as a complimentary part of the study. For two dimensional modelling of the direct shear tests FLAC, (Itasca, 1994) was used to simulate strain softening, an intrinsic behaviour of overconsolidated clay mass, for the unfissured and fully-fissured specimens. Then by using the FLAC programming, FLACish (FISH), and the experimental results, a model was developed to estimate the effective shear strength of fissured specimens subjected to direct shear tests for any arbitrary combination of the parameters which are impractical or impossible to be simulated experimentally.

For the three dimensional modelling of the triaxial samples, ANSYS (1996) was used to study the effects of orientation of discontinuous and continuous fissures and confining pressures on the effective peak shear strength of the specimens subjected to triaxial tests.

After calibration of the coefficients which were necessary for the simulation of the triaxial specimens, the batch files were written to study the effects of orientation of discontinuous and continuous fissures, as well as the effects of confining pressure on the behaviour of the partially and fully-fissured clays and finally the effect of arrangement of fissures on the shear strength.

1.4 LAYOUT OF THE THESIS

Experimental and numerical methods, including two and three dimensional analyses, as well as programming are presented.

The thesis has the following eight chapters: chapter 1 contains the Introduction, sets the background of the research topic and defines the problem.

Chapter 2 presents a literature review of previous studies on the selected relevant materials covering how fissures are formed, how they can be classified, and how they affect the shear strength of fissured clay mass, as well as which kinds of tests, and what dimensions of specimens have been used to evaluate shear strength, compressibility and hydraulic conductivity of fissured clays. However, the more important issues are further discussed in the pertinent sections of the thesis.

Chapter 3 presents a preliminary study on the simulation of the parameters in the laboratory in order to carry out laboratory tests and determine the effect of different parameters, initialisation of the type of clays used for the preparation of artificial consolidated specimens in the laboratory, the shape of the stress- strain curve of the clay materials, rate of shearing the specimens, disturbance of the specimens, effect of locked-in stresses, and method of fissuring the specimens used for both direct shear and triaxial tests, constructing devices needed to prepare artificially consolidated specimens both for direct shear tests and triaxial tests are investigated and discussed.

Chapter 4 presents the experimental program on the direct shear tests and reports the results. For the unfissured, partially and fully-fissured specimens prepared artificially in the laboratory, for three different sizes, 60 mm × 60 mm , 100 mm × 100 mm and 300 mm × 300 mm. At the end of the chapter, the results are discussed in detail to find a formulation for the assessments of the effects of parameters on the effective shear strength parameters, c' and ϕ' of an unfissured overconsolidated specimen subjected to direct shear tests.

Chapter 5 presents the FLAC (Fast Lagrangian Analysis of Continua) modelling of direct shear tests and also strain softening behaviour of the artificially overconsolidated clay specimens for fully fissured and unfissured clay specimens. After verifying the FLAC models for these specimens, models were used to simulate the partially fissured specimens to study the effect of spacing and the width of discontinued fissures in the samples subjected to direct shear tests. At end of the chapter, the procedures used to write the program using FLAC programming language, FISH (FLACish), is reported in detail. This program was used to estimate the effective shear strength of the specimens subjected to direct shear tests which in the laboratory was impractical or impossible.

Chapter 6 presents the experimental program for unfissured, partially and fully-fissured artificially overconsolidated clay specimens subjected to triaxial tests and the results with respect to the effect of preconsolidation pressure, overconsolidation ratio and for the fully or partially fissured samples and the effect of orientation of fissure or discontinued fissure on the effective shear strength, are discussed.

In order to investigate the effect of confining pressure and the orientation of fissures with a complex arrangement, a finite element program, ANSYS (1996), is used to simulate three dimensional triaxial specimens.

Chapter 7 introduces first the ANSYS software for three dimensional modelling artificial specimens then reports on the calibration of the coefficients used in ANSYS modelling for triaxial specimens by using the experimental results from direct shear and triaxial tests. Then ANSYS is used to model other cases which are not practical or possible to simulate in the laboratory. At the end of the chapter, experimental and numerical results are discussed to formulate the effects of orientation of fissures and confining pressures on the effective shear strength of the specimens subjected to triaxial tests.

A summary of the main points, conclusions and recommendations for further study are presented in Chapter 8.

CHAPTER 2

LITERATURE REVIEW

2.1 INTRODUCTION

Fissures are defects in clays which affect their physical and mechanical properties, including shear strength. Many factors influence the shear strength of a fissured clay mass and these have been considered by a number of researchers. This chapter reviews the literature and includes the following aspects:

- The formation of fissures and joints in soils
- Fissure formation
- Classification, techniques of measurement, recording, and description of fissures
- Factors and parameters which influence the shear strength of fissured clays
- Sampling of fissured clays
- Statistical surveys of fissure parameters
- The effect of fissures on other parameters such as ν, E, K_v, K_0, and C_c
- Shear strength suggested for analysis of slope stability in a fissured clay mass
- Test methods for residual, fully softened and peak shear strength

- The effect of fissures on the slope stability and failure surface in a fissured clay mass
- Laboratory shear strength tests of naturally fissured clays
- In-situ shear strength tests on naturally fissured clays
- Laboratory shear strength tests on artificial fissured clays
- Effect of fissure orientation on the estimation of shear strength from an analytical point of view

2.2 FISSURES AND JOINTS IN SOILS

Soils and rocks have many structural weaknesses that significantly decrease the shear strength of the mass below that of the intact material . These discontinuities also have a controlling influence on the movement of ground water through the mass.

This section explains the nature and origin of discontinuities in soil and rock masses with most emphasis on the origin and formation of fissures in clayey soils.

2.2.1 The origin and nature of discontinuities

Discontinuities in soil and rock have a range of methods of formation and this determines their nature and properties. Recognition of the type of discontinuity and its origin will assist in allowing the mechanical properties be assessed and extrapolated (Hencher, 1987). Extrapolation is not valid if the geological history of formations in which discontinuities occur differs for different locations. Hencher (1987) classifies discontinuities into two groups and Tables (2.1) and (2.2) provide a simple classification of common types of discontinuity and list their typical characteristics and geotechnical significance.

Table (2.1) deals with discontinuities that are usual in all rock types and Table (2.2) lists discontinuities which are more common in particular types of rocks and to a lesser extent, soils. These discontinuities are described below.

2.2.1.1 Tectonic joints

Tectonic joints, formed as the result of orogenic stress in the earth's crust, are common to all rock types and may even be found in recent sediments (Burford and

Dixon, 1981). They are often in distinct "sets" a term that is sometimes used to define a series of parallel joints (Herget, 1977).

The geometrical relationship between sets may sometimes be interpreted if there is a regional stress pattern or a local geological structure such as a fault or a fold (Price, 1966).

In many cases, to relate the joint pattern to a known cause is very difficult. The joints formed as the result of shear stresses are commonly less rough than those formed under tension and then might be expected to exhibit lower shear strengths (Hencher, 1987).

2.2.1.2 Faults

Faults are fractures that occur singly or in groups forming shear zones and are often discordant to other geological structures, particularly lithological boundaries and bedding, and are rarer discontinuities than joints.

Where a zone of intense and discordant jointing is available, the term shear zone or fault might be used even though there is no clear evidence of displacement along the zone (Herget, 1977). Faults often cause geotechnical problems, not only in slopes and tunnels, but sometimes in the foundation of large dams.

Faults can be identified by many features, particularly the displacement of beds and by the intensity of jointed or crushed zones of rock. Major faults are often eroded and can be distinguished by air photographs.

2.2.1.3 Lithological boundaries

Geological boundaries between different soils and rocks and between soil and rock often cause sharp changes in engineering properties and are, therefore, important for stability analysis. Where the lithological boundary shows a change from "soil" to "rock", different methods of analysis will be required for the two component materials of the slope.

2.2.1.4 Sheeting joints

Sheeting joints in hard rocks are typically rough and extensive and parallel to the topography of the present-day, or that of the recent geological past. Tensile stresses

following unloading due to erosion or perhaps the removal of ice load can cause these kinds of joints. Sheeting joints occur in all lithology and in quite recent sediments (Fookes, 1965, Skempton et al., 1969). They decrease in frequency with depth in the ground and may cross geological boundaries.

2.2.1.5 Bedding surfaces and bedding surface joints

Change in sediment type or a break in continuity of deposition is displayed as bedding surfaces in sedimentary rock and sedimentary soils. A marked anisotropy is imposed on the rock or soil mass. Bedding surfaces are often closed and may have strong cohesion but because of unloading or weathering, they may open up. Most are fairly planar and smooth but sedimentary features, such as ripple marks or load casts associated with bedding surface, may cause the surface to be of rough texture.

2.2.1.6 Fissures

Fissures are usual in unlithified clays and silts, are generally discontinuous and are often random in orientation (Herget, 1977), even though some authors have tried to relate them to specific stress fields (Skempton et al., 1969; Fookes et al., 1969; McGown et al., 1974).

In the following section the formation of fissures will be discussed in more detail.

2.2.1.7 Cooling joints

In igneous rock, joints form as the magma cools. The most distinguishing examples are the columnar joints formed perpendicular to the cooling surface in lava.

The form of cooling joints in large intrusions are often dome-like with cross-joints (Gamon and Finn, 1984).

Layering of igneous rocks due to density segregation of minerals on cooling can also be found, as well as flow banding, and these features will cause anisotropic engineering behaviour.

2.2.1.8 Metamorphic fabrics

Metamorphic rocks created under pressure usually contain well-defined sets of discontinuities. Slaty cleavage, a close pattern of parallel planar discontinuities, is

formed in rocks by regional stresses and causes significantly anisotropic properties (Brown et al., 1977). Phyllities and Schists are higher grades of metamorphism and exhibit foliation. The foliation surfaces are often coated with minerals such as chlorite, talc and mica that may have low frictional properties. This kind of foliation is generally more wavy than slaty cleavage and this will have an influence on the shear strength.

2.3 FISSURE FORMATION

The origin, formation, and types of fissures will be discussed in this section.

2.3.1 Fissures in Stiff Clays

Fissured clays occur naturally in overconsolidated clays and weathered shales (Bishop and Garga, 1969; Skempton, 1964; Terzaghi, 1936, Jennings, 1970).Fissures develop in these clays for the following reasons:

-During the consolidation process (Casagrande, 1949)

-During swelling of the clay as a result of a decrease in overburden pressure, or stress release perpendicular to exposure and ground surfaces (Casagrande, 1949)

-As a result of syneresis, a colloidal phenomenon (Eide, 1967)

-From chemical reactions in the clay that can induce volume distortion (Kallstenius, 1963)

-As the clay dries, swelling and shrinkage in clay soils (Corte and Higashi, 1964)

-Inherited from the bed rock (Fookes, 1965)

-From large lateral stresses that can induce fissuring of the clay (Atchinsin, 1953; Terzaghi, 1961

-Tectonic movements and landslides (Skempton, 1966)

-Depositional environment (Thorne, 1984)

2.3.1.1 Fissures formed from chemical reactions in the clay which induce volume distortion, chemical and physical weathering, and decomposition

In tropical and subtropical climates chemical action is the dominant weakening process (Irfan, 1988). Physical effects, such as the opening of discontinuities, the

formation of new discontinuities by rock fracture, the opening of grain boundaries and the fracturing of individual grains, generally accompany decomposition. Continued weathering activity for a long time, results in the conversion of rock to a soil which finally loses its original rock fabric and becomes a true residual soil. In tropical regions, intensive weathering may cause a leached, sometimes hardened, rock-like surface layer called laterite as a result of the removal of silica and bases, and cementation of the residual soil by iron and aluminium-oxides.

Physical changes such as reductions in porosity and permeability help to retard chemical reaction during weathering. Interaparticle rehydration of expandable clay minerals will occur in response to physical changes. In dispersive clay, colloidal particles will be gradually washed and will result in microfissures in the clay mass.

Hydrothermal alteration is another weathering weakening process of soil and rock mass in tropical and subtropical climates, the result of hot aqueous solutions penetrating the mass, especially along discontinuities, and producing mineralogical changes, like chemical weathering (Irfan et al., 1988).

2.3.1.2 Fissures formed during the swelling of the clay as a result of a decreasing overburden pressure

Passive failure, following removal of overburden (unloading by erosion or excavation), creates fissures during the swelling of the clay. Unloading by dredging causes an important decrease in strength and stiffness and an increase in K_o (Thorne, 1984).

Vertical stress release due to the removal of overburden pressure perpendicular to an exposure seems to have significant influence when nearly perpendicular to bedding (Fookes et al., 1969).

Figure (2.1) illustrates the concept of fissuring as result of a decreasing overburden pressure. Clays which are deposited during a period of coastal submergence may be fissured as a result of exposure during temporary recessions of the sea level (Thorne, 1984). This was noted by the measured strengths of fissures formed by passive failure which were much below peak intact strengths and in situ tests showed high horizontal stresses (Thorne, 1984). Most fissures are generally closed but there is

some evidence to indicate that they may open because of stress-release, probably associated with their inability to resist the high suction implied by the unloading.

2.3.1.3 Fissures formed as a result of syneresis, a colloidal phenomenon (depositional / syneresis fissures)

The spontaneous throwing-off of a liquid by a gel during ageing, resulting in shrinkage and in the formation of joints or fissures, is called syneresis (Bates and Jackson, 1988). These kinds of cracks with a dull or shiny surface are sometimes planar and show no sign of relative movement. Subaqueous joints differ from subaerial desiccation joints. Subaqueous shrinkage joints are not so well-developed, rather narrow and do not posses well-developed v-shapes in transverse sections. In general, subaqueous shrinkage joints are less regular in form and often incomplete and sometimes they have preferred orientation.

2.3.1.4 Fissures formed during the non-uniformed consolidation process

Fissures can be created in clay beds distorted as the result of consolidation of underlying peat beds by the weight of deposition. Figure (2.2) illustrates the concept of fissuring as a result of a non-uniform consolidation process.

At Botany Bay (Australia) there are many peat deposits and it is estimated that they are now only about 20% of their original thickness, therefore the over lying clays have been distorted substantially by the deposits (Thorne, 1984).

2.3.1.5 Fissures formed when the clay dries (swelling and shrinkage of clay soils)

Fissures can form from the swelling and shrinkage of highly reactive clays when they are exposed as a land surface and subsequently as an inundated surface. Such movements can cause passive failure in wet seasons and ingest the sand and debris into the vertical fissures in dry seasons (Stapledon, 1970) as shown schematically in Fig. (2.3). Moris et al. (1992) investigated the factors which can affect the depth of cracks. They found that surface cracking and fissuring in unsaturated soils undergoing drying is controlled by soil suction and soil properties such as compression modulus, Poisson's ratio, shear strength, tensile strength, and specific

gravity. They derived some relationships for finding the depth of cracks based on electricity theory, linear elastic fracture mechanics, and the transition between tensile and shear failure.

Any decrease in water content as a result of drying causes close arrangement of soil particles and shear straining. Surface-tension as a result of shrinkage generates negative pressures (matrix suction) below atmospheric pressure in the remaining pore water. Matrix suction is measured by the difference (u_a - u_b) between the pore-air pressure and the pore-water pressure and it produces two counteracting effects, one is isotropic contraction of the soil and the other is the development of vertical fissures below horizontal drying surfaces (Morris et al., 1992).

The intensity of cracks depends on the mineralogy of the soil, climatic conditions such as temperature and rainfall, and surface vegetation cover (Morris et al., 1992). Plastic clays which contain more water than lean (low plasticity) clays have larger volumetric contractions on drying. Plastic clays also have a larger effective cohesion c' and larger tensile strength (Barker, 1981). This causes wider, deeper cracks in the plastic clays than in the lean clays. Wide and deep cracking is associated with plastic soils and high temperatures during dry seasons when the water table drops to considerable depth in the soil profile (Morris et al., 1992).

Reinforcement by roots provides additional tensile resistance and reduces cracking. Shrinkage cracks are usually vertical (or sub vertical), although a few are horizontal. They extend almost to the depth of seasonal moisture changes in the ground.

Slickensided joints generally sub-horizontal, may also be present and extend to a considerable depth. Slickensides are the result of shear displacements which may be caused by horizontal pressures that follow re wetting in active clays after infilling has washed into previously open cracks (Morris et al., 1992). Alternatively they may result from differential shrinkage because the soil is non-uniform or the vegetation cover is variable (Stapledon, 1970). They may also be caused by tectonic effects (Morris et al., 1992).

2.3.1.6 Discontinuities formed from the weathering of the rocks

Rocks contain structural discontinuities such as joints, faults, fractures, cleavage and foliation, and lithological structures such as bedding planes, unconformities, laminations, dykes, mineral alignment, etc.

Weathering action is continuously concentrated along these weaknesses. The layer of clay soil overlying the weathered rocks can be affected by non-uniform deformations of the bed rock and this causes some of the clay overlaid to fissure. Figure (2.4) illustrates the concept of fissuring as a result of deformation in bed rock.

Many different infillings and minerals may be present along relict discontinuities. These may be formed from the parent rock, washed in from higher horizons or created in place by weathering or alteration. Inherited infillings may be hard or soft depending on their origin, for example, hard quartz veins or soft clay fault gouge. The infilling can be from a very thin veneer to tens of millimetres. Slickensided or polished relict discontinuities are usual in saprolites (St. John et al., 1969; Koo, 1982a).

Slickensides may be very old features caused as a result of tectonic movements in parent rock and preserved in the weathered rock. They may also have been formed by differential displacements occurring within the saprolitic soil as a result of the weathering process, for example, stress release resulting from gradual erosion of the overlying weathered soils. The quick removal of a deep thickness of weathered soil by mechanical excavation may also cause the development of slickensiding and polishing. Usually for old slickensides there may be more than one direction of polishing (striation) on the relict discontinuity surface (Irfan, 1988).

It has been observed that slickensides occur in materials which have a plasticity index greater than 30 and also a clay fraction (less than 2μm diameter) greater than 30 percent. In fact, the occurrence of slickensides is more possible in clays with an Activity greater than 0.7 or clays classified 'very high' potential expensiveness, or perhaps even 'high' expensiveness when plotted on the Activity chart (Williams, 1958).

The occurrence of slickensided fissures has been observed in depths of up to 15 m, usually above the ground water. Where there is an active soil profile and a climate of a particular and appropriate seasonal moisture variation, the slickensides are numerous. Where one of these two factors is absent, there may be very few slickensides at inclined angles of dip (Williams et al., 1977).

2.3.2 Fissures Formed in Earth Dams During Construction

Fissures form in the clay core of earth dam sections during construction for the following reasons:(Sherard et al., 1963; Marsal, 1979)

a) Differential settlement caused by volume changes in the embankment material, as well as those caused by compaction or consolidation of the foundations, form and develop fissuring in the earth dam.

b) Embankment zones dry and cracked in the sun during construction and subsequently covered up and left in place will contain cracks / fissures.

c) Localised cracks during the deformation of the entire mass can be developed in embankment zones formed by a brittle layer, sandwiched between relatively plastic layers.

d) Insufficient compaction of individual layers or a weak bond between them can cause fissures at the interface.

e) Horizontal shear stresses caused by heavy rollers passing on an embankment will cause horizontal fissures in the earth dam.

According to Covarrubias (1969), fissures or cracks exist in the core section of earth dams as a result of the following factors:

1- Deformation of the materials in the dam or in the foundations due to weight.

2- Abrupt changes in the cross-section of a valley.

3- Large deformations caused by saturation of the materials in the dam.

4- Large rates of strain caused by rapid filling of the reservoir, especially if the materials suffer substantial movements upon saturation.

5- Large transient stresses caused by earthquakes.

6- Large differences in stress-strain properties of materials in adjacent zones or layers.

2.4 CLASSIFICATION, TECHNIQUES OF MEASUREMENT, RECORDING, AND DESCRIPTION OF FISSURES

The objective of this section is to review the different methods used in the classification of fissures in terms of size, surface characters and geometry, and

intensity. "Fabric", which is a general term describing fissures, bedding, joints, etc in soil, can dominate engineering behaviour. The term "microfabric" refers to the size, shape and arrangement of solid particles, the organic inclusions and associated voids. Clay particle arrangements are described as "microfabric", whereas the arrangement of particle groups, for example, in layers having different particle sizes or the fissures or joints in the soil comes under "macrofabric" (Rowe, 1972).

The first method detailed to describe fabric based on the terms relating to type of fissure and fissure surface and fissure fabric and intensities was proposed by Fookes et al. (1969). McGown et al. (1980) further developed and modified Fookes (1969) concepts. This method is discussed briefly below.

2.4.1 McGown et al. 's Method

In this method the nature and form of all macrofabric features commonly found in soil are described and a suggested approach given to the assessment of the arrangement of these features. The fabric description is limited to layering and discontinuities. McGown et al. (1980) suggested that the characterisation of soil fabric can be considered in two parts, one describing the features themselves and the other describing their spatial arrangement.

Features formed by soil particles may be composed of organic or inorganic materials. They may be arranged in three forms, linear (1 Dimensional extensive) termed lineation, planar (2 D extensive) termed layers and three dimensional features (3 D extensive) termed lobes. Examples of various features which fall into these groupings are given in Table (2.3). Macro-Pore spaces also show various forms and can be similarly presented like macro fabric features as linear features (1 D extensive) termed ducts, planar features (2 D extensive) termed discontinuities and three dimensional features (3 D extensive) termed defects. Examples of features falling into these groupings are also given in Table (2.3)

The arrangement of soil macrofabric should be considered in two distinct parts, firstly the orientation of fabric features should be considered, secondly, spacing of the features should be determined. To obtain a full appreciation of the arrangement of fabric, three levels of analysis should be carried out as follows :

(i): the basic level, which is the arrangement of like individuals with regard to one another, e.g. the spacing of silt laminations in a layered clay

(ii): the related level, which is the arrangement of like individuals with regard to other groups of individuals, e.g. the dips of clean fissures compared with the dips of coated fissures .

(iii): the referred level, which is the arrangement of like individuals with regard to specific reference axes or surfaces, e.g. the spatial orientation of low dip angle fissures compared with the original ground surface. In layered soils, the basic spacing of laminations etc. is usually obtained but in soils containing discontinuities, the spacing with respect to a reference axis is more generally obtained (McGown et al., 1980).

McGown et al. (1980) indicate that from a consideration of the nature, form and arrangement of the organic and inorganic materials and pore spaces in a soil, the complete array of data obtainable from a fabric investigation may be formulated as shown in Table (2.4). In most cases, one or two types of fabric features will dominate soil behaviour and rarely will there be a need for all the possible data points to be measured or calculated when investigating a particular soil for a purpose. For convenience in this method, the measurement of layers and discontinuities are treated separately:

2.4.1.1 Layered soils

Most alluvial deposits are laid down periodically e.g. from the annual flooding of a river and variations of sedimentation occur and the soil particles comprising them are, therefore, generally found in distinct units of organisation, variable in thickness, particle gradation, density and perhaps mineralogy (McGown et al., 1980). In this method describing the nature of the features, then their form and lastly their spatial arrangement is suggested.

Two groups of data will be needed to describe the nature of these features, a physical description using standard terms and a classification of the soil particles comprising them. The forms of the layers should be described by their thickness, continuity and surface geometry. For their spatial arrangement, two sets of data, first their orientation and then their spacing are needed as indicated in Table (2.5).

2.4.1.2 Soil containing discontinuities

Many overconsolidated clay soils, normally consolidated soils and a few sandy and silty soils contain discontinuities (McGown et al., 1980). For studying the discontinuities, either a cavity is excavated in undisturbed soil or an oriented undisturbed block sample is obtained for detailed investigation. For both procedures, the volume of soil investigated should include approximately 200 discontinuities in order to obtain a representative population (Radwan, 1974). Description of the discontinuities so exposed in terms of their nature, form and spatial arrangement is necessary. Table (2.6) shows a recommended layout for a record sheet and typical data obtained from a study in a drumlinised till in West Central Scotland by McGown et al. (1980).

McGown et al. (1980) describe the nature of discontinuities in four groups of data. The first is their mode of origin, either depositional, stress relief or shear induced ; the second , their surface roughness; the third, whether the surface is clean , coated or weathered ; the fourth , the nature of any surface coating. To describe the form of discontinuities ,their areal extent and surface geometry are considered .The basic orientation of each discontinuity is simply defined in terms of its strike and dip angles but, for easy handling of the large amount of data generated in an investigation, it is necessary to plot them on equal angle stereographic pole projections (Phillips, 1971).

Measuring the basic spacings of discontinuities is much more complex and McGown et al. (1980) indicated that up to that time, the spacings of discontinuities had been measured with respect to a specific, but arbitrarily chosen, axis or set of axes, which gave only referred spacing data from which basic and related measurements could not be expected . To correct this, McGown et al. (1980) offered an alternative measurement technique that calculates the spacing of discontinuities within sets along the line normal to their average plane and passing through the centroid of the block or cavity being investigated. The spacings of different sets of discontinuities can then be compared to give related and referred spacings. This method is more complex than previous methods and requires computers to analyse the data. However, it is the only method that permits the accumulation of basic spacing data. A

complete description of the method is not within the scope of this study. Details of the methods used and the classifications adopted are found in Appendices (A) and (B), McGown et al. (1980).

2.5 PARAMETERS WHICH INFLUENCE THE SHEAR STRENGTH OF FISSURED CLAYS

An analysis of stability slopes in fissured clays requires a knowledge of the fissure characteristics (or pattern) and the engineering properties of the fissured clay mass which is determined by the strength and characteristics of the fissures and the soil substance.

The pattern and the type of fissures is determined by the formation of the fissure. If the dominant factors for the formation or origination of fissures are known, then it is possible to predict the pattern and orientation of fissures in the fissured mass. As discussed in section 2.1, the major factors that influence the fissure patterns are: depositional environment, stresses release, lithology, bedding, tectonics, diagenesis, weathering, and age of exposure. One or more of these factors can be the major influence on the fissure patterns (dominant factors) and it may be expected that the fissured mass has an uniform pattern of fissures for the affected zone or area when these dominant factors are constant. According to Fookes et al. (1968), the fissures are randomly orientated, but locally they have some preferential orientations. In Australian situations, the fissures have preferred orientations as quoted by MacGregor et al. (1990) in the example.

Parameters such as spacing, length, shape, orientation, type of infilling material, water content, the plasticity index, kind of clay mineral, stress history, the duration of exposure, being closed or open or slickensided, smooth etc. are effective in determining the overall effective shear strength of the fissured clay mass. These factors can categorised into fissure parameters, substance parameters, and environmental parameters.

Fissure parameters include spacing; orientation; length, shape of fissures and infilling materials; substance parameters include soil type; peak, fully softened, residual strength and plasticity; and environmental parameters include stress history and overconsolidation ratio OCR and boundary conditions.

The intensity or spacing of fissures is influenced by near surface desiccation cracks and the mechanical properties of the material (Fookes et al., 1969). Skempton et al.(1967) reported that fissures in London Clay are generally not greater than a few square centimetres in area and the fissure size increases with depth for the three sites investigated by them. A mean dimension of about 30 mm was observed in upper layers and 75 mm in the deeper layers in clay. In most places the frequency of the fissures decreases with depth and the number of fissures per unit volume increases rapidly as the fissure size decreases.

In shape, the fissures are plane, curved (conchoidal) or sometimes of more irregular or undulating form. Skempton et al. (1969) indicate that in their experience (on English clays) the fissures have mounds and depressions of the order of .1 mm in height.

Fissures can be closed, or open, slickensided or rough surface. In situ, most fissures are almost closed but they may be open because of stress-release probably associated with their inability to resist the high suction induced by unloading (Ward, 1967; Garga, 1970).

Skempton et al. (1969) indicated that roughly only 5% of the fissures investigated in the sites studied by them had polished or slickensided surfaces. This contrasts markedly with fissures in some residual basaltic and tuffaceous soils in Australia which are usually slickensided (MacGregor et al., 1990).

Many types of infillings and minerals may be present along the discontinuities and fissures in soils. These may be inherited from the original rock or formed in place by weathering or alteration. Inherited infillings may be hard or soft depending on their origin and the thickness of infillings can vary from very thin to up to tens of millimetres (Irfan et al., 1988).

Slickensided fissures may be formed as a result of tectonic movements in the parent rock or by differential movements occurring within the soil as a result of the weathering process or the rapid removal of a large thickness of soil by mechanical excavation or by alteration of horizontal stress as a result of shrinkage and

subsequent swelling ,wetting and drying (St. John et al., 1969; Koo, 1982; Irfan et al., 1988).

The water content can affect the shear strength of fissured clays. Chen (1991) indicated that there is a specific water content for each kind of soil at which pre-existing fissures in the sample will be closed during the test for the water content greater than the specific amount, and open for water content less than that specific water content.

The kind and percentage of clay minerals has an influence on the effective shear strength (Skempton, 1985). For clays formed from montmorilonite, the shear strength is likely to be less than for other clay minerals. Because of these factors, the plasticity index can have a relationship with the overall shear strength of the fissured mass (Skempton, 1985).

Most parameters mentioned previously also have an influence on the representative sampling or sample size and testing required. The change of stresses, which is applied on the soil, during sampling and the interval of time between sampling and testing, can also have an influence on the shear strength of the fissured clays.

2.6 SAMPLING, AND SAMPLE SIZE EFFECT OF FISSURED SOILS

Examining, describing and recording the fabric of consecutive soil samples are important tasks in the study of fissured soils. For sampling in the fissured mass, the kind of fabric as well as the location, quantity, quality, and size of specimens are important. The quality and the size of specimens are effective in the drilling technique and the cost of site investigation.

Testing in the field can eliminate the sample size effect as well as the effect of fabric in the results. Taking large samples of fissured clay mass for testing in the laboratory can improve results, but the samples should be representative of the fissured soils. The prediction of strength of fissured soil can be completely erroneous if the specimens are not sufficiently representative of the strata and of their geological structure, and of the stress state in the field (Rowe, 1972). It is notable in sampling, the surface of fissures in samples can be roughened by thin deposits of sand or smooth (slickensided). In addition to the kind of fissure surface, the spacing,

orientation and surface condition are important in the sampling. They are effective on the stress component of strength (Rowe, 1972).

The spacing, as well as orientation of fissures, is an essential preliminary step towards representative sampling and testing and it is important to explain a permeable fabric in its location.

The dominance of fabric both in engineering problems and in drilling, sampling and testing should be considered in the study of this kind of soil. The extent of consideration depends on the class of study which is appropriate to the proposed work, on the ground conditions and on the related available finance (Rowe, 1972).

The details of fabric, the description of the principal strata, which should be supported by photographic records, as well as the method of drilling, sampling and testing, and reasons for their choice, should be included in the site investigation report (Rowe, 1972).

Disturbance due to drilling in boreholes, excavations in trial pits, sampling in tubes and laboratory preparation of test specimens, should all be considered and where possible avoided by using appropriate techniques (Rowe, 1968).

Therefore, for the preparation of artificial fissured samples, the effect of stress state as well as trimming the sample and scaling should have to be taken into account. The strength measured in field and laboratory tests depends on the extent of fissuring, the size of sample or specimen tested with regard to the spacing, fissure orientation, shape, surface roughness of the fissures, and the stress changes which occur during boring, excavation, sampling and testing of the clay, and the length of time that the clay remains under each stress history. These factors should, therefore, be modelled and studied for artificial fissured samples. These factors will affect the properties of the clay substance and the shear strength of the fissured mass depends on some or all of these factors.

For clays containing fissures with an uniform arrangement of fissures, laboratory and field tests of a reasonable size can give reliable measures of large-scale strength. It should be noted that these strengths are only applicable to the clay at the time of

sampling and testing and the possibility of further deterioration should be considered in the case of long-term stability problems (Marsland, 1972).

2.7 STATISTICAL SURVEYS OF FISSURE PARAMETERS

Variations of fissure parameters in a field is expected, therefore, a statistical analysis is needed to identify their general behaviour. Although the accuracy of statistical and probabilistic analysis for jointed rock is better than for fissured soils, for the local study of fissured mass, statistical analysis results can predict locally the overall behaviour of fissured mass for specific cases.

Williams et al. (1977) from an analysis of all joint data from South Africa, found that the distribution of values of the dip angle followed a Normal or Gaussian distribution.

Figure(2.5) shows the histogram for data collected in yellow brown clay at Vereeniging imposed by the theoretical Gaussian frequency distribution curve. Figure (2.5) shows a fairly good fit either side of 47°.

Williams et al. (1977) in an analysis of many observations of dip directions showed that the orientation of slickensided joints is quite random and an example of a histogram is shown in Figure (2.6).

They showed that there is a distinct positive skewness in the histograms for the data on joint lengths. It was found that a logarithmic normal distribution fits the experimental values fairly well. In other words, the logarithms of the lengths are normally distributed. In Figure (2.7) it can be observed that the log normal distribution gives a fairly good fit in this typical case.

For joint spacing, following the work of Hudson et al. (1975), a negative exponential distribution can fit the joint spacing as indicated in Figure (2.8).

The roughness parameter of a discontinuity is an index of the unevenness and waviness of the adjacent discontinuity wall.

This index refers to mean discontinuity plane. A waved discontinuity is characterised by large scale undulations, an uneven discontinuity is characterised by small scale roughness (Giani, 1988). The shear strength of a discontinuity is affected by the

roughness of its walls. Waviness influences the initial direction shear displacements relative to the mean discontinuity plane; unevenness affects the shear strength of samples in the laboratory or in situ, with direct shear tests at medium scale (ISRM, 1978). The shear strength due to the roughness decreases as the result of any increase of displacement.

Discontinuity roughness can be defined qualitatively or quantitatively. Figure (2.9) shows the roughness profile shape for each qualitative term (Giani, 1988).

2.8 THE EFFECT OF FISSURES ON PHYSICAL AND MECHANICAL PROPERTIES SUCH AS K, ν, E, C_C, AND K_0

Recent field and laboratory investigations on fissured soils have emphasised the importance of fissures on the physical and mechanical properties of these soils and also the dangers of using data obtained from laboratory tests on small samples in the design of both temporary and permanent works (Marsland, 1971a, 1971b, 1972; Thorne, 1984; Morris et al., 1992) .

2.8.1 The Effect of Fissures on the Permeability (k)

Apted (1977) in laboratory investigations and Garga (1970 and 1988) in field and laboratory investigations, considered the effect of fissures on permeability and found that the presence of fissures increases the permeability of the material even if they are apparently closed .

2.8.2 The Effect of the Fissures on the Other Mechanical Parameters (ν, E, k_V, c_c, and k_0)

The effect of open or closed cracks and pores in a rock mass on its elastic properties was recognised by Walsh (1965). The same consideration can be realised for features such as joints and fissures in a soil mass. Walsh (1965) showed for closed cracks, the effective bulk modulus (K_V) of a mass containing closed cracks is equal to its intact bulk modulus, and the effective Young's modulus for a body containing closed cracks is less than its intact Young's modulus if the surfaces of the cracks side relatively to each other, moreover, the effective Poisson's ratio for a body containing closed cracks is greater than its intrinsic Poisson's ratio. Another approach was used by

Costa-Filho (1980). He used triaxial specimen containing a single closed fissure inclined at an angle i across it.

$$E_A = \frac{E_i}{(H + \frac{\sin^2 i \cos i}{H} \frac{E_i}{K_s})} \qquad (2.1)$$

where E_A and E_i are the apparent Young's modulus and intact Young's modulus for the London clay respectively, H is the height of the specimen and K_s is the shear stiffness of the fissures as defined by Goodman (1976).

Garga (1988) investigated the effect of the specimen size on the volumetric compressibility and found that if all fissures are closed, there should be no sample-size effect under the isotropic state of stresses (Figure 2.10) .

The effect of sample size on stiffness was inspected by Agrawal (1967) on different diameters (300, 38, and 18 mm) and lower stiffnesses were obtained in the tests on large specimens. Marsland reported that the specimens with 38 mm dia. yield and higher moduli than those with 98 mm dia. but the magnitude of the difference was about 10-20%. Maguire (1975) in brecciated upper Lias Clay showed that there was a tendency for the modulus to decrease with increasing sample size.

Lo (1970) performed a series of triaxial tests on Nanticoke stiff fissured clay using specimens of different diameters under undrained conditions, and no distinction can be made in the stress-strain curves for the low stress levels. Marsland and Butler (1967) observed that the stress-strain curves from consolidated drained triaxial tests carried out in fissured Barton clay using specimens with different diameters, had no distinct trend . In these cases, it seems that there is no real trend of decreasing stiffness with increasing sample size for fissured clays provided with the initial effective stresses.

Laboratory triaxial tests, using specimens with different fissure configurations and with no fissures at all performed by Webb (1966), are shown in Figure (2.11). This figure shows the results of three isotropically-consolidated drained tests in London Clay corresponding to an intact specimen, a specimen which failed completely along a fissure and a specimen which failed partly along a fissure. The maximum shear

strength clearly differed, but for the initial stages of shearing up to an axial strain of about 1.5%, they behaved similarly. It seems that the specimens with fewer fissures or having fissures inclined in more favourable inclinations indicate a stiffer behaviour.

A soil with cracks or fissures is more compressible than an intact version of the same soil with the same water content. Wetting and drying cycles lead to increasing overconsolidation towards the surface, and this reduces the compressibility. The transition with depth from overconsolidated states close to the surface to normally consolidated states below the water table is relatively smooth.

As plastic clays contain more water than lean clays, they therefore experience larger volumetric contractions on drying and also have a larger effective cohesion c′ and larger tensile strength. This leads to wider, deeper cracks in plastic clays than in lean clays. So for larger effective cohesion c′, the clay has wider and deeper cracks and is more plastic.

Thorne (1984) in an investigation of fissured clays from Botany Bay and Newcastle in Australia, assessed the strength of these clays which were fissured as a result of desiccation as the clays were exposed during temporary recessions of the sea level, and by deferential settlement due to consolidation of peat layers. He found that the measured fissure strengths were much below the peak intact strengths and in-situ tests showed high horizontal stresses.

The amount of coefficient of earth pressure at rest increases for fissured clays. An increase in K_0 of consolidated clays can induce passive failure and cause fissure surfaces.

2.9 SHEAR STRENGTH SUGGESTED FOR ANALYSIS OF SLOPE STABILITY IN A FISSURED CLAY MASS

Direct shear and triaxial tests have being used to investigate the drained and undrained shear strength of a stiff fissured clay mass. When an overconsolidated clay sample is sheared slowly in a drained condition (so that there is sufficient time for dissipation of pore pressure induced by shearing), the stress-strain curve will take the general form shown in Figure (2.12). Different shearing mechanisms are recognised

in the shear box tests with somewhat different values of strength. Peak effective shear strength and fully softened and residual shear strength are different types which are obtainable in laboratory tests.

The behaviour stress-strain is dependent on clay fraction (finer than 0.002 mm) content and whether it is normally consolidated or overconsolidated (Skempton, 1985). The curve has the following common features:

- A peak effective shear strength was obtained at a small displacement

- A reduction of strength to critical state or fully softened strength then occurs with further displacement. The fully softened strength corresponds to the critical state (Skempton, 1985) i.e. when continuing displacement occurs without further change in volume or water content.

-With continuing displacement, after fully softened displacement, particle reorientation occurs which results in a further reduction in shear strength. The minimum value of shear strength achieved at large displacement is "residual" strength.

For assessing the long-term stability of natural in stiff fissured clays and shales, a knowledge of the drained shear strength of these materials is required (Skempton, 1964; Skempton et al., 1967; Rizkallah, 1977; Moon, 1984). For the short-term stability of slopes, the undrained strength of the materials may be needed (Sherard, 1973; Skempton et al., 1965) and for the landslip which already exists, or if there are pre existing shear surfaces, Skempton (1964) suggested that residual shear strength parameters are required.

Fissures in an overconsolidated clay slope can produce stress concentrations that will force the clay beyond its peak strength and then the non-uniformly mobilised strength of the mass can cause the progressive failure of the slope (Skempton, 1977). In other words, the progressive failure of slopes in stiff fissured clays refers to the non-uniform mobilisation of shear strength along a potential slip surface (Morgenstern, 1977). In this potential failure surface, some elements have obtained peak strength before others and when failure finally occurs, some elements of the soil will be beyond peak strength while others have just reached it . It can be said that the average shear strength available at failure is less than the peak strength but generally greater

than the residual strength . This average shear strength has been called by Skempton (1970) "fully softened strength".

Skempton (1970) and Moon (1984) suggested that the overall shear strength of stiff fissured clay at first failure corresponded to the fully softened shear strength which is obtainable in the shear test when further deformation at constant stress fails to cause any further change in volume or water content i.e. it is the same as the actual state condition.

The fully softened condition was considered by Moon (1984) as a practical approximation of the critical state and the peak strength of normally consolidated and the remoulded clay is also the theoretical limiting strength of a stiff fissured clay which has undergone complete softening.

In a review of the slope stability of cuttings in Brown London clay, Skempton (1977) reported that the fully softened angle of friction was equivalent to the peak angle of friction determined in laboratory tests on undisturbed samples. Chandler and Skempton (1974) calculated the cohesion intercept by back analysing, and argued that although the field cohesion at the time of first failure was small, it could not be zero. They suggested c' values of between 1 and 2 kpa for London clay. These values were similar to the residual cohesion determined in the laboratory tests by Moon (1984). Therefore, the effective shear strength parameters suggested by Moon (1984) for the analysis of first time slides were, the fully softened angle of friction (ϕ'_{fs}) assumed to be equal to the peak angle of friction (ϕ'_{fs}) determined by laboratory tests and the fully softened cohesion c'_{fs}, assumed to be equal to the cohesion obtained in residual tests (c'_r).

James (1971) and Palladino and Peck (1972) have revealed that the deformations required to reach this "fully softened strength" are smaller than the ones needed to produce residual strength conditions along a potential slip surface in slopes made of stiff fissured clays.

Moon (1984) showed that the residual and fully softened effective friction angles depend on the plasticity. The lower plasticity samples had a higher strength than the higher plasticity samples. In addition, the effect of the plasticity on the ϕ' of residual

and fully softened effective shear strength, the overconsolidation ratio, OCR, also has an effect on this parameter.

2.10 TEST METHODS FOR RESIDUAL, FULLY SOFTENED AND PEAK SHEAR STRENGTHS

2.10.1 Residual Shear Strength

The form of the load displacement curve leading to residual strength depends on the mechanism of shearing (Lupini, et al. 1981; Moon, 1983; Skempton, 1985).

Lupini et al. (1981) in three series of tests on different artificial mixtures, showed three modes of residual shear; a turbulent mode in soils with a high proportion of rotund particles or with platy particles of high interparticle friction, in which preferred platy particle orientation does not occur, a sliding mode in which a low strength shear surface of strongly orientated low friction platy particles forms, and a transitional mode involving both turbulent and sliding shear. These results were summarised by Skempton (1985) and are reproduced in Figure (2.13).

Skempton (1985) presented results of field residual and ring shear tests on a range of soils as displayed in Figure (2.14).

Moon (1983) showed that samples with a plasticity index below 40% failed by turbulent shear and did not develop shear planes, while samples with a plasticity index above 55% failed by sliding shear and developed continuous shear surfaces. Samples which failed by turbulent shear had a higher residual strength and produced different load displacement curves to samples which failed by sliding shear (Figure 2.15).

Peak effective shear strength is obtained on the first run for an undisturbed sample subjected to direct shear test but a number of further runs is required to establish the residual strength at each normal pressure. Typical load displacement curves for two types of failures are shown in Figure (2.16).

Moon (1984) showed that there was a tendency for the load to drop a little from run to run until the residual state was reached in samples failing by turbulent shear. However, the load usually remained approximately constant (flat curve) during each

run. In samples failing by sliding shear, some of the later runs could be completed after less than 1 mm displacement. The values of effective residual cohesion, c'_r, and effective residual friction angle, ϕ'_r, were obtained by linear regression analysis.

2.10.2 Fully Softened Strength

Fully softened strength parameters can be measured by consolidated undrained triaxial tests and by direct shear tests. Laboratory strength testing on disturbed samples may be expected to provide an estimate of the fully softened angle of friction (ϕ') but will generally overestimate the fully softened cohesion (Moon, 1984). The five different methods used to determine (ϕ') by Moon (1984) are shown in Table (2.7). He believes that tests on undisturbed samples are preferable to tests on remoulded samples because remoulding destroys any diagenetic bonds or preferred particle orientation which may occur in natural soils.

Figure (2.17) shows the p-q diagram for the staged triaxial test used by Moon (1984) to determine the fully softened shear strength. Back pressure was applied to all the samples and pore pressure parameter B (Skempton parameter) was checked that the samples were being fully saturated.

The strain rate used was about 0.003 percent per minute. Two definitions of failure used by Moon (1984) are, the maximum ratio of principal stresses occurred at a low strain and the minimum difference of principal stresses, i.e. the deviator stress, occurred when the strain is significantly higher. The different definitions of failure resulted in different values of c' and ϕ'. It is also noted that staged testing may have influenced the results because of strain weakening.

Figure (2.16) shows the first forward run of each shear box test for the peak shear strength and the "post peak" shear strength recorded by Moon (1984). The post peak strength was defined as the strength at the end of the first run which was standardised at a shear box displacement of 7 mm. The box drive rate used for these tests was about 0.005 mm/min. From these tests, Moon concluded that the failure envelopes defined by the post peak strength provided a better estimate of the fully softened friction angle.

This conclusion of fully softened friction angle is experimental. Today by using computer monitoring of the testing, the curve of volumetric changes vs horizontal strain can readily be obtained to measure the fully softened (critical state) shear strength accurately.

A series of shear box tests also was carried out by Moon (1984) on remoulded normally consolidated samples. Remoulded soil with a consistency close to the liquid limit was placed in the shear box and allowed to consolidate overnight before being tested. The peak effective friction angle ϕ' was a little lower than the fully softened effective friction angle obtained from tests on undisturbed samples.

Moon (1984) drew the relationship between angle of friction , ϕ', and plasticity index, PI, for the soils tested in Fig. (2.15). The post peak results were obtained by analysing groups of samples with similar plasticity. Group A represents ϕ' obtained by linear regression analysis of test results of samples whose PI ranged from 25 to 33% . Group B represents the analysis of the samples whose PI ranged from 59 to 67%. This figure shows that fully softened effective friction angle has a similar pattern of dependence on plasticity as previously demonstrated for the residual friction angle by Lupini et al. (1981) and Moon (1983). To establish the correlation between plasticity and strength, the recognition of different residual shearing mechanisms is necessary. For the soil which fails by turbulent shear, the fully softened strength will be slightly higher than the residual strength whereas for the soil fails by sliding shear the fully softened strength is likely to be much greater than the residual strength. For the transitional zone, both strength parameters of these kinds of soils will be sensitive to small changes in plasticity.

Moon (1984) showed that the difference between post peak strength and residual strength for low plasticity and low clay fraction percentage (passer by 2μm) is not great. But for high plasticity and clay fraction percentage the difference relatively is great.

2.11 THE EFFECT OF FISSURES ON SLOPE STABILITY AND FAILURE SURFACE IN A FISSURED CLAY MASS

2.11.1 The Development of Failure Surface in Real Cases of Fissured Clays

In heavily over-consolidated or over-consolidated clays, as the strain increases, the stress falls from a peak to a much smaller residual stress. Slopes made from such a clay often collapse progressively many years after construction (Palmer et al., 1973). Sliding occurs on a concentrated slip surface, and it is found that the mean resolved shear stress on that surface is markedly less than the peak shear strength. The components of this slip surface or failure surface are some parts of pre-existing crack surfaces and the others are surfaces passed through the soil substances.

Fissures permit that the movement of blocks of intact clay through them with a minimum passing length through the soil substances (Fookes et al., 1969) and for a site with the conditions of unfavourable orientation of fissures, the major part of a failure plane can follow fissures and so may be near the residual strength of the material. They indicate that the overall strength of the mass can be further reduced by the separation of the walls of closed fissures. This separation can occur on near vertical fissures along the steeply inclined back part of the failure zone. They believe that where the intact clay has a low tensile strength, there is no resistance at all to the opening of a fissure and once it is open there will be no shear resistance along the fissure itself.

To study the possible mechanism of failure in a fissured clay mass and assessing the viability of various methods of stability analysis, Williams et al. (1977) conducted a full-scale experiment in Vereeniging in South Africa.

The behaviour of a vertical bank was observed while excavation proceeded to a depth at which failure was induced. They emphasised that the pre-existing pattern of fissures in the mass had a major influence in the initiation of the stress concentration around fissures and propagation of the secondary cracks. In the cases investigated, the overall stability of the mass was most probably governed by the residual strength along the joints.

In the stability analysis of the slides of the Santa Barbara open mine, Esu et al. (1969) assumed c' equal to zero, and ϕ' equal to its peak value along bedding planes and joints, and to the residual one along faults. Calabresi et al. (1973) confirmed the hypothesis previously advanced by Esu and et al. (1969) and they pointed out that the latter assumption seems quite reasonable, since large displacements had occurred

along fault planes and their surfaces appear polished, slickensided and oxidised. Along bedding planes and joints, however, no displacement had occurred previously and their surfaces appeared remarkably rough and plumose before sliding, and polished and slickensided afterwards.

For the mechanical characteristics of Santa Barbara, Clay Calabresi et al. (1973) found that along joints and bedding planes, the same peak value of friction angle held as in a clay substance with very small cohesion. They realised that the intact clay was more brittle when sheared along planes parallel to the bedding planes and this could have some influence on the development of progressive failure.

Pitts (1985) believes that there is a strong relationship between slope failures and sheeting in the Old Alluvium in Singapore. He suggested two approaches considering the existence of discontinuities in soil masses in respect to slope stability. First, they might be considered to generate an anisotropic decrease in mass strength, which might be a reasonable view of apparently random sets. Second, where a well-ordered tectonic fabric is imposed on the mass, the view may be one of defining sliding blocks and wedges.

For these two cases, sampling and testing of materials for shear strength properties for use in stability analyses can only satisfactorily be undertaken when the geological setting of the site has been well established. This includes careful logging of both lithological and structural characteristics. For the newly cut slopes, future stability may depend on structural weaknesses which do not even exist until the slope is excavated. Pitts (1985) suggested that stress relief effects may well initiate long term destabilisation of slopes in the manner described by Skempton (1970), and that the time period to failure is about 30 years.

By back-analyses and field observations, Pitts (1985) found that joint roughness in soils to be unreliable in terms of enhancing shearing resistance and pre-existing discontinuities like joints, bedding, stress relief and cleavage control the form of many slope failures.

Relict discontinuities are one of the most significant geologic factors affecting the stability of slopes in saprolites. St. John et al., (1969) ; Koo (1982 a), Massad and Teixeira (1985) have shown that landslips in saprolites are associated with relict

discontinuities which generally have lower shear strength than the surrounding weathered intact soil materials.

Sowers (1985) pointed out that many cut slopes which would otherwise be considered stable, fail as a result of water ingress into relict joints opened up by stress relief and that failure occurs along the lower strength relict discontinuities. Invariably, rainfall acts as the final triggering agent and many failures occur during or shortly after heavy rainfall.

The major adverse effects of relict discontinuities recognised by Irfan et al. (1988) on slopes are:

a) Lower shear strengths than the intact soil either through the clayey or more intensely weathered infill or along infill-weathered rock contacts,

b) Particularly low shear strength values along slickensided discontinuities,

c) Reduction of the mass strength, and

d) Locally high water pressure due to damming effects by clayey infills or pipe development resulting from ground water flow.

Deere and Patton (1971) illustrated that as weathering continues, the strength on a discontinuity surface approaches a residual value. Irfan et al. (1988) stated that in highly and completely weathered rocks, the strength of irregularities along discontinuities is reduced so that even at relatively low stress levels these irregularities are very easily sheared off, and the peak strength approaches the residual value. The residual friction angle, ϕ_r , may also vary because of mineralogical changes in most rocks with weathering. In addition, discontinuities in soil zones generally contain thin clayey coatings or infillings which may be polished, resulting in a further reduction in shear strength. As a result, the strength available along relict discontinuities is invariably lower than that of the intact soil and their cohesion intercept is generally zero.

Irfan et al. (1988) suggested that the common form of failures in slopes is discontinuity controlled failures. In addition to simple planar or wedge sliding type failures, involving one or two planes, more complex failures, conditioned by a number of unfavourably oriented relict discontinuities, may occur. They point out

that failures may also be started by the opening up of discontinuities as a result of stress relief. The damming up of ground water along discontinuities may directly cause landslips even though the discontinuities themselves do not act as release planes. Irfan et al., (1988) mentioned the characteristic of failure in saprolitic soil as follows:

Generally, failures are rapid and commonly happen during or shortly following heavy rainfall. They may however also occur in prolonged dry weather during excavation, due to removal of support.

Koo (1982 a) found that edge or planar sliding failures generally occur in soils which are not closely fractured. St. John et al. (1969) and Wolle (1985) recognised that sheeting joints, formed as a result of stress release, can also cause planar slides, particularly in areas of uniform geologic environment where such discontinuities are of common occurrence. Relict joints, as well as relict cleavage planes, foliation planes and faults, are recognised by Irfan et al. (1988) and can be reasons for simple or complex failures in complex folded metamorphic rocks. The strain softening effects of weathering can play an important role in the initiation of some failures in slopes that may be stable when first formed. As explained previously, the shear strength along a discontinuity may decrease with time. Toppling of single blocks or progressive mass toppling are possible modes of failure in jointed saprolitic soils containing vertical or near vertical relict discontinuities (Irfan et al., 1988).

Moon (1992) developed a model to assess the overall shear strength of fissured soils. In this method, he quantified a range of shear strengths which intermediate between fully softened and residual based on observations of the fissures (defects) occurring at particular test locations. He supposed that the strength of the weak layer is in proportion to potential failure surfaces which may occur along pre-existing defects. But the shape and roughness of fissures and boundary condition, including the conditions of geometry and load have not been considered.

2.11.2 The Development of Failure Surface in the Artificial Fissured Clay Specimens in Laboratory

Stiff clays have stress-strain relationships that very closely approximate those of a linear elastic material (Marsland, 1972; Bishop et al., 1975). Vallejo (1985)

concluded that linear elastic fracture mechanics can be used to obtain normal and shear stress in regions near an open fissure located in a clay element that is subjected to gravity-induced stresses,σ and τ. By using the results of Lawn and Wilshaw (1975), he obtained the normal stresses, σ_{xx}, σ_{yy} and shear stresses τ_{xy} on a point close to the fissure (Figure 2.18) and calculated the principal stresses, σ_1 and σ_3. For soil elements near the toe of a slope and located on a potential slip surface in agreement with Peck (1967), he considered only shear strength with no normal stress. Vallejo (1985) showed that compressive, as well as tensile stresses, are very large in regions close to the fissure walls and the fissure acts as stress concentrator. By considering the low amount of tensile strength of over consolidated clays rather than compressive strength (Bishop and Garga, 1969), he concluded the stiff clay failed first in tension, rather than in compression in areas close to the fissure walls. In summary, the fissures can be one cause of progressive failure in slopes of stiff fissured clays and promote tensile stresses in regions close to them. Therefore, in these regions failure in tension will prevail over failure by compression or shear.

Ignoring the method used for preparing the samples (Vallejo, 1985) that in that method of preparation, drying in air caused suction in the samples, the state of stresses is an important parameter in developing the secondary fissures from the tip of pre-existing fissures in the tested samples. For low amounts of normal stress and the brittle behaviour of material, the development of secondary fissures might be based on maximum tensile stress, but for high amounts of normal stress and for more ductile behaviour of material (saturated), the development of secondary fissures should be as the result of shear displacement.

The assumed model for fissure by Vallejo (1985), an open fissure without friction on the surfaces, seems different to what happens in a real case in over-consolidated and saturated clays. Because fissure surfaces have some shear strength and are almost closed, even for slickensided fissures, there is some shear strength and the effect of shear stiffness of fissure surfaces should be taken into account in the development of secondary fissures or fissure propagation.

Vallejo (1986) used the principles of linear Elastic Fracture Mechanics in calculating the propagation direction of cracks as well as the results of laboratory investigations

involving uniaxial compressive tests on samples of stiff Kaolinite clay with pre-existing cracks for confirming and supporting the applied theoretical method.

As indicated in Figure (2.19), σ_r, σ_θ,and $\tau_{r\theta}$ are the radial, tangential and shear stresses respectively, r is the radius between the tip of the crack and a point in the clay surrounding the crack where the stresses are being measured, θ is the angle that the radius r makes with the axis of the crack where β is the angle between the axis of the crack and the direction of the uniaxial compressive stress σ_c, and c is the half length of the inclined pre-existing crack.

Vallejo (1986) used the Maximum Tangential Stress Criterion developed by Erdogan and Sih (1963) for finding the direction of crack propagation (α) .

$$\tan\beta \sin\alpha + (3\cos\alpha - 1) = 0 \qquad (2.2)$$

Figure (2.20) shows the plot showing the variation of crack propagation angle α versus the pre-existing crack angle β for theoretical (Equation 2.2) and laboratory results for five water contents of 3%, 9%, 15%, 22%, and 27%. Equation (2.2) shows the relationship between α and β is independent of the water content of the samples and also state of stress. Although Vallejo (1988d) estimated the amount of $\alpha = \beta/2 + 2\phi$, where ϕ is the angle of internal friction of the intact plastic clay, α depends on the water content of the clay and for the ductile clay sample, the angle of propagation (α) is independent of preconsolidation pressure and confining pressure. Meanwhile, these factors are effective on the direction of secondary fissures from the tips or edges of pre-existing fissure in an overconsolidated clay sample subjected to direct shear or triaxial tests.

2.11.3 Approaches to the Stability Analysis of Overconsolidated Clay Mass with Non-Continuous Defects

In summary, the following approaches appear to be used for assessing the effective strength parameters for slope designs in stiff fissured clays with non-continuous defects:

- Using fully softened parameters

- Using residual strength parameters
- Using the intermediate values between fully softened and residual and in some cases peak effective shear strength

Skempton (1977) used the first approach for London Clay because Skempton et al. (1969) indicated that most fissures (defects) were short (less than 100 mm) and were not slickensided and polished and were flat lying or steeply dipping. But for fissured clays with longer, slickensided and /or polished, inclined defects, using the fully softened strength may lead to an overestimate of shear strength (Moon, 1990).

The second approach is applicable to the slopes which have movement or any form of movement or continuous pre-existing failure surfaces. This approach can underestimate the shear strength, if it applies to slopes where, continuous, unfavourably oriented, slickensided and / or polished defects do not occur (Moon, 1990).

The third approach has been used by Thorne (1984) and MacGregor et al. (1990). The intermediate strength values were based on laboratory testing and observations in material and also by back analysing the failed past slopes. This approach is applicable to the material where closely spaced, slickensided, and polished fissures occur.

2.12 LABORATORY SHEAR TESTS ON NATURALLY FISSURED CLAY MASS

By obtaining block samples from trial pits, Pitts (1985) used a shear box for testing. The samples were carefully trimmed 100 mm square and in the mode of closely spaced soils and because of the difficulty of sampling, he used remoulded samples with a plane pre-cut by a thin wire to form a discontinuity. He emphasised that sampling and testing of weathered rocks and sedimentary soils for use in stability analyses can only satisfactorily be undertaken when the geological setting of the site has been well established. This includes careful logging of both lithological and structural characteristics.

Remoulding and trimming the samples, as well as releasing them from the confined stresses applied naturally, will cause high disturbance of soil substance. Therefore the

behaviour of remoulded samples tested by Pitts (1985) was completely different from the natural closely spaced samples and the shear strength was underestimated.

Skempton et al. (1967), Marsland (1971), and Thorne (1984) carried out a series of tests on intact specimens (unfissured specimens) from a number of sites as well as natural fissures with varying degrees of movement along them. Figure (2.21) shows the results.

From the results, Thorne (1984) recognised that the effective strength on dull fissures gave $c'_f = 0$ but $\phi'_f = \phi'_u$ peak of the intact material, while slickensided surface showed effective strengths essentially the same as laboratory residual values. Thorne (1984) concluded that for the tests in Botany Bay and Newcastle in Australia, the strength would be generally overestimated. Laboratory tests on samples of fissured clay carried out by normal procedures tend to produce a large scatter of results and usually over-estimate the strength for the following reasons.

a) The size of sample is less than the fissure spacing and the samples are free of defects. In other words, the size of sample should be big enough to contain the defects or the sample should be a real representative of the fissured mass.

b) The effect of the presence of end platens modifies the overall strength

c) Destruction of highly fissured samples and having weaker samples as a result of ejection and preparation techniques

d) Samples size effect, in a material with randomly oriented fissuring, the larger the sample, the higher the probability that the failure plane will contain properly oriented fissures.

As demonstrated by Skempton et al. (1967), Lo (1970), McGown et al. (1974) in fissured clays, the size of the test specimen has a major effect on shear strength. A relationship between substance strength (intact strength), mass strength and sample size (defined as the area of the failure surface) has been suggested by Lo (1970). Figure (2.22) is based on the substance and mass strengths from tests on different sizes of samples. As this figure shows, small samples overestimated the mass strength by 3-7 times and for a test to approximate the mass strength a failure surface of at least 50 and desirably 200 times, the area of potential failure plane is required.

Thorne (1984) suggested that the relative strength of the soil substance and the fissure surface can be affected by the orientation of the fissure and the general stress level. This is illustrated in Figure (2.23) for fully fissured samples. Figure (2.23) shows the results of normal effective stresses on the samples with fissures at 25° and 60° angles shown by Mohr circles A, B, and C. The full lines represent the true effective strengths of the soil substance (top line) and fissure surface (bottom line).

Points a, b, c show the strength along the fissures and points b′ and c′ shows the strength of the substance. In Fig. (2.23a), the first stage circle A fails along the fissure when the stresses along the fissure surface reach the fissure failure line (point a) and there is no substance failure. The next stage, circle B has a higher lateral pressure-in this case the stresses on the fissure plane (point b) reach the fissure surface failure line at the same time as the stresses in the soil substance reach the substance failure line (point b′) and so failure occurs both in the body of the soil substance and along the fissure . The next stage, again (circle c) an even higher lateral pressure reaches failure in the soil substance (point c′) before the stresses along the fissure plane reach failure (point c) and so failure surface passes only through the soil substance. Figure (2.23b) shows a similar sequence but for a 60° angle and in this case all stages fail along the fissure.

In these figures heavy dotted lines show the apparent failure envelopes obtained. Thorne (1984) concluded that It could be expected that in addition to the effects of orientation of fissure and general stress level, the overall strength of the fissured samples, would be affected by the roughness of the fissure surface.

Marsland (1972) compared the results of triaxial tests on 38 mm diameter block samples obtained by Ward et al. (1959) during tunnel operations and concluded that the action of tube sampling reduced both the shear strength and the Young's modulus of the clay.

Marsland et al. (1967) in an investigation of strength parameters of highly fissured Barton Clay from Fawley, observed that the stress-strain curves obtained from tests on the 75 and 125 mm diameter specimens, which were allowed to swell under low effective stresses prior to shearing, did not have any pronounced peaks. Other evidence of the absence of peaks from stress-strain curves is the specimens tested

under low effective stresses on 98 mm dia. specimens of highly fissured unweathered blue London Clay from Wrayebury (Marsland, 1972) with a mean spacing of fissures about 40 mm. The 98 mm diameter triaxial specimens also were allowed to come as near as possible to the equilibrium state under the consolidation or swelling pressure. The samples were sheared with a rate of strain of about 0.0002 percent / min. Figure (2.24) shows the stress-strain and volume-strain curves obtained from these tests.

Marsland (1972) showed that at low effective stresses, the fissured clay behaved more like a gravel and the effects of high over consolidation pressures were retained only inside the hard lumps and the lumps of clay remained almost intact. At medium stress levels, the lumps remained tightly interlocked and a larger proportion of the shear plane passed through intact over consolidated clay, therefore the stress-strain curves had well-defined peaks, more representative of the behaviour of over consolidated clays. Marsland (1972) explained that any reduction of stability, with time is due entirely to a gradual decrease in ϕ' and c' component due to softening and lubrication of the fissure surface, and softening of the corners of lumps.

Marsland (1971) indicated that testing on specimens which were allowed to swell under low effective stresses prior to shearing will give different results in comparison with undisturbed specimens, because in situ stresses, which remain in the samples as locked in stresses, will be released due to swelling.

Figure (2.25) shows the effective stresses at the maximum deviator stress and at the maximum strain reached during shear.

The failure envelope obtained from these tests was curved. Marsland (1972) showed that $c' = 0$ for the tested specimens and he believed that the absence of pronounced peaks in the stress-strain curves obtained from specimens tested under low effective stresses will be particularly important for considering the stability of natural slopes and excavations.

Typical results obtained by Marsland (1972), from tests on 38 mm dia. specimens of fissured London Clay trimmed from a single block sample, are given in Figure (2.26).This figure displays the effects of spacing and orientation on the measured strengths. The lowest strengths belonged to specimens containing a single fissure which passed right through the specimen at an inclination corresponding to the plane

of maximum applied shear stress. Intermediate strengths were obtained on specimens containing either rough, irregular shaped fissures, or fissures with steeper or shallower inclinations.

The highest strengths were measured of the specimens containing no obvious fissures, or fissures which were roughly parallel or perpendicular to the longitudinal axis of the specimens.

Figure (2.27) shows the relationship between the ratio measured strength in the laboratory to the estimated strength from in-situ tests against the ratio of specimen diameter to fissure spacing. By increasing the spacing of fissures in the specimens, the difference between measured strength of laboratory and in situ tests will increase. This graph shows the effect of sample size on the shear strength of closely arranged fissured clays.

The shape of the fissures can have an influence on the strength of the clay . The greater the curvature and complexity of the fissures, the greater the strengths (Marsland, 1972).

The interval of time that clay remains under stresses lower than normal in-situ stresses has also an effect on the properties measured both in the laboratory and in the field.

More careful inspection of articles displays that the wide range of strengths measured on small specimens from a particular level and location is due to differing shapes, roughnesses and orientations of fissures in each specimen.

The relationships between ϕ'_{fs} and ϕ'_{r} with p'_{c} and also type of mineral need more investigation.

2.13 IN-SITU SHEAR STRENGTH TESTS ON A NATURALLY FISSURED CLAY MASS

Fissured soils are difficult to sample and test, so in-situ tests are sometimes used for measuring the strength. Closed fissures will be opened as a result of unloading (excavation, erosion, dredging, etc.) and interval time from sampling to testing will be effective to open the closed fissures.

The size of sample, as well the characteristics of the fabric of the soil, has an important effect on the overall strength of the fissured mass.

Many of the parameters which are effective in the effective shear strength of fissured clays will be eliminated for in-situ tests, therefore, there is a tendency to conduct in-situ tests, however, the expansive costs such tests and also their specific and limited applications, limit their usage. The results of different in-situ apparatus used in different sites, as well comparisons with the laboratory test results, will be the aim of this section.

2.13.1 Experimental evidence

Marsland (1972) showed that the measured strength on different sized specimens of London Clay and Barton Clay, which is highly fissured, decreased as the size of the specimen was increased. As a consequence of these findings, he initiated a study of in-situ tests using different sizes and types of equipment. By loading tests on 38 mm diameter probes and on a 152 mm diameter plate at Ashford Common, Ward et al. (1965) showed the importance of the size of the test equipment in relation to the spacing of the fissures. The larger scatter was obtained from loading tests in London Clay on plates with diameters less than 200 mm.

Marsland (1971a) measured the undrained properties by means of loading tests on plates with diameters of up to 865 mm at various depths in boreholes and the effective strength parameters by in-situ tests using a 610 mm square shear box.

The following factors were estimated to have an influence on the result of the undrained properties of stiff fissured clays tested by in-situ plate loading tests (Marsland, 1971a).

a) The mineralogical compositions, strength, and the type of discontinuities present in the stiff clays contain numerous discontinuities in the form of bedding surface, joints, shear dislocations, and fissures. Even in clays with similar mineralogical properties, the discontinuities can vary in size, continuity, inclination and surface roughness with both depth and location.

b) the forces and restraints imposed on the ground around the test levels by different arrangements adopted for the tests.

c) Dimensions of the test equipment and in particular the relative dimensions of the loaded plate and the spacing of the fissures in the clay.

d) The reduction in stress and the accompanying strains which occur in the clay during drilling and insertion of the tests equipment.

e) The interval of time between drilling the hole and loading the plate.

f) The rate of penetration during loading.

Morsland (1971a) found out the influence of the interval of time between excavation and loading from the decrease of deformation moduli determined from plate loading tests with time in the base of Ashford Common shaft. He used loading tests on a 865 mm diameter plate in 900 mm diameter bore holes to keep the interval of time between drilling and testing as short as possible.

Figure (2.28) shows the comparison of shear strength of London Clay calculated from 865 mm diameter plate tests at Chelsea with triaxial tests on 38 mm and 98 mm diameter specimens and also laboratory penetration tests in which a 5.5 mm loading plate was used. At this particular site, the average spacing of fissures was reported from about 15 mm at a depth of 4 to about 100 mm at a depth of 15 mm (Marsland, 1971a).

At this site the strength measured on both the 38 and 98 mm diameter specimens from a depth of about 15 m were about 1.75 times those calculated from the plate tests. The result of the 5.5 mm diameter penetration tests provided an approximate measure of the strength of the 'intact' clay or clay substance within the lumps between fissures. As Figure (2.28) shows, the shear strengths measured from the penetrometer tests increased from about twice to more than four times the large-scale strength of the clay as calculated from the large in-situ test results between depths of 5 and 15 m.

Marsland (1971a) used large in-situ shear box tests to determine the effective stress parameters of stiff fissured clays. From the large differences between undrained strengths obtained by in-situ tests and laboratory tests, he suspected to the effective stress parameters determined from tests on small laboratory specimens. He concluded that these differences were largely attributed to the fact that the proportion of the

shear planes which passed through hard intact clay between the fissures were larger in the laboratory than in the field tests.

2.13.2 Typical results obtained from drained large in-situ shear box tests

Figure (2.29) shows shear stress-displacement curves obtained by using the large in-situ shear box.

The peak and post-peak values from these tests are shown in Figure (2.30) together with the upper and lower limits of the peak strengths on 75 to 125 mm diameter specimens and residual strengths obtained by reversal tests in 60 mm square shear box.

The most significant feature of the results obtained from large in-situ shear tests carried out by Marsland (1971a) was the very small cohesion intercept and relatively large angle of internal friction under low stresses. Large in-situ shear tests showed that under low effective stresses fissured clays behaved like a granular material composed of interlocking lumps of clay.

Williams et al. (1977) carried out a large number of in-situ shear tests using a Swedish vane of 30 mm diameter and 60 mm height in an alluvial clay in South Africa. They stated that the jointing of fissured clays in South Africa is due to either tensile stresses in upper horizons or large stress differences in lower horizons causing shear failure. Both fairly rapid (undrained) and very slow (drained) tests were conducted at rotational speeds giving about 94 mm/min and 0.04 mm/min at the periphery. Figure (2.31) shows some results of undrained tests carried out by them. The lower values were measured from the remoulded, or perhaps residual, strengths obtained after about 50 mm displacement. Loading tests on 150 mm dia. plates were also conducted at various depths in unlined boreholes and the estimated shear strengths (undrained strengths) were also shown in the figure. These values of strength lie between the peak vane values, which presumably give the strength of the clay substance and the remoulded vane values, which probably reflect the strength along an existing shear plane. Williams et al. (1977) also measured the strength on the slickensided surfaces and observed that the shear strength along a slickenside

surface appears to be near the residual value which may be determined in a shear box after repeated reversals of strain.

Thorne (1984) doubted of the values of the undrained Young's modulus of the clays estimated from unloading/reloading loops at appropriate stress levels in oedometer tests for assumed Poisson's ratio of 0.2 because they were too low and also the horizontal stresses were high. The latter were important since an increase in k_0 after dredging, could conceivably have induced passive failure and caused fissure surfaces to link up. He used a self-boring pressuremeter of the type described by Wroth & Hughes (1973). The measured in-situ horizontal stresses are indicated in Fig. (2.32). Almost all the results lie above the $(1-\sin\phi'_s)$ line. Figure (2.33) shows the undrained modulus results against depth for dredged and undredged areas .The results for undredged areas were much higher than from the oedometer tests and in the dredged areas, the moduli values were markedly less than those in the undredged regions. The dredging was carried out only two weeks before the testing and these results showed that the softening process occurred rapidly. The clays, therefore, were highly stressed horizontally, had a high modulus, softened rapidly on unloading and gave some indications that the fissure strength affected the soil mass behaviour.

2.14 LABORATORY SHEAR STRENGTH TESTS ON ARTIFICIAL FISSURED CLAYS

The purpose of this section is to review the work in which the effect of fissure parameters on the strength of the artificial fissured specimens in the laboratory have been studied. How fissures have been created in the artificial specimens or how the fissure parameters have been considered in the laboratory tests and what kind of apparatus has been used for special investigation of the artificial fissured specimens, are the most important points that will be discussed.

2.14.1 Preparation of fissured clay samples

Vallejo (1985-89) used laboratory-prepared samples of brittle kaolinite clay (with a liquid limit equal to 58% and a plastic limit equal to 28%) with pre-existing fissures for the experimental investigation on the effect of fissures in stiff clays subjected to direct shear tests.

Kaolinite clay or any other of clay mineral can provide homogeneity which is an important factor for laboratory investigation on the artificial samples.

Vallejo (1985-89) reported the procedure used for the preparation of the artificial specimens as follows:

Dry Kaolinite was mixed with distilled water to form a soft soil mass with a water content of about 40% . Then the clay water mixture was placed into an oedometer 30 cm in diameter and consolidated under a normal pressure of 25.7 kpa for a period of 5 days. After unloading the oedometer, specimens measuring 12.7 cm in length, 11.40 cm in width and 3.17 cm in thickness were cut from a clay block. Immediately after cutting the prismatic specimens, when their water content was equal to 30%, fissures were artificially made in the samples by inserting and removing thin glass sheets 1 mm in thickness and 3 cm in width, in a direction normal to the samples' free faces (Vallejo, 1985-89).

After the fissures had been made, the samples were allowed to dry in the air for two days so that their degree of brittleness would be increased (Vallejo, 1985-89).

The above method of producing fissures in samples of clay is different from the natural method of fissuring in soils. By inserting the glass and removing it, the direction of roughness of fissure surfaces in two surfaces of fissure is the same and if the fissures are created by shear displacement, the direction of roughness for both surfaces is opposite to each other.

This action causes desiccation of the samples and the susceptibility of uncontrolled dried fissures increases, thus the specimens will not be saturated when they are sheared, and because of the matrix suction in the specimens, the measured strength will not show the real strength of fissured specimens.

Vallejo (1987) developed a direct shear box. Since the sample of soil in the direct shear box had a free face that was normal to the third direction, the new version of direct shear equipment was called the Plane Stress Direct Shear Apparatus (PSDSA). The development of the shear zone and the influence of fissures in this zone could be observed directly for a sample with 12.7 cm in length, and 11.40 cm in thickness. On

account of its small size and free face, the apparatus could not be used for a complicated arrangement of fissures or high normal pressure.

The samples of fissured clay were tested in the PSDSA at a shearing rate of 1 mm/min. This rate for kaolinite clay is too quick to get drained situation for specimens.

2.14.2 Laboratory tests and discussion

Vallejo (1985) used linear elastic fracture mechanics to obtain the state of stresses around a fissure in stiff fissured clays. He analysed the stresses around a fissure and showed that compressive, as well as tensile stresses, existed and were very large in regions close to the fissure wall. Since in stiff clays tensile stresses are lower than the compressive stresses, he concluded that in the fissured clay, clay failed first in tension rather compression. He believed that the fissures promoted tensile stresses in regions close to them. He proved his hypothesis by conducting a few uniaxial compression tests during which he observed the occurrence of fractures from the tips of pre existing fissures toward the edges of samples.

Taking into account the previous study, Vallejo (1989) concluded that the upper-right and lower-left regions of the crack tips are regions of intensified tensile stresses as shown in Figure (2.34). Since soils are weaker in tension than in compression, the regions in the prismatic samples of clay with pre-existing fissures that develop tensile stresses will be those that first fail in the samples, as shown in Figure (2.34).

Vallejo (1987) tried to confirm his previous hypothesis about the propagation of secondary fissures based on linear elastic fracture mechanics. He ran a few tests with the direct shear apparatus (PSDSA) on the brittle kaolinite clay. He showed that secondary fissures developed from either the tips or the edges of the pre-existing fissures in a direction normal to that of the maximum tensile stress and moreover, the failure surface was irregular and formed by linking the pre existing and secondary fissures. The failure surface of the brittle fissured Kaolinite clay did not resemble the smooth failure plane that specimens of clay are expected to develop when subjected to direct shear testing (Bowles, 1978).

He could not explain the development of secondary fissures based on his hypothesis about maximum tensile stress criterion for the samples with the fissures inclined at 30° to the horizontal. For these samples, the pre-existing fissures extended in a direction which followed that of their own planes. Moreover the failure surface was plane and smooth in these tests. This was expected to happen because when a crack or fissure in a stiff clay is subjected to a combination of shear and normal stresses, it will propagate in the direction that follows that of the plane of the pre-existing crack (Bjerrum, 1967; Palmer & Rice, 1973; and Chowdhury, 1978).

He also showed that the type of arrangement of fissures in a sample subjected to the PSDSA test influenced not only the type of stresses, but also the distribution of stresses in the sample. Figure (2.35) shows schematically the different arrangements of the fissured samples studied by Vallejo (1987). The orientation of the fissures in this figure were 60° with respect to direction of uniaxial compressive load. Vallejo (1987) showed that the two pre- existing fissures inclined at 30° to the horizontal (Figure 2.35b) extended themselves in the direction of their own planes and no interaction occurred between the fissures. But, when the two pre-existing fissures were inclined at 120° to the horizontal (Figure 2.35c) secondary fissures developed from the edges of the pre-existing fissures in such a way that pre-existing and secondary linked together.

Vallejo (1986) used linear elastic fracture mechanics to predict the direction of the propagation of secondary fissures in stiff fissured clays. To prove his prediction, he carried out a few uniaxial compression tests. He could show that for brittle kaolinite samples, theoretical predictions for crack propagation were compatible with experimental results (Figure 2.20). Vallejo (1989) used laboratory-prepared samples of brittle Kaolinite clay with pre-existing fissures to investigate the influence that fissure parameters such as inclination, length, number of fissures, and their arrangement have on the unconfined compressive strength of stiff clay. The number and arrangement of the fissures in the samples used for testing are shown in Figure (2.36). He used five crack orientations of 15, 30, 45, 60, and 75° with respect to the direction of the uniaxial compressive load for the samples containing a single crack and the inclination of 60° for the samples with two fissures. For testing the effect of

crack length on the uniaxial compressive strength of fissured clays, he used single pre-existing fissures with measured lengths, 1 cm, 1.5 cm, and 2.5 cm. The single fissures all made caused at an angle β equal to 60° with respect to the direction of the compressive load.

To consider the effect of the clay's water content in the uniaxial compressive strength of the fissured Kaolinite clay, three groups of clay samples with different water content were tested in the laboratory. The final water content in the samples amounted to 15, 9, and 3%. The rate of deformation used in the testing was 0.5 mm/min (0.0197 in / min).

2.14.3 Influence of crack inclination and water content

In Figure (2.37), the maximum values of the compressive stress σ_c at which secondary fissures developed in the clay samples and the corresponding pre-existing crack inclinations β have been plotted. Figure (2.37) shows that the inclinations of the pre-existing fissures have a marked influence on the compressive strengths. The results show that the strengths reached minimum values when the pre-existing fissures in samples reached a critical angle β_c.

Vallejo (1989) showed that if the crack inclination is either increased or decreased from β_c, the compressive strength increases with respect to its minimum value. In addition, the critical crack inclinations β_c are also found to be a function of water content in the samples. The higher the water content, the higher are the values of β_c. Vallejo (1989) noted that the higher the water content in the samples, the greater their compressive strengths (Figure 2.37) and he related this finding to the negative pore water pressures developed by the prismatic samples after they were cut from the cylindrical block samples prepared in the oedometer.

2.14.4 Influence of crack length

The results of testing are shown in Figure (2.38). This figure shows that the unconfined compressive strength of the samples , σ_c , is directly influenced by the length of the fissures in the samples. The smaller the crack length in a sample, the larger is its unconfined compressive strength. Vallejo (1989) supported the laboratory

findings by Linear Elastic Fracture Mechanics (LEFM) theory (Gdoutos, 1984 ; Ingraffea). According to this theory, the magnitude of the tensile and compressive stresses in regions around the tip of a crack (Figure 2.34) is directly related to the length of the crack. In other words, larger fissures concentrate larger stresses in the intact material surrounding them (Ashby and Verral, 1977).

2.14.5 Influence of number and arrangement of fissures

The stress-strain relationship, the failure mode, and the type of stresses induced in the samples by the compressive load and the fissures are shown in Figures (2.39) and (2.40). Figure (2.39) shows that the unconfined compressive strength (given by the peak values of σ_c) of the samples containing one crack was greater than the unconfined compressive strength of the samples with two fissures.

Figure (2.34) shows that the effect of one fissure in the sample under compression is to cause the overstressing of the clay in regions surrounding the crack tips. The presence of more than one crack in the samples will, therefore, cause increased overstressing of the intact material surrounding the fissures as a result of the overlapping of the stresses induced by each crack (Figure 2.40b). Due to this overstressing effect, Vallejo (1989) explained that the sample with more than one crack will, therefore, require a smaller value of uniaxial compressive stress in order to cause their failure than the one required by the sample with a single crack. He showed that the number of fissures is an important factor that needs to be taken into account when testing clays for their unconfined compressive strength.

With respect to the influence of crack arrangement on the unconfined compressive strength stiff fissured clay, Figure (2.39) shows that the sample with the right-stepping fissures (Figure 2.40c) has an unconfined compressive strength larger than the sample with the left-stepping fissures (Figure 2.40b). Thus the way the fissures are arranged seems to have also an influence on the unconfined compressive strength of stiff fissure clay.

An explanation for the measured difference in compressive strength can be obtained from an analysis of Figures (2.40b and 2.40c). These figures depict the way the intensified zones of tensile and compressive stresses overlap depending upon the

arrangement of the fissures in a prismatic sample of brittle material under compressive loads (Vallejo, 1989).

2.15 THE EFFECT OF ORIENTATION OF FISSURE ON THE ESTIMATION OF SHEAR STRENGTH FROM AN ANALYTICAL POINT OF VIEW

Designers have made many attempts or predicting c' and ϕ' of a fissured clay mass. Analytical methods like experimental, numerical or empirical methods have been used in estimation or interpretation of shear strength of the fissured specimens. In this section a brief review has been given to the analytical methods used for triaxial specimens.

2.15.1 Undrained Shear Strength

The effect of a single fissure in the triaxial sample for undrained test was modelled as shown in Figure (2.41). Figure (2.41a) shows a single fissured sample of triaxial test for undrained triaxial test and Figure (2.41b) shows the influence of a single fissure on the undrained shear strength of a triaxial test specimen.

McGown et al. (1986) related the undrained shear strength of a single fissure to a function of both its mass strength and its inclination. The undrained shear strength of the specimen, c_u, was related to the shear strength of the discontinuity, c_f, and the inclination of the fissure,

$$c_u = \frac{c_f}{\sin 2i} \qquad (2.3)$$

where i was the inclination of the discontinuity with respect to the major principal plane. McGown et al. (1980) developed this model for a sample cut by a number of discontinuity sets. They considered the value of $\frac{1}{\sin 2i}$ as a simple weight factor for the presence of a discontinuity at inclination i. McGown et al. (1980) believed that this weight factor was appropriate for a single group of discontinuities with an average inclination i. For a sample cut by a number of discontinuity sets with n_1 discontinuities inclined at angle i_1, and n_2 inclined at angle i_2,..., n_n inclined at angle

i_n, for overall undrained strength-weight factor, they suggested the following equation on the basis of simple summation,

$$R = \frac{n_1}{\sin 2i_1} + \frac{n_2}{\sin 2i_2} + \ldots + \frac{n_n}{\sin 2i_n} \qquad (2.4)$$

where R is the overall undrained strength- weight factor. Therefore, the ratio of the undrained strength of two specimens of the same soil containing the same number of discontinuities, but in different orientations, is the same as the ratio of their R values. In this equation McGown et al. (1980) assumed that the strength as the discontinuity, C_f, is related only to the number of discontinuities (n_i), inclination angles (i), and the undrained shear strength (c_u). Whereas it is also a function of roughness of discontinuity, the area of fissure surface, and the amount of confining pressure in a triaxial test. If the state of stress is chosen high, the possibility of passing the failure surfaces through the clay substance will increase(Thorne, 1984). Moreover considering linearly, the effect of different inclinations and even the number of discontinuities for the same inclination with regarding to the interaction of stresses, needs more probing and investigation.

2.15.2 Drained Shear Strength

For the case of drained strength Lo et al. (1970) assumed that the effective cohesion was negligible and in undrained tests the intact material behaved stronger than the discontinuities whereas in drained tests the differences between the matrix and the discontinuities were much smaller and thus, the drained strength was governed by both mass and discontinuity strength.

They indicated that for each group of inclination of fissures, three cases should have been considered as described in Figure (2.42).

(a) when the discontinuity angle was:

$$i_1 = 45° + \frac{\phi'_f}{2} \qquad (2.5)$$

where ϕ'_f was the angle of friction of the discontinuity. In this case the strength was equal to the strength of the discontinuity plane (Figure 2.42a).

(b) when the discontinuity was oriented at very low or very high angles. For this case the failure occurred in the soil mass. The two critical angles of discontinuity plane have been displayed in Figure (2.42b).

Below and above of these two critical angles (Equations 2.5 and 2.6), i_{c1} and i_{c2} respectively, the failure plane passed through the mass.

$$i_{c1} = \frac{1}{2}\phi'_f + \sin^{-1}\frac{\sin\phi'_f}{\sin\phi'_r} \tag{2.6}$$

$$i_{c1} = 90° + \phi'_f - i_{c1} \tag{2.7}$$

where ϕ'_f was the angle of friction of soil mass.

(c) when the discontinuity angle was between i_{c1} and i_{c2}. The strength of the sample was governed by the discontinuity plane as shown in Figure (2.42c) and Equation (2.8).

$$\sin\phi' = \frac{\sin\phi'_f}{\sin(2i - \phi'_r)} \tag{2.8}$$

The problems with these analytical prediction of shear strength are the elimination of effective cohesion both for mass and discontinuity plane and also independency of these relationships with fissure strength (c'_f and ϕ'_f), fissure area, and confining pressure.

2.16 SUMMARY AND CONCLUSION

This chapter has reviewed the formation, classification, and effect of fissures on shear strength, as well as experimental and analytical methods, including laboratory and in-situ tests on the natural and artificial specimens for determining the shear strength of intact, partially and fully fissured clay specimens. Critical comments were presented in pertinent sections.

Taking into account the continuous effect of weathering on the discontinuity surfaces, it seems that fully softened and residual shear strength are not constant and change with time. In other words, the stability of slopes in fissured clays should be considered for a specific duration of time when the weathering has not any influence in the effective shear strength parameters (c' and ϕ').

Research carried out by Vallejo (1986-89) on the development of secondary fissures showed the direction of developing of failure surface through the fissured clay mass in a slope is affected by pre-existing fissures and linked with them, and then these secondary developed fissures with pre-existing fissures, form the failure surface in fissured clay slopes. In this way it might be possible to predict the most probable failure surface and the overall shear strength of the fissured mass for any prescribed boundary condition just by studying the state of stresses around the fissures and also the interaction of stresses within the fissured mass, if the fissured slope is numerically modelled and the discontinuous fissures are allowed to propagate in the model.

Therefore, it can be said, the overall shear strength or full-scale strength or fully softened shear strength depends on the form and shape of failure surface. For example, if the failure surface is mostly formed of fissure surfaces, the amount of overall strength is near the amount of residual strength of the mass and if the failure surface is passed through the soil substances, the amount of overall strength is close to the peak strength of the soil material. It seems for intermediate failure surfaces, the orientation and arrangement of fissures and the stress level of fissured clay elements located in the path of assumed failure surface and also the roughness of fissure surfaces located along failure surface, can affect the overall strength or fully softened strength of the fissured clay mass.

It is possible to consider these factors from two different approaches, the first, experimental and laboratory approach and the second, the statistical approach. The latter is not the purpose of this investigation.

Strengths measured both in the laboratory and in field tests on the natural fissured clay mass or specimens, indicate that the extent, spacing, inclination, shape and surface roughness of the fissures and fabric of soils are influencing parameters. For laboratory tests, in addition to these parameters, the strengths depend on the stress changes which occur during sampling, boring and testing and also the length of time that the clay remains under particular stresses, the size of specimen and the amount of stresses used for testing in laboratory apparatus, specially in triaxial apparatus.

However, the expensive costs of in-situ tests and also their specific and limited applications limit usage in site investigation.

The laboratory results obtained from the artificial brittle Kaolinite specimens subjected to the uniaxial compressive tests carried out by Vallejo (1986-89) indicate that there is a critical fissure inclination of the compressive strength reaches a minimum value and also the longer the length of a crack or the larger the number of fissures in a sample, the lower was its unconfined compressive strength, and samples with fissures arranged in a left stepping manner were weaker in compression than samples containing right stepping fissures.

Noticeable problems with the laboratory and in-situ tests on the naturally fissured specimens or mass have been the lack of sufficient control of the effect of parameters discussed previously and the natural variability of the material properties on the effective shear strength of the natural fissured mass tested by in-situ tests or natural fissured specimens tested in the laboratory. Therefore, the simulation of the parameters artificially in the laboratory for the drained condition is highly recommended.

Although the research carried out by Vallejo (1986-89) on the artificial specimens prepared from brittle Kaolinite clay gives an indication of the impact of orientation, length, and arrangement of fissures on the unconfined compressive strength of the artificial fissured specimens, the need for more investigation for the study of these parameters on the effective shear strength of the artificially overconsolidated unfissured, partially and fully fissured specimens with considering the effect of strain softening, is noted.

To record the effect of spacing that fissures have in the development of the failure surface in stiff fissured clays subjected to direct shear testing conditions for different arrangements and lengths, a large direct shear box is needed and for different orientations, triaxial apparatus is needed. It is expected that in direct shear testing as is currently conducted in engineering practice, the development of the failure surface during testing, as well as the effect that oriented fissures have on the development of this surface, can not be investigated.

For experimental programs synthetic clay soil mixtures must be designed to simulate the strain softening behaviour of over consolidated clays as well as to prepare the artificial fissured clay specimens. To create the fissures, Vallejo (1986-89) produced artificial fissures in the specimens by inserting and removing a glass with 1 mm thickness after consolidating the mixture of Kaolinite with water in the consolidation apparatus. Another method was used by Pitts (1985) for creating a pre-cut is using a thin wire to form a discontinuity in the remoulded samples. Placing a thin plastic sheet (used for transparency) inside the artificial sample before consolidating and removing it after finishing the consolidation of sample is recommended as another variant for creating fissures in artificial specimens.

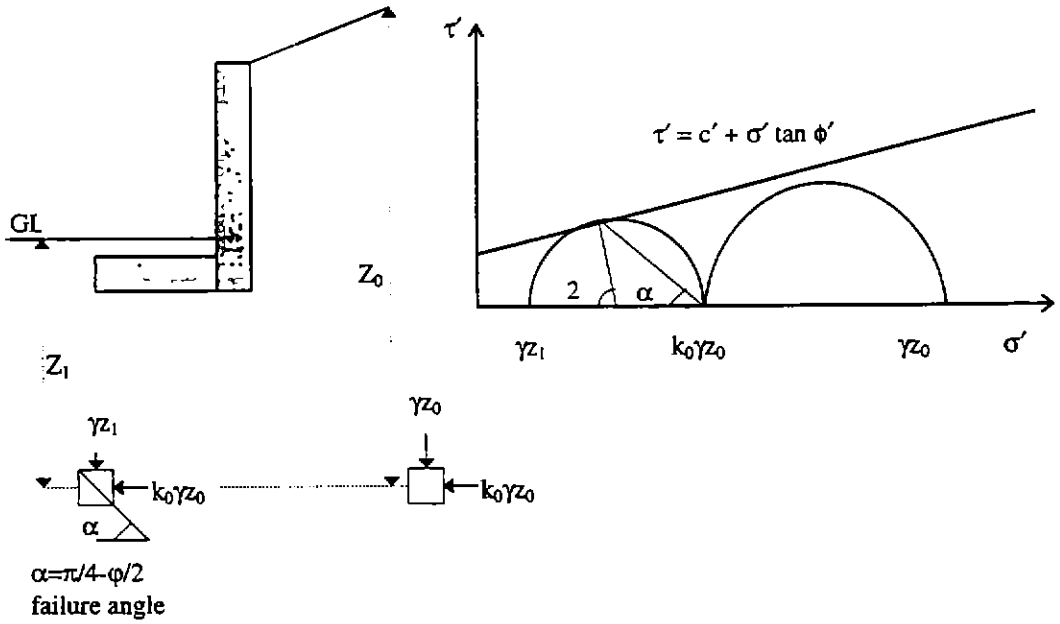

Figure (2.1): Illustration of concept of fissuring as a result of stress releasing.

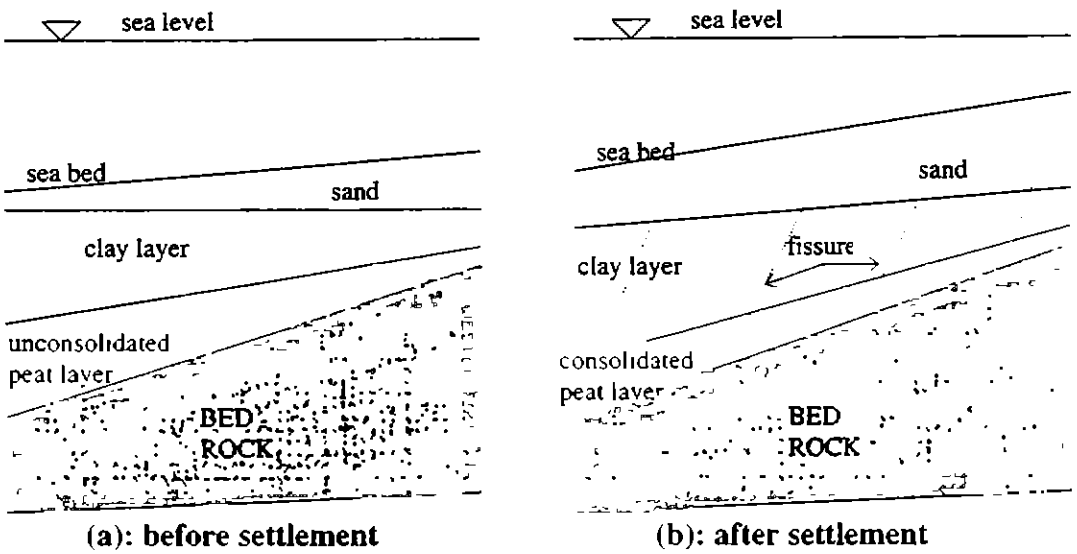

Figure (2.2): Illustration of fissuring as a result of non-uniform consolidation process of peat layer; (a), before consolidation of peat layer ; (b), after consolidation of peat layer.

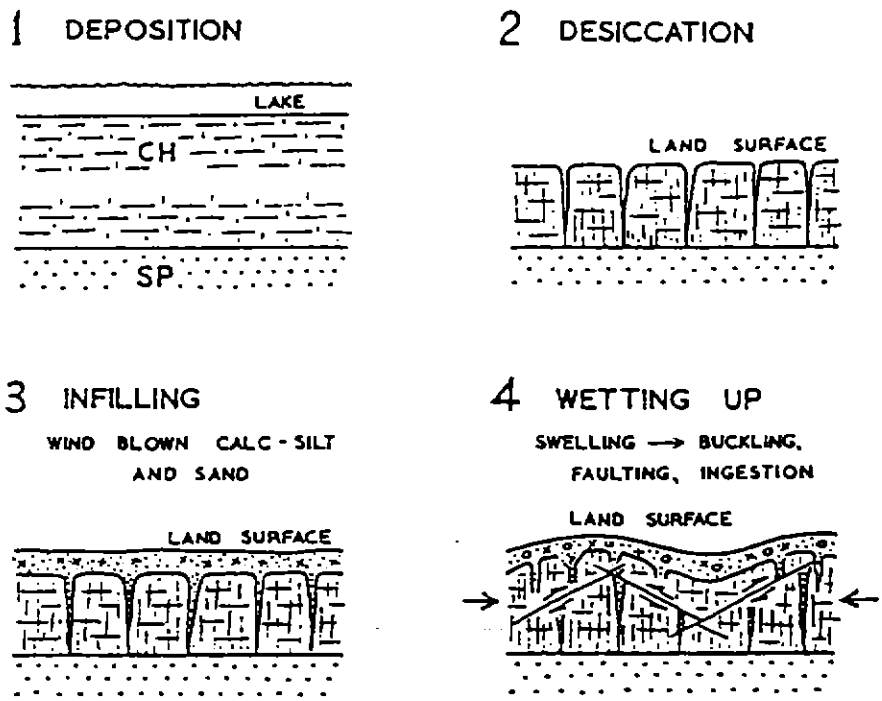

Figure (2.3) Suggested origin of macro-structures in Pleistocene clays, (Stapledon, 1970).

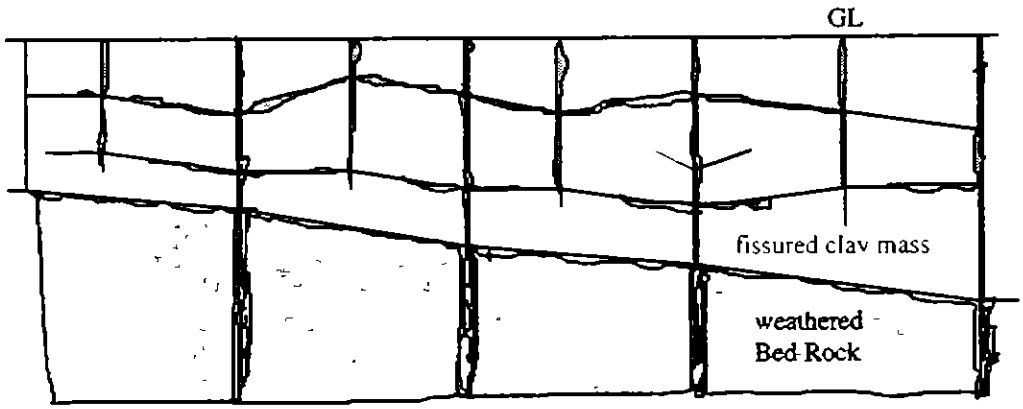

Figure (2.4): Illustration of fissuring as a result of relative deformation in the weathered Bed Rock.

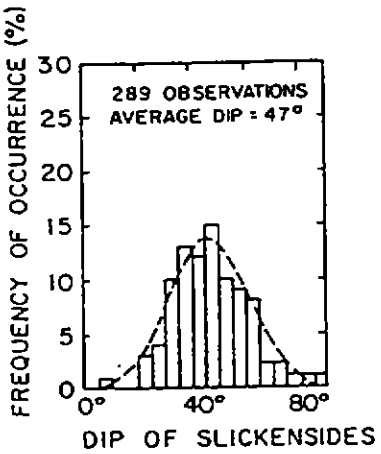

Figure (2.5): Normal frequency distribution of dip angle, (Williams et al., 1977).

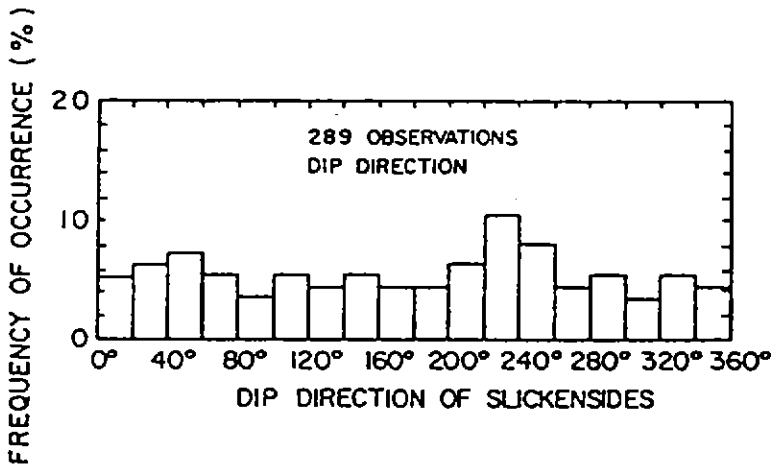

Figure (2.6): Random frequency distribution of dip direction, (Williams et al., 1977).

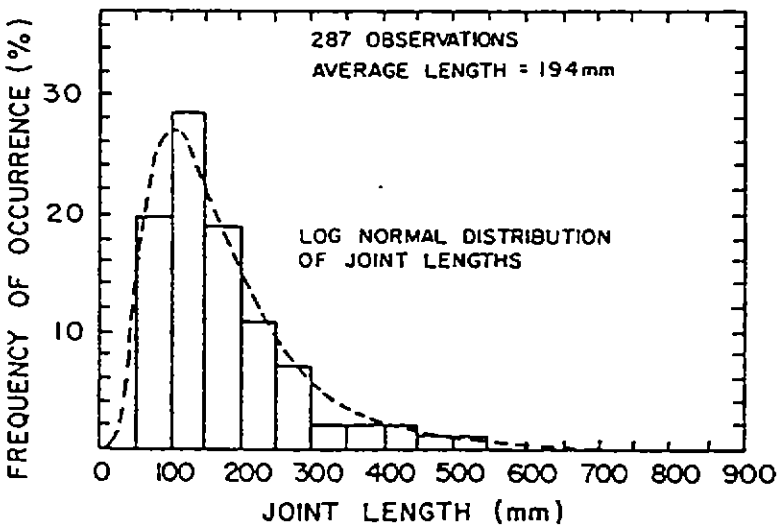

Figure (2.7): Log normal frequency distribution of joint length (Williams et al., 1977).

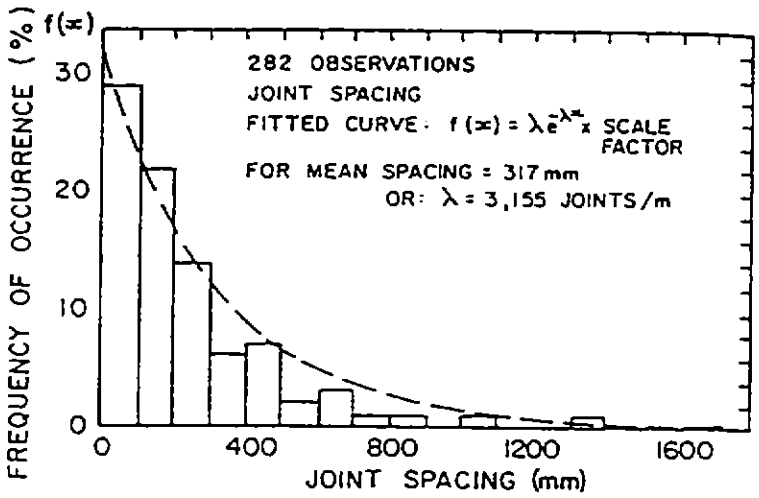

Figure (2.8): Negative exponential frequency distribution of joint spacings, (Williams et al., 1977).

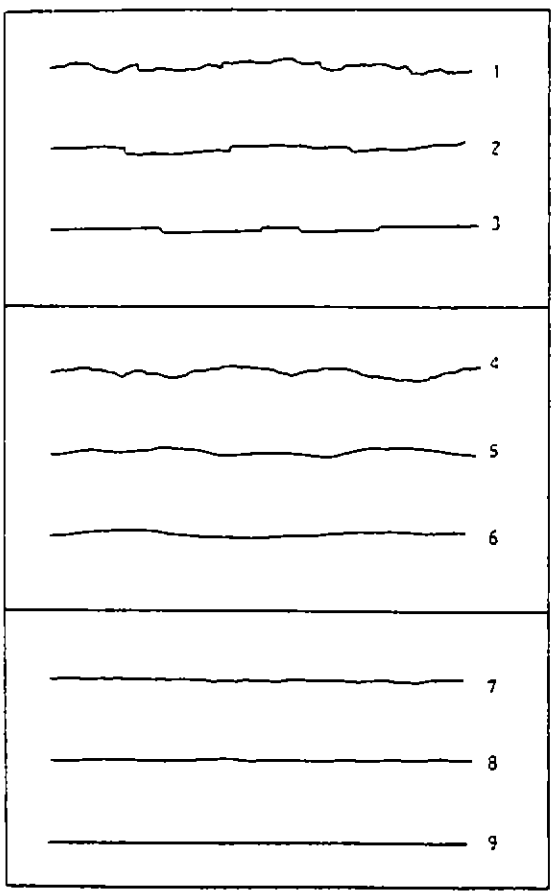

Figure (2.9): Discontinuity roughness classification: 1) Rough or irregular, stepped; 2) Smooth, stepped; 3) Slickenside, stepped; 4) Rough or irregular, waviness; 5) Smooth, waviness; 6) Slickenside, waviness; 7) Rough or irregular, planar; 8) Smooth, planar; 9) Slickenside, planar, (Giani, 1988).

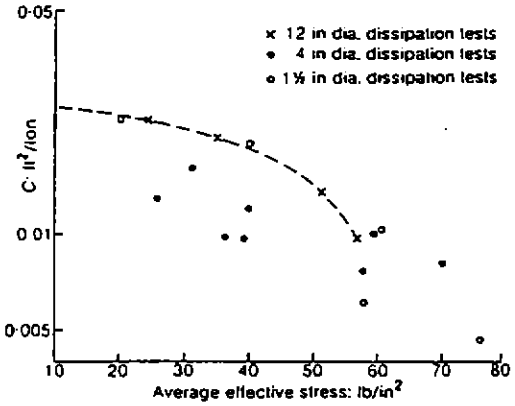

Figure (2.10) Effect of specimen size on all-around compressibility of London Clay from Wraysbury, (Garga, 1970).

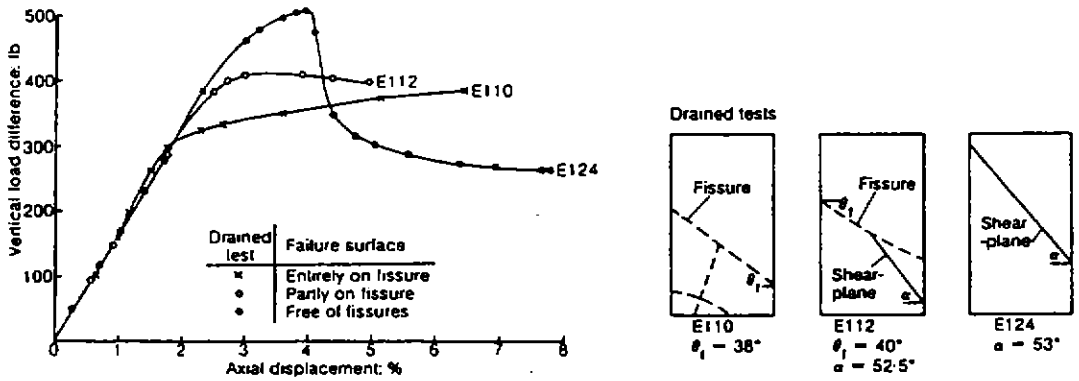

Figure (2.11): Effect of fissure on the stress-strain curve for London Clay .drained triaxial tests, (Webb, 1966).

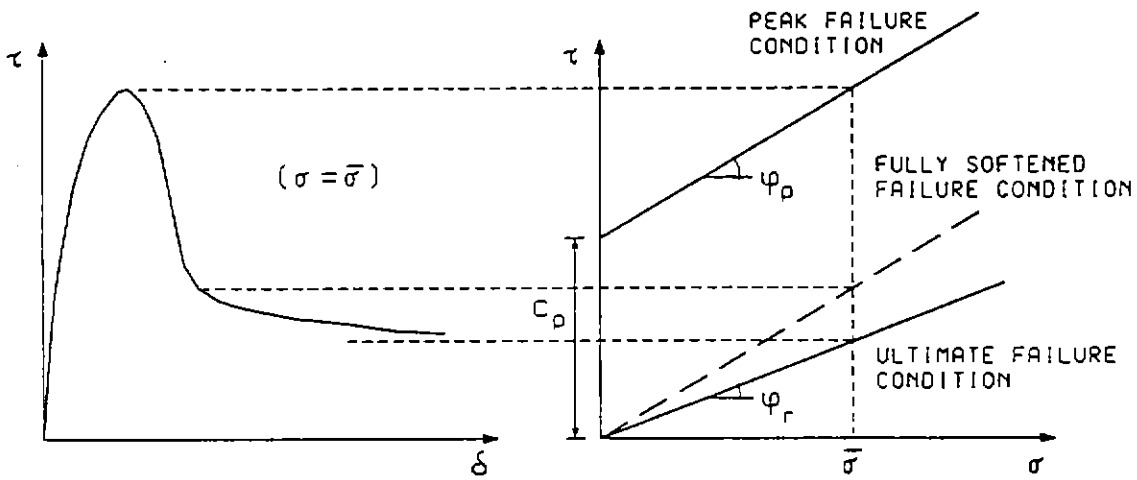

Figure (2.12): Different types of shearing of an overconsolidated clay specimen subjected to direct shear test.

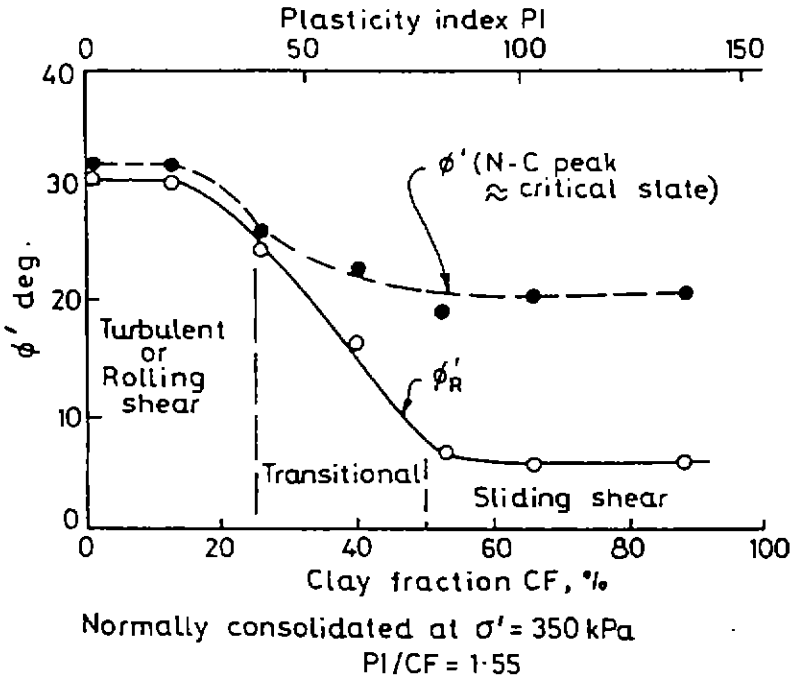

Figure (2.13): Ring shear tests on sand-bentonite mixtures (from Skempton 1985 after Lupini et al. 1981).

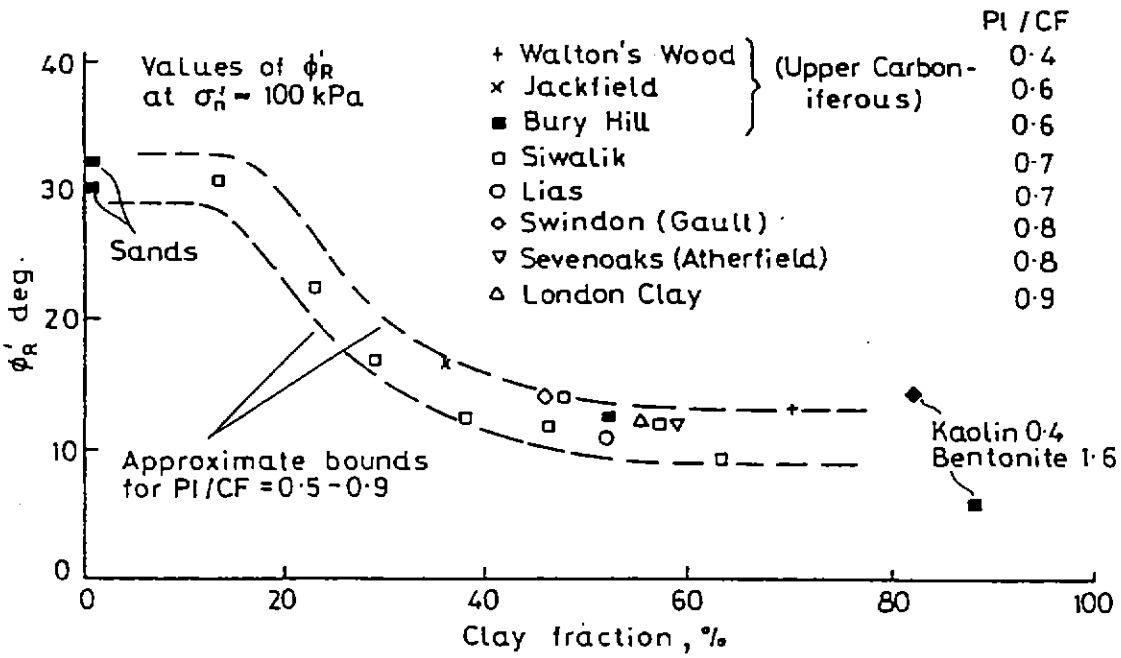

Figure (2.14): Field residual and ring shear tests on sands, kaolin and bentonite (Skempton 1985).

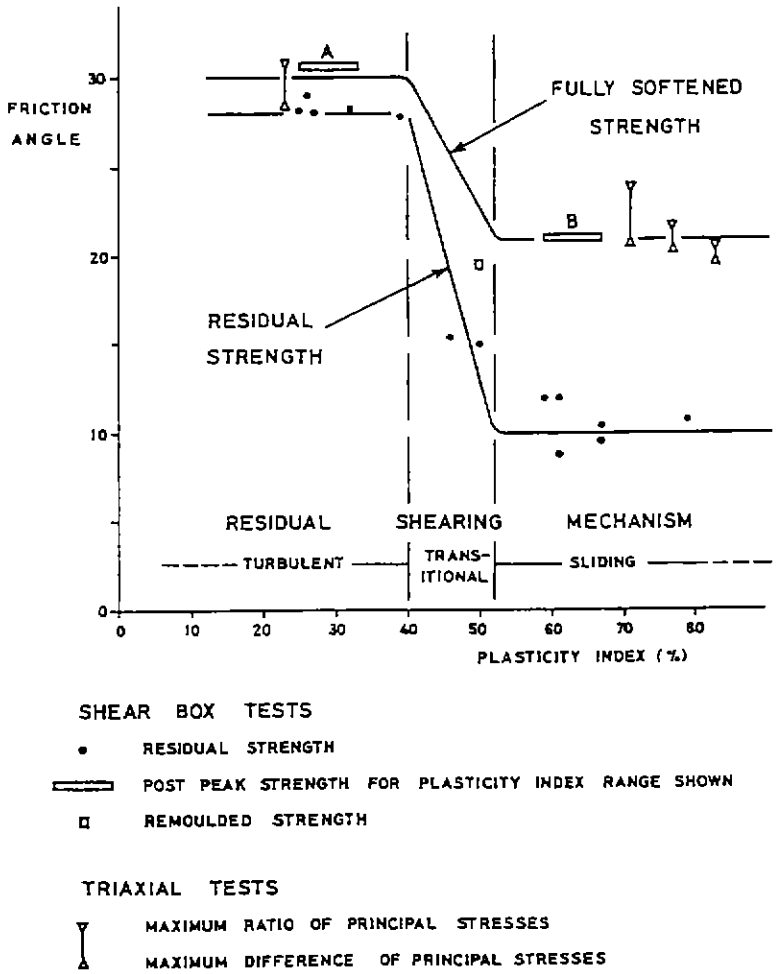

Figure (2.15): Relation between strength and plasticity, (Moon, 1984).

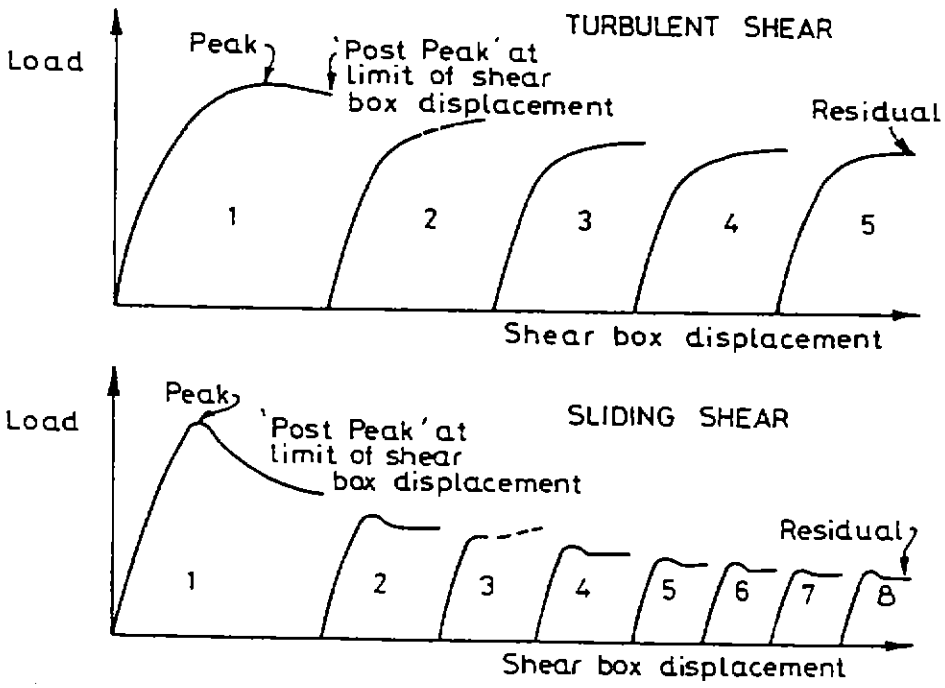

Figure (2.16): Typical load displacement curves for direct shear test (Moon, 1984).

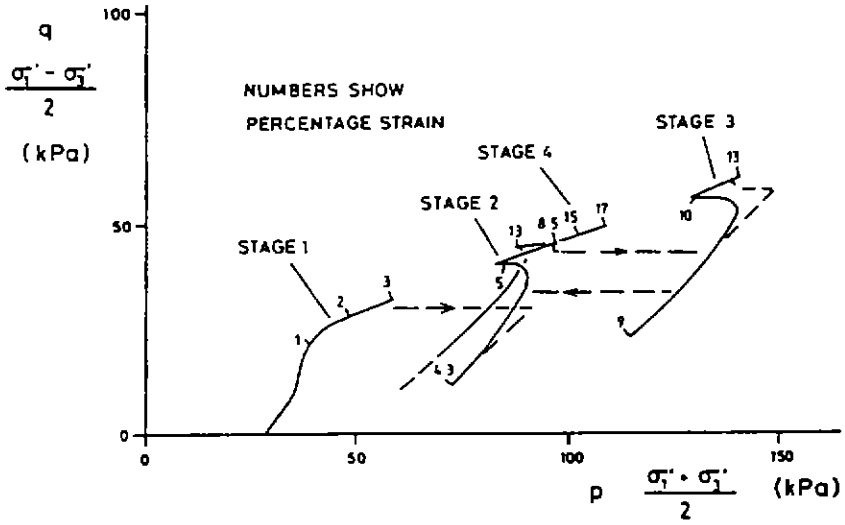

Figure (2.17): P-Q Diagram for staged triaxial test (Moon, 1984).

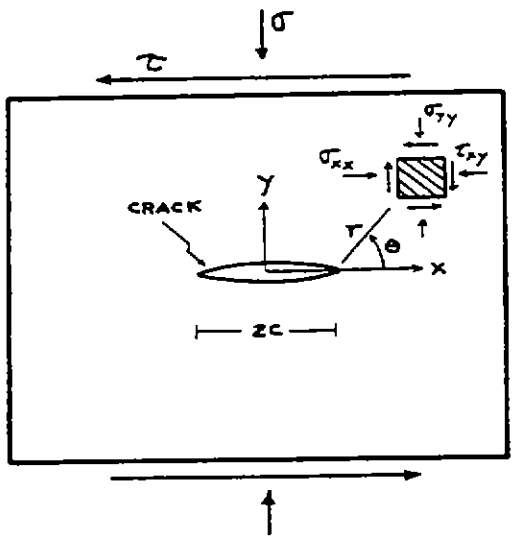

Figure. (2.18): Soil element containing an open crack or fissure, (Vallejo 1985).

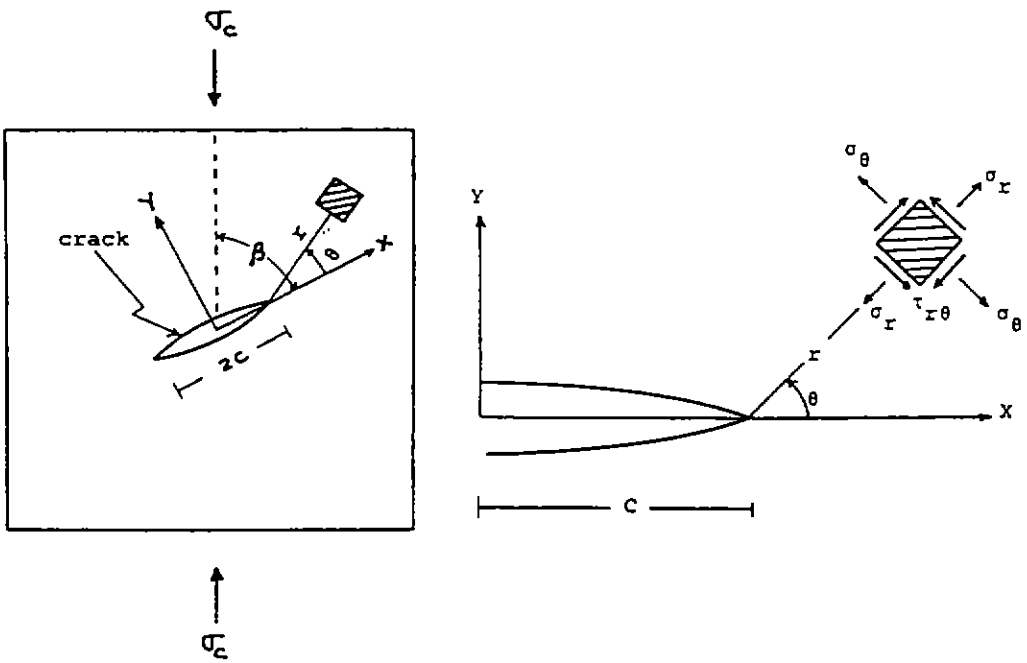

Figure (2.19): Crack tip stresses and system of reference, (Vallejo 1986).

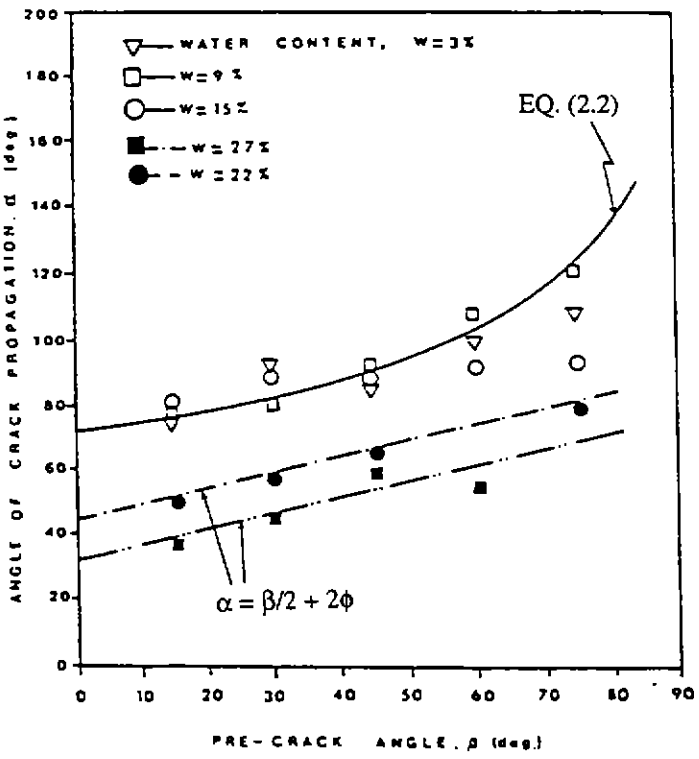

Figure (2.20) Crack propagation angle, α, verses pre-existing crack angle, β, in the brittle and ductile samples of clay. (Vallejo, 1988).

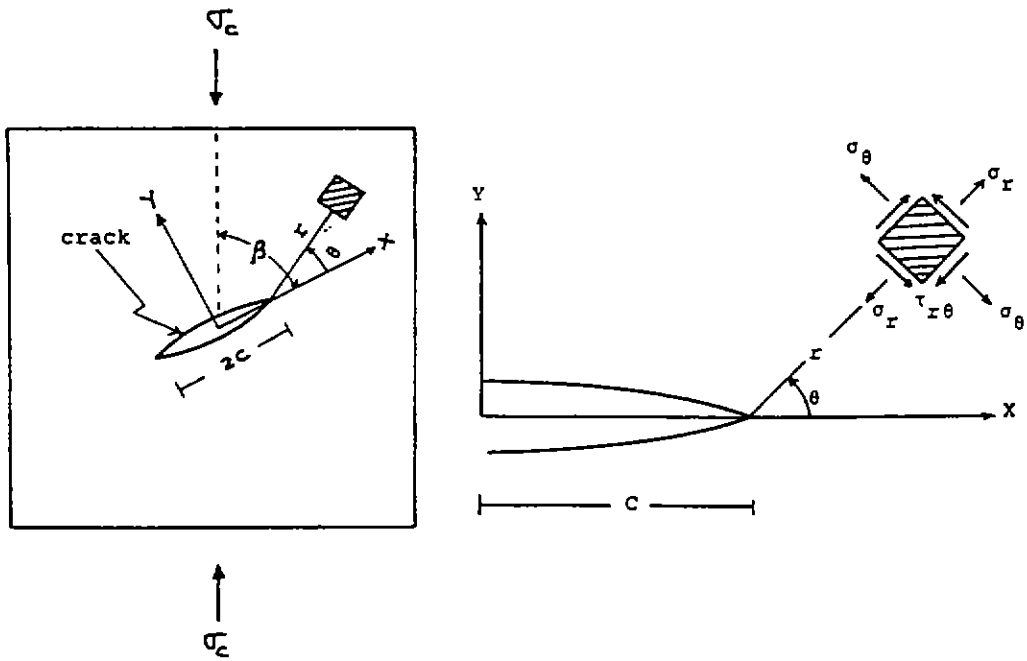

Figure (2.19): Crack tip stresses and system of reference, (Vallejo 1986).

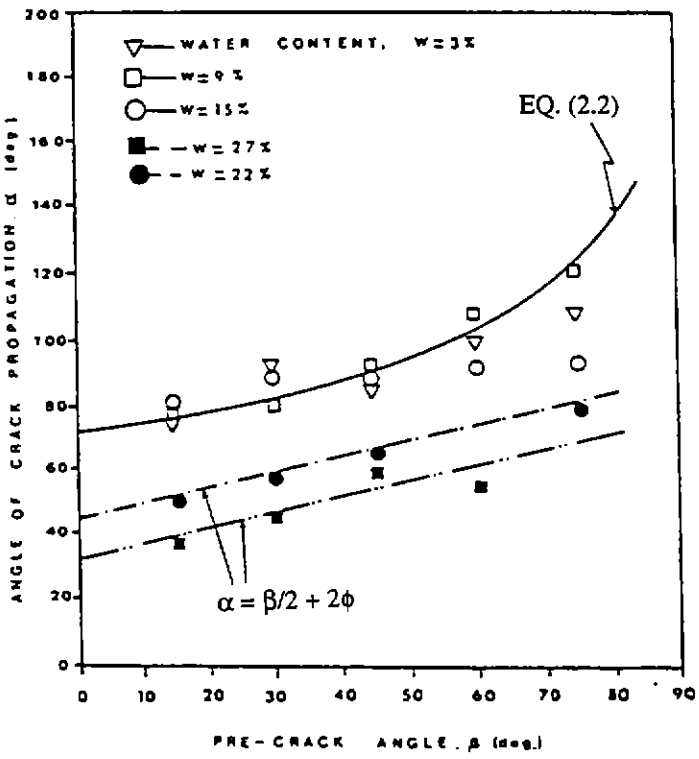

Figure (2.20) Crack propagation angle, α, verses pre-existing crack angle, β, in the brittle and ductile samples of clay, (Vallejo, 1988).

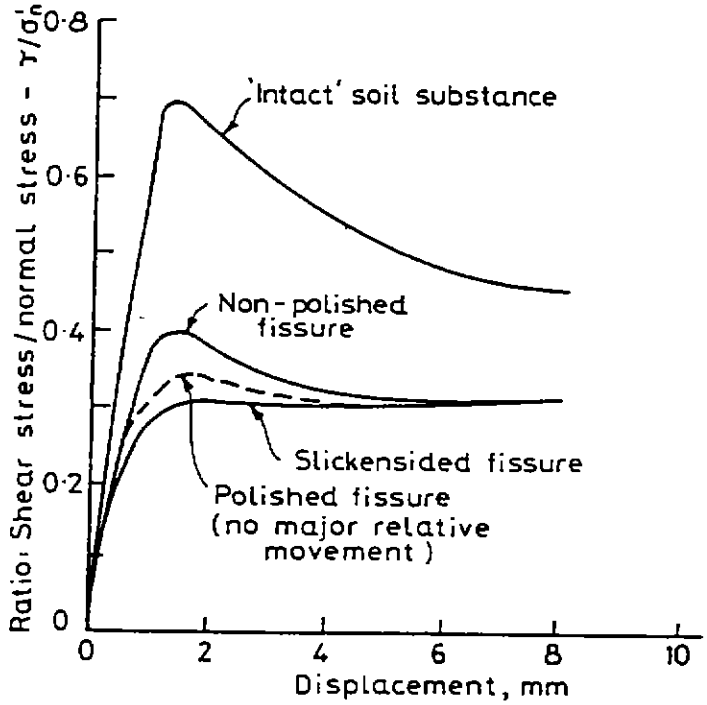

Figure (2.21): Shear tests on soil substance and on various types of fissure surface, (Thorne, 1984).

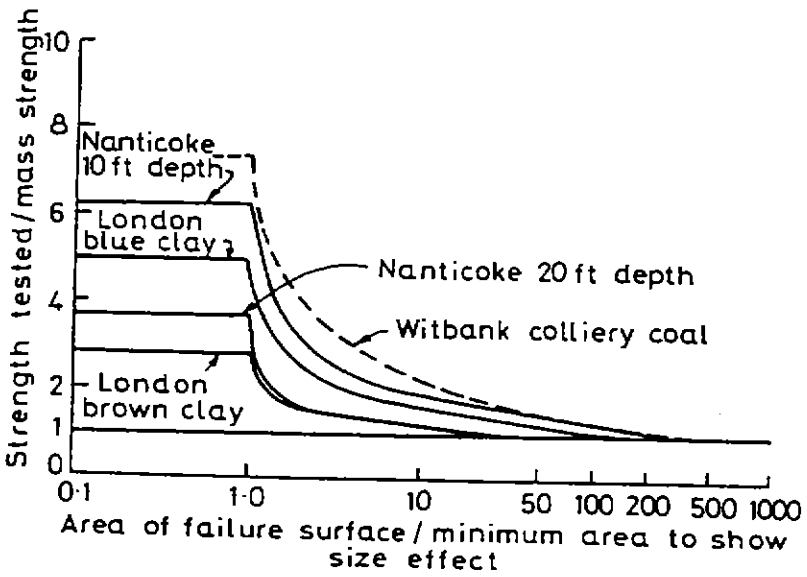

Figure (2.22): Effect of sample size on measured strength, (Thorne, 1984).

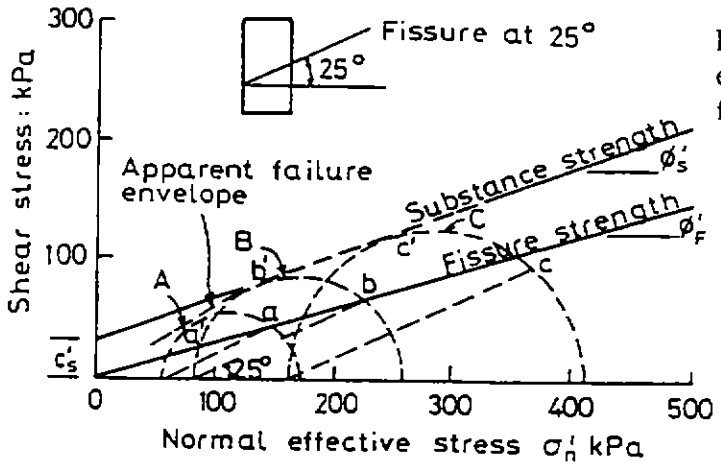

Figures. (2.23): Mohr-Coulomb envelopes at: (a) 25° and (b) 60° fissure inclinations, (Thorne, 1984).

(a)

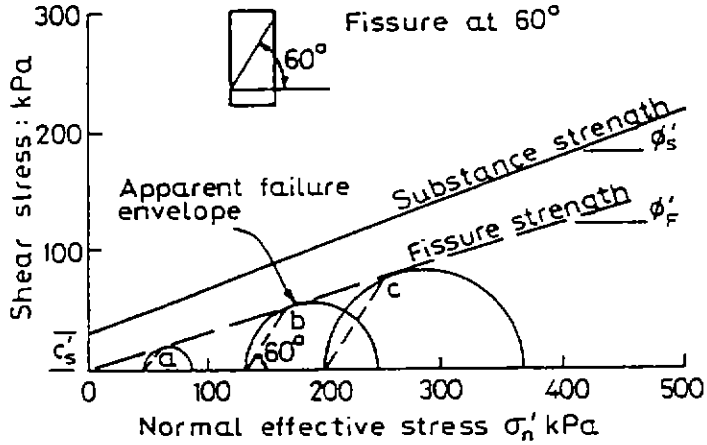

(b)

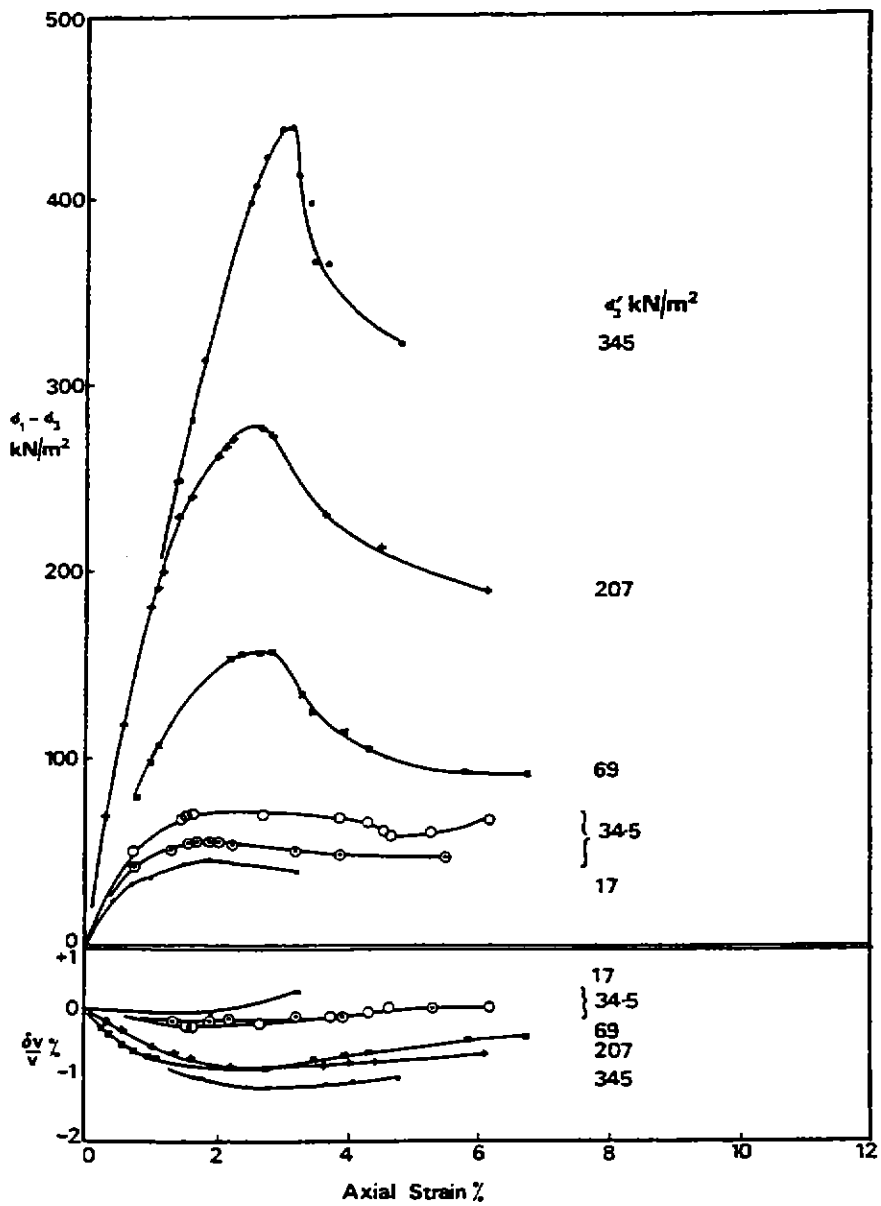

Figure (2.24): Stress strain curves for drained triaxial tests on 98 mm diameter specimens of London Clay from Wraysbury, longitudinal axes 45° to Vertical, (Marsland, 1971)

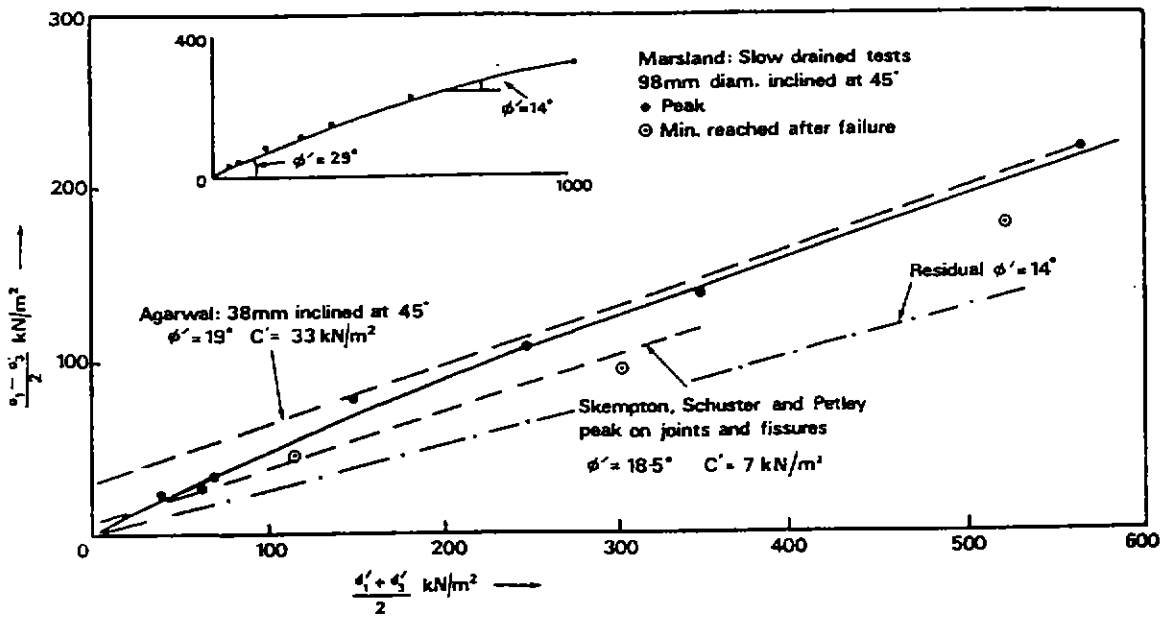

Figure (2.25): Strength of highly fissured London Clay from Wraysbury in terms of effective stresses, (Marsland, 1971).

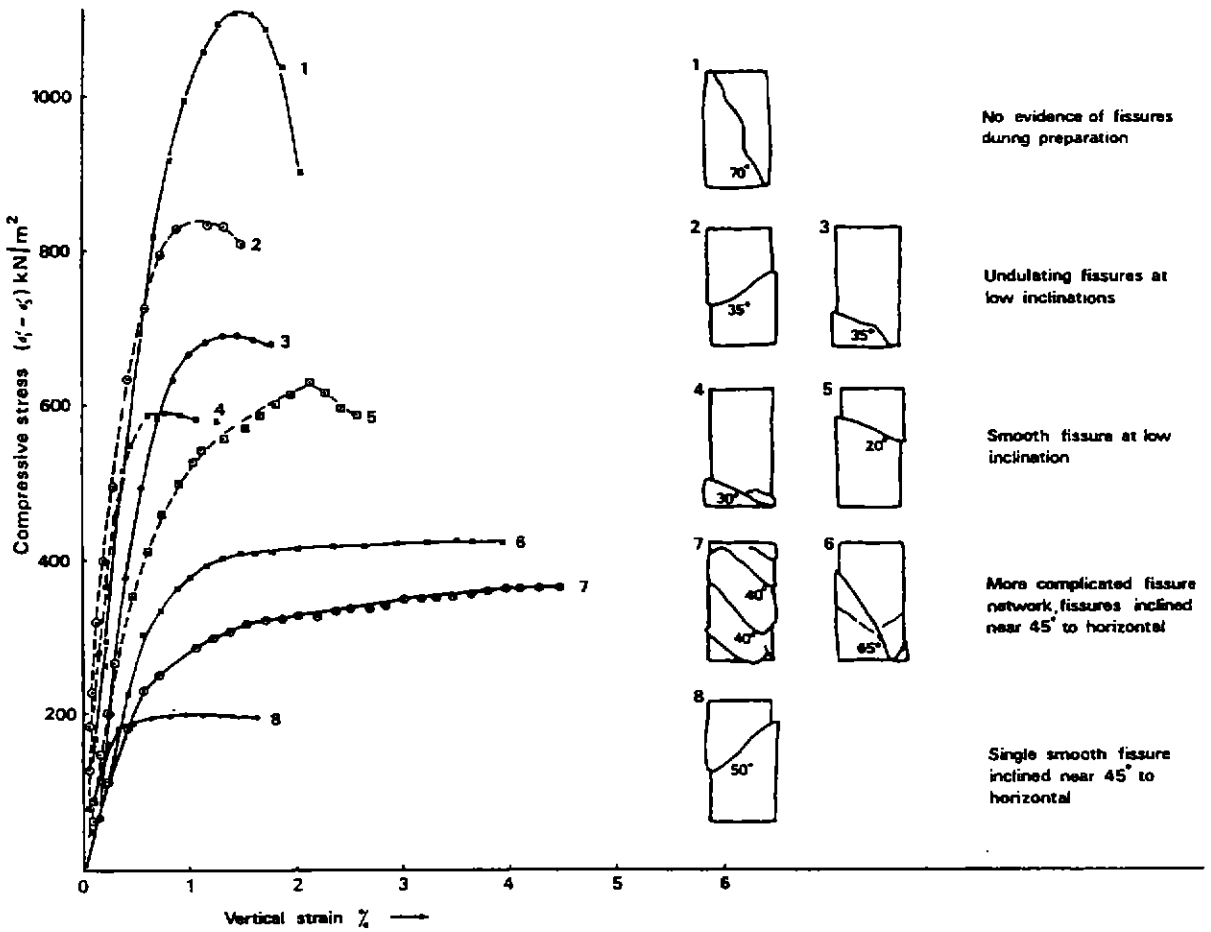

Figure (2.26) Relation of strength measured in triaxial tests on 38 mm diameter specimens to the fissures in the specimens, (Marsland, 1971).

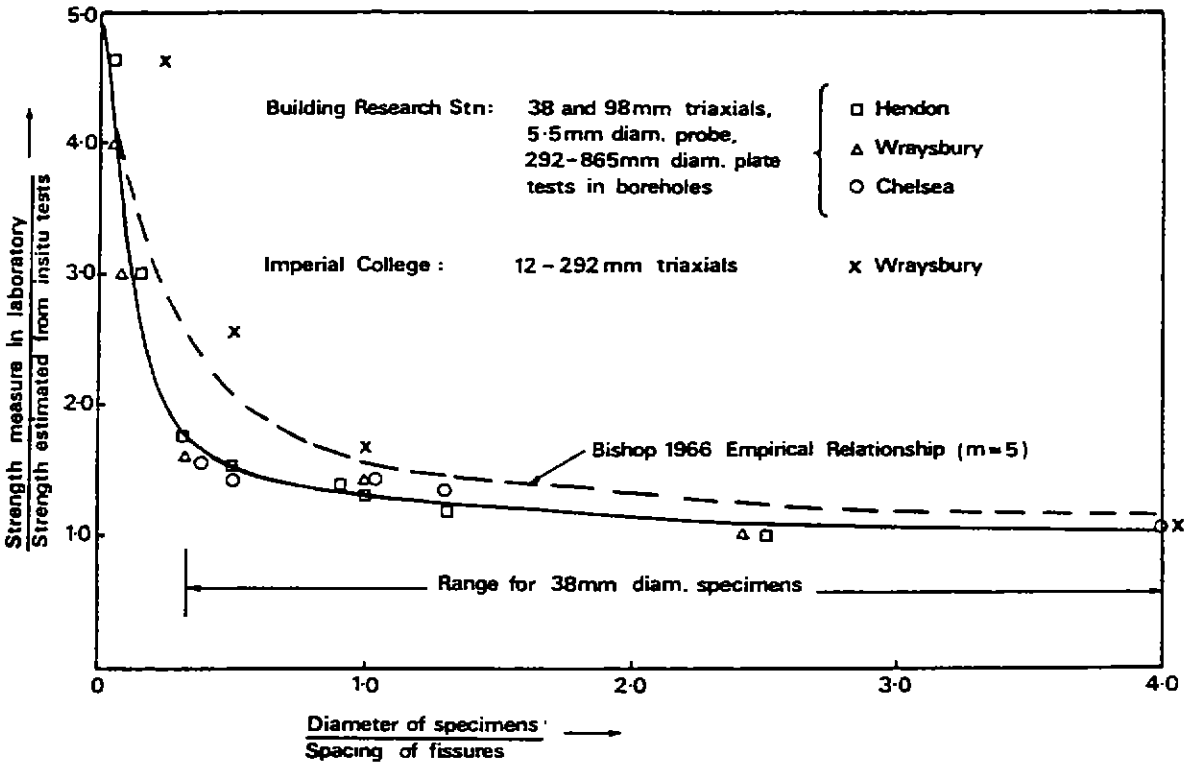

Figure (2.27): Influence of the ratio of sample size to the fissure spacing on the strengths measured in measured laboratory tests, (Marsland, 1971)

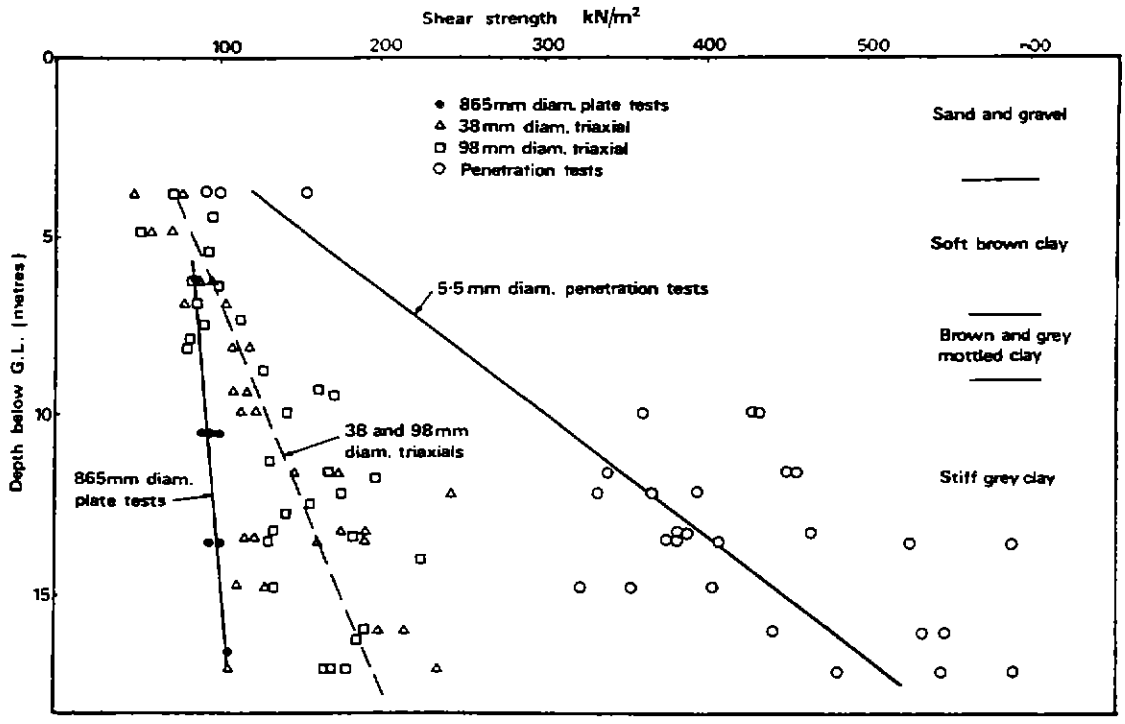

Figure (2.28): Comparison of the undrained shear strengths estimated from 865 mm diameter plate tests and laboratory test on 38 mm and 98 mm diameter specimen in London Clay at Chelsea, (Marsland, 1971b).

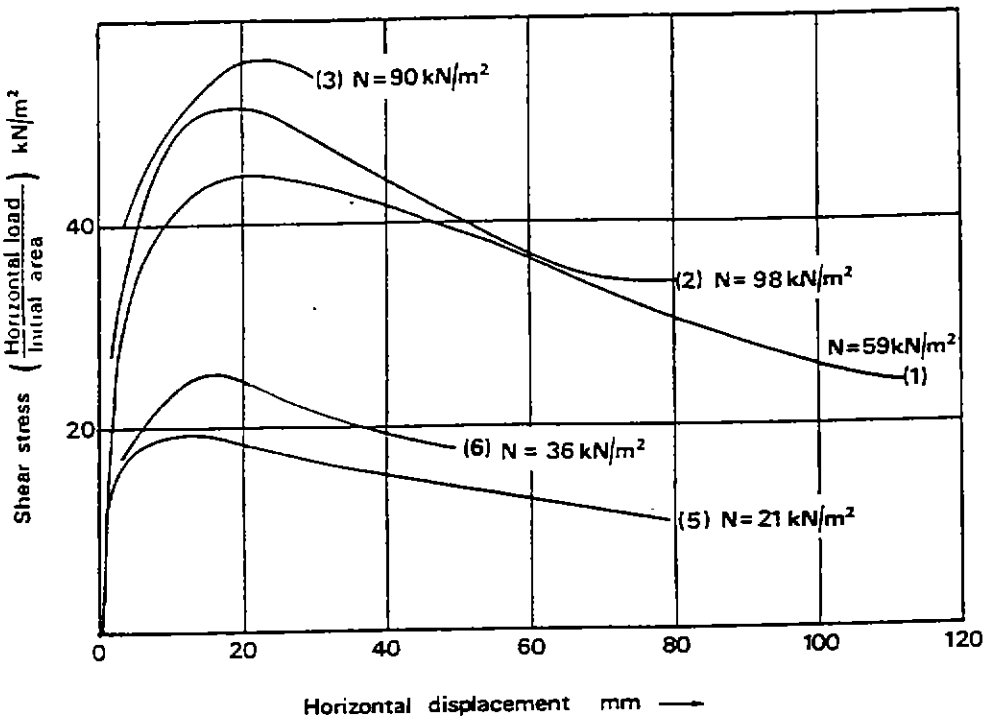

Figure (2.29): Shear stress-displacement curves obtained form drained test on Barton Clay using the large in-situ shear box, (Marsland, 1971b).

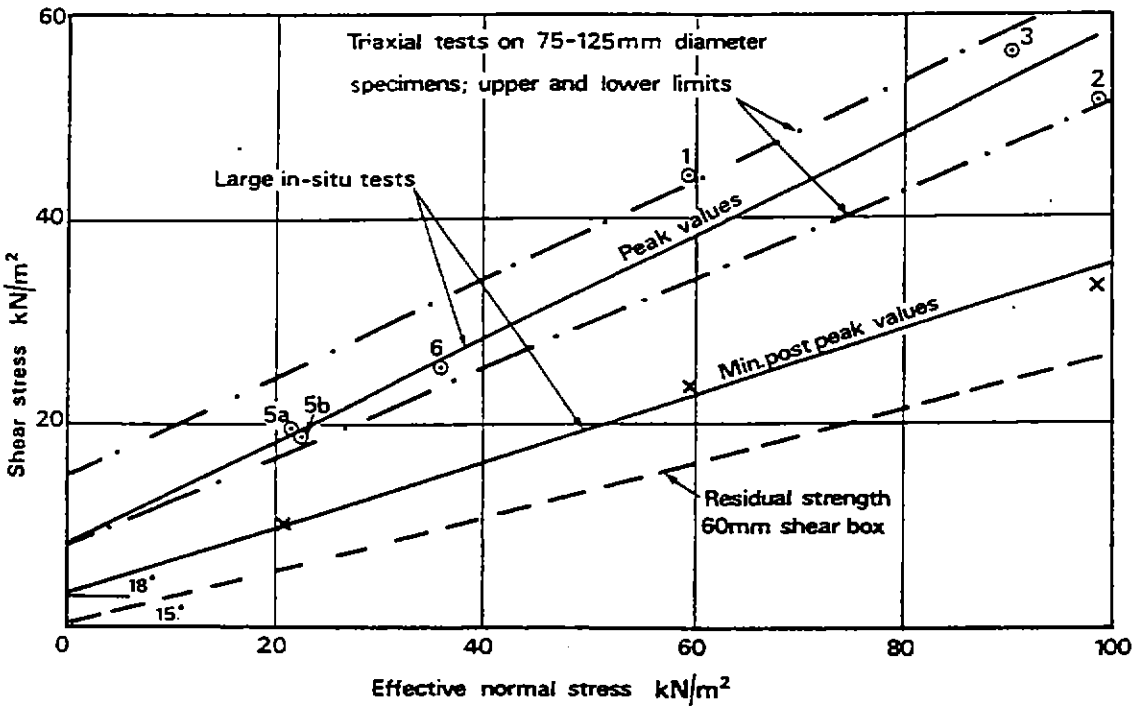

Figure (2.30): Results of in-situ shear tests expressed in terms of effective Marsland (1971b)stresses.

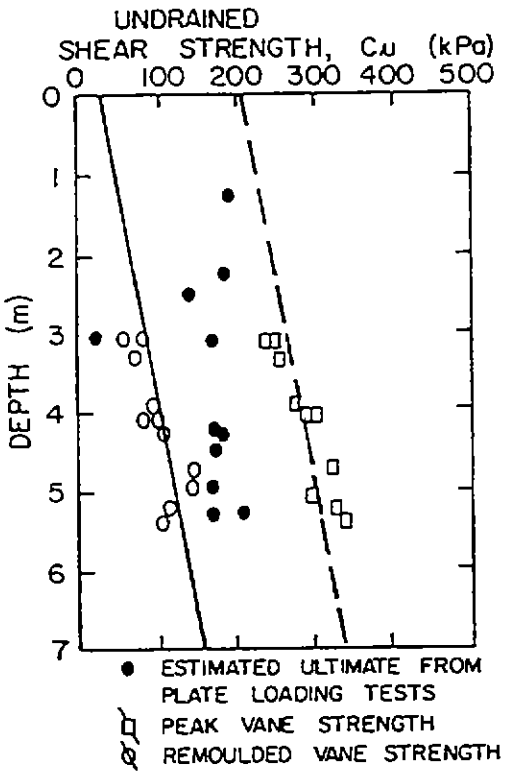

Figure (2.31): Shear strength estimated from in situ tests, (Williams et al., 1977).

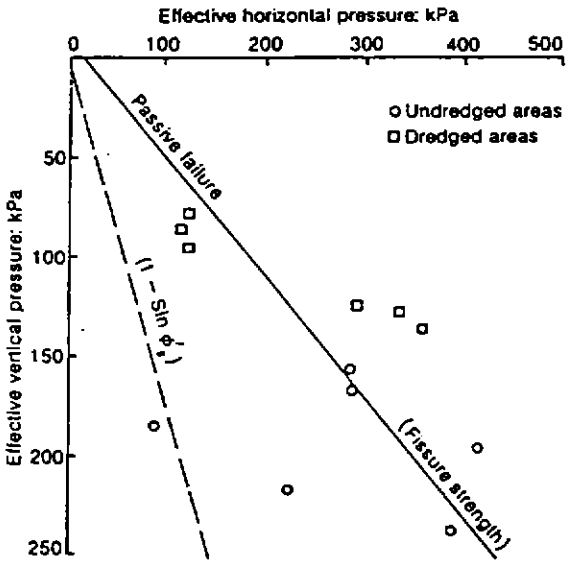

Figure (2.32): In-situ measurement of horizontal stresses (Thorne 1984).

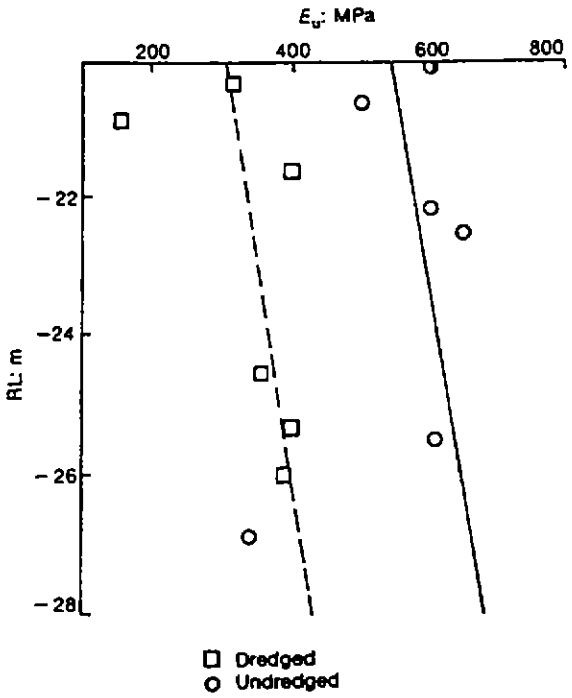

Figure (2.33): Undrained modulus from pressuremeter tests Stresses, (Thorne 1984).

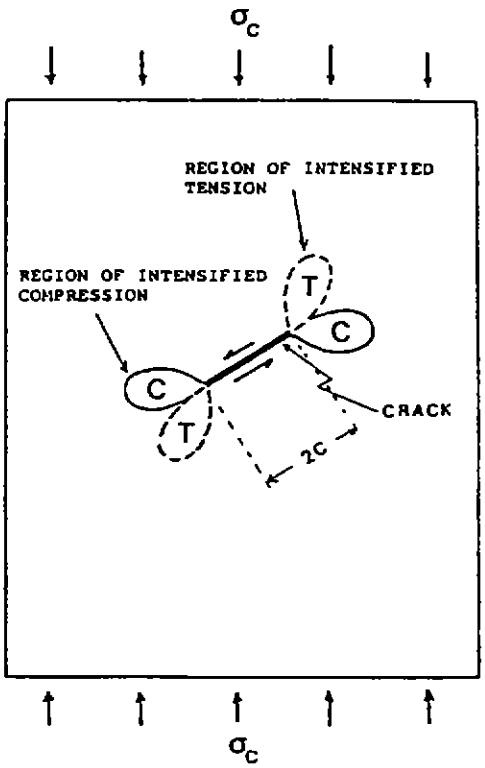

Figure (2.34): Tensile and compressive stresses at open inclined crack in prismatic brittle material under uniaxial compression, (Vallejo, 1989).

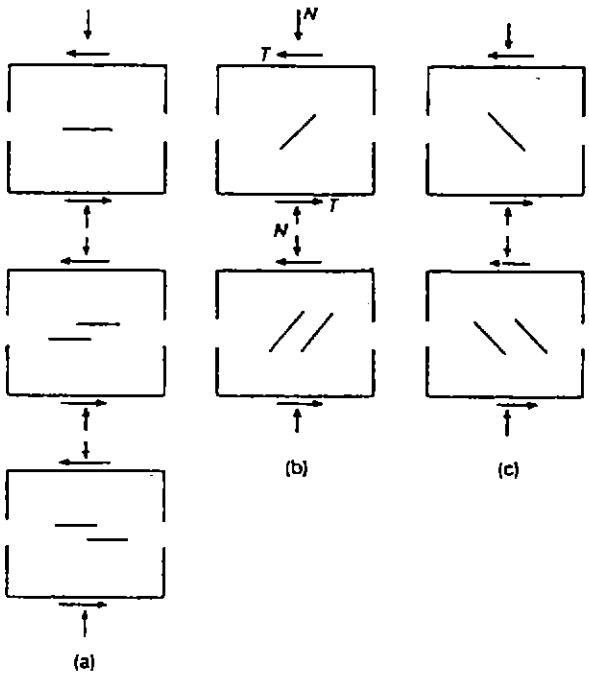

Figure (2.35): (a) Samples of clay with a horizontal crack, two left stepping cracks and two right stepping cracks; (b) samples of clay with one and two cracks inclined at 30° to the horizontal; (c) samples of clay with one and two cracks inclined at 120° to horizontal, (Vallejo, 1989).

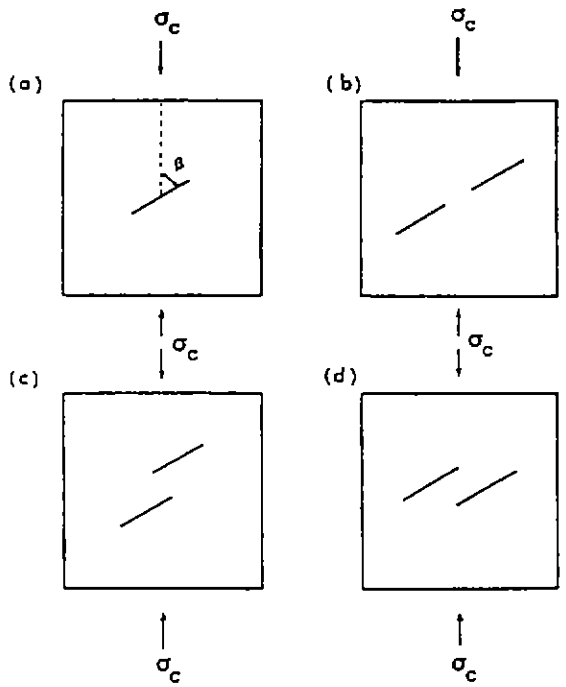

Figure (2.36): Sample with: (a) One inclined fissure;(b) Two aligned fissures;(c) Two left-stepping fissures; (d) Two right-stepping fissures, (Vallejo, 1989).

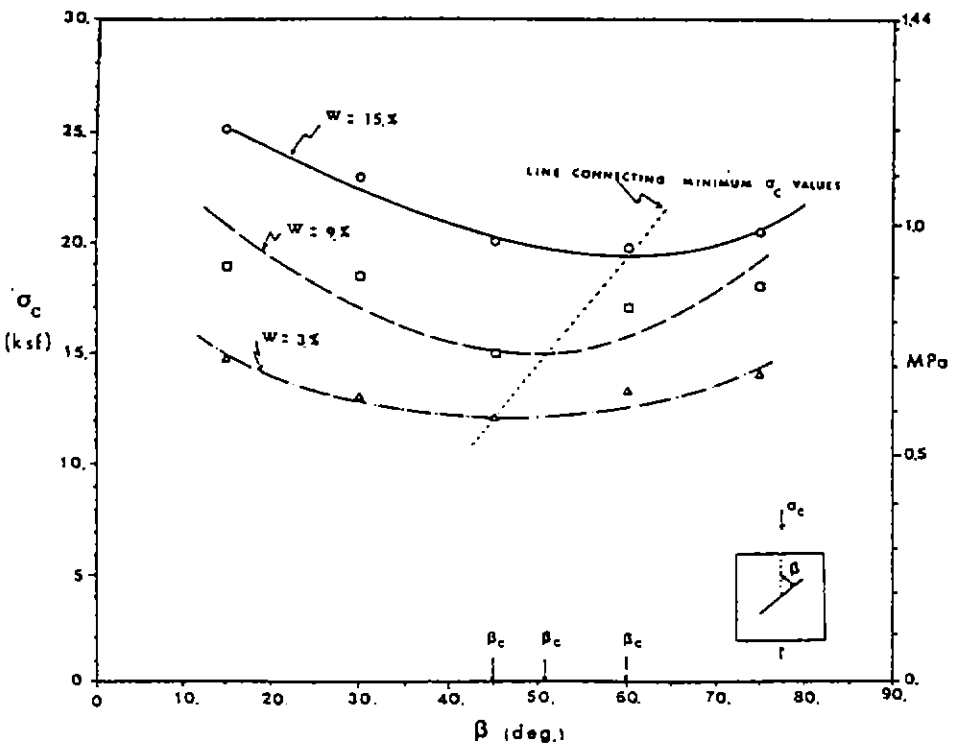

Figure (2.37): Relationships between uniaxial compressive strength and crack inclination in clay samples (Vallejo, 1989).

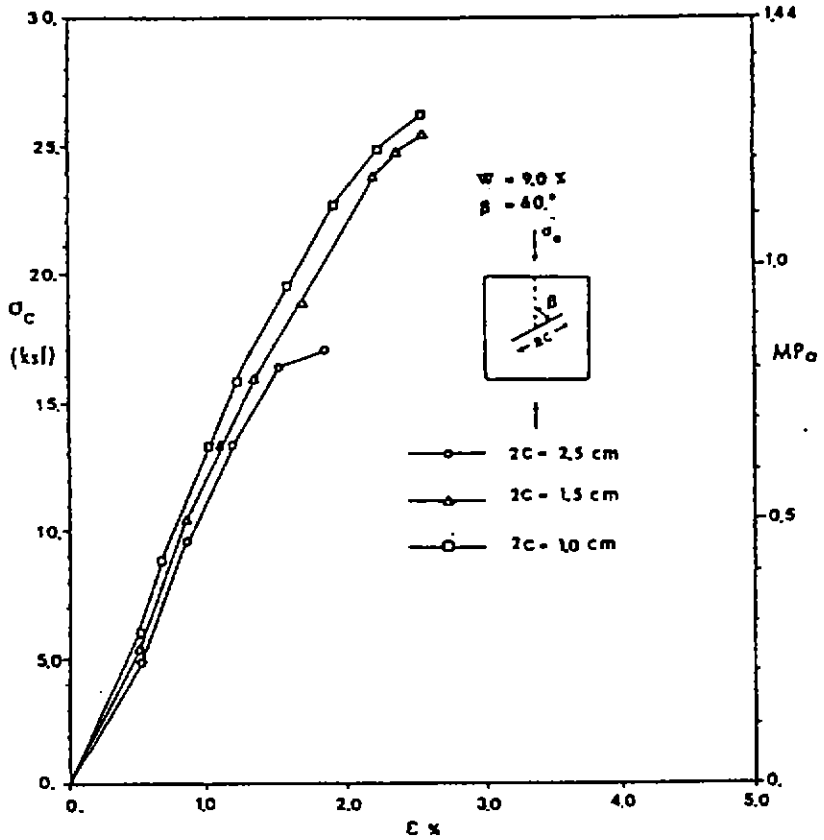

Figure (2.38): Effect of crack length on stress -strain characteristics of clay samples with one crack and water content of 9%, (Vallejo, 1989).

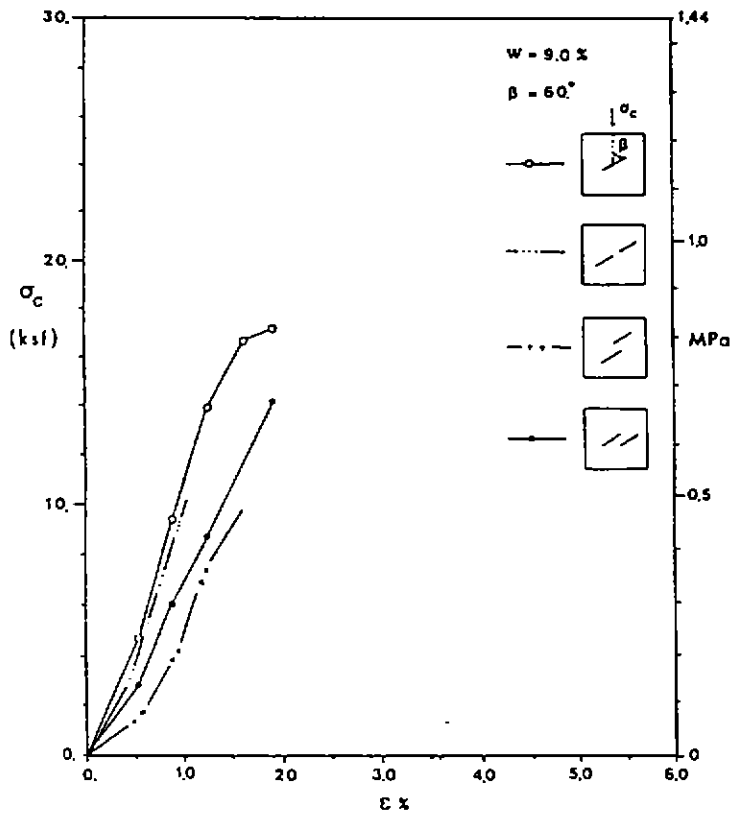

Figure (2.39): Effect of number of crack arrangement on stress strain characteristics of fissured clay samples with water content of 9 %, (Vallejo, 1989).

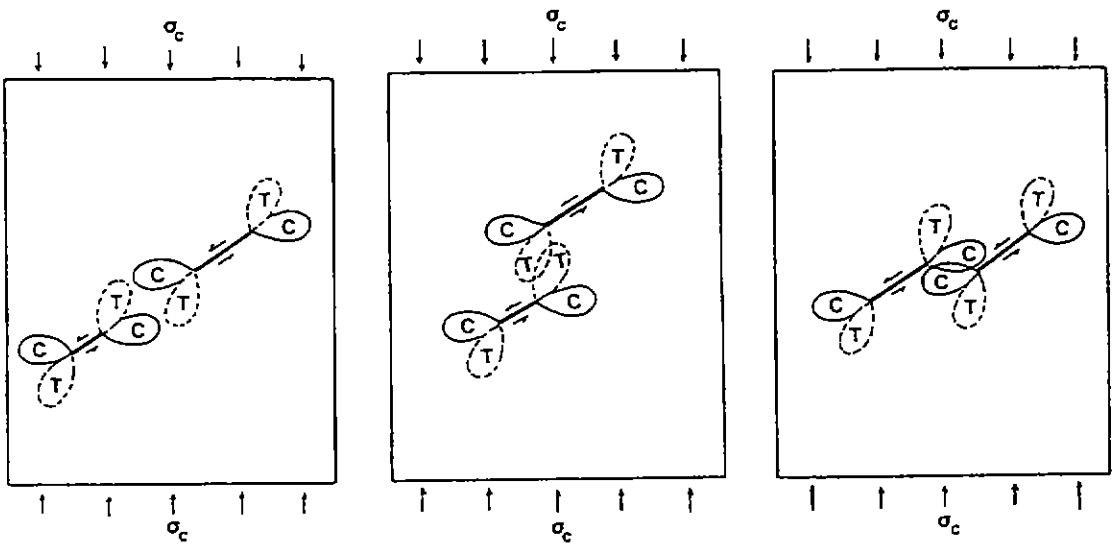

Figure (2.40): Tensile and compressive stresses in prismatic brittle material under uniaxial compression at : (a) two aligned open fissures ; (b) two open left-stepping pre existing fissures; (c) two open right-stepping fissures , (Vallejo 1989).

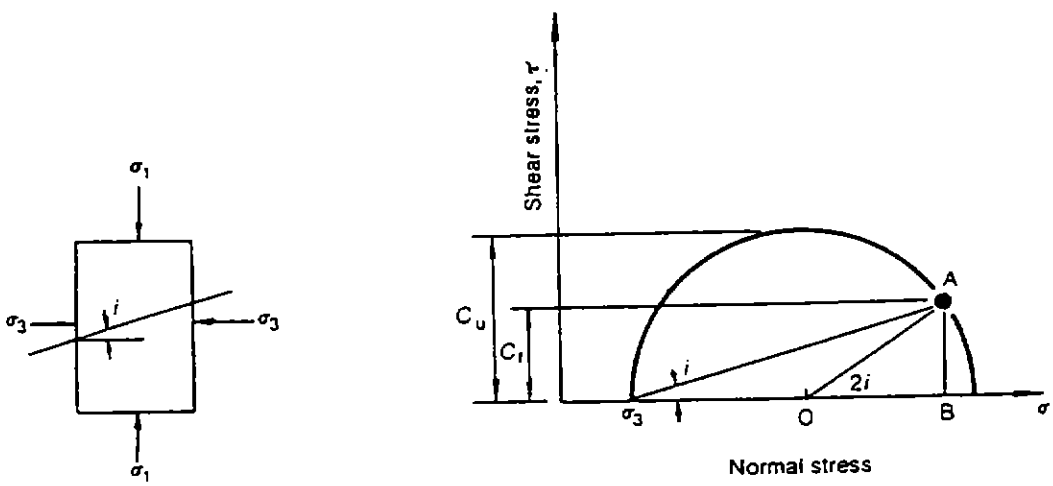

C_U = Undrained strength ≤ intact soil strength (C_m)of sample
C_f = Undrained strength of discontinuity

From Δ OAB: AB/AO = sin (2i) $\therefore C_U = C_f$ sin (2i) $\therefore$ 1/sin (2i) can be considered as a weight factor, which accounts for the weakness induced by an inclined discontinuity of strength C_f

Figure (2.41): The influence of a single discontinuity on the undrained shear strength of a triaxial compression test specimen: a) A single discontinuity in a triaxial test; b) derivation of the weight factor, (McGown et al., 1980).

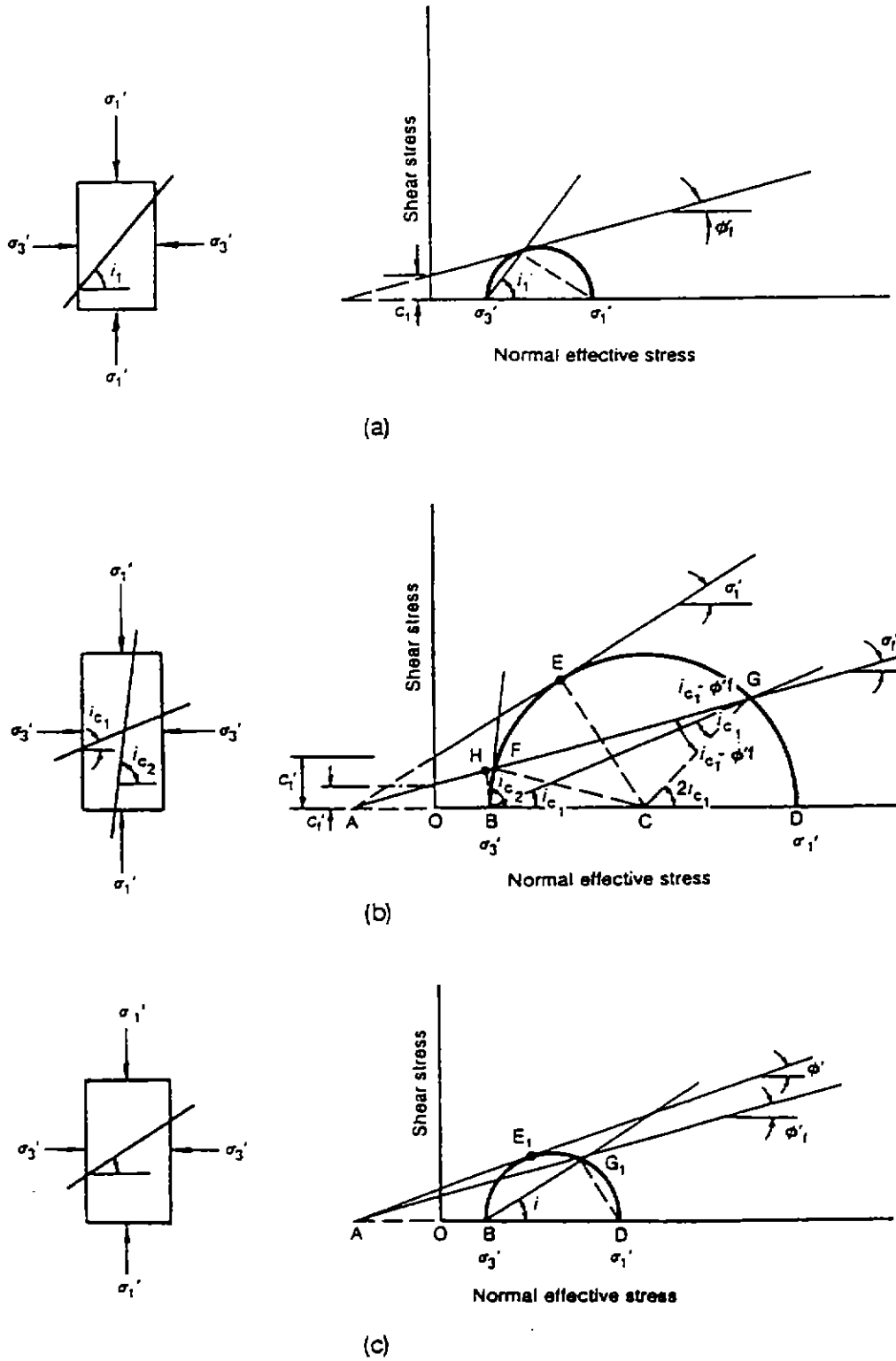

Figure (2.42): The influence of a single discontinuity on the drained shear strength of a triaxial compression test specimen: fissure plane dipping at (a) $i_1 = 45° + \phi'_f/2$; (b) critical angles i_{c1} and i_{c2}; (c) angle $i_{c1} < i < i_{c2}$.

Discontinuity Type	Physical Characteristics	Geotechnical Aspects	Comments
Tectonic joints	Persistent fractures resulting from tectonic stresses. Joints often occur as related groups or 'sets'. Joint systems of conjugate sets may be explained in terms of regional stress fields.	Tectonic joints are classified as 'shear' or 'tensile' according to probable origin. Shear joints are often less rough than tensile joints. Joints may die out laterally resulting in impersistence and high strength.	May only be extrapolated confidently where systematic and where the geological origin is understood.
Faults	Fractures along which displacement has occurred. Any scale from millimetres to hundreds of kilometres. Often associated with zones of sheared rock.	Often low shear strength particularly where slickensided or containing gouge. May be associated with high groundwater flow or act as barriers to flow. Deep zones of weathering may occur along faults. Recent faults may be seismically active.	Mappable, especially where rocks either side can be matched. Major faults often recognized as photo lineations due to localized erosion.
Sheeting joints	Rough, often widely spaced fractures; parallel to the ground surface; formed under tension as a result of unloading.	May be persistent over tens of metres. Commonly adverse (parallel to slopes). Weathering concentrated along them in otherwise good quality rock.	Readily identified due to individuality and relationship with topography.
Lithological boundaries	Boundaries between different rock types. May be of any angle, shape, and complexity according to geological history.	Often mark distinct changes in engineering properties such as strength, permeability and degree and style of jointing. Commonly form barriers to groundwater flow.	Mappable allowing interpolation and extrapolation providing the geological history is understood.

Table (2.1): Geotechnical classification of discontinuities common to all rock and soil types, (Hencher, 1987).

Rock or Soil type	Discontinuity type	Physical characteristics	Geotechnical aspects	Comments
Sedimentary	Bedding planes/ bedding plane joints	Parallel to original deposition surface and marking a hiatus in deposition. Usually almost horizontal in unfolded rocks.	Often flat and persistent over tens or hundreds of metres. May mark changes in lithology, strength and permeability. Commonly close, tight, and with considerable cohesion. May become open due to weathering and unloading.	Geologically mappable and therefore, may be extrapolated providing structure understood. Other sedimentary features such as ripple marks and mud-cracks may aid interpretation and affect shear strength.
	Shaley cleavage	Close parallel discontinuities formed in mudstones during diagenesis and resulting in fissility.		
	Random fissures	Common in recent sediments probably due to shrinkage and minor shearing during consolidation. Not extensive but important mass feature.	Controlling influence for strength and permeability for many clays.	Best described in terms of frequency.
Igneous	Cooling joints	Systematic sets of hexagonal joints perpendicular to cooling surfaces are common in lavas and sills. Larger intrusions typified by doming joints and cross joints.	Columnar joints have regular pattern so easily dealt with. Other joints often widely spaced with variable orientation and nature.	Either entirely predictable or fairly random.
Metamorphic	Slaty cleavage	Closely spaced, parallel and persistent planar integral discontinuities in fine grained strong rock.	High cohesion where intact but readily opened due to weathering or unloading. Low roughness.	Formed by regional stresses and therefore mappable over wide areas.
	Schistosity	Crenulate or wavy foliation with parallel alignment of minerals in coarser grained rocks.	Often foliations coated with minerals such as talc, and chlorite giving a low shear strength.	Less mappable than slaty cleavage but general trends recognizable.

Table (2.2): Geotechnical classification of discontinuities characteristic of particular rock and soil types, (Hencher, 1987).

Nature of features	Form of features	Description
Solids (organic or inorganic)	Linear (1D extensive)	Lineations, which includes thin channel infillings and rootlets
	Planar (2D extensive)	Layers, which includes laminations, bands beds, seams, partings, dustings, strata
	Equidimensional (3D extensive)	Lobes, which includes lumps, peds, pockets, nodules, lenses
Pore space	Linear (1D extensive)	Ducts, which includes open channels and passageways
	Planar (2D extensive)	Discontinuities, which includes bedding planes, shear surfaces, faults, joints, fissures, cracks
	Equidimensional (3D extensive)	Defects, which includes packing voids, solution cavities, vessicles

Table (2.3): Macrofabric features commonly found in soils, (McGown et al., 1980).

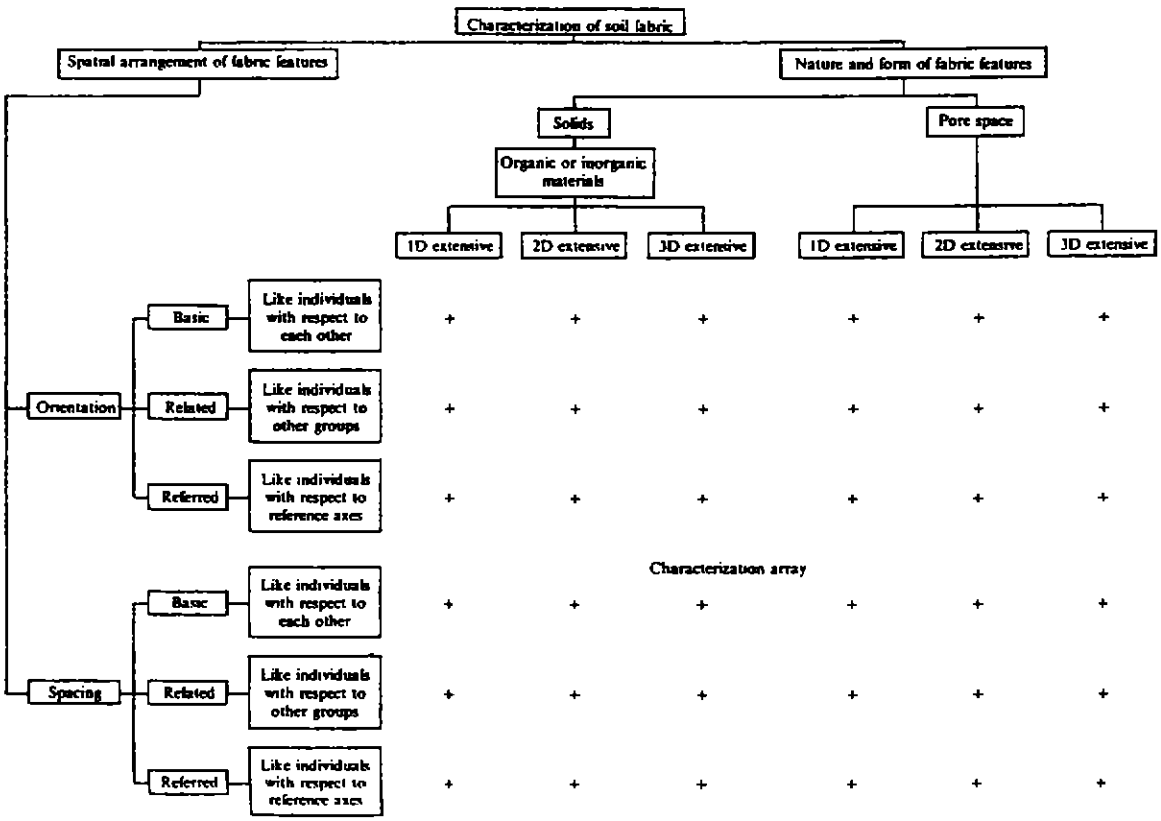

Table (2.4) The characterisation array for soil macrofabric (McGown et al., 1980).

1. Site: Clyde Estuary
2. Date: February 1977
3. Block core or cavity details. Depth: 15·75 to 16·65 m Piston sample; size 54 mm. dia
4. Orientation of basic axis: Vertical
5. Soil description: Silty clay
6. Observed related or referred features: None
7. Measurements:

No. of feature	Nature		Form			Orientation		Spacing
	Feature type	Soil classification	Thickness *t*: mm	Continuity assessment*	Surface geometry	Strike	Dip	*S*: mm
1	Dusting	Fine sand	0·3	Continuous	Planar	Horizontal		2
2	Dusting	Fine sand	0·3	Continuous	Planar	Horizontal		2
3	Lamination	Fine sand	1·0	Continuous	Planar	Horizontal		4
4	Lamination	Fine sand	1·0	Continuous	Planar	Horizontal		7
5	Lamination	Fine sand	2·0	Continuous	Planar	Horizontal		4
6	Dusting	Fine sand	0·3	Continuous	Planar	Horizontal		4
7	Dusting	Fine sand	0·3	Continuous	Planar	Horizontal		4
8	Dusting	Fine sand	0·3	Continuous	Planar	Horizontal		4

8. Derived data

Measurement on like features	Feature type (a)	(b)	(c)
Average thickness, t_{av}: mm = 0·4	—	—	—
Average spacing (S_{av}): mm = 5·0			
No. of features in depth measured, N = 63 in 454 mm			
Frequency per metre f = 138 per metre			
Relative overall thickness of feature per metre ($t_{av}F$) = R.O.T. = 6·2%			

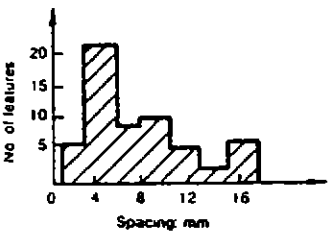

Table (2.5) Macrofabric record sheet for layered sediments, (McGown et al., 1980).

1. Site: Glasgow
2. Date: June 1977
3. Block or cavity details. Depth: 6·5 m; Size: 1 m × 1 m × 1 m.
4. Orientation of basic axes: N–S, E–W, vertical
5. Soil description: Glacial lodgement till
6. Observed related or referred features: Drumlin surface above (Strike 70°, Dip 14°)
7. Measurements:

No. of Discontinuity	Nature				Form		Orientation		Spacing		
	Discontinuity type	Surface roughness	Surface staining or coating	Intact soil type	Dimensions: mm	Surface geometry	Strike	Dip	Centre point co-ordinates mm X_c	Y_c	Z_c
1	Stress relief	1·5 mm	Clean	Well graded	80 × 90	Planar	180	85	125	80	60
2	Stress relief	2·0 mm	Clean	Stoney	70 × 110	Planar	183	88	200	70	50
3	Stress relief	2·0 mm	Clean	Sandy	110 × 90	Planar	148	87	210	65	45
4	Bedding feature	4·5 mm	Silt coated	Silty	150 × 100	Planar	75	5	220	107	80
5	Bedding feature	5·5 mm	Silt coated	Clay	160 × 120	Planar	78	9	250	130	120

Table (2.6): Macro fabric record sheet for discontinuities, (McGown et al., 1980)..

Apparatus	Sample Type	Failure Definition
Triaxial	Undisturbed	maximum ratio of principal stresses
Triaxial	Undisturbed	maximum difference of principal stress
Shear box	Undisturbed	peak strength
Shear box	Undisturbed	post peak strength (at 7 mm displacement)
Shear box	Remoulded	peak strength of normally consolidated sample

Table (2.7): Method used to determine fully softened strength, (Moon, 1984).

CHAPTER 3

PRELIMINARY STUDY ON THE LABORATORY PREPARATION OF SPECIMENS

3.1 INTRODUCTION

Laboratory simulation provides accurate solutions in many research studies especially where there are parameters and each needs to be monitored, controlled, and quantified or the interaction of a few simultaneously investigated.

In geotechnical engineering, laboratory simulation has been used to simulate geotechnical problems such as the interaction between substructure and soil or the interaction within water flow, soil, and external static or dynamic loads.

The simulation of materials, especially in rock mechanics, has been useful in many recent investigations. In the geomechanics area, clayey soils were imitated by using artificial clays such as kaolin and bentonite to avoid the effect of nonhomogeneity of material. Fissures in stiff fissured clays and naturally overconsolidated clays, like discontinuities in rocks such as faults, joints, cracks and micro cracks, have been studied in the laboratory. These studies were conducted for special purposes but are insufficient to study the drained shear strength of these materials.

Laboratory simulation of fissures in stiff fissured clays and the parameters influencing the effective shear strength of these materials, as well as measuring their effects, could be useful in estimating the effective shear strength of the naturally over-consolidated fissured clay mass.

Fissure parameters such as spacing, orientation, width of fissures and stress history parameters like preconsolidation pressure, OCR and material parameters, the type of the minerals, and clay fraction, the effects of sampling, the size of specimens, and the rate of shearing, are very important parameters influencing the effective shear strength of a fissured clay mass.

In naturally overconsolidated fissured specimens, because of a lack of control of these parameters, studies have not been satisfactory enough to qualify and identify them individually.

Many attempts have been made to estimate the effective shear strength of a naturally fissured clay mass based on the situation in the field, from physical and mechanical points of views, and a few experimental approaches have been suggested. Some researchers stated that the fully softened strength of unfissured specimens of a naturally over-consolidated clay would give a good estimation of the effective shear strength of the naturally overconsolidated fissured clayey mass (Skempton, 1970; Moon, 1984). Ignoring the effects of fissure parameters, material parameters and boundary conditions, and relating the overall effective shear strength of a naturally overconsolidated fissured mass just to the fully softened shear strength of the unfissured overconsolidated clayey specimens, would be erroneous. Therefore, in addition to laboratory tests on the fissure surfaces and unfissured specimens, mapping and monitoring fissure parameters such as size, orientation, spacing and arrangement of fissures are necessary for a realistic estimation of the effective shear strength of the naturally over-consolidated fissured mass.

As the behaviour of strain-softening is a common behaviour observed in stiff fissured clay mass or naturally overconsolidated fissured clay mass in this chapter, particular attention has been paid to simulate this behaviour for the artificial clay materials used to prepare the laboratory specimens.

This research has not been designed to stimulate a particular type of stiff fissured clay mass. Therefore, satisfying all similitude conditions as explained by Langharr (1951), Devendra (1968), and Einstein et al. (1970) is not within its scope.

However, the similarity of the materials used for artificially prepared specimens in the laboratory and the natural materials found in stiff fissured clay mass or naturally overconsolidated clay mass, as well as the similarity of the type of stress-strain curves, have been satisfied and they are two important conditions which may be involved in seeking similitude conditions.

The scaling factor, induced as a result of geometry and boundary conditions, is an important parameter in the study of similarity. The study of this factor is not within the scope of this study because this research has not been designed for a particular type of material or a particular field problem.

However, this factor could be taken into account by qualifying and identifying the effects of fissure parameters and arrangements, sampling, and size of specimens for different loadings on the effective shear strength of unfissured, partially and fully fissured specimens as discussed in Chapter 5.

In this chapter firstly, the development of the artificial mixed clays used for the research with regard to the strain-softening behaviour, is discussed, then, the physical and mechanical properties of the artificial materials are introduced, and finally the laboratory preparation of artificially overconsolidated clay specimens, as well as the simulation of the parameters from a practical point of view, are explained or discussed briefly.

From the results of this chapter, the material types used, the method of preparation of specimens tested in the experimental program and initial experimental programming for the study of the parameters were concluded.

3.2 PARAMETER STUDIES FOR THE LABORATORY PREPARATION OF THE SPECIMENS

In this section, the effect of parameters and methods involved in the preparation of the laboratory specimens for both direct shear and triaxial tests are discussed.

3.2.1 Strain Softening

Strain-softening in simplistic terms may be defined as a part of the stress-strain curve for which a decrease in strength is associated with an increase in strain. An example of the strain-softening behaviour of soil is depicted in Figure (3.1). This behaviour originally was reported by Skempton (1964).

In recent studies on granular materials, Chu et al. (1992, 1996) observed and classified three different types of strain-softening behaviour. The first was due to boundary imperfections such as end restraints in conventional triaxial testing without effective free ends. Banding softening was reported as the second type. Chu et al. (1996) indicated that this was always associated with shearing in the post-failure regime. The last type was reported as the result of material softening which can happen both in pre-failure and post-failure regimes.

Strain softening in the stress-strain curve is one of the most significant characteristics of the stiff fissured clays or overconsolidated clayey mass (Skempton, 1948; Bishop et al., 1965). Although many researchers have tried to relate the strain softening effect to the clay fraction or plastic indices (Lupini et al., 1981; Moon, 1984), few researches believe it because of the material type, OCR and fissure existence in the material (Kenny, 1967; Skempton, 1964; Skempton et al., 1969). For this study, a mixture of kaolin and bentonite clays was used for laboratory simulation of the strain softening behaviour of clayey specimens. However, the stress strain curve of specimens prepared of kaolin shows that little strain softening happens after a large amount of displacement.

Figure (3.2) shows the stress-strain curve obtained from an overconsolidated K specimen tested with the preconsolidation pressure of 440 kpa and an OCR = 10 with a rate of shearing of 0.0005 mm/min. As this figure shows, the stress-strain curve is ductile and there is no significant decrease of strength because of the effect of strain-softening. Therefore, a combination of Kaolin (50% of dry weight) with fine uniform sand (50% of dry weight) was tried. The existence of fine sand increased and improved the effective shear strength of the specimens prepared of Kaolin and sand (KS), but did not change the behaviour of the stress strain curve to a different

behaviour observed from Kaolin specimens (K). As Figure (3.3) shows, there is an increase of effective shear strength for the KS specimens but no improvement of strain softening behaviour is observed. A mixture of Kaolin (50%), bentonite (40%) and fine sand (10%) was used in another attempt to simulate strain softening behaviour for the artificially consolidated clay specimens. Figure (3.4) depicts the stress-strain curve obtained from a KBS specimen. There was a nice strain-softening behaviour in the curve, but the time needed for the consolidation of this type of material (KBS) was too long to accept this mixture as an artificial clayey material for this research (about 4-5 days loading).

A mixture of Kaolin (75%) and Bentonite (25%) was used in another attempt. A good strain softening behaviour was observed (Figure 3.5). The time needed to consolidate this mixture (KB), about 2 days, was suitable for this research taking into account the number of tests needed for the study of the parameters. However, another mixture of KB (50% K and 50% B) was also tried. The improvement of strain-softening behaviour was not significant compared with the increase of time needed for the consolidation process. Therefore, the best ratio in view of the number of tests needed to study the purposed parameters was 1/3 bentonite to kaolin of the dry weights.

For this ratio, about two days, loading for a specimen with a thickness of 25 mm was needed. Figure (3.6) shows the stress strain curves of these two materials (K and KB) for the same rate of shearing and OCR, and that the effective shear strength of KB specimens is less than that of K specimens.

Di Maio et al. (1994) studied the residual strength of kaolin and bentonite specimens subjected to drained direct shear tests. They observed by scanning electron micrographs that the difference in roughness of shear surfaces resulted in a difference in the residual shear strength. Although, this study was conducted on the residual shear strength, it can be implied that difference in roughness of shear surfaces could be an explanation of the differences in the peak shear strength of K and KB specimens as well.

Figure (3.6) also shows the effect of fissures on the behaviour of stress-strain curves for two types of materials. In spite of the ductile behaviour of unfissured overconsolidate K specimens, the fully fissured K specimens for the same initial conditions showed a significant strain softening behaviour.

3.2.2 Preparation of the Materials

In the early stage of the study, the Kaolin specimens (100% K) were compacted based on the optimum water content and maximum dry density.

Figure (3.7) shows the results of compaction tests on the Kaolin powder. In conducting these 5 to 6 different water contents were added to the dry powder of Kaolin, mixed uniformly and then kept in plastic bags to avoid any change in the water content during curing which was about 12 hours for K specimens and 24 hours for KB specimens. Later, it was found that the assessment of the effects of preconsolidation pressure, as well as the overconsolidation ratio (OCR) on the effective shear strength, would be impossible for specimens prepared initially by the compaction method. Moreover, the possibility of air bubbles being entrapped during compaction was very high a factor which could affect the effective shear strength of the specimens. Therefore, the method of preparation was changed to the consolidation of the pastes of clay materials for any prescribed standard preconsolidation pressure.

For specimens, either K (100% Kaolin) specimen or KB (25% Bentonite 75% Kaolin), a paste of K or KB with a suitable water content of about 53% and 67% respectively, was prepared.

Particular attention was given in the preparation of KB specimens. Kaolin and bentonite powders, with a ratio of 1/3 of the dry weights, were mixed uniformly to make a homogenised mixed powder and then tap water for a water content of about 67% was added. The paste was thoroughly mixed using paint scrapers and a steel float, wrapped in plastic bag, put in a monitored temperature store and cured for an average of 24 hours. For the preparation of the paste required for each large specimen, about 2.5 hours was needed. Figures (3.8, 3.9, 3.10) show the three stages

of weighing and mixing the Kaolin and Bentonite powders and adding water to make the paste.

3.2.2.1 The Physical and Mechanical Properties of the K and KB Materials

Taking into account the workability of the paste, water contents of about 67 and 53% were used in the preparation of the KB and K specimens respectively. The typical physical and chemical properties of the two types of clays, bentonite and kaolin, used in this research, are reported in Appendix A(3.1).

However, Table (3.1) shows the results of some physical and mechanical tests such as consolidation, Atterberg limits, specific gravity (G_s) carried out on K and KB materials. The results of consolidation tests on K and KB materials are depicted in Figures (3.11) and (3.12) respectively.

3.2.3 Disturbance of the Specimens As Result of Trimming

Another factor that had to be taken into account in the artificial preparation of the specimens, was disturbance as a result of trimming. In order to have less trimming and disturbance of the laboratory specimens, the amount of raw material and the thickness of the unconsolidated specimens had to be estimated first. To do this an oedometer test was conducted on each material (Figures 3.11, and 3.12). From the curve of e-log P'_c, the amount of the void ratio ($e_{p'_c}$) for the applied proposed consolidation pressure (P'_c) was estimated. Then by relating the ($e_{p'_c}$) to the thickness of the consolidated specimen (H_f), the initial thickness (H_0) was estimated for the proposed pre-consolidation pressure (P'_c) in order to have less trimming of the specimen. This procedure was important and useful for the fissured or partially fissured specimens prepared for direct shear boxes. Running the shearing surfaces through the fissure surfaces was very important for accurate estimation of the effects of fissure parameters in this study. In other words, the alignment of the failure plane in the shear box with the fissure surfaces was very important to estimate accurately the effective shear strength of the fully or partially fissured specimens. By using this procedure, the initial thickness of the unconsolidated material needed for each size of specimen, was estimated for any proposed pre-consolidation pressure.

$$H_0 = H_f (1+\omega G_s) / (1+(e_{p'_c}) \quad (3.1)$$

where H_0 and H_f are the initial and final thicknesses of the samples (mm), ω is the initial water content of the paste, G_s is the specific gravity of the material and e_{pc} is the final void ratio of the pre-consolidation pressure (P'_c). The details of the derivation of Equation (3.1) are given in Appendix A(3.2).

3.2.4 Consolidation in One Stage or Multistage

In order to reduce the time needed for the consolidation of the laboratory specimens, they were loaded in one stage. To control the effect of this factor, a few specimens were loaded in a few stages and the effective shear strength results showed no difference, from the effective shear strength point of view, between specimens consolidated in one stage and those consolidated in multistage.

Figure (3.13) shows the effective shear strength of two artificially overconsolidated Kaolin clay specimens prepared by one stage and multistage loading.

3.2.5 Non Flooded Samples

Another point that had to be considered for laboratory specimen preparation, was the presence of water during the consolidation process. Two options were studied. In the first option, specimens were consolidated in the box of consolidation without water and in the second option, they were flooded or submerged.

This factor had to be taken into account specially for the preparation of the large direct shear box specimens. These were prepared in a detachable box as explained in this chapter. It was not practical to provide another external container in order to submerge the specimens during the consolidation processes.

Figures (3.14) and (3.15) depict the effect of this factor on the effective shear strength of artificially overconsolidated clay specimens prepared from K (Kaolin) and KBS (Kaolin, Bentonite and Sand) respectively.

3.2.6 Locked-In Horizontal Stress

Another important parameter was the effect of the horizontal locked-in stresses for the laboratory prepared specimens. Lateral stresses are available in the field for in-situ tests. By sampling, these lateral stresses are released and the uniformity of material is changed especially around the surfaces, edges and corners of the natural specimens. For the laboratory, this parameter also was considered. and specimens were, therefore, prepared for two situations, locked-in horizontal stress specimens (as an abbreviation, locked specimens) and unlocked-in horizontal stress specimens (unlocked specimens). Figures (3.16) and (3.17) indicate the effect of locked-in horizontal stresses on the two types of materials (K and KB) for the same P'_c, OCR and rate of shearing. The results obtained for the effects of type of mineral, size and preconsolidation pressure and this parameter are discussed in Chapter 4.

3.2.7 The Effect of the Rate of Shearing

In order to have a fully drained situation in the direct shear tests, the rate of shearing was estimated based on an empirical derivation (Gibson et al., 1954). To find the maximum rate of shearing, several consolidation tests were conducted and the t_{100} was estimated from the curve s-$\sqrt{T}$ or s-log t for each material type and purposed consolidation pressure and then by using the Equation (3.2):

$$T_f = 12.7\ t_{100} \qquad (3.2)$$

T_f was measured, where T_f (min) is the time required to fail the specimen.

The rate of shearing mainly influences the shear strengths of the unfissured and partially fissured specimens. The rate for the fully drained test depends on the type of material and presence of fissure in the specimen and the preconsolidation pressure. To take into account the effect of the rate of shearing, three specimens levels were studied for the locked and unlocked for both types of materials (K and KB), and also for the unfissured, partially and fully fissured specimens as reported in Chapter 4.

Figures (3.18) and (3.19) show the effect of two different rates of shearing on the two types of materials for locked and unlocked situations of horizontal stresses. Figure (3.20) indicates the effect of the rate of shearing on the fissured KB and K specimens.

3.2.8 The Specimen Size Effect

As discussed in Chapter 2, the size of a specimen is an important parameter for laboratory testing of a stiff fissured clay mass or naturally overconsolidated fissured clay mass.

In order to reduce the effect of sample size in naturally fissured specimens, the specimen should be representative of the naturally fissured mass. In other words, fissure parameters such as size, width, spacing, orientation and fissure surface shape must be taken into account.

But for homogenous, isotropic and unfissured specimens, specimen size effect has not been discussed enough. Taking into account the effect of strain softening behaviour, a study of the specimen size effect was necessary for artificial overconsolidated K and KB specimens. This parameter was investigated for three different sizes subjected to direct shear tests and the results are given in Chapter 4.

The specimen size effect for unfissured specimens can be explained from the strain softening behaviour point of view.

For strain softening material, the Mohr Coulomb parameters (c'_p & ϕ'_p) are related to plastic strain (Skempton, 1970; Itasca, 1993). Therefore, for the larger specimens, the plastic flow of material as a result of strain softening takes place faster than for the smaller specimens. In other words, the mobilisation of shear strength to the peak for the smaller specimens is uniformly faster than the larger specimens. Moreover, the shear stress distribution along the shear band for smaller specimen is more uniform than for the larger specimens. It means for larger specimens along the shearing surfaces, locally for some parts, the shear strength is mobilised to the peak, whereas the other part is still under the peak magnitude and for a moment after, those parts which have passed the peak stress enter post peak stress, other parts enter the peak or even need more time to be mobilised to peak shear stress.

This phenomenon can be explained by another expression. If the displacement required to reach peak shear strength of specimens with length l_1 is assumed Δl_1., when this displacement is applied to another specimen with a length $l_2 > l_1$, the extra

part of the second specimen, ($\Delta l_1 = l_2 - l_1$), is still not mobilised. This causes the nonuniformity of shear stresses along the shearing surfaces and also a decrease of the average shear strength of the larger specimen (l_2) compared with the average shear strength of the smaller specimen (l_1). When more displacement is applied to a larger specimen, the shear strength of the extra part is mobilised to the peak, whereas the shear strength of the initial part passes from the peak and causes more decrease in the average shear strength of the larger specimen. Based on this phenomenon, the time needed to obtain the maximum mobilisation of shear strength is roughly the same for different sizes of specimens with the same initial conditions of preconsolidation pressure, OCR, material type, and rate of shearing. In other words, the peak shear strength for the larger specimens is smaller and occurs with a smaller percentage of shearing strain than for the smaller specimen in the same initial conditions.

Figure (3.21) shows the effect of specimen size on the effective shear strength of the unfissured KB specimens.

Figure (3.22) gives the effect of fissures on the position of the effective shear strength. As this figure shows, the peak effective shear strength in fissured clay specimens takes place sooner than unfissured specimens for the same initial conditions.

3.2.9 The Simulation of P'_c and OCR in the Laboratory

The P'_c and OCR also influence the effective shear strength of a naturally over-consolidated clay mass. To take into account the effect of P'_c, the specimens were consolidated at three levels of stress, 660 kpa, 440 kpa, and 330 kpa. The maximum level was considered based on the availability and possibility of tools and devices for both processes of consolidating and shearing the specimens. The minimum level was considered based on the minimum normal pressure required to overcome the effect of swelling pressure as a result of expansion for OCR > 1.0. Moreover, Di Miao et al. (1994) also indicated that for K and B preconsolidation pressures less than 200 kpa, the Mohr Coulomb envelop is not linear. In order to have the effect of OCR, three levels of normal stresses in direct shear boxes or confined pressures in triaxial cells have been applied. The ratio of P'_c (pressure applied during consolidation) to σ_N

(pressure applied during the shearing process) for direct shear boxes, is similar to the OCR (over consolidation ratio). Almost three of the OCR's 1, 1.5, 2.5, 3.3, 5 and 10 have been used for different material types (K and KB) and sizes of direct shear box specimens.

For an OCR greater than one after the consolidation process, it was necessary to wait for the specimen to reach an equilibrium. The amount of dilation as a result of unloading and swelling had to be considered in the preparation of the fully or partially fissured specimens.

For triaxial specimens, to make different OCR's was a little more complicated than the direct shear box specimens. By using results for each level of P'_c of the specimens subjected to direct shear tests, the magnitude of σ_3 was estimated from the Mohr circle for different normal stresses and based on the magnitude of applied back pressure, the magnitude of confined pressure was calculated for each OCR proposed.

Although applying the σ'_3 (effective confined pressure) using this concept, caused little change in the behaviour of the specimens as result of applying an isotropic confined pressure, the difference was not important. Meanwhile, another solution was to carry out the K_0 consolidation test or zero lateral strain test in the triaxial cell (Menzies et al. 1977; Nikraz 1985 and 1990; Menzies, 1988). The basic concept behind of consolidation is that the volume change in the pore water duct must at all times be equal to the volume of the axial deformation, times the original average cross-sectional area. This rule is only applicable to saturated soils. It is possible to simulate any proposed OCR by the K_0 consolidation concept.

Figure (3.23) shows the effect of P'_c for three different levels of stresses on the KB specimens. Figure (3.24) displays the effect of OCR on one level of P'_c on the K and KB specimens.

3.2.10 The Defined Residual Strength of the Specimens

In Chapter 2, the methods used by Skempton (1964) and Moon (1984) to obtain residual and fully softened shear strengths were explained.

To relate the effective shear strength of a naturally overconsolidated fissured mass or stiff fissured mass or stiff fissured mass to the fully softened shear strength of the unfissured strength mass is not reasonable and can not be generalised as a solution for any type of stiff fissured clay mass. However, establishing the effective shear strength of a stiff fissured mass, based on qualifying and identifying the effects of the parameters influence, is highly recommended and reasonable.

Identifying the fully softened strength of the specimens tested for each parameter was, not therefore, necessary, but it was necessary for the residual shear strength to be discussed and determined.

The problems with the method suggested by Skempton (1964) to obtain residual shear strength were the time required to run very slowly a number of reverses in a drained situation and the unpredictable effects that a number of further runs for establishment of the residual strength, sometimes could have on the accuracy of the results of the experimental tests. Therefore, this matter was investigated and some assumptions were applied for the establishment of the residual strength of the specimens prepared artificially for the study of each parameter. However, these assumptions arose and were initiated from results obtained in the laboratory study of the residual shear strength of the artificially overconsolidated clay specimens prepared from K and KB materials.

The first assumption, was the residual shear strength of KB specimens was obtainable after a full running of the direct shear box.

The second assumption, was the residual shear strength of an unfissured specimens was the same as the fully fissured specimen with the same initial conditions such as preconsolidation pressure, overconsolidation ratio, same rate of shearing, same size of specimen, and same material.

Figure (3.25) shows the results obtained from the first and a few reverse runs of a KB specimen. This figure shows, for the first run, the residual strength is roughly the same as that of the first and second reverses.

Another interesting point is depicted in Figure (3.26). The residual shear strength of the fully fissured KB specimens is the same as the residual shear strength of the unfissured KB specimens after a few runs. Figure (3.27) indicates the first run and a few reverse runs of a k specimen, and Figure (3.28) shows the residual shear strength obtained from the fully fissured specimen of K for same initial conditions applied for the unfissured specimen of K.

As these two figures show, the second assumption was not far from the reality of the material behaviour.

Another matter that arose from the study of the residual strength of the specimens, was the reduction of strength as a result of stopping the direct shear test for at least 20 hours. In the study of the effect of different high rates on the shear strength of a specimen which was sheared initially, a reduction of strength was observed as a result of stopping the tests for a few hours.

Figure (3.29) indicates the effect of different high rates on the shear strength of a pre sheared K specimen. As this figure shows, for different rates, no effect as a result of differentiation of suction was observed. There were, however, reductions of strengths as a result of stopping the tests. Figure (3.30) shows a comparison between the residual effective shear strength obtained from the same specimen with the results obtained from the quick tests of different rates. As this figure shows, the residual shear strength obtained at a very slow rate (0.005 mm/min) still shows some suction effect on the estimation of the real residual shear strength . The real residual shear strength was obtained by eliminating the suction effects which in this study was conducted by stopping the tests for at least 20 hours.

The reason behind this phenomenon might be related to the size of the clay particles. When a clay specimen is sheared at a very slow rate e.g. 0.005 mm, the relative movement of the particles on the surfaces of the upper half is huge in comparison with the clay particles on the surface of the lower half. Therefore, even under this very slow rate of shearing, some suction will still be created along the shearing surfaces and when the machine or test is stopped, this suction is eliminated and there

will be a reduction on the effective shear strength. In Figure (3.31) this concept can be seen for a KB specimen.

3.3 FISSURIZING THE SPECIMENS

In order to fissurise the specimens, the following methods have been used:

1- cutting them with a very sharp thin object (blade or wire specimen cutter) to make inclined fissures in direct shear box specimens, or partially fissured triaxial specimens as shown schematically in Figure (3.32).

2- putting strips of plastic material like a transparency or Teflon sheets and after the consolidation process, pulling out the strips. This procedure was used to make fully fissured and partially fissured specimens for direct shear box specimens. Figure(3.33) depicts this method schematically.

3- cutting the specimens, then putting and leaving the separator material like a filter paper inside the specimen before the consolidation process. This procedure is useful for partially fissured specimens for discontinuous fissured triaxial specimens.

4- designing, constructing a specific system of loading and preparing the triaxial fully fissured specimens for different orientations of fissures as discussed in Chapter 6.

5- consolidating the specimens in two or three layers. This procedure was used to create closed fully fissured specimens for both direct shear box and triaxial specimens. This type of closed fissure was like a bedding discontinuity.

3.4 FISSURE PARAMETERS

The effect of fissure parameters, mainly three parameters of size, spacing and orientation of fissures were studied but the effect of parameters like shape and roughness the artificially prepared specimens was not studied. More discussion, the laboratory plan for the study of the parameters and the results are discussed in Chapter 4.

3.4.1 The Size of fissures

It is obvious that by increasing the width of fissure in the partially fissured specimens, the effective shear strength decreases. In order to study the effect of this

parameter for one level of consolidation pressure, for two OCR's 1 & 2.5, some large specimens (300 mm × 300 mm) for the large direct shear box were prepared for zero, 10, 30, 50, and 100 percentages of the fissure surfaces and by doing regression analysis on the obtained results, the effect of fissure size was estimated. Figure (3.34) shows schematically different percentages of fissure surfaces.

3.4.2 The Spacing of Fissures

By increasing the spacing of the fissures in an over-consolidated fissured mass, the overall effective shear strength increases. To estimate the effect of spacing of the fissures for a constant fissure surface, a set of large fissured specimens for three different spacings was prepared. The results were used for regression analysis to estimate the effect of the spacing. Figure (3.35) displays schematically different spacing of fissures in large direct shear tests for 50% of fissure surfaces.

3.4.3 The Orientation of Fissures

To study parameters for the direct shear box, a few specimens with 45° orientated fissures to the horizontal were prepared. For the triaxial apparatus, a sample maker was designed and used to prepare the fully or partially fissured specimens for orientations of 30°, 45° and 90° to the horizontal. The details of this sample maker are discussed in Chapter 6.

3.5 DIRECT SHEAR BOX SAMPLE MAKERS

These sample makers were used to prepare three different sizes of unfissured, fully fissured, and partially fissured specimens (60×60 mm, 100×100 mm and 300×300 mm).

Figure (3.36) shows a pair of sample makers designed for the consolidation of medium sized specimens (100 mm by 100 mm). By modifying and using the bases of oedometer apparatuses, these sample makers were designed. These boxes of consolidation, hangers and yokes were the main parts designed for sample makers. However, particular attention was given to drainage, the stability of the boxes, and preventing paste from squeezing as a result of loading.

For the three sizes, three different types of boxes and moulds were designed and constructed. The sizes of the boxes and moulds were estimated based on minimising the effect of trimming the specimens. The characteristics of the boxes and moulds, specially for the large direct shear box, were the detachability of the parts and also the possibility of drainage as a result of the consolidation process and enough resistance against rust. Figure (3.37) shows the boxes designed for 300 mm by 300 mm and 100 mm by 100 mm specimens.

A detachable mould was designed for each size of direct shear specimen. The mould was used to have the same amount of material for each specimen and also to shape the paste and prepare initially the unconsolidated specimens before the consolidation process. The thickness of the mould was estimated based on the procedure already explained by Equation (3.1). Figure (3.38) shows schematically the moulds used for unfissured, partially and fully fissured specimens.

The paste, which had been cured for one day, was put into the detachable mould, tamped and refilled, then the top and bottom surfaces were trimmed. Figure (3.39) shows filling the mould for preparation of the specimens. Then the paste having been shaped by the mould was put in the box of consolidation designed for that mould and the load was applied to consolidate the specimen.

3.5.1 The Homogeneity of the Material in the Partially Fissured Specimens

For the preparation of partially or fully fissured specimens, another detachable mould was used. The height of this mould was half the height of the mould used for unfissured specimens. After the preparation of the two halves, two sets of strips of Teflon were attached at two ends and at points along the joints put on the top trimmed surface of each half. The two halves were put together the number. of strips depended on the different widths of fissure in the specimens.

The important point that had to be taken into account was the homogeneity of the unfissured parts of the specimens which were supposed as unfissured parts in the partially fissured specimens.

Figure (3.40) shows the scratched parts of a partially fissured specimen which should be retamped to make homogenous parts and Figure (3.41) displays the situation of the partially fissured specimen after consolidation in the box and in Figure (3.42), the situation of the specimen after pulling out the Teflon strips is displayed.

To do this, the two halves were put in the original mould used for unfissured specimens and then the parts which were supposed to be unfissured, were tamped again to mix the material of the two halves and to obtain homogeneity.

The width of each strip which had been put inside the material was estimated based on the cohesive and frictional surface strength applied during the pulling out of the consolidated specimen to each strip and the tension strength of each strip. In order to reduce the surface friction between each Teflon strip and the consolidated clay, two layers of strips were used for each proposed width of fissure.

For each width, the strips were put together and attached at two or three points along the joints by pieces of adhesive tape. The length of the strips for each width of fissure was about 10 mm longer than the size of the specimen so that enough projected to enable them to be pulled out easily. After being prepared and shaped by the mould, each specimen was consolidated, then taken out of the box. The tip of each Teflon strip was then held between two pieces of small brass plate and pulled out with pliers. To insert the Teflon strips, putting in the paste and filling the mould to shape the specimen, about 4 hours was required.

3.5.2 Reducing the Time Needed for the Consolidation Process of the Large Specimens

Two perforated reinforced concrete blocks (see Figure 3.41) were designed and constructed to drain the bottom and top of the specimen during the consolidation process of the large direct shear box specimens. The thickness of these perforated concrete blocks minimised the usage of unconsolidated clay material needed for the preparation of each specimen.

To avoid squeezing paste into the holes of the perforated concrete blocks, two fibre filters were put on each side between the specimen and concrete block.

This figure also shows the arrangement of the different parts including concrete blocks, fibber filters and specimen with two layers of Teflon strips for each width of fissure after the consolidation of the specimen in the large direct shear box.

To measure the magnitude of the settlement of each specimen, a strain gauge with a magnetic base was attached to one edge of the box.

3.5.3 The Loading System of the Large Direct Shear Box Sample Maker

The box was placed on the base of a triaxial frame. Because of the high load for consolidation of the large specimens (300 mm × 300 mm), a consolidation pressure of 330 kpa was chosen. To avoid changing the initial pressure as a result of settlement, a digital controller, GDS unit (Menzies, 1988), was connected to a hydraulic jack. The pressure applied by the GDS unit was calibrated by a transducer. This was also calibrated based on the deformation of the proving ring of the triaxial loading frame. The GDS unit was able to apply constant pressure during the consolidation process.

Therefore, by releasing pressure in the hydraulic jack as a result of settlement, the pressure was compensated by the GDS unit. The prescribed pressure was kept constant by pumping oil automatically by the GDS to the jack through a T connection with a hydraulic jack. Figure (3,43) shows the system of loading designed for preparation of the large specimens.

When the consolidation process ended and the settlement had been monitored by the strain gauge, pressure of the GDS was released. Then the box was separated and the consolidated partially, fully or unfissured specimen taken out.

In the next stage, if a specimen was fissured, the strips were pulled out one by one and the specimen weighed and its thickness determined. It was then completely wrapped, named and stored in a room in which the temperature was controlled by an air conditioning unit, until required for testing.

3.6 DISCUSSIONS AND CONCLUSIONS

The preparations of the material and specimens artificial were investigated in the laboratory. The K specimens showed less strain softening than the KB specimens. Adding the bentonite in the KB specimens decreased the effective shear strength significantly and softened the specimens during shearing.

For this study it was necessary to have significant strain softening with large displacement. It appears that the type of clay material is very important in the strain softening behaviour.

The presence of the fissures in the K specimens caused a significant strain softening. For the fissured K specimens, the strain softening occurred faster than in the unfissured K specimens. This is consistent with the findings of Skempton et al. in 1969. Moreover the KB specimens even for the OCR of 1 showed strain softening behaviour.

The pastes prepared for the K and KB specimens with water contents of 53 and 67 precents were wet enough to work, shape and avoid entrapping air bubbles while filling the moulds for the consolidation process and wet enough for the full saturation after consolidation.

The estimation of the amount of unconsolidated material needed for the preparation of each specimen was necessary specially for the partially and fully fissured specimens. Passing the shearing surfaces in the direct shear tests through the fissures was important in order to investigate the effects of fissure parameters.

For the artificial consolidation of the specimens, both options of loading, in one stage and multistage, were studied. The results of the direct shear test showed no difference for this feature.

Because of sufficiency of the proposed water contents for the pastes, the submergence of the specimens during the consolidation process did not influence the effective shear strength of the artificially consolidated specimens. The results from the tests on both types of the prepared specimens (submerged and unsubmerged specimens) showed there was no difference from the effective shear strength point of

specimens) showed there was no difference from the effective shear strength point of view, even if the prepared specimens sheared without the presences of water (unflooded). However, for this research, the specimens were flooded during the shear process. The only effect of this parameter during the shearing of the specimens was dryness of the sheared surfaces specially when the rate was so slow.

For the unfissured locked specimens, the lateral stresses were not released. Therefore, during shearing, the clay particles were flattened and the sheared surfaces were smooth and even. But for the unlocked specimen, the lateral stresses were released. Therefore, the clay particles were not flattened and the sheared surfaces were more bumpy and uneven. For this reason, the shear strength of unfissured unlocked specimens was greater than the unfissured locked specimens for the same initial conditions, such as water content, OCR, material type, size and rate of shearing. The magnitude of differences depends mainly on the type of mineral.

For the unfissured locked specimens, the rate of shearing had less influence on the shear strength than the unfissured unlocked specimens. Because of the bumpy surfaces created during shearing, there was a little suction in the quicker rates of shearing. Therefore, the shear strength was a little greater than the unfissured unlocked specimens sheared by the slower rates of shearing . But for the unfissured locked specimens, the difference as a result of changing the rates of shearing was very little.

The fissure surfaces created from the proposed methods of fissurising were flattened, non polished, or somewhat polished fissure surfaces but useful for this study.

The rate of shearing for the drained tests was slow enough to dissipate extra pore pressure created during the shearing. For the fully fissured, as well as for the unfissured locked in horizontal specimens, the rate of shearing was not so effective. But for the unfissured unlocked specimens, the rate was effective. For faster rate sheared specimens, because of the negative pore pressure created as a result of suction, the shear strength was greater than the slow rate sheared specimens.

The results of the specimen size effect showed that the peak shear strength mainly and the residual shear strengths somewhat were influenced by the size of the

The results of the specimen size effect showed that the peak shear strength mainly and the residual shear strengths somewhat were influenced by the size of the specimen for the same initial conditions. By increasing the size of the specimens, the effective peak shear strength decreased a little.

The results for different P'_c either K or KB showed that by increasing P'_c, effective peak shear strength increased because of increase of density and decrease of void ratio or porosity of the specimens.

For different OCR's the swelling of the specimens as a result of unloading should have been considered specially for the partially and fully fissured specimens.

The specially designed and constructed sample makers and the commissioning of the tools either for the direct shear box tests or triaxial tests were positive steps to study the effects of these parameters in the laboratory.

These sample makers were used for the size and specification of the specimens proposed and defined in this study. The procedures used to make the artificially over-consolidated unfissured, partially or fully fissured specimens, could be useful for further studies in this area.

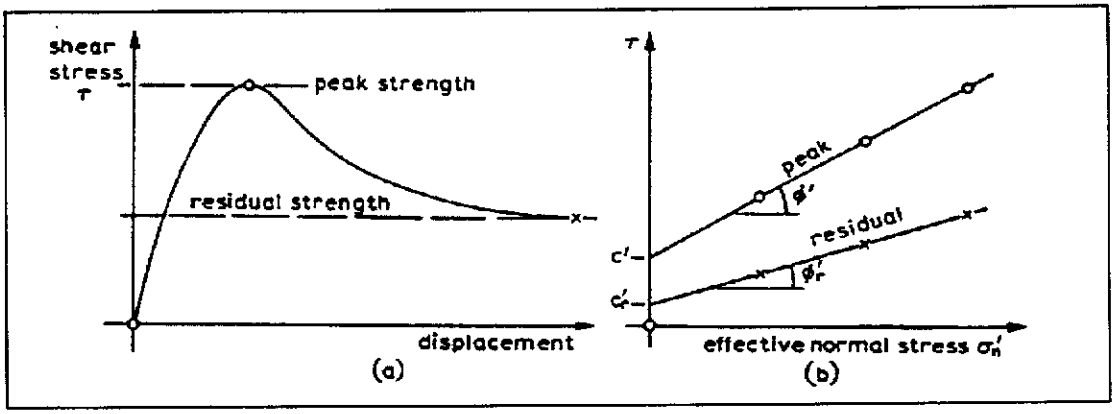

Figure (3.1): (a) Peak and residual shear strength, (b) Coulomb envelops for peak and residual conditions, (Skempton, 1964).

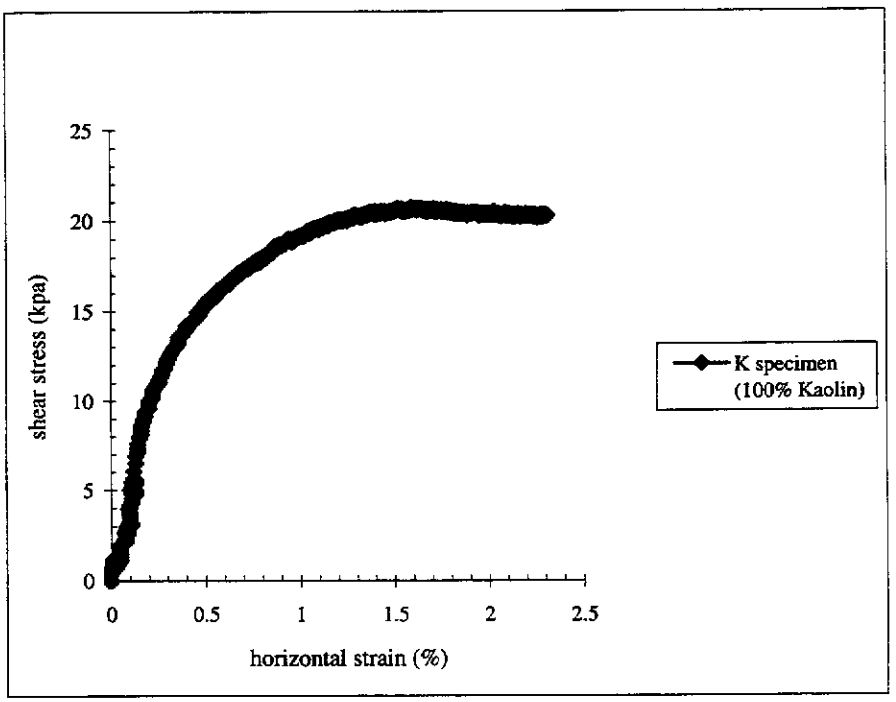

Figure (3.2): Stress-strain curve of a K specimen (100% Kaolin).

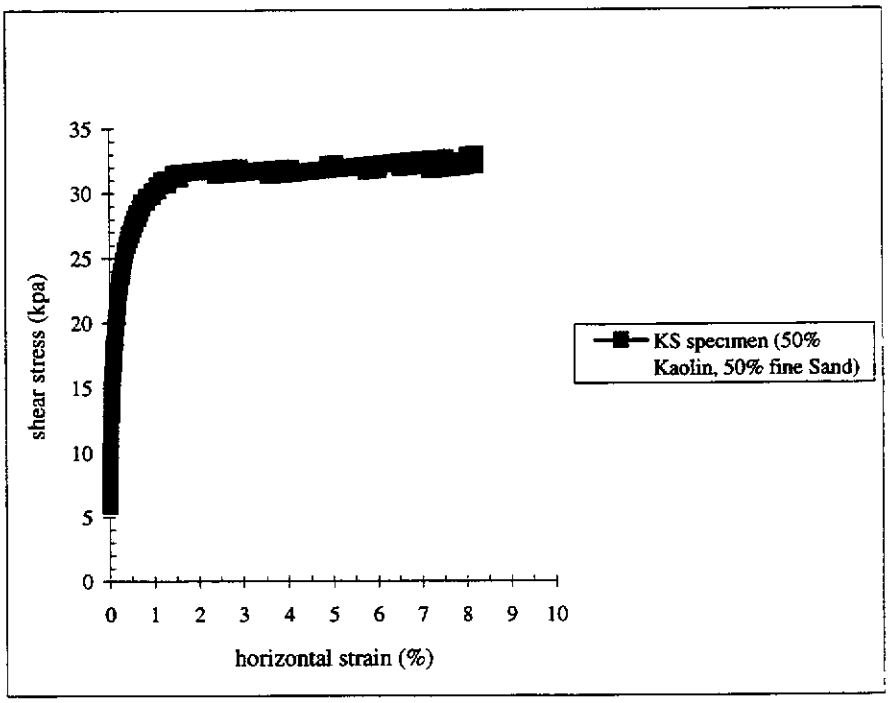

Figure (3.3): stress-strain curve of a KS specimen (50% Kaolin and 50% fine Sand).

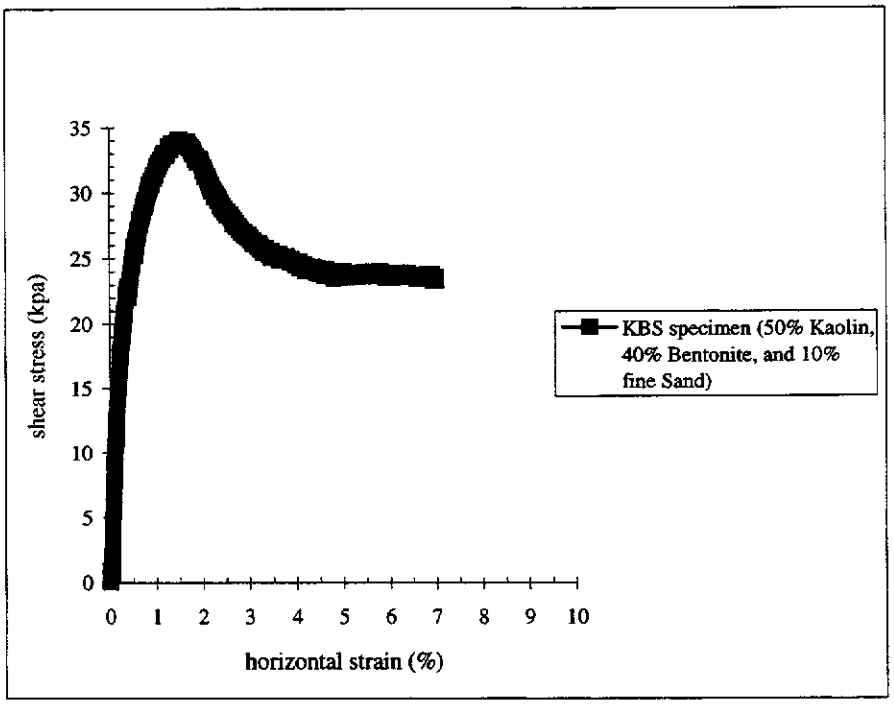

Figure (3.4): stress-strain curve of a KBS specimen (50% Kaolin, 40% Bentonite and 10% fine Sand).

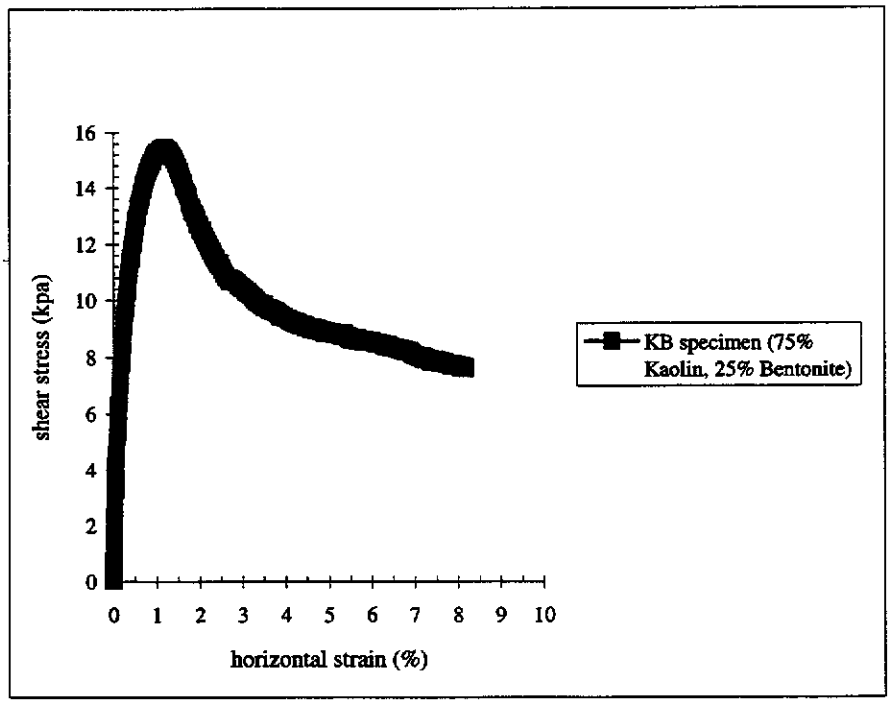

Figure (3.5): stress-strain curve of a KB specimen (75% Kaolin and 25% Bentonite).

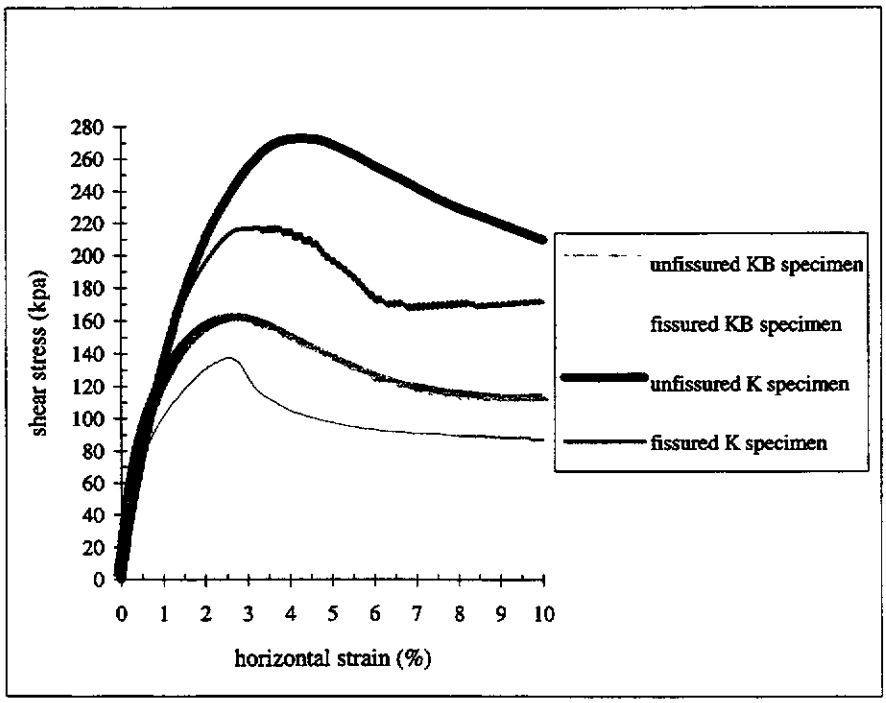

Figure (3.6): stress-strain curves of the fully fissured and unfissured K and KB specimens.

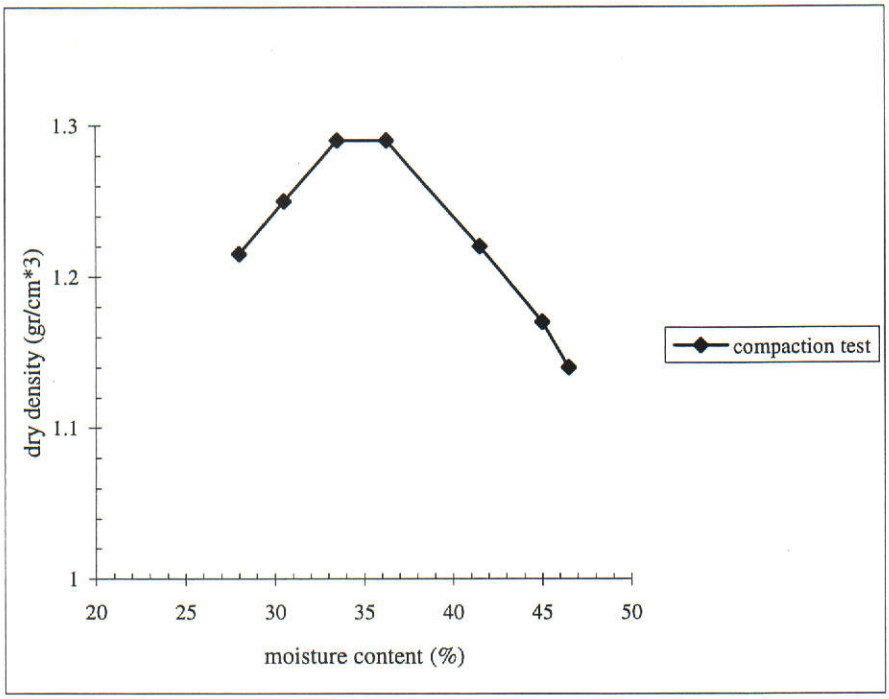

Figure (3.7): Relationship between dry density of the K material (100% Kaolin) and moisture content.

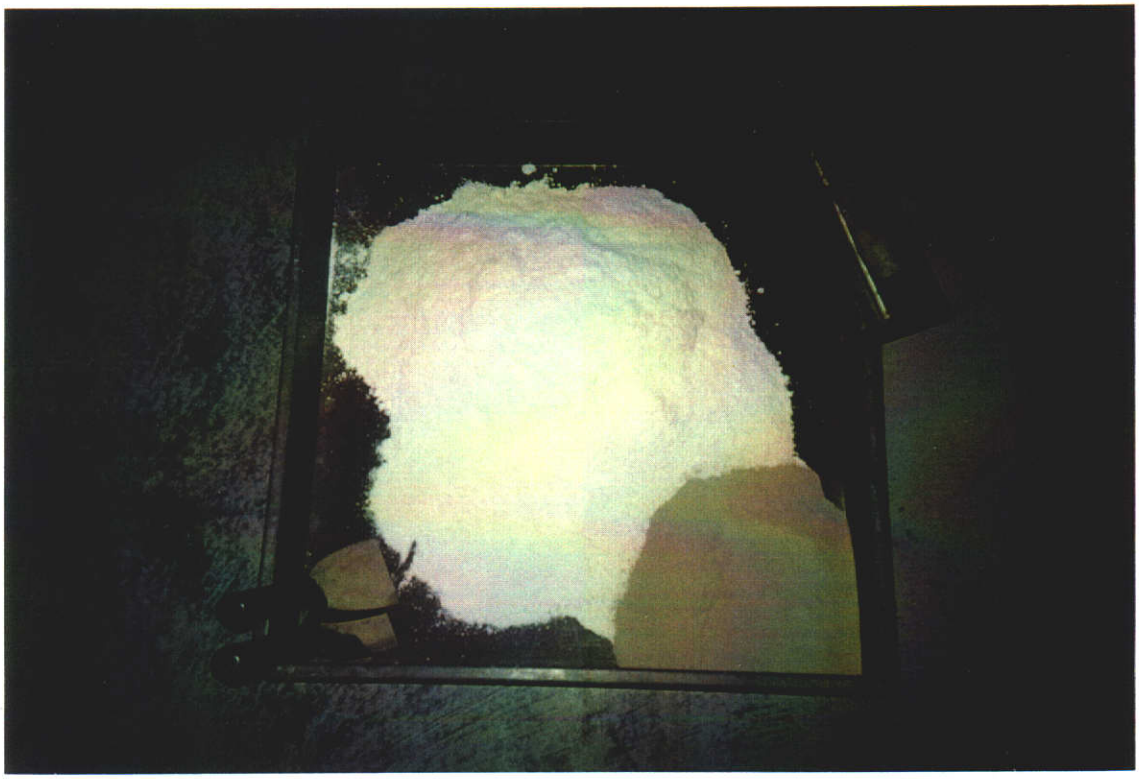

Figure (3.8): Preparation process of the KB paste; weighing of the powders required for the preparation of the paste.

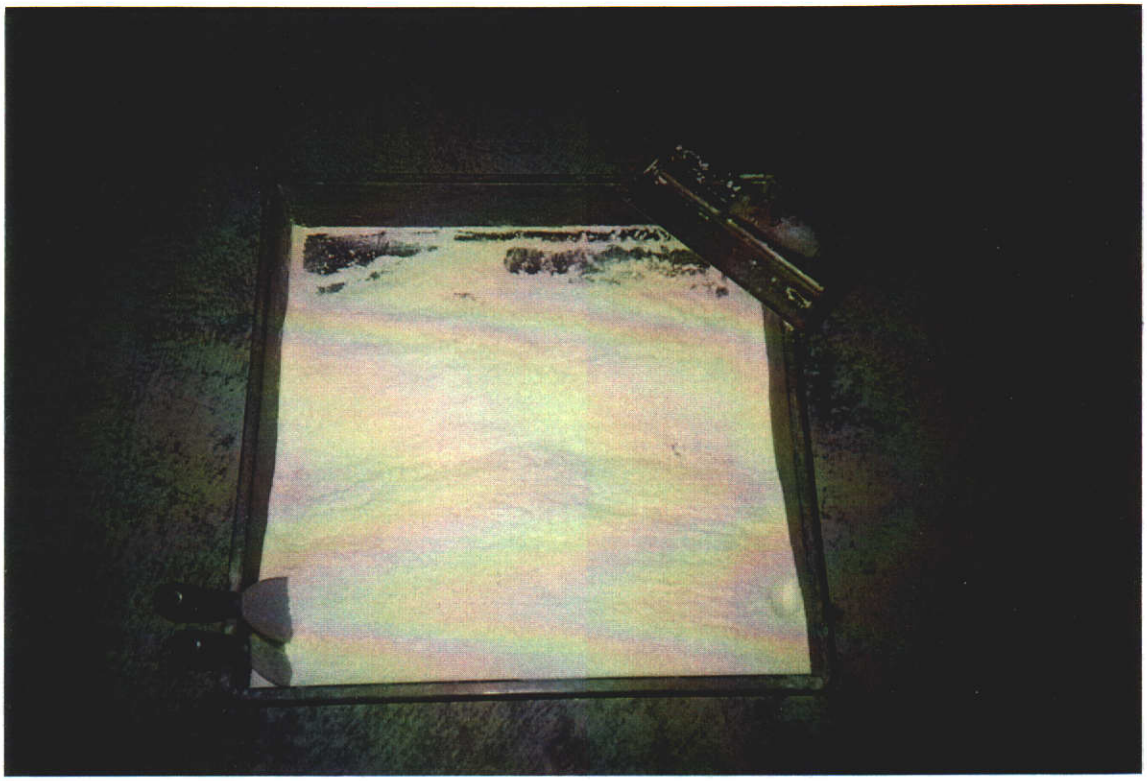

Figure (3.9): Preparation process of the KB paste; mixing the powders in order to have homogenous material.

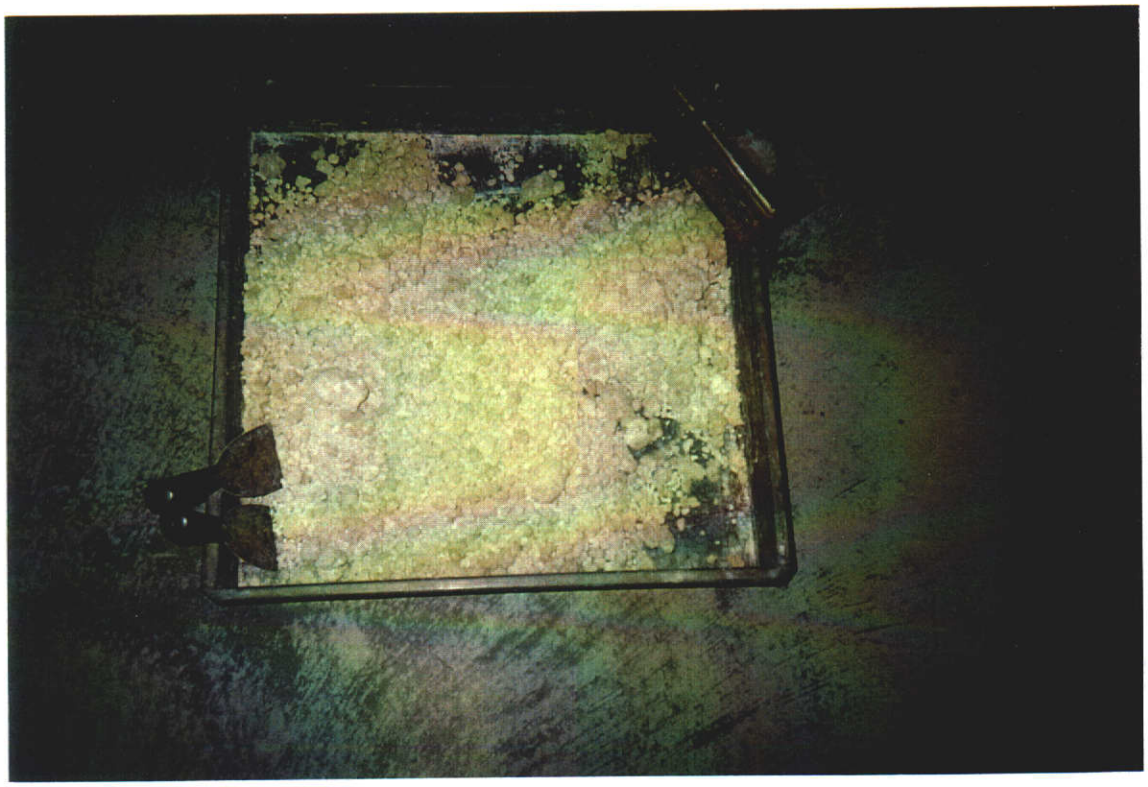

Figure (3.10): Preparation process of the KB paste; adding water to the mixed powders.

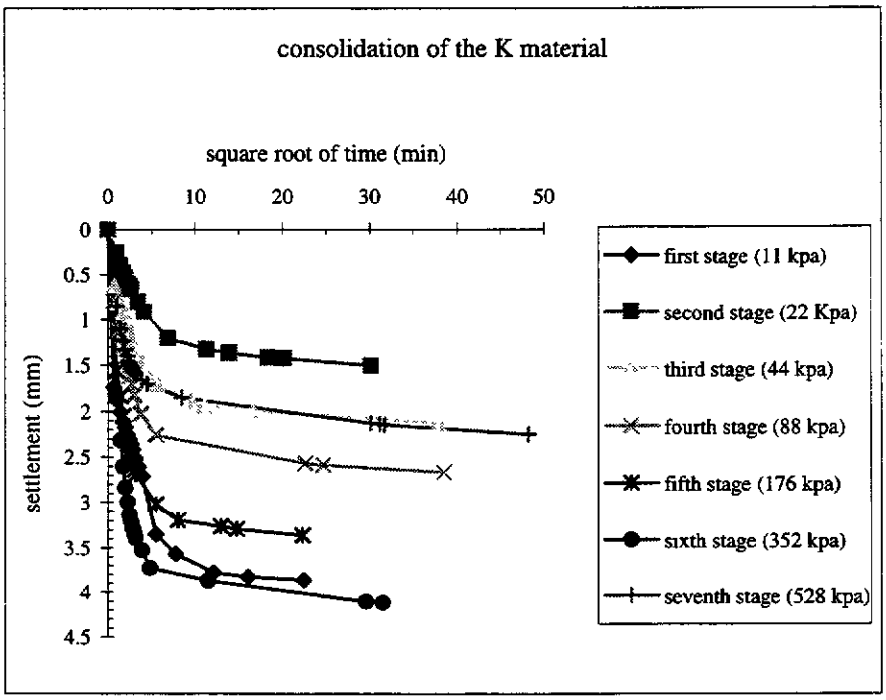

(a)

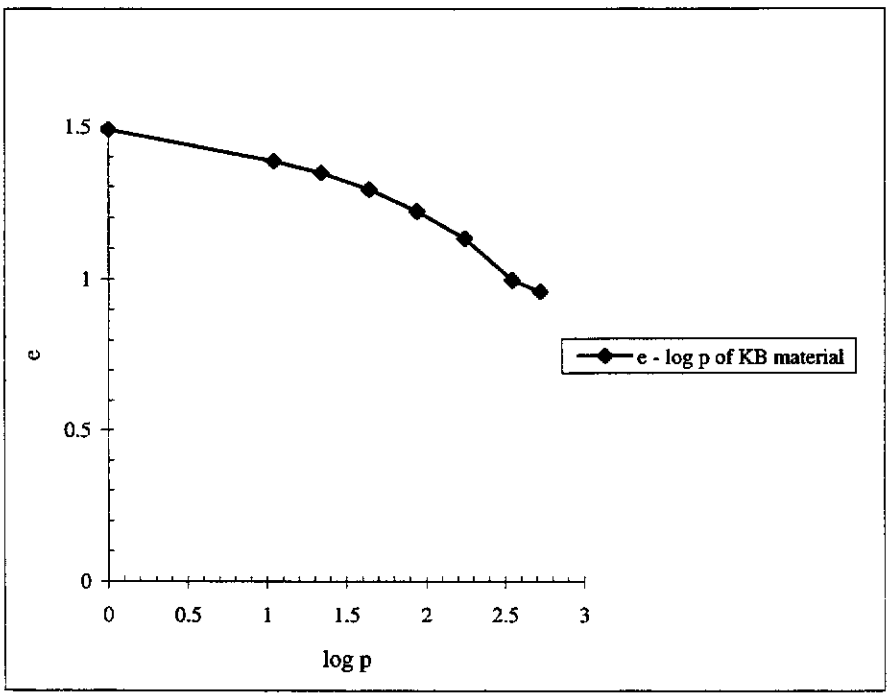

(b)

Figure (3.11): Consolidation results of the K material, (a): the $\Delta s - \sqrt{t}$ curves, (b): e-log p'_c curve.

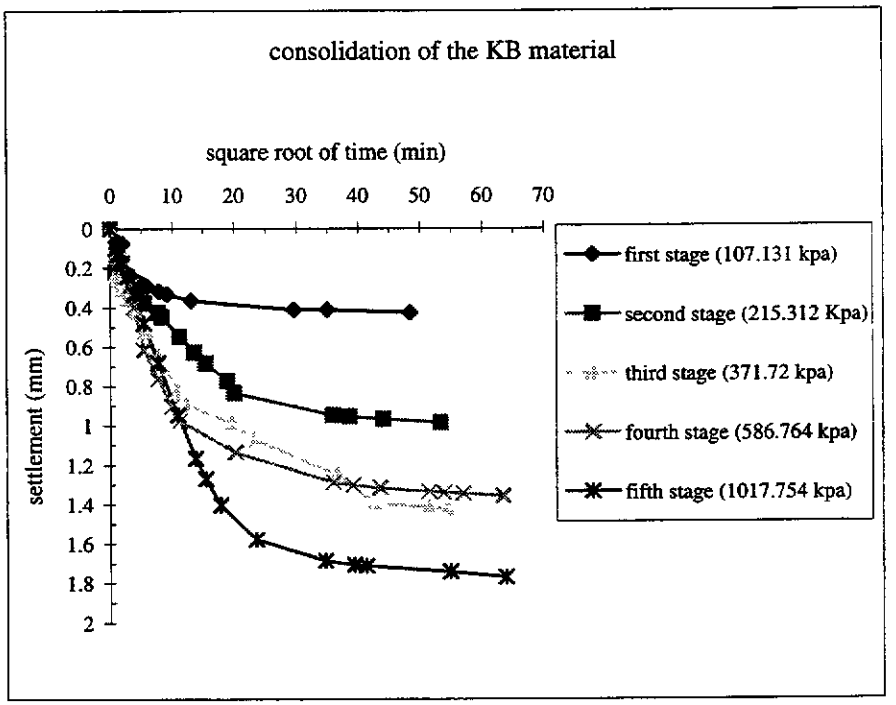

(a)

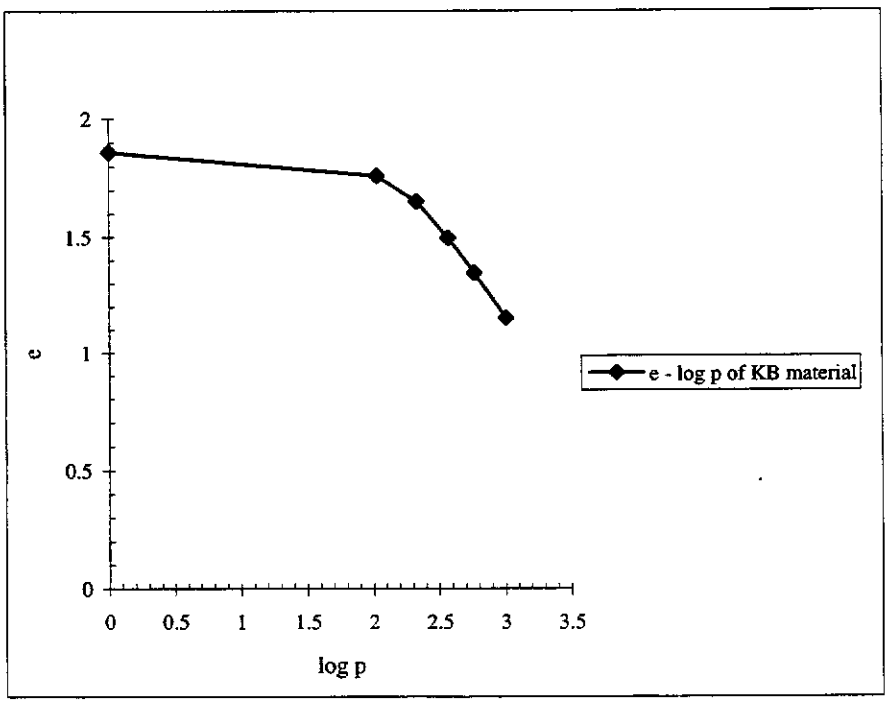

(b)

Figure (3.12): Consolidation results of the KB material, (a): the $\Delta s - \sqrt{t}$ curves, (b): e-log p'_c curve.

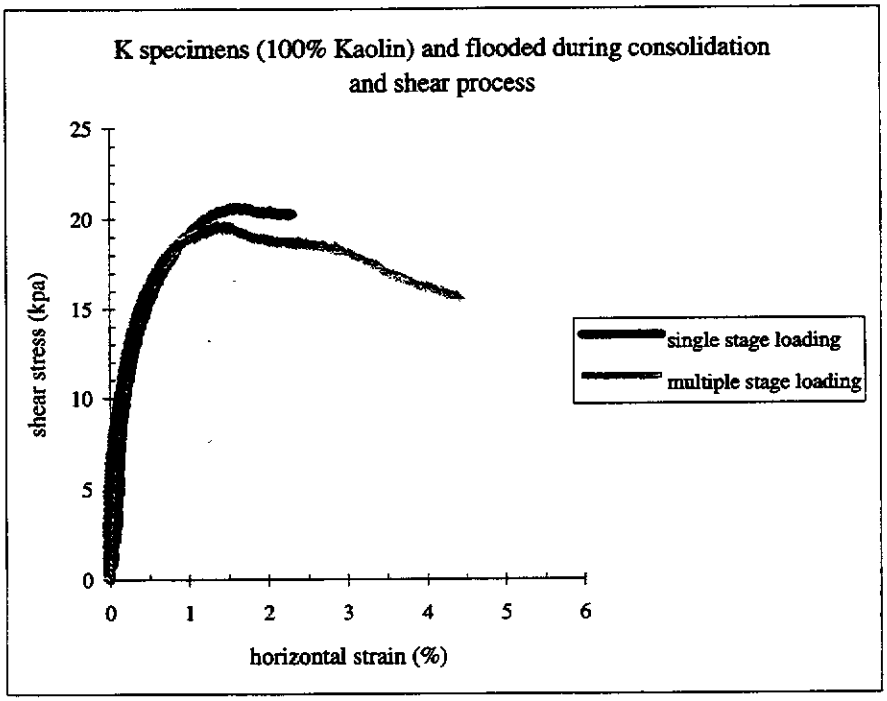

Figure (3.13): The stress strain curves of the K specimens consolidated by the single and multiple stage of loading.

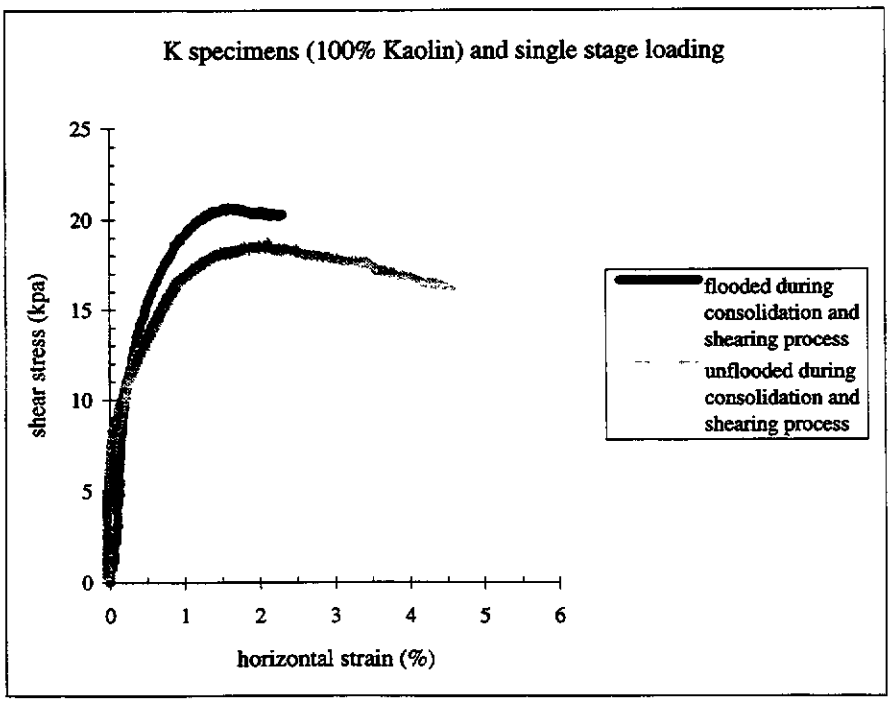

Figure (3.14): The stress strain curves of the K specimens consolidated and sheared with and without of the existence of water in the container of the box of direct shear machine.

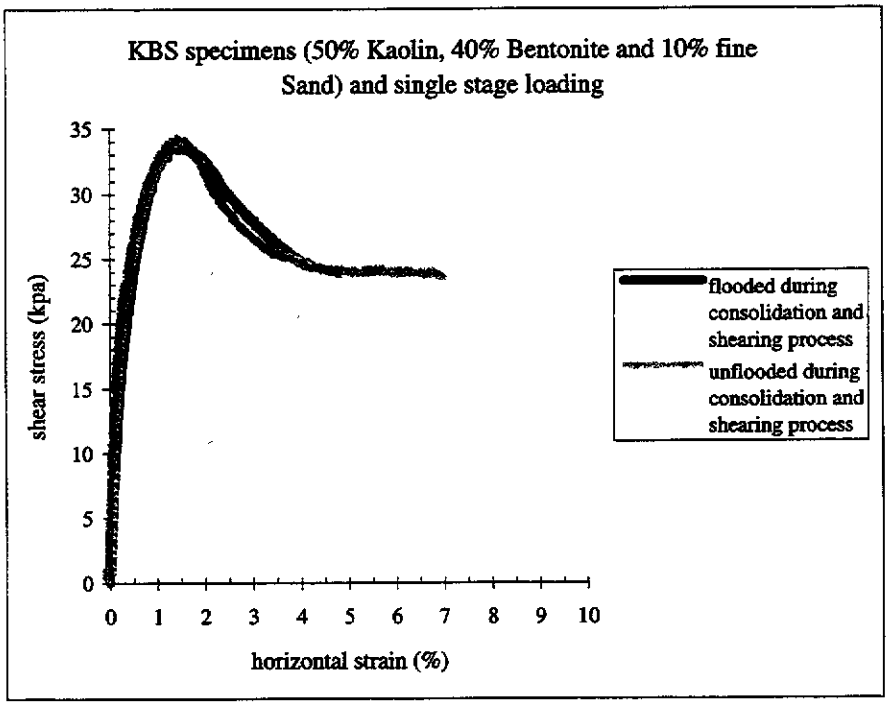

Figure (3.15): The stress strain curves of the KBS specimens consolidated and sheared with and without of the existence of water in the container of the box of direct shear machine.

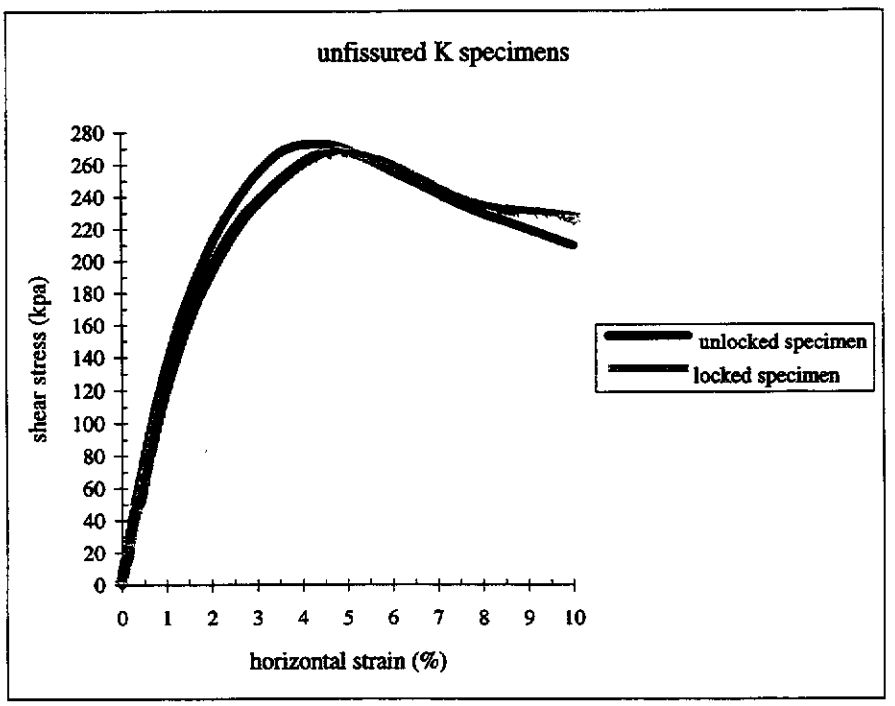

Figure (3.16): The stress strain curves of the locked and unlocked K specimens.

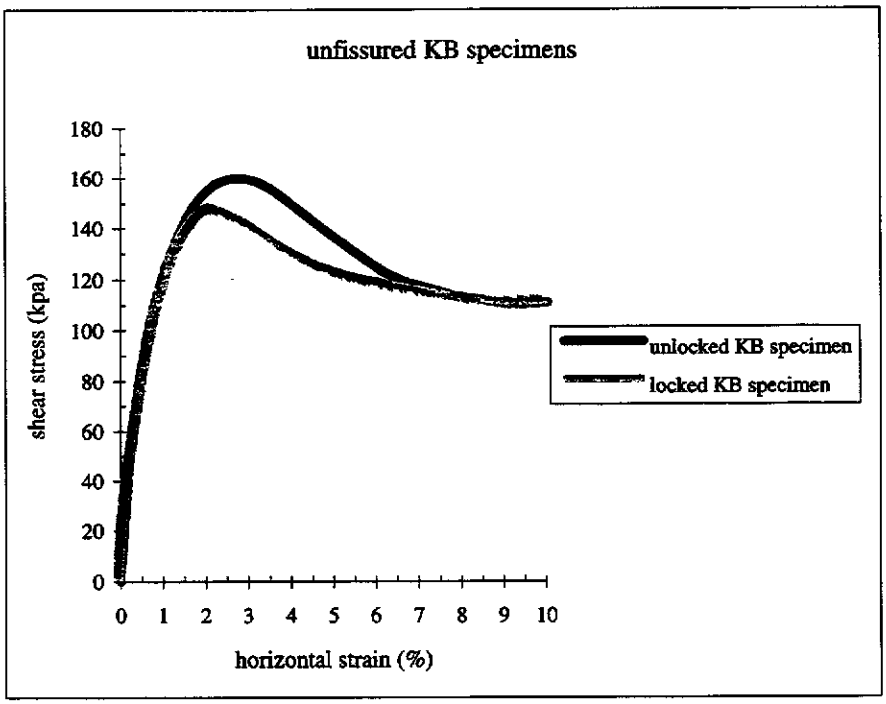

Figure (3.17): The stress strain curves of the locked and unlocked KB specimens.

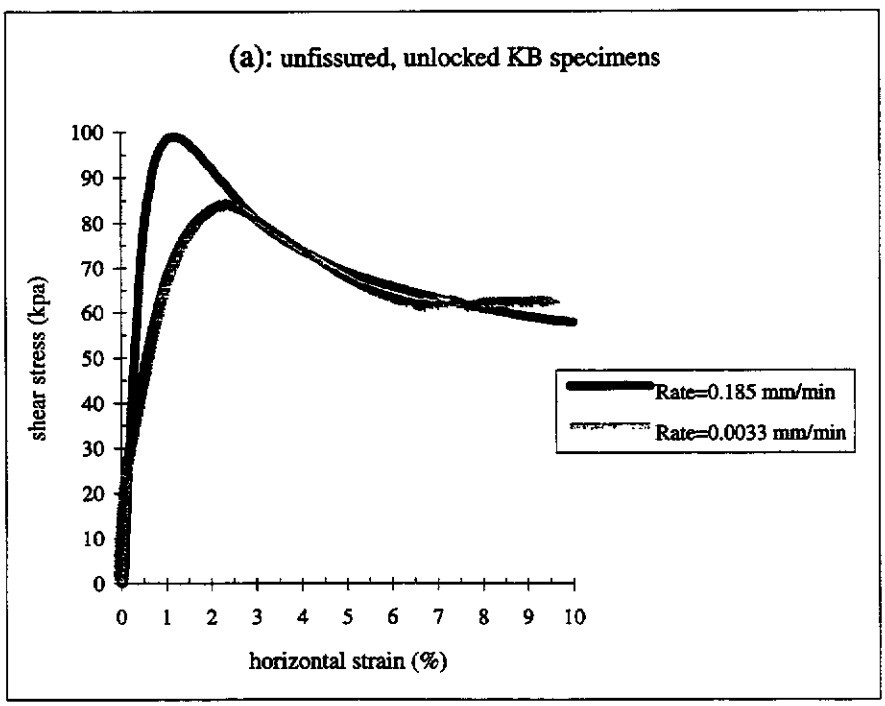

Figure (3.18): The stress strain curves of the KB specimens sheared with two different rates for, (a); unlocked specimens, (b); locked specimens.

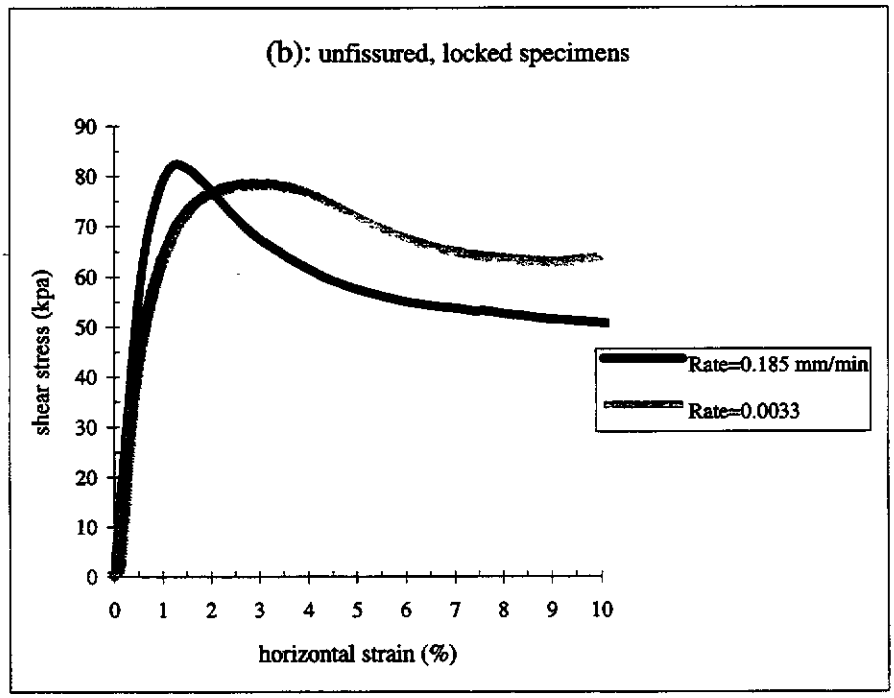

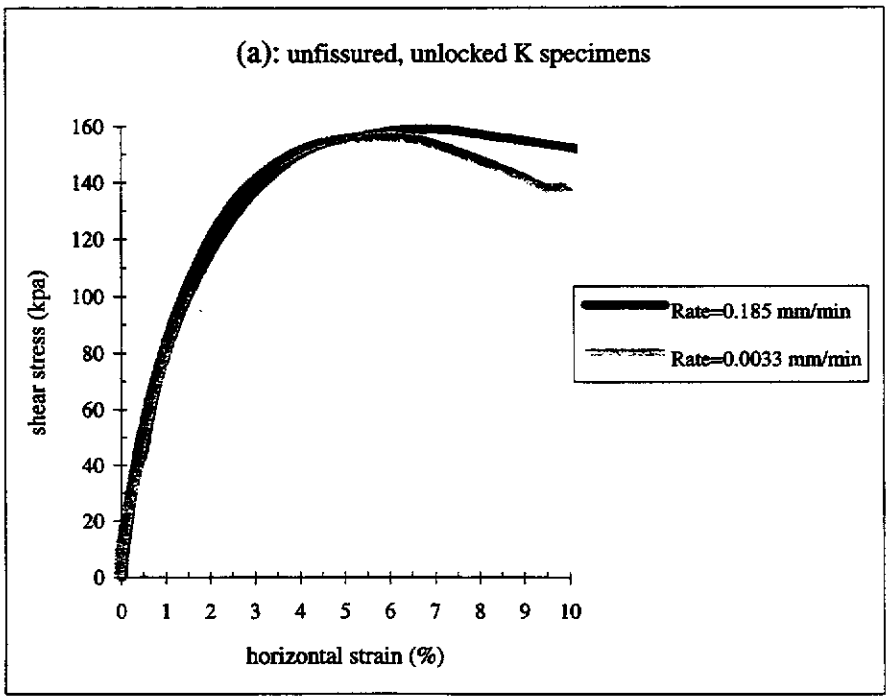

Figure (3.19): The stress strain curves of the K specimens sheared with two different rates for. (a); unlocked specimens, (b); locked specimens.

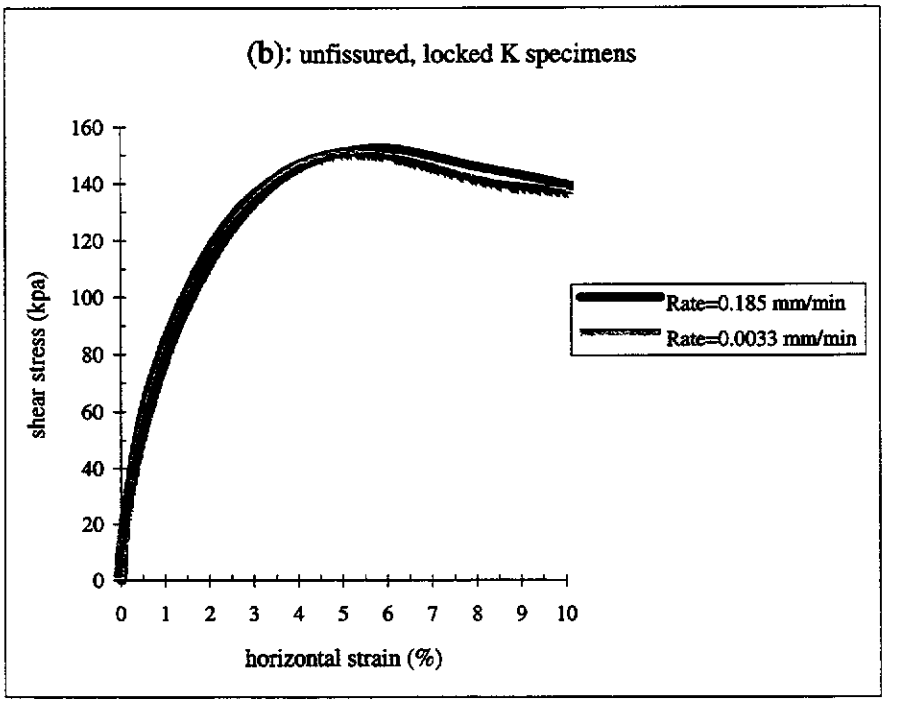

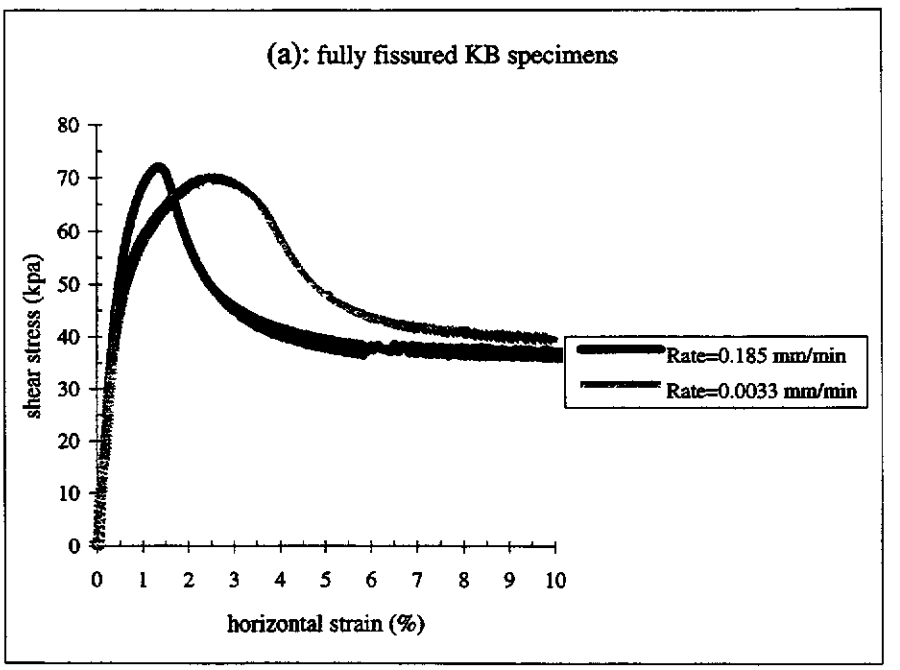

Figure (3.20): The stress strain curves of the fully fissured specimens sheared with two different rates for, (a); KB specimens, (b); K specimens.

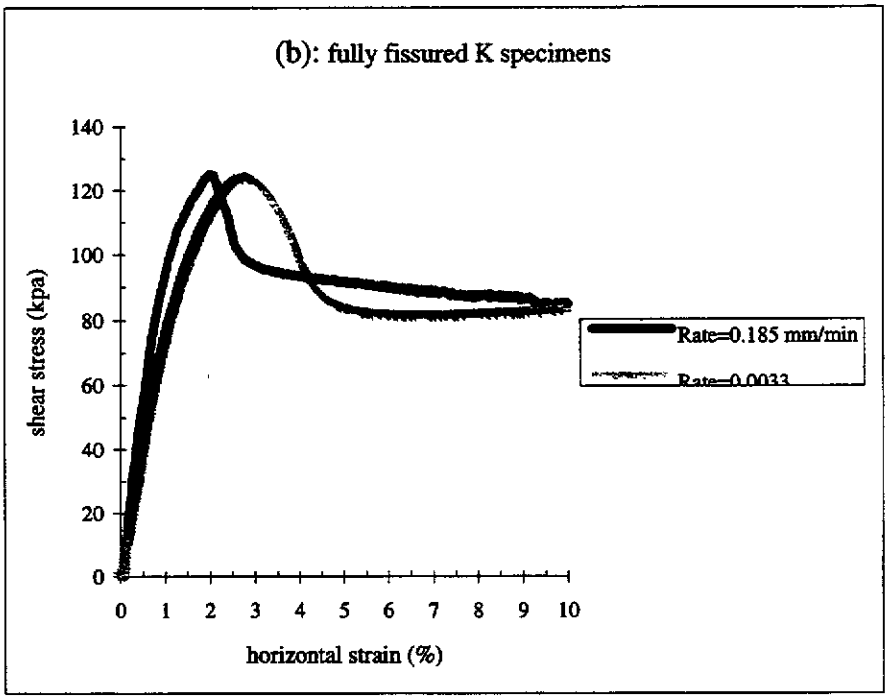

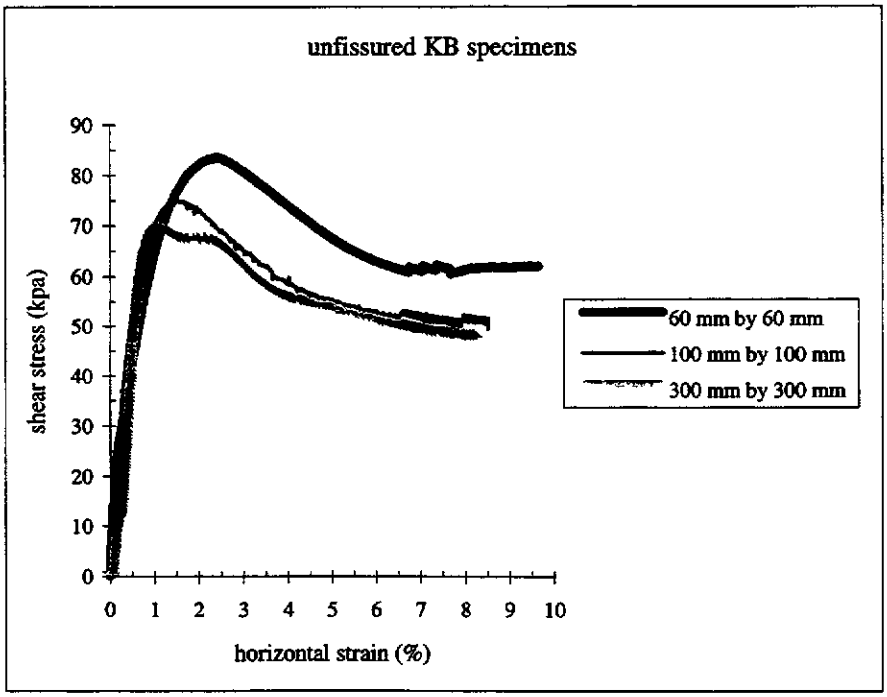

Figure (3.21): The stress strain curves of the KB specimens for three different sizes of 60 mm, 100 mm and 300 mm.

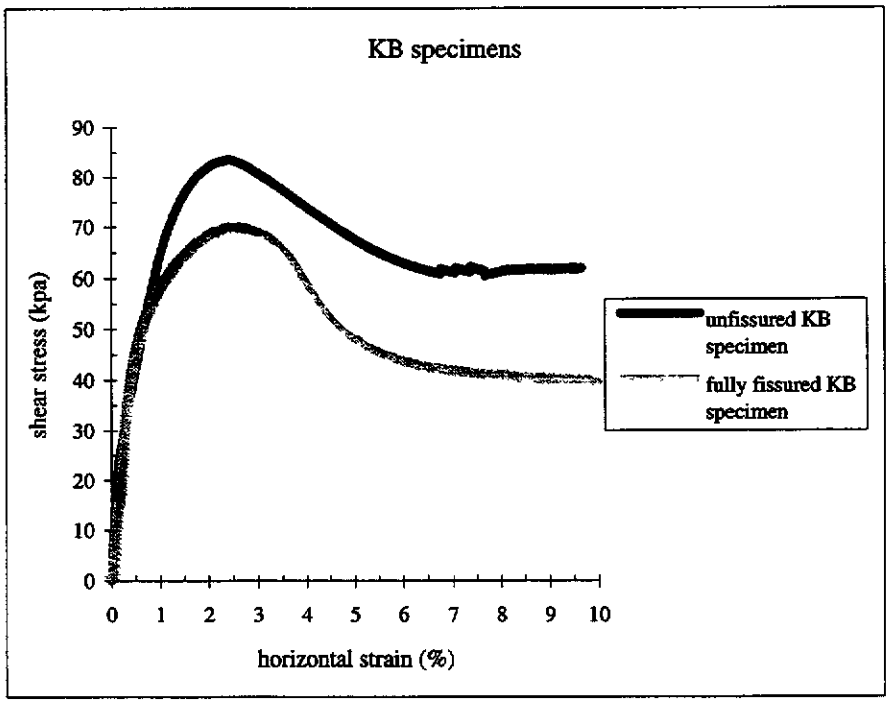

(a)

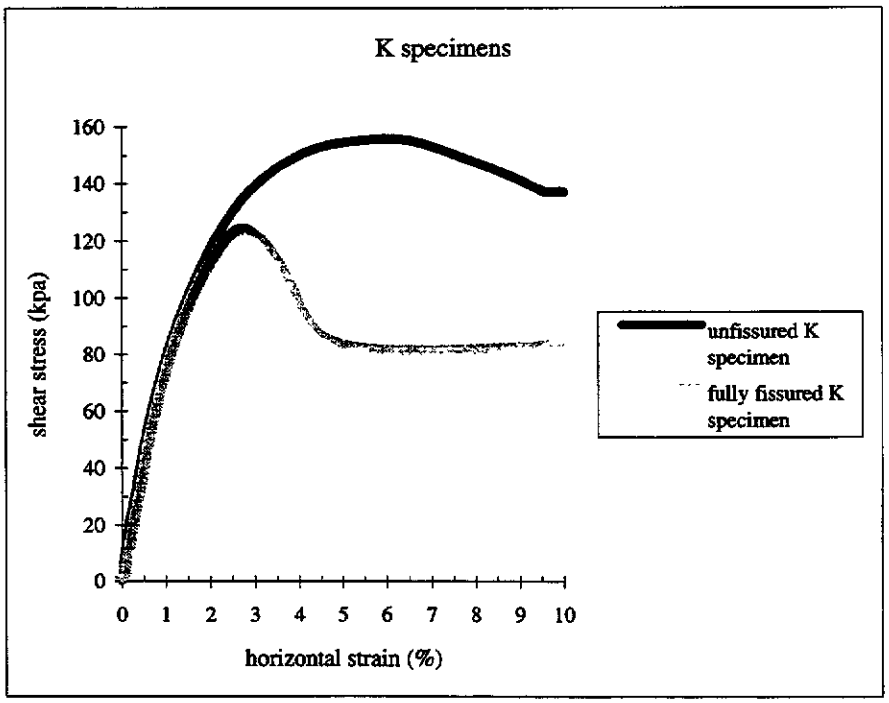

(b)

Figure (3.22): The effect of fissure on the behaviour of the stress strain curve, (a); KB specimens, (b); K specimens.

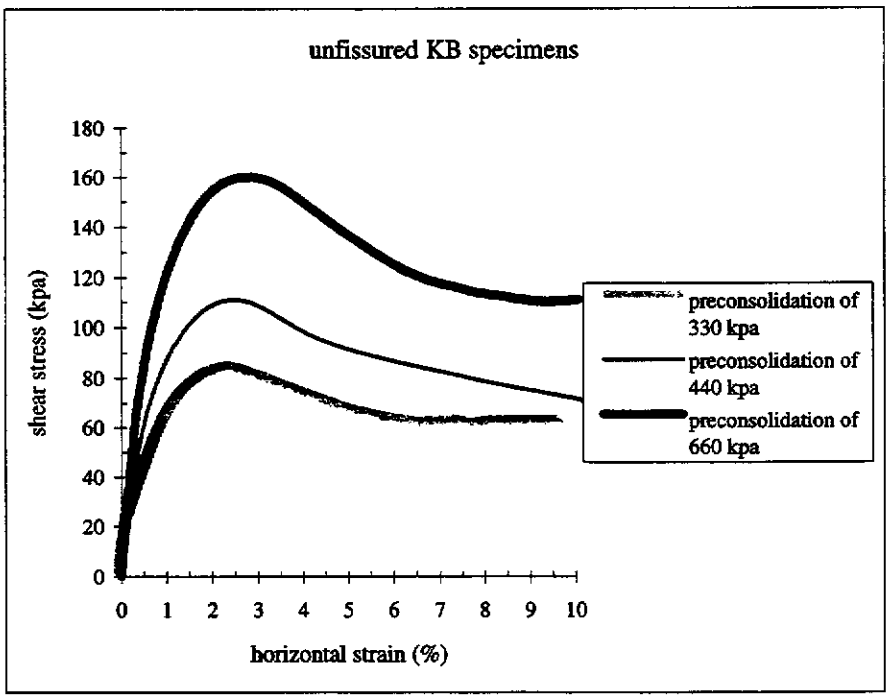

Figure (3.23): The stress strain curves of the KB specimens consolidated by three different p'_c of 330 kpa, 440 kpa and 660 kpa.

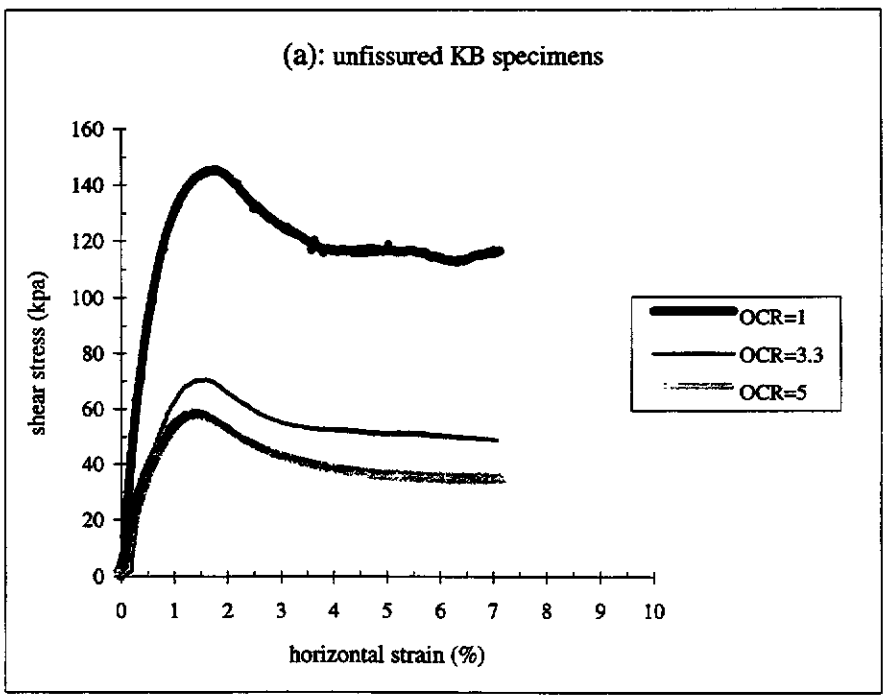

Figure (3.24): The effect of OCR on the specimens, (a); KB specimens, (b); K specimens.

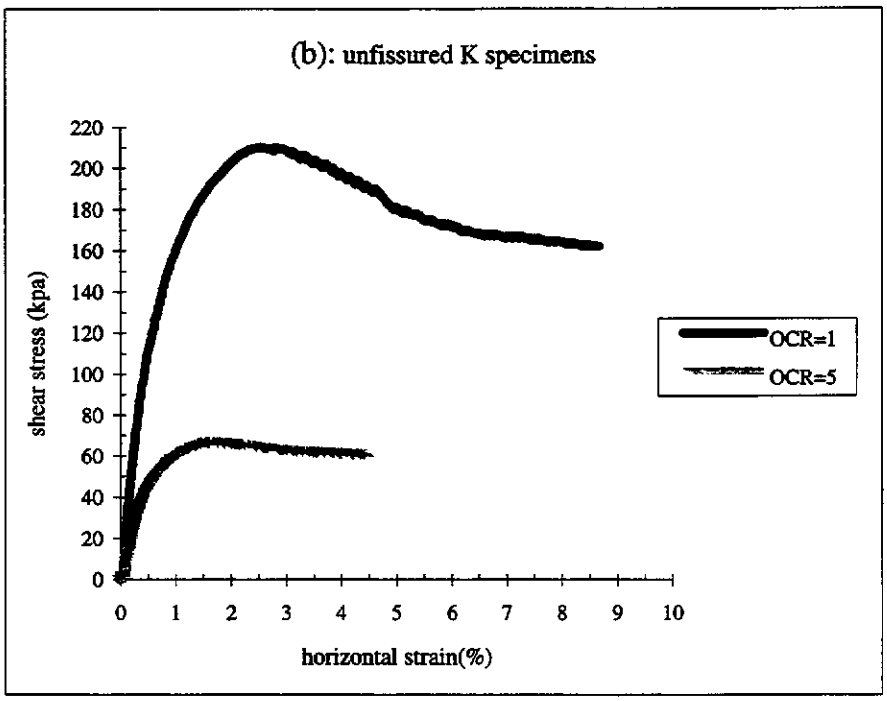

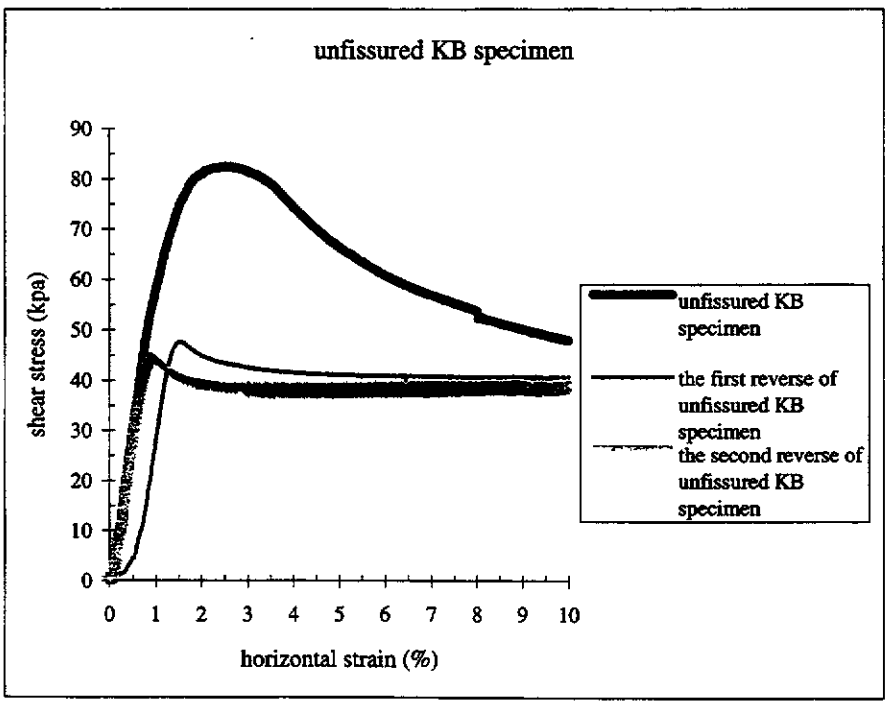

Figure (3.25): The stress strain curves of the unfissured KB specimen sheared three times.

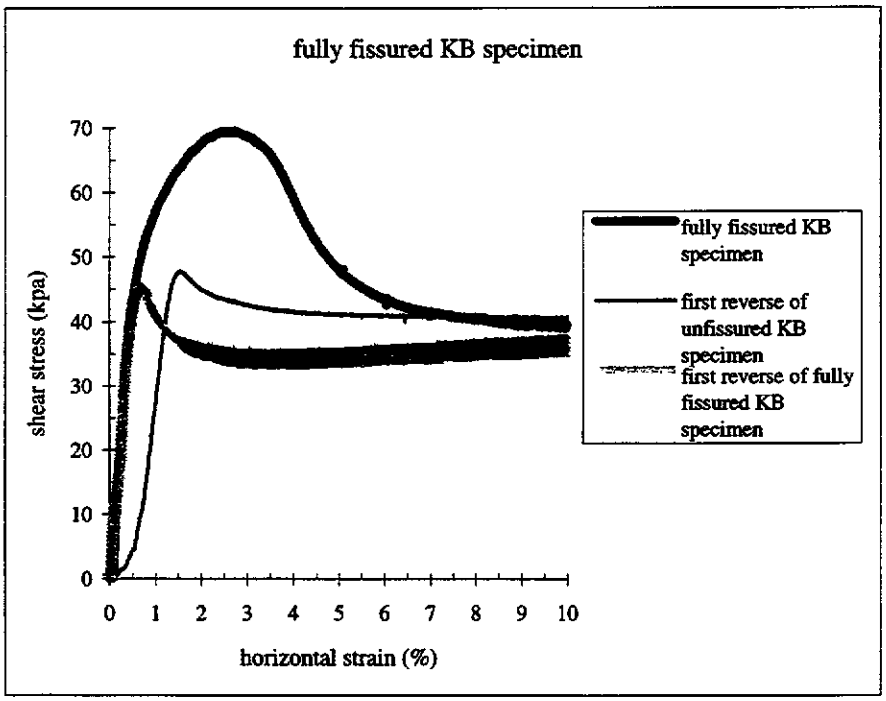

Figure (3.26): The stress strain curves of the fully fissured KB specimen sheared two times and compared with the residual shear strength of the unfissured KB specimen.

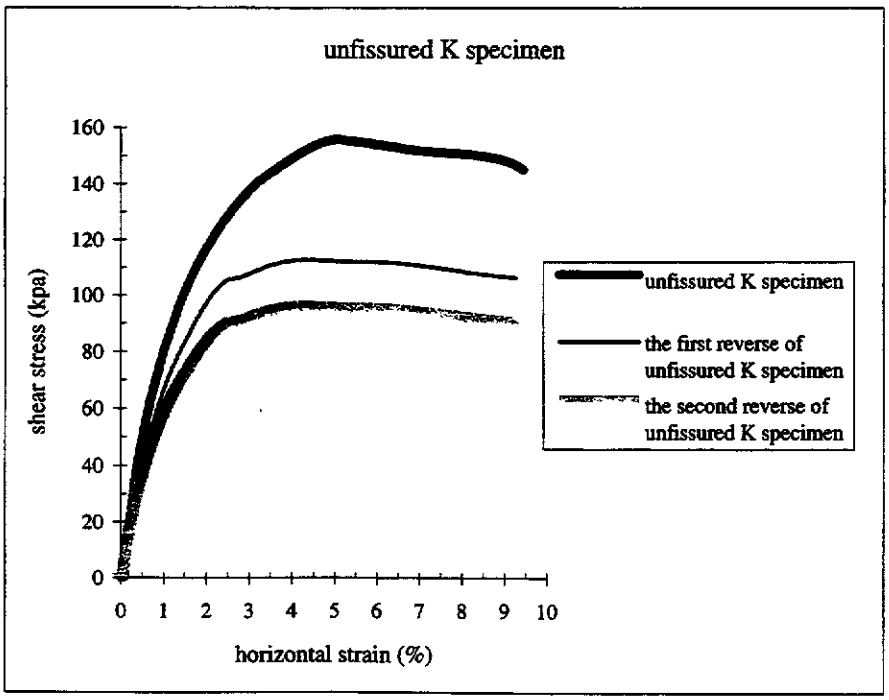

Figure (3.27): The stress strain curves of the unfissured K specimen sheared three times.

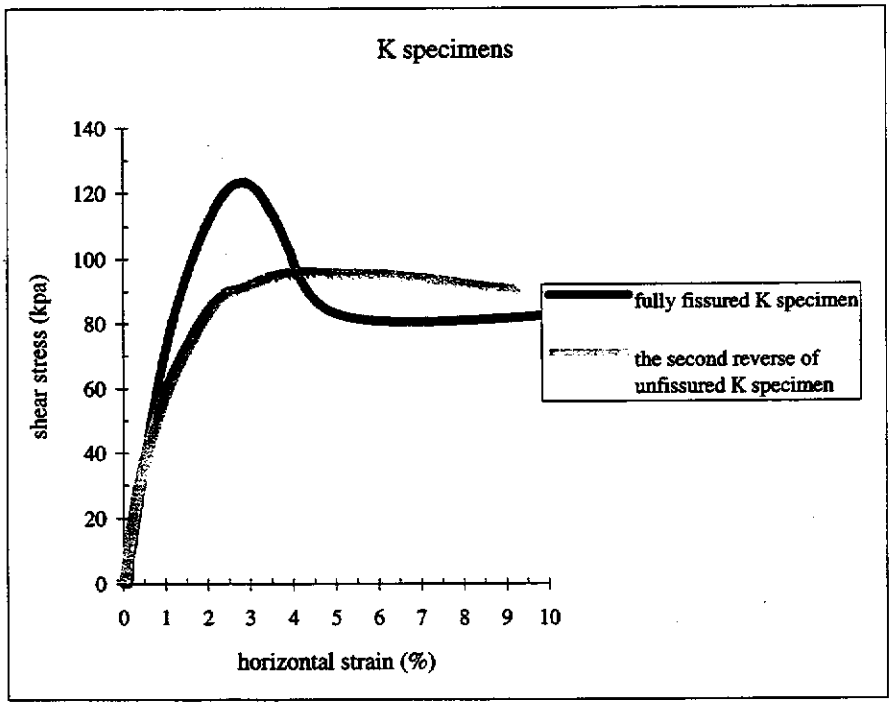

Figure (3.28): The stress strain curves of the fully fissured K specimen and compared with residual shear strength of the unfissured K specimen.

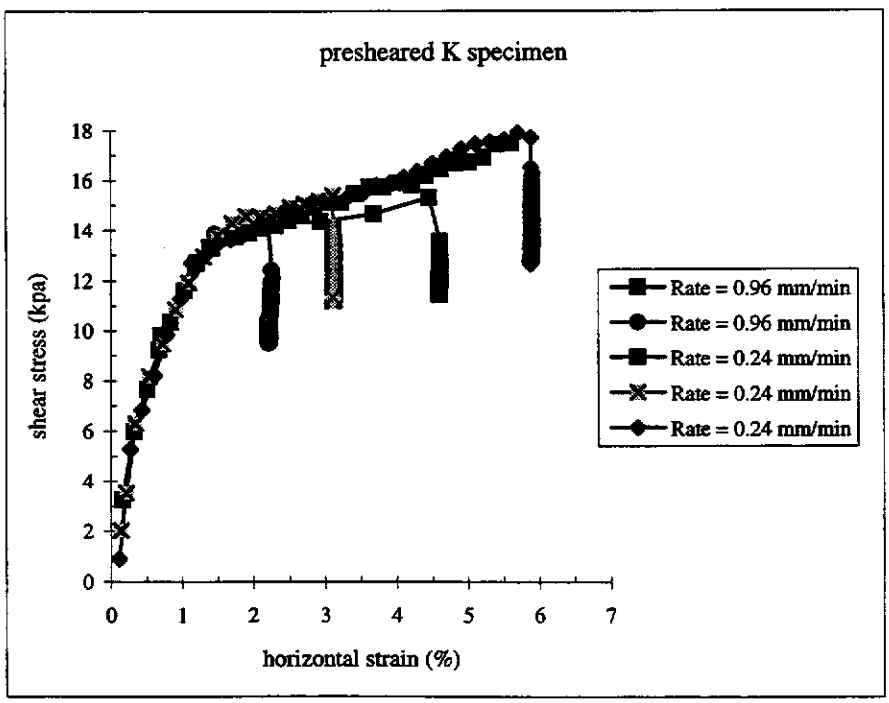

Figure (3.29): The effect of different high rates on the shear strength of a pre-sheared K specimen.

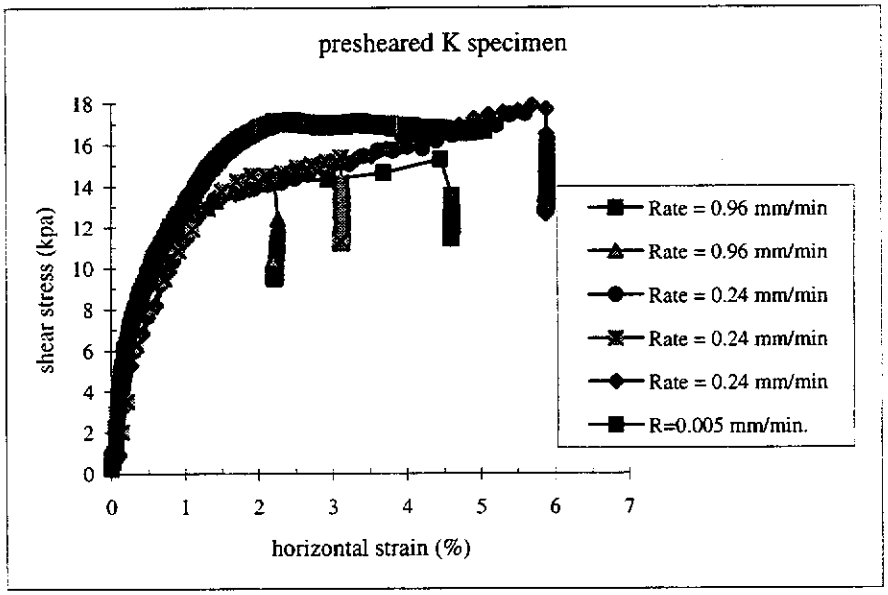

Figure (3.30): The reduction of the shear strength of the pre-sheared K specimen and a comparison with the residual shear strength of the specimen.

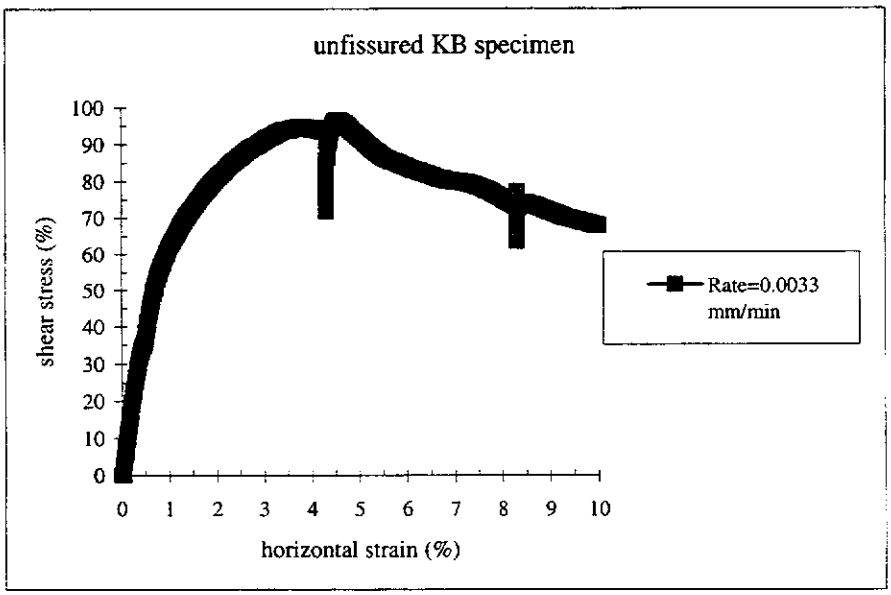

Figure (3.31): The reduction of the effective shear strength of the KB specimen.

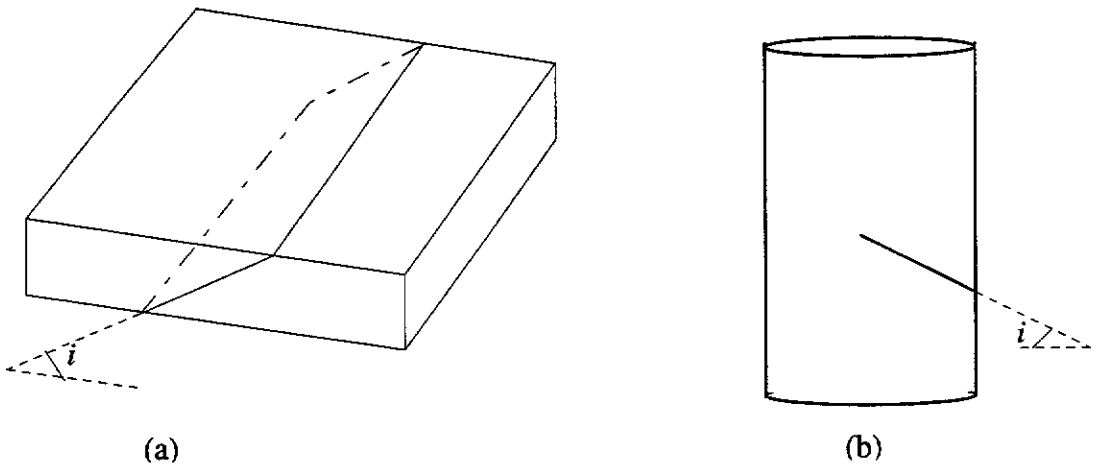

Figure (3.32): Illustration of pre cut specimens used wire cutter for creating the inclined fissures, (a); for the inclined direct shear specimens, (b); for the triaxial partially fissured specimens.

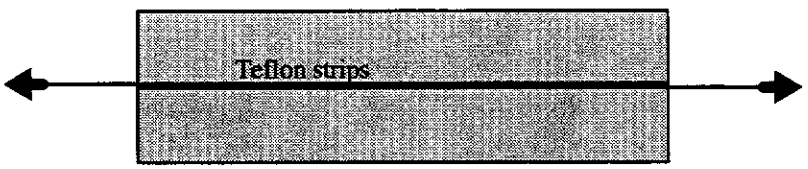

Figure (3.33): Illustration of the Teflon strips inside the direct shear box specimen and the direction of pulling out the strips

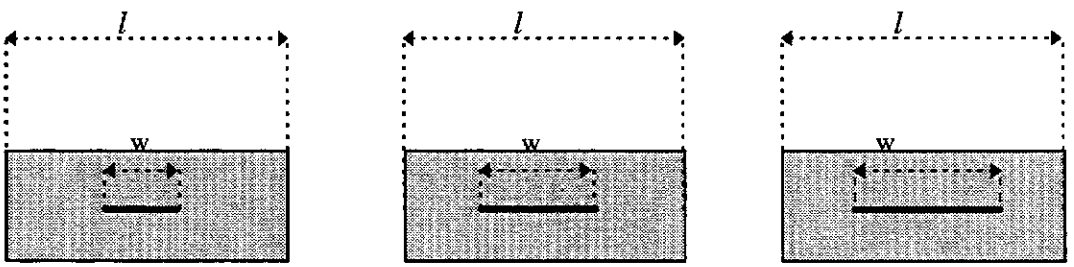

(a): $\alpha_f=w/l=10\%$ (b): $\alpha_f=w/l=30\%$ (c): $\alpha_f=w/l=50\%$

Figure (3.34): Illustration of different fissure surface; (a): $\alpha_f=w/l=10\%$, (b); $\alpha_f=w/l=30\%$, (c); $\alpha_f=w/l=50\%$, (α_f stands for percentage of the fissures, w is the width of fissures and l is the length of the specimens).

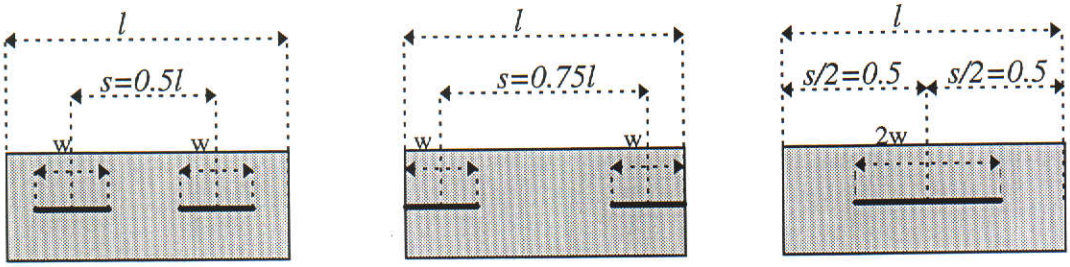

(a): $s=0.5l$ (b): $s=0.75l$ (c): $s=l$

Figure (3.35): Illustration of different fissure spacing; (a): $s=0.5l$, (b); $s=0.75l$, (c); $s=l$, (s stands for spacing of the fissures).

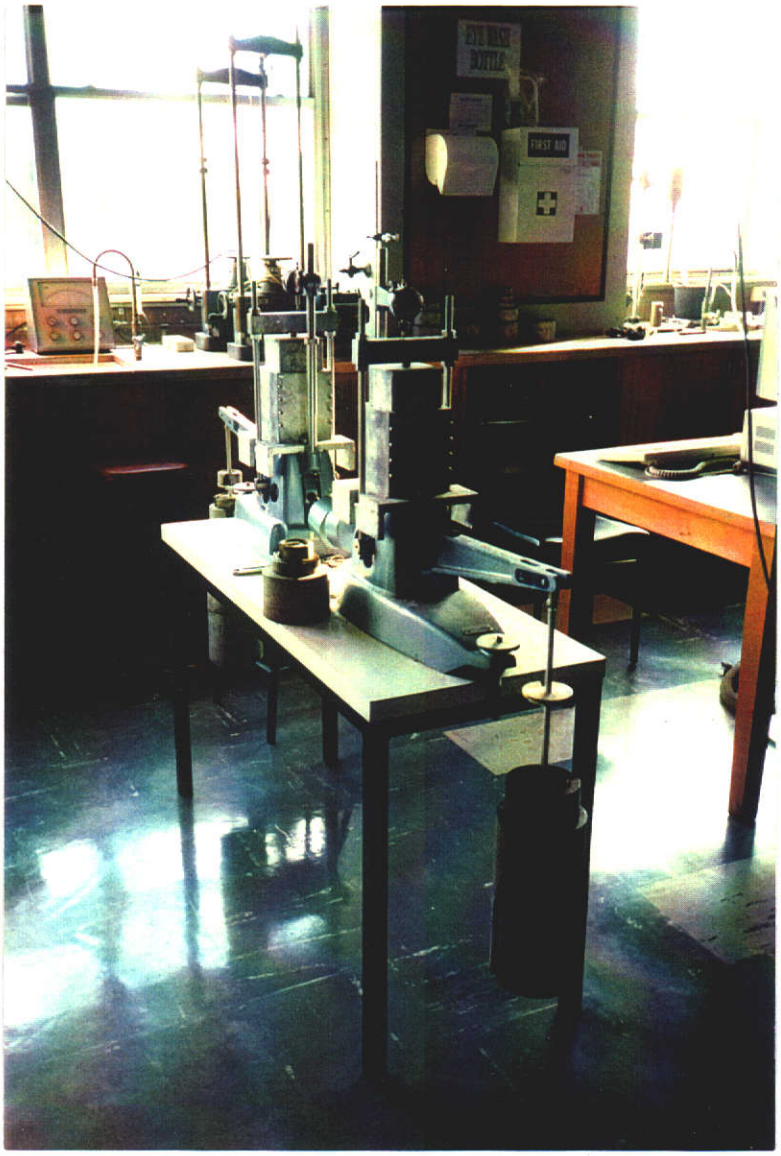

Figure (3.36): Direct shear box sample maker for the specimen size of 100 mm.

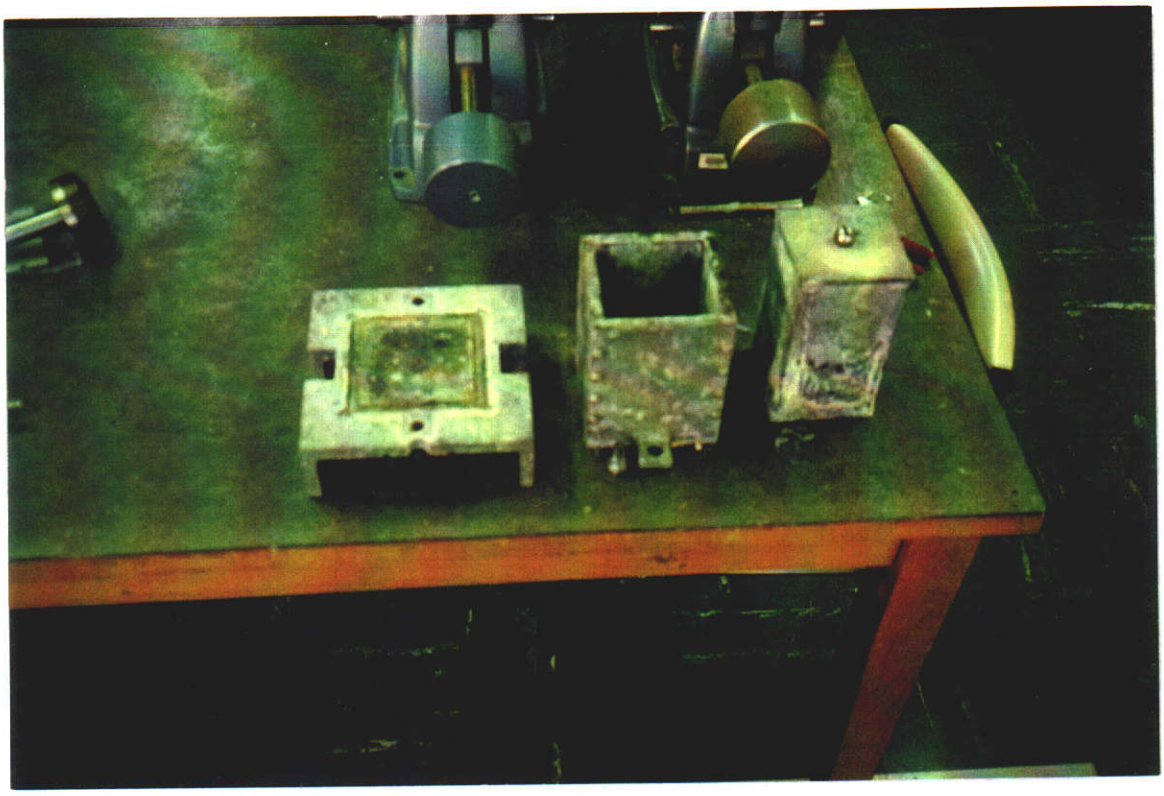

(a)

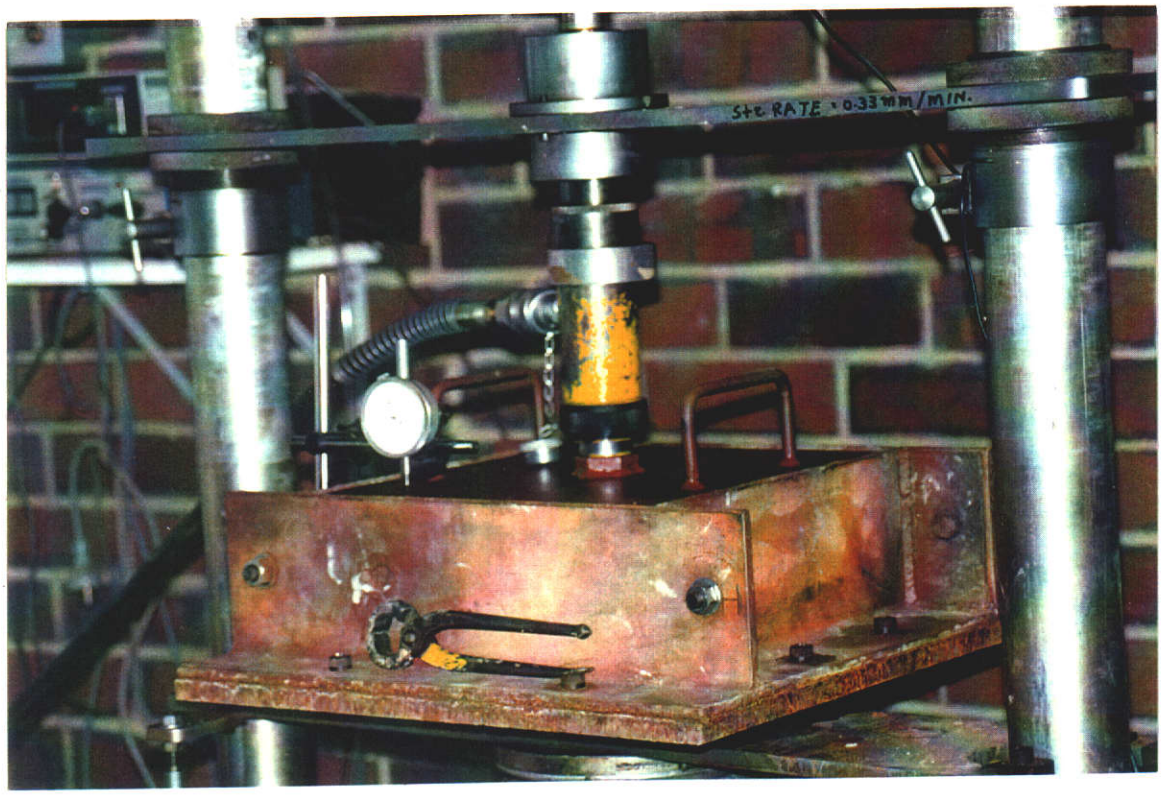

(b)

Figure (3.37): Direct shear boxes for the specimen size of (a); 100 mm, (b); 300 mm.

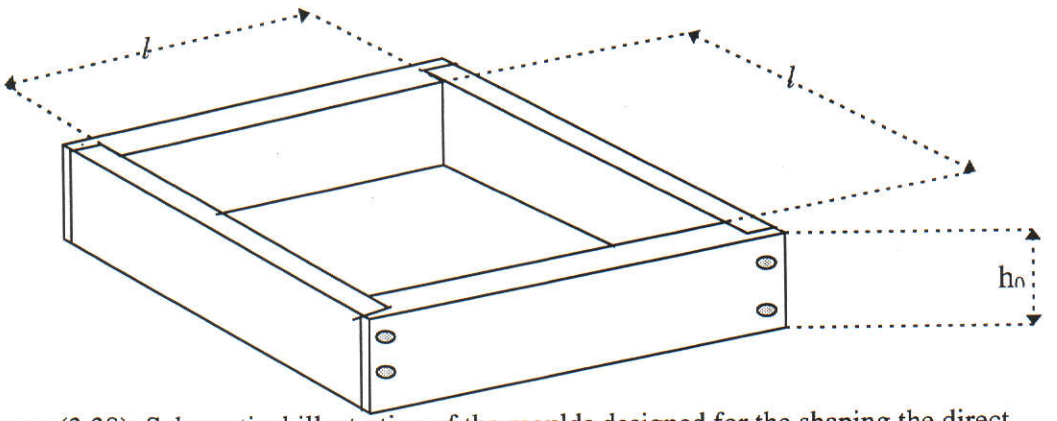

Figure (3.38): Schematical illustration of the moulds designed for the shaping the direct shear box specimens. The thickness of the mould (h_0) for the fissured specimens was half of the unfissured specimens.The lengths of the moulds were 60 mm, 100 mm, and 300 mm.

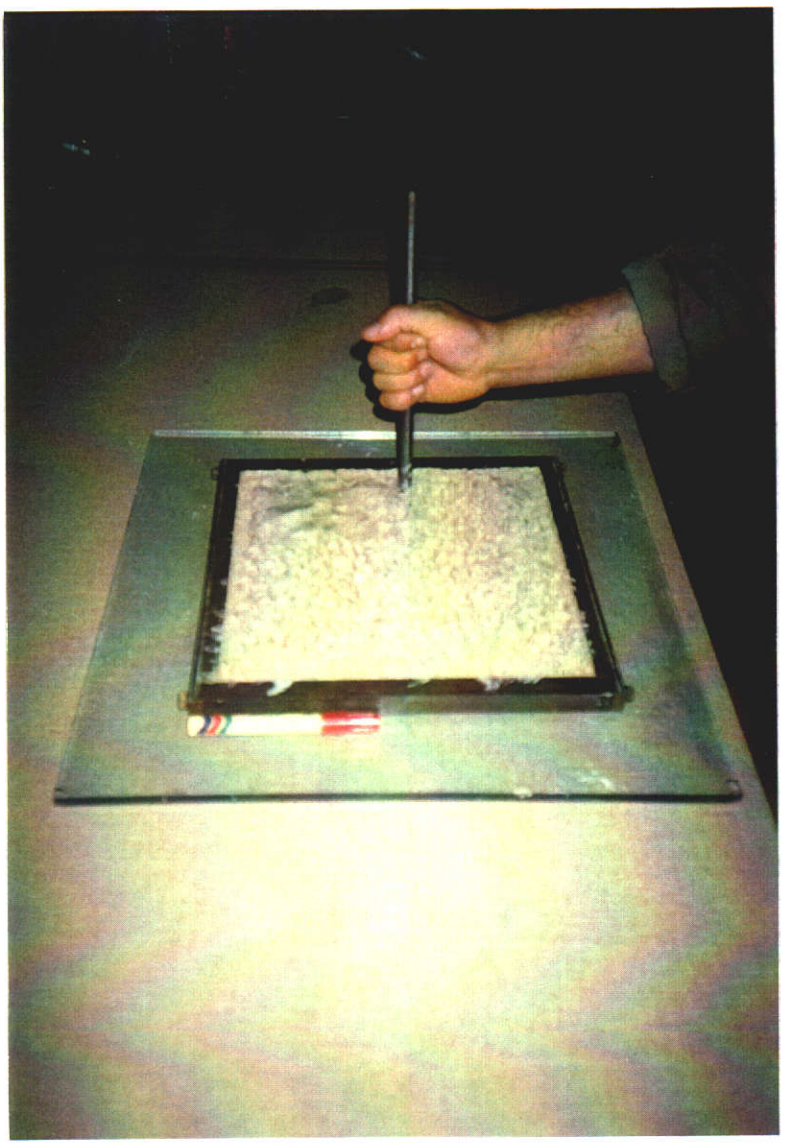

Figure (3.39): Illustration of the filling of the mould.

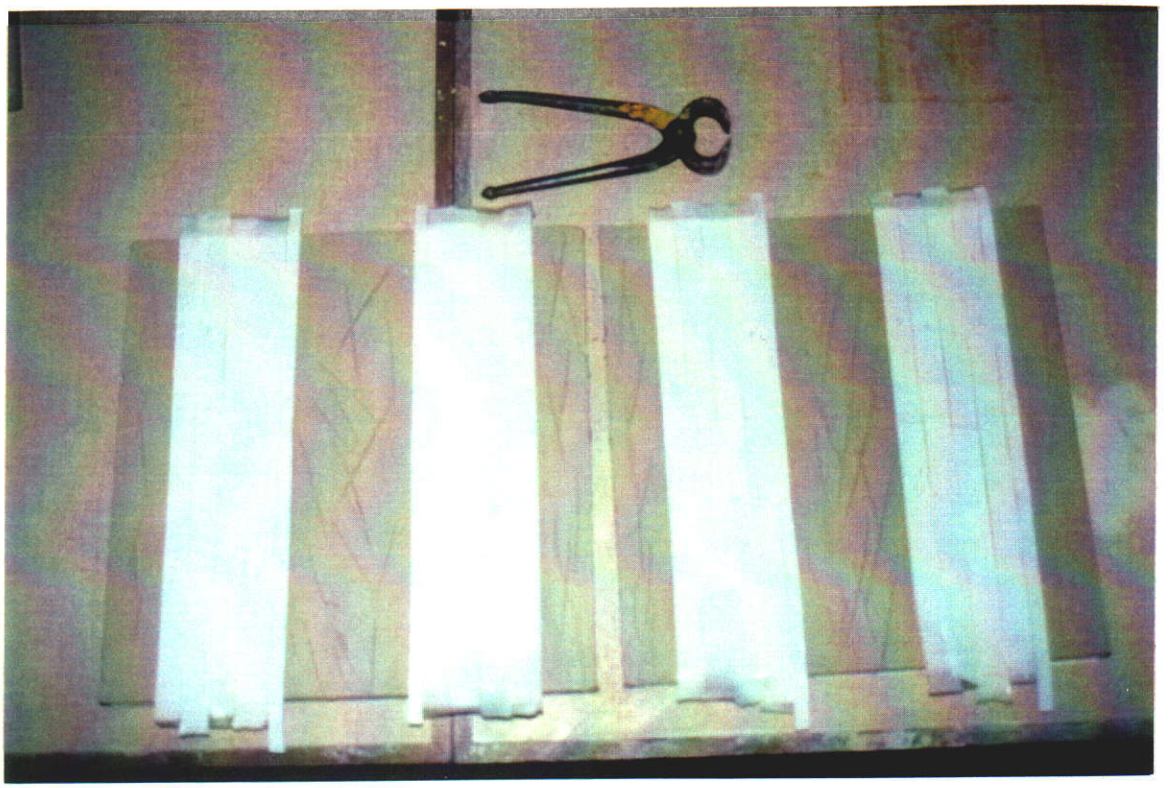

Figure (3.40): The two halves of a partially fissured Kb specimens with the position of the Teflon strips.

Figure (3.41):The arrangement of a partially fissured KB specimen in the box of sample maker.

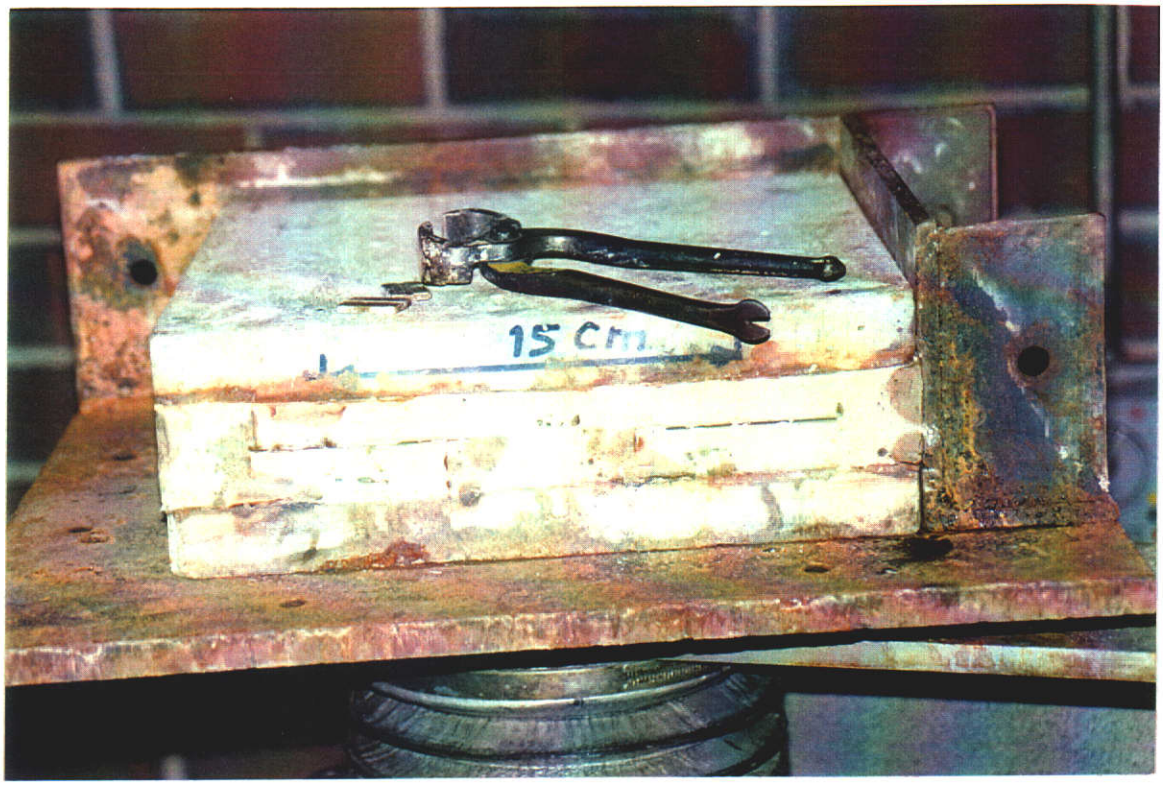

Figure (3.42): Illustration of a partially fissured KB specimen.

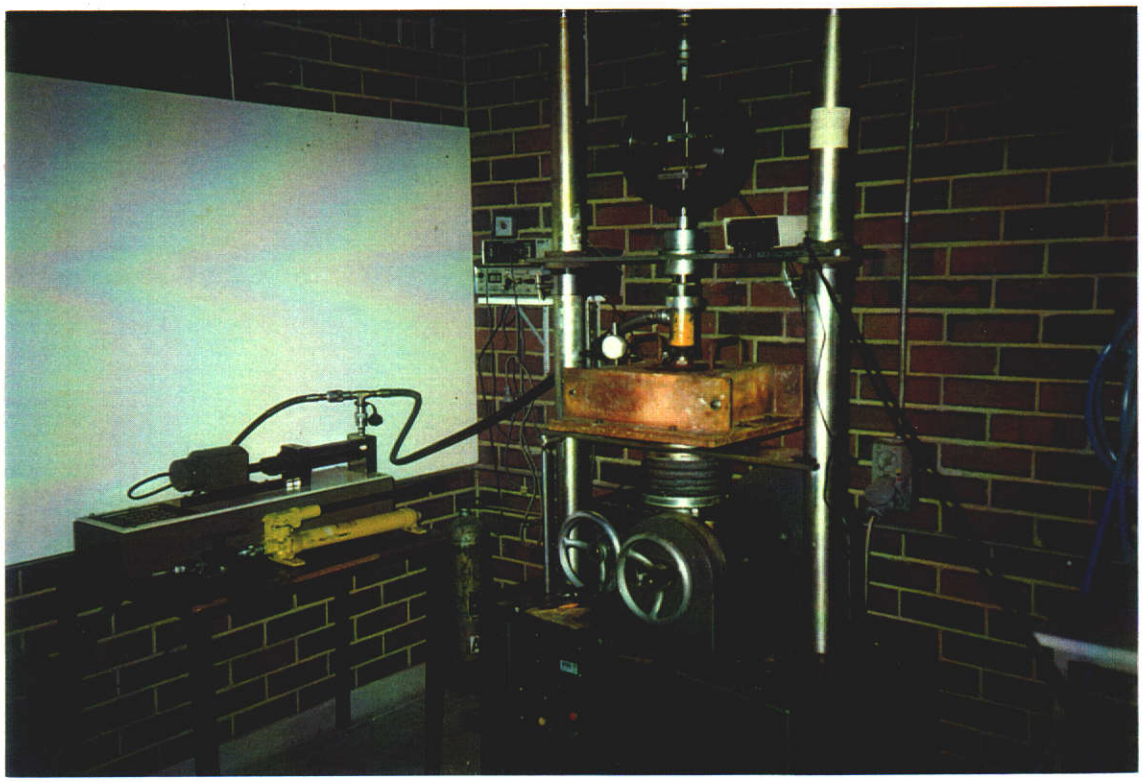

Figure (3.43): Illustration of the loading system of the direct shear box sample maker.

material type	ω (%)	e_0	C_v (cm^2/min)	PL (%)	LL (%)	PI (%)	G_s	PH	γ_T (gr/cm^3)
K	53	1.489	0.0406	42	68	26	2.67	6.0	1.686
KB	67	1.86	0.001975	50	155	105	2.6375	9.5	1.54

Table (3.1): Some physical and mechanical properties of K and KB materials used in this research.

Appendix A(3.1):

The physical and mechanical characteristics of Kaolin and Bentonite clays.

Appendix A(3.2):

Derivation of Equation (3.1).

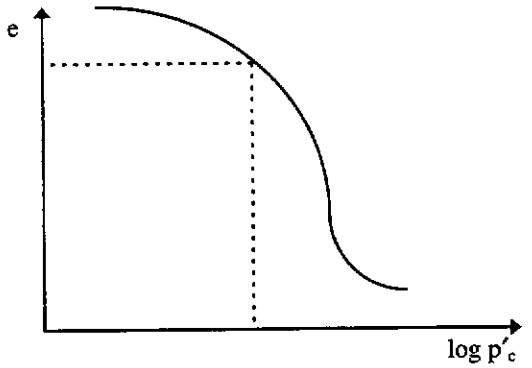

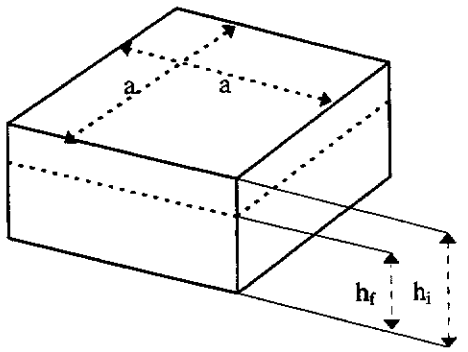

$$s.e_{p'_c} = \omega_f .G_s \qquad s = 100\% \qquad \text{A(3.1)}$$

$$V_f = h_f. a^2 \qquad \text{A(3.2)}$$

$$W_f = W_s(1 + \omega_f) \qquad \text{A(3.3)}$$

$$\gamma_f = \frac{W_f}{V_f} = \frac{G_s\,(1+\omega_f)}{1+e_{p'_c}} \Rightarrow W_f = V_f.\gamma_f \Rightarrow W_f = V_f \frac{G_s\,(1+\omega_f)}{1+e_{p'_c}} \Rightarrow W_s = \frac{V_f.G_s}{1+e_{p'_c}} \qquad \text{A(3.4)}$$

$$s.e_0 = \omega_i\, G_s \qquad s = 100\% \qquad \text{A(3.5)}$$

$$V_i = h_0\, a^2 \qquad \text{A(3.6)}$$

$$W_i = W_s(1 + \omega_i) \qquad \text{A(3.7)}$$

$$\gamma_i = \frac{W_i}{V_i} = \frac{G_s\,(1+\omega_i)}{1+e_0} \Rightarrow W_i = V_i.\gamma_i \Rightarrow W_f = W_i\left(\frac{1+e_0}{G_s\,(1+\omega_i)}\right) \qquad \text{A(3.8)}$$

$$h_0 = \frac{V_i}{a^2} \qquad \text{A(3.9)}$$

the substitution of Equations A(3.4) and A(3.8), into Equation A(3.9):

$$h_0 = h_f \frac{(1+e_0)}{1+e_{p'_c}} \Rightarrow h_f \frac{(1+\omega_i.G_s)}{1+e_{p'_c}} \qquad \text{A(3.10)}$$

The subscriptions of f and i stand for final and initial values or magnitudes of the parameters subsequently. W: wet weight of the specimens; W_s: dry weight of the specimen; γ: density of the specimen; h_0: initial thickness of the specimen; h_f, final thickness of the specimen after consolidation process; e_0: initial void ratio; $e_{p'_c}$: final void ratio for the applied p'_c and G_s: Specific Gravity of the material; V: volume of the specimen; *s*: degree of saturation; ω: water content.

CHAPTER 4

DIRECT SHEAR TESTS

4.1 INTRODUCTION

In this chapter, the results of three series of direct shear tests for three different sizes of specimens prepared artificially in the laboratory, are presented.

Except for the large direct shear box, whose specimens were prepared from one type of material (KB) and one level of preconsolidation pressure (P'_c) and for the unlocked-in horizontal stresses but for fully, partially fissured and unfissured specimens, the other sizes (100 mm by 100 mm and 60 mm by 60 mm) were prepared from two different materials (K and KB) for both unfissured locked and unfissured unlocked or fully fissured unlocked specimens and also for three different preconsolidation pressures, two or three different OCR's and three different rates of shearing.

This chapter aims to investigate in detail and evaluate the effects of parameters such as preconsolidation pressure, size of specimens, the situation of horizontal stresses, rates of shearing, and fissure parameters like width, spacing and orientation on the effective peak shear strength parameters (c'_p & ϕ'_p). In some cases the relationships

within the parameters and their effects on the Mohr Coulomb effective peak shear strength parameters (c'_p & ϕ'_p) of unfissured unlocked specimens are described.

4.2 TESTING EQUIPMENT

In addition to the boxes of consolidation and moulds and also the sample makers designed and constructed for the preparation of the direct shear box specimens, three strain controlled direct shear boxes for three different sizes of specimens were utilised.

Figures (4.1) and (4.2) show the direct shear boxes for 300 mm by 300 mm and 60 mm by 60 mm specimens.

These apparatuses were equipped with electronic measuring and monitoring systems for vertical, horizontal displacements and forces.

Transducers were used for the measurement of displacement and loads. Electronic signal conditioning automatically processed the voltage output from these transducers and showed the readings as a digital display in engineering units. The data obtained were stored on the hard disk of the microcomputer system for later processing, thus the task of observing and reading results was easy and the likelihood of errors was greatly reduced.

By connecting the transducers to a compatible data logging system, the numerical results were transferred to the hard disk for computational processes. In Appendix A(4.1) an example of the computer program written for converting the electronic signals to an engineering digital display is given.

The main reason for the use of these transducers was calibration. The transducers for vertical and horizontal displacement were calibrated by a very accurate micrometer with an accuracy of 0.0005 mm.

The transducers used for small and medium sizes (60 mm by 60 mm and 100 mm by 100 mm) were calibrated directly by loading in compression or tension modes with an accuracy of 50 grams. The transducers used for load measuring of the large direct shear box (300 mm by 300 mm), however, were calibrated by a triaxial frame and improving ring with an accuracy of 1 kg.

4.3 MATERIAL, SPECIMEN PREPARATION AND TESTING PROCEDURE

Because of the artificial nature of the specimens tested in this research, particular attention was given to the preparation of the pastes and specimens and then to the consolidation process of the specimens and finally to their testing.

As discussed briefly in Chapter 3, the pastes of K (100% Kaolin) and KB (75% Kaolin and 25% Bentonite) were prepared with desirable and workable water contents of about 53% and 67% respectively.

For KB material, a mixture of Kaolin (K) and Bentonite (B) was prepared whenever necessary. The desirable ratio was 1/3 of dry weight of Bentonite and Kaolin respectively.

Before the preparation of the KB pastes, the water content of K and B powders was determined and then the amount of water required for a water content of 67% was added to the uniformly mixed powder of K and B. For K specimens (100% Kaolin), enough water to reach a water content of 53% was added and then directly mixed with the K powder.

After preparation, the pastes were wrapped in plastic bags, dated, numbered, and finally stored in a temperature monitored room to cure for 24 hours.

Different separable moulds were designed for the preparation of pasty specimens to shape specimens to the required sizes. The interiors of the moulds used for large specimens (300 mm by 300 mm) were lubricated a little by grease to facilitate the separation of the pasty and sticky specimens shaped from the moulds.

Plastic separators were put between the moulds and the thin glass base board to ease the separation of pasty and sticky contact surfaces of the specimens from the glass base board. When the pastes were cured and the moulds were ready to use, they were placed in the moulds, tamped and refilled. The top and bottom surfaces were trimmed with a metallic ruler and the pasty shaped specimens were taken out of the moulds and put in the boxes of consolidation. Based on the time required to consolidate the specimens by monitoring the settlement through the attached dial gauge for vertical

displacement, the specimens were loaded for consolidation pressure. The loading system of the direct shear box sample makers has been explained in Chapter 3. For small and medium specimens, the loads were directly applied on the top of specimens, but for the larger sizes, the loads were applied through a hydraulic jack connected to a GDS unit (Menzies, 1988). That GDS unit was able to keep and apply constant pressures programmed or targeted for the consolidation of the specimens.

The water content, the weight and the dimensions of specimens before and after the consolidation process were determined or measured for the further engineering usages such as determination of density.

For fully fissured or partially fissured unlocked specimens, the heights of moulds were half of the heights of unfissured unlocked specimens. When the two halves of a pasty specimen were prepared, based on the specimen characteristics required, two sets of Teflon strips were put together and attached at two or three points along the joints by pieces of adhesive tape and put on the top of the trimmed surfaces of each half. Then the two halves were put together and placed in the original moulds used for preparation of the unfissured specimens. To have homogeneity in the unfissured parts of the partially fissured specimens, those parts assumed to be unfissured parts were tamped again and trimmed before being put in the boxes of consolidation.

The length of the strips for each proposed size of specimen was about 10 mm longer than the size of the specimen so there was enough strip projecting out of the specimens for them to be pulled out easily. To pull out the strips, the tip of each Teflon strip was held between two pieces of small plate brass and pulled out with pliers.

After the consolidation process, the specimens were weighed, their dimensions measured and they were then wrapped properly to prevent any water content change and finally numbered, dated, and stored in the temperature monitored room until required for testing.

In order to prepare unfissured locked-in horizontal stress specimens (unfissured locked specimens), the boxes of direct shear apparatuses were used for the consolidation process of the specimens. Because of technical problems with the box

of large direct shear apparatus, just unlocked-in horizontal stress specimens, including unfissured, partially fissured or fully fissured unlocked specimens, were tested with the apparatus.

In the next stage after the consolidation process of the specimens, they were prepared for shearing in the boxes of direct shear apparatuses.

Driving motors and data loggers were turned on to start shearing the specimens and logging the data. When the specimens were seated and loaded for the purposed normal stresses in the shear boxes and the one millimetre gap between the two halves was provided, the clamping screws were opened. The shearing machines were set up for the purposed rates of shearing through the gear boxes of the apparatus, and the shear and normal transducers and normal load cell were mounted in the correct locations.

For the unlocked and locked specimens sheared with an OCR of one, a few hours before shearing were required to stabilise the deformation of the specimens as result of a one millimetre gap between two halves of the boxes of shear apparatuses.

But for the unlocked or locked specimens sheared with an OCR > 1, about 24 hours for KB specimens and 12 hours for K specimens time were required so that the vertical displacement could reach an equilibrium from the unloading, expansion or swelling of the specimens as result of water absorption, and deformation of specimens as a result of a one millimetre gap between the two halves of the boxes.

The magnitudes of the applied shear load, the normal and horizontal displacement for small and medium sizes of direct shear boxes and normal load extra for large direct shear boxes were monitored simultaneously at a frequent intervals prescribed or defined by the operator during the tests and stored in the memory of the computer system connected for later processing.

The specimens for drain tests were sheared at a rate of 0.005 or 0.0033 mm/min. The other two rates used in this research were 0.01 mm/min and 0.185 mm/min.

The specimens prepared for the medium size direct shear box (100 mm) were tested for three different OCR's of 1, 3.3 and 5 or 10. The specimens prepared for the small (60 mm) and large (300 mm)sizes were sheared for two different OCR's of 1 and 2.5.

The preconsolidation pressures applied were 330, 440 and 660 kpa for the small and medium specimens and 330 kpa for the large specimens in view of the technical problems of the large direct shear box.

Fully fissured and 50% fissured unlocked specimens were prepared for all sizes of specimens, but for the study of different widths and spacing of fissures, just large specimens were prepared and tested. Figure (4.3) shows schematically the definition of width (w) and spacing (s) of fissures.

Figure (4.4) shows the photograph of a set of the different types of large unlocked specimens (300 mm by 300 mm) prepared for testing. In this figure, the numbers refer to fully fissured unlocked specimen (1), partially fissured unlocked specimen with w = 75 mm, s= 150 mm α_f = 50% (2), partially fissured unlocked specimen with w = 75 mm, s = 225 mm and α_f = 50 % (3), partially fissured unlocked specimen with w = 150 mm, s = 300 mm and α_f = 50 % (4), partially fissured unlocked specimen with w = 90 mm, s = 300 mm and α_f = 30 % (5), partially fissured unlocked specimen with w = 30 mm, s = 300 mm and α_f = 10 % (6), unfissured unlocked specimen with bedding (7), and unfissured unlocked specimen without bedding (8).

A few small inclined fissured unlocked specimens with an inclination of 45° to the horizontal direction also were prepared and tested. Figure (4.5) shows the photograph of a small KB specimen with a fissure inclination of 45°.

In the partially fissured specimens, there were two options for placing and shearing the specimens in the boxes of shear apparatuses. The first was shearing the specimens along the length of fissures (the shearing direction was parallel to the fissure lengths), the second option was shearing the specimens along the width of specimens (the shearing direction was perpendicular to fissure length). Figure (4.6) shows schematically both directions of shearing. Direction ① is perpendicular to the fissure length and direction ② is parallel to the fissure length. The effect of the direction of shearing was investigated only on the large specimens.

4.4 THE TESTING PROGRAM FOR DIRECT SHEAR TESTS

Three sizes of specimens, each designed for particular cases of study, were prepared and tested. They were 60 mm by 60 mm (small), 100 mm by 100 mm (medium), and 300 mm by 300 mm (large).

The laboratory test program for these three sizes consisted of more than 180 direct shear tests. The specimens were prepared from the same raw materials under the same initial conditions of preparation. These tests were conducted under constant normal stress conditions for both types of materials (one stage loading). The main aims of these tests have been:

(a) to investigate the effective shear strength of K and KB specimens

(b) to investigate the effect of preconsolidation pressures

(c) to investigate the effect of overconsolidation ratio (OCR)

(d) to investigate the effect of size of specimens

(e) to investigate the effect of rate of shearing

(f) to investigate the effect of releasing the locked-in horizontal stresses

(g) to investigate the effect of fissure parameters for different width and spacing and orientation of fissures

(h) to investigate the effect of the direction of shearing

The testing programs for direct shear tests have been summarised in Tables (4.1) - (4.9).

4.5 THE RESULTS OF DIRECT SHEAR BOX SPECIMENS

The experimental results of the specimens subjected to direct shear tests have been reported in Table (4.10). The underlined part of the specimen number indicates the normal stress applied during the shearing process.

For each test, the graph of shear stress (τ) against horizontal strain have been plotted. For brevity, only selected test results are presented in the figures of this chapter. However, all test data are included in the analysis of the results. Typical results are

presented in Figures (4.7) - (4.26). The components of Table (4.10) are explained as follows:

size: size of specimen (three sizes 60 mm by 60 mm, 100 mm by 100 mm and 300 mm by 300 mm were prepared and tested in this research)

K: a 100% Kaolin specimen with a water content of 53% of density of 1.686 g/cm^3 before the consolidation process

KB: a specimen of 75% Kaolin and 25% Bentonite with a water content of 67% and density 1.540 g/cm^3 before the consolidation process

UFS: an unfissured unlocked specimen or unfissured locked specimen

FFS: a fully fissured unlocked specimen

PFS: a partially fissured unlocked specimen

IFS: an inclined fissured unlocked specimens

Locked specimen: a locked in horizontal stress specimen

Unlocked specimen: an unlocked in horizontal stress specimen

Without bedding specimen: a specimen prepared in one layer of material

With bedding specimen: a specimen prepared in two layers of material

Rate: rate of shearing (mm/min) eg. for drained tests, rate of 0.005 or 0.0033 mm/min was applied. The other two rates of 0.01 mm/min and 0.185 mm/min also were also applied to study the effect of the rate of shearing.

P'_c: preconsolidation pressure, three different preconsolidation pressures (330 kpa, 440 kpa, and 660 kpa) were applied to consolidate the specimens artificially.

OCR: overconsolidation ratio which is a fraction of p'_c over the normal stress applied during shearing.

Fissure parameters: fissure length (l), width of fissure (w) and spacing of fissure (s) based on mm, and orientation of fissure to the horizontal direction (i, based on degree) and percentage of fissured surface, α_f which is:

$\alpha_f = w/l \times 100$ for one fissure with width of w (4.1)

$\alpha_f = nw/l \times 100$ for n fissures with width of w (4.2)

Peak: peak shear strength (kpa) of the shear stress-horizontal strain graph of the specimen

Residual: residual shear strength (kpa) of the stress - strain graph of the specimen

Shearing Direction ①: shearing direction is perpendicular to the fissure length

Shearing Direction ②: shearing direction is parallel to the fissure length

4.5.1 Typical Behaviour of Specimens Sheared by Direct Shear Boxes

The sheared surfaces of all specimens were observed carefully. The parts of the shearing surfaces passed through the intact material were polished or slickensided, indicating the specimens failed by the shear mode rather than by the tension mode.

As typical results of KB specimen graphs (Figure 4.7) show, the behaviour of stress strain can be divided approximately into three zones. In all KB specimens in the pre-peak zone, an almost linear elastic response up to a pronounced peak shear strength was observed (first zone). With further relative displacement beyond the peak, a rapid reduction in the shear strength occurred (second zone). With further shearing, a third zone was finally defined when the shear stress reached an approximately constant value, residual strength.

These three zones occurred for K specimens but with relatively larger shearing displacements (Figure 4.10).

The first zone is the peak shear strength at an early stage of shearing, strains usually in the range of 0.5% to 2% for KB unfissured unlocked or locked specimens with a size of 100 mm and 2.5 % to 5% for K unfissured unlocked or locked specimens with a size of 100 mm, and 0.5 to 1.1 % for fully fissured unlocked KB specimens of 100 mm.

The second zone occurred at shearing strains that were in the range of 2% to 5% for KB unfissured unlocked or locked specimens, 5% to 10% for K unfissured unlocked or locked specimens and 1.0 to 4% for fully fissured unlocked KB specimens. The third zone showed more than 5% for KB unfissured unlocked or locked specimens, 10 % and more for K unfissured unlocked or locked specimens and 4% for fully fissured unlocked specimens (Figures 4.9 and 4.10).

For unfissured locked specimens for both materials peak shear strength happened with greater displacement than with the unfissured unlocked specimens (Figures 4.7, 4.8, 4.21 and 4.22). By increasing the P'_c, or decreasing the overconsolidation ratio, greater horizontal strains were required (Figures 4.7 and 4.25).

For smaller than 100 mm specimens, greater horizontal strains were required. On the contrary, for larger than 100 mm specimens, smaller horizontal strains for occurrence of peak shear strength were observed (Figures 4.7 and 4.18).

These findings can be explained by the maximum disturbance required for the specimens and clay particles at the time of peak shear strength. For unfissured locked specimens, the disturbance is less than unfissured unlocked specimens. Therefore, more time is required to reach the maximum disturbance at peak. But for unfissured unlocked specimens, because the release of horizontal locked in stresses, some disturbance occurs before the shearing process. Thus less time is required to reach maximum disturbance at peak.

For specimens consolidated with higher p'_c, the clay particles are flattened and reoriented therefore, more time is required to reach maximum disturbance at the time of peak shear strength. In other words, more shearing displacement is required to disturb again the clay particles reorientated to reach peak shear strength.

The specimens are sheared with higher OCR's, because of the dilation of the specimens and disturbance of the clay particles before shearing. Some part of the disturbance required to reach peak will occur before shearing. Therefore, for these specimens less time is required to reach the maximum disturbance at peak shear strength.

The effect of size on the situation of peak shear strength can also be explained by the concept of strain softening behaviour. Assuming that the shearing displacement required for a 60 mm specimen is 2 mm, it means for further displacement after 2 mm, the average shear stresses decreases from the peak shear strength. If the size of specimen increases from 60 mm to 100 mm and 2 mm shearing displacement is applied, the shearing stresses would reach the peak shear strength for some part of the 100 mm specimen, but other parts would be under peak shear strength and when

further shearing displacement is applied, the former part passes from peak and the latter part just reaches the peak. It means the total average of shearing stresses of the specimen with a size of 100 mm never has a chance to increase more than the peak shear strength obtained from the specimen with a size of 60 mm. Therefore, the 2 mm shearing displacement would be the peak displacement required for the 100 mm specimen too, whereas the horizontal strain for a smaller size with this 2 mm displacement would be 3.3% ($\frac{2.0}{6.0}\times$ 100), for 100 mm would be 2% and for a specimen of 300 mm would be 0.66%.

4.5.2 Peak and Residual Shear Strength Parameters

In order to define the shear strength parameters, peak and residual shear stresses were plotted against horizontal shearing stresses for each set of tests for the same p'_c.

The Mohr Coulomb parameters (c'_p and ϕ'_p or c'_r and ϕ'_r). of each set of tests are listed in Tables (4.11) and (4.12). The peak shear strength predicted by the Mohr-Coulomb criterion is defined by the Equation (4.3) and the residual shear strength is defined by Equation (4.4).

$$\tau_p = c_p + \sigma \tan \phi_p \qquad (4.3)$$

$$\tau_r = c_r + \sigma \tan \phi_r \qquad (4.4)$$

In these equations the subscription p and r are refer to peak shear strength and residual shear strength respectively. Although the results of shear strengths showed that the Mohr Coulomb envelopes were curves, for the stress ranges applied in this research, straight lines were assumed and fitted.

As these results, show the shear strengths of the specimens increase if the P'_c increases or OCR decreases. The existence of fissures resulted in the decrease of shear strengths. The material K displayed a higher strength than KB material for the sample P'_c, OCR, size and rate. Increasing the rate of shearing in locked or unlocked unfissured specimens resulted in the increase of shear strength. For fully fissured specimens, the increase of shearing rate did not increase significantly the shear strength. The unfissured unlocked specimens displayed higher shear strengths than

the unfissured locked specimens. By increasing the size of specimens, the shear strength decreased for both materials.

4.6 COMPARISON OF THE SHEAR STRENGTHS

The effect of different parameters on the peak shear strength and Mohr Coulomb parameters of the artificially overconsolidated clay specimens subjected to direct shear tests are discussed and the results are plotted or listed comparatively in the following subsections.

4.6.1 The Effect of P'_c on the Peak Shear Strength

The increase of P'_c resulted in the increase of density and this increased or improved the mechanical properties of the material. Therefore, the increase of P'_c for both material types increased the shear strengths.

The Mohr Coulomb envelopes for the peak shear strengths have been plotted in Figures (4.27)-(4.32) for KB specimens and in Figures (4.33)-(4.37) for K specimens.

As these two sets of figures show, two different behaviours have been observed for two different materials. Although the peak shear strengths and cohesions for both materials have increased as the p'_c increased, the friction angles for both materials have displayed different trends by increasing the P'_c. The friction angles of KB specimens have increased but on the contrary, the friction angles of K specimens have decreased.

For KB specimens, the normally consolidated lines did not pass from the centre of normal and shear stress coordinate axes; however, the intercepts (cohesion) were not significant (less than 10 kpa). The friction angle of the normally consolidated specimens (ϕ'_{NCL}) were greater than the friction angles obtained from the overconsolidated specimens (ϕ'_{OCL}) for different preconsolidation pressures. For fully fissured KB specimens, the intercepts for normally consolidated specimens were negligible and the friction angles of normally consolidated lines (ϕ'_{NCL}) were roughly the same as those of the overconsolidated lines (ϕ'_{OCL}). In other words, the effective peak cohesion (c'_p) and friction (ϕ'_p) of the fully fissured KB specimens showed

much less stress dependency than the effective peak c'_p and ϕ'_p of the unfissured KB specimens.

The normally consolidated lines (ϕ'_{NCL}) of K specimens also did not pass from the origin of the normal and shear stress axes. The intercepts of K specimens were significant and almost more than 30 kpa, even more for the fully fissured K specimens.

The friction angles of normally consolidated K specimens (ϕ'_{NCL}), for both unfissured and fully fissured unlocked specimens, were less than the friction angles of overconsolidated specimens (ϕ'_{OCL}) in contrast to KB specimens.

In both materials, the changes of the effective peak cohesion (c'_p) as result of the changes of preconsolidation pressure (P'_c) were more significant than the effective friction (ϕ'_p).

As these figures show, the envelopes of overconsolidated KB specimens for different preconsolidation pressures (P'_c) approached from the above to the normally consolidated line (NCL). On the contrary, the envelopes of overconsolidated K specimens for different preconsolidation pressures approached from below the NCL. However, for both types of materials, the extremity of ϕ'_{OCL} for overconsolidated lines by increasing the P'_c would be the same as ϕ'_{NCL} of the normally consolidated lines.

Figures (4.38) and (4.39) show the normally consolidated lines (NCLs) including the fully fissured unlocked, unfissured locked and unlocked KB specimens for 60 mm and 100 mm and Figures (4.40) and (4.41) show NCLs for the K specimens.

These figures show that by transferring the normally consolidated lines (NCLs) from fully fissured unlocked condition to unfissured locked condition and also from unfissured locked condition to unfissured unlocked condition, the c' and ϕ' both were increased. in other words, the effects of locked in horizontal stresses in the unfissured locked specimens and also fissure parameters in the partially or fully fissured unlocked specimens can be related to the Mohr Coulomb effective peak shear strength parameters of the unfissured unlocked specimens.

As these results show, c' and ϕ' have been changed by changing P'_c, whereas, the plastic index either for all the KB specimens or for all the K specimens has been constant. In other words, there is no relationship between plastic index and cohesion or friction angle for the specimens prepared of the same material type but different P'_c.

The extreme increase of c'_p and ϕ'_p for unfissured unlocked KB specimens or increase of c'_p and decrease of ϕ'_p for unfissured unlocked K specimens with the increase of P'_c would be limited to the magnitudes which they should be estimated based on the trends of the c'_p and ϕ'_p with P'_c for each particular size of specimen. These limits are discussed in Chapter 5.

4.6.2 The Effect of Specimen Size on the Peak Shear Strength

The peak effective shear strength parameters (c'_p and ϕ'_p) of the three different sizes of unfissured and fully fissured unlocked KB specimens consolidated by 330 kpa are listed in Table (4.13).

As this table shows, an increase in size decreased the shear strengths which mainly reduced the ϕ'_p rather than c'_p. The fully fissured unlocked specimens showed less size dependency than unfissured unlocked specimens. The extreme reductions of c'_p and ϕ'_p of unfissured specimens with an increase in the size of specimens would be limited to the magnitudes based on the trends of c'_p and ϕ'_p with size for the particular P'_c of the specimens. Theses limits have been discussed in Chapter 5.

4.6.3 The Effect of Horizontal Stresses on the Peak Shear Strength

This effect was investigated for both materials for three levels of preconsolidation pressures and for two sizes, 60 mm and 100 mm specimens. The ratios of the shear strengths of unfissured locked in horizontal stress specimens to unfissured unlocked in horizontal stress specimens, as well as the ratios for the Mohr Coulomb effective peak shear strength parameters, are listed in Table (4.14).

The ratio of one means no difference is observed between the shear strengths of the unfissured locked and unfissured unlocked specimens. If the reductions are less than

one, there are differences. This table shows that specimens prepared from KB were more sensitive to the disturbance as a result of releasing locked in horizontal stresses than specimens prepared from the K material. The increase in size for both materials resulted in the decrease of the ratios of shear strengths of unfissured locked specimens to shear strengths of the unfissured unlocked specimens.

This phenomenon is attributed to the increase of the disturbed volume for larger specimens as a result of releasing the horizontal locked in stresses. By increasing the size of specimens, the amount of the disturbed volumes increased. For example, if the disturbance as a result of releasing horizontal stresses affects the material of specimens to a depth of 5 mm, the volume affected for a specimen with dimensions of 60 mm by 60 mm by 20 mm would be 22 cm^3 (20×55×4×5) which is the product of the thickness of specimen × effective length of specimen × four sides × depth of disturbance. For a specimen 100 mm by 100 mm by 20 mm it would be 38 cm^3 (20×95×4×5) and for one 300 mm by 300 mm by 20 mm, it would be 118 cm^3 (20×295×4×5). Therefore, by releasing the locked in horizontal stresses, the smaller specimens would show less differences than the larger specimens.

Thus the ratios of locked in horizontal stress to unlocked in horizontal stress for the smaller specimens are greater than the ratios of the larger specimens. The KB specimens showed shear strength increases between 8%-12% and K specimens between 4%-6% as a result of releasing locked in horizontal stresses. Equations (4.5) and (4.6) display these results for KB and K specimens respectively.

$$\tau'_{unlocked} = \tau'_{locked}\,(1.08\text{-}1.12) \tag{4.5}$$

$$\tau'_{unlocked} = \tau'_{locked}\,(1.04\text{-}1.06) \tag{4.6}$$

4.6.4 The Effect of the Rate of Shearing on the Peak Shear Strength

The effect of the rate of shearing on peak shear strength has been reported in Table (4.15) , and on the Mohr Coulomb parameters in Table (4.16). By increasing the rate of shearing in the unfissured unlocked KB specimens, the negative pore pressure, as a result of interparticle suction, was developed along the shearing surfaces. This phenomenon resulted in a false increase in shear strength. As Table (4.15) shows, for

unfissured unlocked KB specimens, the effect of increase of rate was more significant than the unfissured locked KB specimens.

Specimens consolidated with lower preconsolidation pressure or sheared with lower normal stresses (higher OCR) showed higher increases of shear strength for the higher rates of shearing rather than the specimens consolidated with higher preconsolidation pressures or sheared with higher normal stresses (lower OCR). In other words, the percentages of the increase of shear strength for the higher rate sheared specimens consolidated and sheared with higher pressures, were less than the specimens consolidated and sheared with lower pressures. The impacts of increase of rate for fully fissured KB specimens and also unfissured locked KB specimens were negligible. These effects were not pronounced for unfissured unlocked K specimens either.

Figure (4.42) shows the effect of different rates of shearing on the peak shear strength of unfissured locked KB specimens with a size of 60 mm and consolidated and sheared with 330 kpa. For high rates of shearing an increase of a maximum of 6% was observed.

As K material is more permeable than KB material, the K specimens did not show significant increases of shear strengths with the applied fast rates of shearing. The fissured KB specimens also did not display pronounced increases of shear strengths as a result of higher rates because of the impact of the fissures in increasing the permeability of the specimens and therefore, reducing the effect of suction during the shearing process.

The unfissured locked KB specimens also were not affected significantly by the applied high rates. The clay particles in the unfissured locked specimens were more flattened, reorientated and behaved like the fully fissured specimens. The observed shear surfaces of unfissured locked specimens were relatively more smooth than those of unfissured unlocked KB specimens.

4.6.5 The Effect of Bedding Surfaces on the Peak Shear Strength

Specimens consolidated in two layers with the closed contact surfaces were designated as specimens with beddings. others prepared in one layer were considered without beddings. Table (4.17) lists the experimental results of these two types of specimens. As this table shows, the shear strengths of specimens prepared with bedding were about the same as the shear strengths of fully fissured specimens, with a little increase in shear strengths as the result of the roughness of the closed contact surfaces.

4.6.6 The Effect of Fissure Parameters on the Peak Shear Strength

Discontinued fissures or finite sized fissures have been created artificially along the shearing surfaces of the large specimens subjected to direct shear tests.

Three sizes of fissures with the same spacing were investigated to consider the effect in fissure widths. But the effect of spacing for the same width of fissure and fissure surface percentage was just investigated for two different spacings Although it was possible to prepare artificially another set of specimens with the same percentage of fissure surfaces and width of fissures, but different spacing, for the study of the effect of spacing of fissures, the accuracy of the results was highly affected and doubtful due to an increase in the disturbance of the material within the fissures in the closely fissured specimens. Moreover, a study of the effect of spacing for the widely spaced fissured specimens of a very large size (more than 300 mm) was neither feasible nor programmed in the scope of the experimental tests. Therefore, as discussed in Chapter 5, the numerical modellings with FLAC (Fast Lagrangian Analysis of Continua) have been used to investigate the effects of width and spacing of fissures on the shear strength parameters of the specimens subjected to direct shear tests.

4.6.6.1 The Effect of Width and Spacing of Fissures

The test results are listed in Table (4.18). This table shows an increase in the width of a fissure resulted in a decrease of shear strength. On the contrary, an increase in the spacing of fissures, increased the shear strength of the partially fissured specimens. Closely spaced fissured specimens behaved like the fully fissured specimens and the largely spaced fissured specimens behaved like the unfissured specimens.

Thus, for each width of fissure and size of specimen, there should be a maximum limit of spacing after which, the partially fissured specimen can be considered as an unfissured specimen and a minimum limit of spacing, which below that spacing the partially fissured specimen can be considered as a fully fissured specimen. Between these two limits, the spacing is meaningful and its effect should be determined. For these reasons, the size of specimen and choice of representative specimen are critical in determining the effective shear strength parameters of the naturally fissured clay masses.

Ignoring the effect of the spacing of fissures which influences the shear stress concentration and magnitude around the tips of fissures located along the shear surfaces, a simplified formulation has been suggested for the prediction of shear strength for the partially fissured unlocked specimens subjected to direct shear tests. The basic concept behind Equation (4.7) is the superposition of the material properties and shear strengths along the shear surfaces.

$$\tau_{pf} = \alpha_f \tau_f + (1 - \alpha_f) \tau_u \tag{4.7}$$

$$\alpha_f = \frac{nw}{l} \times 100 \tag{4.8}$$

In this equation, α_f is the percentage of fissure surfaces and dimensionless, τ_f is the shear strength of the fully fissured unlocked specimens, τ_u is the shear strength of the unfissured unlocked specimens for the same initial conditions with fully fissured unlocked specimens and n is the number of fissures in a specimen, w and l are width and length of fissure respectively. As can be seen in Equation (4.7), the effect of spacing, and preconsolidation pressures, size of specimen and strain softening behaviour have been ignored and require more investigation and development. The results of shear strength predicted by the this equation are also reported in Table (4.18).

4.6.6.2 The Effect of Orientation of Fissures

A few direct shear box specimens were prepared with a single inclined fissure with an angle of 45° to the direction of the shearing surfaces. The results are plotted comparatively in Figure (4.43) with results obtained from the unfissured unlocked

specimens for the same initial conditions. As this figure shows, no significant difference was observed. In other words, the direct shear box is not a useful apparatus for the study of the effect of inclination or orientation of fissures. In a plane strain direct shear box (standard direct shear box), the possibility of sliding along the inclined fissures was zeroed by the existence of two perforated or solid grid plates located at the top and bottom of the specimen. Moreover, the specimens in direct shear box failed in the shear mode rather than in the tension mode (tensile failure), because in the standard direct shear box, the specimens are constrained to fail along a predetermined plane of shear and failure is mainly dominated by the shear. Thus the opening of the discontinuous or continuous inclined fissures or sliding along the inclined fissures with the presence of the normal stresses in the inclined fissured overconsolidated clay specimens subjected to direct shear tests, were not possible. However, in Chapter 6 the effect of orientations of fissures, investigated experimentally on the triaxial fully or partially fissured specimens, is described.

4.6.7 The Effect of Direction of Shear on the Peak Shear Strength

In shearing the partially fissured unlocked specimens subjected to direct shear tests, there are two options for placing specimens in the box. In the first option, the direction of shearing was perpendicular to the length of the fissures and in the second it was parallel to the length of fissures. Different results were observed for two specimens prepared with the same specifications of materials, fissures and testing procedures including rates, normal stresses and OCR's, while they were sheared in two different directions.

The shear strengths of the specimens sheared parallel to the length of fissures were higher than those sheared perpendicular to the length of fissures. Figures (4.44) and (4.45) show the surfaces of the two specimens sheared in the two directions. As can be seen from the photos, the amplitudes or depth of uneven surfaces for the specimens sheared in a parallel direction (Figure 4.44) were higher than those of specimens sheared in a perpendicular direction (Figure 4.45). In other words, specimens sheared in a parallel direction had more chance of developing shear surfaces through the depth of the material than the specimens sheared in a perpendicular direction. In this phenomenon, the maximum length of the unfissured

parts of a partially fissured specimen or the widths of unfissured parts which are parallel to the direction of shearing, are very important and effective for the development of the shearing surfaces into the depth of specimen. Longer length means deeper depth of the unevenness of the shearing surfaces. It is obvious for deeper depth of unevenness in a specimen, the curved shearing surfaces will increase resulting in an increase of shearing force needed for moving and sliding the top shearing surface of the upper half over the bottom shearing surfaces of the lower half.

The results of the effect of the direction of shearing have been listed in Table (4.19). According to this table, the shear strengths for the specimens sheared in a parallel direction were greater than the specimens sheared in perpendicular direction for the same initial conditions of fissure, material and stress specifications.

It seems that for specimens sheared in a parallel and perpendicular direction, the spacings of the fissures are influential or meaningful.

4.7 THE RESIDUAL SHEAR STRENGTH RATIO AND PARAMETERS

The residual shear strength parameters for both KB and K for three different sizes for fully fissured, unfissured locked and unfissured unlocked specimens are reproduced in Tables (4.20))-(4.24). In these tables, the residual shear strength ratios (τ_r/P'_c) for the OCR of one are also listed.

The effects of P'_c, size and rate of shearing have been studied statistically on the residual shear strength ratios and parameters by calculating the mean and standard deviation values eg. as displayed in Table (4.24), the standard deviations of KB fully fissured unlocked specimens were less than those of the KB unfissured unlocked specimens which means that the KB fully fissured unlocked specimens showed much less dependency on that particular parameter of study which in this table was the effect of the rate of shearing on the residual shear strength ratios and parameters.

4.7.1 The Effect of P'_c on Effective Residual Shear Strength Ratio and Parameters

Table (4.25) shows the standard deviations of the residual strength ratios and effective residual shear strength parameters calculated for three levels of P'_c (330

kpa, 440 kpa and 660 kpa). The minimum standard deviations belonged to the effective residual shear strength ratios and parameters of the fully fissured KB and K specimens. In other words, the fully fissured specimens showed too much less stress dependency than the locked unfissured or unlocked unfissured specimens.

The unfissured locked specimens showed a small increase of effective residual friction angle in comparison to the unfissured unlocked specimens. This phenomenon might be related to the reorientation of the clay particles of the unfissured unlocked specimens and on the contrary, the increase of the disturbance of the clay particles in the unfissured locked specimens with the increase of shearing displacement.

4.7.2 The Effect of Size on Effective Residual Shear Strength Ratio and Parameters

The effect of size on the effective residual shear strength ratios and parameters can be seen in Tables (4.26) and (4.27), for fully fissured and unfissured KB specimens consolidated with 330 kpa respectively.

The KB fully fissured specimens showed too much less size dependency than the KB unfissured specimens. In other words at residual, the shear strength ratios and parameters show size independency.

4.7.3 The Effect of Rate of Shearing on Residual Shear Strength Ratio and Parameters.

Tables (4.28) and (4.29) show the statistical evaluations of the effect of the rate of shearing on the residual shear strength ratios and parameters of the specimens consolidated with 330 kpa and a size of 60 mm for the fully fissured and unfissured unlocked KB and K specimens respectively.

The fully fissured specimens at residual showed much less standard deviation with a change of rate of shearing than the unfissured specimens and also the K fully fissured specimens showed less change in the residual shear strength ratios and parameters than the KB fully fissured specimens. This finding can be related to the higher permeability of the K material than the KB material.

4.7.4 Changes of Moisture Content on the Residual Shear Strength

The water content of the specimens at residual depends on preconsolidation pressure, normal stress during shearing and type of clay mineral in drained tests and additionally, the rate of shearing in the undrained tests. Thus, for the Mohr Coulomb effective residual shear strength parameters, different water contents for each specimen sheared with different normal stresses, would be expected. For undrained tests (undrained unconsolidated tests), however, it is possible to have the same water content for the specimens sheared with different normal stresses if the normal stresses are applied very quickly and there is no time for the absorption of water from the container of the shear box or intrusion of water into the specimens. Thus, in drained test, the water content of the specimens consolidated with the same p'_c and sheared with the same rate of shearing and residual would give different water contents for different OCR's.

4.8 THE EFFECT OF TYPE OF WATER

Taking into account the nature of the mineral composition of these two types of clays used in this research, it was necessary to investigate the influence of the type of water used in the preparation of the pastes of these clays and also for testing the specimens. A few specimens of both materials (K and KB) were prepared and tested with distilled water and the results are reported in Table (4.30). In this table, the results of specimens prepared and tested with tap water are listed. No significant difference was observed. The PH of both types of water were measured./ Both types of water were nearly neutralise or somewhat with a PH $\leq$ 7, whereas the presence of some elements like sodium chloride in the solution can influence the shear strength of the clayey materials which require a PH greater than 7.

4.9 THE EFFECT OF THE NUMBER OF REPETITION OF EACH TEST

Great care was given over each test and the factors which influenced the scattering of the results such as type of material, water content of powders and pastes, procedures for mixing of the powders, preparation and curing of the pastes, shaping, loading or consolidating, and shearing of the specimens. Moreover, factors such as the temperature at the time of preparation, the curing of the pastes, storing the specimens

or consolidating and finally shearing, were monitored and carefully controlled to minimise the scattering the results of the specimens tested for the same initial conditions. However, systematic errors as a result of the accuracy of the data logging system, load cell and transducer calibrations, and possibly unknown factors, have been investigated on the effective shear strengths of the different specimens and are reported in Table (4.31). This table also displays the statistical evaluation of the results obtained from the repetitions of some of tests for different specimen sizes and preconsolidation pressures.

The type of distribution of the test repetition would be bell-shaped or normal distribution with negligible standard deviations ranging between 0.7 and 3. As this table shows, the standard deviations for KB specimen were smaller than those of K specimens for the same size and P'_c. By increasing the size, the standard deviations decreased. On the contrary, by increasing the P'_c, the standard deviations increased.

For the engineering design of Mohr Coulomb parameters, at least three repetitions for each test are recommended, but taking into account the number of parameters that should have been investigated experimentally in this research and also paying careful attention to the preparation of the materials, pastes, curing the pastes, shaping, consolidating and shearing the specimens which had direct impact on the scattering of the results and also the negligible amount of variation as a result of systematic errors or unknown factors, the result of one specimen test or one repetition for each case was taken into consideration for further analysis. However, in each case, there were many mechanisms for controlling the results, such as a comparison between the results obtained for different OCR's, rates, sizes, and preconsolidation pressures and whenever some result were suspicious or the trends were not acceptable or reasonable, tests were repeated to obtain reasonable results or to discover the real behaviour expected from such cases.

4.10 DISCUSSION AND CONCLUSION

The effects of parameters such as type of clay material, preconsolidation pressure , size of specimen, situation of the horizontal stresses, rate of shearing, bedding in the specimens, and fissure parameters like width, spacing and orientation, have been investigated experimentally on the artificially prepared materials and specimens in

the laboratory by utilising the standard direct shear test for three different sizes of specimens.

An increase of P'_c resulted in an increase of the effective peak and residual shear strength of both materials. But in detail the increase of P'_c resulted in the increase of the effective peak shear strength parameters (c'_p & ϕ'_p) mainly and the effective residual shear strength parameters (c'_r & ϕ'_r) somehow in the unfissured locked or unlocked KB specimens.

In the fully fissured unlocked KB specimens, the increase of P'_c increased the effective peak shear strength parameters and did not have any significant influence on the effective residual shear strength parameters of the fully fissured unlocked KB specimens.

In the unfissured locked or unlocked K specimens, the increase of P'_c increased c'_p and c'_r and decreased the ϕ'_p and ϕ'_r. In the fully fissured unlocked K specimens, the increase of P'_c increased the c'_p and decreased ϕ'_p, but had no significant impact on the c'_r & ϕ'_r of the fully fissured unlocked K specimens.

The extreme points of the changes of the c'_p & ϕ'_p by increasing the P'_c can be estimated from the trends of the graphs of c'_p & ϕ'_p with P'_c for each particular specimen size .

The increase in size of specimens for each constant prescribed preconsolidation pressure decreased the effective peak and residual shear strengths of both materials. The increase in size resulted in the decrease of c'_p & ϕ'_p of the unfissured locked or unlocked KB and K specimens mainly and the c'_r & ϕ'_r of the unfissured locked and unlocked KB and K specimens somewhat. But in the fully fissured locked KB and K specimens, the increase in size decreased the c'_p & ϕ'_p of the specimens and did not have any influence on the c'_r & ϕ'_r of the fully fissured unlocked KB and K specimens. The extreme reductions of the c'_p & ϕ'_p for the unfissured unlocked KB and K specimens should have been estimated by the results of the changes of c'_p & ϕ'_p with size for each prescribed preconsolidation pressure.

The effect of locked in horizontal stresses can be applied through the reduction functions or factors on the effective peak shear strength parameters of the unfissured unlocked specimens. Both materials showed that by increasing the shearing displacements, the differences between the unlocked and locked in horizontal stresses decreased. In other words at residual, this effect is negligible.

An increase in the rate of shearing increased the shear strength of the unfissured unlocked specimens, but it did not influence the peak shear strengths of the fully fissured unlocked specimens significantly.

In the fully fissured unlocked specimens, the increase in the rate of shearing did not have any effect on the residual shear strengths.

The effect of rate of the shearing can be applied as functions or factors on the effective peak shear strength parameters of the unfissured unlocked specimens.

For any particular size in the partially fissured unlocked specimens, an increase in width of fissures decreased the effective peak shear strength of the specimens. On the contrary, the increase of spacing increased the effective peak shear strength for that particular size.

There are two limits of spacing for each size and width of specimen before the minimum limit of spacing. The partially fissured specimen behaves like a fully fissured specimen and after the maximum limit of spacing, it behaves like an unfissured specimen. These limits can be defined from the trends of the changes of peak shear strength with spacing experimentally on very large specimens or numerically by modelling the partially fissured specimens.

Testing the very large specimens was not within the scope of this research but a numerical study of the effect of width and spacing of the fissures in the partially fissured specimens has been one of the objectives of the following chapter.

The inclined fissured specimens subjected to direct shear test did not show any impact of the inclination of fissure on the shear strength. Thus this effect is covered and described in Chapter 6 in the partially and fully fissured triaxial specimens.

In the partially fissured specimens, the direction of shearing with respect to the length of fissures was important. The specimens sheared parallel to the length of fissures showed an increase of effective peak shear strength rather than those sheared perpendicularly to the length of fissure for the same initial conditions including material, size, and fissure specification.

The type of the water used in the research did not have any significant change on the effective shear strength.

The residual shear strength parameters (c'_r & ϕ'_r) of the fully fissured unlocked specimens did not show any change with an increase in the P'_c, size and rate of shearing.

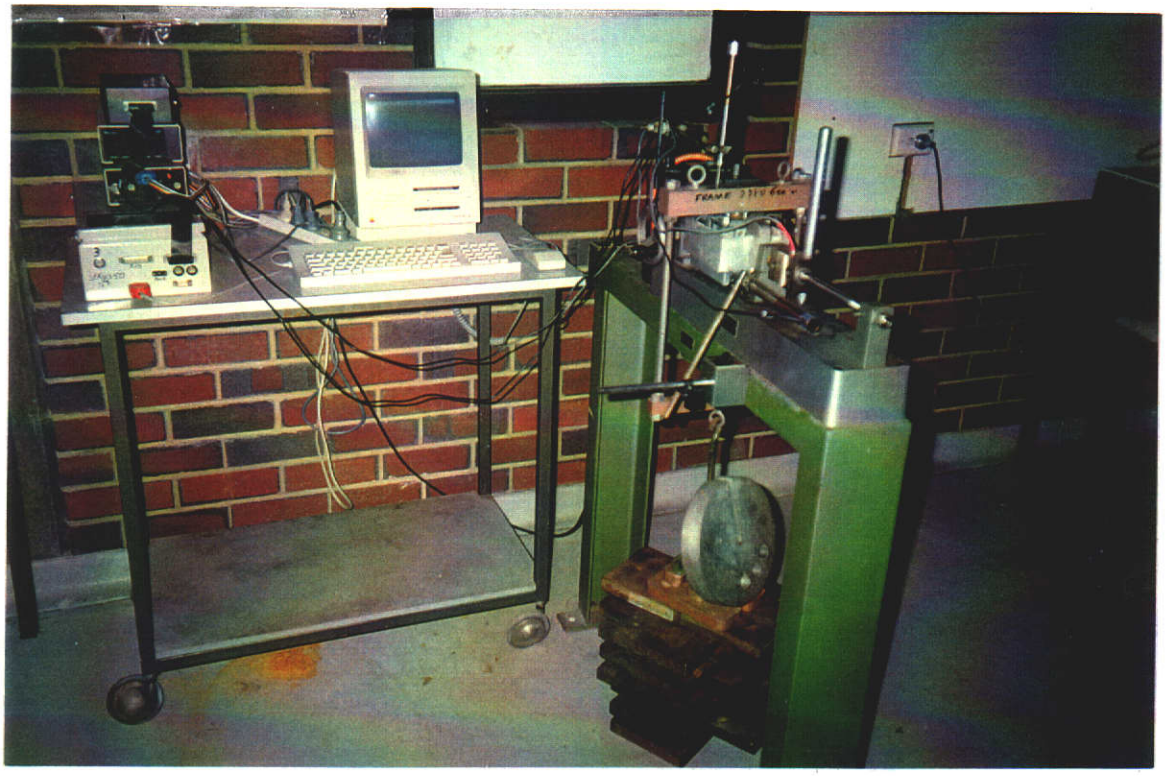

Figure (4.1): Illustration of the small direct shear machine used for the specimens with a size of 60 mm.

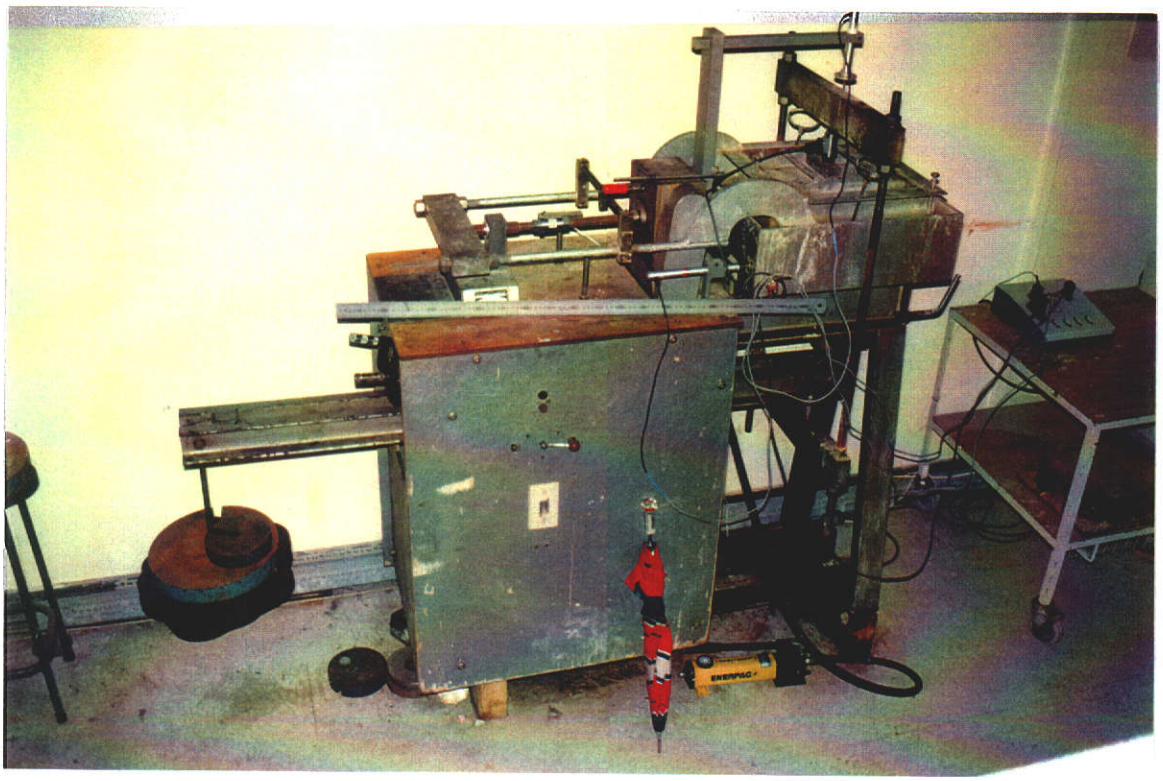

Figure (4.2): Illustration of the large direct shear machine used for the specimens with a size of 300 mm.

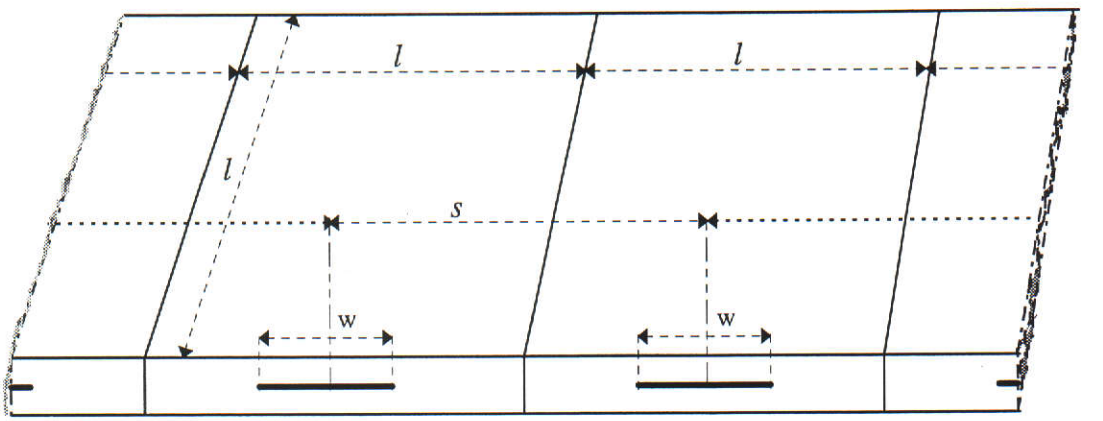

Figure (4.3): Schematical illustration for the definition of the width (w) and spacing (*s*) of the fissures.

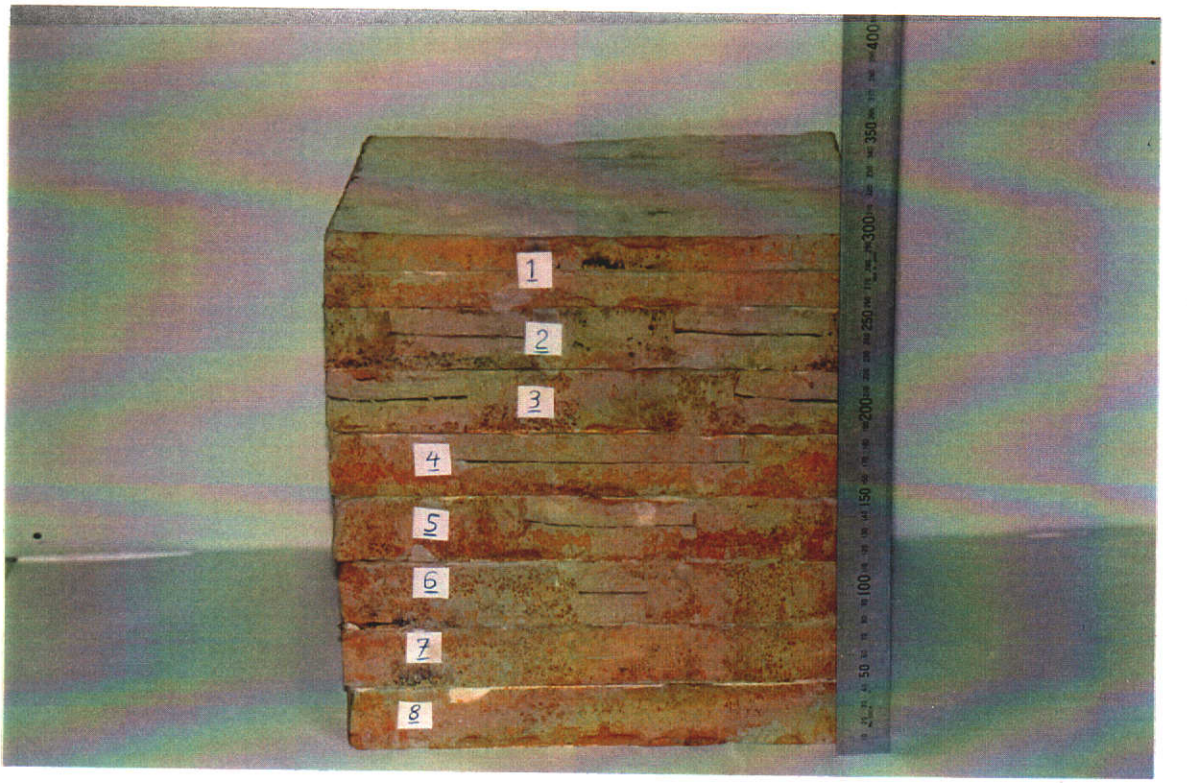

Figure (4.4): Illustration of different types of large KB specimens; ① is fully fissured unlocked specimen, ② is partially fissured unlocked specimen with w= 75 mm, s= 150 mm and α_f= 50%; ③ is partially fissured unlocked specimen with w = 75 mm, s= 225 mm, and α_f= 50%;; ④is partially fissured specimen with w = 150 mm, s = 300 mm and α_f= 50%; ⑤is partially fissured unlocked specimen with w= 90 mm, s = 300 mm, and α_f= 30%; ⑥ is partially unlocked specimen with w = 30 mm, s = 300 mm, and α_f= 10%; ⑦ is unfissured unlocked specimen with bedding, ⑧ is unfissured unlocked specimen without bedding.

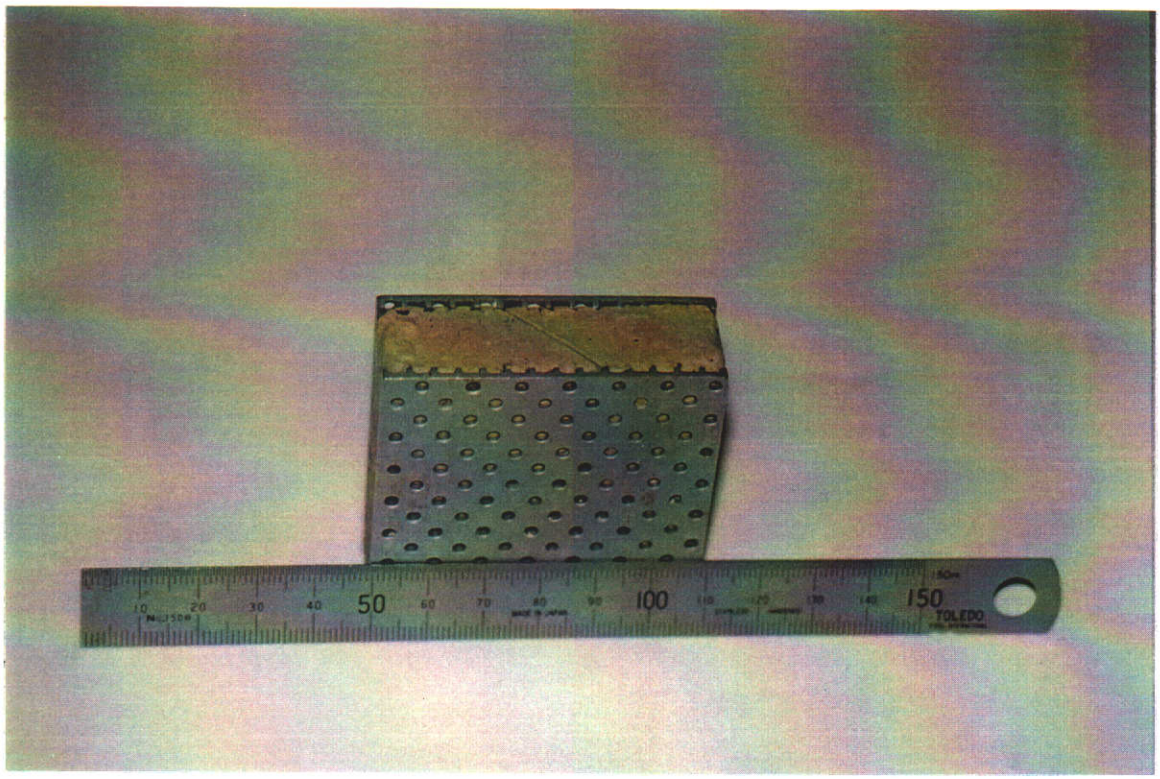

Figure (4.5): Illustration of an inclined fissured small KB specimen with an angle of 45 °.

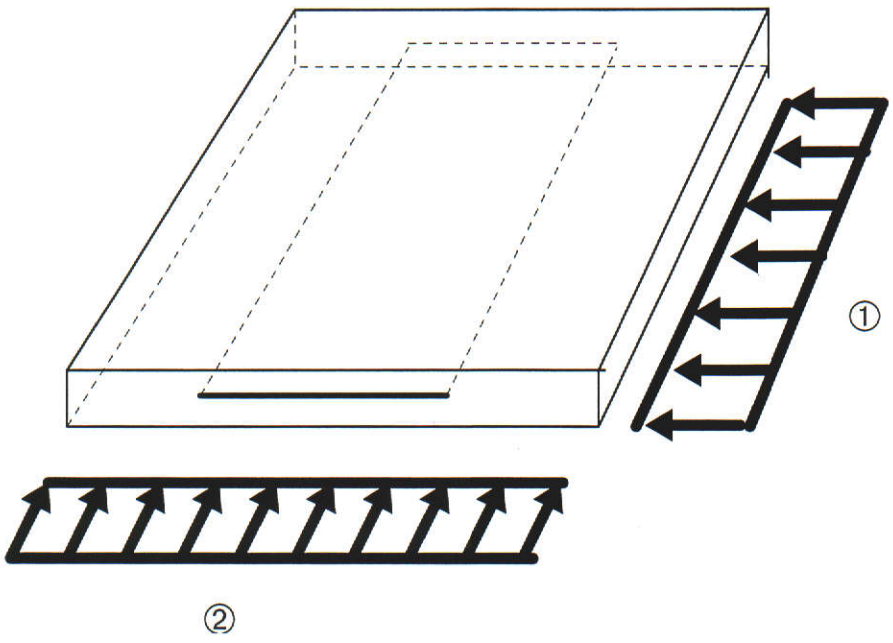

Figure (4.6): Schematical illustration of the both direction of shearings,. Direction ① is perpendicular to the fissure length and direction ② is parallel to the fissure length.

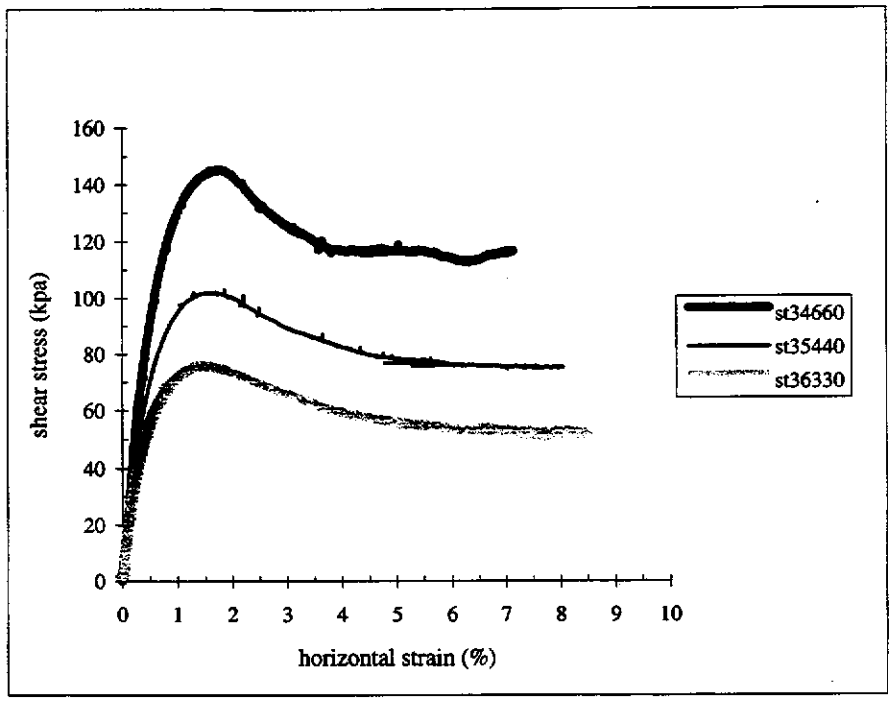

Figure (4.7): The stress strain curves of the 100 mm unfissured unlocked KB specimens consolidated and sheared with three different pressures of 330 kpa, 440 kpa and 660 kpa and rate of 0.005 mm/min.

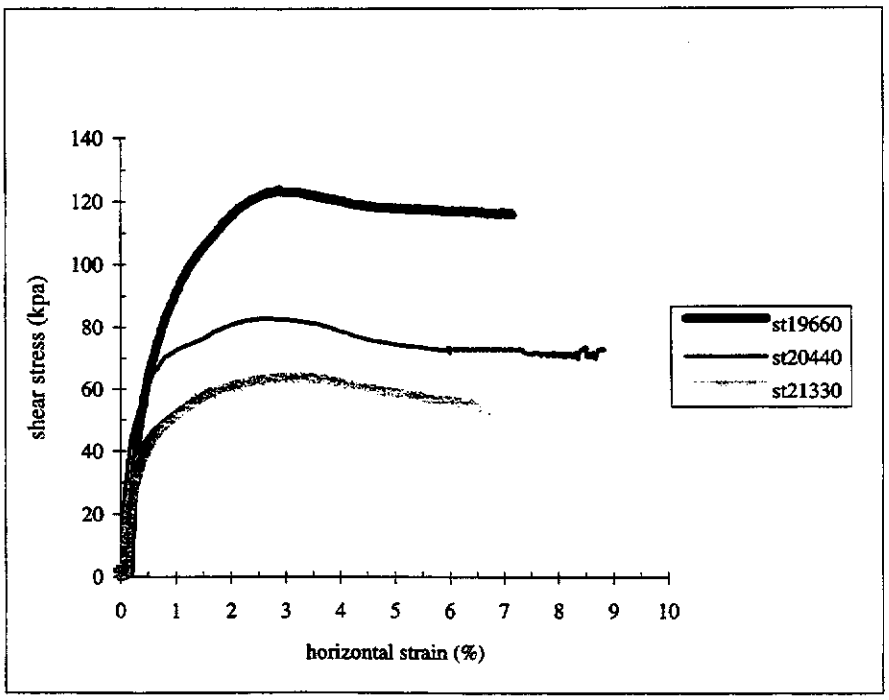

Figure (4.8): The stress strain curves of the 100 mm unfissured locked KB specimens consolidated and sheared with three different pressures of 330 kpa, 440 kpa and 660 kpa and rate of 0.005 mm/min.

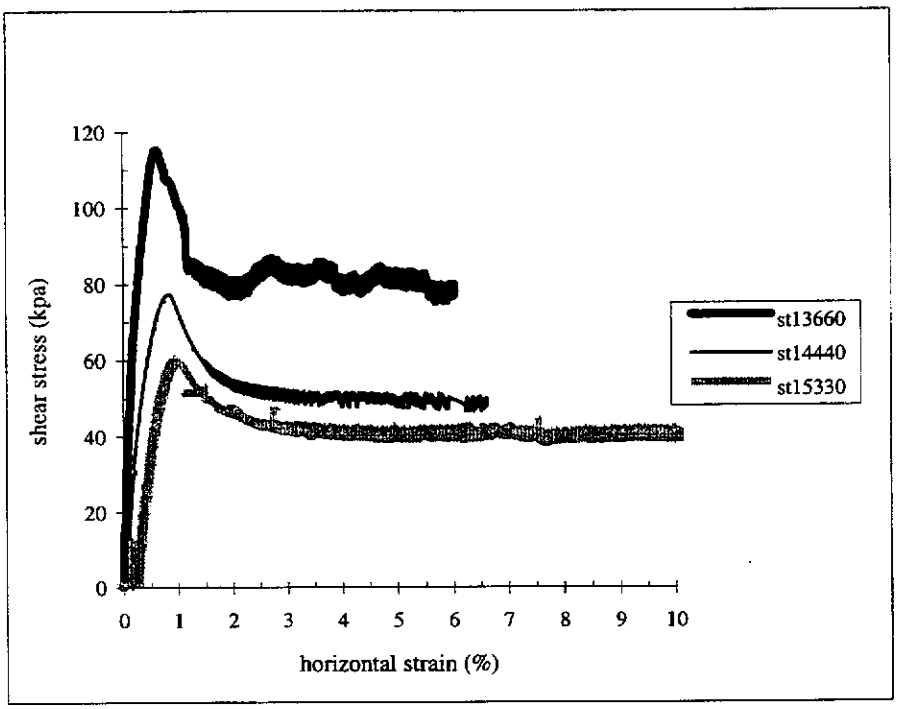

Figure (4.9): The stress strain curves of the 100 mm fully fissured unlocked KB specimens consolidated and sheared with three different pressures of 330 kpa, 440 kpa and 660 kpa and rate of 0.005 mm/min.

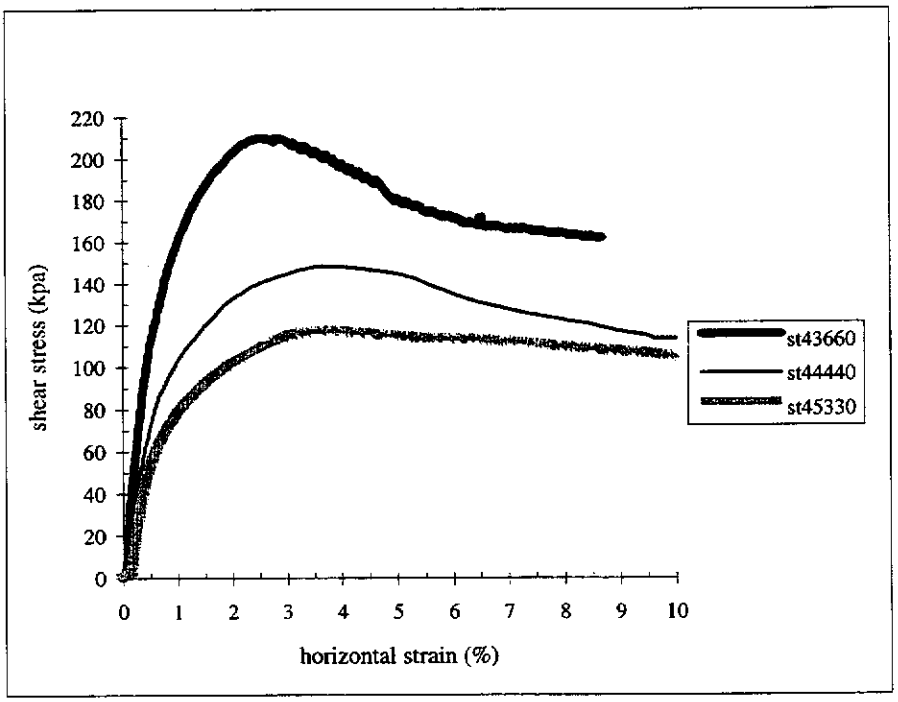

Figure (4.10): The stress strain curves of the 100 mm unfissured unlocked K specimens consolidated and sheared with three different pressures of 330 kpa, 440 kpa and 660 kpa and rate of 0.005 mm/min.

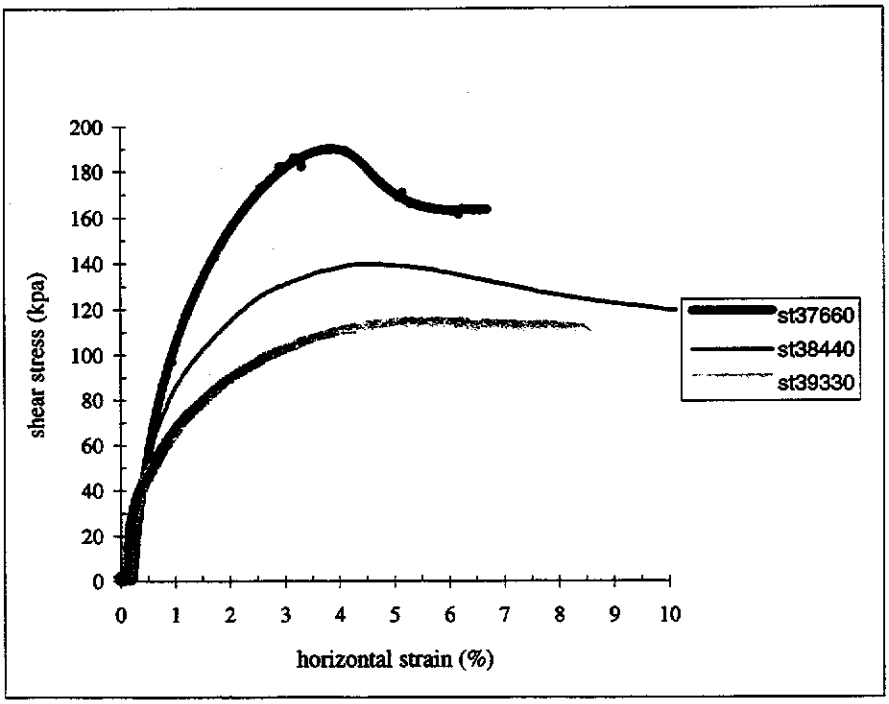

Figure (4.11): The stress strain curves of the 100 mm unfissured locked K specimens consolidated and sheared with three different pressures of 330 kpa, 440 kpa and 660 kpa and rate of 0.005 mm/min.

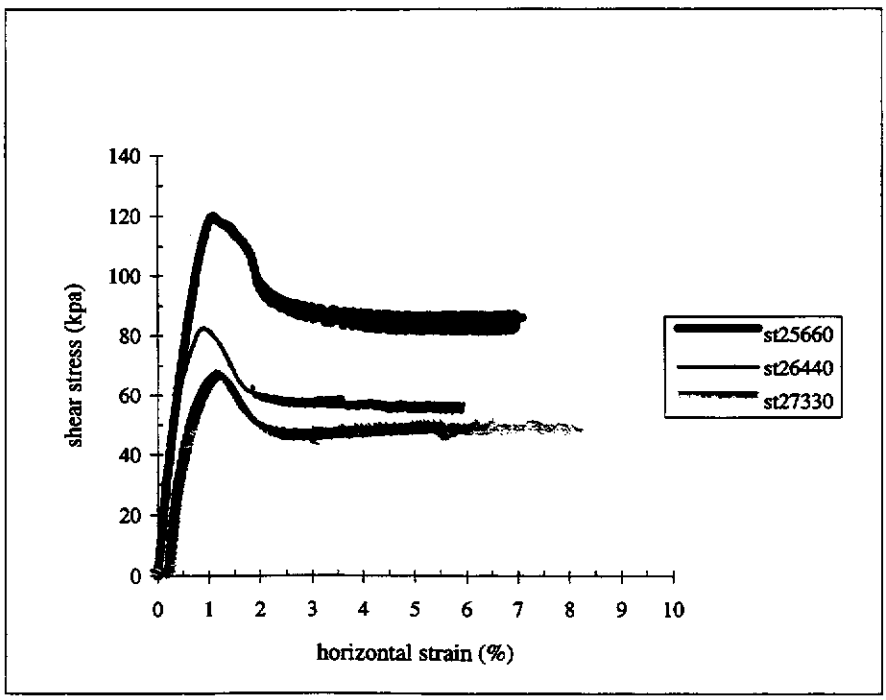

Figure (4.12): The stress strain curves of the 100 mm and 50% fissured unlocked KB specimens consolidated and sheared with three different pressures of 330 kpa, 440 kpa and 660 kpa and rate of 0.005 mm/min.

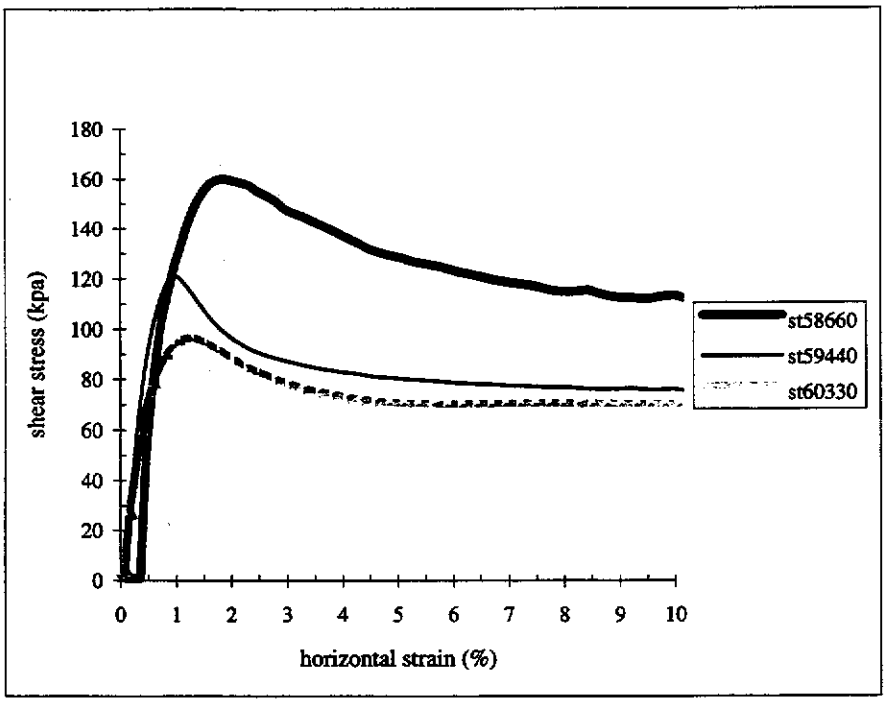

Figure (4.13): The stress strain curves of the 100 mm unfissured unlocked KB specimens consolidated and sheared with three different pressures of 330 kpa, 440 kpa and 660 kpa and rate of 0.185 mm/min.

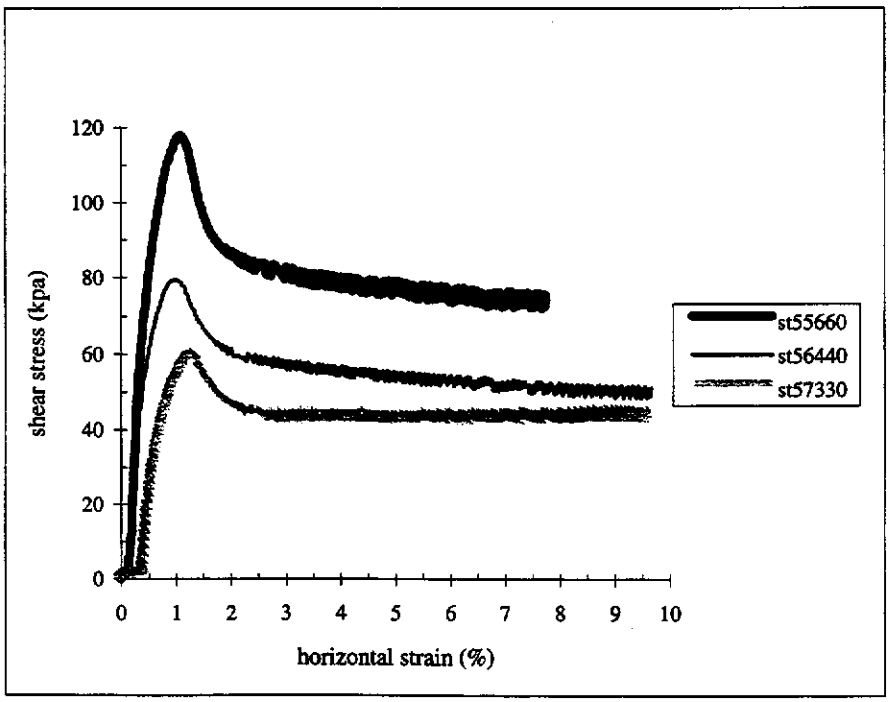

Figure (4.14): The stress strain curves of the 100 mm fully fissured unlocked KB specimens consolidated and sheared with three different pressures of 330 kpa, 440 kpa and 660 kpa and rate of 0.185 mm/min.

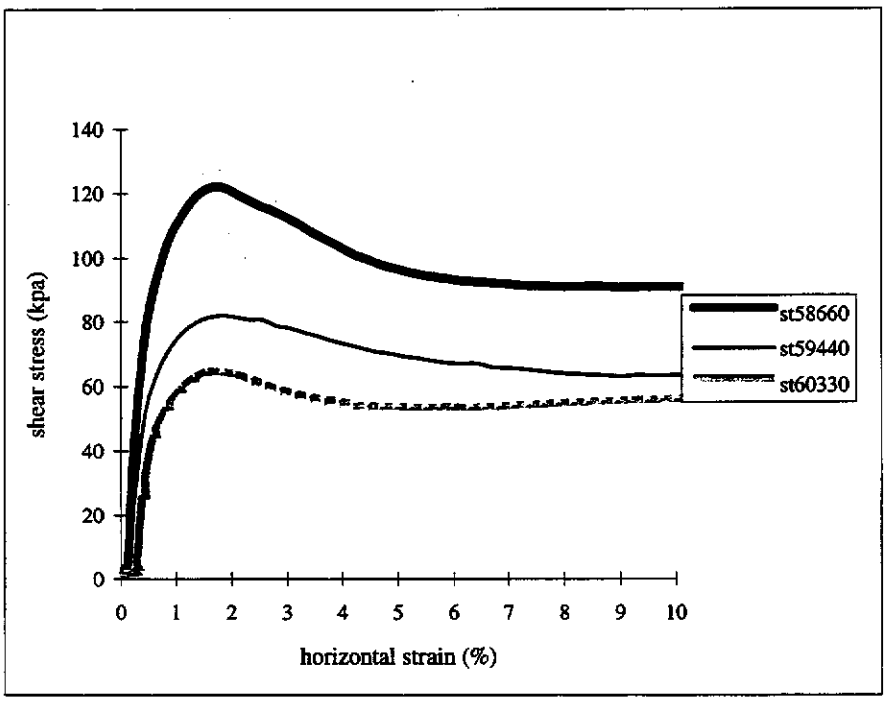

Figure (4.15): The stress strain curves of the 100 mm unfissured locked KB specimens consolidated and sheared with three different pressures of 330 kpa, 440 kpa and 660 kpa and rate of 0.185 mm/min.

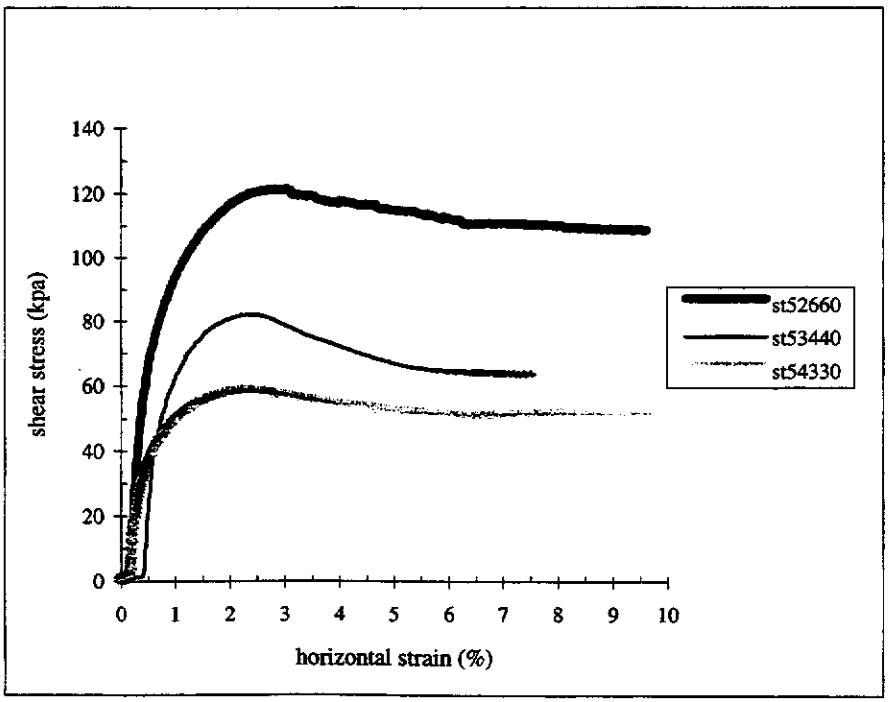

Figure (4.16): The stress strain curves of the 100 mm unfissured locked KB specimens consolidated and sheared with three different pressures of 330 kpa, 440 kpa and 660 kpa and rate of 0.01 mm/min.

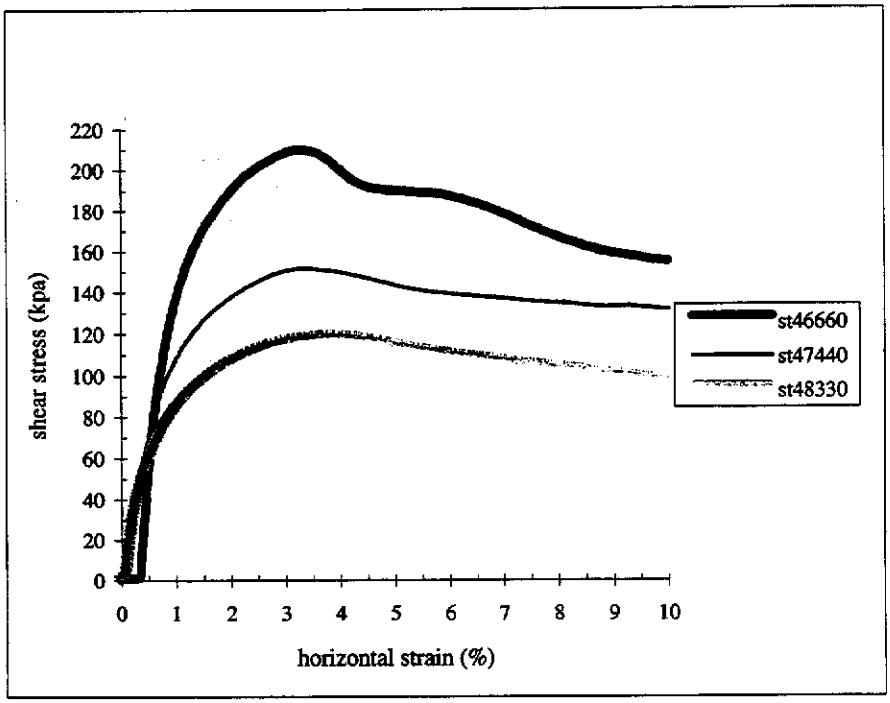

Figure (4.17): The stress strain curves of the 100 mm unfissured unlocked K specimens consolidated and sheared with three different pressures of 330 kpa, 440 kpa and 660 kpa and rate of 0.01 mm/min.

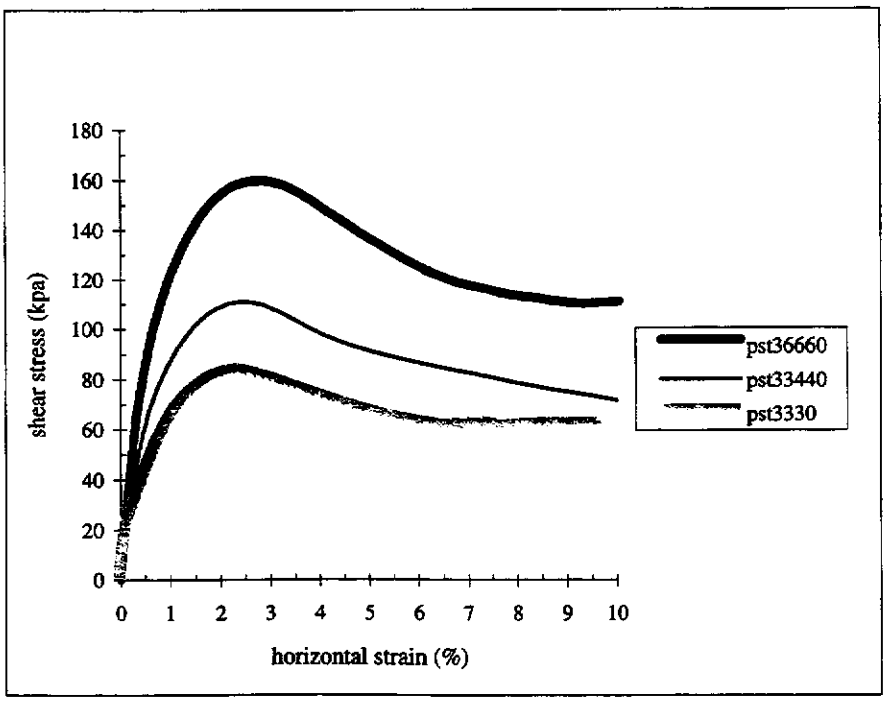

Figure (4.18): The stress strain curves of the 60 mm unfissured unlocked KB specimens consolidated and sheared with three different pressures of 330 kpa, 440 kpa and 660 kpa and rate of 0.0033 mm/min.

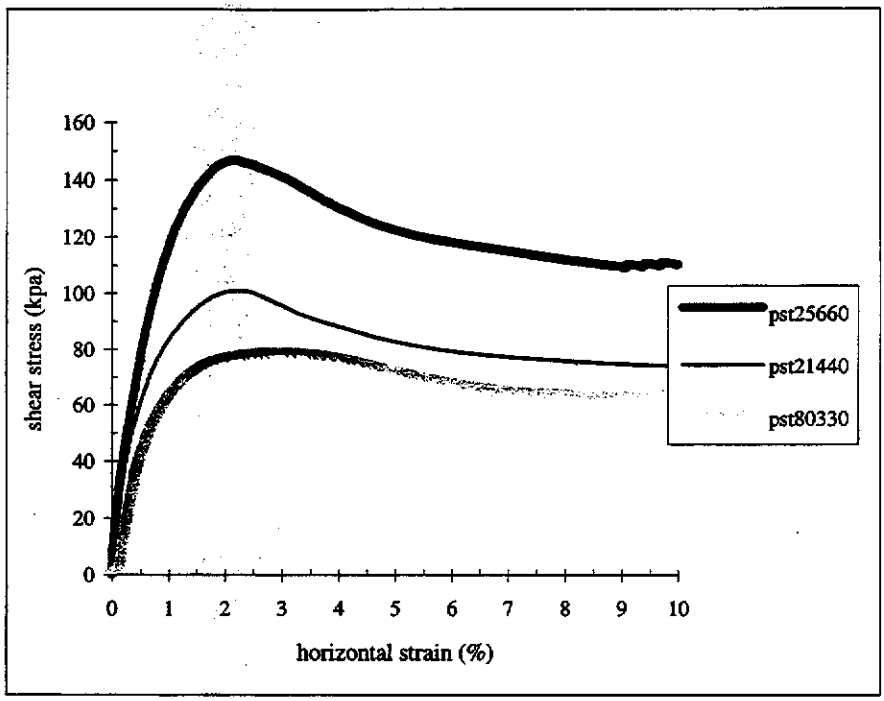

Figure (4.19): The stress strain curves of the 60 mm unfissured locked KB specimens consolidated and sheared with three different pressures of 330 kpa, 440 kpa and 660 kpa and rate of 0.0033 mm/min.

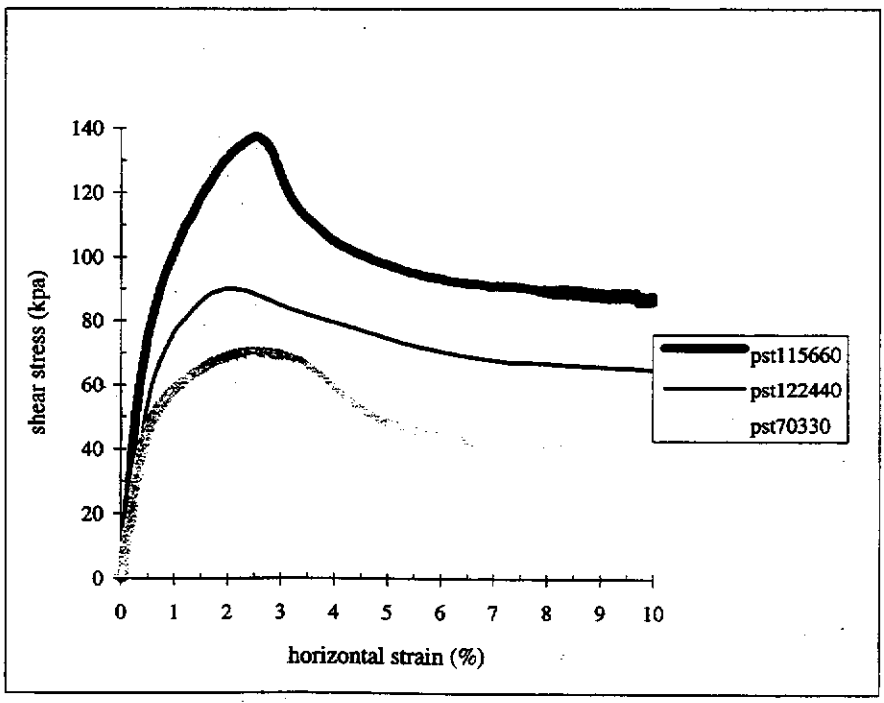

Figure (4.20): The stress strain curves of the 60 mm fully fissured unlocked KB specimens consolidated and sheared with three different pressures of 330 kpa, 440 kpa and 660 kpa and rate of 0.0033 mm/min.

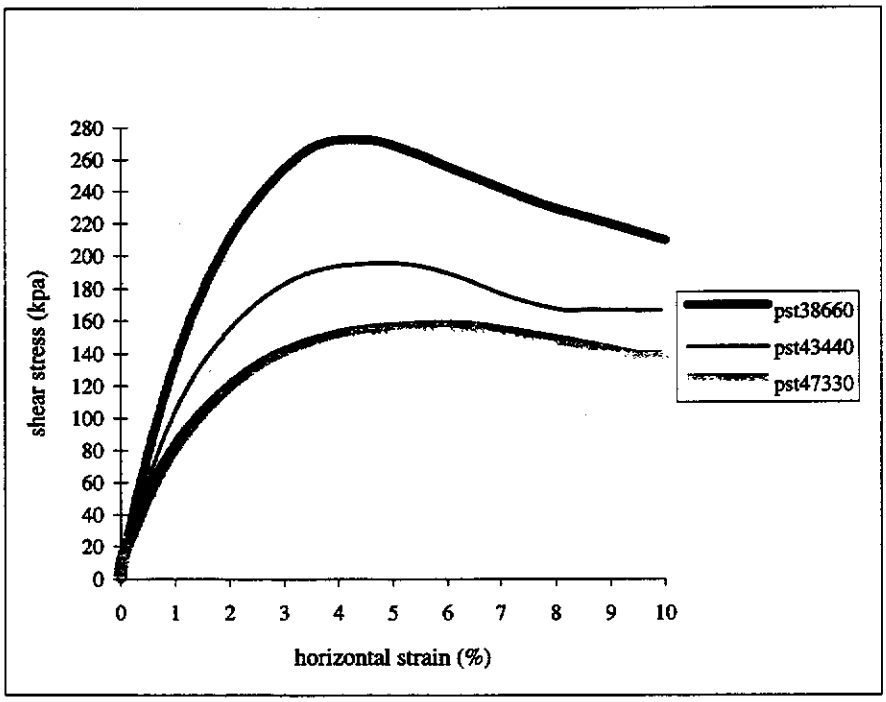

Figure (4.21): The stress strain curves of the 60 mm unfissured unlocked K specimens consolidated and sheared with three different pressures of 330 kpa, 440 kpa and 660 kpa and rate of 0.0033 mm/min.

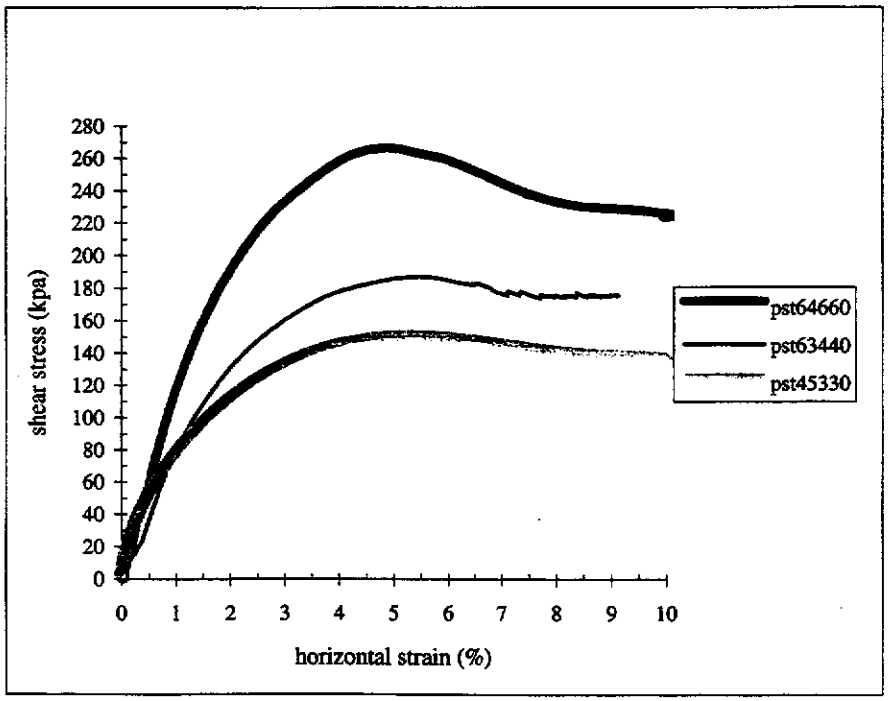

Figure (4.22): The stress strain curves of the 60 mm unfissured locked K specimens consolidated and sheared with three different pressures of 330 kpa, 440 kpa and 660 kpa and rate of 0.0033 mm/min.

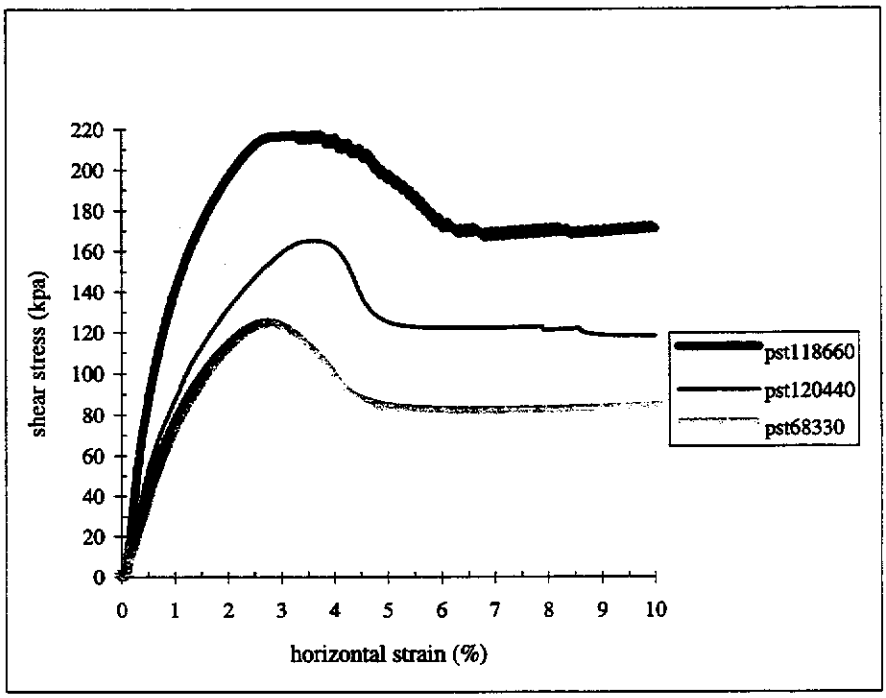

Figure (4.23): The stress strain curves of the 60 mm fully fissured unlocked K specimens consolidated and sheared with three different pressures of 330 kpa, 440 kpa and 660 kpa and rate of 0.0033 mm/min.

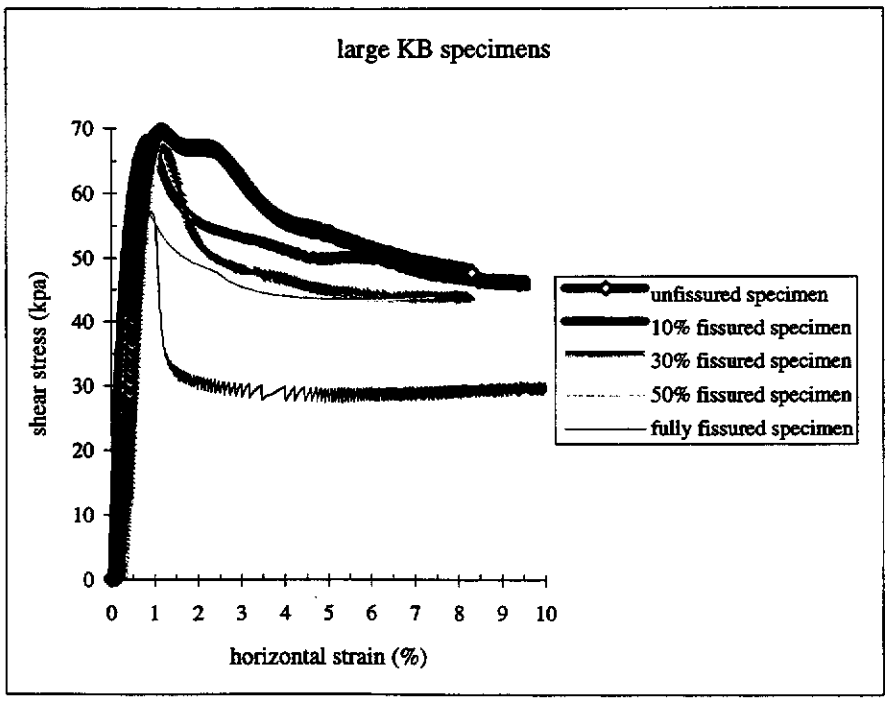

Figure (4.24): The stress strain curves of the 300 mm unfissured, fully, and partially fissured unlocked KB specimens consolidated and sheared with pressure of 330 kpa and rate of 0.005 mm/min.

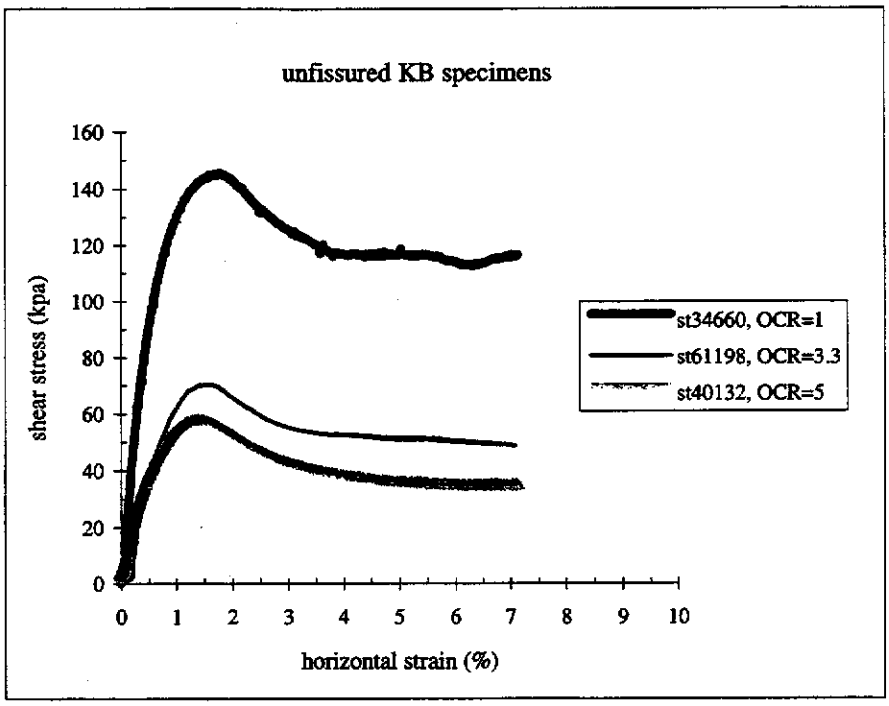

Figure (4.25): The stress strain curves of the 100 mm unfissured unlocked KB specimens consolidated with 660 kpa and sheared with three different OCR's of 1, 3.3 and 5 and rate of 0.005 mm/min.

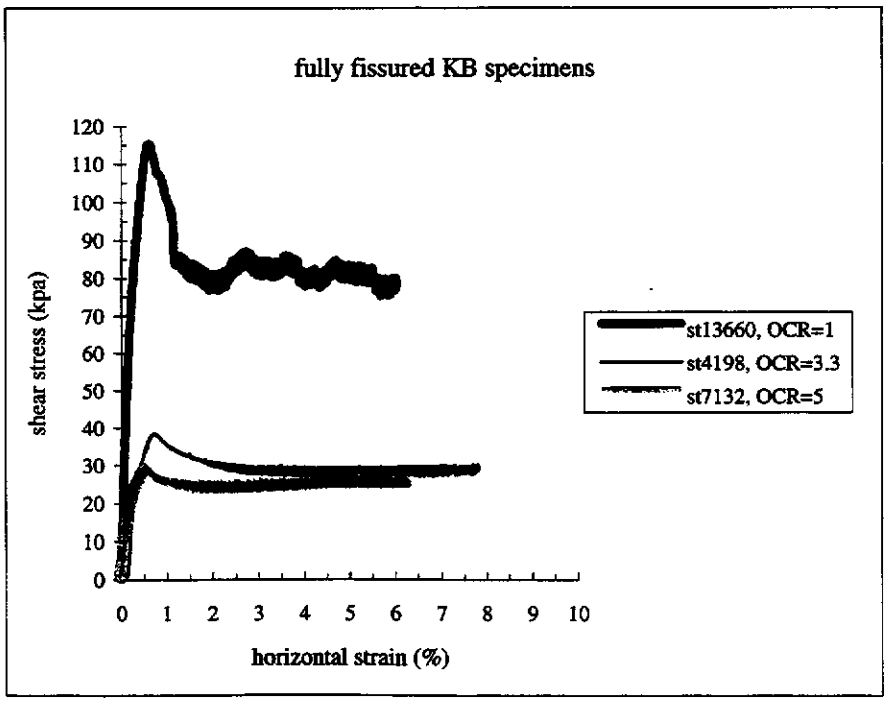

Figure (4.26): The stress strain curves of the 100 mm fully fissured unlocked KB specimens consolidated with 660 kpa and sheared with three different OCR's of 1, 3.3 and 5 and rate of 0.005 mm/min.

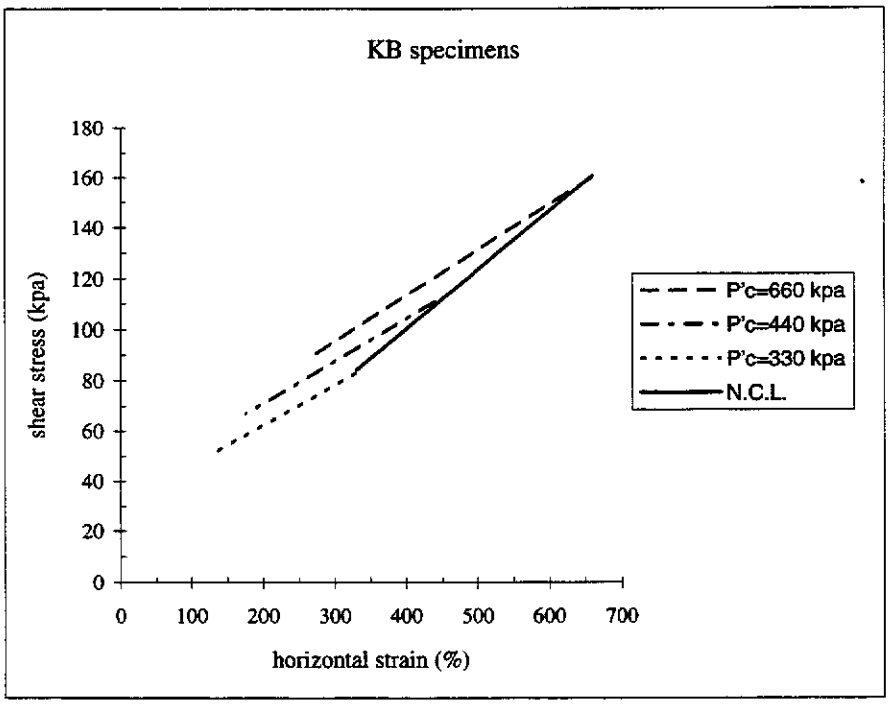

Figure (4.27): The Coulomb envelopes and normally consolidated line of the 60 mm unfissured unlocked KB specimens and sheared with a rate of 0.0033 mm/min.

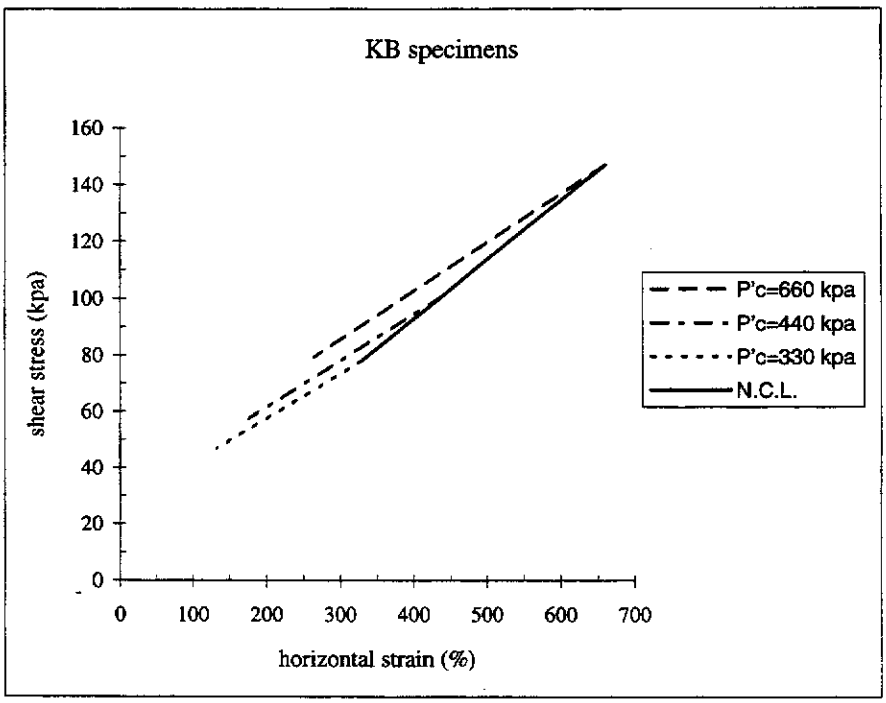

Figure(4.28): The Coulomb envelopes and normally consolidated line of the 60 mm unfissured locked KB specimens and sheared with a rate of 0.0033 mm/min.

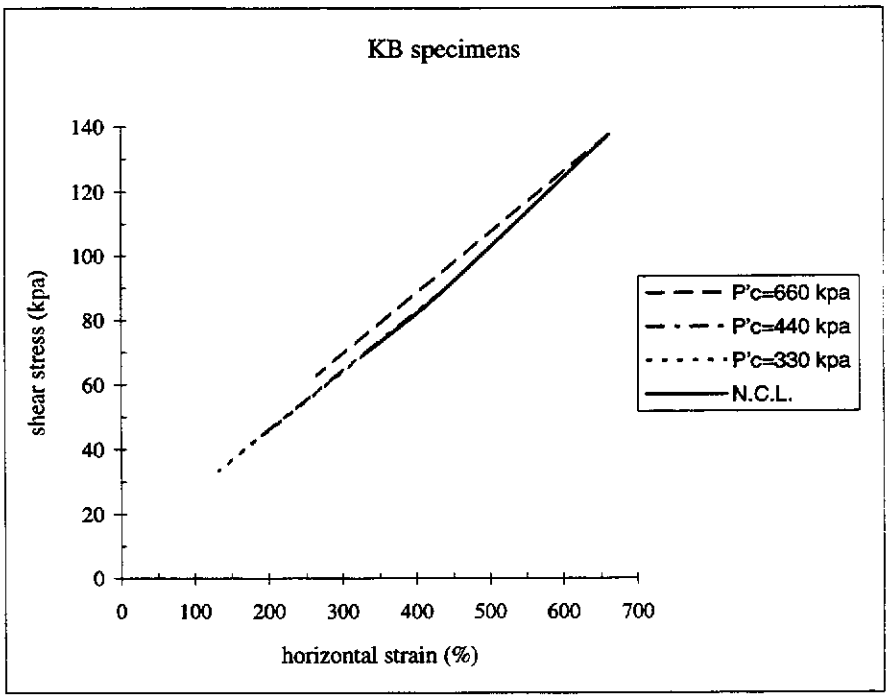

Figure (4.29): The Coulomb envelopes and normally consolidated line of the 60 mm fully fissured unlocked KB specimens and sheared with a rate of 0.0033 mm/min.

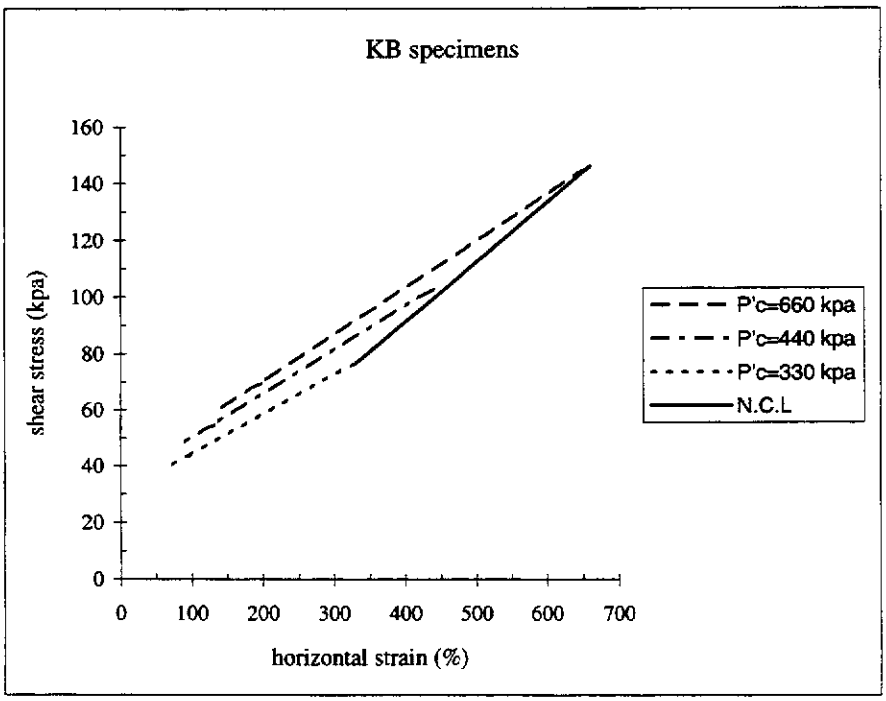

Figure (4.30): The Coulomb envelopes and normally consolidated line of the 100 mm unfissured unlocked KB specimens and sheared with a rate of 0.005 mm/min.

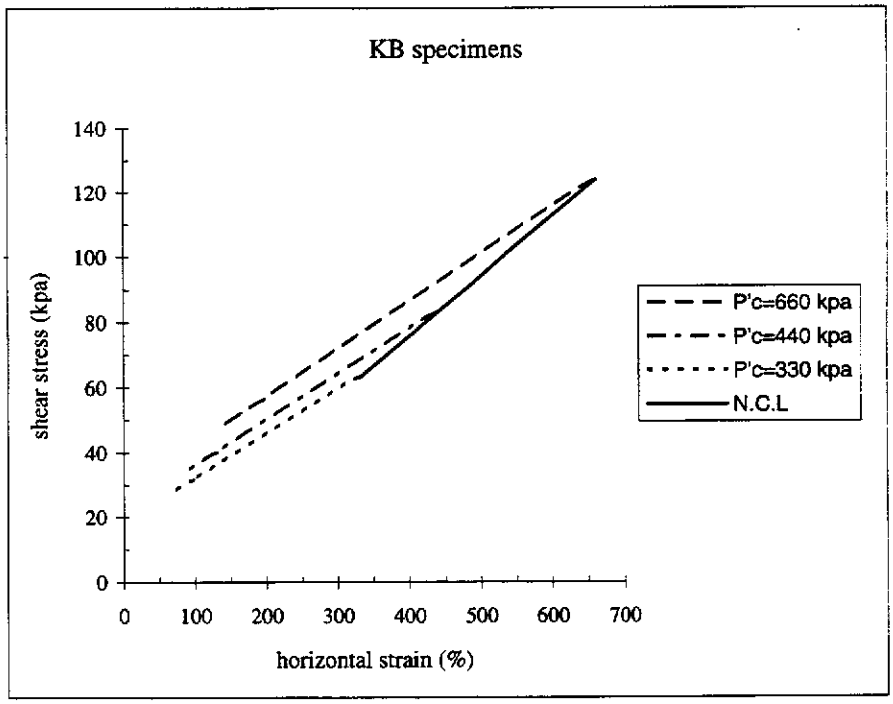

Figure (4.31): The Coulomb envelopes and normally consolidated line of the 100 mm unfissured locked KB specimens and sheared with a rate of 0.005 mm/min.

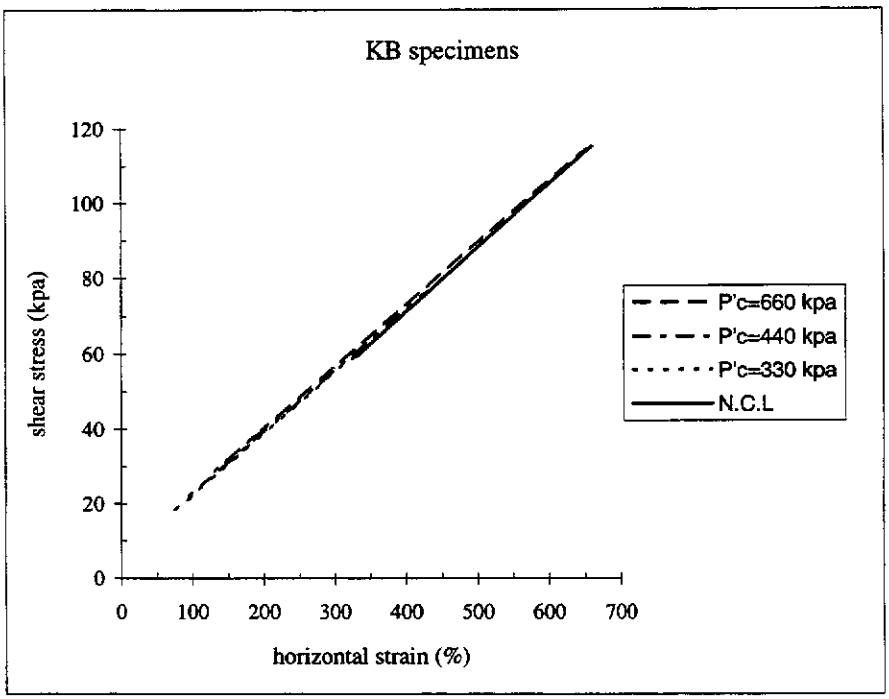

Figure (4.32): The Coulomb envelopes and normally consolidated line of the 100 mm fully fissured unlocked KB specimens and sheared with a rate of 0.005 mm/min.

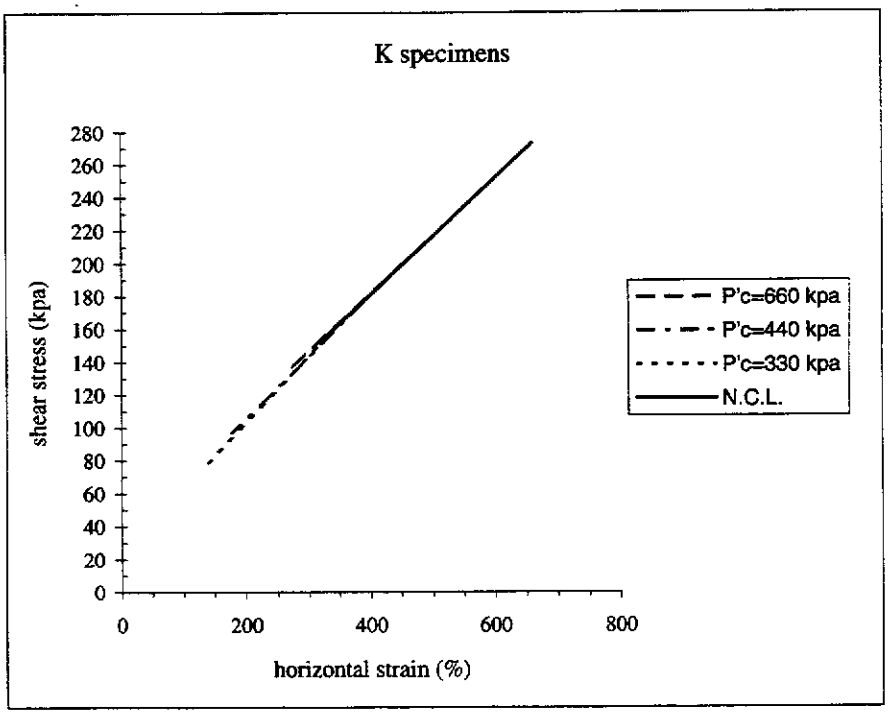

Figure (4.33): The Coulomb envelopes and normally consolidated line of the 60 mm unfissured unlocked K specimens and sheared with a rate of 0.0033 mm/min.

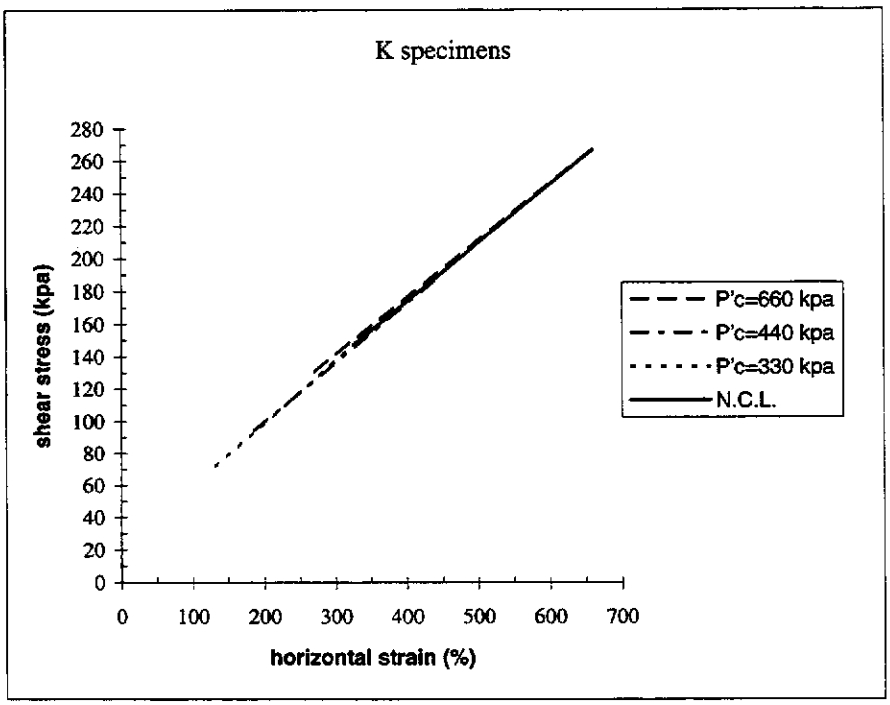

Figure (4.34): The Coulomb envelopes and normally consolidated line of the 60 mm unfissured locked K specimens and sheared with a rate of 0.0033 mm/min.

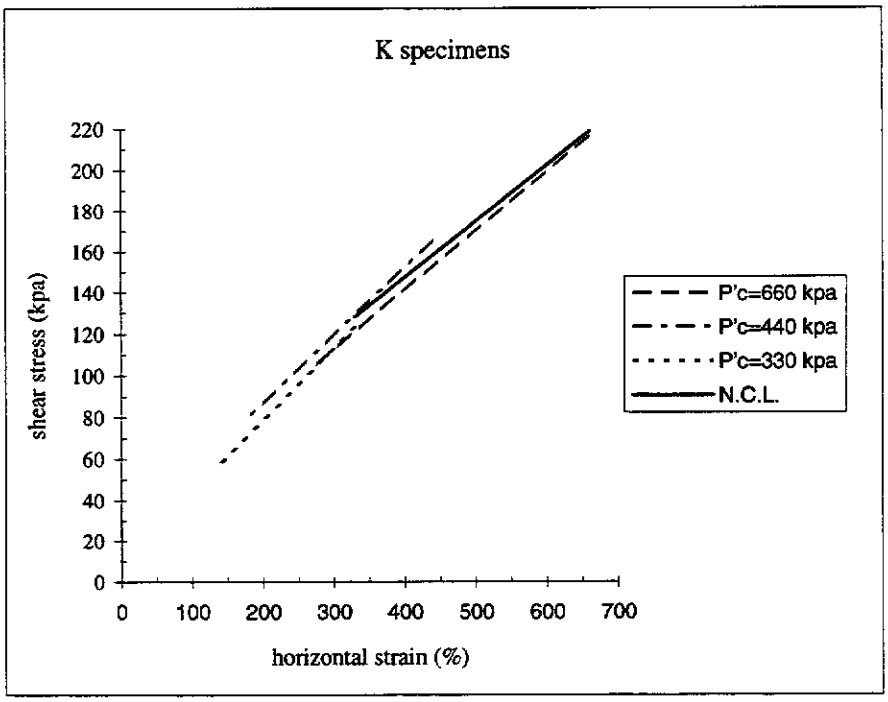

Figure (4.35): The Coulomb envelopes and normally consolidated line of the 60 mm fully fissured unlocked KS specimens and sheared with a rate of 0.0033 mm/min.

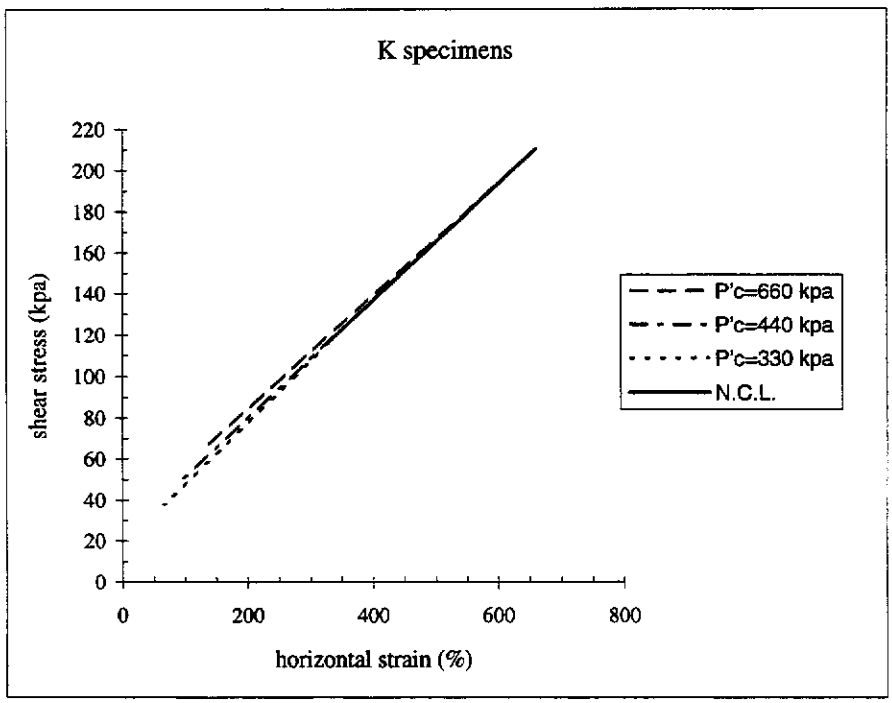

Figure (4.36): The Coulomb envelopes and normally consolidated line of the 100 mm unfissured locked K specimens and sheared with a rate of 0.0033 mm/min.

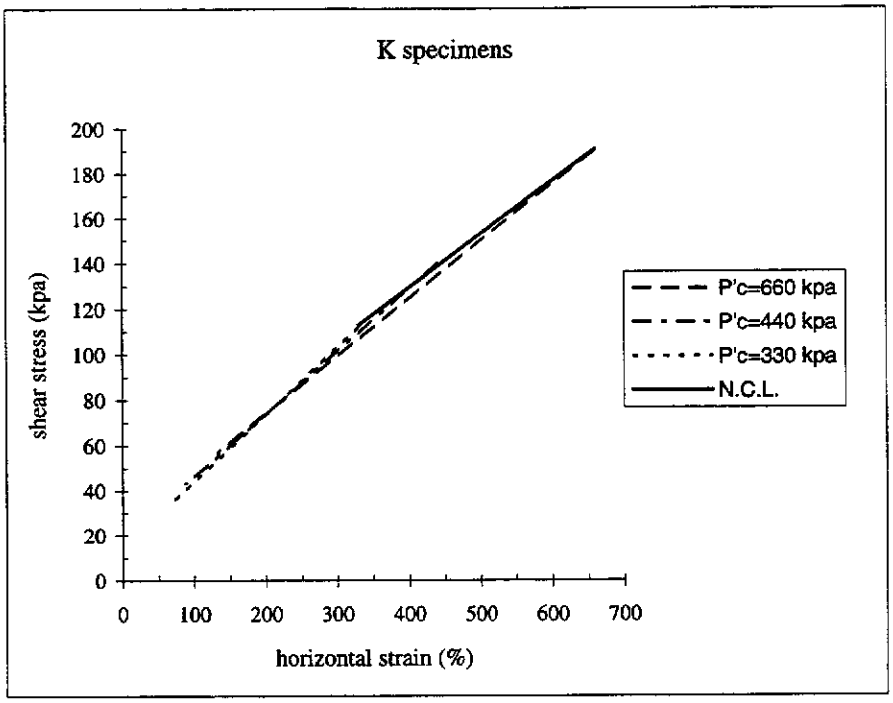

Figure (4.37): The Coulomb envelopes and normally consolidated line of the 100 mm unfissured locked K specimens and sheared with a rate of 0.005 mm/min.

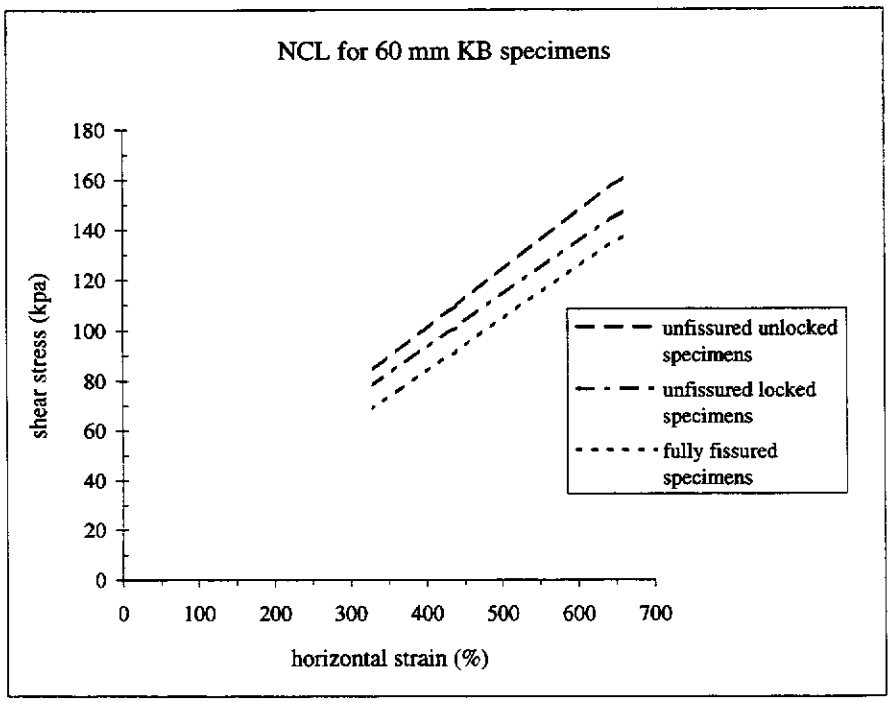

Figure (4.38): The normally consolidated lines of the 60 mm KB specimens sheared with a rate of 0.0033 mm/min.

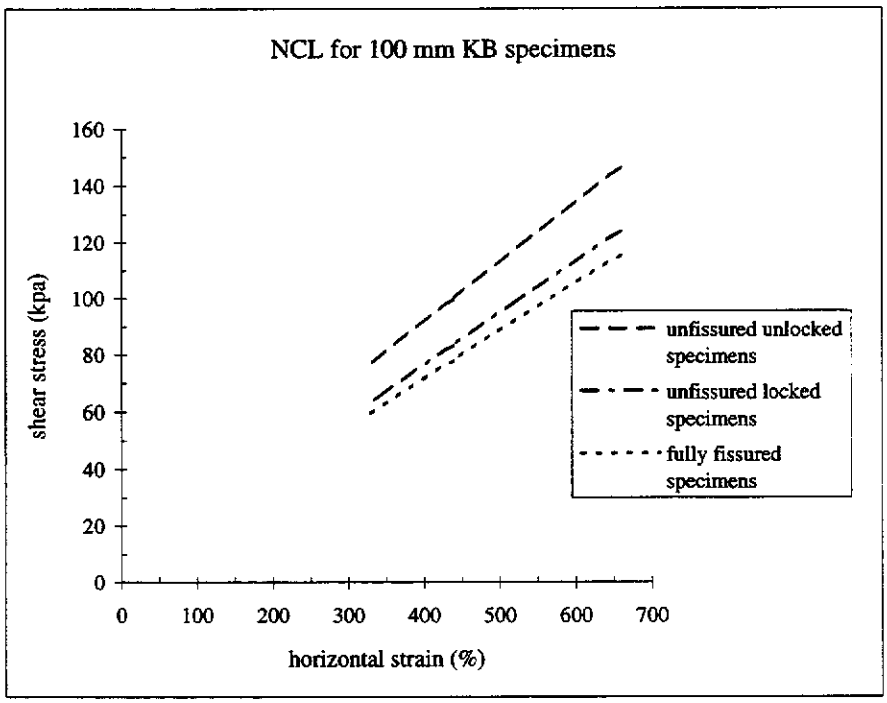

Figure (4.39): The normally consolidated lines of the 100 mm KB specimens sheared with a rate of 0.005 mm/min.

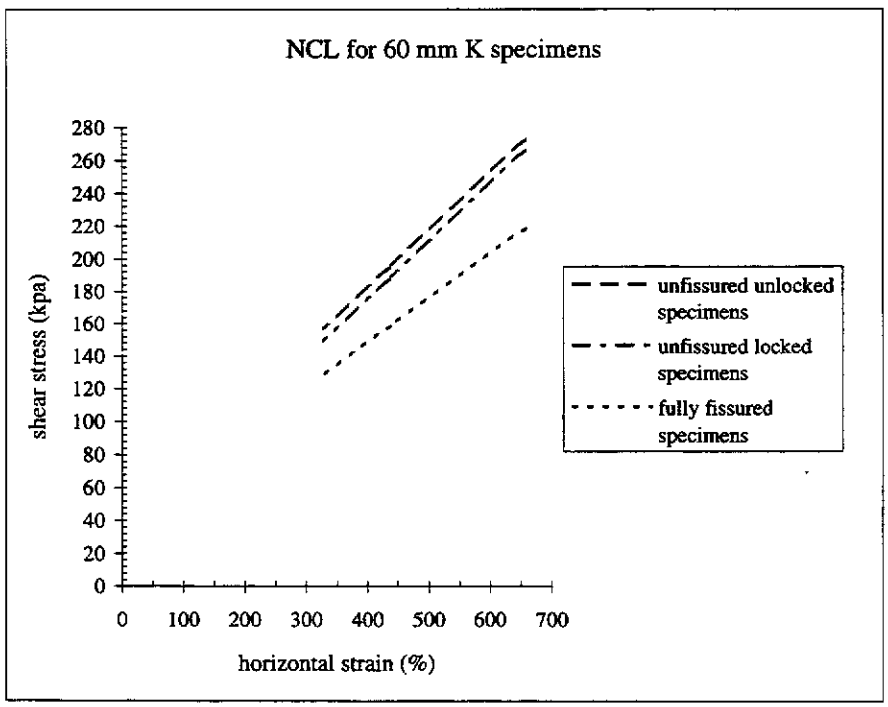

Figure (4.40): The normally consolidated lines of the 60 mm K specimens sheared with a rate of 0.0033 mm/min.

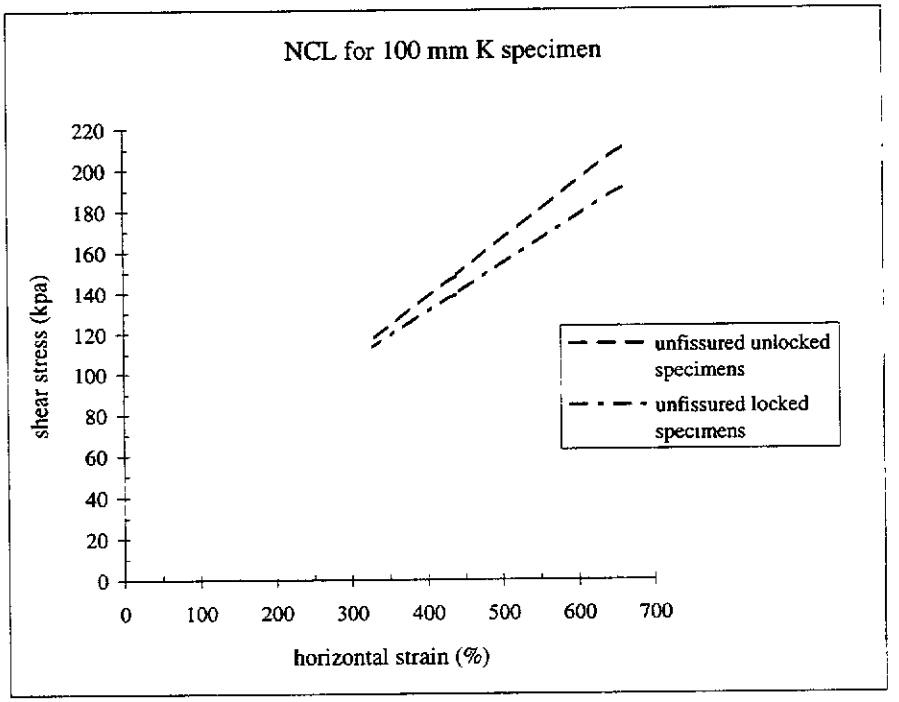

Figure (4.41): The normally consolidated lines of the 100 mm KS specimens sheared with a rate of 0.005 mm/min.

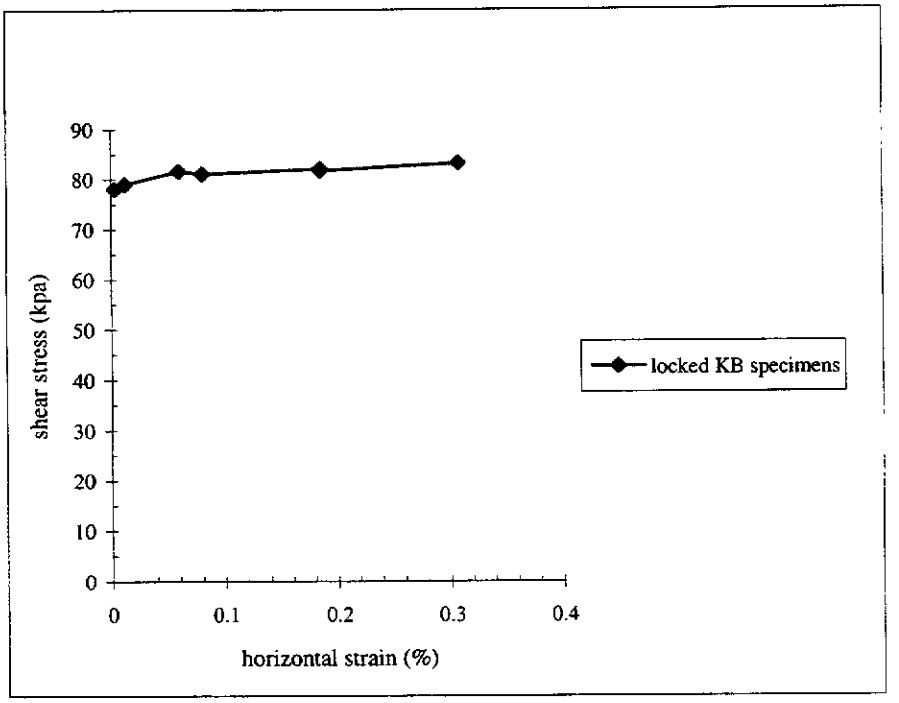

Figure (4.42): The relation between rate and shear strength of the unfissured locked KB specimen consolidated and sheared with a pressure of 330 kpa.

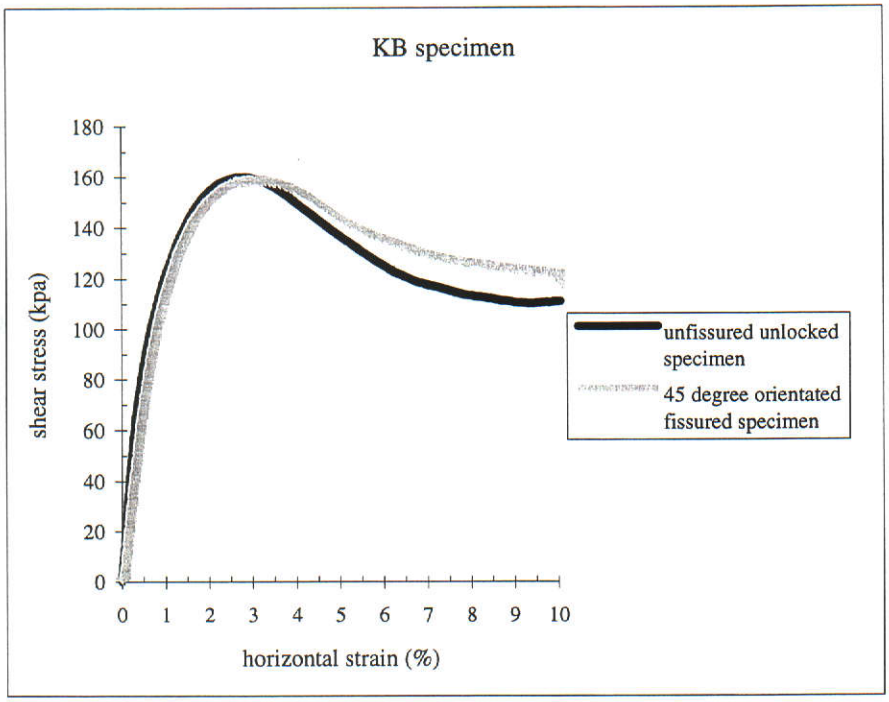

Figure (4.43): The stress strain curves of the inclined fissured and unfissured unlocked 60 mm KB specimens consolidated and sheared with 660 kpa.

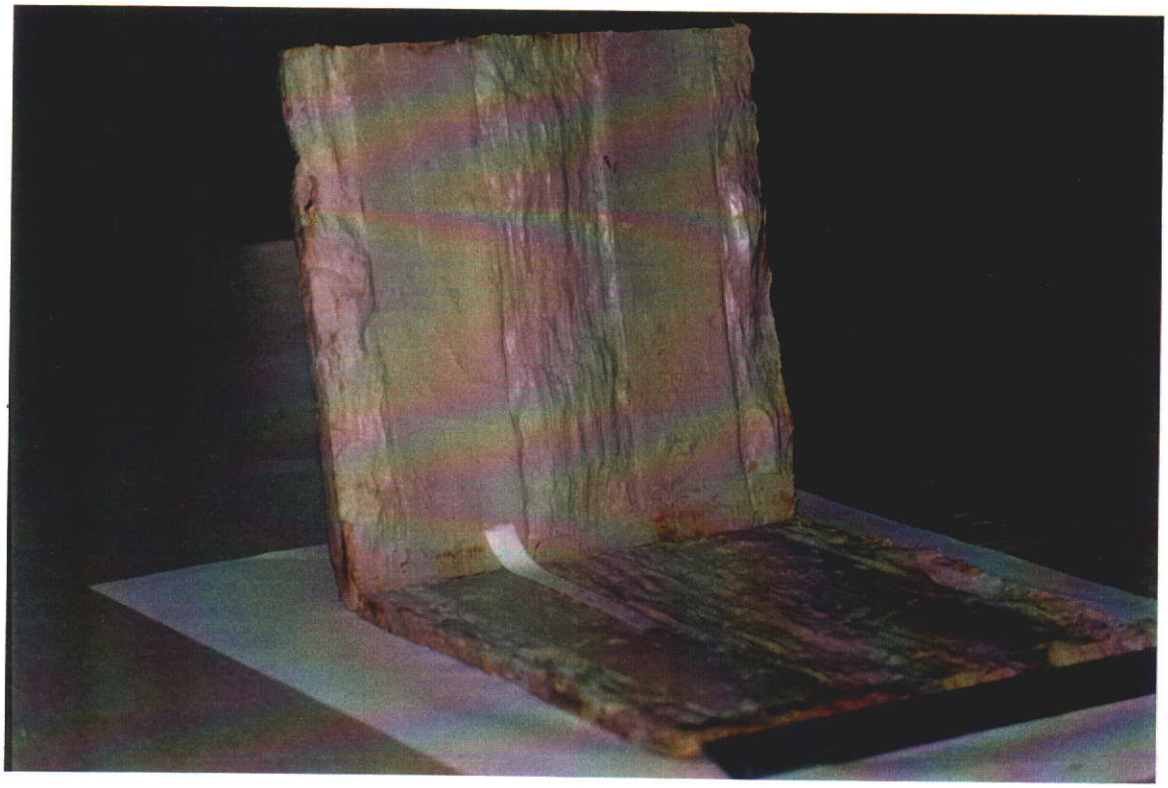

Figure (4.44): Illustration of the presheared partial fissured unlocked large KB specimen consolidated and sheared with a pressure of 330 kpa: The direction of shear is parallel to the length of the fissure.

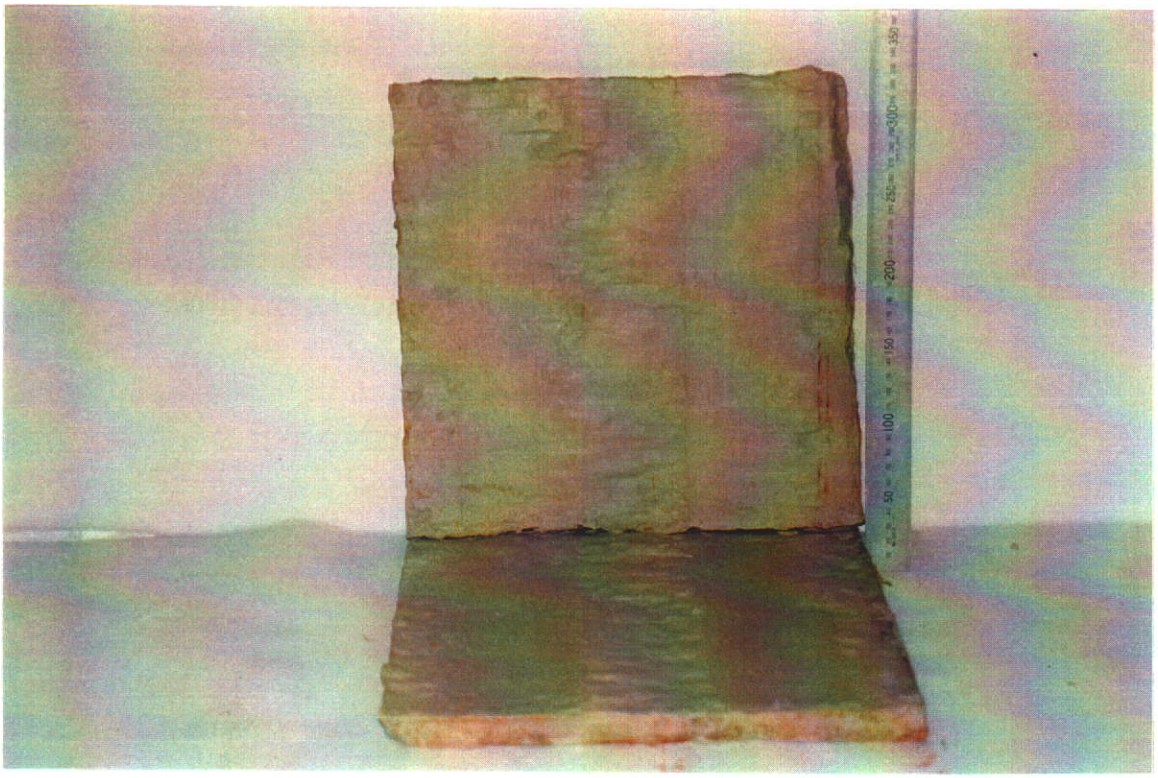

Figure (4.45): Illustration of the presheared partially fissured unlocked large KB specimen consolidated and sheared with a pressure of 330 kpa. The direction of shear perpendicular to the length of the fissure.

Specification for 100 mm size KB specimens	p'_c (kpa)	OCR = 1 R =0.005 (mm/min)	OCR = 1 R = 0.01 (mm/min)	OCR = 1 R =0.185 (mm/min)	OCR=3.3 R =0.005 (mm/min)	OCR=5 R = 0.005 (mm/min)
Unfissured and unlocked in horizontal stress specimens	330	st36330	—	st60330	st6399	st4266
	440	st35440	—	st59440	st62132	st4188
	660	st34660	st70660	st58660	st61198	st40132
Unfissured and locked in horizontal stress specimens	330	st21330	st54330	st60a330	st399	st3366
	440	st20440	st 53440	st59a440	st2132	st3288
	660	st19660	st 52660	st58a660	st1198	st31132
Fully fissured and unlocked in horizontal stress specimens	330	st15330	—	st57330	st699	st966
	440	st14440	—	st56440	st5132	st888
	660	st13660	—	st55660	st4198	st7132
50% fissured and unlocked in horizontal stress specimens	330	st27330	—	—	st1899	st2466
	440	st26440	—	—	st17132	st2388
	660	st25660	—	—	st16198	st22132

Table (4.1): Test program for KB specimens with a size of 100 mm.
The underlined part of each test name shows the applied normal stress during the shearing of the specimen.

KB: 75% Kaolin and 25% Bentonite material
p'_c: preconsolidation pressure (kpa)

OCR: overconsolidation ratio ($\frac{p'_c}{\text{normal stress}}$)

R: rate of shearing (mm/min)

unlocked specimens: unlocked in horizontal stress specimens
locked specimens: locked in horizontal stress specimens
fully fissured specimens: fissure length is 100% of the specimen length or size
50% fissured specime: fissure length is 50% of the specimen length or size

specification for 60 mm size KB specimens	p'_c (kpa)	OCR = 1 R = 0.0033 (mm/min)	OCR = 1 R = 0.01 (mm/min)	OCR = 1 R = 0.185 (mm/min)	OCR=3.3 R = 0.0033 (mm/min)	OCR=2.5 R = 0.01 (mm/min)	OCR=2.5 R = 0.185 (mm/min)
Unfissured and unlocked in horizontal stress specimens	330	pst3330	pst17330	pst29330	pst32132	pst31132	pst30132
	440	pst33440	—	—	pst34176	—	—
	660	pst36660	—	—	pst35264	—	—
Unfissured and locked in horizontal stress specimens	330	pst80330	st9330	pst13330	pst102132	pst19132	pst20132
	440	pst 21440	—	—	pst22176	—	—
	660	pst25660	—	—	pst24264	—	—
Fully fissured and unlocked in horizontal stress specimens	330	pst70330	pst105330	pst109330	pst59132	pst106132	pst111132
	440	pst122440	—	—	pst123176	—	—
	660	pst115660	—	—	pst116264	—	—
50% fissured and unlocked in horizontalstress specimens	330	pst60330	—	—	pst61132	—	—

Table (4.2): Test program for KB specimens with a size of 60 mm.

Specification for the unlocked 300 mm size KB specimens consolidated with 330 kpa		Fissure specifications				First level of normal stress		Second level of normal stress	
Specimen type	Shearing direction	w (mm)	s (mm)	α_i (%)	i (deg.)	R = 0.0033 (mm/min)	R = 0.185 (mm/min)	R= 0.0033 (mmimin)	R = 0.185 (mm/min)
UFS, without bedding	—	—	—	—	—	plt38333	plt63320	plt39220	plt64221
UFS, with bedding	—	—	—	—	—	plt31330	—	plt37221	—
FFS	—	300	0.0	100	0.0	plt7333	plt11335	plt10217	plt12218
FFS	—	300	0.0	100	0.0	plt8334	—	—	—
FFS	—	300	0.0	100	0.0	plt9334	—	—	—
PFS, without bedding	ℵ	30	300	10	0.0	plt40332	—	plt41225	—
PFS, without bedding	ℵ	90	300	30	0.0	plt42333	—	plt43221	—
PFS, without bedding	ℵ	150	300	50	0.0	plt44333 plt69318	—	plt45222	—
PFS, without bedding	ℵ	75	225	50	0.0	plt67323 plt48331	—	plt49221	—
PFS, without bedding	ℵ	75	150	50%	0.0	plt46323	—	plt68221 plt47222	—

Table (4.3): Test program for unlocked KB, 300 mm size specimens consolidated with 330 kpa.

UFS: unfissured specimen
FFS: fully fissured specimen
PFS:partially fissured specimen
w: width of fissure (mm)
s: spacing of fissure (mm)
i: inclination of fissure (degree)

without bedding: consolidated in one layer
with bedding: consolidated in two layers
shear direction ℵ: shear direction is perpendicular to the fissure length
shear direction ℑ: shear direction is parallel to the fissure length

α_i: fissure surface percentag e.g. for single fissure $\alpha_i = \frac{w}{l \text{ (length of fissure)}} \times 100$

Table (4.3): continued

PFS, with bedding	ℵ	30	300	10	0.0	plt35335	—	plt3622	—
PFS, with bedding	ℵ	90	300	30	0.0	plt33333	—	plt34222	—
PFS, with bedding	ℵ	150	300	50	0.0	plt19333	plt18332	plt15166	plt20231
PFS, with bedding	ℵ	75	225	50	0.0	plt29332	—	plt32221	—
PFS, with bedding	ℵ	75	150	50	0.0	plt21334	plt25335	plt22220	plt26233
PFS, without bedding	ℑ	30	300	10	0.0	plt54332	—	plt55223	—
PFS, without bedding	ℑ	90	300	30	0.0	plt56332	—	plt57220	—
PFS, without bedding	ℑ	75	225	50	0.0	plt60321	—	plt61221	—
PFS, without bedding	ℑ	150	300	50	0.0	plt59332	—	plt14218	—
PFS, without bedding	ℑ	75	150	50	0.0	plt62320	—	plt65219	—
PFS, with bedding	ℑ	150	300	50	0.0	plt16332	—	plt17218	—
PFS, with bedding	ℑ	75	150	50	0.0	plt23330	—	plt24230	—

Specification for 100 mm size K specimens	p'_c (kpa)	OCR = 1 R =0.005 (mm/min)	OCR = 5 R = 0.005 (mm/min)	OCR = 1 R =0.01 (mm/min)
unfissured and	330	st45330	st6666	st48330
unlocked in horizontal	440	st44440	st6588	st47440
stress specimens	660	st43660	st64132	st46660
unfissured and locked	330	st39330	st5166	—
in horizontal stress	440	st38440	st 5088	—
specimens	660	st37660	st 49132	—

Table (4.4): Test program for K specimens with a size of 100 mm ;K: 100% Kaolin material.

Specification for K 60 mm size specimens	p'_c (kpa)	OCR = 1 R =0.0033 (mm/min)	OCR = 1 R = 0.01 (mm/min)	OCR = 1 R= 0.185 (mm/min)	OCR=2.5 R =0.0033 (mm/min)	OCR=2.5 R = 0.01 (mm/min)	OCR=2.5 R = 0.185 (mm/min)
Unfissured and	330	pst47330	pst51330	pst55330	pst48132	pst52132	pst56132
unlocked in horizontal	440	pst43440	—	—	pst44176	—	—
stress specimens	660	pst38660	—	—	pst40264	—	—
Unfissured and locked	330	pst45330	pst49330	pst53330	pst46132	pst50132	pst54132
in horizontal stress	440	pst 63440	—	—	pst42176	—	—
specimens	660	pst64660	—	—	pst39264	—	—
Fully fissured and	330	pst68330	pst107330	pst112330	pst69132	pst108132	pst113132
unlocked in horizontal	440	pst120440	—	—	pst121176	—	—
stress specimens	660	pst118660	—	—	pst119264	—	—

Table (4.5): Test program for K specimens with a size of 60 mm.

Specification of specimens		OCR = 1 first test	OCR = 1 second test	OCR = 1 third test
KB, l = 60 mm,	locked	pst80330	pst78330	—
p'_c = 330 kpa	unlocked	pst3330	pst27330	pst71330
K, l = 60 mm,	locked	pst45330	pst97330	pst77330
p'_c = 330 kpa	unlocked	pst47330	pst98330	pst79330
KB, l = 100 mm,	locked	st19660	st19a1660	st19a2660
p'_c = 660 kpa				
KB, l = 300 mm,	unlocked	plt7333	plt8334	plt9334
p'_c = 330 kpa				

Table (4.6): Test program for the study of the test repeatation.

Specimen type	Rate (mm/min)	Test name
KB, locked l=60 mm p'_c = 330 kpa OCR=1	0.0033	pst80330
	0.01	pst9330
	0.06	pst12330
	0.08059	pst10330
	0.185	pst13330
	0..185	pst14330
	0.3076	pst11330

Table (4.7): Test program for the study of the different shearing rates on the locked KB specimens with a size of 60 mm, p'_c = 330 and sheared with OCR = 1.

Specimen type	OCR = 1	OCR = 2.5
KB, locked l= 60 mm R = 0.0033 mm/min	pst66330 pst67330	pst72132
K locked l = 60 mm R = 0.0033 mm/min	pst73330	pst65132

Table (4.8): Test program for the effect of type of water used for the preparation of the specimens.

Specimen type (IFS)	Rate (mm/min)	Test name
unlocked , l = 60 mm p'_c = 660 kpa, i = 45° R = 0.0033 mm/min	pst81660	pst82264

Table (4.9): Test program for the study the effect of inclined fissures on the shear strength of specimens subjected to direct shear test; IFS: Inclined Fissured Specimen.

Specimen. no.	Size (mm)	Material type	Type of specimen	Fissure specification				Horizontal stress situation	Rate (mm/min)	P'_c (kpa)	OCR	Shear strength (kpa)			
				w (mm)	s (mm)	α_f (%)	i (deg.)					peak	strain	residual	strain
st36330	100	KB	UFS	—	—	—	—	unlocked	0.005	330	1	75.0	1.507	51.318	8.532
st35440	100	KB	UFS	—	—	—	—	unlocked	0.005	440	1	102.0	1.699	75.079	7.205
st34660	100	KB	UFS	—	—	—	—	unlocked	0.005	660	1	145.41	1.79	114.2	5.004
st6399	100	KB	UFS	—	—	—	—	unlocked	0.005	330	3.3	55.0	1.383	31.64	6.449
st62132	100	KB	UFS	—	—	—	—	unlocked	0.005	440	3.3	61.0	1.418	37.091	6.751
st61198	100	KB	UFS	—	—	—	—	unlocked	0.005	660	3.3	70.55	1.5	50.54	7.0
st4266	100	KB	UFS	—	—	—	—	unlocked	0.005	330	5.0	28.8	1.811	18.387	5.0
st4188	100	KB	UFS	—	—	—	—	unlocked	0.005	440	5.0	42.0	1.667	21.622	6.99
st40132	100	KB	UFS	—	—	—	—	unlocked	0.005	660	5.0	57.421	1.48	32.52	6.01
st60330	100	KB	UFS	—	—	—	—	unlocked	0.185	330	1	95.0	1.347	68.594	5.88
st59440	100	KB	UFS	—	—	—	—	unlocked	0.185	440	1	121.007	0.954	76.136	8.915

Table (4.10): Summary of test results.

Table (4.10): continued

st58660	100	KB	UFS	—	—	—	—	unlocked	0.185	330	1	160.0	1.815	113.193	9.994
st70660	100	KB	UFS	—	—	—	—	unlocked	0.01	660	1	156.0	1.605	98.56	6.703
st21330	100	KB	UFS	—	—	—	—	locked	0.005	330	1	63.0	3.245	54.135	8.003
st20440	100	KB	UFS	—	—	—	—	locked	0.005	440	1	83.0	2.586	72.049	8.0
st19660	100	KB	UFS	—	—	—	—	locked	0.005	660	1	123.9	2.5	116.84	5.0
st399	100	KB	UFS	—	—	—	—	locked	0.005	330	3.3	34.0	1.414	21.954	6.999
st2132	100	KB	UFS	—	—	—	—	locked	0.005	440	3.3	43.0	1.668	28.138	5.0
st1198	100	KB	UFS	—	—	—	—	locked	0.005	660	3.3	56.78	1.31	40.56	8.0
st3366	100	KB	UFS	—	—	—	—	locked	0.005	330	5	25.0	0.83	18.192	5.0
st3288	100	KB	UFS	—	—	—	—	locked	0.005	440	5	31.5	1.58	24.756	5.0
st31132	100	KB	UFS	—	—	—	—	locked	0.005	660	5	46.78	1.84	36.74	5.0
st54330	100	KB	UFS	—	—	—	—	locked	0.01	330	1	58.0	2.47	50.43	6.01
st53440	100	KB	UFS	—	—	—	—	locked	0.01	440	1	82.40	2.43	63.62	7.57
st52660	100	KB	UFS	—	—	—	—	locked	0.01	660	1	121.66	3.03	108.8	8.0
st60a330	100	KB	UFS	—	—	—	—	locked	0.185	330	1	63.3	1.847	52.42	6.018
st59a440	100	KB	UFS	—	—	—	—	locked	0.185	440	1	82.0	1.842	62.981	9.012
st58a660	100	KB	UFS	—	—	—	—	locked	0.185	660	1	122.0	1.833	90.933	8.031
st15330	100	KB	FFS	100	0.0	100	0.0	unlocked	0.005	330	1	59.5	0.988	39.869	3.999
st14440	100	KB	FFS	100	0.0	100	0.0	unlocked	0.005	440	1	77.46	0.837	50.26	3.994
st13660	100	KB	FFS	100	0.0	100	0.0	unlocked	0.005	660	1	115.348	0.617	80.472	3.999
st699	100	KB	FFS	100	0.0	100	0.0	unlocked	0.005	330	3.3	22.0	0.547	15.833	4.001
st5132	100	KB	FFS	100	0.0	100	0.0	unlocked	0.005	440	3.3	30.24	0.895	19.88	3.0
st4198	100	KB	FFS	100	0.0	100	0.0	unlocked	0.005	660	3.3	38.484	0.712	28.471	4.0
st966	100	KB	FFS	100	0.0	100	0.0	unlocked	0.005	330	5	16.5	0.959	14.028	4.998
st888	100	KB	FFS	100	0.0	100	0.0	unlocked	0.005	440	5	18.0	0.689	15.238	5.0

Table (4.10): continued

st7132	100	KB	FFS	100	0.0	100	0.0	unlocked	0.005	660	5	28.96	0.588	25.604	4.995
st57330	100	KB	FFS	100	0.0	100	0.0	unlocked	0.01	330	1	60.0	1.324	42.46	4.004
st56440	100	KB	FFS	100	0.0	100	0.0	unlocked	0.01	440	1	79.46	1.008	52.42	7.991
st55660	100	KB	FFS	100	0.0	100	0.0	unlocked	0.01	660	1	118.0	1.06	72.697	6.994
st27330	100	KB	PFS	50	100	50	0.0	unlocked	0.005	330	1	66.26	1.25	46.64	3.998
st26440	100	KB	PFS	50	100	50	0.0	unlocked	0.005	440	1	82.54	0.92	55.32	3.997
st25660	100	KB	PFS	50	100	50	0.0	unlocked	0.005	660	1	120.04	1.084	85.94	5.001
st1899	100	KB	PFS	50	100	50	0.0	unlocked	0.005	330	3.3	29.996	0.44	21.857	3.0
st17132	100	KB	PFS	50	100	50	0.0	unlocked	0.005	440	3.3	31.999	0.756	20.744	5.001
st16198	100	KB	PFS	50	100	50	0.0	unlocked	0.005	660	3.3	43.66	0.602	30.22	5.003
st2466	100	KB	PFS	50	100	50	0.0	unlocked	0.005	330	5	24.246	0.658	18.09	4.0
st2388	100	KB	PFS	50	100	50	0.0	unlocked	0.005	440	5	34.425	0.918	20.709	4.99
st22132	100	KB	PFS	50	100	50	0.0	unlocked	0.005	660	5	35.59	0.917	25.838	4.003
pst3330	60	KB	UFS	—	—	—	—	unlocked	0.0033	330	1	83.01	2.417	61.509	9.65
pst33440	60	KB	UFS	—	—	—	—	unlocked	0.0033	440	1	111.04	2.55	72.56	10.0
pst36660	60	KB	UFS	—	—	—	—	unlocked	0.0033	660	1	160.01	2.85	110.946	10.0
pst32132	60	KB	UFS	—	—	—	—	unlocked	0.0033	330	2.5	51.51	1.233	31.259	10.0
pst34176	60	KB	UFS	—	—	—	—	unlocked	0.0033	440	2.5	67.03	1.483	39.578	10.0
pst35264	60	KB	UFS	—	—	—	—	unlocked	0.0033	660	2.5	89.02	1.45	58.41	10.0
pst17330	60	KB	UFS	—	—	—	—	unlocked	0.01	330	1	82.57	1.567	59.683	8.967
pst31132	60	KB	UFS	—	—	—	—	unlocked	0.01	330	2.5	52.0	1.15	32.071	6.15
pst29330	60	KB	UFS	—	—	—	—	unlocked	0.185	330	1	98.88	1.183	57.734	10.0
pst30132	60	KB	UFS	—	—	—	—	unlocked	0.185	330	2.5	64.23	1.533	29.906	9.967
pst80330	60	KB	UFS	—	—	—	—	locked	0.0033	330	1	78.01	2.933	62.254	10.0
pst21440	60	KB	UFS	—	—	—	—	locked	0.0033	440	1	101.03	2.233	74.585	8.933

Table (4.10): continued

pst25660	60	KB	UFS	—	—	—	—	locked	0.0033	660	1	147.0	2.167	109.575	8.933
pst102132	60	KB	UFS	—	—	—	—	locked	0.0033	330	2.5	46.726	1.567	31.576	10.0
pst22176	60	KB	UFS	—	—	—	—	locked	0.0033	440	2.5	57.47	1.2	39.625	9.2
pst24264	60	KB	UFS	—	—	—	—	locked	0.0033	660	2.5	79.294	0.85	50.104	8.933
pst9330	60	KB	UFS	—	—	—	—	locked	0.01	330	1	79.0	2.717	62.888	7.25
pst19132	60	KB	UFS	—	—	—	—	locked	0.01	330	2.5	48.0	0.933	26.587	8.933
pst13330	60	KB	UFS	—	—	—	—	locked	0.185	330	1	82.0	1.2	51.506	8.933
pst20132	60	KB	UFS	—	—	—	—	locked	0.185	330	2.5	49.0	0.75	27.087	8.967
pst70330	60	KB	FFS	60	0.0	100	0.0	unlocked	0.0033	330	1	69.53	2.733	39.5	10.0
pst122440	60	KB	FFS	60	0.0	100	0.0	unlocked	0.0033	440	1	90.06	2.1	60.5	10.0
pst115660	60	KB	FFS	60	0.0	100	0.0	unlocked	0.0033	660	1	137.53	2.55	84.5	7.783
pst59132	60	KB	FFS	60	0.0	100	0.0	unlocked	0.0033	330	2.5	33.52	0.817	19.0	10.0
pst123176	60	KB	FFS	60	0.0	100	0.0	unlocked	0.0033	440	2.5	41.9	1.25	28.093	5.8
pst116264	60	KB	FFS	60	0.0	100	0.0	unlocked	0.0033	660	2.5	63.08	1.333	36.7	10.0
pst105330	60	KB	FFS	60	0.0	100	0.0	unlocked	0.01	330	1	72.07	2.4	36.526	10.0
pst106132	60	KB	FFS	60	0.0	100	0.0	unlocked	0.01	330	2.5	35.05	0.867	19.199	10.0
pst109330	60	KB	FFS	60	0.0	100	0.0	unlocked	0.185	330	1	71.99	1.383	34.37	10.0
pst111132	60	KB	FFS	60	0.0	100	0.0	unlocked	0.185	330	2.5	36.05	0.883	18.043	8.583
pst60330	60	KB	PFS	30	60	50	0.0	unlocked	0.0033	330	1.0	76.077	2.633	57.714	4.83
pst61132	60	KB	PFS	30	60	50	0.0	unlocked	0.0033	330	2.5	37.291	0.866	20.301	10
plt38333	300	KB	UFS without bedding	—	—	—	—	unlocked	0.0033	330	1.0	69.54	1.204	47.664	8.304
plt39220	300	KB	UFS without bedding	—	—	—	—	unlocked	0.0033	330	1.5	55.7	1.0728	35.217	7.91

Table (4.10): continued

plt63320	300	KB	UFS without bedding	—	—	—	—	unlocked	0.185	330	1.0	81.66	0.663	46.642	9.844
plt64221	300	KB	UFS without bedding	—	—	—	—	unlocked	0.185	330	1.5	68.807	0.631	38.057	9.516
plt31330	300	KB	UFS with bedding	—	—	—	—	unlocked	0.0033	330	1.0	60.2	0.852	37.5	9.0
plt37221	300	KB	UFS with bedding	—	—	—	—	unlocked	0.0033	330	1.5	47.25	0.745	24.5	9.131
plt40332	300	KB	PFS, ① without bedding	30	300	10	0.0	unlocked	0.0033	330	1.0	68.48	0.884	45.399	9.565
plt41225	300	KB	PFS, ① without bedding	30	300	10	0.0	unlocked	0.0033	330	1.5	54.08	0.876	35.091	9.885
plt42333	300	KB	PFS, ① without bedding	90	300	30	0.0	unlocked	0.0033	330	1.0	67.02	0.934	42.0	8.296
plt43221	300	KB	PFS, ① without bedding	90	300	30	0.0	unlocked	0.0033	330	1.5	52.741	0.803	28.0	9.778
plt44333	300	KB	PFS, ① without bedding	150	300	50	0.0	unlocked	0.0033	330	1.0	65.437	0.573	45.0	8.026
plt69318	300	KB	PFS, ① without bedding	150	300	50	0.0	unlocked	0.0033	330	1.0	62.3	0.540	42.672	8.247
plt45222	300	KB	PFS, ① without bedding	150	300	50	0.0	unlocked	0.0033	330	1.5	51.04	0.467	32.075	9.246

Table (4.10): continued

plt67323	300	KB	PFS, ① without bedding	75	225	50	0.0	unlocked	0.0033	330	1.0	63.41	1.409	41.373	9.016
plt48331	300	KB	PFS, ① without bedding	75	225	50	0.0	unlocked	0.0033	330	1.0	66.17	0.909	51.374	10.0
plt49221	300	KB	PFS, ① without bedding	75	225	50	0.0	unlocked	0.0033	330	1.5	52.23	0.606	39.156	9.827
plt46332	300	KB	PFS, ① without bedding	75	150	50	0.0	unlocked	0.0033	330	1.0	59.01	0.794	40.929	9.565
plt68221	300	KB	PFS, ① without bedding	75	150	50	0.0	unlocked	0.0033	330	1.5	48.57	1.040	26.279	9.835
plt47222	300	KB	PFS, ① without bedding	75	150	50	0.0	unlocked	0.0033	330	1.5	48.33	0.532	28.826	7.837
plt35335	300	KB	PFS, ① with bedding	30	300	10	0.0	unlocked	0.0033	330	1.0	60.07	0.893	31.704	8.157
plt36222	300	KB	PFS, ① with bedding	30	300	10	0.0	unlocked	0.0033	330	1.5	47.23	0.737	22.901	7.968
plt33333	300	KB	PFS, ① with bedding	90	300	30	0.0	unlocked	0.0033	330	1.0	61.1	0.868	31.932	8.320
plt34222	300	KB	PFS, ① with bedding	90	300	30	0.0	unlocked	0.0033	330	1.5	46.13	0.688	21.253	9.205
plt19333	300	KB	PFS, ① with bedding	150	300	50	0.0	unlocked	0.0033	330	1.0	60.5	0.672	33.5	8.181

Table (4.10): continued

plt15166	300	KB	PFS, ① with bedding	150	300	50	0.0	unlocked	0.0033	330	2.0	34.14	0.213	17.1	7.789
plt18332	300	KB	PFS, ① with bedding	150	300	50	0.0	unlocked	0.185	330	1.0	60.56	0.418	31.817	3.202
plt20231	300	KB	PFS, ① with bedding	150	300	50	0.0	unlocked	0.185	330	1.43	46.38	0.434	23.465	9.221
plt29332	300	KB	PFS, ① with bedding	75	225	50	0.0	unlocked	0.0033	330	1.0	61.05	0.835	—	—
plt32221	300	KB	PFS, ① with bedding	75	225	50	0.0	unlocked	0.0033	330	1.5	47.03	0.770	22.597	7.928
plt 21334	300	KB	PFS, ① with bedding	75	150	50	0.0	unlocked	0.0033	330	1.0	58.944	0.573	34.0	5.004
plt22220	300	KB	PFS, ① with bedding	75	150	50	0.0	unlocked	0.0033	330	1.5	42.668	0.672	22.5	7.534
plt25335	300	KB	PFS, ① with bedding	75	150	50	0.0	unlocked	0.185	330	1.0	60.57	0.237	29.612	5.397
plt26233	300	KB	PFS, ① with bedding	75	150	50	0.0	unlocked	0.185	330	1.42	44.39	0.459	20.565	5.192
plt54332	300	KB	PFS,② without bedding	30	300	10	0.0	unlocked	0.0033	330	1.0	69.26	0.810	49.744	9.794
plt55223	300	KB	PFS, ② without bedding	30	300	10	0.0	unlocked	0.0033	330	1.5	55.15	0.631	35.473	9.582

Table (4.10): continued

plt56332	300	KB	PFS, ② without bedding	90	300	30	0.0	unlocked	0.0033	330	1.0	68.13	0.835	49.9	8.713
plt57220	300	KB	PFS,② without bedding	90	300	30	0.0	unlocked	0.0033	330	1.5	53.21	0.753	37.033	7.804
plt60321	300	KB	PFS, ② without bedding	75	225	50	0.0	unlocked	0.0033	330	1.0	63.27	0.614	46.1	9.279
plt61221	300	KB	PFS, ② without bedding	75	225	50	0.0	unlocked	0.0033	330	1.5	53.12	0.753	35.0	8.976
plt59332	300	KB	PFS, ② without bedding	150	300	50	0.0	unlocked	0.0033	330	1.0	66.12	0.442	47.0	9.836
plt14218	300	KB	PFS, ② without bedding	150	300	50	0.0	unlocked	0.0033	330	1.5	50.11	0.377	30.5	9.811
plt62320	300	KB	PFS, ② without bedding	75	150	50	0.0	unlocked	0.0033	330	1.0	59.012	0.688	45.431	6.347
plt65219	300	KB	PFS, ② without bedding	75	150	50	0.0	unlocked	0.0033	330	1.5	49.23	0.639	33.232	7.787
plt16332	300	KB	PFS, ② with bedding	150	300	50	0.0	unlocked	0.0033	330	1.0	58.14	0.581	32.428	7.002
plt17218	300	KB	PFS, ② with bedding	150	300	50	0.0	unlocked	0.0033	330	1.5	43.18	0.369	23.894	8.501
plt23330	300	KB	PFS, ② with bedding	75	150	50	0.0	unlocked	0.0033	330	1.0	55.67	0.369	33.228	6.830

Tabe (4.10): continued

plt24230	300	KB	PFS, ② with bedding	75	150	50	0.0	unlocked	0.0033	330	1.43	45.64	0.606	24.402	8.410
plt7333	300	KB	FFS	300	0.0	100	0.0	unlocked	0.0033	330	1.0	57.24	0.934	34.361	10.0
plt10217	300	KB	FFS	300	0.0	100	0.0	unlocked	0.0033	330	1.5	41.12	0.197	23.313	8.467
plt11335	300	KB	FFS	300	0.0	100	0.0	unlocked	0.185	330	1.0	60.13	0.606	35.766	5.487
plt12218	300	KB	FFS	300	0.0	100	0.0	unlocked	0.185	330	1.5	45.91	0.328	24.7	8.623
st45330	100	K	UFS	—	—	—	—	unlocked	0.005	330	1.0	116.34	3.95	104.14	10.0
st44440	100	K	UFS	—	—	—	—	unlocked	0.005	440	1.0	148.5	3.66	113.792	10.0
st43660	100	K	UFS	—	—	—	—	unlocked	0.005	660	1.0	210.16	2.53	162.006	8.67
st6666	100	K	UFS	—	—	—	—	unlocked	0.005	330	5.0	37.7	1.922	30.0	6.997
st6588	100	K	UFS	—	—	—	—	unlocked	0.005	440	5.0	48.0	2.026	38.871	6.182
st64132	100	K	UFS	—	—	—	—	unlocked	0.005	660	5.0	66.0	1.612	57.334	4.536
st48330	100	K	UFS	—	—	—	—	unlocked	0.01	330	1.0	118.34	3.92	97.12	10.0
st47440	100	K	UFS	—	—	—	—	unlocked	0.01	440	1.0	151.76	3.43	131.7	10.0
st46660	100	K	UFS	—	—	—	—	unlocked	0.01	660	1.0	210.0	3.25	155.039	10.0
st39330	100	K	UFS	—	—	—	—	locked	0.005	330	1.0	112.12	5.000	111.36	8.0
st38440	100	K	UFS	—	—	—	—	locked	0.005	440	1.0	140.1	4.74	119.56	10.0
st37660	100	K	UFS	—	—	—	—	locked	0.005	660	1.0	190.3	3.8	163.52	6.5
st5166	100	K	UFS	—	—	—	—	locked	0.005	330	5.0	34.0	2.62	31.375	6.57
st5088	100	K	UFS	—	—	—	—	locked	0.005	440	5.0	43.0	3.17	40.111	6.18
st49132	100	K	UFS	—	—	—	—	locked	0.005	660	5.0	57.0	2.6	51.507	7.6
pst47330	60	K	UFS	—	—	—	—	unlocked	0.0033	330	1.0	155.9	5.95	136.876	10.0
pst43440	60	K	UFS	—	—	—	—	unlocked	0.0033	440	1.0	195.61	4.767	166.38	9.917
pst38660	60	K	UFS	—	—	—	—	unlocked	0.0033	660	1.0	272.793	4.25	209.262	10.0

Table (4.10) continued

pst48132	60	K	UFS	—	—	—	—	unlocked	0.0033	330	2.5	75.625	6.25	68.497	10.0
pst44176	60	K	UFS	—	—	—	—	unlocked	0.0033	440	2.5	96.534	6.5	91.169	10.0
pst40264	60	K	UFS	—	—	—	—	unlocked	0.0033	660	2.5	134.03	5.2	120.927	10.0
pst51330	60	K	UFS	—	—	—	—	unlocked	0.01	330	1.0	156.17	5.533	134.183	9.067
pst52132	60	K	UFS	—	—	—	—	unlocked	0.01	330	2.5	75.675	5.317	57.652	10.0
pst55330	60	K	UFS	—	—	—	—	unlocked	0.185	330	1.0	159.19	6.967	152.256	10.0
pst56132	60	K	UFS	—	—	—	—	unlocked	0.185	330	2.5	77.432	6.533	69.136	10.0
pst45330	60	K	UFS	—	—	—	—	locked	0.0033	330	1.0	149.51	5.2	136.145	10.0
pst63440	60	K	UFS	—	—	—	—	locked	0.0033	440	1.0	187.03	5.45	175.485	10.0
pst64660	60	K	UFS	—	—	—	—	locked	0.0033	660	1.0	266.93	4.933	224.002	10.0
pst46132	60	K	UFS	—	—	—	—	locked	0.0033	330	2.5	72.05	6.083	67.636	10.0
pst42176	60	K	UFS	—	—	—	—	locked	0.0033	440	2.5	91.01	3.867	85.881	10.0
pst39264	60	K	UFS	—	—	—	—	locked	0.0033	660	2.5	129.04	5.517	116.457	10.0
pst49330	60	K	UFS	—	—	—	—	locked	0.01	330	1.0	148.03	4.45	133.453	9.067
pst50132	60	K	UFS	—	—	—	—	locked	0.01	330	2.5	72.91	7.433	71.807	10.0
pst53330	60	K	UFS	—	—	—	—	locked	0.185	330	1.0	152.54	5.95	139.617	10.0
pst54132	60	K	UFS	—	—	—	—	locked	0.185	330	2.5	70.743	3.3	65.17	10.0
pst68330	60	K	FFS	60	0.0	100	0.0	unlocked	0.0033	330	1.0	123.512	2.9	82.474	10.0
pst120440	60	K	FFS	60	0.0	100	0.0	unlocked	0.0033	440	1.0	165.33	3.617	119.654	10.0
pst118660	60	K	FFS	60	0.0	100	0.0	unlocked	0.0033	660	1.0	216.49	2.85	170.345	10.0
pst69132	60	K	FFS	60	0.0	100	0.0	unlocked	0.0033	330	2.5	55.105	2.567	36.554	10.0
pst121176	60	K	FFS	60	0.0	100	0.0	unlocked	0.0033	440	2.5	79.26	2.533	52.361	10.0
pst119264	60	K	FFS	60	0.0	100	0.0	unlocked	0.0033	660	2.5	102.43	2.833	70.598	10.0
pst107330	60	K	FFS	60	0.0	100	0.0	unlocked	0.01	330	1.0	126.41	2.7	86.812	10.01
pst108132	60	K	FFS	60	0.0	100	0.0	unlocked	0.01	330	2.5	55.46	1.95	41.792	10.0

Table (4.10) continued

pst112330	60	K	FFS	60	0.0	100	0.0	unlocked	0.185	330	1.0	125.11	2.0	85.674	10.0
pst113132	60	K	FFS	60	0.0	100	0.0	unlocked	0.185	330	2.5	53.87	2.367	40.598	10.0
pst78330	60	KB	UFS	—	—	—	—	locked	0.0033	330	1.0	79.1	3.5	58.994	10.01
pst27330	60	KB	UFS	—	—	—	—	unlocked	0.0033	330	1.0	84.0	2.267	56.631	10.0
pst71330	60	KB	UFS	—	—	—	—	unlocked	0.0033	330	1.0	82.5	2.663	51.142	10.0
pst97330	60	K	UFS	—	—	—	—	locked	0.0033	330	1.0	151.0	5.433	126.465	9.383
pst77330	60	K	UFS	—	—	—	—	locked	0.0033	330	1.0	153.0	6.25	124.483	10.0
pst98330	60	K	UFS	—	—	—	—	unlocked	0.0033	330	1.0	153.0	5.083	130.056	10.0
pst79330	60	KB	UFS	—	—	—	—	unlocked	0.0033	330	1.0	157.0	7.48	131.491	10.0
pst12330	60	KB	UFS	—	—	—	—	locked	0.06	330	1.0	81.6	1.483	58.987	10.0
pst10330	60	KB	UFS	—	—	—	—	locked	0.08	330	1.0	81.0	1.0	55.367	10.0
pst14330	60	KB	UFS	—	—	—	—	locked	0.185	330	1.0	81.6	1.183	52.367	10.0
pst11330	60	KB	UFS	—	—	—	—	locked	0.3	330	1.0	83.11	1.417	52.468	10.0
st19a1660	100	KB	UFS	—	—	—	—	locked	0.005	660	1.0	125.65	3.32	109.84	6.53
st19a2660	100	KB	UFS	—	—	—	—	locked	0.005	660	1.0	119.8	2.89	112.36	7.0
plt9334	300	KB	FFS	300	0.0	100	0.0	unlocked	0.0033	330	1	58.48	0.385	30.123	7.0
plt8334	300	KB	FFS	300	0.0	100	0.0	unlocked	0.0033	330	1	57.19	0.45	31.613	8.533
pst81660	60	KB	IFS	28	60	—	45	unlocked	0.0033	660	1	158.0	3.0	121.048	10.0
pst82264	60	KB	IFS	28	60	—	45	unlocked	0.0033	660	2.5	86.0	1.266	58.115	9.967
pst66330	60	KB	UFS distilled water	—	—	—	—	locked	0.0033	330	1.0	79.0	4.167	63.443	10.0
pst67330	60	KB	UFS distilled water	—	—	—	—	locked	0.0033	330	1.0	78.5	2.85	60.442	10.0

Table (4.10) continue:

pst72132	60	KB	UFS distilled water	—	—	—	—	locked	0.0033	330	1.0	46.677	1.683	26.439	10.0
pst73132	60	K	UFS distilled water	—	—	—	—	locked	0.0033	330	1.0	69.669	4.9	64.071	10.0
pst65330	60	K	UFS distilled water	—	—	—	—	locked	0.0033	330	1.0	149.1	6.667	131.5	10.0

Material type	p'_c (kpa)	Size (mm)	Horizontal stress situation	Shearing rate (mm/min)	Specimen type	Fissure specification				Mohr Coulomb parameters			
						w (mm)	s (mm)	α_f (%)	i (deg.)	c_p (kpa)	ϕ_p (deg)	c_r (kpa)	ϕ_r (deg.)
KB	330	100	unlocked	0.005	UFS	—	—	—	—	29.433	8.105	15.604	6.286
KB	440	100	unlocked	0.005	UFS	—	—	—	—	33.859	8.905	13.499	8.046
KB	660	100	unlocked	0.005	UFS	—	—	—	—	36.694	9.366	16.7586	8.445
KB	330	100	locked	0.005	UFS	—	—	—	—	18.035	7.810	8.770	7.819
KB	440	100	locked	0.005	UFS	—	—	—	—	21.645	7.984	11.424	7.822

Table (4.11): Mohr Coulomb parameters for peak and residual shear strength.

K: 100% Kaolin
KB: 75% Kaolin + 25% Bentonite
UFS: unfissured locked or unlocked specimen
FFS: fully fissured unlocked specimen
PFS: partially fissured unlocked specimen
IFS: inclined fissured unlockedspecimen
p'_c: preconsolidation pressure (kpa)

locked: locked in horizontal stress
unlocked: unlocked in horizontal stress
w, s: width and spacing of fissures respectively (mm)
i: inclination of fissure (degree)
α_f: fissure surface percentag
c_p, c_r : peak and residual cohesion respectively (kpa)
ϕ_p, ϕ_r: peak and residual friction respectively (degree)

Table (4.11): continued

KB	660	100	locked	0.005	UFS	—	—	—	—	27.715	8.294	13.021	8.902
KB	330	100	unlocked	0.005	FFS	100	0.0	100	0.0	5.82	9.202	6.721	5.717
KB	440	100	unlocked	0.005	FFS	100	0.0	100	0.0	6.002	9.258	6.64	5.664
KB	660	100	unlocked	0.005	FFS	100	0.0	100	0.0	6.6	9.348	9.506	6.113
KB	330	100	unlocked	0.005	PFS	50	100	50	0.0	14.04	8.998	11.071	6.154
KB	440	100	unlocked	0.005	PFS	50	100	50	0.0	17.362	8.351	9.906	5.907
KB	660	100	unlocked	0.005	PFS	50	100	50	0.0	12.994	9.198	8.945	6.635
K	330	100	unlocked	0.005	UFS	—	—	—	—	18.04	16.588	11.465	15.686
K	440	100	unlocked	0.005	UFS	—	—	—	—	22.875	15.935	20.141	12.016
K	660	100	unlocked	0.005	UFS	—	—	—	—	29.975	15.765	31.166	11.213
K	330	100	locked	0.005	UFS	—	—	—	—	14.47	16.484	11.379	16.855
K	440	100	locked	0.005	UFS	—	—	—	—	18.725	15.422	20.249	12.719
K	660	100	locked	0.005	UFS	—	—	—	—	23.6675	14.169	23.504	11.977
KB	330	60	unlocked	0.0033	UFS	—	—	—	—	30.5	9.039	11.092	8.686
KB	440	60	unlocked	0.0033	UFS	—	—	—	—	37.667	9.462	17.59	7.121
KB	660	60	unlocked	0.0033	UFS	—	—	—	—	41.668	10.165	23.377	7.559
KB	330	60	locked	0.0033	UFS	—	—	—	—	25.87	8.979	11.124	8.807
KB	440	60	locked	0.0033	UFS	—	—	—	—	38.43	9.369	16.318	7.543
KB	660	60	locked	0.0033	UFS	—	—	—	—	34.156	9.702	10.456	8.540
KB	330	60	unlocked	0.0033	FFS	60	0.0	100	0.0	9.513	10.308	5.333	5.911
KB	440	60	unlocked	0.0033	FFS	60	0.0	100	0.0	9.793	10.338	6.688	6.934
KB	660	60	unlocked	0.0033	FFS	60	0.0	100	0.0	13.447	10.648	4.833	6.882
KB	330	60	unlocked	0.0033	PFS	30	60	50	0.0	11.434	11.083	-0.641	9.026
K	330	60	unlocked	0.0033	UFS	—	—	—	—	22.108	22.069	22.911	19.052
K	440	60	unlocked	0.0033	UFS	—	—	—	—	30.483	20.571	41.028	15.902

Table (4.11): continued

K	660	60	unlocked	0.0033	UFS	—	—	—	—	41.523	19.311	62.037	12.575
K	330	60	locked	0.0033	UFS	—	—	—	—	20.412	21.366	21.967	19.085
K	440	60	locked	0.0033	UFS	—	—	—	—	26.997	19.987	26.145	18.747
K	660	60	locked	0.0033	UFS	—	—	—	—	37.113	19.198	44.76	15.194
K	330	60	unlocked	0.0033	FFS	60	0.0	100	0.0	9.5	19.059	5.941	13.057
K	440	60	unlocked	0.0033	FFS	60	0.0	100	0.0	21.88	18.057	7.5	14.3
K	660	60	unlocked	0.0033	FFS	60	0.0	100	0.0	26.39	16.0679	4.1	14.138
K	330	60	unlocked	0.01	FFS	60	0.0	100	0.0	8.16	19.714	11.779	12.81
K	330	60	unlocked	0.185	FFS	60	0.0	100	0.0	6.377	19.789	10.547	12.825
KB	330	60	unlocked	0.01	FFS	60	0.0	100	0.0	10.37	10.59	7.648	5.001
KB	330	60	unlocked	0.185	FFS	60	0.0	100	0.0	12.09	10.288	7.158	4.714
KB	330	60	unlocked	0.01	UFS	—	—	—	—	27.333	8.898	13.663	7.938
KB	330	60	unlocked	0.185	UFS	—	—	—	—	27.0	9.462	10.808	7.031
KB	330	60	locked	0.01	UFS	—	—	—	—	31.62	8.777	15.33	7.655
KB	330	60	locked	0.185	UFS	—	—	—	—	41.137	9.923	11.354	8.0
K	330	60	unlocked	0.01	UFS	—	—	—	—	22.012	22.124	6.631	21.133
K	330	60	unlocked	0.185	UFS	—	—	—	—	22.959	22.425	14.556	22.649
K	330	60	locked	0.01	UFS	—	—	—	—	22.83	20.776	30.71	17.294
K	330	60	locked	0.185	UFS	—	—	—	—	16.212	22.446	15.539	20.606
KB	660	60	unlocked	0.0033	IFS	28	60	0.0	45	38.0	10.305	16.159	9.03
K	330	60	locked	0.0033	UFS distilled water	—	—	—	—	16.717	21.859	19.119	18.806
KB	330	60	locked	0.0033	UFS distilled water	—	—	—	—	25.117	9.274	8.437	9.463

Specification for unlocked 300 mm size KB specimens consolidated with 300 kpa		Fissure specification				Mohr Coulomb parameters			
rate of shearing	specimen type	w (mm)	s (mm)	α_f (%)	i (deg.)	c_p (kpa)	ϕ_p (deg.)	c_r (kpa)	ϕ_r (deg.)
0.0033	UFS, without bedding	—	—	—	—	28.488	7.029	10.748	6.327
0.0033	UFS, with bedding	—	—	—	—	20.617	6.855	-1.858	6.801
0.185	UFS, without bedding,	—	—	—	—	40.176	7.369	18.933	4.939
0.0033	FFS	300	0.0	100	0.0	10.761	7.939	3.320	5.260
0.185	FFS	300	0.0	100	0.0	19.292	6.953	4.100	5.400
0.0033	PFS, without bedding,①	30	300	10	0.0	23.800	7.665	13.415	5.503
0.0033	PFS, with bedding, ①	30	300	10	0.0	22.005	6.483	5.607	4.455
0.0033	PFS, without bedding,①	90	300	30	0.0	24.565	7.266	0.375	7.125
0.0033	PFS, with bedding, ①	90	300	30	0.0	16.190	7.681	-0.105	5.495
0.0033	PFS, without bedding,①	150	300	50	0.0	22.246	7.390	6.225	6.642
0.0033	PFS, with bedding, ①	150	300	50	0.0	7.938	6.852	0.798	5.609
0.0033	PFS, without bedding,①	75	150	50	0.0	26.776	5.546	4.400	6.279
0.0033	PFS, with bedding, ①	75	150	50	0.0	11.258	8.125	0.307	5.760
0.0033	PFS, without bedding,①	75	225	50	0.0	24.223	7.222	14.609	6.338
0.0033	PFS, with bedding, ①	75	225	50	0.0	19.116	7.199	—	—
0.0033	PFS, without bedding,②	30	300	10	0.0	26.283	7.376	6.276	7.459
0.0033	PFS, without bedding,②	90	300	30	0.0	23.903	7.588	11.759	6.554
0.0033	PFS, without bedding,②	150	300	50	0.0	19.494	7.994	-1.053	8.236
0.0033	PFS, with bedding, ②	150	300	50	0.0	14.572	7.476	7.575	4.281
0.0033	PFS, without bedding,②	75	150	50	0.0	28.02	5.532	6.781	6.887
0.0033	PFS, with bedding, ②	75	150	50	0.0	22.571	5.728	4.102	5.044
0.0033	PFS, without bedding,②	75	225	50	0.0	30.689	5.796	10.469	6.334
0.185	PFS, with bedding, ①	150	300	50	0.0	13.949	7.992	4.363	4.727
o.185	PFS, with bedding, ①	75	150	50	0.0	7.430	9.014	-0.101	5.069

Table (4.12): Peak and residual shear strength parameters of the unlocked KB specimens consolidated with 330 kpa and with a size of 300 mm.

p'_c =330 (kpa)	KB unfissured, unlocked specimens				KB fissured, unlocked specimens			
size (mm)	c'_p (kpa)	c'_r (kpa)	ϕ'_p (deg.)	ϕ'_r (deg.)	c'_p (kpa)	c'_r (kpa)	ϕ'_p (deg.)	ϕ'_r (deg.)
60	30.50	11.092	9.039	8.686	9.513	5.333	10.308	5.911
100	29.43	15.604	8.105	6.286	5.820	6.721	9.202	5.717
300	28.02	10.748	7.029	6.327	10.761	3.320	7.939	5.260

Table (4.13) The peak and residual effective shear strength parameters for three different sizes of 60 mm, 100 mm and 300 mm unlocked, unfissured and fully fissured KB specimens consolidated with 330 kpa.

Specimen type		Size of 60 mm			Size of 100 mm		
Material type	p'_c (kpa)	$\frac{\tau'_{p\ (locked)}}{\tau'_{p\ (unlocked)}}$	$\frac{c'_{p\ (locked)}}{c'_{p\ (unlocked)}}$	$\frac{\phi'_{p\ (locked)}}{\phi'_{p\ (unlocked)}}$	$\frac{\tau'_{p\ (locked)}}{\tau'_{p\ (unlocked)}}$	$\frac{c'_{p\ (locked)}}{c'_{p\ (unlocked)}}$	$\frac{\phi'_{p\ (locked)}}{\phi'_{p\ (unlocked)}}$
	660	0.9188	0.8161	0.9544	0.8521	0.7552	0.8836
KB	440	0.9100	0.8318	0.9773	0.8137	0.6392	0.8950
	330	0.0.938	0.8306	0.9841	0.8400	0.6127	0.9630
Average ratio		0.9228	0.8262	0.9710	0.8350	0.6690	0.9139
	660	0.9785	0.8934	0.9937	0.9062	0.7898	0.9043
K	440	0.9560	0.8859	9689	0.9434	0.8186	0.9662
	330	0.9590	0.9195	0.9655	0.9636	0.8039	0.9954
Average ratio		0.9645	0.8971	0.9760	0.9378	0.8041	0.9553

Table (4.14): The ratios of locked in horizontal stresses to unlocked in horizontal stresses for both material types, two different sizes and three different levels of preconsolidation pressures.

The ratios of $\frac{\tau'_{p\ (locked)}}{\tau'_{p\ (unlocked)}}$ are for OCR = 1

Specime type	p'_c (kpa) OCR = 1	τ_p (kpa) for KB - 100 × 100 mm			τ_p (kpa) for KB - 300 × 300 mm		τ_p (kpa) for K - 100 × 100 mm	
		R = 0.005 (mm/min)	R = 0.01 (mm/min)	R = 0.185 (mm/min)	R = 0.0033 (mm/min)	R = 0.185 (mm/min)	R = 0.005 (mm/min)	R = 0.01 (mm/min)
Unlocked	660	145.51	156.0	160.0	—	—	210.1	210.0
	440	102.0	—	121.0	—	—	148.5	151.76
	330	75.0	—	95.0	69.54	81.66	116.34	118.36
Locked	660	123.9	121.66	122.0	—	—	—	—
	440	83.0	82.4	82.0	—	—	—	—
	330	63.0	58.0	63.3	—	—	—	—
100% fissured	660	115.34	118.0	—	—	—	—	—
	440	77.46	79.46	—	—	—	—	—
	330	59.5	60.0	—	57.24	60.13	—	—

Table (4.15): The effect of rate of shearing on the peak shear strengths of the specimens.

p'_c = 330 (kpa)			Mohr	Rate of shearing		
Size (mm)	Material type	specimen type	Coulomb parameters for peak	R = 0.0033 (mm/min)	R = 0.01 (mm/min)	R = 0.185 (mm/min)
		unlocked	c_p (kpa)	30.5	27.333	27.0
			ϕ_p (deg.)	9.039	8.898	9.462
60	KB	locked	c_p (kpa)	25.870	31.62	41.137
			ϕ_p (deg.)	8.979	8.777	9.923
		fully	c_p (kpa)	9.513	10.37	12.09
		fissured	ϕ_p (deg.)	10.308	10.59	10.288

Table (4.16): Mohr Coulomb parameters for the peak shear strengths of the specimens consolidated with 330 kpa and sheared with the three different rates of shearing.

Table (4.16): continued

60	K	unlocked	c_n (kpa)	22.108	22.012	22.959
			ϕ_p (deg.)	22.069	22.124	22.425
		locked	c_n (kpa)	20.412	22.83	16.212
			ϕ_p (deg.)	21.366	20.776	22.446
		fully fissured	c_n (kpa)	9.5	8.16	6.377
			ϕ_p (deg.)	19.057	19.714	19.789
300	KB	unlocked	c_n (kpa)	28.488	—	40.176
			ϕ_p (deg.)	7.029	—	7.369
		fully fissured	c_n (kpa)	10,761	—	19.292
			ϕ_p (deg.)	7.939	—	6.953

KB material size = 300 mm p'_c = 330 kpa	R = 0.0033 (mm/min)				R = 0.185 (mm/min)			
	τ'_p (kpa)	σ_n (kpa)	c'_p (kpa)	ϕ'_p (kpa)	τ_p (kpa)	σ_n (kpa)	c_n (kpa)	ϕ_p (kpa)
Unfissured without bedding	69.54	332.95	28.488	7.029	81.66	320	40.176	7.369
Unfissured with bedding	60.2	330	20.617	6.855	—	—	—	—
fully fissured	57.24	333.3	10.761	7.939	60.13	335	19.292	6.953

Table (4.17): Effect of bedding on the shear strength for KB specimens with size of 300 mm and consollidated with 330 kpa.

Specimen specification	Unlocked KB specimens with size of 300 mm consolidated with 330 kpa						
	Unfissured without bedding	Fully fissured	Partially fissured specimens without bedding				
s (mm)	∞	0.0	300	300	300	225	150
α_f (%)	0.0	100	10	30	50	50	50
w (mm)	—	300	30	90	150	75	75
σ_N (kpa)	332.95	333.3	332.6	333.29	332.94	331.03	332.59
τ'_p (kpa)	69.54	57.24	68.48	67.02	65.44	66.17	59.01
τ'_p (kpa) from Eq. (4 7)	69.54	57.24	68.261	65.879	63.365	63.114	63.114
c'_p (kpa)	28.488	10.761	23.80	24.565	22.246	24.223	26.776
ϕ'_p (deg.)	7.029	7.939	7.665	7.266	7.39	7.222	5.546

Table (4.18): Effect of width, spacing of horizontal fissures on the effective peak shear strngths of KB specimens with size of 300 mm consolidated with 330 kpa and sheared with a rate of 0.0033 mm/min.

Fissure specification		KB partially fissured specimens with size of 300 mm consolidated with 330 kpa				
α_f (%)		10	30	50	50	50
w (mm)		30	90	150	75	75
s (mm)		300	300	300	225	150
	τ'_p (kpa)	69.26	68.13	66.12	63.27	59.01
parallel	σ_N (kpa)	332.25	332.08	332.08	320.58	320.59
direction, ℑ	c'_p (kpa)	26.283	23.903	19.494	30.689	28.02
	ϕ'_p (deg.)	7.376	7.588	7.994	5.796	5.532
	τ'_p (kpa)	68.48	67.02	65.44	63.4	59.01
perpendicular	σ_N (kpa)	332.60	333.29	332.94	323.2	332.59
direction, ℵ	c'_p (kpa)	23.80	24.565	22.246	24.223	26.776
	ϕ'_p (deg.)	7.665	7.266	7.39	7.222	5.546

Table (4.19): The effect of direction of shearing on the effective peak shear strength parameters of the KB partially fissured specimens with a size of 300 mm and consolidated with 330 kpa and sheared with a rate of 0.0033 mm/min. σ_n is the normal stress applied on the specimen during the shearing process for each τ'_p.

KB specimens	Rate (mm/min)	0.005			0.01			0.185		
size = 100 mm	p'_c (kpa)	660	440	330	660	440	330	660	440	330
Unfissured unlocked	τ_f/p'_c	0.177064	0.170634	0.155509	—	—	—	0.171505	0.173036	0.207860
	c_r (kpa)	21.741	13.499	15.604	—	—	—	—	—	—
	ϕ_r (deg.)	8.28	8.046	6.286	—	—	—	—	—	—
Unfissured locked	τ_f/p'_c	0.177030	0.163840	0.164045	0.164848	0.143227	0.152818	0.137777	0.143138	0.158848
	c_r (kpa)	13.021	11.424	8.770	—	—	—	—	—	—
	ϕ_r (deg.)	8.902	7.822	7.819	—	—	—	—	—	—
Fully fissured unlocked	τ_f/p'_c	0.121927	0.114227	0.120815	0.110146	0.119136	0.128666	—	—	—
	c_r (kpa)	9.506	6.640	6.721	—	—	—	—	—	—
	ϕ_r (deg.)	6.113	5.664	5.717	—	—	—	—	—	—

Table (4.20): Residual shear strength ratios and parameters of KB specimens with a size of 100 mm; τ_f/p'_c is calculated for OCR = 1.

KB specimens	Rate (mm/min)	0.0033			0.01	0.185
size = 60 mm	p'_c (kpa)	660	440	330	330	330
Unfissured unlocked	τ_f/p'_c	0.1681	0.162636	0.186391	0.180857	0.174951
	c_r (kpa)	23.377	17.590	11.092	13.663	10.808
	ϕ_r (deg.)	7.559	7.121	8.686	7.938	7.031
Unfissured locked	τ_f/p'_c	0.166022	0.169511	0.188648	0.190545	0.156078
	c_r (kpa)	10.456	16.318	11.124	15.33	11.354
	ϕ_r (deg.)	8.540	7.543	8.807	7.655	8.0
Fully fissured unlocked	τ_f/p'_c	0.128030	0.13750	0.119696	0.110684	0.104151
	c_r (kpa)	4.833	6.688	5.333	7.648	7.158
	ϕ_r (deg.)	6.882	6.934	5.911	5.001	4.714

Table (4.21): Residual shear strength ratios and parameters of KB specimens with a size of 60 mm; τ_f/p'_c is calculated for OCR = 1.

K specimens size = 60 mm	Rate (mm/min)	0.0033			0.01	0.185
	p'_c (kpa)	660	440	330	330	330
Unfissured unlocked	τ_f/p'_c	0.31706	0.378136	0.414776	0.406615	0.461382
	c_r (kpa)	62.037	41.028	22.911	6.631	14.556
	ϕ_r (deg.)	12.575	15.902	19.052	21.133	22.649
Unfissured locked	τ_f/p'_c	0.339396	0.398829	0.412561	0.404403	0.423082
	c_r (kpa)	44.76	26.145	21.967	30.710	15.539
	ϕ_r (deg.)	15.194	18.747	19.085	17.294	20.606
Fully fissured unlocked	τ_f/p'_c	0.258098	0.271941	0.249921	0.263066	0.259624
	c_r (kpa)	4.1	7.5	5.941	11.779	10.547
	ϕ_r (deg.)	14.138	14.300	13.057	12.81	12.825

Table (4.22): Residual shear strength ratios and parameters of K specimens with a sizeof 60 mm; τ_f/p'_c is calculated for OCR = 1.

K specimens size = 100 mm	Rate (mm/min)	0.0033		
	p'_c (kpa)	660	440	330
Unfissured unlocked	τ_f/p'_c	0.245463	0.258618	0.315575
	c'_r (kpa)	31.166	20.14	11.465
	ϕ'_r (deg.)	11.213	12.016	15.686
Unfissured locked	τ_f/p'_c	0.247757	0.271727	0.343515
	c'_r (kpa)	23.504	20.249	11.379
	ϕ'_r (deg.)	11.977	12.719	16.855

Table (4.23): Effective residual shear strength ratios and parameters of K specimens with a size of 100 mm; τ_f/p'_c is calculated for OCR = 1

KB specimens size = 300 mm	p'_c (kpa)	330		Mean	Standard
	Rate (mm/min)	0.0033	0.185		deviation
Unfissured unlocked without bedding	τ_r/p'_c	0.143135	0.145756	2.1444	0.0019
	c_r (kpa)	10.748	18.933	14.8405	5.7877
	ϕ_r (deg.)	6.327	4.939	5.5880	0.9178
Fully fissured unlocked	τ_r/p'_c	0.102102	0.106764	0.1044	0.0033
	c_r (kpa)	3.32	4.1	3.7100	0.5515
	ϕ_r (deg.)	5.26	5.4	5.3300	0.0990

Table (4.24): Residual shear strength ratios and parameters of KB specimens with a size of 300 mm and p'_c = 330 kpa. τ_r/p'_c is calculated for OCR = 1.

Statistical evaluation for three levels of p'_c		KB size 60 mm		KB size 100 mm		K size 60 mm		K size 100 mm	
		Mean	Standard deviation	Mean	Standard deviation	Mean	Standard deviation	Mean	Standard deviation
Fully	τ_r/p'_c	0.1284	0.0089	0.1190	0.0042	0.2600	0.0111	—	—
fissured	c'_r (kpa)	5.6180	0.9598	7.6223	1.6318	5.8470	1.7019	—	—
	ϕ'_r (deg.)	6.5757	0.5762	5.8313	0.2454	13.8317	0.6758	—	—
Unfissured	τ_r/p'_c	0.1724	0.0124	0.1677	0.0111	0.3700	0.0494	0.3066	0.0571
unlocked	c'_r (kpa)	17.3530	6.1459	16.9480	4.2822	41.9920	19.5808	20.9237	9.8739
	ϕ'_r (deg.)	7.7887	0.8074	7.5373	1.0900	15.8430	3.2389	12.9717	2.3847
Unfissured	τ_r/p'_c	0.1747	0.0122	0.1683	0.0076	0.3836	0.0389	0.2877	0.0498
locked	c'_r (kpa)	12.6327	3.2090	11.0717	2.1473	30.9573	12.1346	18.3773	6.2754
	ϕ'_r (deg.)	8.2967	0.6662	8.1810	0.6244	17.6753	2.1555	13.8503	2.6284

Table (4.25): Statistical evaluations for the effect of p'_c on the effective residual shear strength ratios and parameters of KB and K specimens.

Fully fissured KB specimens for p'_c = 330 kpa				Statistical evaluation	
Size (mm)	60	100	300	Mean	Standard deviation
τ_r/p'_c	0.119696	0.120815	0.103186	0.1146	0.0099
c'_r (kpa)	5.333	6.721	3.320	5.1247	1.7100
ϕ'_r (deg.)	5.911	5.717	5.260	5.6293	0.3342

Table (4.26): Statistical evaluations for the effect of size on the effective residual shear strength ratios and parameters of the fully fissured of KB specimens.

Unfissured unlocked KB specimens for p'_c = 330 kpa				Statistical evaluation	
Size (mm)	60	100	300	Mean	Standard deviation
τ_r/p'_c	0.186391	0.155509	0.143135	0.1617	0.0223
c'_r (kpa)	11.092	15.604	10.748	12.4813	2.7098
ϕ'_r (deg.)	8.686	6.286	6.327	7.0997	1.3740

Table (4.27): Statistical evaluations for the effect of size on the effective residual shear strength ratios and parameters of the unfissured unlocked KB specimens.

Fully fissured	KB material			K material		
Rate (mm/min)	τ_r/p'_c	c'_r (kpa)	ϕ'_r (deg.)	τ_r/p'_c	c'_r (kpa)	ϕ'_r (deg.)
0.0033	0.119696	5.333	5.911	0.249921	5.941	13.057
0.01	0.110684	7.648	5.001	0.263066	11.779	12.81
0.185	0.104151	7.158	4.714	0.259624	10.547	12.825
Mean	0.1115	6.7130	5.2087	0.2575	9.4223	12.8973
Standard deviation	0.0078	1.2200	0.6249	0.0068	3.0772	0.1385

Table (4.28): Statistical evaluation for the effect of rate of shearing on the residual shear strength ratios and parameters of the fully fissured KB and K specimens with a size of 60 mm and p'_c = 330 kpa.

Unfissured unlocked	KB material			K material		
Rate (mm/min)	τ_f/p'_c	c'_r (kpa)	ϕ'_r (deg.)	τ_f/p'_c	c'_r (kpa)	ϕ'_r (deg.)
0.0033	0.186391	11.092	8.686	0.414776	22.911	19.052
0.01	0.180857	13.663	7.938	0.406615	6.631	21.133
0.185	0.174951	10.808	7.031	0.461382	14.556	22.649
Mean	0.1807	11.8543	7.8850	0.4276	14.6993	20.9447
Standard deviation	0.0057	1.5728	0.8288	0.0295	8.1409	1.8059

Table (4.29): Statistical evaluation for the effect of rate of shearing on the residual shear strength ratios and parameters of the unfissured unlocked KB and K specimens with a size of 60 mm and p'_c = 330 kpa.

Material type	Shear strength parameters	with distilled water PH = 6.5	With tap water PH = 7
Unfissured locked KB	τ' (kpa) OCR = 1	79.0	78.01
		79.0	78.01
	c' (kpa)	25.117	25.870
	ϕ'(deg.)	9.274	8.979
locked K	τ' (kpa) OCR = 1	149.1	149.5
	c' (kpa)	16.717	20.412
	ϕ'(deg.)	21.859	21.366

Table (4.30): The effect of type of water on the effective peakshear strength and parameters of the specimens.

Specimen specification	Effective peak shear strength (kpa)				Statistical evaluation	
	Repeatation	First test	Second test	Third test	Mean value	Standard deviation
KB, l = 60 mm	locked	78.01	79	—	78.555	0.771
p'_c = 330 kpa	unlocked	83.01	84	82.5	83.170	0.763
K, l = 60 mm	locked	149.51	151	153	151.17	1.751
p'_c = 330 kpa	unlocked	155.9	153	157	155.30	2.066
KB, l = 100 mm p'_c = 660 kpa	locked	123.9	125.65	119.8	123.117	3.003
KB, l = 300 mm p'_c = 330 kpa	unlocked	57.0	58.48	57.19	57.557	0.805

Table (4.31): The statistical evaluation of the number of repeatation of test.

Appendix A(4.1):

An example of the program written for data logging of the direct shear tests.

```
Datataker 0 Version 3.33
Initializing...Done.

50_3/_Ali
3658   432
; CARDID="50_3/_Ali"  ' Version 3.33  D.E. October 1995
; P10=20 P22=9 P25=7 P15=0  P31=1 P33=8 P39=0 /n/m/e/u/T
; Y1=12,-5.735589332E-3"mm" 'LVDT 23       25 mm  Amp  G
; Y2=15,-9.127502077E-3"mm" 'LVDT 24       50 mm  Amp  G
; Y3=4.47962362,3.3424068E-2"KG"              'Transducer
; BEGIN
;  RA1M
; 1V(Y3,FF3) 3+V(X,Y1,FF2)  3-V(X,Y2,FF2)
; '  Trans      LVDT 23    LVDT 24
; END
; LOGON
; GA
; CARDID 4SV
; /M/N/U STATUS8 /m/n/u
```

CHAPTER 5

FLAC MODELLING OF DIRECT SHEAR BOX

5.1 INTRODUCTION

As discussed in Chapter 4, to study the effect of spacing required a large direct shear box (larger than 300 mm) or a numerical solution. The former was neither feasible nor within the scope of this research. Thus, in order to study numerically the effect of fissure parameters like width of spacing on the effective shear strength, it was necessary first to simulate numerically, the strain softening behaviour which is an intrinsic characteristic of the naturally overconsolidated fissured clay masses (Skempton, 1948, Bishop et al., 1965). FLAC (Fast Lagrangian Analysis of Continua, Itasca, 1994), combined with a programming section (FISH) of the FLAC were used for numerical simulations of the strain softening behaviours observed experimentally for both fully fissured and unfissured specimens subjected to direct shear tests. Then, after verifying the models with the available experimental results, the interaction of fissure parameters on the effective shear strength parameters (c'_u and ϕ'_u) of the unfissured material was studied by taking into account the effect of the strain softening behaviour of the materials.

After numerically investigating the effects of fissure parameters by modelling direct shear boxes for three different spacings but with the same width of fissure and

percentage of fissure surface and also for three different widths of fissures but with the same spacing, and formulating the available experimental results on the effects of P'_c, size, situation of horizontal stresses, a model was written by using the programming section of the FLAC. That model was designated as the Homogenised Strain Softening Model (HSSM). In it, first the effects of the different parameters were estimated individually by using the experimental and numerical relationships and then the effects were applied as functions or factors on the functions of the effective shear strength parameters of the unfissured material (c'_u and ϕ'_u) with respect to the strain softening formulations.

The HSSM was used to estimate the effective shear strengths of the specimens which in laboratory simulations were neither possible nor practical. For example, it was used for the estimation of the effective shear strength of the partially or fully fissured locked specimens or estimation of the effective shear strength of the very large specimens, 600 mm.

The procedures to simulate the effects of these parameters can be used in the evaluation of the interaction of the parameters on the effective shear strength parameters of a naturally overconsolidated fissured clay mass.

5.2 INTRODUCING FLAC PROGRAM AND FISH

The FLAC program (Itasca, 1993)is essentially a continuum stress analysis code, with a range of nonlinear models available for soil or rock material, interfaces, and structural elements for modelling rock bolts, tunnel linings, etc.

Using the strain softening/hardening model available in the FLAC program for the material, the user can represent arbitrary non-linear hardening and softening behaviour of the material, based on the variation of cohesion, friction, and dilatancy with plastic strain. The user can define the cohesion, friction and dilation of the material as functions of the total plastic strain. These are defined as piecewise linear segments of a generally non-linear function of the total plastic strain. In reality, these functions are non-linear, however, they may be approximated as a set of linear segments for use in FLAC.

Interfaces are desirable to represent planes on which sliding or separation can occur and FLAC provides interfaces that are characterised by Coulomb sliding or tensile separation. They are defined with the properties of friction, cohesion, normal and shear stiffness, and tensile strength supposed constant for use in FLAC.

Joint or fissure properties are conventionally derived from laboratory testing (eg. triaxial and direct shear tests). These tests can produce physical properties for joint or fissure friction angles, cohesion, dilation angles, and tensile strength, as well as joint or fissure normal and shear stiffnesses.

FISH (short for FLACish) is a programming language embedded within FLAC which enables the user to define new variables and functions. These functions may be used to extend FLAC's usefulness or implement new constitutive models. For example, new variables may be plotted or printed, special grid generators may be implemented, servo control may be applied to a numerical test, unusual distributions of properties may be specified, and parameter studies may be automated.

FISH is a compiler rather than an interpreter. Programs entered via a FLAC data file are translated into a list of instructions stored in FLAC's memory space; the original source program is not retained by FLAC. Whenever a FISH function is invoked, its compiled code is executed. The use of a compiled code rather than an interpreted source code enables programs to run much faster . However, unlike a compiler, variable names and values are available for printing at any time; values may be modified by the user by using FLAC's **SET** Command.

The rotation of principal stresses and the strength weakening of the material by the increase of the plastic deformation cause the non-uniformity of stress and strain of the zones or elements located along the sheared zone or sheared band in the direct shear box modelling. Therefore, assuming constant properties for the interface when simulating the strain-softening behaviour for the material, is not valid.

Assigning a strength weakening model of the properties to the interface due to the shear displacement is not referred in the FLAC program. However, there is a possibility that variable material properties can be assigned to the interface during each step through the FISH programming by the user.

5.3 NUMERICAL SIMULATION OF THE DIRECT SHEAR BOX

5.3.1 Background

The direct shear box test is used to determine the strength and deformation properties of soils. In spite of defects reported by researchers (Horslev, 1960; Saada et al., 1981), this test remains popular in practice owing to its simplicity and the results are consistent with results from more sophisticated ones.

Specimens in the direct shear box test have received some study. Optical observations have been made by some researchers (Morgenstern et al., 1967). Some numerical and mathematical models for the investigation of the physical or mechanical behaviour of the specimens subjected to direct shear test have been reported in the literature (Noona et al., 1972; Potts et al., 1987; Dounies et al., 1988; Duan et al., 1991; Cividini et al., 1992;).

In the computer modelling of the direct shear box, providing the possibility of sliding or separation and shearing the upper half over the lower half through the shear band or sheared zone is very important to simulate the behaviour of the tests properly and this point has been ignored in almost all the research conducted by the using finite element method.

Another important point in the modelling of strain-softening behaviour is to relate the reduction of the cohesion and friction angle to the increase of the total horizontal deformation (sliding and plastic deformation). In the research reported by Potts et al. (1987), Dounias et al. (1988) and Cividini et al. (1992) for the direct shear box computer modelling by using Finite Element method programs, the reduction of cohesion or friction angle was just related to the increase of the plastic deformation and conditions for the possibility of sliding in the formulation of the plastic deformation have been ignored.

However, in some numerical modellings of the direct shear box, the large strain model has been used for the elements in the sheared zone or shear bound. The mesh dependency of the results has been also pointed out strongly in these modellings (Potts et al. 1987, Dounias et al. 1988).

5.3.2 The Simulation of the Direct Shear Box Using FLAC

Figure (5.1) shows the generated mesh for the modelling of the direct shear box consisting of a grid of 4 × 8 (which means 4 rows and 8 columns) or 32 zones for the simulation of the clay specimen, of 100 mm by 100 mm and 20 mm thick, and 22 zones for the simulation of the shear box including lower, upper and cap loading parts. These parts were modelled through very stiff elements. Both vertical and horizontal displacement of the lower part of the box were constrained. The vertical displacement of the upper part was free and horizontal displacement was controlled by the applied constant horizontal rate of shearing simulated to the constant horizontal velocity applied by the direct shear box machine during the shearing of the specimen.

In order to provide the possibility of the sliding of the upper half over the lower half, a continuous interface was located along the surfaces of the shearing planes of the direct shear box between the two halves. The material properties of the interface were defined for both unfissured and fully fissured unlocked specimens.

Assuming and assigning an interface for the direct shear box was reasonable, because in the direct shear box test, the shear band, sheared zones and slipping surfaces are located along the plane surfaces of the two halves of the box. Even for the simulation of the partially fissured specimens with a horizontal pre-existing crack or fissure, in a plane strain direct shear box, because the propagation of the fissure is in the direction of the plane of the pre-existing crack (Bjerrum, 1967; Palmer et al., 1973; and Chowdhury, 1978), this assumption was reasonable and valid.

But for the simulation of triaxial specimens, because the direction of the creating or growing of shearing surfaces or slip surfaces, as well as the direction of the propagation of pre-existing fissure in the orientated partially fissured triaxial specimens is not known initially, and is stress dependent, this approach is not applicable and practical and needs more investigation.

In addition to assigning an interface for sliding (interface ②), for each two non homogenised contact surfaces such as contact surfaces ①, ③, ④, ⑤, ⑥, ⑦, ⑧, an interface was assigned.

The numbers ④, ⑤, ⑥, ⑦, and ⑧, were defined glue interfaces to prevent any slip or separation for these interfaces. The values of friction, cohesion and tensile strength were not needed and ignored (Itasca, 1993) but the shear and normal stiffnesses were provided. For interfaces ⑤ and ⑦ K_n = 1e14 pa/m and K_s = 1e14 pa/m and for interfaces ⑥ and ⑧ K_n = 1e12 pa/m and K_s = 1e4 pa/m were estimated and for interface ④ K_n = 1e12 pa/m and K_s = 5e10 pa/m were estimated. The basic concept in the estimation of K_n and K_s for interface ⑥ was the similarity of vertical and horizontal displacements of grid points located in both sides of the interface.

The K_n = 1e14 pa/m and K_s = 1 pa/m were assigned for interfaces ① and ③. K_s = 1 pa/m was assigned in order to minimise the force needed for the sliding of elements attached to these interfaces.

The E, K_V, G, and γ (elastic, bulk shear module, Poisson's ratio and density respectively) for steel parts (stiff parts) were assumed E = 200 Gpa, , K_v = 1.1 e11 pa, G = 8e10 pa, ν = 0.2 and γ = 7 t/m^3.

The type of interface assigned for number ② was real type. This interface is designated as a main interface. The material properties of the main interface were defined based on laboratory tests. For each preconsolidation pressure, the c′and ϕ' were estimated from laboratory tests for both fully fissured and unfissured unlocked 100 mm specimens.

E, K_v, G, ν, and γ were estimated for KB specimens, E= 44e6 pa, K_v = 6.25e7 pa, G = 1.4e7 pa, ν = 0.3958, γ = 1.660 t/m^3. The K_n and K_s were estimated from the results of direct shear box tests. The assigned values were K_n = 1.8384e10 pa/m K_s = 1.8384e10 pa/m in the model.

Normal stress was applied on the top of the upper half of the box. The shear rate applied was xvel = 8.33e-8 m/step. Although in the model simulated by FLAC, the rate of shearing has no relation with the rate applied for drained tests in the laboratory, and also has no impact on the behaviour of the test, it could have a shock effect on the behaviour of the stress-strain of the material if it were assigned faster than the applied rate in the model.

In order to provide enough rigidity for the frame of the direct shear box in the upper half as well as the rigidity of cap, the same velocity was applied for both sides of the stiff parts.

5.3.3 The Constitutive Model

An elastic material constitutive model was assigned for stiff parts and primarily Mohr Coulomb plasticity for the clay specimens. After calibrating and confirming all the parameters needed to be defined for the simulation of the fully fissured and unfissured unlocked specimens, primarily the simple Mohr Coulomb model was assigned to the clay specimens. Figures (5.2) and (5.3) show the results of FLAC modellings of the unfissured and fully fissured unlocked KB specimens consolidated and sheared with a P'_c of 660 kpa for the simple Mohr Coulomb model. As can be seen from these two figures, the type of stress-strain is not a strain softening one. A few models with different numbers of layers with simple Mohr Coulomb models were run to study the effect of the number of layers on the results. Table (5.1) displays the results for four different models for fully fissured and unfissured unlocked KB specimens consolidated and sheared with 660 kpa pressure. As the results indicate, the increase of the layers increased the shear strength somewhat, but taking into account the time and memory of the hard disc required to run the models for the higher number of layers, layers were chosen for subsequent models. In the next attempt, strain softening models, available in the FLAC program which is only applied to the material by relating the changes of $c'$and ϕ' to the plastic strain, were used to simulate the strain softening behaviour of the material.

Table (5.2) shows the changes of the c' and ϕ' with the horizontal strain for both fully fissured and unfissured unlocked KB specimens of 100 mm and P'_c = 660 kpa and the rate of shearing = 0.005 mm/min.

From Figures (4.25) and (4.26), the variation of c' and ϕ' with shear displacement of unfissured and fully fissured KB specimens consolidated with P'_c = 660 kpa were estimated. Figures (5.4) and (5.5) show the relationships between c' and ϕ' of the unfissured and fully fissured unlocked KB specimens consolidated by P'_c = 660 kpa with shear strain.

In Figures (5.4a) and (5.4b), the c′ and ϕ′ are reduced from the peak values to residual values within 3% of horizontal strain. Cohesion reduction is more than 50% but friction reduction is about 10-15%. In other words, the type of strain-softening behaviour is a brittle rather than a ductile type. In Figure (5.4a), before ϕ′ reaches residual magnitude, there was a drop in the graph which is about the horizontal percentage of strain for the happening of the fully softened shear strength.

For the fully fissured KB specimens as shown in Figure (5.5a), the friction is reduced from the peak to residual value within 1% from the peak horizontal strain. At residual, the friction is about 30%. The friction angle obtained from unfissured and fully fissured specimens for the peak is the same, but at residual displacement, the friction angle of the fully fissured unlocked specimens is much less than that the unfissured unlocked specimens.

In Figure (5.5b), the cohesion of the peak point is reduced and increased to the residual value within 1% of the horizontal strain from the peak horizontal strain. Although the cohesion is increased at residual, the cohesion of fully fissured specimens is reduced drastically in comparison with the cohesion of the unfissured unlocked specimens.

By being fissured a specimen, a cohesion reduction of 70% at peak and 60% at residual values took place, but for friction angle, almost no reduction at peak and 30% at residual values was observed.

Figure (5.6) shows the FLAC modelling results of the unfissured unlocked KB specimens on which the strain softening model was applied to the material by the Table Command. In that model, the c′ and ϕ′ were related to the plastic strain as piecewise linear systems of the total shear strain by using the Table Command of the FLAC programme.

It can be seen that the drop from the peak to the residual shear strength happened in a few connected linear pieces of lines and was not a continuous curve. In order to modify the trend of the strain softening behaviour as a continuous curved line, the relationships between c′ and ϕ′ of the unfissured and fully fissured unlocked KB specimens consolidated by P'_c = 660 kpa with shear strain as depicted in Figures

(5.4) and (5.5) respectively, were estimated by using the curve fitting of a statistical program like SPSS. The relationships were displayed in Equations (5.1) to (5.4) for the fully fissured unlocked KB specimens, and in Equations (5.5)-(5.8) for the unfissured unlocked KB specimens.

Taking into account the condition for the best curve fit that is appeared in correlation coefficient r or coefficient of determination (r^2), a high value of r^2 is a strong confirmation of the proposed model.

For the relationships between friction and shear strain (ε_h) of the fully fissured unlocked KB specimens:

$0.91033 \leq \varepsilon_h \leq 1.4601189$

$$\phi'_F = 8.426501846 + 3.6183\ \varepsilon_h^2 - 2.7532\ \varepsilon_h^3 \qquad (5.1)$$

$1.4601189 < \varepsilon_h \leq 2.01033$

$$\phi'_F = 17.41666234 - 8.2484\ \varepsilon_h + 0.7058\ \varepsilon_h^3 \qquad (5.2)$$

cohesion with shear strain (ε_h):

$0.91033 \leq \varepsilon_h \leq 1.11033$

$$C'_F = 18131.574776 - 12660.65578\ \varepsilon_h \qquad (5.3)$$

$1.11033 < \varepsilon_h \leq 2.01033$

$$C'_F = e^{(9.811561365 - \frac{1.6645}{\varepsilon_h})} \qquad (5.4)$$

For the relationships between the friction and shear strain (ε_h) of the unfissured unlocked KB specimens:

$1.8844 \leq \varepsilon_h \leq 4.794$

$$\phi'_U = 11.00410705 - 0.9302\ \varepsilon_h + 0.0173\ \varepsilon_h^3 \qquad (5.5)$$

$4.794 < \varepsilon_h \leq 12$

$$\phi'_U = 8.454666 - 8.05462\ e^{-4\varepsilon_h} \qquad (5.6)$$

cohesion with shear strain (ε_h):

$1.8844 \leq \varepsilon_h \leq 4.794$

$$C'_U = 644438.2549 - 18322\,\varepsilon_h - 1908.75\,\varepsilon_h^2 \quad (5.7)$$

$4.794 < \varepsilon_h \leq 12$

$$C'_U = 22948.911740 - 515.859312\,\varepsilon_h \quad (5.8)$$

Figures (5.7) and (5.8) display the relationships between C'_U and ϕ'_U with shear strain for three different P'_c of 330 kpa, 440 kpa and 660 kpa of the unfissured unlocked KB 100 mm specimens and Figures (5.9) and (5.10) depict the relationships between C'_F and ϕ'_F with shear strain for three different P'_c of 330 kpa, 440 kpa, and 660 kpa of the fully fissured unlocked KB 100 mm specimens.

As can be seen from these figures, the trend of strain softening behaviour is independent of the P'_c. In other words, it is possible that the formulation of the strain softening behaviour be normalised and be used for different P'_c and size specimens but for the same material type.

There were three options for applying the strain softening model. The first was applied only to the clay specimen, the second only to the main interface and the third to both the clay specimens and main interface.

By applying strain softening only to the clay material (specimens), the sliding part of the deformation of the material for the assigned and calibrated values of K_n and K_s of the main interface was negligible and total deformation was induced by plastic deformation. By reducing the K_s in order to provide enough sliding, the shear strength was reduced significantly and also no strain-softening occurred in the stress strain curve of the material in spite of assigning the strain softening model to the material for the reduced K_s.

Another aspect of the results of this section of the study was the strain-softening of the clay material around the main interface. From the running of the different initial models to which strain softening models were applied in the different layers around the interface, it was discovered that strain-softening behaviour took place in the layers very close to the main interface. It did not make any difference to the results if the simple Mohr Coulomb plastic models were assigned for the other layers.

However, for all the models in which strain softening was applied to the material, the problem of sliding was observed.

In the second option, it was necessary to use FISH programming and write a program to assign variable material properties by changing the horizontal strain to the main interface for each substep during the execution of the FLAC model.

In the third option, strain-softening models were applied to both the materials and main interfaces. There was a little reduction of strength for the same initial conditions applied in the two previous options. The reduction was negligible. Moreover, it was observed that strain-softening happened in the layers very close to the sheared zone in the models run by the authors. For these reasons, in subsequent models, only the strain-softening was assigned to the main interface.

5.3.4 Simulation of the Strain-Softening Behaviour Using FISH Programming

Taking into account all the drawbacks and short-comings explained in the preceding section, two programs were written for the simulation of the strain-softening behaviour of fully fissured and unfissured unlocked specimens. The two models have been reproduced in Appendices A(5.1) and A(5.2). In these two programs, the strain-softening behaviour as mathematical functions were related to the average percentage of horizontal displacement or shear deformation in each time-stepping and applied only to the main interface. As explained previously, these functions were estimated by using the curve fitting option of SPSS software. The simple Mohr Coulomb plasticity model (perfect plastic) was defined or assigned for the material.

In order to relate the changes of shear deformation to the changes of c' and ϕ' of unfissured and fully fissured unlocked KB specimens, the average shear deformation in each substep or the average shear strain was calculated through the subroutine written by using FISH. For each substep of loading, the c' and ϕ' were calculated and then based on the new magnitude of the $c'$and ϕ', the numerical models were resolved and subsequently the new magnitudes of the average shear deformation was calculated and then the $c'$and ϕ' were calculated based on the new average shear deformations. For each substep this process was repeated to reach the total number of step prescribed at the beginning of the running the model by using a loop command.

Figures (5.11) and (5.12) show the effective shear stress (kpa) against horizontal shear strain of the unfissured and fully fissured (respectively) KB specimens (100 mm by 100 mm) subjected to direct shear test and consolidated with P'_c =660 kpa and sheared for the OCR of one.

As can be seen from Figure (5.12), because the fissure in the fully fissured specimen was closed, even for fully fissured specimens, strain-softening behaviour was observed, but changes of strengths from peak values to residual values happened very fast. In other words, brittle failure happened in the fully fissured unlocked specimens in comparison with unfissured unlocked KB specimens.

Figures (5.13) and (5.14) show the numerical results obtained from the FLAC models (using FISH programming) for the simulation of the unfissured and fully fissured KB specimens for the same initial conditions indicated for the experimental tests depicted in Figures (5.11) and (5.12). By comparing the numerical results (pa) with the experimental results, it can be seen that they almost match.

Table (5.3) shows the effect of the variation of K_n and K_s of the main interface on the effective shear strengths for the fully fissured and unfissured unlocked KB specimen models. Increasing the normal and shear stiffnesses, the magnitude of peak did not show a significant increase but the mobilisation of the shear strength happened with less shear strain.

Table (5.4) displays the numerical results obtained from the modelling of unfissured unlocked KB specimens for different mesh sizes. A grid of 4×8 means a grid with 4 rows and 8 columns located in two separate sets, one the upper half, the other the lower half of the direct shear box specimen.

By increasing the number of layers from 4 to 8, no significant increase happened. But for models with less than 4 layers, the peak effective shear strength showed a little decrease. Altogether for the finer mesh, the increase of peak effective shear strength was negligible. Taking into account the increase of time and memory for running the finer mesh models and negligible effect of mesh size the grid of 4×8 was chosen for subsequent models.

In contrast to the mesh dependency of the direct shear box models using finite elements in the research conducted by Potts et al. (1987) and Fortin et al. (1990), the numerical results obtained from the FLAC models for the unfissured and fully fissured specimens showed the independency of the models to the variations of K_n and K_s as well as the size of the mesh.

5.4 SIMULATION OF THE EFFECTS OF OTHER PARAMETERS BY FLAC

In the preceding section, the simulations of strain softening for the unfissured and fully fissured KB specimens consolidated with a P'_c of 660 kpa for 100 mm have been explained numerically by using FLAC and FISH programming. In this section, specific considerations have been given to simulate or formulate the effects of other parameters such as rate of shearing, situation of horizontal stresses or to formulate the effects of the parameters such as P'_c, size of specimens and fissure parameters like, width, spacing and orientation of fissures by using FLAC programme and FISH programming.

5.4.1 The Velocity or Shearing Rate

The modelling of problems which involve the coupled response of fluid flow and mechanical behaviour is possible and considered in FLAC, but the effect of negative pore pressure during the shearing process as a result of the increase of rate of shearing, can not be considered unless through an empirical or experimental formulation defined by the FISH programming. Moreover, the displacement cannot be controlled or applied directly in FLAC. In order to apply a given displacement to a boundary, it is necessary to prescribe the boundary's velocity for a given number of steps. If the desired displacement is D, a velocity of V, over N steps (where N = D/V) may be applied. In practice, V should be kept small and N large in order to minimise shocks to the system being modelled. The magnitude of V = 8.37e-8 m/step was applied for the models. By applying this magnitude of shearing rate to the models, a step of 150000 was needed to obtain a displacement of 10-12 mm which corresponded to a maximum shear deformation of 10% -12%.

5.4.2 The Simulation of the Effect of Locked in Horizontal Stress

Another parameter in the laboratory simulation is the effect of horizontal locked-in stresses or lateral stresses in the in-situ tests. In the field, the clay particles are well oriented. By sampling these, lateral stresses are released and the uniformity of the material is changed, especially around the surfaces, edges and corners of the natural specimens.

In order to simulate the horizontal locked in stresses in the FLAC model, the model was run initially for a number of steps without applying the shearing rate to the upper half of the shear box model, while the vertical displacement of the grid points located in the lower half was fixed in order to have uniform layers on the top of the interface. In the next stage, the model was run by applying the shearing rate. The appearance of the horizontal locked-in stresses established from the first stage, as well as fixing the vertical displacement of the grid points on the lower half, could reduce the average shear strength obtained from the model.

There was a good agreement with the experimental results for the high level of normal stresses but for the low levels, the agreement was not satisfactory. For this reason, in the final model explained next, the effects of horizontal locked in stresses for different types of material and different preconsolidation pressures, estimated from the experiments on the c' and ϕ', were applied as coefficients of functions to the homogenised strain softening model as will be explained in the following section.

5.4.3 Formulation of the Effects of P'_c and Size

As discussed in Chapter 4, the results of the laboratory tests for the different P'_c of the KB specimens showed that by increasing P'_c, both c' and ϕ' were increased. To estimate the effect of different OCR's, different normal stresses for each prescribed P'_c were applied, based on the OCR of 1,2.5,5 and in some cases 10 (σ_N: normal stress = P'_c/OCR). The trend of the results showed that there was a P'_c for each size and material type and that after that particular P'_c, no more increase in c' and ϕ' took place in the laboratory tests.

Tests conducted to note the effect of size showed that by increasing specimen sizes, both c' and ϕ' decreased and the trend showed that there was a size for each type of

material or for each magnitude of P'_c after that the specimen size effect was negligible. In other words, after increasing the size from a particular size and for each P'_c, no more reduction in c' and ϕ' was observed. The results obtained in these two discussions have been used in writing the homogenised strain softening model explained subsequently.

5.4.4 The Simulation and Formulation of the Effects of Fissure Parameters

As discussed in the proceeding chapter, the fissure parameters such as width, spacing, and orientation were simulated experimentally for the direct shear tests. The results from the study of inclined fissured specimens subjected to direct shear tests showed no difference. For this reason as discussed in Chapter 6, the problem has been investigated experimentally on triaxial specimens. Meanwhile, there was a problem to study experimentally the effect of the spacing of the fissures for the same percentage of fissure surfaces and fissure widths because of the lack of accuracy of the data logging system and tools as well as the high disturbance of the specimens for the closely spaced fissures for the available long specimens (300 mm) Therefore, from the two options discussed in Chapter 4 numerical simulation was used for the study of the effect of fissure parameters such as width and spacing.

In order to simulate numerically the partially fissured specimens, a combination of strain softening models for the fully fissured and unfissured models was used. For the unfissured parts, the formulation of strain softening models for unfissured specimens and for the fissured parts, fully fissured specimens were applied. A typical model prepared for the modelling of partially fissured KB specimens is explained in Appendix A(5.3).

For three different combinations of widths and spacings of fissures, the partially fissured models were prepared and run to estimate the effects of these two parameters on the c' and ϕ'. Figure (5.15) shows schematically the different models were run for the study of the effect of fissure surfaces. The number of blocks was eight. In the partially fissured specimens, the blocks assumed fissured were marked by horizontal lines in the middle of the blocks. Figure (5.16a) shows the seven different cases run for the 25% fissured specimen models. The 50% and 75% fissured specimen models for the same spacing are depicted in Figure (5.16b) and Figure (5.16c) respectively.

In Figure (5.16a), seven different possible arrangements of fissures were depicted for a specimen with an eight block or zone arrangement. Thus, the effect of any possible numerical error as a result of the arrangement of the fissures was eliminated. The average result of each case of study of fissure percentage was taken into account for further analysis.

Figure (5.17) shows schematically the different arrangements of fissures for studying the effect of spacing on the effective shear strength. Figure (5.17a) shows fissures of 75 mm with spacing of 150 mm. As can be seen from these configurations, four possible arrangements were depicted for an eight block specimen. The other three spacings were 112.5 mm, 300 mm and 187.5 depicted in Figures (5.17b), (5.17c) and (5.17d) respectively.

In each model, three levels of normal stresses corresponding with OCRs of 1, 3.3 and 5 were applied. Table (5.5) shows the numerical results obtained from the running of these models for three levels of OCR's for the unfissured and fully fissured unlocked KB specimens of 100 mm and P'_c = 660 kpa.

Table (5.6) displays the Mohr Coulomb parameters obtained numerically from the study of the width of fissures and average peak shear strength for each percentage of fissure surfaces. Table (5.7) shows the Mohr Coulomb parameters obtained numerically from the study of the effect of spacing of fissures and average peak shear strength for each spacing of the fissures.

The trends of the results for this particular size (100 mm) showed that by increasing the width of fissure, the shear strength was reduced reaching the shear strength of a fully fissured specimen and by increasing the spacing, the shear strength was increased reaching the shear strength of an unfissured specimen. The changes of fissure parameters influenced mainly the peak effective cohesion rather than the peak effective friction. These results were used in writing the homogenised strain-softening program explained in the following section.

The effects of the orientation of fissures in the direct shear box were estimated by running the FLAC model for the inclined fissured specimens. The model was run for every 5 degrees of inclination to the horizontal direction of the direct shear box

model. The results for the range 20° to 90° inclinations showed little reduction in shear strength because of the presence of the inclined fissure. The maximum reduction in strength of partially oriented fissured specimens happened for the model with an inclination of 60° to the horizontal direction.

Figure (5.18) shows the shear strengths obtained numerically from the inclined fissured specimens against the inclinations of fissure.

5.5 THE HOMOGENISED STRAIN SOFTENING MODEL

The models developed for the simulation of strain-softening of the fully fissured and unfissured specimens were able to simulate models for defined initial conditions. As initial conditions were changed, the models should have been modified for new conditions.

To eliminate this drawback, the results of experimental, as well as numerical modellings designed for the estimation of the effects of fissure parameters, were used in a new model and all the effects estimated experimentally or numerically were applied on the new model as functions or coefficients. The size, P'_c, percentage, width, and spacing of fissures, type of material and the situation of the horizontal stress as a locked in or unlocked in horizontal stress, were introduced initially as input data to the model.

The effects of these parameters were estimated as functions and coefficients and were applied to the main part of the model. In other words, the effects were estimated, homogenised and then applied on the C'_U and Φ'_U of the basic strain softening model written for an unfissured specimen. The following steps were taken into account to write the homogenised strain-softening model (HSSM).

1- Formulation of the strain-softening behaviour for the different materials for the particular size and preconsolidation pressure of an unfissured specimen. From the experimental results, the mathematical relationships between c' and ϕ' of the unfissured unlocked specimens with percentages of horizontal displacement for different types of materials were established using SPSS software. These formulations of strain-softening were considered as base formulations of the strain softening for each type of material.

2- Formulation of the interactions of P'_c and size with c' and ϕ' for each type of material. Figure (5.19) shows schematically the relationships between p'_c and size with c' or ϕ' for the KB unfissured unlocked specimens. From the experimental results the formulations were estimated by using SPSS regression analyses and mathematical formulation of the plane surfaces in a three dimensional space of P'_c, size and c' or ϕ'. The numbers in this figure refer to the number of plane surfaces.

The mathematical equation for each plane surface for both c' and ϕ' with P'_c and size (l) are reported in Appendix (A 5.4). The basic formulation regressed is displayed in Equation (5.9).

$$Y = e^{(b_0 + \frac{bl}{t})} \qquad (5.9)$$

In this equation, Y is referred to C'_U and Φ'_U, b_0 is a constant and b_1 is the regression coefficient and t is an independent variable which for the relation between C'_U and Φ'_U with size (l) it was size (l) of the specimen or for the C'_U and Φ'_U with P'_c, it was the P'_c (kpa). For example, for the P'_c = 330 kpa the Equations (5.10) and (5.11) were regressed (with $r^2 = 1$) for the relationships between c' or ϕ' with size (l):

$$C'_U = e^{(3.3139 + \frac{6.3606}{l})} \qquad (5.10)$$

$$\Phi'_U = \text{Arc tan}\,(e^{(-2.1294 + \frac{17.5980}{l})}) \qquad (5.11)$$

and for 60 mm, the Equations (5.12) and (5.13) were regressed (with r^2 = 0.960 - 0.984) for the relationships between c' and ϕ' with P'_c (kpa) or Equations (5.14) and (5.15) were regressed (with r^2 = 0,971 - 0.976) for the size of 100 mm.

$$C'_U = e^{(4.0600 - \frac{205.90}{p'_c})} \qquad (5.12)$$

$$\Phi'_U = \text{Arc tan}\,(e^{(-1.6036 - \frac{78.900}{p'_c})}) \qquad (5.13)$$

$$C'_U = e^{(3.8331 - \frac{145.55}{p'_c})} \qquad (5.14)$$

$$\Phi'_U = \text{Arc tan}\left(e^{(-1.6479 - \frac{96.918}{P'c})}\right) \quad (5.15)$$

In order to formulate mathematically the surfaces created from the intersections of the curves estimated for the P'_c with the curves estimated for the size, the curved surfaces were simplified with a few discontinuous plane surfaces. Then, for each plan surface, two three dimensional vectors were defined The normal vector to the plane surface which passes through these two vectors is the cross product of these two three dimensional vectors.

$$\vec{p}_1 = a_1\vec{i} + b_1\vec{j} + c_1\vec{k} \quad (5.16)$$

$$\vec{p}_2 = a_2\vec{i} + b_2\vec{j} + c_2\vec{k} \quad (5.17)$$

$$|p_1| = \sqrt{a_1^2 + b_1^2 + c_1^2} \quad (5.18)$$

$$|p_2| = \sqrt{a_2^2 + b_2^2 + c_2^2} \quad (5.19)$$

$$\vec{p}_1 = \vec{n}_1 . |p_1| \quad (5.20)$$

$$\vec{p}_2 = \vec{n}_2 \ |p_2| \quad (5.21)$$

$$\vec{N} = \vec{p} \times \vec{p}_2 \quad (5.22)$$

$$|N| = |p_1| \times |p_2| . \sin\alpha \quad (5.23)$$

$$\vec{N} = |N| \times \vec{n}_v \quad (5.24)$$

$$\vec{n}_v = \vec{n}_1 \times \vec{n}_2 \quad (5.25)$$

The $\vec{n}_v$ is the direction vector or unit vector of the plane surface which passes through the $\vec{p}_1$ and $\vec{p}_2$.

$$\vec{n}_v = a\,\vec{i} + b\,\vec{j} + c\,\vec{k} \quad (5.26)$$

For any arbitrary vector located in this plane such as $\vec{p}$ vector with the components of:

$$\vec{p} = (x-x_0)\ \vec{i} + (y-y_0)\ \vec{j} + (z-z_0)\vec{k} \quad (5.27)$$

the dot product of the $\vec{n}_v$ with arbitrary vector, $\vec{p}$ would be zero.

$$\vec{n}_v \cdot \vec{p} = 0 \tag{5.28}$$

$$a(x-x_0) + b(y-y_0)\, c(z-z_0) = 0 \tag{5.29}$$

$$aX + bY + cZ = d \tag{5.30}$$

$$d = aX_0 + bY_0 + cZ_0 \tag{5.31}$$

$$a'X + b'Y + c'Z = 1 \tag{5.32}$$

$a' = a/d$

$b' = b/d$

$c' = c/d$

In these equations: a_1, b_1 and c_1 or a_2, b_2 and c_2 are the component vectors $\vec{p}_1$ and $\vec{p}_2$ respectively. $|p_1|$ or $|p_2|$ is the length of the vector. $\vec{n}_1$ or $\vec{n}_2$ is the cosine direction vector or unit vector of $\vec{p}_1$ or $\vec{p}_2$ respectively. $\vec{N}$ is the cross product or vector product of the two vectors ($\vec{p}_1$ and $\vec{p}_2$). $|N|$ is the magnitude of $\vec{N}$. α is the angle between vectors $\vec{p}_1$ and $\vec{p}_2$. $\vec{n}_v$ is the unit vector of $\vec{N}$. $\vec{p}$ is an arbitrary vector located in the plane of ($\vec{p}_1$ and $\vec{p}_2$. d or a′, b′, and c′ are constant coefficients.

These procedures can be applied for each type of material in order to formulate the relationships within c′ and ϕ' of unfissured unlocked specimens with P'_c and size of the specimens.

3- Formulation of the interactions of the width (w) and spacing (s) with c′ and ϕ' from the results obtained from laboratory tests, as well as numerical modelling for the particular size (100 mm) and preconsolidation pressure (P'_c = 660 kpa) by using SPSS regression analyses and mathematical formulation of the plane surfaces in a three dimensional space (s, w, and c′ or ϕ'). For each material and for any particular size and P'_c, these interactions should be estimated. In order to generalise the results of the interactions of s and w with c′ or ϕ', for different sizes, the results from numerical modelling were normalised with the size of the specimen. Therefore, the relationships were formulated based on s/l and w/l with c′ or ϕ'. Figures (5.20) and (5.21) show schematically the relationships within s/l, w/l with ϕ' or c′ respectively.

For example, the relationships between c′ and ϕ′ with s/*l* for the constant width of fissure (w/*l* = 0.25) were depicted in Equations (5.33) and (5.34) respectively and the relationships between c′ and ϕ′ with w/*l* for the constant spacing of fissure (s/*l* = 1) in Equations (5.34) and (5.36) respectively.

$$c' = 3.8154 + 45.7264\ (s/l) - 21.7110\ (s/l)^2 \tag{5.33}$$

$$\phi' = 8.3568 + 1.3316\ (s/l) - 0.7965\ (s/l)^2 \tag{5.34}$$

$$c' = 35.9519 - 31.181\ (w/l) \tag{5.35}$$

$$\phi' = 9.0109 - 0.0063\ (w/l) \tag{5.36}$$

In these figures the numbers refer to the number of plane surfaces and the equations for each plane number have been reported in (A5.5).

4- Calculating and applying the effects of the parameters indicated in steps 2 and 3, as well as the experimental tests conducted for the study of different parameters as defined functions or determined coefficients on the base formulation of the strain softening behaviour for each particular material type.

Altogether three types of coefficients or functions were applied on the Mohr Coulombs parameters (C'_U and Φ'_U) for strain-softening formulations of each type of material. The first set of coefficients was determined based on the prescribed P'_c and the size introduced as a part of input data. By using the formulation of size and P'_c with c′ or ϕ′ , the c′ and ϕ′ for the prescribed size and P'_c of that particular material type were calculated and, then the coefficients β_1 and β_2 were calculated as follows:

$$\beta_1 = 1 - \frac{c'_{\text{calculated from the formulation of } p'_c, \text{ size with c}}}{c'_{\text{peak used for the base formulation of strain softening model (C')}}} \tag{5.37}$$

$$\beta_2 = 1 - \frac{\phi'_{\text{calculated from the formulation of } p'_c, \text{ size with } \phi'}}{\phi'_{\text{peak used for the base formulation of strain softening model } (\Phi')}} \tag{5.38}$$

The second set was calculated based on the presence of fissures in a specimen. Based on the fissure parameters (s/l and w/l), the magnitude of c′ and ϕ′ were

calculated from the formulation of the interaction of s/l and w/l with c′ and ϕ′ then the coefficients of θ_1 and θ_2 were calculated as follows:

$$\theta_1 = \frac{c'_{\text{calculated from the formulation of s/l and w/l with c'}}}{c'_{\text{peak used for the base formulation of strain softening model (C')}}} \quad (5.39)$$

$$\theta_2 = \frac{\phi'_{\text{calculated from the formulation of s/l and w/l with } \phi'}}{\phi'_{\text{peak used for the base formulation of strain softening model } (\Phi')}} \quad (5.40)$$

The third set was calculated for the effect of horizontal locked-in stresses. As explained in the preceding section, the results from FLAC modelling in this regard were not satisfactory Therefore, based on the experimental results for different types of material and different magnitudes of P'_c and size of specimens, the coefficients were estimated experimentally and programmed in the homogenised strain-softening model (HSSM). Based on the prescribed input data, the coefficients were estimated by the program itself.

γ_1= coefficient for modifying c′ for the effect of locked in horizontal stress (5.41)

γ_2= coefficient for modifying ϕ′ for the effect of locked in horizontal stresses (5.42)

In addition to these three main homogenising factors, another set of coefficients or functions was applied to the c′ and ϕ′ because of an error estimation of plane surfaces instead of curved surfaces in the three dimensional spaces of p'_c and size with c′ and ϕ′.

In the formulation of the interaction of P'_c and size with c′ and ϕ′ as well as s/l and w/l with c′ and ϕ′ , the curved surfaces were simplified as plane surfaces. For this assumption, this set of coefficients or functions was also introduced and applied to the homogenised strain-softening model.

ψ_1= correction factor for the effect of curve surface for c′ (5.43)

ψ_2= correction factor for the effect of curve surface for ϕ′ (5.44)

Therefore, these four sets of factors were applied to the base c′ and ϕ′ strain softening formulation. The coefficients α_1 and α_2 were applied as constants to the c′ and ϕ′ strain-softening formulations during the execution of the program.

$$\alpha_1=(1-\beta_1).\theta_1.\gamma_1.\ \psi_1 \tag{5.45}$$

$$\alpha_2=(1-\beta_2).\theta_2.\gamma_2.\ \psi_2 \tag{5.46}$$

A typical program of HSSM has been listed in Appendix (A5.6).

5.6 VERIFICATION AND PREDICTION OF THE EXPERIMENTAL TESTS

Verifying the available experimental results and then predicting the shear strength for cases in which laboratory simulation was impractical or impossible, were also other parts of this study. Table (5.8) shows the numerical results obtained by the HSSM compared with experimental results for the same initial conditions. The numerical results were verified by the experimental results.

For cases in which experimental simulations were not practical and possible, the shear strengths were predicted by the homogenised strain-softening model. For instance, the effective shear strength could be predicted by the HSSM for a partially or fully fissured horizontal locked-in stress specimen. It was possible to estimate experimentally the shear strengths of the horizontal locked-in stress specimens which were not partially or the fully fissured. Also it was possible to estimate experimentally the shear strengths of fully or partially fissured specimens which were not horizontal locked-in stress. But the experimental prediction for a combination of partially or fully fissured specimen with a horizontal locked-in stress condition was not possible and practical in the laboratory. From evaluating the experimental and numerical results and combining the results, these types of predictions and estimations were possible by the homogenised strain-softening model.

Figure (5.22) shows the experimental results obtained from direct shear tests on the 50% fissured and unlocked-in horizontal stress KB specimen (100 mm by 100 mm) consolidated and sheared with 660 kpa. Comparatively, Figure (5.23) shows the results estimated by FLAC model for the same initial conditions.

Figure (5.24) shows the experimental results for the 50 % fissured and unlocked-in horizontal stress KB sample (300 mm by 300 mm) consolidated and sheared with 330 kpa. The numerical results obtained from the FLAC model is indicated in Figure (5.25).

Table (5.8) lists the results obtained from HSSM (Homogenised Strain-Softening Model) for verification and comparison with the experimental results and also the prediction of HSSM for cases in which laboratory simulations were impossible or impractical.

5.7 DISCUSSION AND CONCLUSION

The objectives of this chapter were to simulate strain-softening behaviour by using FLAC programming (FISH) and also to simulate the effects of the parameters which were effective on the evaluation of effective shear strengths of the overconsolidated, unfissured, partially and fully fissured specimens subjected to direct shear tests and finally to write a program by using FISH to estimate or predict the effective shear strength of the specimens by homogenising the effects of the parameters discussed previously and applying the strain softening model written for the unfissured unlocked specimen.

In FLAC, shear strength softening is simulated by making Mohr Coulomb properties (cohesion and friction) functions of plastic strain and these functions are specified as linear piecewises by using the TABLE command. Tabulation of the c' and ϕ', instead of introducing the functions for them and only relating these parameters to the plastic deformation and ignoring to provide the conditions for the possibility of sliding or separation of the upper half of the specimen in the direct shear box model, could influence the prediction of the behaviour of the models in comparison with real behaviour observed in the laboratory tests.

In a direct shear box, sliding and plastic deformation happens along the shear band or shearing surfaces. Therefore, in this study, the reductions of c' and ϕ' due to strain were related to the horizontal strain or shear deformation which is a combination of sliding and plastic deformation.

An interface was also assigned along the shearing surfaces. The interface could simulate properly the behaviour of the material along the sheared zone or shearing surfaces by providing conditions for the sliding of the material, as well as the plastic deformation along the sheared zone or shearing surfaces.

Applying the strain-softening behaviour to the main interface in the direct shear box simulation by the FLAC showed much less mesh dependency in comparison with finite element modelling of the direct shear box.

The results from KB specimen tests showed that by increasing P'_c, the c' and ϕ' were increased. Also the trends of the results showed that there was a limit for the P'_c after which no more significant increases happened in c' and ϕ'. Also by increasing the size of a KB specimen for a particular P'_c, c' and ϕ' were decreased and there was a limit for the size after which no more pronounced reduction was noted in c' and ϕ'. These limits were estimated from the trends of the tests and were used in the programming. In order to consider the effects of fissure parameters, some limits also were defined. They were estimated from the trends of the experimental results.

The reduction of effective shear strength because of the presence of oriented fissures in the direct shear box modelling was negligible and should be studied experimentally or numerically on the three dimensional models.

The simulation of the effect of locked-in horizontal stress by the possible numerical approach proposed in this chapter was not satisfactory. However, the effects were applied through the coefficients obtained by the results of the vast experimental tests.

In direct shear box numerical modelling, because the shearing surfaces coincide with the plane surface of the two halves of the box, an interface can be assigned along the shearing surfaces to provide the possibility of sliding which happens during shearing. This procedure is not applicable in the case where the direction of the shear band shearing zone, as well as the direction of the propagation of a pre-existing fissure, eg. (in a triaxial sample) is not predictable. The propagation of discontinued fissures in the partially fissured specimens subjected to triaxial tests needs more numerical and experimental investigation.

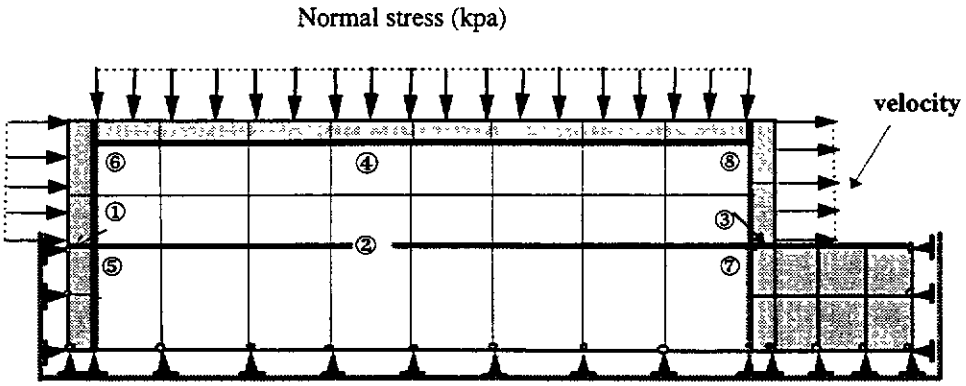

Figure (5.1): The generated mesh for the modelling of the direct shear box. **①,②,③,④,⑤,⑥,⑦ and ⑧ are interfaces**

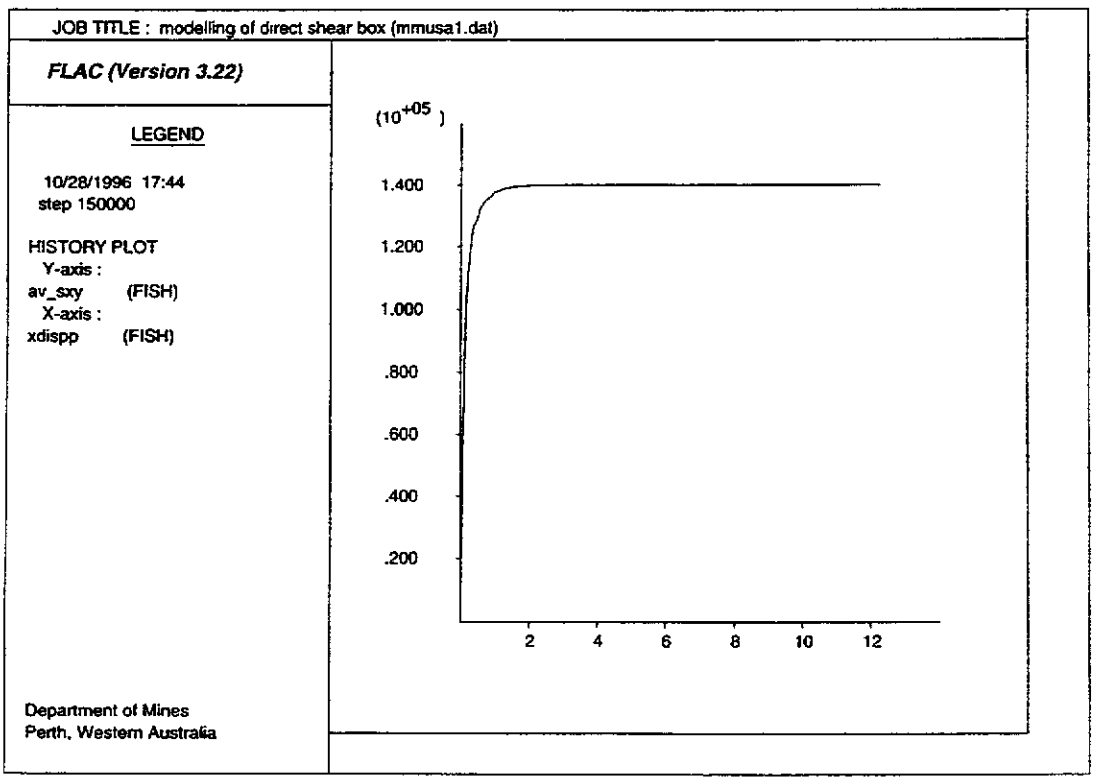

Figure (5.2): The stress strain curve obtain from the FLAC model for an unfissured unlocked KB specimen consolidated and sheared with a P'_c 660 kpa.

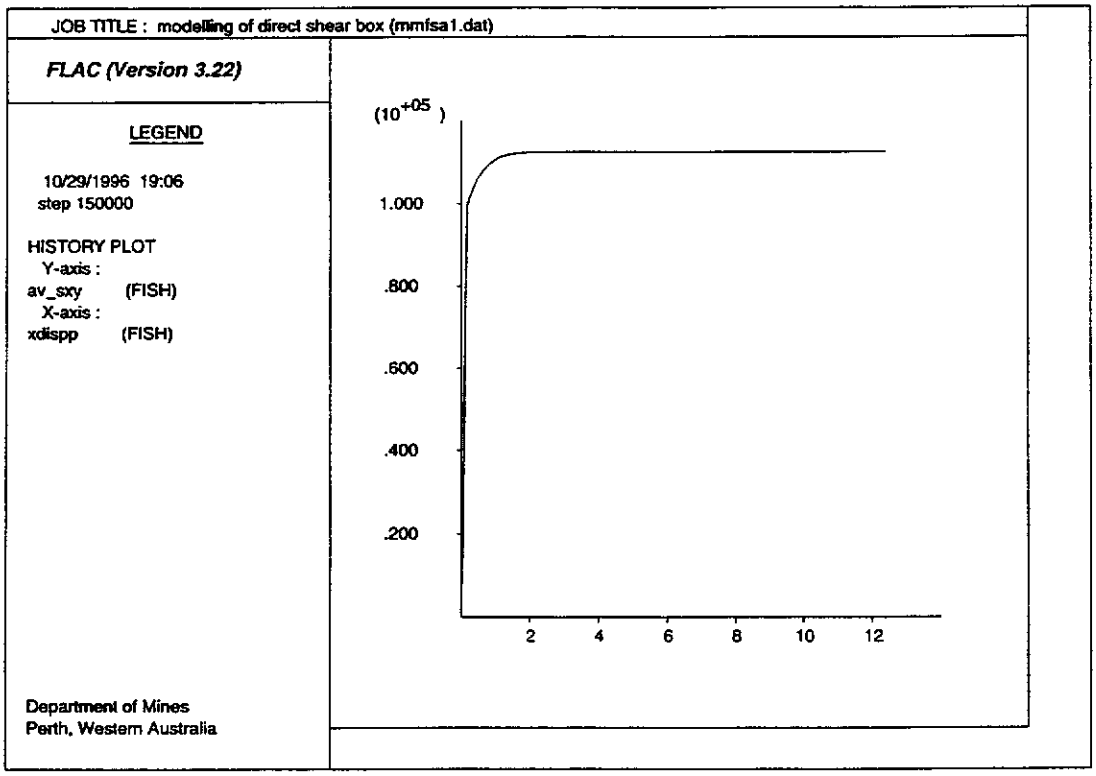

Figure (5.3): The stress strain curve obtain from the FLAC model for a fully fissured unlocked KB specimen consolidated and sheared with a P'_c 660 kpa.

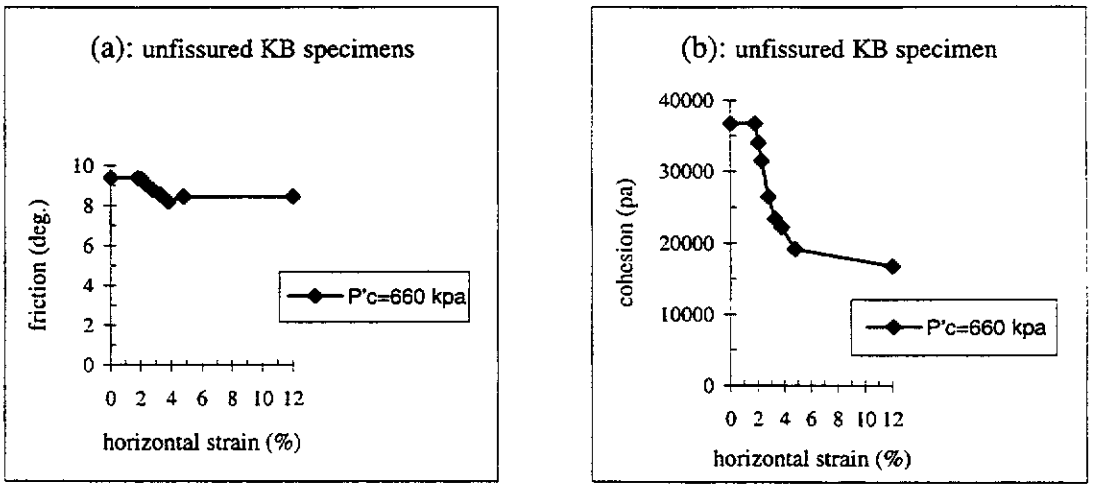

Figure (5.4): The relationships between c′ and ϕ′ with shear displacement of an unfissured unlocked KB specimens consolidated with a P'_c 660 kpa, (a); ϕ′ with shear displacement, (b); c′ with shear displacement.

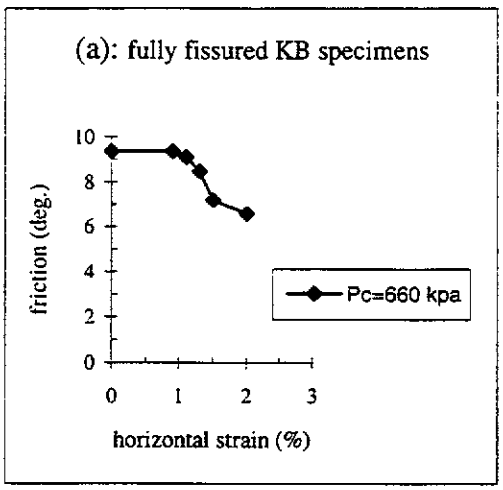

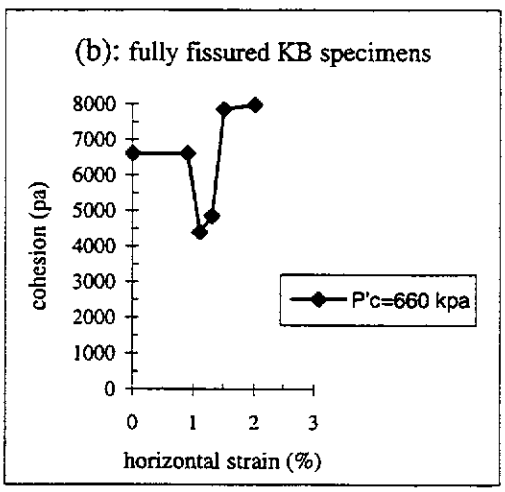

Figure (5.5): The relationships between c′ and ϕ′ with shear displacement of a fully fissured unlocked KB specimens consolidated with a P'_c 660 kpa, (a); ϕ′ with shear displacement, (b); c′ with shear displacement.

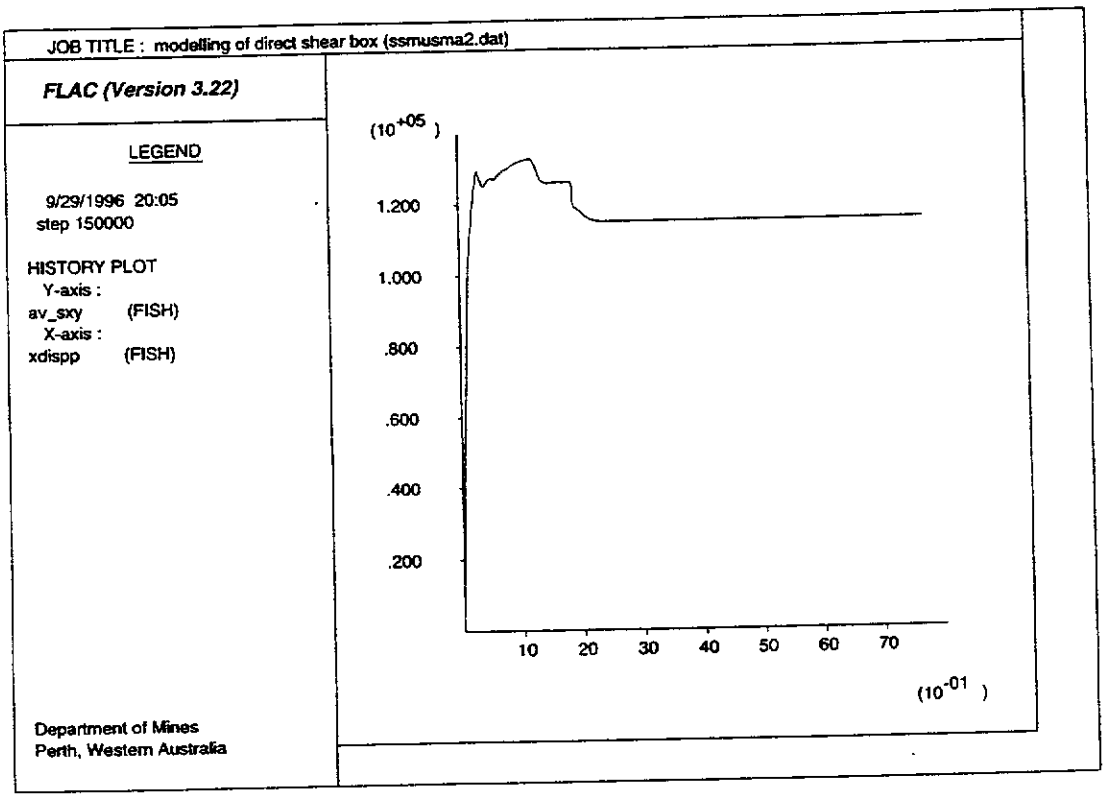

Figure (5.6): The stress strain curve obtained from the FLAC model for an unfissured unlocked KB specimen consolidated and sheared with a p'_c = 660 kpa.

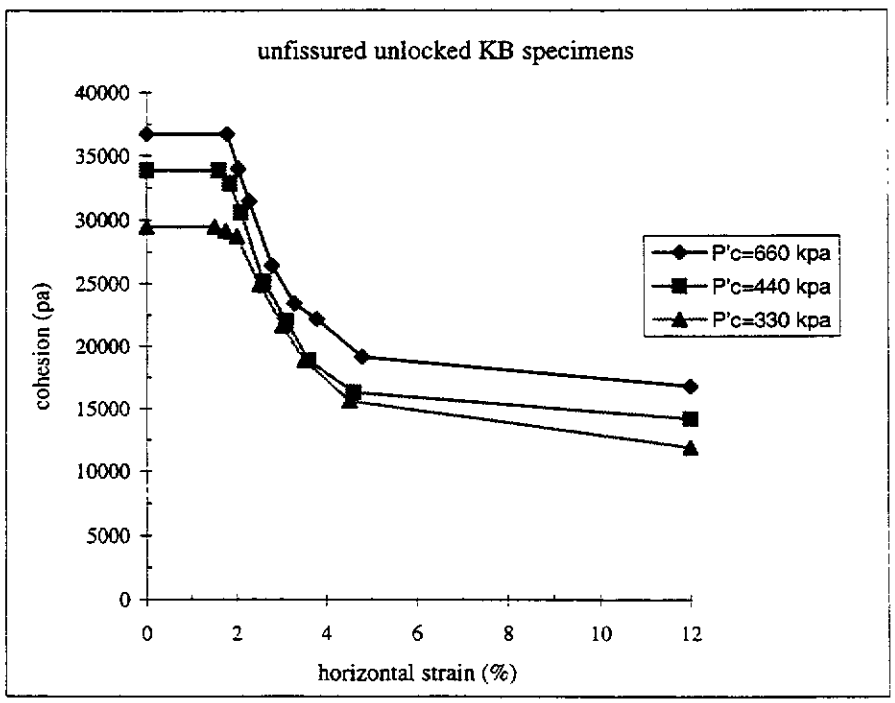

Figure (5.7): The relationships between C'_u and shear strain of the 100 mm unfissured unlocked KB specimens sheared with three different P'_c of 330 kpa, 440 kpa, and 660 kpa and a rate of 0.005 mm/min.

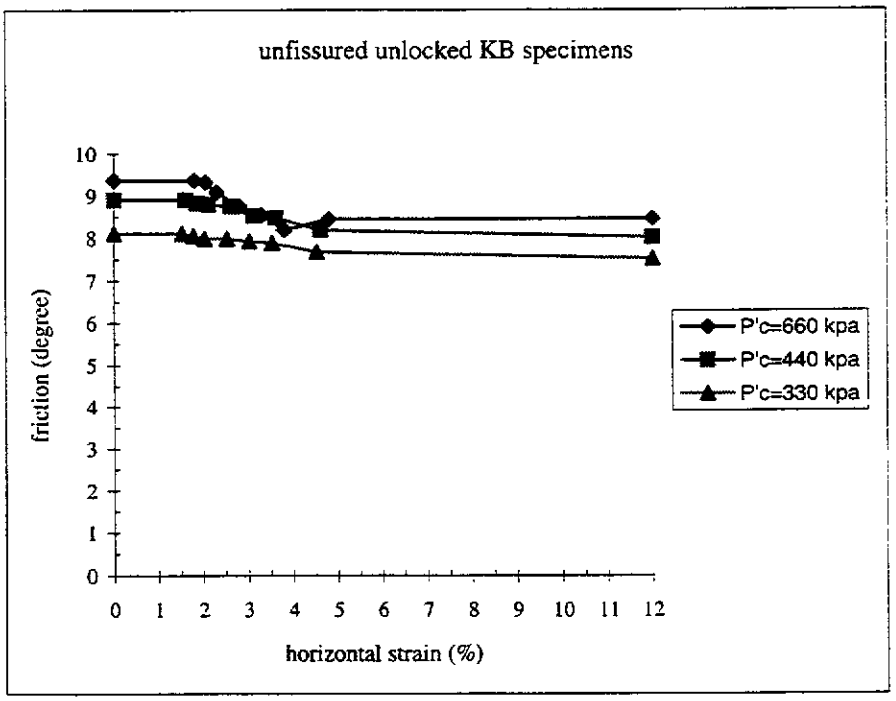

Figure (5.8): The relationships between Φ'_u and shear strain of the 100 mm unfissured unlocked KB specimens sheared with three different p'_c of 330 kpa, 440 kpa, and 660 kpa and a rate of 0.005 mm/min.

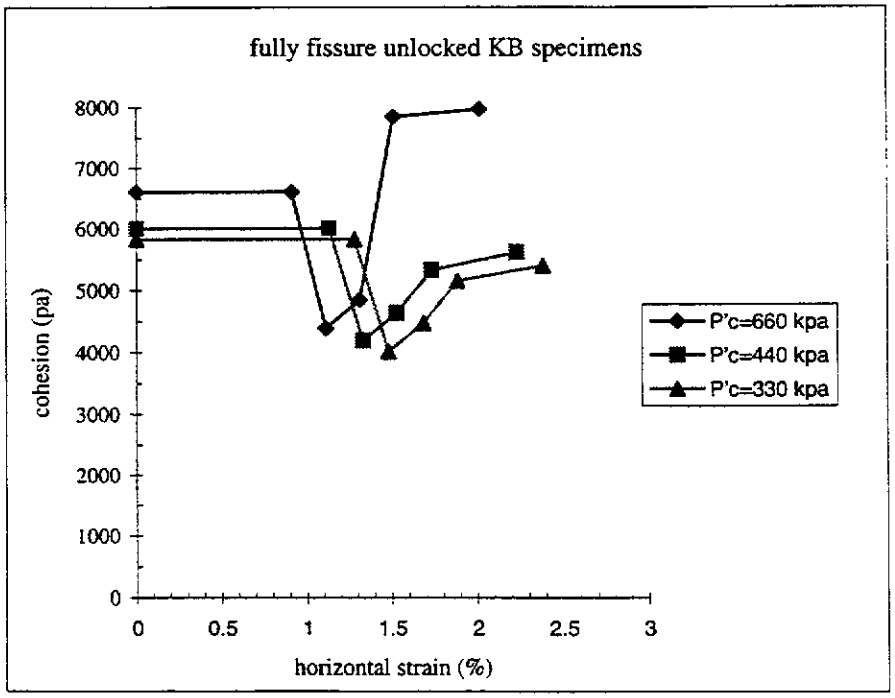

Figure (5.9): The relationships between C'_F and shear strain of the 100 mm fully fissured unlocked KB specimens sheared with three different P'_c of 330 kpa, 440 kpa, and 660 kpa and a rate of 0.005 mm/min.

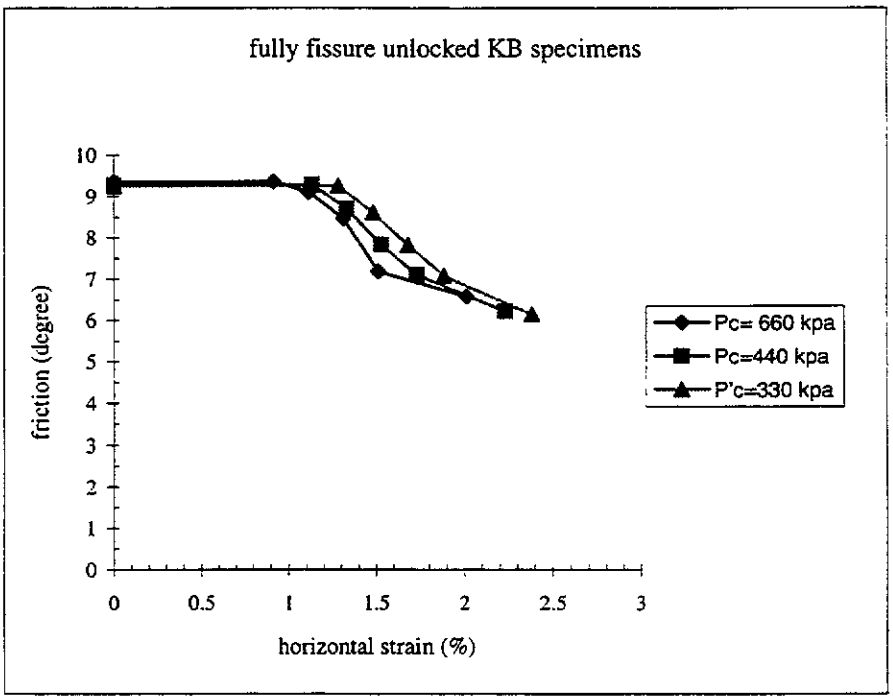

Figure (5.10): The relationships between Φ'_F and shear strain of the 100 mm fully fissured unlocked KB specimens sheared with three different P'_c of 330 kpa, 440 kpa, and 660 kpa and a rate of 0.005 mm/min.

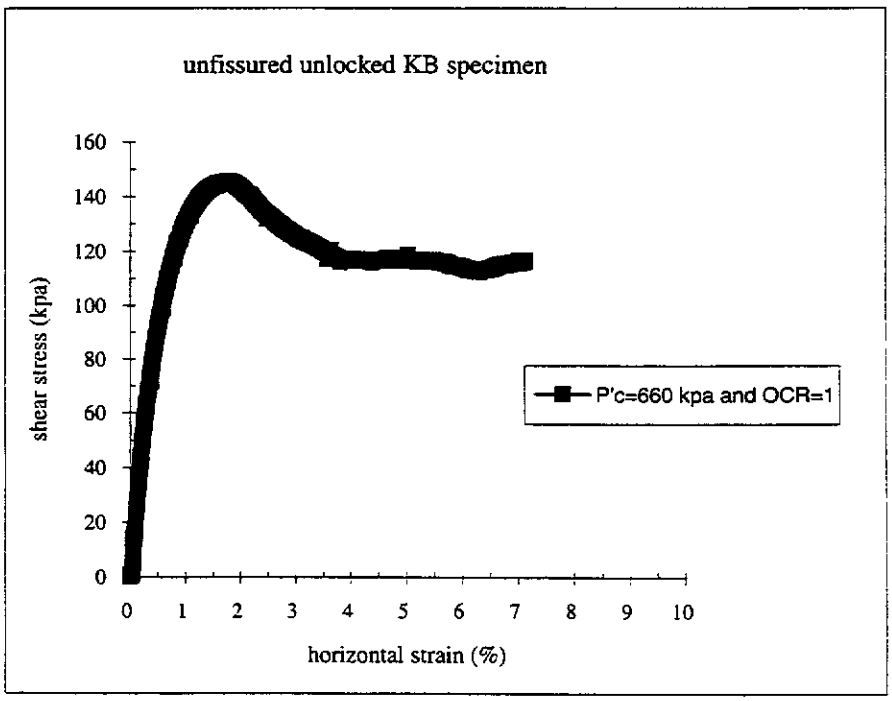

Figure (5.11): The stress strain curve obtained experimentally for the 100 mm unfissured unlocked KB specimen consolidated and sheared with a pressure of 660 kpa and rate of 0.005 mm/min.

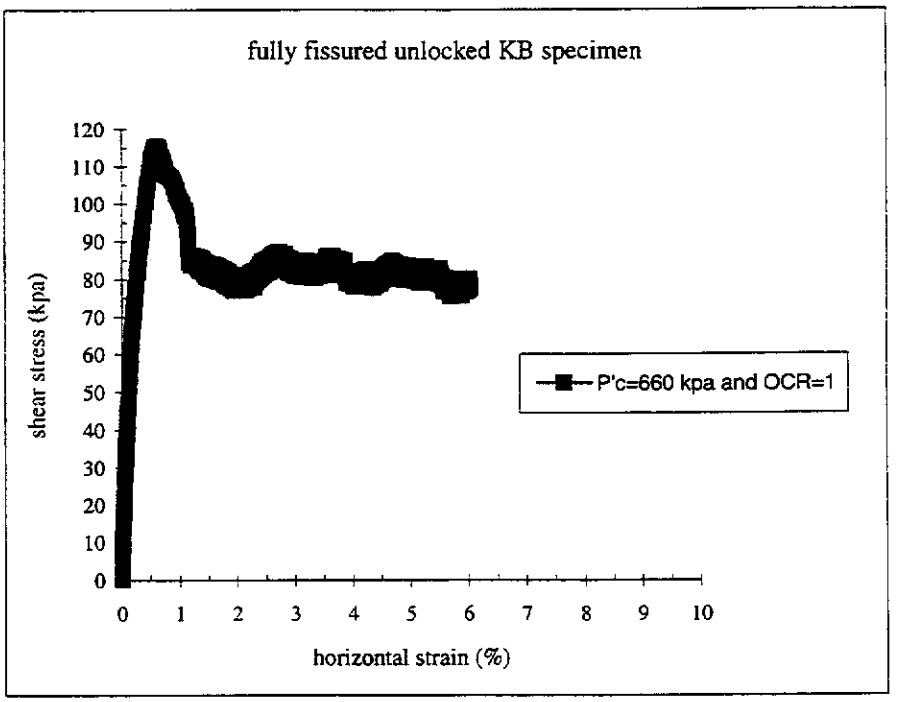

Figure (5.12): The stress strain curve obtained experimentally for the 100 mm fully fissured unlocked KB specimen consolidated and sheared with a pressure of 660 kpa and rate of 0.005 mm/min.

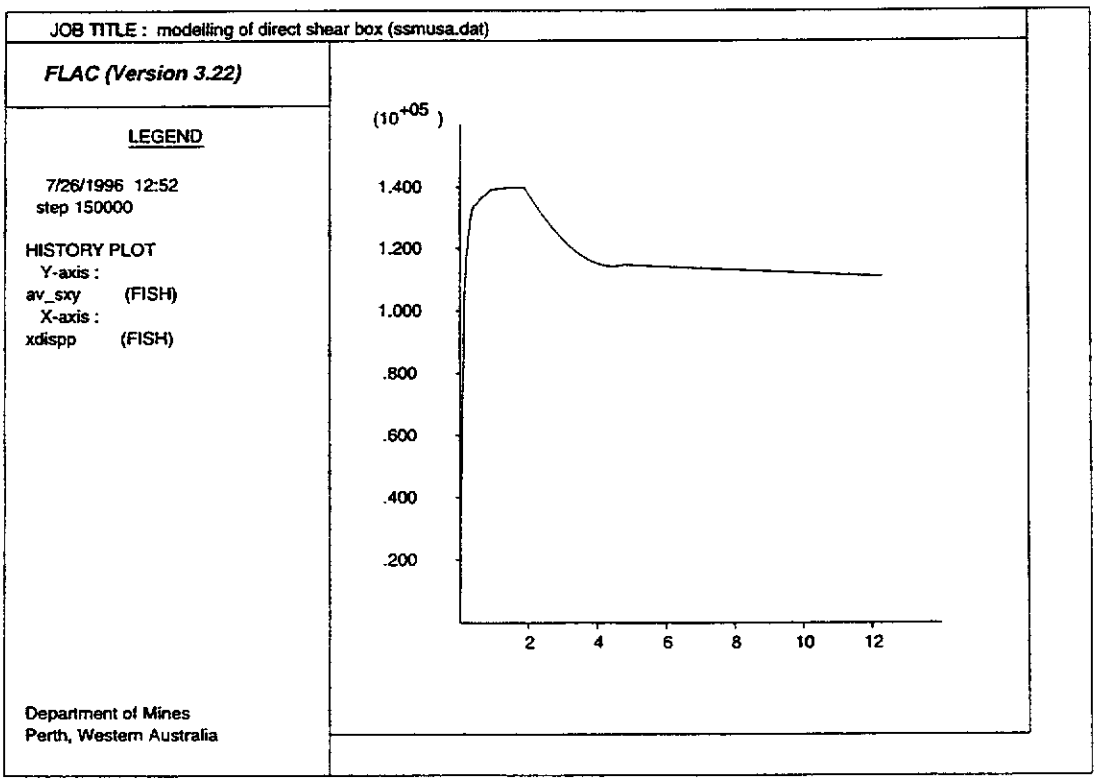

Figure (5.13): The stress strain curve obtained numerically for the 100 mm unfissured unlocked specimen model for the same conditions indicated in Figure (4.11).

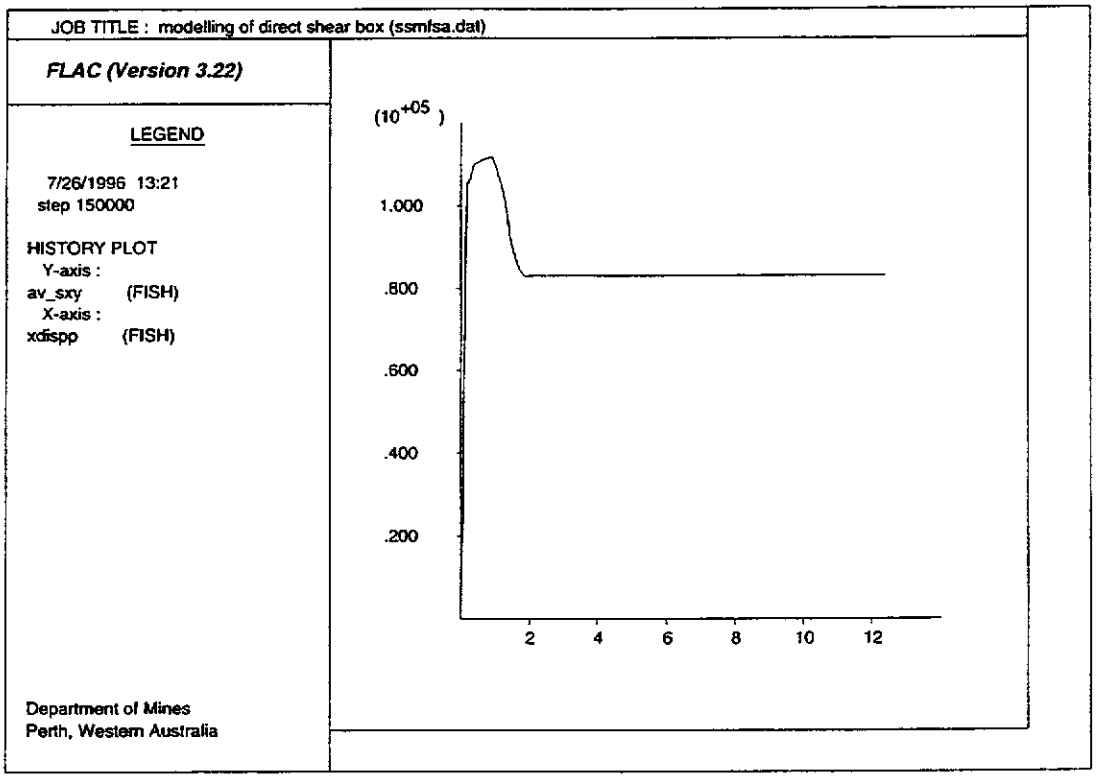

Figure (5.14): The stress strain curve obtained numerically for the 100 mm unfissured unlocked specimen model for the same conditions indicated in Figure (4.12).

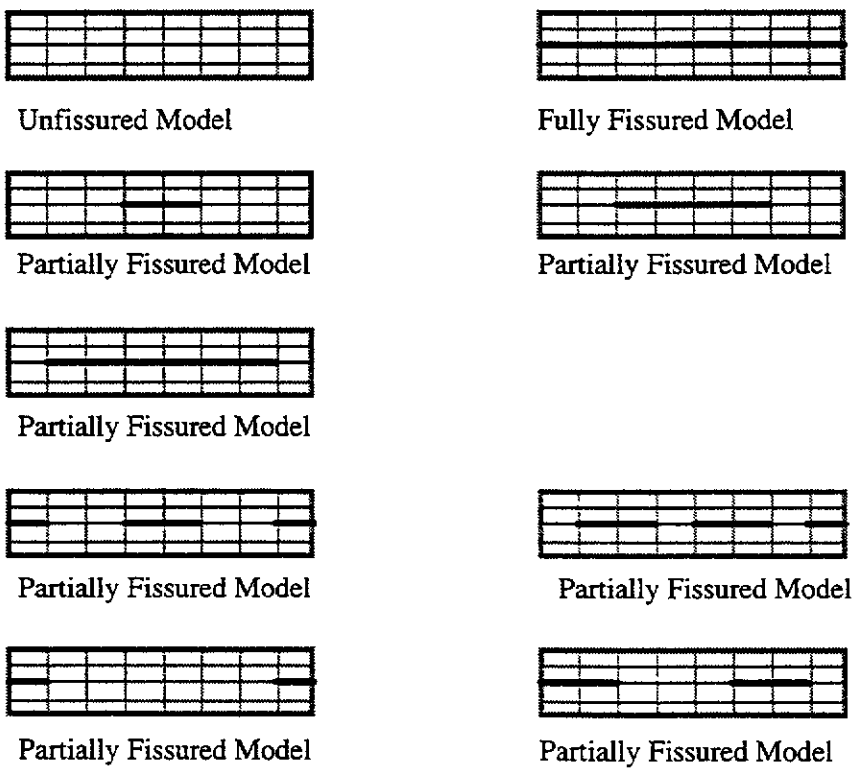

Figure (5.15): Schematical illustration of the models generated for the study of the width (w) and spacing (s) of the fissures.

Model: ssmpfsa5

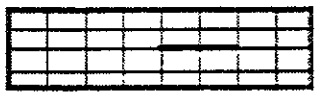

Model: ssmpfsa9

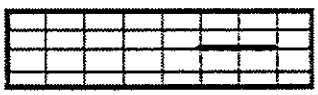

Model: ssmpfsa10

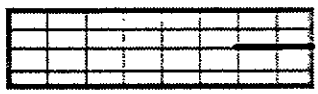

Model: ssmpfsa11

Model: ssmpfsa7

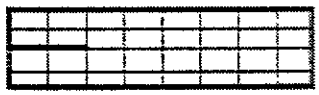

Model: ssmpfsa12

Model: ssmpfsa13

(a): w=75 mm and α_f=25%

Model: ssmpfsa1

Model: ssmpfsa14

Model: ssmpfsa15

Model: ssmpfsa16

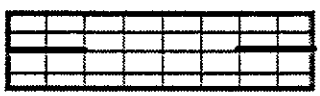

Model: ssmpfsa3

Model: ssmpfsa17

Model: ssmpfsa18

Model: ssmpfsa19

(b): w=150 mm and α_f=50%

Figure (5.16): Schematical illustration of the partially fissured specimen models with length and spacing of 300 mm generated for the study of the effect of fissure surface percentage and width,(a); w=75 mm and α_f=25%,(b). w=150 mm and α_f=50% ,(c). w=225 mm and α_f=75%.

Model: ssmpfsa4

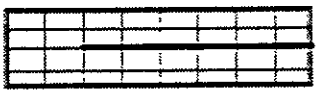

Model: ssmpfsa20

Model: ssmpfsa21

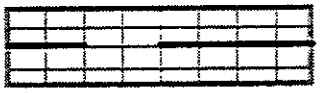

Model: ssmpfsa22

Model: ssmpfsa6

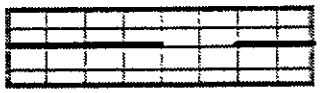

Model: ssmpfsa23

Model: ssmpfsa124

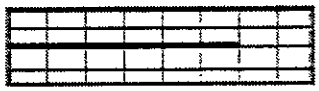

Model: ssmpfsa25

(c): w=225 mm and α_t=75%

Model: ssmpfsa8

Model: ssmpfsa26

Model: ssmpfsa2

Model: ssmpfsa27

(a): s=150 mm and w=75 mm

Figure (5.17): Schematical illustration of the partially fissured specimen models with length of 300 mm and width of 75 mm generated for the study of the effect of fissure spacing, (a); s=150 mm, (b); s=112.5 mm, (c); s=300 mm, (d); s=187.5 mm.

Model: ssmpfsa28

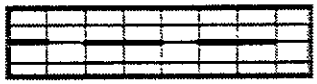

Model: ssmpfsa29

Model: ssmpfsa30

(b): s=112.5 mm and w=75 mm

Model: ssmpfsa12

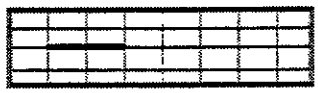

Model: ssmpfsa13

Model: ssmpfsa35

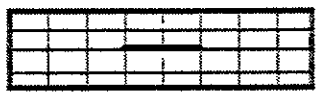

Model: ssmpfsa5

Model: ssmpfsa9

Model: ssmpfsa10

Model: ssmpfsa7

(c): s=300 mm and w=75 mm

Model: ssmpfsa5

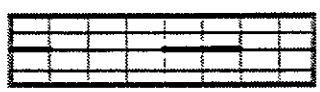

Model: ssmpfsa31

Model: ssmpfsa32

Model: ssmpfsa33

Model: ssmpfsa34

(d): s=187.5 mm and w=75 mm

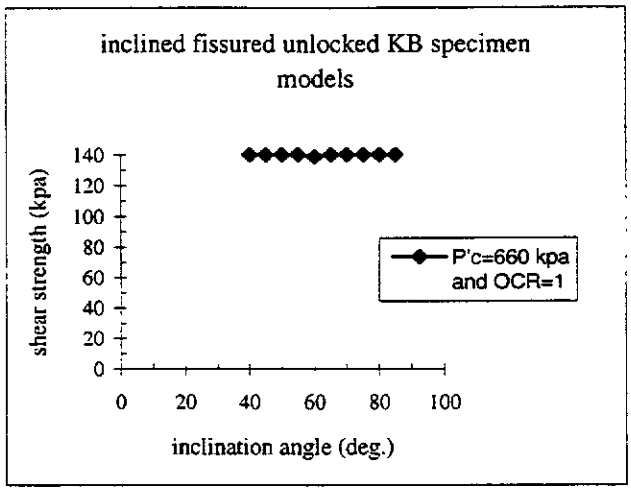

Figure (5.18): Relationship between the numerical results obtained from the inclined fissured specimen models and inclination angle.

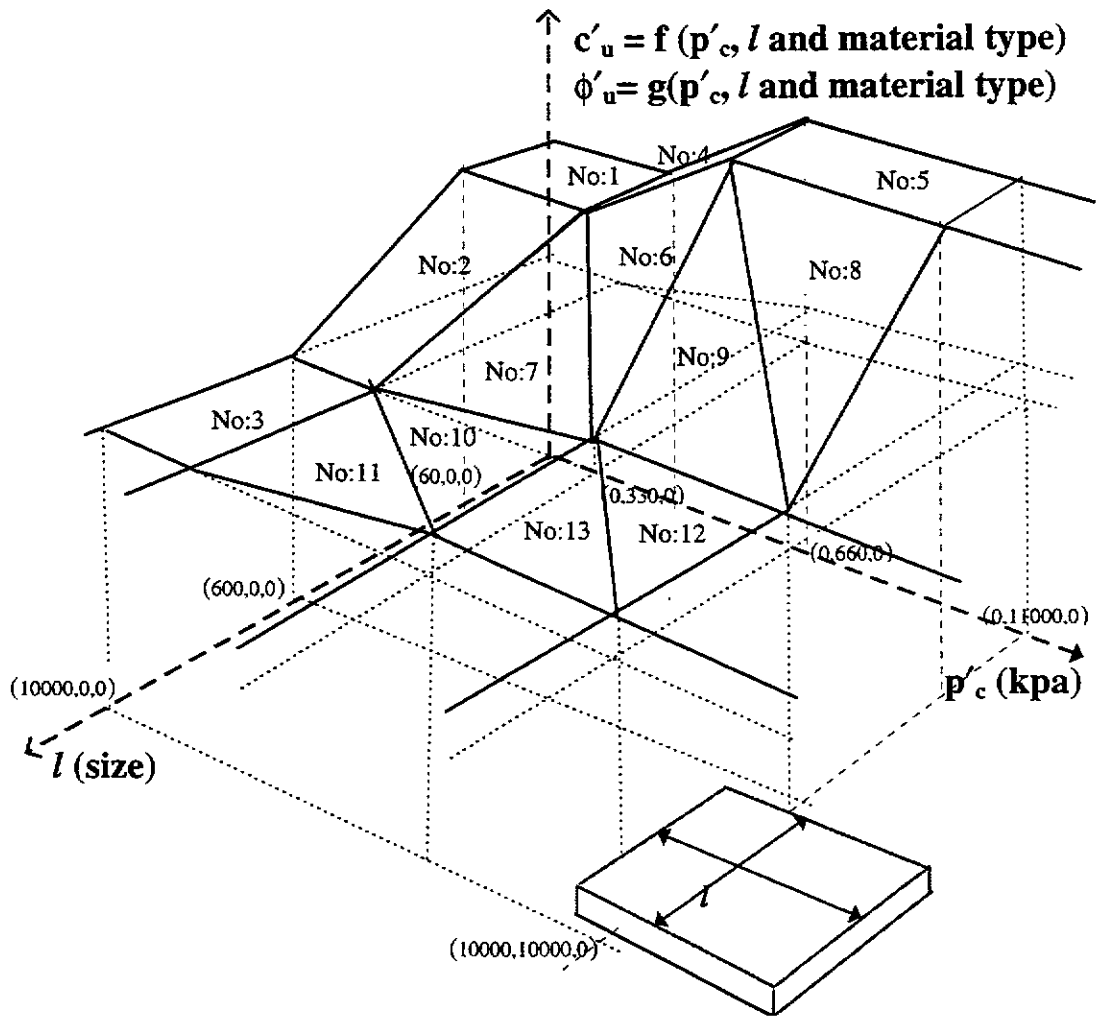

Figure (5.19): Schematical illustration of the relationships within P'_c, size (l), and C′ or ϕ' for the unfissured unlocked KB specimens sheared with a rate of 0.005mm/min.

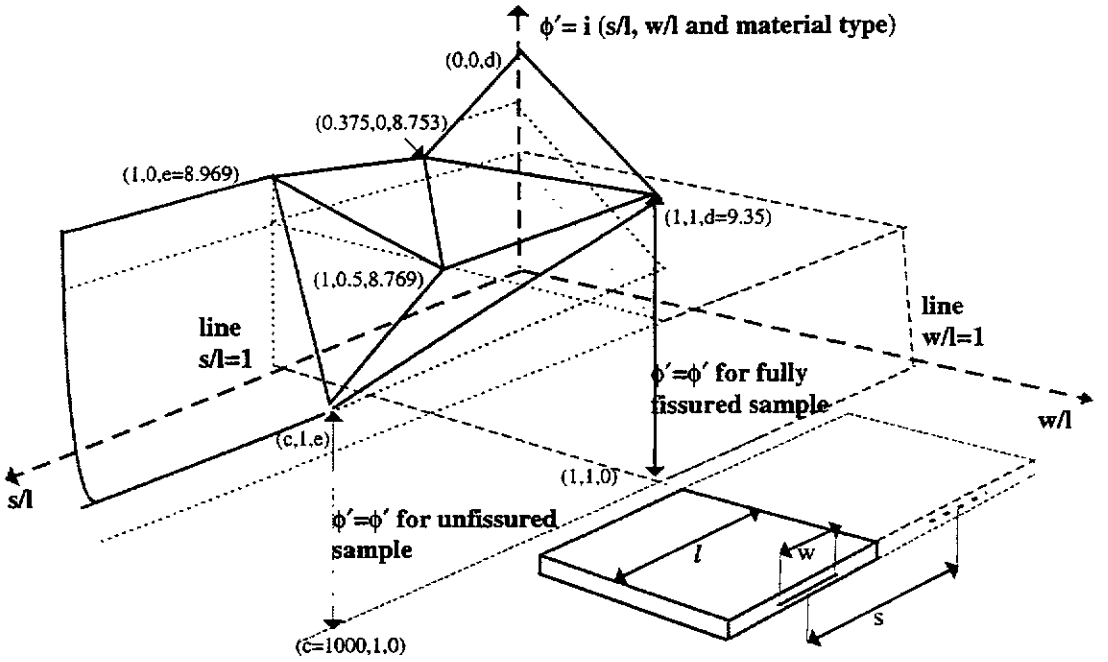

Figure(5.20): Schematical illustration of the relationships within s/l, w/l and ϕ′ for the partially fissured unlocked KB specimen models.

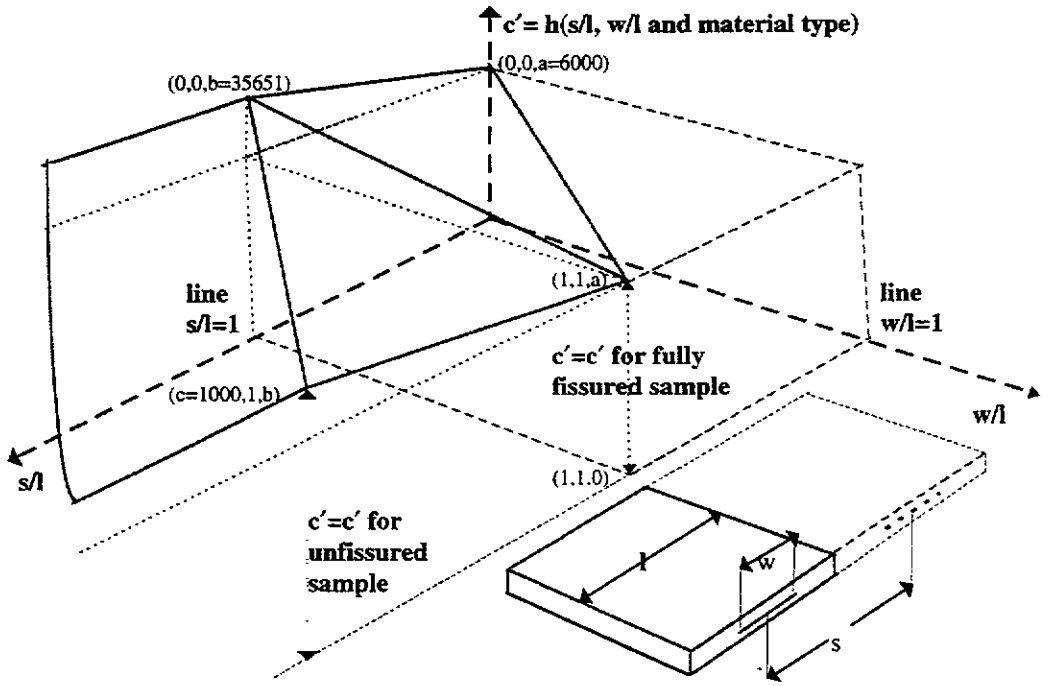

Figure (5.21): Schematical illustration of the relationships within s/l, w/l, and c′ for the partially fissured unlocked KB specimen models.

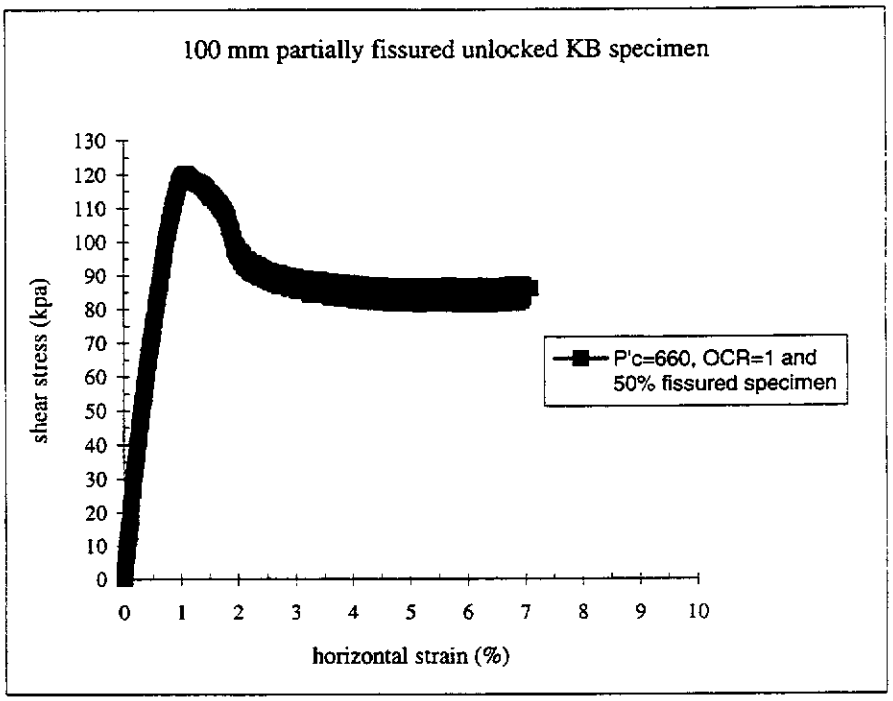

Figure (5.22): The stress strain curve of the 100 mm partial fissured (α_f = 50%, w = 50 mm, and s= 100 mm) unlocked KB specimen consolidated and sheared with a pressure of 660 kpa and with a rate of 0.005 mm/min.

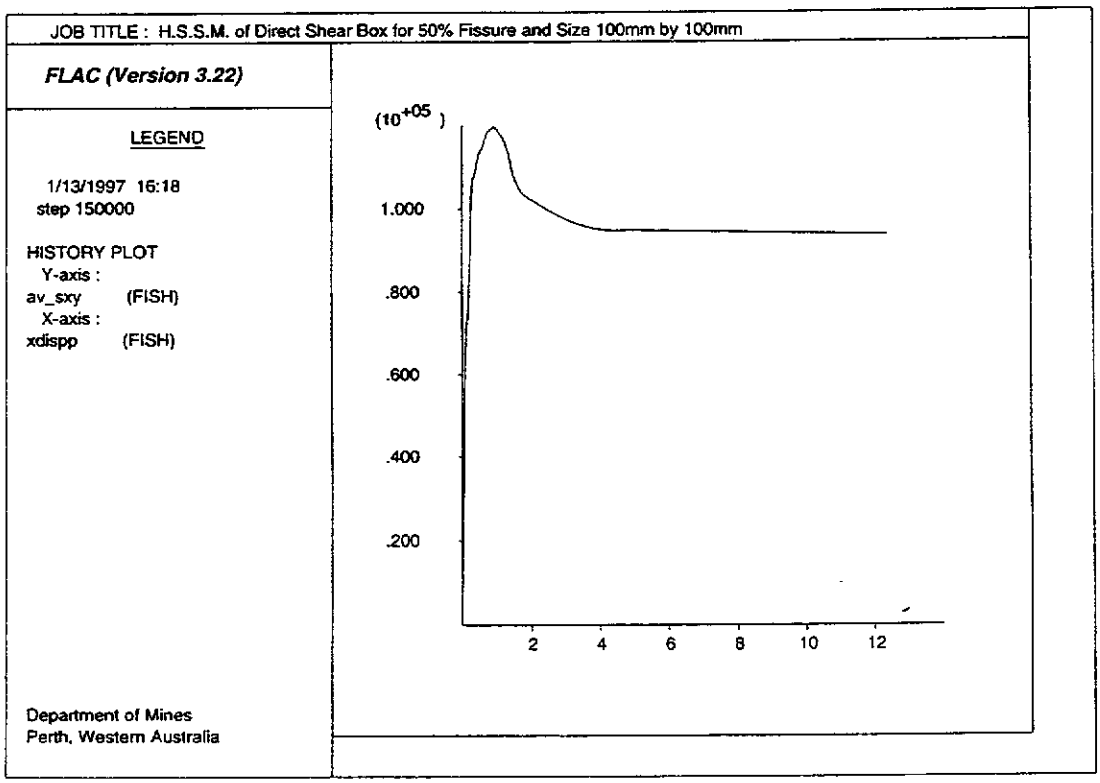

Figure (5.23): The stress strain curve of the model run for the same conditions indicated in Figure (5.22).

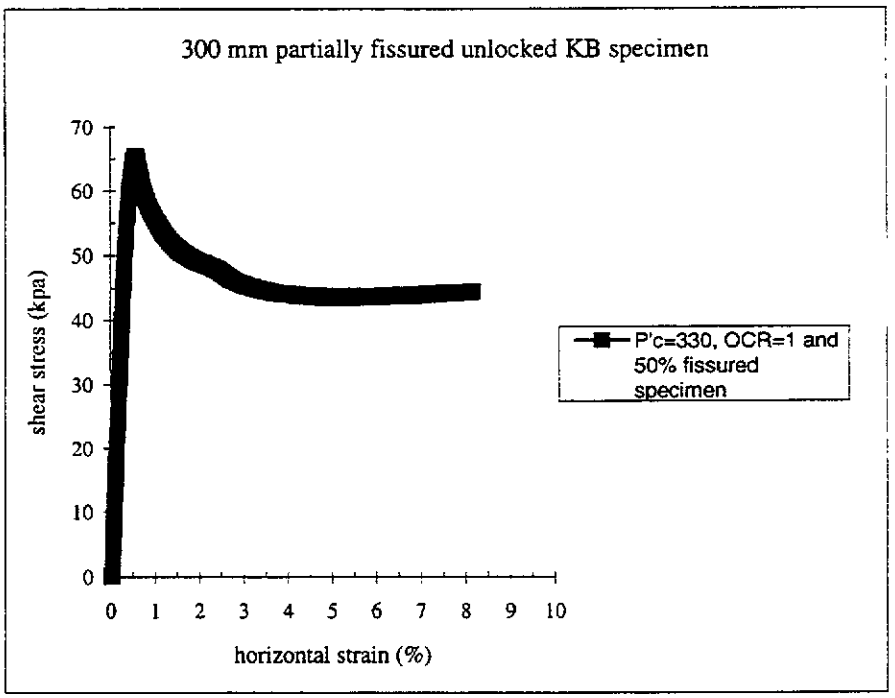

Figure (5.24): The stress strain curve of the 300 mm partially fissured (α_f = 50%, w = 150, mm, and s= 300 mm) unlocked KB specimen consolidated and sheared with a pressure of 330 kpa and with a rate of 0.005 mm/min.

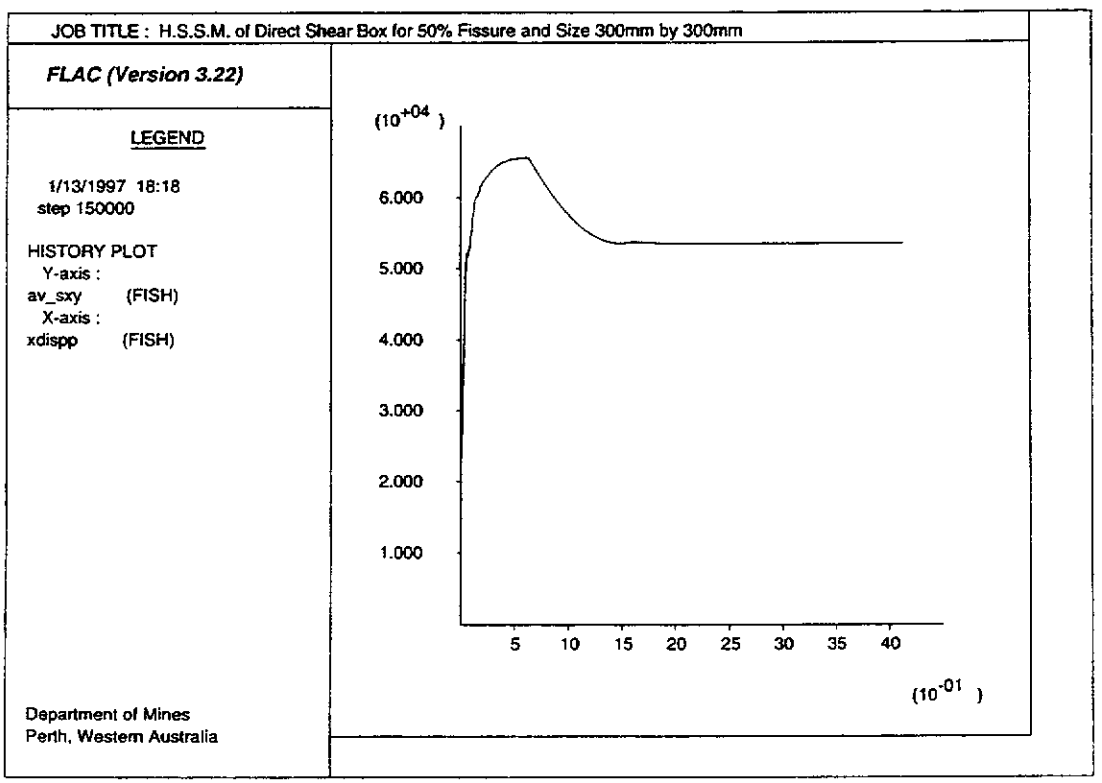

Figure (5.25): The stress strain curve of the model run for the same conditions indicated in Figure (5.24).

KB specimens p'_c = 660 kpa OCR =1		4 × 8 symmetric	6 × 8 symmetric	6 × 8 non symmetric	8 × 8 symmetric
Fully fissured	Model nam e	mmfsa1.dat	mmfsa2.dat	mmfsa3.dat	mmfsa4.dat
model	Shear stress (kpa)	112.48	114.08	115.87	114.89
Unfissured	Model name	mmusa1.dat	mmusa2.dat	mmusa3.dat	mmusa4.dat
model	Shear stress (kpa)	140.1	142.98	146.57	144.21

Table (5.1): FLAC model results for the study of the effect of number of layers. Stress - strain of the material is perfect plastic.

Unfissured unlocked specimens			Fully fissured unlocked specimens		
horizontal strain (%)	c′ (pa)	ϕ′ (deg.)	horizontal strain (%)	c′ (pa)	ϕ′ (deg.)
0.0	36695.79	9.367	0.0	6606.2	9.348
1.794	36695.79	9.36	0.91	4387.90	9.09
2.044.	33983.33	9.319	1.11	4387.90	9.09
2.294	31457.89	9.081	1.31	4846.14	8.46
2.794	26411.4	8.761	1.51	4846.11	7.18
3.294	23403.16	8.537	2.01	7970.70	6.57
3.794	22155.61	8.186	12	7970.70	6.57
4.794	19129.12	8.443	—	—	—
12	16758.6	8.445	—	—	—

Table (5.2): The relationships between the c′ and ϕ′ with shear strain (horizontal strain for fully fissured and unfissured unlocked KB specimens consolidated by P'_c = 660 kpa.

Normal and shear stiffness (pa/m)	Peak shear strength (kpa)			
	Model name	KB fully fissured unlocked model	Model name	KB unfissured unlocked model
$k_n = k_s$ = 1e8	kssintmfsa1.dat	107	kssintmusa1.dat	135.5
$k_n = k_s$ = 1e9	kssintmfsa2.dat	110	kssintmusa2.dat	137
$k_n = k_s$ = 1e10	kssintmfsa3.dat	11.5	kssintmusa3.dat	140
$k_n = k_s$ = 1.838e10	ssmfsa.dat	111.85	ssmusa.dat	140.01

Table (5.3): Numerical study of the effect of normal and shear strength of the KB specimen models for the P'_c = 660 kpa and OCR= 1

model name	σ_n (kpa)	Peak shear strain (kpa)	Type of grid
ssmusa.dat	660	140.01	4 × 8
ssmusb.dat	198	65.456	
ssmusc.dat	132	57.754	
ssmusga3.dat	660	136.35	4 × 16
ssmusgb3.dat	198	64.879	
ssmusgc3.dat	132	59.905	
ssmusga4.dat	660	138.65	4 × 4
ssmusgb4.dat	198	67.465	
ssmusgc4.dat	132	57.315	
ssmusga1.dat	660	142.15	8 × 16
ssmusgb1.dat	198	67.614	
ssmusgc1.dat	132	57.197	
ssmusga5.dat	660	143.95	8 × 8
ssmusgb5.dat	198	68.797	
ssmusgc5.dat	132	58.026	
ssmusga2.dat	660	133.89	2 × 4
ssmusgb2.dat	198	64.365	
ssmusgc2.dat	132	56.266	
ssmusga6.dat	660	131.35	2 × 8
ssmusgb6.dat	198	62.265	
ssmusgc6.dat	132	53.825	

Table (5.4): Numerical study of the effect of mesh size on the peak effective shear strength of the KB specimen models for P'_c = 660 kpa.

Model name	Specimen type	σ_n (kpa)	Peak shear strength (kpa)
ssmusa.dat	UFS	660	140.01
ssmusb.dat	UFS	198	65.456
ssmusc.dat	UFS	132	57.754
ssmfsa.dat	FFS	660	111.85
ssmfsb.dat	FFS	198	35.915
ssmfsc.dat	FFS	132	26.417
ssmpfsa1.dat	PFS	660	119.27
ssmpfsb1.dat	PFS	198	46.801
ssmpfsc1.dat	PFS	132	37.606
ssmpfsa2.dat	PFS	660	122.62
ssmpfsb2.dat	PFS	198	49.452
ssmpfsc2.dat	PFS	132	39.577
ssmpfsa3.dat	PFS	660	124.85
ssmpfsb3.dat	PFS	198	54.389
ssmpfsc3.dat	PFS	132	44.759

Table (5.5): The numerical results for the peak effective shear strengths obtained from the running of the models depicted in figures (5.16) and (5.17).

Table (5.5) continued:

ssmpfsa4.dat	PFS	660	113.19
ssmpfsb4.dat	PFS	198	39.291
ssmpfsc4.dat	PFS	132	27.502
ssmpfsa5.dat	PFS	660	130.43
ssmpfsb5.dat	PFS	198	56.220
ssmpfsc5.dat	PFS	132	47.114
ssmpfsa6.dat	PFS	660	116.23
ssmpfsb6.dat	PFS	198	46.353
ssmpfsc6.dat	PFS	132	36.241
ssmpfsa7.dat	PFS	660	134.90
ssmpfsb7.dat	PFS	198	62.758
ssmpfsc7.dat	PFS	132	52.759
ssmpfsa8.dat	PFS	660	124.70
ssmpfsb8.dat	PFS	198	52.851
ssmpfsc8.dat	PFS	132	43.348
ssmpfsa9.dat	PFS	660	128.45
ssmpfsb9.dat	PFS	198	57.607
ssmpfsc9.dat	PFS	132	46.868
ssmpfsa10.dat	PFS	660	130.02
ssmpfsb10.dat	PFS	198	57.567
ssmpfsc10.dat	PFS	132	48.058
ssmpfsa11.dat	PFS	660	132.37
ssmpfsb11.dat	PFS	198	59.113
ssmpfsc11.dat	PFS	132	49.876
ssmpfsa12.dat	PFS	660	133.82
ssmpfsb12.dat	PFS	198	61.301
ssmpfsc12.dat	PFS	132	52.799
ssmpfsa13.dat	PFS	660	130.85
ssmpfsb13.dat	PFS	198	56.958
ssmpfsc13.dat	PFS	132	48.049
ssmpfsa14.dat	PFS	660	120.07
ssmpfsb14.dat	PFS	198	47.058
ssmpfsc14.dat	PFS	132	36.890
ssmpfsa15.dat	PFS	660	122.71
ssmpfsb15.dat	PFS	198	50.251
ssmpfsc15.dat	PFS	132	40.157
ssmpfsa16.dat	PFS	660	124.79
ssmpfsb16.dat	PFS	198	53.904
ssmpfsc16.dat	PFS	132	43.785
ssmpfsa17.dat	PFS	660	124.03
ssmpfsb17.dat	PFS	198	54.068
ssmpfsc17.dat	PFS	132	45.742
ssmpfsa18.dat	PFS	660	123.30
ssmpfsb18.dat	PFS	198	51.995

Table (5.5) continued:

ssmpfsc18.dat	PFS	132	42.557
ssmpfsa19.dat	PFS	660	122.79
ssmpfsb19.dat	PFS	198	47.609
ssmpfsc19.dat	PFS	132	39.200
ssmpfsa20.dat	PFS	660	112.76
ssmpfsb20.dat	PFS	198	40.468
ssmpfsc20.dat	PFS	132	30.469
ssmpfsa21.dat	PFS	660	119.46
ssmpfsb21.dat	PFS	198	43.299
ssmpfsc21.dat	PFS	132	33.296
ssmpfsa22.dat	PFS	660	117.46
ssmpfsb22.dat	PFS	198	46.287
ssmpfsc22.dat	PFS	132	35.486
ssmpfsa23.dat	PFS	660	116.27
ssmpfsb23.dat	PFS	198	46.342
ssmpfsc23.dat	PFS	132	35.958
ssmpfsa24.dat	PFS	660	119.79
ssmpfsb24.dat	PFS	198	44.908
ssmpfsc24.dat	PFS	132	36.328
ssmpfsa25.dat	PFS	660	112.44
ssmpfsb25.dat	PFS	198	43.509
ssmpfsc25.dat	PFS	132	33.414
ssmpfsa26.dat	PFS	660	123.28
ssmpfsb26.dat	PFS	198	54.231
ssmpfsc26.dat	PFS	132	43.492
ssmpfsa27.dat	PFS	660	123.08
ssmpfsb27.dat	PFS	198	51.090
ssmpfsc27.dat	PFS	132	40.259
ssmpfsa28.dat	PFS	660	119.05
ssmpfsb28.dat	PFS	198	47.252
ssmpfsc28.dat	PFS	132	37.272
ssmpfsa29.dat	PFS	660	118.25
ssmpfsb29.dat	PFS	198	47.495
ssmpfsc29.dat	PFS	132	36.984
ssmpfsa30.dat	PFS	660	121.37
ssmpfsb30.dat	PFS	198	50.007
ssmpfsc30.dat	PFS	132	40.851
ssmpfsa31.dat	PFS	660	128.29
ssmpfsb31.dat	PFS	198	55.302
ssmpfsc31.dat	PFS	132	46.405
ssmpfsa32.dat	PFS	660	125.67
ssmpfsb32.dat	PFS	198	52.727
ssmpfsc32.dat	PFS	132	43.596
ssmpfsa33.dat	PFS	660	124.56

Table (5.5) continued:

ssmpfsb33.dat	PFS	198	51.952
ssmpfsc33.dat	PFS	132	41.286
ssmpfsa34.dat	PFS	660	127.15
ssmpfsb34.dat	PFS	198	57.311
ssmpfsc34.dat	PFS	132	45.348
ssmpfsa35.dat	PFS	660	129.48
ssmpfsb35.dat	PFS		55.613
ssmpfsc35.dat	PFS		46.855

Partially fissured unlocked KB specimen models with p'_c = 660 kpa and s/l = 1			Mohr Coulomb parameters	
w/l	σ_N (kpa)	Average peak shear strength (kpa)	c'_P (kpa)	ϕ'_P (kpa)
0.25	660	131.548	28.309	8.886
	198	58.789		
	132	49.360		
0.5	660	122.726	20.542	8.796
	198	50.759		
	132	41.337		
0.75	660	115.95	12.951	8.869
	198	43.807		
	132	33.586		

Table (5.6): Average peak effective shear strength and Mohr Coulomb parameters for the study of the effect of fissure width for the models depicted in Figure (5.16).

Partially fissured unlocked KB specimen models with p'_c = 660 kpa and s/l = 1			Mohr Coulomb parameters	
s/l	σ_N (kpa)	Average peak shear strength (kpa)	c'_P (kpa)	ϕ'_P (kpa)
0.5	660	123.42	21.242	8.800
	198	51.906		
	132	41.669		
0.375	660	119.556	17.913	8.753
	198	48.251		
	132	38.369		
1.0	660	131.135	27.831	8.890
	198	58.289		
	132	48.928		
0.625	660	127.22	23.920	8.893
	198	54.702		
	132	44.749		

Table (5.7): Average peak effective shear strengths and Mohr Coulomb parameters for the study of the effect of fissure spacing for the models depicted in Figure (5.17).

Specimen type	Shear trength (kpa) of the KB material with p'_c = 330 kpa					
	Size (mm)	60	100	300	200	600
Unfissured unlocked in horizontal stress	Lab test	83	75	69.54	—	—
	HSSM prediction	83.11	75.11	69.79	72.55	62.25
100% fissured unlocked in horizontal stress	Lab test	69.5	59.5	57.24	—	—
	HSSM prediction	64.46	58.11	53.23	55.65	46.22
50% fissured unlocked in horizontal stress	Lab test	76.08	66.26	65.44	—	—
	HSSM prediction	77.48	—	65.65	68.34	57.95
Unfissured locked in horizontal stress	Lab test	78	63	—	—	—
	HSSM prediction	79.87	63.18	58.81	60.8	52.34
100% fissured locked in horizontal stress	Lab test	—	—	—	—	—
	HSSM prediction	54.29	48.85	44.97	46.90	39.04

Table (5.8): Shear strength obtained from the experiments and numerical modelling of KB specimens.

Appendix A(5.1):

The FLAC model for the simulation of strain softening behaviour of the 100 mm unfissured unlocked KB specimens consolidated with P'_c of 660 kpa and sheared with a rate of 0.005 mm/min.

```
title
modelling of direct shear box (ssmusa.dat)
grid 14,7
m m i=3,10 j=1,2
m m i=3,10 j=4
m m i=3,10 j=5
m e i=1 j=1,2
m e i=1 j=4,5
m e i=12,14 j=1,2
m e i=12 j=4,5
m e i=3,10 j=7
gen 0,0 0,0.035 0.175,0.035 0.175,0
ini x=0.00075 i=2
ini x=0.14925 i=12
ini y add -0.005 i=1,2 j=4,6
ini y add -0.005 i=3,4 j=4,6
ini y add -0.005 i=5,6 j=4,6
ini y add -0.005 i=7,8 j=4,6
ini y add -0.005 i=9,13 j=4,6
ini y add -0.01 i=1,13 j=7,8
ini y=0.02075  i=3,11 j=8
interface 1, aside from 1,3 to 2,3 bside from 1,4 to 2,4
interface 2, aside from 3,3 to 11,3 bside from 3,4 to 11,4
interface 3, aside from 12,3 to 13,3 bside from 12,4 to 13,4
interface 4, aside from 3,6 to 11,6 bside from 3,7 to 11,7
int 1 kn 1e14 ks 1
int 3 kn 1e14 ks 1
int 4 glue kn 1e12 ks 5e10
ini x add 0.02425 i=1,2 j=1,6
ini x add -0.02425 i=12,15 j=1,6
interface 5, aside from 2,1 to 2,3 bside from 3,1 to 3,3
interface 6, aside from 2,4 to 2,6 bside from 3,4 to 3,6
interface 7, aside from 11,1 to 11,3 bside from 12,1 to 12,3
interface 8, aside from 11,4 to 11,6 bside from 12,4,to 12,6
int 5 glue kn 1e14 ks 1e4
int 6 glue kn 1e12 ks 1e4
int 7 glue kn 1e14 ks 1e4
int 8 glue kn 1e12 ks 1e4
fix x y  i=1,2 j=1
fix x  i=1,2 j=2,3
fix  x y  i=12,15 j=1
```

```
fix  x   i=12,15 j=2,3
fix x y i=3,11 j=1
app nv=-8.33e-8 i=1 j=4,6
app nv=8.33e-8 i=2 j=4,6
app nv=-8.33e-8 i=3 j=4,6
app nv=8.33e-8 i=11 j=4,6
app nv=-8.33e-8 i=12 j=4,6
app nv=8.33e-8 i=13 j=4,6
app xv 8.33e-8 i=3,11 j=7
app xv 8.33e-8 i=3,11 j=8
app syy=-660000 i=3,11 j=6
prop den=7000 she 8e10 bul 1.1e11  i=1 j=1,2
prop den=1 she 8e10 bul 1.1e11  i=1 j=4,5
prop den=1660 she 1.4e7 bul=6.252565417e7   i=3,10 j=1,2
prop fric 9.367 cohe=36695.79   i=3,10 j=1,2
prop den=1660 she 1.4e7   bul=6.252565417e7   i=3,10 j=4,5
prop fric 9.367 cohe=36695.79   i=3,10 j=4,5
prop den=7000 she 8e10 bul 1.1e11  i=12,14 j=1,2
prop den=1 she 8e10 bul 1.1e11  i=12 j=4,5
prop den=1 she 8e10 bul 1.1e11  i=3,10 j=7
plot bou fix apply stress
def xdispp
while_stepping
sum=0
loop i (3,11)
sum=sum+ xdisp(i,4)
end_loop
xdispp=(sum/9)*1000
end
def av_sxy
while_stepping
sum1=0
loop i (4,9)
sum1=sum1+ sxy(i,4)
end_loop
av_sxy=sum1/6
end
his unbal
hist xdis i=1 j=4
hist xdis i=2 j=4
hist xdis i=3 j=4
hist xdis i=4 j=4
hist xdis i=5 j=4
hist xdis i=6 j=4
hist xdis i=7 j=4
hist xdis i=8 j=4
hist xdis i=9 j=4
hist xdis i=10 j=4
hist xdis i=11 j=4
hist xdis i=12 j=4
hist xdis i=13 j=4
hist sxy i=1 j=4
```

```
hist sxy i=2 j=4
hist sxy i=3 j=4
hist sxy i=4 j=4
hist sxy i=5 j=4
hist sxy i=6 j=4
hist sxy i=7 j=4
hist sxy i=8 j=4
hist sxy i=9 j=4
hist sxy i=10 j=4
hist sxy i=11 j=4
hist sxy i=12 j=4
hist sxy i=13 j=4
hist xdispp
hist av_sxy
def fuint2
while_stepping
xdisavp=1.8844
xdisavf=4.794
xdisavr=12
if xdispp<=xdisavp then
fuint2=9.367
end_if
if xdispp>xdisavp then
if xdispp<=xdisavf then
fuint2=11.00410705-0.9302*(xdispp)+0.0173*(xdispp^3)
end_if
end_if
if xdispp>xdisavf then
if xdispp<=xdisavr then
fuint2=8.454666-8.05462e-4*xdispp
end_if
end_if
if xdispp>xdisavr then
fuint2=8.445
end_if
end
def cuint2
while_stepping
if xdispp<=xdisavp then
cuint2=36695.79
end_if
if xdispp>xdisavp then
if xdispp<=xdisavf then
cuint2=64443.82549-18322*(xdispp)+1908.75*(xdispp^2)
end_if
end_if
if xdispp>xdisavf then
if xdispp<=xdisavr then
cuint2=22948.911740-515.859312*xdispp
end_if
end_if
if xdispp>xdisavr then
```

```
cuint2=16758.60
end_if
end
his cuint2
his fuint2
def ampif_model
loop nn (1,150000)
xdisavp=1.8844
xdisavf=4.794
xdisavr=12
if xdispp<=xdisavp then
fuint2=9.367
cuint2=36695.79
end_if
if xdispp>xdisavp then
if xdispp<=xdisavf then
fuint2=11.00410705-0.9302*(xdispp)+0.0173*(xdispp^3)
cuint2=64443.82549-18322*(xdispp)+1908.75*(xdispp^2)
end_if
end_if
if xdispp>xdisavf then
if xdispp<=xdisavr then
fuint2=8.454666-8.05462e-4*xdispp
cuint2=22948.911740-515.859312*xdispp
end_if
end_if
if xdispp>xdisavr then
fuint2=8.445
cuint2=16758.60
end_if
command
interface 2 ks=1.83846417e10 kn=1.83846417e10 cohe=cuint2 fric=fuint2
step=1
end_command
end_loop
end
ampif_model
save ssmusa.sav
plot g mag
plot his 15 vs 2
plot his 16 vs 3
plot his 17 vs 4
plot his 18 vs 5
plot his 19 vs 6
plot his 20 vs 7
plot his 21 vs 8
plot his 22 vs 9
plot his 23 vs 10
plot his 24 vs 11
plot his 25 vs 12
plot his 26 vs 13
plot his 27 vs 14
```

Appendix A(5.2):

The FLAC model for the simulation of strain softening behaviour of the 100 mm fully fissured unlocked KB specimens consolidated with P'_c of 660 kpa and sheared with a rate of 0.005 mm/min.

```
title
modelling of direct shear box (ssmfsa.dat)
grid 14,7
m m i=3,10 j=1,2
m m i=3,10 j=4
m m i=3,10 j=5
m e i=1 j=1,2
m e i=1 j=4,5
m e i=12,14 j=1,2
m e i=12 j=4,5
m e i=3,10 j=7
gen 0,0 0,0.035 0.175,0.035 0.175,0
ini x=0.00075 i=2
ini x=0.14925 i=12
ini y add -0.005 i=1,2 j=4,6
ini y add -0.005 i=3,4 j=4,6
ini y add -0.005 i=5,6 j=4,6
ini y add -0.005 i=7,8 j=4,6
ini y add -0.005 i=9,13 j=4,6
ini y add -0.01 i=1,13 j=7,8
ini y=0.02075  i=3,11 j=8
interface 1, aside from 1,3 to 2,3 bside from 1,4 to 2,4
interface 2, aside from 3,3 to 11,3 bside from 3,4 to 11,4
interface 3, aside from 12,3 to 13,3 bside from 12,4 to 13,4
interface 4, aside from 3,6 to 11,6 bside from 3,7 to 11,7
int 1 kn 1e14 ks 1
int 3 kn 1e14 ks 1
int 4 glue kn 1e12 ks 5e10
ini x add 0.02425 i=1,2 j=1,6
ini x add -0.02425 i=12,15 j=1,6
interface 5, aside from 2,1 to 2,3 bside from 3,1 to 3,3
interface 6, aside from 2,4 to 2,6 bside from 3,4 to 3,6
interface 7, aside from 11,1 to 11,3 bside from 12,1 to 12,3
interface 8, aside from 11,4 to 11,6 bside from 12,4,to 12,6
int 5 glue kn 1e14 ks 1e4
int 6 glue kn 1e12 ks 1e4
int 7 glue kn 1e14 ks 1e4
int 8 glue kn 1e12 ks 1e4
fix x y  i=1,2 j=1
fix x  i=1,2 j=2,3
fix  x y  i=12,15 j=1
fix  x  i=12,15 j=2,3
```

```
fix x y i=3,11 j=1
app nv=-8.33e-8 i=1 j=4,6
app nv=8.33e-8 i=2 j=4,6
app nv=-8.33e-8 i=3 j=4,6
app nv=8.33e-8 i=11 j=4,6
app nv=-8.33e-8 i=12 j=4,6
app nv=8.33e-8 i=13 j=4,6
app xv 8.33e-8 i=3,11 j=7
app xv 8.33e-8 i=3,11 j=8
app syy=-660000 i=3,11 j=6
prop den=7000 she 8e10 bul 1.1e11  i=1 j=1,2
prop den=1 she 8e10 bul 1.1e11  i=1 j=4,5
prop den=1660 she 1.4e7 bul=6.252565417e7   i=3,10 j=1,2
prop fric 9.367 cohe=36695.79   i=3,10 j=1,2
prop den=1660 she 1.4e7   bul=6.252565417e7   i=3,10 j=4,5
prop fric 9.367 cohe=36695.79  i=3,10 j=4,5
prop den=7000 she 8e10 bul 1.1e11  i=12,14 j=1,2
prop den=1 she 8e10 bul 1.1e11  i=12 j=4,5
prop den=1 she 8e10 bul 1.1e11  i=3,10 j=7
plot bou fix apply stress
def xdispp
while_stepping
sum=0
oop i (3,11)
sum=sum+ xdisp(i,4)
end_loop
xdispp=(sum/9)*1000
end
def av_sxy
while_stepping
sum1=0
loop i (4,9)
sum1=sum1+ sxy(i,4)
end_loop
av_sxy=sum1/6
end
his unbal
hist xdis i=1 j=4
hist xdis i=2 j=4
hist xdis i=3 j=4
hist xdis i=4 j=4
hist xdis i=5 j=4
hist xdis i=6 j=4
hist xdis i=7 j=4
hist xdis i=8 j=4
hist xdis i=9 j=4
hist xdis i=10 j=4
hist xdis i=11 j=4
hist xdis i=12 j=4
hist xdis i=13 j=4
hist sxy i=1 j=4
hist sxy i=2 j=4
```

```
hist sxy i=3 j=4
hist sxy i=4 j=4
hist sxy i=5 j=4
hist sxy i=6 j=4
hist sxy i=7 j=4
hist sxy i=8 j=4
hist sxy i=9 j=4
hist sxy i=10 j=4
hist sxy i=11 j=4
hist sxy i=12 j=4
hist sxy i=13 j=4
hist xdispp
hist av_sxy
def ffint2
while_stepping
xdisavp=0.91033
xdisavf=1.11033
xdisavh=1.4601189
xdisavr=2.01033
if xdispp<=xdisavp then
ffint2=9.348
end_if
if xdispp>xdisavp then
if xdispp<=xdisavh then
ffint2=8.426501846+3.6183*(xdispp^2)-2.7532*(xdispp^3)
end_if
end_if
if xdispp>xdisavh then
if xdispp<=xdisavr then
ffint2=17.41666234-8.2484*(xdispp)+0.7058*(xdispp^3)
end_if
end_if
if xdispp>=xdisavr then
ffint2=6.569
end_if
end
def cfint2
while_stepping
if xdispp<=xdisavp then
cfint2=6606.2
end_if
if xdispp>xdisavp then
if xdispp<=xdisavf then
cfint2=18131.574776-12660.65578*xdispp
end_if
end_if
if xdispp>xdisavf then
if xdispp<=xdisavr then
cfint2=(exp(1))^(9.811501365-(1.6645/xdispp))
end_if
end_if
if xdispp>=xdisavr then
```

```
cfint2=7970.702
end_if
end
his cfint2
his ffint2
def ampfif_model
loop nn (1,150000)
xdisavp=0.91033
xdisavf=1.11033
xdisavh=1.4601189
xdisavr=2.01033
if xdispp<=xdisavp then
ffint2=9.348
end_if
if xdispp>xdisavp then
if xdispp<=xdisavh then
ffint2=8.426501846+3.6183*(xdispp^2)-2.7532*(xdispp^3)
end_if
end_if
if xdispp>xdisavh then
if xdispp<=xdisavr then
ffint2=17.41666234-8.2484*(xdispp)+0.7058*(xdispp^3)
end_if
end_if
if xdispp>=xdisavr then
ffint2=6.569
end_if
if xdispp<=xdisavp then
cfint2=6606.2
end_if
if xdispp>xdisavp then
if xdispp<=xdisavf then
cfint2=18131.574776-12660.65578*xdispp
end_if
end_if
if xdispp>xdisavf then
if xdispp<=xdisavr then
cfint2=(exp(1))^(9.811501365-(1.6645/xdispp))
end_if
end_if
if xdispp>=xdisavr then
cfint2=7970.702
end_if
command
interface 2 kn=1.83846417e10 ks=1.83846417e10 cohe=cfint2 fric=ffint2
step=1
end_command
end_loop
end
ampfif_model
save ssmfsa.sav
plot g mag
```

```
plot his 15 vs 2
plot his 16 vs 3
plot his 17 vs 4
plot his 18 vs 5
plot his 19 vs 6
plot his 20 vs 7
plot his 21 vs 8
plot his 22 vs 9
plot his 23 vs 10
plot his 24 vs 11
plot his 25 vs 12
plot his 26 vs 13
plot his 27 vs 14
plot his 29 vs 28
```

Appendix A(5.3):

The FLAC model for the simulation of strain softening behaviour of the 100 mm partially fissured unlocked KB specimens consolidated with P'_c of 660 kpa and sheared with a rate of 0.005 mm/min.

```
title
modelling of direct shear box (ssmpfsa1.dat)
grid 14,7
m m i=3,10 j=1,2
m m i=3,10 j=4
m m i=3,10 j=5
m e i=1 j=1,2
m e i=1 j=4,5
m e i=12,14 j=1,2
m e i=12 j=4,5
m e i=3,10 j=7
gen 0,0 0,0.035 0.175,0.035 0.175,0
ini x=0.00075 i=2
ini x=0.14925 i=12
ini y add -0.005 i=1,2 j=4,6
ini y add -0.005 i=3,4 j=4,6
ini y add -0.005 i=5,6 j=4,6
ini y add -0.005 i=7,8 j=4,6
ini y add -0.005 i=9,13 j=4,6
ini y add -0.01 i=1,13 j=7,8
ini y=0.02075  i=3,11 j=8
ini x add 0.02425 i=1,2 j=1,6
ini x add -0.02425 i=12,15 j=1,6
interface 1, aside from 1,3 to 2,3 bside from 1,4 to 2,4
interface 2, aside from 3,3 to 5,3 bside from 3,4 to 5,4
interface 3, aside from 5,3 to 9,3 bside from 5,4 to 9,4
interface 4, aside from 9,3 to 11,3 bside from 9,4 to 11,4
interface 5, aside from 12,3 to 13,3 bside from 12,4 to 13,4
interface 6, aside from 3,6 to 11,6 bside from 3,7 to 11,7
int 1 kn 1e14 ks 1
int 5 kn 1e14 ks 1
int 6 glue kn 1e12 ks 5e10
interface 7, aside from 2,1 to 2,3 bside from 3,1 to 3,3
interface 8, aside from 2,4 to 2,6 bside from 3,4 to 3,6
interface 9, aside from 11,1 to 11,3 bside from 12,1 to 12,3
interface 10, aside from 11,4 to 11,6 bside from 12,4,to 12,6
int 7 glue kn 1e14 ks 1e4
int 8 glue kn 1e12 ks 1e4
int 9 glue kn 1e14 ks 1e4
int 10 glue kn 1e12 ks 1e4
fix x y  i=1,2 j=1
fix x  i=1,2 j=2,3
```

```
fix  x y  i=12,15 j=1
fix  x   i=12,15 j=2,3
fix x y i=3,11 j=1
app nv=-8.33e-8 i=1 j=4,6
app nv=8.33e-8 i=2 j=4,6
app nv=-8.33e-8 i=3 j=4,6
app nv=8.33e-8 i=11 j=4,6
app nv=-8.33e-8 i=12 j=4,6
app nv=8.33e-8 i=13 j=4,6
app xv 8.33e-8 i=3,11 j=7
app xv 8.33e-8 i=3,11 j=8
app syy=-660000 i=3,11 j=6
prop den=7000 she 8e10 bul 1.1e11  i=1 j=1,2
prop den=1 she 8e10 bul 1.1e11  i=1 j=4,5
prop den=1660 she 1.4e7 bul=6.252565417e7  i=3,10 j=1,2
prop fric 9.367 cohe=36695.75   i=3,10 j=1,2
prop den=1660 she 1.4e7 bul=6.252565417e7 i=3,10 j=4,5
prop fric 9.367 cohe=36695.75   i=3,10 j=4,5
prop den=7000 she 8e10 bul 1.1e11  i=12,14 j=1,2
prop den=1 she 8e10 bul 1.1e11  i=12 j=4,5
prop den=1 she 8e10 bul 1.1e11  i=3,10 j=7
plot  g apply velocity
def xdispp
while_stepping
sum=0
loop i (3,11)
sum=sum+ xdisp(i,4)
end_loop
 xdispp=(sum/9)*1000
end
def av_sxy
while_stepping
sum1=0
loop i (4,9)
sum1=sum1+ sxy(i,4)
end_loop
av_sxy=sum1/6
end
his unbal
hist xdis i=1 j=4
hist xdis i=2 j=4
hist xdis i=3 j=4
hist xdis i=4 j=4
hist xdis i=5 j=4
hist xdis i=6 j=4
hist xdis i=7 j=4
hist xdis i=8 j=4
hist xdis i=9 j=4
hist xdis i=10 j=4
hist xdis i=11 j=4
hist xdis i=12 j=4
hist xdis i=13 j=4
```

```
hist sxy i=1 j=4
hist sxy i=2 j=4
hist sxy i=3 j=4
hist sxy i=4 j=4
hist sxy i=5 j=4
hist sxy i=6 j=4
hist sxy i=7 j=4
hist sxy i=8 j=4
hist sxy i=9 j=4
hist sxy i=10 j=4
hist sxy i=11 j=4
hist sxy i=12 j=4
hist sxy i=13 j=4
hist xdispp
hist av_sxy
def fuint2
while_stepping
xdisavpu=1.8844
xdisavfu=4.794
xdisavru=12
if xdispp<=xdisavpu then
fuint2=9.367
end_if
f xdispp>xdisavpu then
if xdispp<=xdisavfu then
fuint2=11.00410705-0.9302*(xdispp)+0.0173*(xdispp^3)
end_if
end_if
if xdispp>xdisavfu then
if xdispp<=xdisavru then
fuint2=8.454666-8.05462e-4*xdispp
end_if
end_if
if xdispp>xdisavru then
fuint2=8.445
end_if
end
def cuint2
while_stepping
if xdispp<=xdisavpu then
cuint2=36695.79
end_if
if xdispp>xdisavpu then
if xdispp<=xdisavfu then
cuint2=64443.82549-18322*(xdispp)+1908.75*(xdispp^2)
end_if
end_if
if xdispp>xdisavfu then
if xdispp<=xdisavru then
cuint2=22948.911740-515.859312*xdispp
end_if
end_if
```

```
if xdispp>xdisavru then
cuint2=16758.60
end_if
end
his cuint2
his fuint2
def ffint2
while_stepping
xdisavpf=0.91033
xdisavff=1.11033
xdisavhf=1.4601189
xdisavrf=2.01033
if xdispp<=xdisavpf then
ffint2=9.348
end_if
if xdispp>xdisavpf then
if xdispp<=xdisavhf then
ffint2=8.426501846+3.6183*(xdispp^2)-2.7532*(xdispp^3)
end_if
end_if
if xdispp>xdisavhf then
if xdispp<=xdisavrf then
ffint2=17.41666234-8.2484*(xdispp)+0.7058*(xdispp^3)
end_if
end_if
if xdispp>=xdisavrf then
ffint2=6.569
end_if
end
def cfint2
while_stepping
if xdispp<=xdisavpf then
cfint2=6606.2
end_if
if xdispp>xdisavpf then
if xdispp<=xdisavff then
cfint2=18131.574776-12660.65578*xdispp
end_if
end_if
if xdispp>xdisavff then
if xdispp<=xdisavrf then
cfint2=(exp(1))^(9.811501365-(1.6645/xdispp))
end_if
end_if
if xdispp>=xdisavrf then
cfint2=7970.702
end_if
end
his cfint2
his ffint2
def amppif_model
loop nn (1,15000)
```

```
xdisavpu=1.8844
xdisavfu=4.794
xdisavru=12
xdisavpf=0.91033
xdisavff=1.11033
xdisavhf=1.4601189
xdisavrf=2.01033
if xdispp<=xdisavpu then
fuint2=9.367
cuint2=36695.79
end_if
if xdispp>xdisavpu then
if xdispp<=xdisavfu then
fuint2=11.00410705-0.9302*(xdispp)+0.0173*(xdispp^3)
cuint2=64443.82549-18322*(xdispp)+1908.75*(xdispp^2)
end_if
end_if
if xdispp>xdisavfu then
if xdispp<=xdisavru then
fuint2=8.454666-8.05462e-4*xdispp
cuint2=22948.911740-515.859312*xdispp
end_if
end_if
if xdispp>xdisavru then
fuint2=8.445
cuint2=16758.60
end_if
if xdispp<=xdisavpf then
ffint2=9.348
end_if
if xdispp>xdisavpf then
if xdispp<=xdisavhf then
ffint2=8.426501846+3.6183*(xdispp^2)-2.7532*(xdispp^3)
end_if
end_if
if xdispp>xdisavhf then
if xdispp<=xdisavrf then
ffint2=17.41666234-8.2484*(xdispp)+0.7058*(xdispp^3)
end_if
end_if
if xdispp>=xdisavrf then
ffint2=6.569
end_if
if xdispp<=xdisavpf then
cfint2=6606.2
end_if
if xdispp>xdisavpf then
if xdispp<=xdisavff then
cfint2=18131.574776-12660.65578*xdispp
end_if
end_if
if xdispp>xdisavff then
```

```
if xdispp<=xdisavrf then
cfint2=(exp(1))^(9.811501365-(1.6645/xdispp))
end_if
end_if
if xdispp>=xdisavrf then
cfint2=7970.702
end_if
cpf=(cuint2+cfint2)/2
fpf=(fuint2+ffint2)/2
command
interface 2 ks=1.83846417e10 kn=1.83846417e10 cohe=cuint2 fric=fuint2
interface 3 kn=1.83846417e10 ks=1.83846417e10 cohe=cfint2 fric=ffint2
interface 4 ks=1.83846417e10 kn=1.83846417e10 cohe=cuint2 fric=fuint2
step=10
end_command
end_loop
end
his cpf
his fpf
amppif_model
save ssmpfsa1.sav
plot g mag
plot his 15 vs 2
plot his 16 vs 3
plot his 17 vs 4
plot his 18 vs 5
plot his 19 vs 6
plot his 20 vs 7
plot his 21 vs 8
plot his 22 vs 9
plot his 23 vs 10
plot his 24 vs 11
plot his 25 vs 12
plot his 26 vs 13
plot his 27 vs 14
plot his 29 vs 28
```

Appendix A(5.4):

The mathematical formulation of the planes indicated in Figure (5.19).

plane No. 1
$l \leq 60$ mm
$P'_c \leq 330$ kpa
$C'_u = 30.8155$ kpa
$\Phi'_u = 0.158914$

plane No.2
60 mm $< l \leq 600$ mm
$P'_c \leq 330$ kpa
$C'_u = 30.8155 - 5.61179629 \times 10^{-3} (l - 60)$
$\Phi'_u = \text{Arctan} (0.158914 - 6.7296293 \times 10^{-5} (l - 60))$

plane No.3
600 mm $< l \leq 10000$ mm
$P'_c \leq 330$ kpa
$C'_u = 27.78513 - 2.930851 \times 10^{-5} (l - 600)$
$\Phi'_u = \text{Arctan} (0.122448 - 3.54255319 \times 10^{-7} (l - 600))$

plane No.4
$l \leq 600$ mm
330 kpa $< P'_c \leq 660$ kpa
$C'_u = 30.8155 + 0.035217909 (P'_c - 330)$
$\Phi'_u = \text{Arctan} (0.158914 + 5.936363 \times 10^{-5} (P'_c - 330))$

plane No.5
$l \leq 600$ mm
660 kpa $< P'_c \leq 11000$ kpa
$C'_u = 42.43741 + 1.3986286 \times 10^{-3} ((P'_c - 660)$
$\Phi'_u = \text{Arctan} (0.178504 + 2.053094778 \times 10^{-6} (P'_c - 660))$

plane No.6
60 mm $< l \leq 600$ mm
330 kpa $< P'_c \leq 660$ kpa
$M_F = 60 + 1.636363 (P'_c - 330)$
if $l \leq M_F$
$C'_u = 20.4324136 + 0.035217909 \times 10^{-3} P'_c - 0.020647062 l$
$\Phi'_u = \text{Arctan} (0.142275115 + 5.93667636 \times 10^{-5} P'_c - 4.918525 \times 10^{-5} l)$

plane No.7
60 mm < $l \leq$ 600 mm
330 kpa < $P'_C \leq$ 660 kpa
if $l > M_F$
$C'_U = 27.64933778 + 0.01061475\ P'_C - 5.611796296 \times 10^{-3}\ l$
$\Phi'_U = \text{Arctan}\ (0.133469812 + 8.9381712 \times 10^{-5}\ P'_C - 6.752962963 \times 10^{-5}\ l)$

plane No.8
60 mm < $l \leq$ 600 mm
330 kpa < $P'_C \leq$ 660 kpa
$N_F = 60 + 0.052224371\ (P'_C - 660)$
if $l \leq N_F$
$C'_U = 43.9722102 + 1.39862862 \times 10^{-3}\ P'_C - 0.040964918\ l$
$\Phi'_U = \text{Arctan}\ (0.178994938 + 2.05309477 \times 10^{-6}\ P'_C - 3.0766344 \times 10^{-5}\ l)$

plane No.9
60 mm < $l \leq$ 600 mm
330 kpa < $P'_C \leq$ 660 kpa
if $l > N_F$
$C'_U = 43.4534565 + 3.37541032 \times 10^{-4}\ P'_C - 0.020647055\ l$
$\Phi'_U = \text{Arctan}\ (0.179465268 + 3.01501054 \times 10^{-6}\ P'_C - 4.918525 \times 10^{-5}\ l)$

plane No.10
600 mm < $l \leq$ 10000 mm
330 kpa < $P'_C \leq$ 660 kpa
$O_F = 600 + 28.484848\ (P'_C - 330)$
if $l \leq O_F$
$C'_U = 24.34481464 + 0.01061475\ P'_C - 1.042577266 \times 10^{-4}\ l$
$\Phi'_U = \text{Arctan}\ (0.093113736 + 8.938171212 \times 10^{-5}\ P'_C - 2.69703085 \times 10^{-7}\ l)$

plane No.11
600 mm < $l \leq$ 10000 mm
330 kpa < $P'_C \leq$ 660 kpa
if $l > O_F$
$C'_U = 25.0043677 + 8.47984051 \times 10^{-3}\ P'_C - 2.930851064 \times 10^{-5}\ l$
$\Phi'_U = \text{Arctan}\ (0.092369797 + 9.17901697 \times 10^{-5}\ P'_C - 3.542553191 \times 10^{-7}\ l)$

plane No.12
600 mm < $l \leq$ 10000 mm
660 kpa < $P'_C \leq$ 11000 kpa
$P_F = 600 + 0.909090\ (P'_C - 660)$
if $l \leq P_F$
$C'_U = 31.17813185 + 3.37541032 \times 10^{-4}\ P'_C - 1.88181557 \times 10^{-4}\ l$
$\Phi'_U = \text{Arctan}\ (0.150055593 + 3.01501054 \times 10^{-6}\ P'_C - 1.692259574 \times 10^{-7}\ l)$

plane No.13

600 mm < $l \leq$ 10000 mm

660 kpa < $P'_c \leq$ 11000 kpa

if $l > P_F$

$C'_U = 31.17813185 + 2.6124664 \times 10^{-4} P'_c - 1.042577266 \times 10^{-4} l$

$\Phi'_U = \text{Arctan}\ (0.149258179 + 3.10635338 \times 10^{-6} P'_c - 1.8996170 \times 10^{-7} l)$

Appendix A(5.5):

Appendix A(5.5): The mathematical formulation of the planes indicated in Figures (5.20) and (5.21).

a = 6000 pa
b = 35651 pa
$c = \frac{s}{l} = 1000$
d = 10°
e = 8.969°

for: $w \le l$

$s \le l$

$s \le \frac{w}{2}$

$s = \frac{w}{2}$

$C'_{PF} = a + (b - a)\ \frac{s}{l} + (a - b)\ \frac{w}{l}$

$\Phi'_{PF} = (e - d)\ \frac{s}{l} + (d - e)\ \frac{w}{l}$

for: $w \le l$

$w < s \le l$

$C'_{PF} = a + (b - a)\ \frac{s}{l} + (a - b)\ \frac{w}{l}$

$\Phi'_{PF} = d + (e - d)\ \frac{s}{l} + (d - e)\ \frac{w}{l}$

for: $w \le l$

$1 < \frac{s}{l} \le c$

$m = (\frac{s}{l}) / (c-1) + (c-2) / (c-1)$

$\frac{w}{l} \le m$

$$C'_{PF} = \frac{(2b - a - bc)}{(1 - c)} + \frac{(a - b)(\frac{s}{l})}{(1 - c)} + (a - b)\ \frac{w}{l}$$

$$\Phi'_{PF} = \frac{(2e - ce - d)}{(1 - c)} + \frac{(d - e)(\frac{s}{l})}{(1-c)} + (d - e)\frac{w}{l}$$

for: $w \le l$

$1 < \frac{s}{l} \le c$

$\frac{w}{l} > m$

$C'_{PF} = b$

$\Phi'_{PF} = e$

for: $w \le l$

$\frac{s}{l} > c$

$C'_{PF} = b$

$\Phi'_{PF} = e$

for: $w > l$

$w = l$

$\frac{s}{l} \le 1$

$$C'_{PF} = a + (b - a)\frac{s}{l} + (a - b)\frac{w}{l}$$

$$\Phi'_{PF} = d + (e - d)\frac{s}{l} + (d - e)\frac{w}{l}$$

Appendix A(5.6):

The HSSM program was written for the estimation of the effective shear strength of the overconsolidated clay specimens subjected to direct shear test.

```
title
Homogenised Strain Softeninig Model of Direct Shear Box (hssmupf2.dat)
grid 14,7
m m i=3,10 j=1,2
m m i=3,10 j=4
m m i=3,10 j=5
m e i=1 j=1,2
m e i=1 j=4,5
m e i=12,14 j=1,2
m e i=12 j=4,5
m e i=3,10 j=7
gen 0,0 0,0.035 0.175,0.035 0.175,0
ini x=0.00075 i=2
ini x=0.14925 i=12
ini y add -0.005 i=1,2 j=4,6
ini y add -0.005 i=3,4 j=4,6
ini y add -0.005 i=5,6 j=4,6
ini y add -0.005 i=7,8 j=4,6
ini y add -0.005 i=9,13 j=4,6
ini y add -0.01 i=1,13 j=7,8
ini y=0.02075  i=3,11 j=8
interface 1, aside from 1,3 to 2,3 bside from 1,4 to 2,4
interface 2, aside from 3,3 to 11,3 bside from 3,4 to 11,4
interface 3, aside from 12,3 to 13,3 bside from 12,4 to 13,4
interface 4, aside from 3,6 to 11,6 bside from 3,7 to 11,7
int 1 kn 1e14 ks 1
int 3 kn 1e14 ks 1
int 4 glue kn 1e12 ks 5e10
ini x add 0.02425 i=1,2 j=1,6
ini x add -0.02425 i=12,15 j=1,6
interface 5, aside from 2,1 to 2,3 bside from 3,1 to 3,3
interface 6, aside from 2,4 to 2,6 bside from 3,4 to 3,6
interface 7, aside from 11,1 to 11,3 bside from 12,1 to 12,3
interface 8, aside from 11,4 to 11,6 bside from 12,4,to 12,6
int 5 glue kn 1e14 ks 1e4
int 6 glue kn 1e12 ks 1e4
int 7 glue kn 1e14 ks 1e4
int 8 glue kn 1e12 ks 1e4
fix x y  i=1,2 j=1
fix x   i=1,2 j=2,3
```

```
fix  x y  i=12,15 j=1
fix  x   i=12,15 j=2,3
fix x y i=3,11 j=1
def propfactors
command
* beta1: the correction factor of c (cohesion) for the effect of size and
*       over-consolidation pressure for KB material
* beta2: the correction factor of friction for the effect of size and
*       over-consolidation pressure for KB material
* beta3: the correction factor of c (cohesion) for the effect of size and
*      over-consolidation pressure for K material
* beta4: the correction factor of friction for the effect of size and
*       over-consolidation pressure for K material
* teta1: the correction factor of c (cohesion) for the effects of fissure
*       parameters(spacing and width of fissure for KB material
* teta2: the correction factor of friction for the effects of fissure
*       parameters(spacing and width of fissure for KB material
* teta3: the correction factor of c (cohesion) for the effects of fissure
*       parameters(spacing and width of fissure for K material
* teta4: the correction factor of friction for the effects of fissure
*       parameters(spacing and width of fissure for K material
* gama1: the correction factor of c (cohesion) for the effects of
*       locked in horizontal stresses for KB material
* gama2: the correction factor of friction for the effects of
*       locked in horizontal stresses for KB material
* gam3: the correction factor of c (cohesion) for the effects of
*       locked in horizontal stresses for K material
* gama4: the correction factor of friction for the effects of
*       locked in horizontal stresses for K material
* sai1:  the correction factor of c (cohesion) for the effects of
*       curve estimation (size and p'c) for KB material
* sai2:  the correction factor of friction for the effects of
*       curve estimation (size and p'c) for KB material
*  uf=1 for unfissured samples
*  uf=0 for fissured samples
*  comb=1     for KB material samples (75% kaolin and 25% bentonite)
*  comb=0     for K material samples (100% kaolin)
*  ns         for normal stress on the sample
*  n          the number of the fissures in a sample
*  w          width of a fissure
*  perc       percentage of fissures in a sample
*  l          the length of a sample
*  s          the spacing of the fissures
*  unlock=1   for unlocked in horizontal stress samples
*  unlock=0   for locked in horizontal stress samples
end_command
pc=330
unlock=1
```

```
ns=-330000
l=300
uf=0
w=90
s=300
n=1
perc=0.3
comb=1
command
* introducing mohr-coulomb parameters for KB material
end_command
if comb=1 then
cu=36695.2
fu=9.367
end_if
command
* introducing mohr-coulomb parameters for K material
end_command
if comb=0 then
cu=29975
u=15.26523621
end_if
command
* introducing the factors for the effect of size and over_consolidation
* pressure for the cohesion and friction of KB material
end_command
if comb=1 then
if l<=60 then
if pc<=330 then
cii=30.8155
ci=cii*1000
fii=0.158914
fi=(180/pi)*atan(fii)
beta1=1-ci/cu
beta2=1-fii/(tan(fu*pi/180))
end_if
end_if
if 60<l then
if l<=600 then
if pc<=330 then
cii=30.8155-5.61179629e-3*(l-60)
ci=cii*1000
fii=0.158914-6.75296293e-5*(l-60)
fi=(180/pi)*atan(fii)
beta1=1-ci/cu
beta2=1-fii/(tan(fu*pi/180))
end_if
end_if
```

```
end_if
if 600<l then
if l<=10000 then
if pc<=330 then
fii=0.122448-3.54255319e-7*(l-600)
cii=27.78513-2.93085106e-5*(l-600)
ci=cii*1000
fi=(180/pi)*atan(fii)
beta1=1-ci/cu
beta2=1-fii/(tan(fu*pi/180))
end_if
end_if
end_if
if l<=60 then
if 330<pc then
if pc<=660 then
cii=30.8155+0.035217909*(pc-330)
ci=cii*1000
fii=0.158914+5.93636363e-5*(pc-330)
fi=(180/pi)*atan(fii)
beta1=1-ci/cu
beta2=1-fii/(tan(fu*pi/180))
end_if
end_if
if 660<pc then
if pc<=11000 then
cii=42.43741+1.3986286286e-3*(pc-660)
ci=cii*1000
fii=0.178504+2.05309477866e-6*(pc-660)
fi=(180/pi)*atan(fii)
beta1=1-ci/cu
beta2=1-fii/(tan(fu*pi/180))
end_if
end_if
end_if
if 60<l then
if l<=600 then
if 330<pc then
if pc<=660 then
mf=60+1.63636363*(pc-330)
if l<=mf then
cii=20.4324136+0.035217909*pc-0.020647062*l
ci=cii*1000
fii=0.142275115+5.93636363E-5*pc-4.918525E-5*l
fi=(180/pi)*atan(fii)
beta1=1-ci/cu
beta2=1-fii/(tan(fu*pi/180))
end_if
```

```
if l>mf then
cii=27.64933778+0.01061475*pc-5.611796296e-3*l
ci=cii*1000
fii=0.133469812+8.9381712e-5*pc-6.752962963e-5*l
fi=(180/pi)*atan(fii)
beta1=1-ci/cu
beta2=1-fii/(tan(fu*pi/180))

end_if
end_if
end_if
if 660<pc then
if pc<=11000 then
nf=60+0.052224371*(pc-660)
if l<=nf then
cii=43.9722102+1.398628627e-3*pc-0.040964918*l
ci=cii*1000
fii=0.178994938+2.05309477e-6*pc-3.076634444-5*l
fi=(180/pi)*atan(fii)
beta1=1-ci/cu
beta2=1-fii/(tan(fu*pi/180))
end_if
if l>nf then
cii=43.4534565+3.37541032e-4*pc-0.020647055*l
ci=cii*1000
fii=0.179465208+3.01501054e-6*pc-4.918525e-5*l
fi=(180/pi)*atan(fii)
beta1=1-ci/cu
beta2=1-fii/(tan(fu*pi/180))
end_if
end_if
end_if
end_if
end_if
if 600<l then
if l<=10000 then
if 330<pc then
if pc<=660 then
of=600+28.48484848*(pc-330)
if l<=of then
cii=24.34481464+.0106147*pc-1.042577266e-4*l
ci=cii*1000
fii=.093113736+8.938171212e-5*pc-2.69703085e-7*l
fi=(180/pi)*atan(fii)
beta1=1-ci/cu
beta2=1-fii/(tan(fu*pi/180))
end_if
if l>of then
```

```
cii=25.0043677+8.4798405e-3*pc-2.930851064e-5*l
ci=cii*1000
fii=.092369797+9.17901697e-5*pc-3.542553191e-7*l
fi=(180/pi)*atan(fii)
beta1=1-ci/cu
beta2=1-fii/(tan(fu*pi/180))
end_if
end_if
end_if
if 660<pc then
if pc<=11000 then
pf=600+.9090909090*(pc-660)
if l<=pf then
cii=31.17813185+3.37541032e-4*pc-1.881815574e-4*l
ci=cii*1000
fii=.15005593+3.01501054e-6*pc-1.692259574e-7*l
fi=(180/pi)*atan(fii)
beta1=1-ci/cu
beta2=1-fii/(tan(fu*pi/180))
end_if
if l>pf then
cii= 31.17813185+2.61246641e-4*pc-1.042577266e-4*l
ci=cii*1000
fii=.149258179+3.10635338e-6*pc-1.899617021e-7*l
fi=(180/pi)*atan(fii)
beta1=1-ci/cu
beta2=1-fii/(tan(fu*pi/180))
end_if
end_if
end_if
end_if
end_if
end_if
command
* introducing the factors for the effect of size and over_consolidation
* pressiure for the cohesion and friction of K material
end_command
if comb=0 then
if l=100 then
beta3=beta3
beta4=beta4
end_if
if l=60 then
beta3=beta3
beta4=beta4
end_if
if l=300 then
beta3=beta3
```

```
beta4=beta4
end_if
end_if
command
* introducing the factors for the effect of locked horizontal
* stress for the cohesion and friction of KB material
end_command
if comb=1 then
if unlock=1 then
gama1=1
gama2=1
end_if
if unlock=0 then
if 440<pc then
if pc<=660 then
if 60<=l then
gama1=0.8
gama2=0.75
end_if
if 60<l then
gama1=0.81
gama2=0.87
end_if
end_if
end_if
if 330<pc then
if pc<=440 then
gama1=0.81
gama2=0.83
end_if
end_if
if pc<=330 then
gama1=0.81
gama2=0.85
end_if
if 660<pc then
gama1=0.82
gama2=0.88
end_if
end_if
end_if
command
* introducing the factors for the effect of locked horizontal
* stress for the cohesion and friction of K material
end_command
if comb=0 then
if unlock=1 then
gama3=1
```

```
gama4=1
end_if
if unlock=0 then
gama3=0.85
gama4=0.97
end_if
end_if
command
* calculating the factors of the effects of unlocked,
* locked and size for unfissured KB and K samples
end_command
if uf=1 then
if comb=1 then
if pc>=440 then
if pc<=660 then
if l<=60 then
sai1=1.2
sai2=1.2
end_if
if l>60 then
if l<=100 then
if pc>=550 then
if pc<=660 then
sai1=1.164100-.002735*l
sai2=1.08805-.001467*l
end_if
end_if
if pc>=440 then
if pc<550 then
sai1=0.98
sai2=1
end_if
end_if
end_if
end_if
if l>100 then
if l<=300 then
sai1=.904150-1.35500e-4*l
sai2=.948-6.7e-5*l
end_if
end_if
if l>300 then
if l<=400 then
sai1=.7585+3.5e-4*l
sai2=.8688+1.97e-4*l
end_if
end_if
if l>400 then
```

```
if l<=500 then
sai1=.7145 +4.6e-4*l
sai2=.8496+2.45e-4*l
end_if
end_if
if l>500 then
if l<=600 then
sai1=.667+5.55e-4*l
sai2=.8326+2.79e-4*l
end_if
end_if
if l>600 then
sai1=1
sai2=1
end_if
end_if
end_if
if pc>330 then
if pc<440 then
if l>60 then
if l<=300 then
sai1=0.95
sai2=0.98
end_if
end_if
if l>300 then
sai1=1
sai2=1
end_if
end_if
end_if
if pc<=330 then
if l<=60 then
sai1=1.2
sai2=1.2
end_if
if l>60 then
sai1=0.95
sai2=0.95
end_if
end_if
if pc>660 then
sai1=1
sai2=1
end_if
alfa1=(1-beta1)*gama1*sai1
alfa2=(1-beta2)*gama2*sai2
end_if
```

```
if comb=0 then
alfa3=(1-beta3)*gama3
alfa4=(1-beta4)*gama4
end_if
end_if
command
*  subroutine for calculating parameters of
*  fissure or partially fissured samples
end_command
if uf=0 then
if comb=1 then
command
*  parameters from the results of the
*  experimental and computer models
end_command
a=6000
b=35651
c=1000
d=10
e=8.969
if w<=l then
if s<=l then
if s<=w/2 then
s=w/2
command
*  relationships for the s/l and w/l with cohesion and friction
*  parameters of partially or fully fissured kb samples
end_command
cpf=a+(b-a)*s/l+(a-b)*w/l
fpf=d+(e-d)s/l+(d-e)w/l
teta1=cpf/cu
teta2=fpf/fu
end_if
if s>w/2 then
sef=(l/n)*(1-perc)
wf=perc*l
w=perc*l/n
wu=n*s*(1-perc)
cpf=a+(b-a)*s/l+(a-b)*w/l
fpf=d+(e-d)s/l+(d-e)w/l
teta1=cpf/cu
teta2=fpf/fu
end_if
end_if
if s/l>1 then
if s/l<=c then
m=(s/l)/(c-1)+(c-2)/(c-1)
if w/l<=m then
```

```
cpf=(2*b-a-b*c)/(1-c)+(a-b)*(s/l)/(1-c)+(a-b)*w/l
fpf=(2*e-c*e-d)/(1-c)+(d-e)*(s/l)/(1-c)+(d-e)*w/l
teta1=cpf/cu
teta2=fpf/fu
end_if
if m<w/l then
cpf=b
fpf=e
teta1=cpf/cu
teta2=fpf/fu
end_if
end_if
end_if
if s/l>c then
cpf=b
fpf=e
end_if
end_if
if w>l then
w=l
if s/l<=1 then
cpf=a+(b-a)*s/l+(a-b)*w/l
fpf=d+(e-d)s/l+(d-e)w/l
teta1=cpf/cu
teta2=fpf/fu
end_if
if s/l>1 then
if s/l<=c then
m=(s/l)/(c-1)+(c-2)/(c-1)
if w/l<=m then
cpf=(2*b-a-b*c)/(1-c)+(a-b)*(s/l)/(1-c)+(a-b)*w/l
fpf=(2*e-c*e-d)/(1-c)+(d-e)*(s/l)/(1-c)+(d-e)*w/l
teta1=cpf/cu
teta2=fpf/fu
end_if
if m<w/l then
cpf=b
fpf=e
teta1=cpf/cu
teta2=fpf/fu
end_if
end_if
end_if
if s/l>c then
cpf=b
fpf=e
end_if
end_if
```

```
if pc>=440 then
if pc<=660 then
if l<=60 then
sai1=1.2
sai2=1.2
end_if
if l>60 then
if l<=100 then
if pc>=550 then
if pc<=660 then
sai1=1.164100-.002735*l
sai2=1.02
end_if
end_if
if pc>=440 then
if pc<550 then
sai1=1
sai2=1.05
end_if
end_if
end_if
end_if
if l>100 then
if l<=300 then
sai1=.904150-1.35500e-4*l
sai2=.948-6.7e-5*l
end_if
end_if
if l>300 then
if l<=400 then
sai1=.7585+3.5e-4*l
sai2=.8688+1.97e-4*l
end_if
end_if
if l>400 then
if l<=500 then
sai1=.7145 +4.6e-4*l
sai2=.8496+2.45e-4*l
end_if
end_if
if l>500 then
if l<=600 then
sai1=.667+5.55e-4*l
sai2=.8326+2.79e-4*l
end_if
end_if
if l>600 then
sai1=1
```

```
sai2=1
end_if
end_if
end_if
if pc>330 then
if pc<440 then
if l> 60 then
if l<=300 then
sai1=0.95
sai2=0.98
end_if
end_if
if l>300 then
sai1=1
sai2=1
end_if
if l<60 then
sai1=1
sai2=1
end_if
end_if
end_if
if pc<=330 then
if l<=60 then
sai1=1.2
sai2=1.2
end_if
if l>60 then
sai1=1.1
sai2=1.1
end_if
end_if
if pc>660 then
sai1=1
sai2=1
end_if
alfa1=(1-beta1)*(gama1*teta1)*sai1
alfa2=(1-beta2)*(gama2*teta2)*sai2
end_if
if comb=0 then
command
* for further research the relationships for s/l, w/l with
* cohesion andfriction of k material samples for differnt
* spacing and size of fissure should be investigated
end_command
cpf=cpf
fpf=fpf
teta3=cpf/cu
```

```
teta4=fpf/fu
if unlock=1 then
gama3=1
gama4=1
end_if
if unlock=0 then
gama3=0.85
gama4=0.97
end_if
alfa3=(1-beta3)*gama3*teta3
alfa4=(1-beta4)*gama4*teta4
end_if
end_if
command
*  calculating the factors of the effects of unlocked,locked
*  and size for the partially or fully fissured KB and K samples
end_command
command
app syy=ns i=3,11 j=6
prop den=1660 she 1.4e7 bul=6.252565417e7   i=3,10 j=1,2
prop fric=fi cohe=ci  i=3,10 j=1,2
prop den=1660 she 1.4e7   bul=6.252565417e7   i=3,10 j=4,5
prop fric=fi cohe=ci  i=3,10 j=4,5
end_command
end
propfactors
app nv=-8.33e-8 i=1 j=4,6
app nv=8.33e-8 i=2 j=4,6
app nv=-8.33e-8 i=3 j=4,6
app nv=8.33e-8 i=11 j=4,6
app nv=-8.33e-8 i=12 j=4,6
app nv=8.33e-8 i=13 j=4,6
app xv 8.33e-8 i=3,11 j=7
app xv 8.33e-8 i=3,11 j=8
prop den=7000 she 8e10 bul 1.1e11  i=1 j=1,2
prop den=1 she 8e10 bul 1.1e11  i=1 j=4,5
prop den=7000 she 8e10 bul 1.1e11  i=12,14 j=1,2
prop den=1 she 8e10 bul 1.1e11  i=12 j=4,5
prop den=1 she 8e10 bul 1.1e11  i=3,10 j=7
plot bou fix apply stress
def xhdispp
while_stepping
sum=0
loop i (3,11)
sum=sum+ xdisp(i,4)
end_loop
xhdispp=(sum/9)*1000
xdispp=(sum/9)*100000/1
```

```
end
def av_sxy
while_stepping
sum1=0
loop i (4,9)
sum1=sum1+ sxy(i,4)
end_loop
av_sxy=sum1/6
end
his unbal
hist xdis i=3 j=4
hist xdis i=4 j=4
hist xdis i=5 j=4
hist xdis i=6 j=4
hist xdis i=7 j=4
hist xdis i=8 j=4
hist xdis i=9 j=4
hist xdis i=10 j=4
hist sxy i=3 j=4
hist sxy i=4 j=4
hist sxy i=5 j=4
hist sxy i=6 j=4
hist sxy i=7 j=4
hist sxy i=8 j=4
hist sxy i=9 j=4
hist sxy i=10 j=4
hist xdispp
hist av_sxy
his xhdispp
def fuint2h
while_stepping
if comb=1 then
xdisavp=1.8844
xdisavf=4.794
xdisavr=12
if xhdispp<=xdisavp then
fuint2=9.367
fuint2h=alfa2*fuint2
end_if
if xhdispp>xdisavp then
if xhdispp<=xdisavf then
fuint2=11.00410705-0.9302*(xhdispp)+0.0173*(xhdispp^3)
fuint2h=alfa2*fuint2
end_if
end_if
if xhdispp>xdisavf then
if xhdispp<=xdisavr then
fuint2=8.454666-8.05462e-4*xhdispp
```

```
fuint2h=alfa2*fuint2
end_if
end_if
if xhdispp>xdisavr then
fuint2=8.445
fuint2h=alfa2*fuint2
end_if
end_if
if comb=0 then
xdisavp=xdisavp
xdisavf=xdisavf
xdisavr=xdisavr
fuint2=fuint2
fuint2h=alfa4*fuint2
end_if
end
def cuint2h
while_stepping
if comb=1 then
if xhdispp<=xdisavp then
cuint2=36695.79
cuint2h=alfa1*cuint2
end_if
if xhdispp>xdisavp then
if xhdispp<=xdisavf then
cuint2=64443.82549-18322*(xhdispp)+1908.75*(xhdispp^2)
cuint2h=alfa1*cuint2
end_if
end_if
if xhdispp>xdisavf then
if xhdispp<=xdisavr then
cuint2=22948.911740-515.859312*xhdispp
cuint2h=alfa1*cuint2
end_if
end_if
if xhdispp>xdisavr then
cuint2=16758.60
cuint2h=alfa1*cuint2
end_if
end_if
if comb=0 then
xdisavp=xdisavp
xdisavf=xdisavf
xdisavr=xdisavr
cuint2=cuint2
cuint2h=alfa3*cuint2
end_if
end
```

```
his cuint2
his fuint2
his cuint2h
his fuint2h
def ampifh_model
loop nn (1,7000)
if comb=1 then
xdisavp=1.8844
xdisavf=4.794
xdisavr=12
if xhdispp<=xdisavp then
fuint2=9.367
fuint2h=alfa2*fuint2
cuint2=36695.79
cuint2h=alfa1*cuint2
end_if
if xhdispp>xdisavp then
if xhdispp<=xdisavf then
fuint2=11.00410705-0.9302*(xhdispp)+0.0173*(xhdispp^3)
fuint2h=alfa2*fuint2
cuint2=64443.82549-18322*(xhdispp)+1908.75*(xhdispp^2)
cuint2h=alfa1*cuint2
end_if
end_if
if xhdispp>xdisavf then
if xhdispp<=xdisavr then
fuint2=8.454666-8.05462e-4*xhdispp
fuint2h=alfa2*fuint2
cuint2=22948.911740-515.859312*xhdispp
cuint2h=alfa1*cuint2
end_if
end_if
if xhdispp>xdisavr then
fuint2=8.445
fuint2h=alfa2*fuint2
cuint2=16758.60
cuint2h=alfa1*cuint2
end_if
end_if
if comb=0 then
xdisavp=xdisavp
xdisavf=xdisavf
xdisavr=xdisavr
fuint2=fuint2
fuint2h=alfa4*fuint2
cuint2=cuint2
cuint2h=alfa3*cuint2
end_if
```

```
command
interface 2 ks=1.83846417e10 kn=1.83846417e10 cohe=cuint2h fric=fuint2h
step=10
end_command
end_loop
end
ampifh_model
step 80000
save hssmupf2.sav
set out = u1
plot pen his 19 vs 18
set out = u2
plot pen g mag
plot g mag
plot his 15 vs 2
plot his 16 vs 3
plot his 17 vs 4
plot his 18 vs 5
plot his 19 vs 6
plot his 20 vs 7
plot his 21 vs 8
plot his 22 vs 9
plot his 23 vs 10
plot his 24 vs 11
plot his 25 vs 12
plot his 26 vs 13
plot his 27 vs 14
plot his 29 vs 28
```

CHAPTER 6

TRIAXIAL TESTS

6.1 INTRODUCTION

Orientation or inclination of fissures has a significant effect on the triaxial compressive strengths and deformation behaviour of the overconsolidated clay specimens.

The testing program described in this chapter was carried out to study the effect of orientation of continuous or discontinuous fissures on the effective compressive strengths as well as the effect of confining pressure on the deformation behaviour of the fully fissured triaxial specimens. These were tested in single stage loading and each orientation for three different OCR's.

In addition to the unfissured specimens, the fully fissured specimens were prepared for three different orientation angles, 30°, 45°, and 60° to the direction of the minimum principal (σ_3) stress. This study is an attempt to prepare artificially consolidated fully or partially fissured clay specimens and also to investigate experimentally the effect of orientation of fissure and confining pressure on the effective compressive strength of the triaxial specimens.

6.2 THE TESTING PROGRAM FOR THE TRIAXIAL TESTS

A sample maker was designed and constructed to prepare artificially the fully, partially fissured or unfissured consolidated specimens.

The size of consolidated cylindrical specimens subjected to triaxial tests was 50 mm diameter by 100 mm height. The unfissured triaxial specimens were consolidated initially by the three different preconsolidation pressures of 660 kpa, 440 kpa and 330 kpa the same as the P'_c applied for the consolidation of the specimens subjected to direct shear tests. But the fully fissured or partially fissured triaxial specimens were only consolidated by the P'_c of 660 kpa.

For the unfissured specimens, an average of a 15 day loading for each KB specimen and an 8 day loading for each K specimen were required to consolidate the specimens in the triaxial sample maker. For the fully fissured specimens, the time increased to 25 or 15 days of loading for KB or K specimens respectively because of the increase of raw material for the fully fissured specimens.

Taking into account the very low permeability of the clay materials, consolidated undrained tests (CU) with pore pressure measurement and with a filter paper side drain, were conducted with an axial rate of 0.1 mm/hr.

The specimens consolidated by P'_c of 660 kpa in the triaxial sample maker, were again consolidated isotropically and then tested in the triaxial cell with the three different effective confining pressures of 600 kpa, 400 kpa, and 1100 kpa. The back pressure applied for the each confining pressure was 400 kpa.

The specimens consolidated by P'_c of 440 kpa or 330 kpa were also consolidated isotropically and then tested in the triaxial cell with pressures of 400 kpa, 200, and 900 kpa or 300 kpa, 100, and 800 kpa respectively. The back pressures were 600 kpa and 700 kpa for the P'_c of 440 kpa and 330 kpa respectively.

The test program and results of the triaxial specimens are summarised in Tables (6.1)-(6.3) . The main objective of these tests has been to investigate the effect of orientation of fissures in the fully and partially fissured specimens.

6.3 THE TRIAXIAL SAMPLE MAKER

Figures (6.1) and (6.2) show schematically the illustration of the photograph of the triaxial sample maker which was developed. It was used to prepare fully, partially fissured and unfissured triaxial specimens with a diameter of 50 mm and height of 100 mm. Three different orientations of 30°, 45° and 60° fissured specimens were prepared by this sample maker.

Except for the support frame, beam, dial gauge, and the weight hanger of the triaxial sample maker, the original parts of an oedometer apparatus, all other parts were developed, designed and constructed to be used for making triaxial fully, or partially, or unfissured consolidated clay specimens.

The basic concept for the preparation of the orientated fissured specimens was to keep the top and bottom drainage surfaces parallel during the consolidation process, for any proposed orientation angle.

6.3.1 System Layout

As shown schematically in Figure.(6.1), the sample maker mainly consisted of the support frame, beam (lever), weight hanger, consolidation cell, locking flange, base and compression pads, load spacer, hollow cylinders, stabilising alignment clamps and a dial gauge. For three orientations 30°, 45° and 60°, three pairs of base and compression pads were designed. To each pad a porous sintered brass was attached for drainage during the consolidation process of the orientated fissured specimens.

The surfaces of the base and compression pads touching the specimen were parallel to the surfaces of the oriented fissure. Therefore the surfaces of the fissure during the consolidation process were parallel, even, and smooth. Figure (6.3) shows a photograph of the orientated fissured specimen for i=60°.

6.3.2 The System Elements

6.3.2.1 The Sample maker consolidation cell

The consolidation cell or reservoir, consisted of a base plate which was ribbed for drainage of the specimen from the bottom as shown in the photograph in Figure

(6.4), the cell body prepared of clear acrylic and three studs. The cell body was connected to the base plate and sealed by an o-ring. There was a locating recess at the bottom of the base plate that allowed the reservoir to be seated on the support frame of the consolidation apparatus.

The base plate was nickel-plated to resist rust. Three studs were located on the base plate to fit the ring retainer around the shoulder of the base cylinder. In order to have parallel surfaces between compression and base pads, there was a reference mark on the external edge of the base plate to adjust the situation of the reservoir to another reference mark located on the surface of the support frames. The compression pad was aligned by a location guide in the load spacer and the base pad was aligned by reference marks on the base cylinder, locking flange, reservoir, and the support frame of the oedemata apparatus.

6.3.2.2 The locking flange

The locking flange or retaining ring was designed and constructed to avoid separating the base cylinder from the base plate as a result of misalignment of the compression pad and also the uplifting pressure of the squeezing paste because of compression loads.

The locking flange had three locating holes and was connected to the base plate by three studs and clamping nuts as shown in Figure (6.4).

On the wing of the flange there was a reference mark that allowed alignment with the mark on the base cylinder.

The base pad was aligned by the marks on the base cylinder, locking flange and base plates and consequently by the mark located on the support frame of the oedometer apparatus.

6.3.2.3 The hollow cylinders

Three brass hollow detachable cylinders were constructed and connected by male and female location steps. This type of connection was easy and practical, specially for removing dirt after the preparation of each specimen. The base cylinder was fixed to

the ribbed base plate of the consolidation cell, the locking flange or retaining ring with three clamping screws. It had a clamping shoulder and the locking flange was located on it. The base cylinder and locking flange were fixed to the consolidation cell by three studs and clamping nuts. A locating screw in the shoulder of the base cylinder connected the base pad to the base cylinder.

The internal diameter of this cylinder was 50 mm and its height was 150 mm. This cylinder was also used for making unfissured specimens.

The middle cylinder had two male and female location steps at each end. The internal diameter was 50 mm and its height was 100 mm.

The top cylinder was used for the preparation of 60 degree oriented fissured specimens. The height and internal diameter were the same as the middle cylinder.

These cylinders made a column and to stabilise it three extra column alignment clamps were used. Three pieces of strip brass with hose clamps were used to keep them connected and closed during the consolidation process and to pull out the consolidated samples from the cylinders. To avoid destroying the consolidated samples from tension stresses, as a result of unloading, these clamps were necessary and worked by friction on the external surface of the cylinders.

6.3.2.4 Base and compression pads

With the exception of the base and compression pads used for the preparation of unfissured specimens, three pairs of brass pads for the 30°,45°and 60 degrees were designed. A few full length holes in each pad were drilled to supply drainage for the specimen during the consolidation process. The surface of the pad was in contact with the specimen with the porous brass filter plate. The porosity of the sintered porous brass was chosen based on the size of the clay particles and the capability of full drainage during the consolidation process. The filters were connected to the pads by screws.

The compression pad also had a locking screw hole and a hole for the locater pin of the loading spacer which was connected to the compression pad by a location pin and

locking screw. As shown in Figure (6.3). The compression pad is connected to the loading spacer by a location and locking screw.

6.3.2.5 The load spacer

This element was designed to be used for all compression pads. It was constructed of brass, had holes to provide drainage from the top of the specimens and was connected to the compression pad by a locking screw and a location pin. It had a ball load seat for loading by the loading bolt and a locating guide. The locating guide aligned the compression pad to provide correct orientation and angular parallel surfaces between the compression and base pads. The length of the locating guide was estimated, based on the maximum settlement of the specimens. This locating guide travelled through a hole in the loading yoke during the consolidation process.

6.3.2.6 The loading frame

The loading frame consisted of a yoke and yoke spacer rods. There was a hole in the yoke for the locating guide of the load spacer. The yoke was manufactured of sufficient depth to work as a rigid element during the loading of the sample. A height adjustable loading bolt was used to apply load to the top of the samples. The yoke was connected to two yoke spacer rods and so as to be able to use the loading frame for different height orientations, the length of the rods was adjustable. Figure (6.5) shows the photograph of the different parts designed and constructed for the preparation of the triaxial specimens including the consolidation cell, locking flange, base and compression pad, loading spacer, loading frame, hollow cylinders, and alignment and stabilising clamps.

6.3.2.7 The stabilising clamp

The assembled cylinders were fixed from the base by a locking flange, and from the top by a stabilising clamp. In order to stabilise the assembled cylinders from the top, the clamp was designed and constructed from pvc material. It consisted of two jaws connected by locating screws. One end of the clamp was fixed to the gauge pillar and the other end was attached to the external surface of the top cylinder.

6.4 THE TRIAXIAL DATA LOGGING SYSTEM

In addition to the triaxial sample maker discussed in the preceding section for the artificial preparation of the fully, partially fissured or unfissured overconsolidated specimens, a computer controlled hydraulic triaxial testing system was also utilised to test the specimens, as shown in Figure (6.6). A computer was linked to the hydraulic triaxial cell via three micro processor controlled hydraulic actuators called "digital controllers" and two subsystems, one for the measurement of axial deformation and the other for the measurement of pore pressure. Figure (6.7) shows the two subsystems. The digital indicator, connected to the bottom of the cell shown at the left, was used for the measurement of the axial deformation and the pressure transducer, shown at the bottom of the triaxial, right side of the cell, was used for the measurement of the pore pressure.

Figure (6.8) shows the photograph of a digital controller. The principles of operation are described by Menzies (1988) and shown schematically in Figure (6.9). De-aerated water in a cylinder was pressurised and displaced by a piston moving in the cylinder. The piston was actuated by a ball screw turned in a captive ball nut by a stepping motor and gear box that moved rectilinearly on a ball side. Pressure was detected by means of an integral solid state pressure transducer. Volume change was measured by counting the steps of the stepping motor. As explained in Chapter 3, this digital controller could be used as a constant pressure source for the consolidation of the specimens. It could be programmed through its own control panel or via the standard IEEE 488 computer interface.

The triaxial compression/extension cell used in this system was based on the design of Bishop and Wesley's (1975a). This versatile cell could be used to carry out classic standard tests, as well as advanced tests. Figure (6.10) shows schematically the lay-out of the triaxial cell depicted by Bishop et al. (1975a).

As shown in this figure, axial force was exerted on the test specimen by means of a piston fixed to the movable base pedestal. The top cap of the test specimen was fixed in the cell with an adjustable rod passing through the top of the cell. The piston could move up and down in a linear guide comprising a cage of ball bearings housed in a

turret joining the cell to the base. The piston was actuated hydraulically from an integral lower chamber in the base of the cell which contained deaerated water.

The piston was sealed into the upper cell and the lower chamber by matched Bellofram rolling diaphragms which swept equal volumes of water. Accordingly the axial ram friction was very small. Equation (6.1) was introduced by Bishop et al. (1975) for the static equilibrium of the loading ram.

$$\sigma_a = p\,(a/A) + \sigma_r\,(1-a/A) - w/A \qquad (6.1)$$

In this equation "σ_a" was the average axial total stress, "σ_r" was the radial total stress or cell pressure, "p" was the pressure in the lower chamber, "A" was the current average cross-sectional area of the test specimen, "a" was the effective area of the Bellofram rolling diaphragm, and "w" was the weight of the loading ram.

The digital controllers precisely regulated the pressure and volume change of deaerated water supplied to the cell to control axial load or axial deformation, cell pressure, and back pressure. This system also could measure axial deformation indirectly by volume change into the lower chamber of the cell or by direct measurement of displacement using a digital indicator. The digital controllers, pore pressure indicator, axial deformation indicator, printer or plotter were connected by interface bus cables to the IEEE 488 standard parallel interface of the computer.

The computer continuously computed directly the average axial total stress just by using Equation (6.1) and there was no need to use an external or internal load cell in this system. The separate system elements and subsystems and also the operation of the system have been described by Menzies (1988). The operation of the system to run tests such as isotropic consolidation tests, K_0 consolidation tests, CU tests, however, is explained later in this chapter.

6.5 MATERIAL AND SPECIMEN PREPARATION FOR TRIAXIAL TESTS

As discussed in Chapter 3, after measuring the water content of kaolin and bentonite powders, they were mixed on the ratio of one part dry bentonite to three parts of dry kaolin for KB specimens or just Kaolin for K specimens and water was added to give

a water content of 67 or 53 percent for KB or K specimens respectively. This formed a paste from which the specimens were prepared.

After curing for one day, the paste was ready to be inserted into detachable moulds for three different angles 30°,45°,and 60° to shape it, as shown in Figure (6.11). For the initial shaping and preparation of each specimen, its mould was assembled. The mould consisted of four parts with three angular separation slots. To keep the parts of the mould together, a split mould outer casing was used. The outer casings and the moulds for three different angles were made of pvc pipe. The outer casings were used as alignment clamps for the moulds.

To keep the mould and outer casing together several Utilox hose clamps were used . In order to shape a specimen before putting it in the triaxial sample maker, paste was put in the mould assembly and filled completely by tamping and refilling. The two ends were then trimmed and the hose clamps and outer casing were removed. By using a wire sample cutter, the specimen was cut through the angular separation slots.

After cutting, two plastic transparency sheets cut in advance to the same size as the cross section of the specimen, were attached to the specimen in the middle slot. For the other two ends, two filter papers were placed and again the four parts were put together and the outer casing with the hose clamps kept them together. Then the assembly mould with the pre-cut specimen was placed in a sample extractor to be pushed out. After pushing out the pre-cut and shaped specimen, the two extra end parts were removed and the two main parts were put in the triaxial sample maker to be consolidated. Figures (6.12) shows photographs of the KB triaxial specimens prepared artificially by the triaxial sample maker. This procedure was applied for all orientated fissured specimens.

The partially fissured triaxial specimens were prepared from the unfissured consolidated triaxial specimens by using a wire sample cutter. The specimens were cut through the separation slots of the moulds designed for shaping the fully fissured specimens.

Figure (6.13) shows schematically a partially fissure specimen cut an inclination of 30°.

The water content of the paste had an important role in the preparation. If it were too liquid or too dry, it was neither practical nor possible to create a well shaped specimen so a water content of 67 percent for KB and 53 percent for K specimens was used to make the pastes. These water contents were enough to work and shape the specimens and to fill the mould without the entrapment of air bubbles.

6.6 TEST PROCEDURE FOR TRIAXIAL SPECIMENS

In order to conduct a triaxial test, initially the computer triaxial systems and specimens were set up and then the GDS triaxial testing system, GDSTTS program, was run for the particular type of test designed for the specimen. The GDSTTS controlled the test parameters, data logging and data presentation. The computer was linked to the test cell by three GDS digital controllers and a digital pressure interface. Data was logged and saved continuously into the computer memory.

The GDSTTS provided the normal test preliminaries of isotropic consolidation and evaluation of the pore pressure parameter B. In addition, saturation ramps and permeability tests by constant rate of flow were also provided. The test menu was as follows:

- unconsolidated - undrained
- consolidated - undrained
- Drained
- K_0 consolidation and swelling
- stress - paths
- cyclic loading

The tests were carried out simply by loading the GDSTTS program and the saved data were used for further analysis by a spreadsheet program like Microsoft Excel. The data saved on the hard disk consisted of information about the dimensions of the test specimen followed by sets of readings from the digital controllers.

6.6.1 Setting Up the Computer and Triaxial Systems

One digital controller was connected to the valve to the lower chamber of the cell, the lower chamber controller, one to the valve to the cell chamber itself, the cell pressure controller, and the third was connected to the valve to the drain to the top cap, the back pressure controller.

To link the digital controllers, a pore pressure transducer, digital indicators and a plotter to the computer, a device code known as an IEEE controller address, was assigned to each. The devices were power on and at each digital controller , the pressure datum was set by holding the open ends of each water filled pressure outlet at mid height of the test specimen (as set up in the test cell) and pressing the PRESSURE ZERO function key on each controller.

The Legris push-fit connectors were checked and the controllers were linked to the test cells ensuring all connections were properly deaired with deaerated distilled water.

After setting up the specimen as described in the following section, the triaxial cell was placed in its place, connected to the base through screws and subsequently filled with deaerated water. Before applying cell pressure, the cell pressure controller was set to zero and the lower chamber pressure, displayed on the lower chamber digital controller, was observed. The pressure in the lower chamber controller was caused by the self weights of the triaxial cell piston and the specimen and associated porous stones and top cap. That pressure should be nulled by pressing the PRESSURE ZERO function key on the lower chamber digital controller. After that the GDS triaxial testing system (GDSTTS) was loaded. The GDSTTS was a user friendly system. All data entry was validated to avoid erroneous entries or so-called "finger trouble". The user interface with the system was based on a dialogue or conversation with the computer. The software asked a sequence of questions such as: the data, time, the IEEE addresses device codes for the controllers. The answers to each question, yes or no were entered "y" or "n" respectively. For a positive answer, the chance of changing the option was given to the user and then the sequence of questions continued to the options of running the tests, plotting the results or

terminating the GDSTTS program. At this stage the computer and triaxial systems were set up and were ready for running the tests or plotting the results.

6.6.2 Setting up the Specimens

Each specimen, before testing, was weighed and its dimensions were determined to an accuracy of 0.01 mm and other specifications, such as the type of material, P'_c applied for consolidation in the triaxial sample maker or for fissured specimens, the orientation of fissures were noted in the laboratory report. Then the specimen was trimmed at the ends to a height of 100 mm. The extra parts from the bottom and top of the untrimmed specimen were weighed and used to determine its water content before testing.

For the fully fissured specimens, particular attention was given that the centre of the fissure surface be located at the middle of the height of the specimen after trimming. The trimmed specimen was weighed again before being tested.

In order to accelerate the drainage of pore water inside the specimen, a saturated filter paper side drain around the specimen also was used, except for specimens designed for K_0 consolidation or CD tests, selected automatic drained testing rate by controlled hydraulic gradient.

After setting up the computer system and the triaxial system, a prepared specimen was placed on the base pedestal or bottom seating cap. Two filter papers were put at both ends of the specimen between the specimen and the deaired saturated porous disc stones located at ends of the specimen. Then the specimen was jacketed with a rubber membrane. A hollow cylinder as membrane stretcher was used to facilitate the jacketing process.

Two "O" rings from the top of specimen were fitted to seal the membrane on the base pedestal. A little water was allowed to moisten the porous disc stone covering the top of the specimen through the drainage valve. Then the upper seating cap was placed on the top of the specimen. The top cap had a spherical seat to accommodate the spherical tip of the hollow reaction rod.

Two more "O" rings used to seal and tighten the membrane to the upper seating cap at the top of the specimen. The "O" rings were fitted by the use of a pvc split tube "O" ring stretcher. The specimen axis was checked that it was vertical and that the top seating cap of the specimen was properly seated. A good fit of the spherical tip of the hollow reaction rod could confirm the proper alignment of the specimen with two seating caps located at both ends of the specimen.

The hollow reaction rod was adjusted so that it would not to hit specimens' top end when placing the cell. The perspex cylinder, called the "triaxial cell", was positioned gently on the base of the cell and the clamping screws, or nuts on the tie rods were progressively tightened. The hollow reaction rod was allowed to fall slowly into contact with the top of the specimen. The deairing and the filling valves were opened to fill up the cell with deaerated and distilled water and to allow the air bubbles to exit the cell via the deairing valve. The computer, printer digital controllers, digital indicators, pore pressure transducers were all turned on and left for at least half an hour before starting the test. The program GDSTTS was run based on the type of test designed for the specimen and the test was automatically carried out as explained in section 6.6.3.

After the test, the pressures applied by the digital controllers were zeroed and the cell pressure valve was turned to evacuate the water from the cell. Then the screws were opened and the cell was removed. The specimen was separated from the pedestal and the membrane and porous stones were removed. The tested specimen was weighed, its dimensions measured and the water content was determined for further analysis.

6.6.3 Running the Tests

After setting up the computer and triaxial system and the specimens and checking the connecting tubes, the Belloframs and Rotolin bearings, the GDS triaxial testing system (GDSTTS), was loaded for each test.

The GDSTTS inspected the devices introduced when setting up the computer and triaxial systems and reported them. At this stage there was a chance to change or modify the previously inserted information. If the computer could not access any of the defined devices, the programs were terminated. If all the devices could be

accessed satisfactorily, the status of each device was reported. Then the program asked about the back pressure controller, whether it was open or closed and a few question about the size of the Bellofram, average diameter and height of the specimen. Each answer was followed by pressing the "ENTER" key and the program asked about the validity of the information by inserting "y" or "n" letters for yes or no respectively. Before starting the test, the computer would carry out a friction check between the Bellofram Rolling Diagram and Rotolin bearing guiding the piston. Specimens which were subject to the friction check showed a correction of about 2 kpa, which was negligible.

After this check, the controllers were maintained automatically a constant volume which meant the program was ready to carry out the different types of tests such as B check or isotropic consolidation test through the pre test menu and K_0 consolidation test, CU or CD tests through the test menu.

6.6.3.1 B check

To evaluate B, a step in cell pressure was made and the undrained change in pore pressure was monitored and used to calculate B. The specimen was considered as a consolidated specimen isotropically when the magnitude of the pore pressure was the same as the back pressure. At this stage the B check was carried out to check the saturation of the specimen at the end of the consolidation test. The B values of the specimens varied between 0.95-0.98.

The B check was one of the tests in the pre test menu of the GDSTTS. The valve to the back pressure was closed and the program asked the required cell pressure change and then the time for plotting the value of B against the square root of time. The test was terminated when the function key F_1 on the keyboard was pushed.

6.6.3.2 The Isotropic consolidation test

As explained previously, the triaxial specimens were consolidated initially in the triaxial sample maker. To minimise the disturbance of the specimens there were two options. The first was to run the K_0 consolidation and the second was to carry out an isotropically consolidation test. Because initially the specimens were consolidated in

the triaxial sample maker, to run a K_0 test without applying isotropic pressure (confining pressure) to consolidate the specimens isotropically was neither useful nor practical. Therefore, for consolidated specimens, the isotropic consolidation test was carried out. From the experimental results obtained from the specimens subjected to direct shear tests, the c'_p and ϕ'_p for each P'_c were estimated. Then for the assumed OCR's, the effective confining pressures (σ'_3) were estimated through Equations (6.2)-(6.6)

$$OCR = \frac{p'_c}{\sigma_N} \tag{6.2}$$

$$\tau'_p = c'_p + \sigma_N \tan \phi'_p \tag{6.3}$$

$$\tau'_p = \frac{\sigma'_1 - \sigma'_3}{2} \sin 2\theta \tag{6.4}$$

$$\sigma_N = \frac{\sigma'_1 + \sigma'_3}{2} + \frac{\sigma'_1 - \sigma'_3}{2} \cos 2\theta \tag{6.5}$$

$$\theta = 45° + \frac{\phi'_p}{2} \tag{6.6}$$

The specimens were consolidated by the σ'_3 estimated from these equations for different OCRs. Ignoring the long time required for the consolidation of each, however, it was possible to put the unconsolidated, but shaped specimens, directly in the cell and the system was set up for the K_0 consolidation test.

In the GDSTTS, isotropic consolidation was allowed to occur by setting a cell pressure and allowing pore water to flow into (swelling) or out (consolidation) of the specimens. The flow of water in the consolidation phase was plotted against the square root of time, as shown in the photograph in Figure (6.14). For KB specimens about 7 days and for K specimens about one day were required to consolidate isotropically the specimens for a cell pressure of 1500 kpa and a back pressure of 400 kpa.

Figures (6.15) and (6.16) show the changes of volume against the square root of time for the KB and K specimens consolidated under the effective confining pressure of

1100 kpa and prepared initially by P'_c of 660 kpa. The value of C_v was calculated from Equation (6.7).

$$C_v = \frac{\pi D^2}{\lambda t_{100}} \qquad (6.7)$$

where C_V (m^2/year) is the coefficient of consolidation, D is the diameter of the specimen (mm), λ is a constant depending on drainage boundary conditions and t_{100} is time for the end of isotropic consolidation process of the specimen (min). Head (1985) stated that the end of consolidation should represent at least 95% dissipation of the excess pore pressure. The value of λ recommended by Head (1985) for the specimens with filter paper side drain is 100. The magnitudes of C_v for KB and K specimens are listed in Table (6.4).

6.6.3.3 The K_0 consolidation test

The K_0 consolidation test could be carried out properly if the specimens initially were consolidated in the cell directly instead of in the triaxial sample maker.

But for the specimens consolidated initially in triaxial sample maker, running the K_0 consolidation test could not simulate the real state of the specimens because for each purposed OCR, a particular confining pressure should be initially applied to consolidate the specimen with no excess pore pressure. Therefore, as result of this confining pressure, there will be some deformation in the dimension of the specimen which is in contrast with the zero lateral strain condition for the simulation of in situ states of the specimens.

Taking into account the time required to run the K_0 consolidation of the specimen directly in the cell and the drawback of conducting the K_0 test on specimens consolidated initially in the triaxial sample maker, the K_0 tests were not carried out for the KB and K specimens and only isotropic consolidation tests were conducted with the predetermined confining pressures as explained in the previous section.

However, the basic rules for the K_0 consolidation test are as follows:

• to calculate the volume of the axial deformation times the original cross-sectional area

• to command the back pressure controller which is under volume change control to stop an equal and opposite volume change

• to command the cell pressure controller to adjust cell pressure to keep the back-pressure constant at the pre-determined value.

These rules result in zero lateral strain which is an essential condition for the simulation of the in situ state of the specimens.

6.6.3.4 CU, the Consolidated undrained test

The problem with a few CD tests, (consolidated drained tests) conducted for KB specimens was the rate of strain. Although the rate was estimated based on the empirical formulation suggested by Heads (1985), during the shearing stage, the excess pore pressure was not dissipated properly for the rate of 0.1 mm/hr. Taking into account the time required for running at least 3% -5% axial strain and also the unsatisfactory dissipation of pore water pressure, only the CU tests with the measurement of the pore water pressure were carried out for the subsequent tests.

This test was carried by the GDSTTS in two stages. After the first stage, the specimens were consolidated isotropically or by a K_0 consolidation test and in the second stage, the specimens were loaded axially with constant radial stresses and by closing the back pressure valve to prevent drainage of the pore water inside the specimens.

The CU test was in the test menu. After setting up the specimen and running the isotropic consolidation test, the GDSTTS reminded the user to dock the top cap against the adjustable reaction head. The system asked for an estimation of the time required to run the test.

The type of test control was questioned in the next step. There were two options, axial total stress and axial deformation. For axial total stress control, the possibility of missing the peak was high, particularly for material with strain softening behaviour. Therefore, axial deformation control, the most common mode in triaxial

testing, was chosen. In the next steps the rate of axial deformation was asked. Although, there was no need to define the very slow rate of strain for the dissipation of pore water pressure induced by the axial strain, the rate of axial strain was applied very slowly to avoid of local failure caused possibly by the high rate of axial strain. The rate of 0.1 mm/hr was inserted for CU tests. The GDSTTS asked the percentage of axial strain required to failure the specimen. A minimum of 3 percentage of axial strain was necessary to mobilise the strength of the specimens to the peak.

The type of plot was subsequently asked by the GDSTTS. There were two options, one plotting the deviator stress and pore pressure and other, the stress ratio. Figure (6.17) shows the typical graphs of stress ratio, deviator stress, and pore pressure against axial strain or stress ratio against axial strain. The test was terminated when the calculated value of axial percentage strain became greater than or equal to the terminal value of percentage axial strain entered by the user.

6.7 TEST RESULTS

The GDSTTS was able to tabulate the basic data relating to the triaxial cell as reproduced in Table (6.5) for a few readings.

At the top of this table, the specifications of the Bellofram, the specimen, the name of the file, and the total number of readings, were recorded. A_0 stands for the specimen area (mm^2), l_0 for specimen height (mm), A_1 for Bellofram area (mm^2), FRICTION for friction value (kpa), RDG for Reading Number, T for Time (min), P_6 for the pressure read from the digital pressure indicator (the pore pressure), P_7 for the pressure read from the radial controller (the cell pressure), V_7 for the volume change read from the radial controller, P_8 the pressure read from the back pressure controller (the back pressure), V_8 the volume change read from the back pressure controller (the specimen volume change), P_9 the pressure read from the lower chamber controller, and V_9 the volume change read from the lower chamber controller.

Each set of data was gathered at the same point in time. All of the other parameters related to the triaxial cell and the test specimen could be calculated from these basic values. For example, the following equations were used for parameters such as, axial

strain (E_1), effective axial stress (S_2), effective radial stress (S_3), deviator stress (D_1) or effective stress ratio (R_6).

$$E_1 = \frac{V_9}{(A_1 \times l_0)} \tag{6.8}$$

$$A = \frac{A_0(1 + \frac{V_8}{A_0 \times l_0})}{(1 - E_1)} \tag{6.9}$$

$$S_1 = (P_9 - P_7) \times \frac{A_1}{A} + P_7 \tag{6.10}$$

$$S_2 = S_1 - P_8 \tag{6.11}$$

$$S_3 = P_7 - P_8 \tag{6.12}$$

$$D_1 = S_1 - P_7 \tag{6.13}$$

$$R_6 = \frac{S_2}{S_3} \tag{6.14}$$

The results are listed in Tables (6.6)-(6.11).

6.7.1 General Behaviour Observed Experimentally

Figure (6.18) shows a photograph of the two KB specimens subjected to triaxial tests. The surfaces of the fully fissured specimen prepared artificially were smooth. In contrast, the shear surfaces of the unfissured specimens were uneven and bumpy but polished and slikensided which means the unfissured specimens failed in shear mode rather than tension or torsion modes. Figure (6.19) shows a photograph of a set of KB specimens tested in the triaxial apparatus for three angles of inclination.

The fully fissured triaxial specimens tested with low pressure (less than 1000 kpa) showed obvious sliding along the fissure surfaces, but at high confining pressure (1500 kpa) showed dependency of angle for the sliding. The fully fissured triaxial specimens with angles of inclination of 60° and 30° showed slight sliding, but an inclination of 45° showed obvious sliding for the confining pressure of 1500 kpa. Because of the limitation of cell pressure (max 1500 kpa), the effect of high confining pressure on the deformation and strength behaviours of the fully, partially

fissured or unfissured specimens, were studied numerically, as will be explained in the next chapter.

6.7.2 Discussion on the Results

As indicated in Table (6.6), the deviator stress increased as the P'_c increased or and effective confining pressure increased.

By increasing P'_c, the ratio of deviator stress to effective confining pressure increased. But this ratio for any particular P'_c increased as the effective confining pressure decreased. The stress ratio or and the ratio of the effective confining pressure to the effective axial pressure increased when P'_c decreased. For any particular P'_c, the stress ratio decreased as the effective confining pressure decreased.

The relationships within the OCR, P'_c, $(\sigma'_3 - \sigma'_1)$, $\frac{\sigma'_1 - \sigma'_3}{\sigma'_3}$, $\frac{\sigma'_3}{\sigma'_1}$ were evaluated statistically from the triaxial test results and reported in Equations (6.16), (6.19). In these equations the effects of OCR and P'_c are included.

$$\frac{1}{OCR} = b_0 + \frac{b_1}{\sigma'_1 - \sigma'_3} \tag{6.15}$$

$$b_0 = 68.5354 + 0.7093\ P'_C \tag{6.17}$$

$$b_1 = 23.7831 - 0.2078\ P'_C \tag{6.18}$$

$$OCR = \frac{P'_c}{\sigma'_3} \tag{6.16}$$

$$\frac{1}{OCR} = b_0 + b_1\left(\frac{\sigma'_1 - \sigma'_3}{\sigma'_3}\right) \tag{6.19}$$

$$b_0 = 0.6030 + \frac{363.924}{P'_c} \tag{6.20}$$

$$b_1 = -0.2806 - \frac{152.86}{P'_c} \tag{6.21}$$

$$\frac{1}{OCR} = b_0 + b_1\left(\frac{\sigma'_3}{\sigma'_1}\right) \tag{6.22}$$

$$b_0 = 0.5601 - \frac{73.260}{P'_c} \tag{6.23}$$

$$b_1 = 27.2983 \frac{30.2280}{P'_c} \tag{6.24}$$

Table (6.7) shows clearly the effect of angle of the inclination of fissure for the KB specimens consolidated initially in the triaxial sample maker with P'_c = 440 kpa. It can be said that by increasing the angle of inclination of fissure, the ratio of deviator stress to effective confining pressure ($\frac{\sigma'_1 - \sigma'_3}{\sigma'_3}$) was decreased and on the contrary, the stress ratio ($\frac{\sigma'_3}{\sigma'_1}$) was increased.

In Equation (6.25) the relationship between the effective axial stress and i (deg.) is evaluated experimentally. This equation would be minimum with an inclination angle of $i = 42.78°$.

$$\sigma'_1 = 473.298 - 1.9763\, i + 0.0231\, i^2 \tag{6.25}$$

Figure (6.20) shows the changes of the effective axial stress (σ'_1) with the inclination angle of the fissures for the KB specimens consolidated initially in the sample maker with P'_c = 440 kpa and a confining pressure of 1000 kpa in the triaxial cell. Around 45°, the effective axial stress (σ'_1) shows a drop in the graph. But it is hard to confirm this angle produces the minimum effective axial stress.

Taking into account the problems related to preparation and testing of the triaxial specimens for other angles of inclination, the triaxial specimens were modelled numerically to study the effect of angles of inclination of fissures as well as the effect of confining pressure on effective deviator stress or the effective shear strength of the triaxial KB specimens.

Table (6.8) shows the effect of confining pressure and inclination of the fissures on the ratio of deviator stress to effective confining pressure ($\frac{\sigma'_1 - \sigma'_3}{\sigma'_3}$) and stress ratio

($\frac{\sigma'_3}{\sigma'_1}$). By increasing the confining pressure, the ratio of $\frac{\sigma'_1 - \sigma'_3}{\sigma'_3}$ was increased, on the contrary the ratio of $\frac{\sigma'_3}{\sigma'_1}$ was decreased. The increase of angle of inclination decreased the ratio of $\frac{\sigma'_1 - \sigma'_3}{\sigma'_3}$ and increased the ratio of. $\frac{\sigma'_3}{\sigma'_1}$ The effect of inclination of fissure was similar to the effect of the decrease of the p'_c.

The relationships within OCR, P'_c, $(\sigma'_3 - \sigma'_1)$, $\frac{\sigma'_1 - \sigma'_3}{\sigma'_3}$, $\frac{\sigma'_3}{\sigma'_1}$ and i (inclination angle) were evaluated statistically from the experimental test results and reported in Equations (6.26), (6.29) and (6.32). In these equations the effect of P'_c, OCR and inclination angle (i)are included.

$$\frac{1}{OCR} = b_0 + \frac{b_1}{\sigma'_1 - \sigma'_3} \tag{6.26}$$

$$b_0 = 539.876 + 2.4835\, i - 0.694\, i^2 \tag{6.27}$$

$$b_1 = -114.11 - 1.4510\, i + 0.0183\, i^2 \tag{6.28}$$

$$\frac{1}{OCR} = e^{(b_0 + b_1 \frac{\sigma'_3}{\sigma'_1 - \sigma'_3})} \tag{6.29}$$

$$b_0 = -0.5902 + 0.0075\, i - .0002\, i^2 \tag{6.30}$$

$$b_1 = 0.2341 - 0.0031\, i - 1.4 \times 10^{-5}\, i^2 \tag{6.31}$$

$$\frac{1}{OCR} = b_0 \left(e^{b_1 \frac{\sigma'_3}{\sigma'_1}}\right) \tag{6.32}$$

$$b_0 = 0.04419 + 0.0141\, i - 0.0003\, i^2 \tag{6.33}$$

$$b_1 = 0.3347 - 0.0613\, i + 0.0015\, i^2 \tag{6.34}$$

The effect of discontinuous fissure with an inclination of 30 degree was negligible. However, other inclinations need more tests and investigation as will be reported in the next chapter.

Table (6.9) displays the Mohr Coulomb parameters obtained for three P'_c of 660 kpa, 440 kpa, and 330 kpa triaxial specimens. In comparison with the direct shear box results, there were differences. The reason is related to the effect of secondary isotropic consolidation of the specimens in the triaxial consolidation of the specimens in the triaxial cell after initial preparation in the sample maker. However, the trend was the same as that observed relating to the direct shear box specimens. By increasing p'_c, the effective shear strength increased which in the triaxial tests, mainly the ϕ' was increased.

Table (6.10) shows the Mohr Coulomb parameters obtained for three angles of inclination. As can be seen from the table, the friction mainly decreased as the angle of inclination increased. As explained previously, this behaviour is similar to the behaviour of specimens with the decreasing of the P'_c.

6.8 CONCLUSION

The partially or fully fissured triaxial specimens were prepared artificially for three angles of inclination. The design and construction of a triaxial sample maker, as well the methods and techniques applied in this research, were positive steps for the simulation of fully or partially fissured clay specimens. However, the study of fissure parameters and their interaction with P'_c and confining pressure need more experimental investigation and time which is beyond the scope of this thesis with the available limited time.

The results showed that by increasing P'_c in the triaxial clay KB specimens, the ϕ' mainly increased.

The ratio of deviator stress to effective confining pressure . $\frac{\sigma'_1 - \sigma'_3}{\sigma'_3}$ was increased by increasing the P'_c. But the ratio of effective confining pressure to effective axial stress was decreased by increasing the P'_c.

In the fully fissured KB specimens, the effective axial stress for the specimens consolidated with the same pressure showed some changes with variation of the

angle of fissure. The angle of inclination of 45° was coincident with the minimum effective axial stress within the available test results for the three inclination angles of 30°, 45° and 60°.

Moreover, by applying high confining pressure (σ_3), the fully fissured KB specimens with inclinations of 30° and 60° showed less sliding along the fissure surfaces than fully fissured specimens with an inclination of 45°.

The partially fissured KB specimens with an inclination angle of 30° (Table 6.11) did not show any obvious effect of discontinuous fissure on the deformation behaviour and effective Mohr Coulomb parameters. The study of the effect of other inclination angles of discontinuous fissures needs more experimental investigation.

In the fully fissured KB specimens, the ratio of $\frac{\sigma'_1 - \sigma'_3}{\sigma'_3}$ was decreased by increasing the inclination angle of fissure (i). But the ratio of $\frac{\sigma'_3}{\sigma'_1}$ was increased by increasing the inclination angle of fissure (i). This behaviour was similar to the behaviour observed for the decrease of P'_c on the unfissured KB triaxial specimens. Taking into account the huge amount of time required for preparing and testing the fully or partially fissured KB specimens for the study of the other angles of inclination, as well as for the study of the effect of confining pressure on the fissured clay triaxial specimens, the numerical modelling of triaxial specimens was applied. In the next chapter, the effect of fissure inclination or orientation and also the effect of confining pressure on the effective shear strength of the triaxial fully or partially fissured clay specimens will be described.

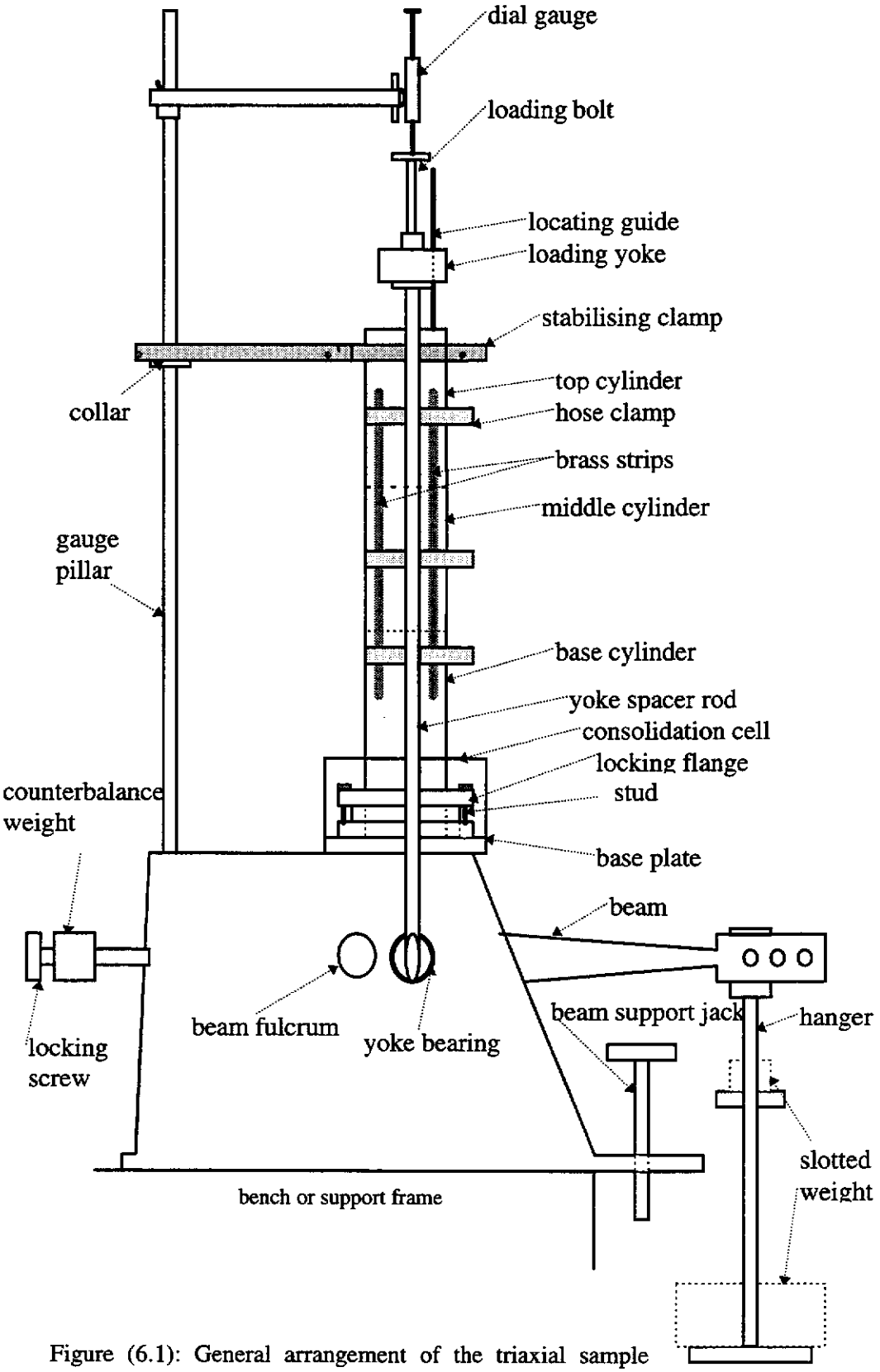

Figure (6.1): General arrangement of the triaxial sample maker.

Figure (6.2): Illustration of the triaxial sample maker.

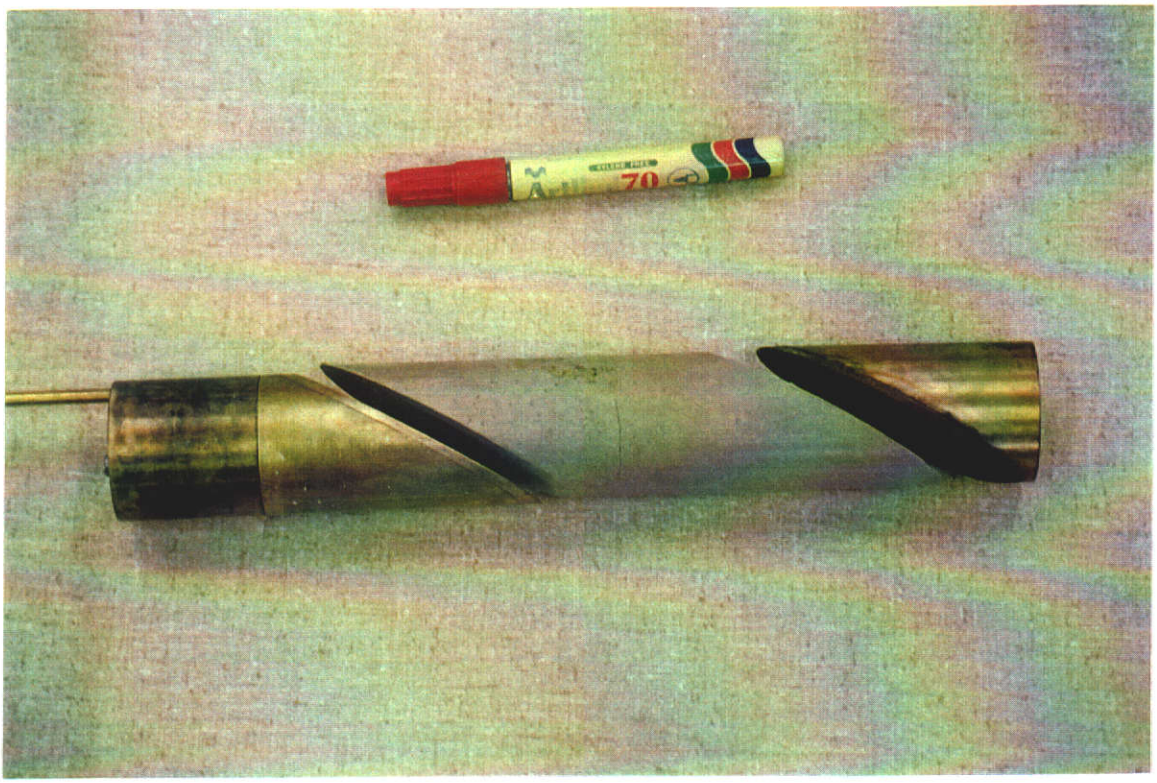

Figure (6.3): Illustration of an orientated fissured triaxial specimen for the inclination angle of 60° to the horizontal direction.

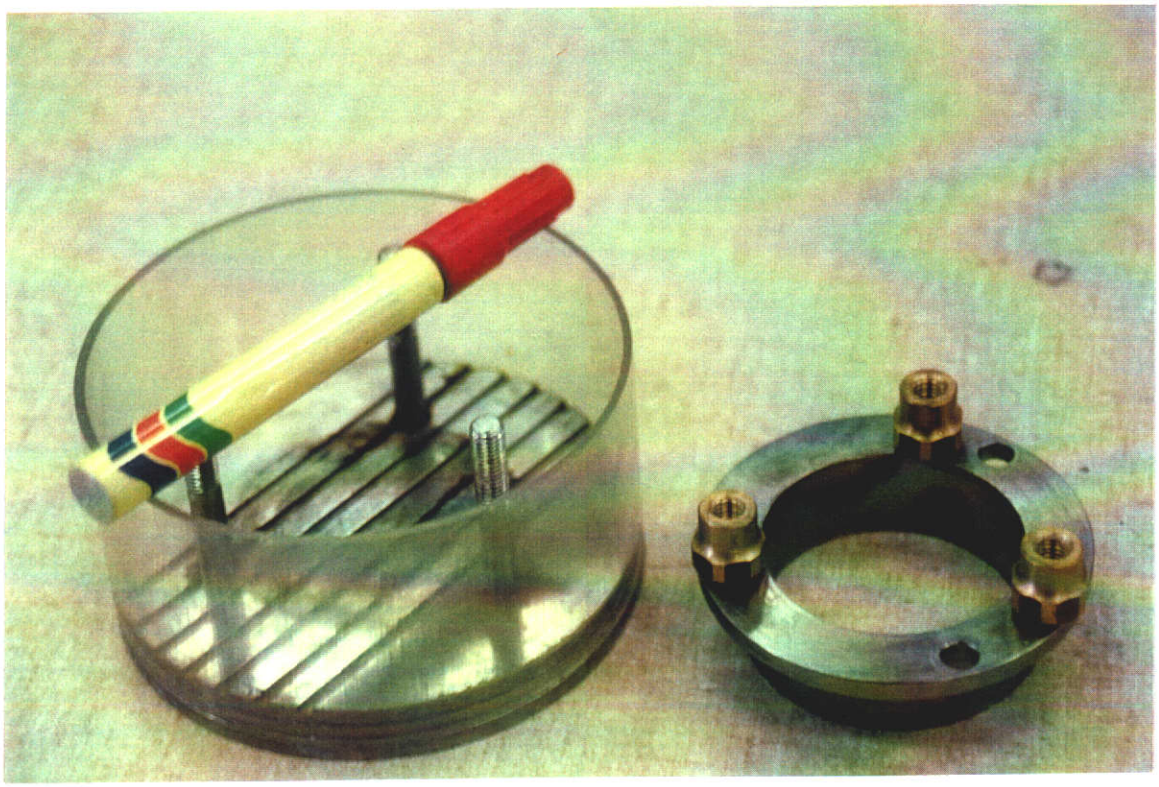

Figure (6.4): Illustration of the reservoir of the triaxial sample maker.

Figure (6.5): Illustration of the different parts designed and constructed for the triaxial sample maker.

Figure (6.6): The computer and triaxial testing system used for the research.

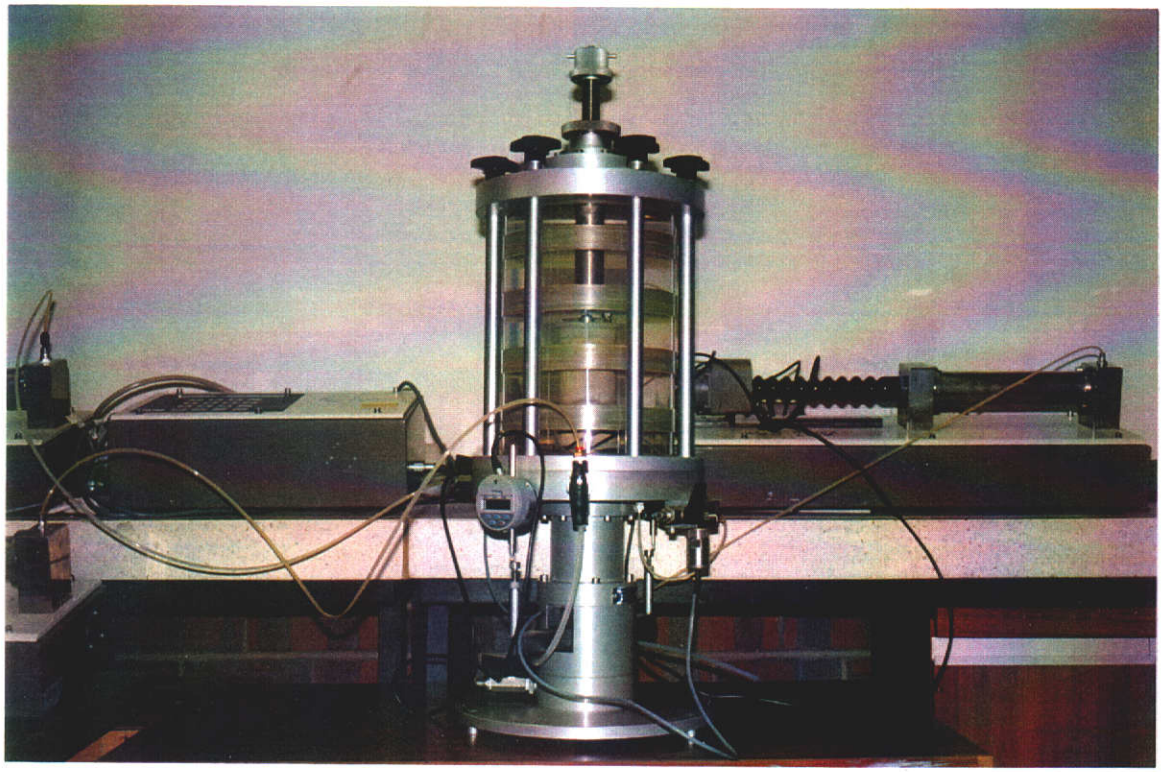

Figure (6.7): Illustration of the triaxial cell with the digital indicator and the pressure transducer.

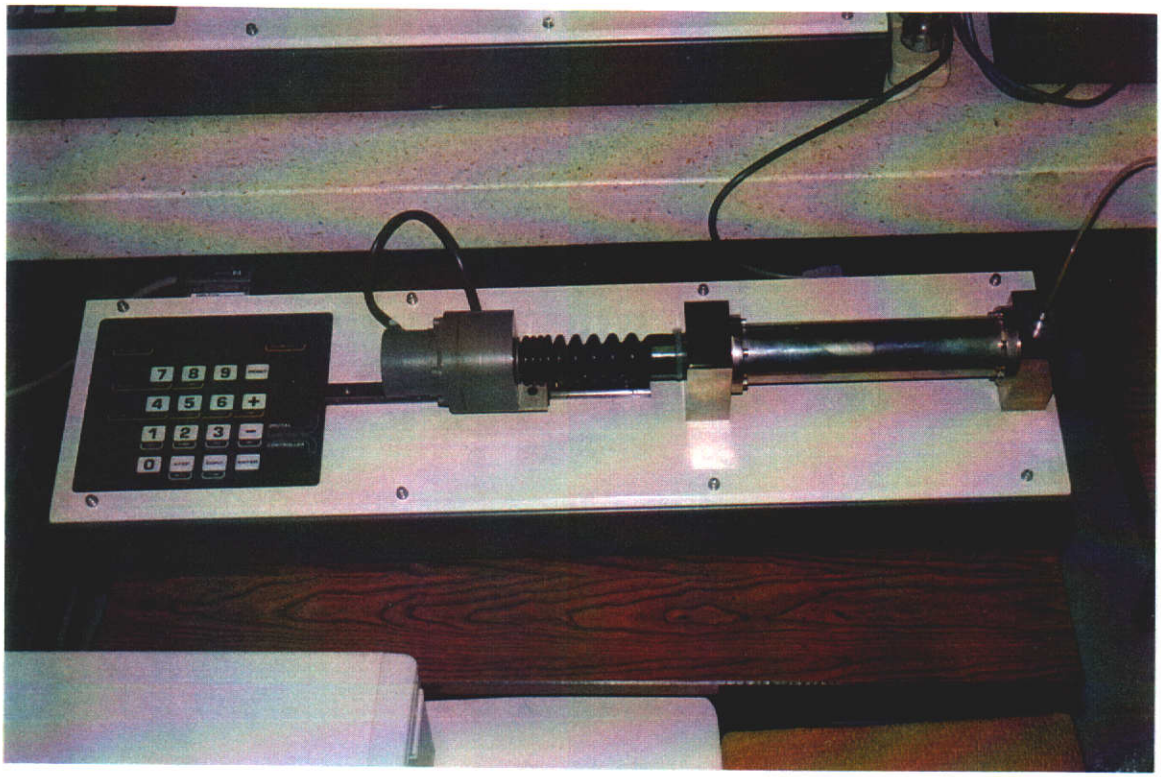

Figure (6.8): Illustration of a digital controller.

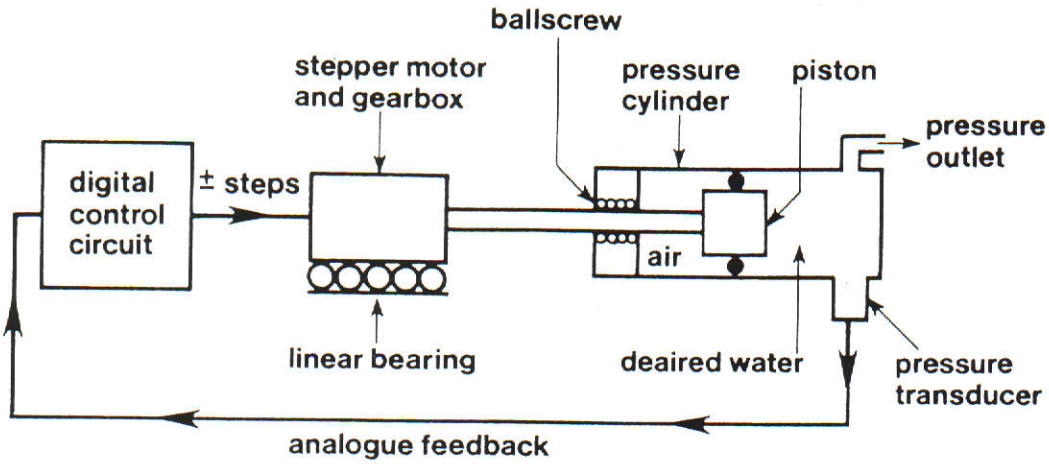

Figure (6.9): Schematical illustration of a digital controller (Menzies, 1988).

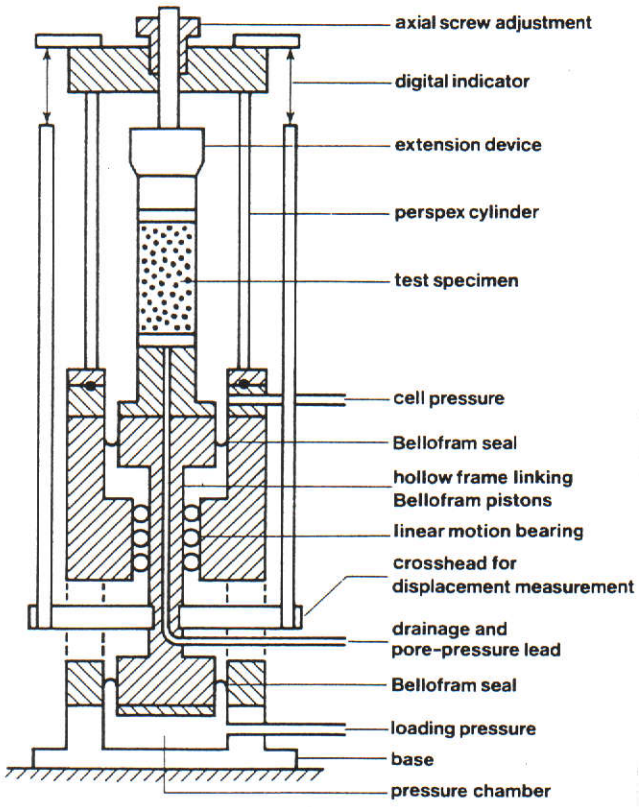

Figure (6.10): Schematical Illustration of the layout of the triaxial cell (Bishop et al., 1975).

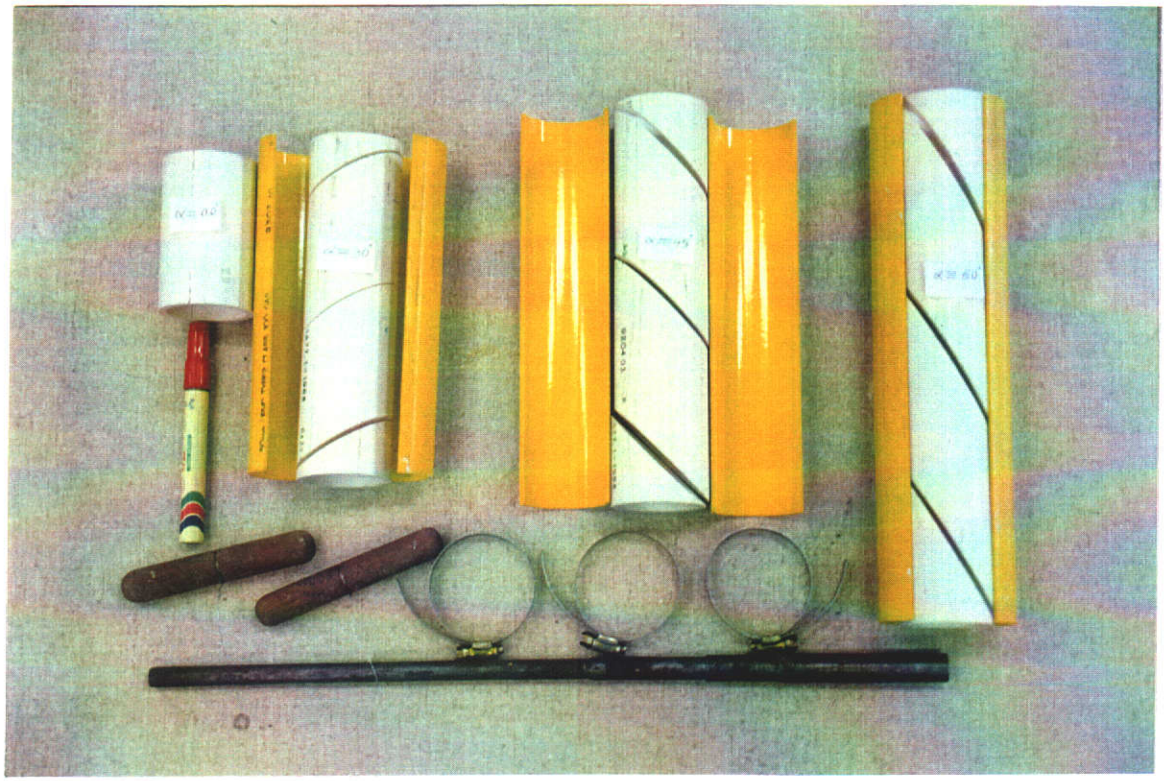

Figure (6.11): Illustration of the detachable mould designed to shape the orientated fissured triaxial specimens for three different angles of 30°, 45° and 60° to the horizontal direction.

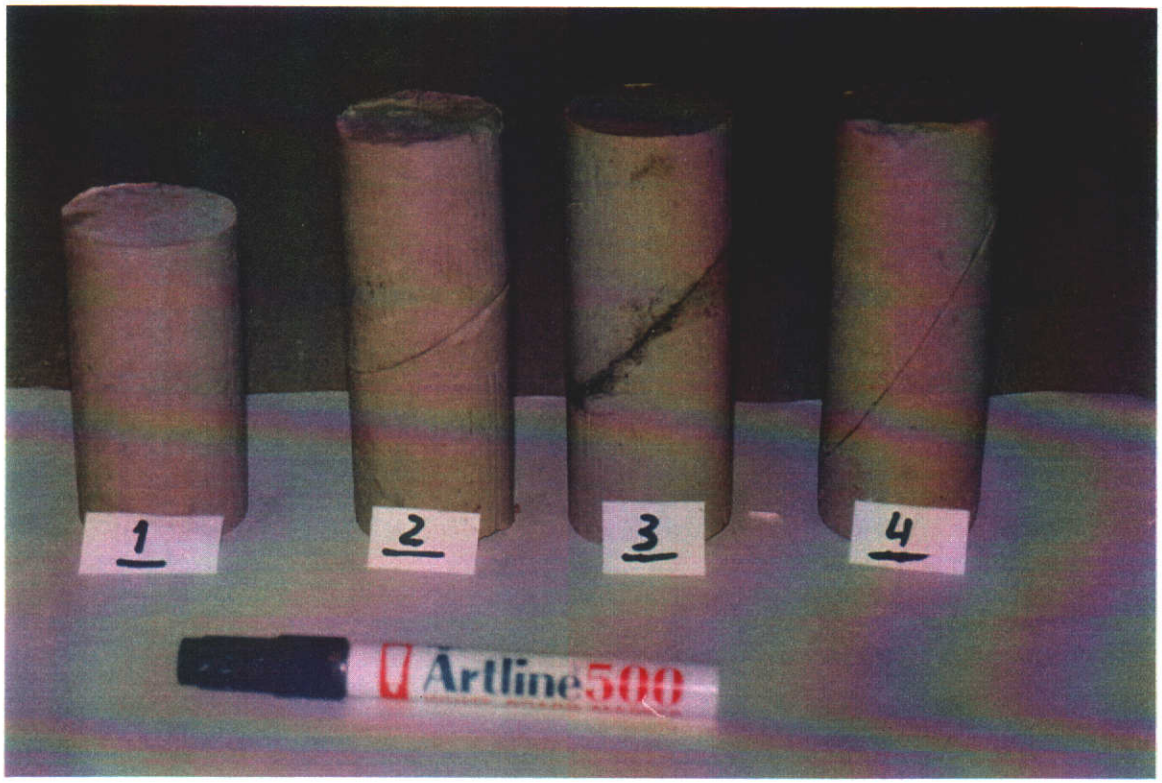

Figure (6.12): Illustration of the unfissured and fully fissured KB triaxial specimens.

Figure (6.13): Illustration of a partially orientated fissured triaxial specimen with an inclination angle of 30° to the horizontal direction.

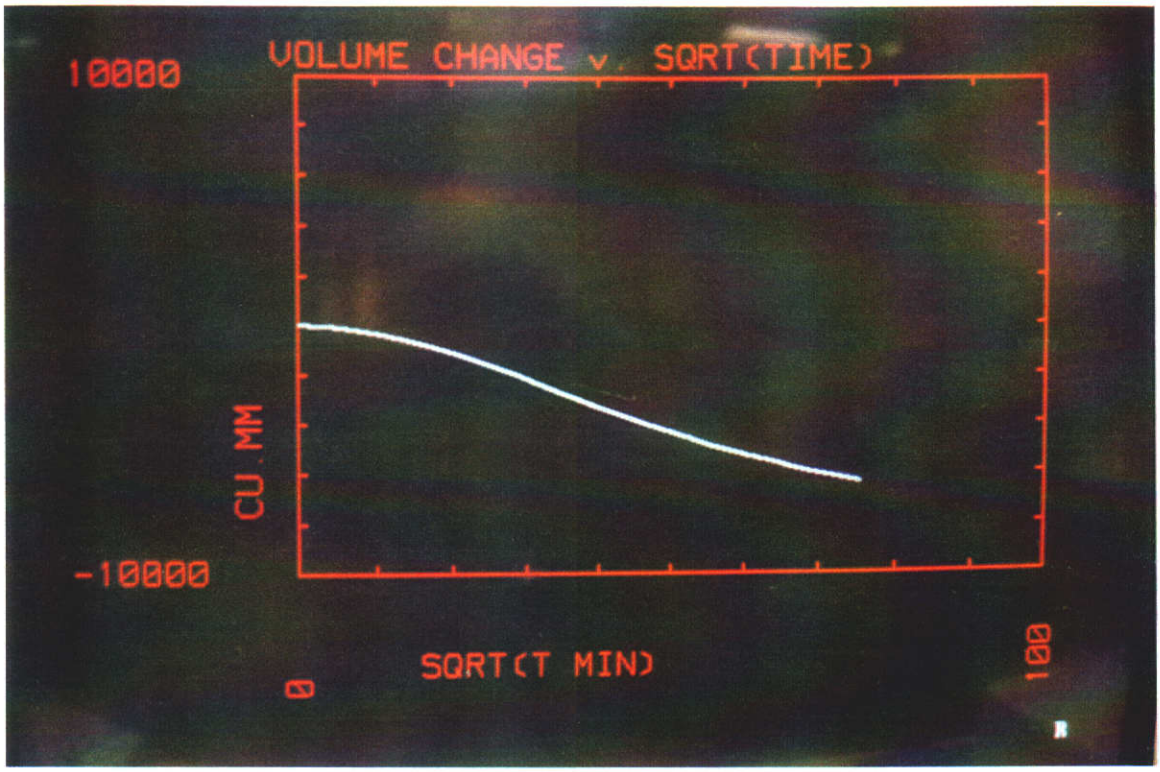

Figure (6.14): Illustration of volume change against the square root of time prepared by the GDSTTS.

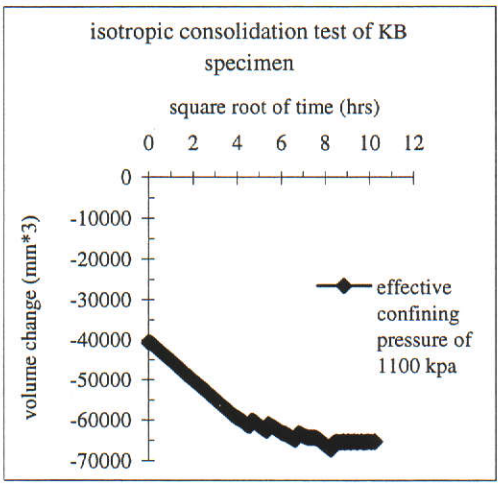

Figure (6.15): The changes of volume change against the square root of time for a KB specimen with an effective confining pressure of 1100 kpa.

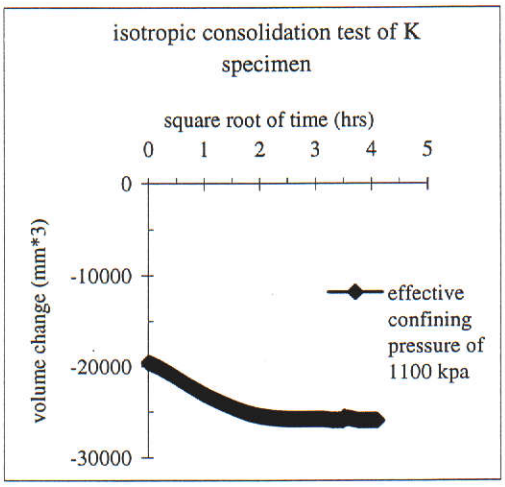

Figure (6.16): The changes of volume change against the square root of time for a K specimen with an effective confining pressure of 1100 kpa.

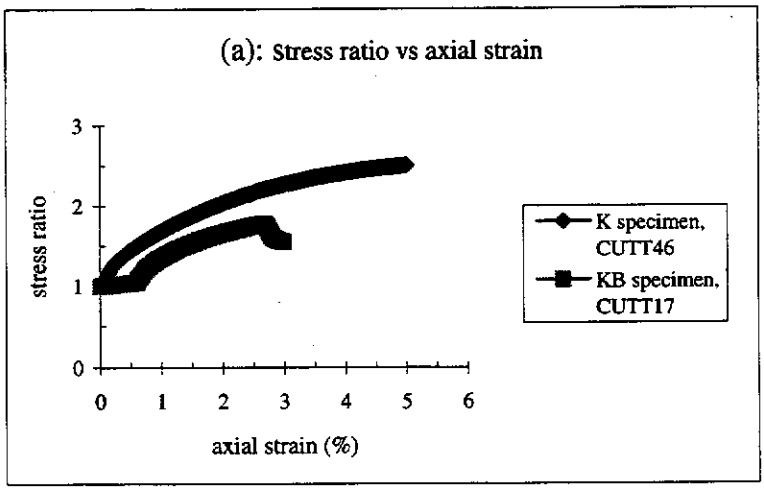

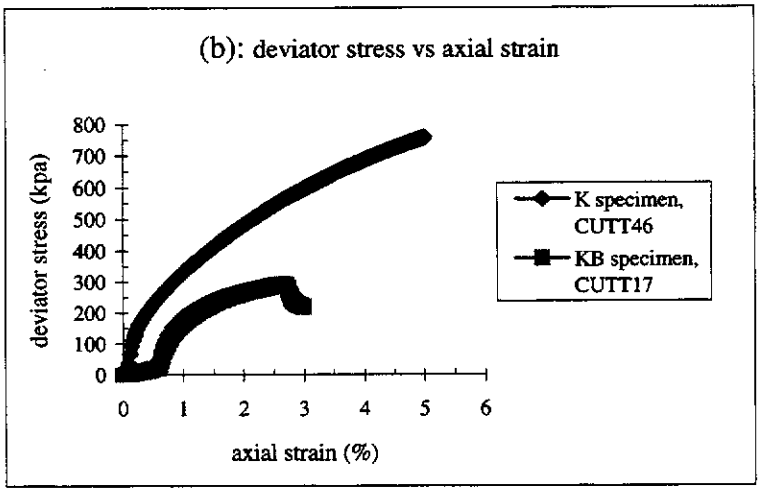

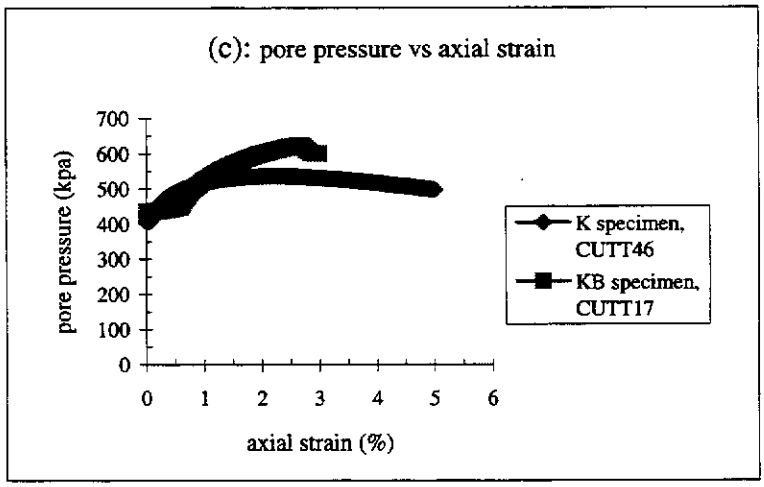

Figure (6.17): The typical graphs of the stress ratio, deviator stress and pore pressure against axial strain obtained from a CU test on K and KB specimens, (a); stress ratio vs axial strain, (b); deviator stress vs axial strain, (c); pore pressure vs axial strain.

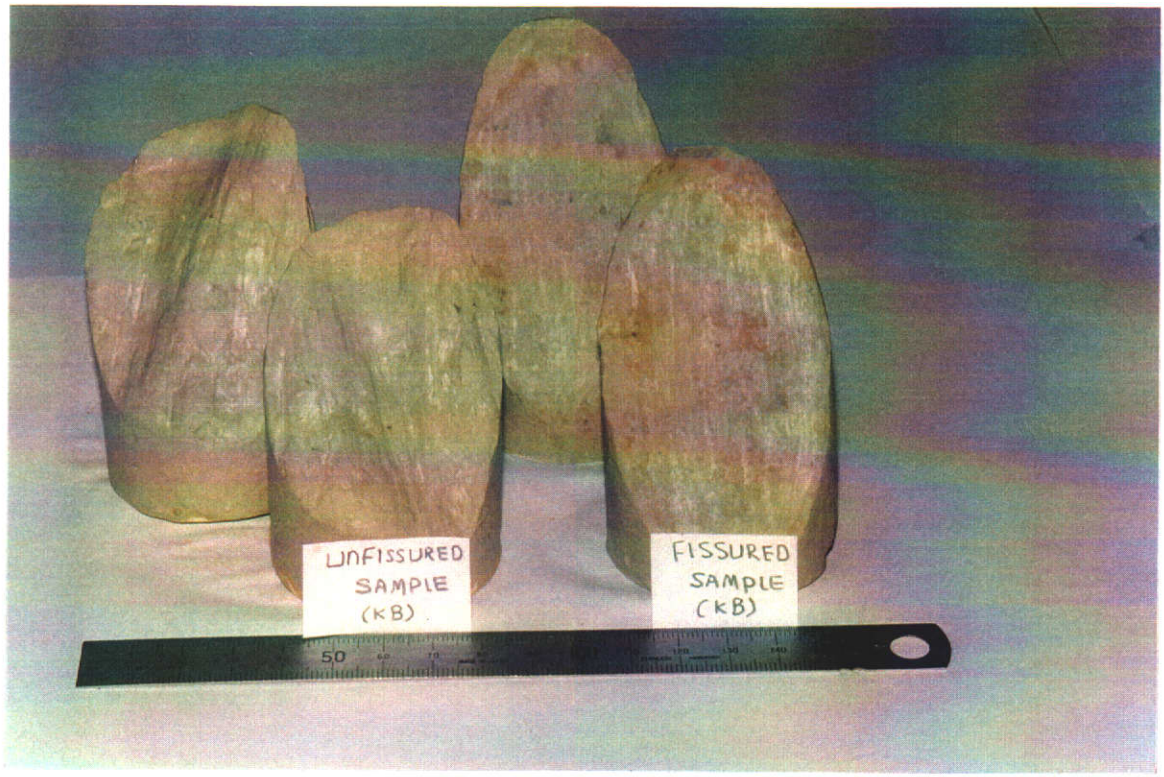

Figure (6.18): Illustration of the surfaces of two KB specimens tested in the triaxial apparatus.:

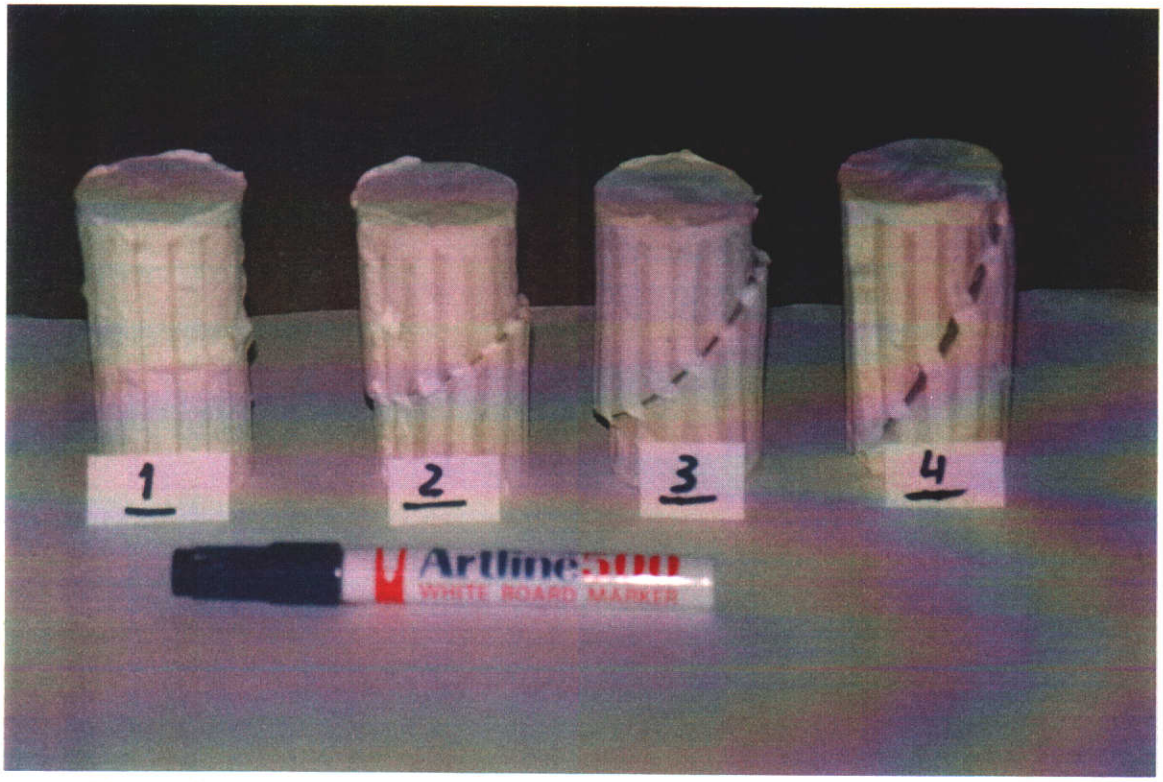

Figure (6.19): Illustration of the KB specimens tested in the triaxial apparatus.

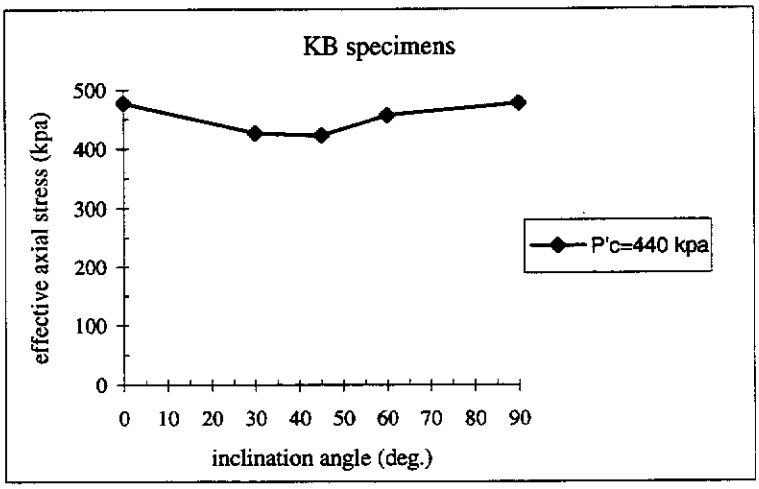

Figure (6.20): The changes of the effective axial stress (σ') against the inclination angle of the orientated fissures.

Triaxial tests on clay specimens R = 0.1 mm/hr					
Specimen type	P'_c (kpa)	Specimen No.	CP (kpa)	BP (kpa)	Type of test
Unfissured KB specimen	660	CUTT35	1500	400	CU
		CUTT28	800	400	CU
		CUTT15 CUTT20	1000	400	CU
	440	CUTT34	1500	600	CU
		CUTT27	800	600	CU
		CUTT14	1000	600	CU
	330	CUTT32	1500	800	CU
		CUTT29	800	800	CU
		CUTT16	1000	800	CU
K Unfissured specimen	660	CUTT44	1500	400	CU
		CUTT39	800	400	CU
		CUTT46	1000	400	CU

Table (6.1): Triaxial tests for the study of the effect of P'_c
CP: Cell pressure (kpa)
BP: Back pressure (kpa)
CU: Consolidated undrained test

Specimen type	Inclination i	Specimen No.	CP (kpa)	BP (kpa)	Type of test
KB $P'_c = 440$	30	CUTT13	1000	600	CU
	45	CUTT12	1000	600	CU
	60	CUTT11	1000	600	CU

Table (6.2): Triaxial tests for the study of the effect of orientation of fissure on the KB specimens consolidated with $P'_c = 440$ kpa.

Triaxial tests on clay specimens R = 0.1 mm/hr					
Specimen type	P'_c (kpa)	Specimen No.	CP (kpa)	BP (kpa)	Type of test
KB fully fissured	30°	CUTT36	1500	400	CU
		CUTT25	800	400	CU
		CUTT21 CUTT17	1000	400	CU
	45°	CUTT37	1500	400	CU
		CUTT24	800	400	CU
		CUTT23 CUTT18	1000	400	CU
	60°	CUTT38	1500	400	CU
		CUTT26	800	400	CU
		CUTT19 CUTT22	1000	400	CU
KB partially fissured	30°	CUTT33	1500	400	CU
		CUTT31	800	400	CU
		CUTT30	1000	400	CU

Table (6.3): Triaxial tests for the study of the effect of orientation of fissure on the KB specimens consolidated with $P'_c = 660$ kpa.

CP (kpa)	BP (kpa)	C_v (m^2/year)	
		KB	K
1500	400	0.012	0.082
1000	400	0.014	0.145
800	400	0.016	0.327

Table (6.4): Coefficients of the consolidation of the triaxial specimens consolidated by P'_c=660 kpa in the triaxial sample maker and with filter paper side drain.

DESC: TRIAXIAL CONSOLIDATED UNDRAINED TEST								
FILE: CUTT20								
NUM_RDGS	240							
INITIAL VALUES								
A0	L0	A1	FRICTION					
1865.115	95.6027	2940	0					
RDG	TIME	P7	V7	P8	V8	P9	V9	P6
1	0	1000	0	419	0	1000.7	0	419
2	435.7	1000.4	-22	419	0	1001.5	36	419
3	871.3	1000.1	-71	419	0	1001.3	71	419
4	1306.9	1000.2	-112	419	0	1001.5	107	419
5	1742.3	1000.4	-151	419	0	1001.8	142	419
6	2178.1	1000.3	-200	419	0	1001.8	178	419
7	2615	1000.1	-249	419	0	1002	214	419
8	3051	1000.1	-293	419	0	1002	249	419
9	3486.9	1000.2	-334	419	0	1002.2	285	419
10	3922.7	999.7	-385	419	0	1001.7	320	419
.....	.....	.....	.....	.....	.....	.....	.....	.....
240	104188.5	1000.4	-8696	618	0	1200.8	8509	618
241	104625.3	1000.5	-8740	618	0	1200.6	8544	618
242	105061.5	1000.3	-8782	619	0	1201	8580	619
243	105066.6	1000.4	-8782	619	0	1201.2	8581	619
244	105066.6	1000.4	-8782	619	0	1201.2	8581	619

Table (6.5): Typical data were logged for CU test by the triaxial and computer systems.

Specimen No.	CP (kpa)	BP (kpa)	σ'_1	σ'_3	$\sigma'_1-\sigma'_3$	$\frac{\sigma'_1-\sigma'_3}{\sigma'_3}$	$\frac{\sigma'_3}{\sigma'_1}$
CUTT35	1500	400	1085.5	637.4	448.12	0.70304	0.58719
CUTT20	1000	400	706.29	381.4	324.89	0.85183	0.54000
CUTT15	1000	400	690.65	379.6	311.05	0.819415	0.549627
CUTT28	800	400	502.945	246.9	256.045	1.0370	0.4909
CUTT34	1500	600	957.4	613.8	343.6	0.55979	0.64111
CUTT14	1000	600	477.3	252.3	225	0.8917	0.528598
CUTT27	800	600	360.84	158.4	202.44	1.27796	0.438975
CUTT32	1500	700	820.2	540.7	279.5	0.51692	0.659229
CUTT16	1000	700	410	184.4	334.6	1.21143	0.452195
CUTT29	800	700	233	90	143.79	1.59766	0.386266
CUTT44	1500	400	1655.05	704.7	950.35	1.349	0.426
CUTT46	1000	400	1262.55	504.8	757.7522	1.501	0.400
CUTT39	800	400	885.195	340.8	544.395	1.597	0.385

Table (6.6): Triaxial test results for the study of the effect of P'_c on the unfissured specimens.

Specimen No	i (deg.)	CP (kpa)	BP (kpa)	σ'_1	σ'_3	$\sigma'_1-\sigma'_3$	$\frac{\sigma'_1-\sigma'_3}{\sigma'_3}$	$\frac{\sigma'_3}{\sigma'_1}$
CUTT14	0.0	1000	600	477.3	252.3	225	0.8917	0.528598
CUTT13	30	1000	600	426.209	259.5	166.709	0.64238	0.60885
CUTT12	45	1000	600	421.98	265.98	156.0	0.5865	0.63024
CUTT11	60	1000	600	456.698	310	146.5981	0.4728	0.678785

Table (6.7): Triaxial test results of the KB specimens consolidated with P'_c = 440 kpa for the study of the effect of orientation of fissures.

Specimen No	i (deg.)	CP (kpa)	BP (kpa)	σ'_1	σ'_3	$\sigma'_1-\sigma'_3$	$\frac{\sigma'_1-\sigma'_3}{\sigma'_3}$	$\frac{\sigma'_3}{\sigma'_1}$
CUTT36	30	1500	400	1052.75	623.8	428.95	0.68764	0.592543
CUTT21		1000	400	664.22	382.5	281.72	0.73652	0.57586
CUTT17		1000	400	668.33	377.8	290.53	0.7690	0.56528
CUTT25		800	400	496.73	271.2	225.53	0.831600	0.54597
CUTT37	45	1500	400	1014.25	631.7	382.55	0.60558	0.622824
CUTT23		1000	400	644.697	399	245.697	0.615782	0.618895
CUTT18		1000	400	656.56	401.9	254.66	0.63364	0.612129
CUTT24		800	400	487.17	281.9	205.29	0.72818	0.5786
CUTT38	60	1500	400	1036.29	671	365.29	0.543748	0.647502
CUTT19		1000	400	667.51	467.3	200.21	0.42843	0.70006
CUTT22		1000	400	647.68	447.6	200.08	0.4470	0.691082
CUTT26		800	400	466.96	296.8	170.16	0.57331	0.6356
CUTT33	30 PFS	1500	400	1084.479	618.7	465.778	0.75283	0.57050
CUTT30		1000	400	658.2058	343.4	314.8058	0.916732	0.521721
CUTT31		800	400	479.6719	224.7	254.972	1.13472	0.468445

Table (6.8): Triaxial test results for the study of the effect of orientation of fissures on the KB specimens consolidated with P'_c = 660 kpa.

P'_c (kpa)	OCR		NCL	
	c' (kpa)	ϕ' (deg.)	c' (kpa)	ϕ' (deg.)
660	65	9.9	53	11.5
440	65	7.8	74	6.2
330	64	6.8	—	—

Table (6.9)): The effective Mohr Coulomb parameters for the study of the effect of P'_c.

i (deg.)	OCR		NCL	
	c′ (kpa)	ϕ′ (deg.)	c′ (kpa)	ϕ′ (deg.)
30	36	11.7	25	13
45	47	8.5	21	11.9
60	51	5.2	56	11.4

Table (6.10): The effective Mohr Coulomb parameters for the study of the effect of orientation of fissure on the KB specimens consolidated with P'_c = 660 kpa.

P'_c=660 kpa	OCL		NCL	
i (deg.)	c′ (kpa)	ϕ′ (deg.)	c′ (kpa)	ϕ′ (deg.)
30	51	12.4	5.3	12.2

Table (6.11): The effective Mohr Coulomb parameters for the partially KB specimens with an angle of 30° and consolidated with P'_c = 660 kpa.

CHAPTER 7

NUMERICAL MODELLING OF TRIAXIAL SPECIMENS

7.1 INTRODUCTION

The effect of the orientation of fissures in the fully or partially fissured specimens subjected to direct shear test was investigated experimentally and numerically. The results showed no significant differences as discussed in Chapters 4 and 5. In order to estimate these effects, the possibility of the opening or sliding of the orientated fissures should be provided both in experimental and numerical simulations.

The effect of the orientation of fissures was investigated experimentally on specimens subjected to triaxial tests for three different angles of inclination 30°, 45°, and 60° to the direction of the minimum principle stress (σ_3) and also on the partially fissured specimens with an inclination angle of 30° to the direction of σ_3.

Having taken into account the huge amount of time required for the preparation and testing of the fully and partially fissured triaxial clay specimens and also the technical problems for applying high confining pressure, the effects of confining pressures and orientation of fissures in the fully or partially fissured specimens were

investigated numerically using a three dimensional finite element program, ANSYS version 5.2 (1996).

Although this software can be used for programming, it was just used to simulate the triaxial fully, partially fissured and unfissured specimens and nor for advanced study of the crack or fissure propagation in the partially fissured overconsolidated clayey specimens. This needs more experimental and numerical investigation which is beyond of the scope of this research.

After defining the coefficients required for the modelling of the unfissured specimens from the experimental results on the unfissured triaxial specimens, the results obtained from direct shear tests on the fully fissured specimens were used to define the coefficients required for the contact elements used for the numerical simulation of the fissures in the fully or partially fissured triaxial specimens. Then, the numerical models prepared for the fully, fissured and unfissured specimens were verified by the available experimental triaxial tests for the fully fissured and unfissured specimens.

To save time in running the program for different models, batch files for different models were prepared for different inclination angles, confining pressures for both the fully and partially fissured specimens.

Numerical models, also for the study of the effect of two different arrangements of fissures in the double fissured specimens, were prepared. Finally, the results from the different parts are discussed and formulated statistically using SPSS software.

7.2 INTRODUCING THE ANSYS

The ANSYS version 5.2, a three dimensional finite element software, was used for the simulation of the fully, partially fissured and unfissured triaxial specimens.

This program provides the user with interactive access to program functions, commands, documentation, and reference material. Users can input data through a mouse, a keyboard or a combination of the two, three or four general methods to instruct the ANSYS program as follows:

- Menus
- Dialogue boxes
- Tool bars
- Direct input of commands

Menus are groupings of related commands and functions for operating the ANSYS program located in individual windows.

Dialogue Boxes are windows that present the user with choices for completing operations or specifying settings. These boxes prompt the user to input data or make decisions for a particular functions.

Tollbars permit the user to place commonly used commands or user-written routines in a top-level palette for instant one-click access.

An input window provides an area for typing ANSYS commands and displays program prompt messages.

A command history is provided for previously typed commands. This allows for cutting and pasting commands from the log file, command history.

The log files are accessible through the program's output window. It permits the user to review a list of commands in the event of an error or to save a list of commands as a file for batch processing.

The ANSYS functions are organised into groups called processors. The ANSYS program has one preprocessor, one solution processor, two post processors and several auxiliary processors such as the design optimiser.

$\therefore$ The ANSYS preprocessor allows the user to create a finite element model and to specify options needed for subsequent solutions. The user can select coordinate systems and element types, define real constants and material properties, create solid models and mesh them, manipulate nodes and elements, and define coupling and constraint equations.

Cartesian, cylindrical, spherical, elliptical, and toroidal coordinate system types are available in the ANSYS and can be located anywhere in space and in any orientation. The global Cartesian coordinate system was used for analyses of the triaxial specimen models.

In the ANSYS program, there are two different methods for generating a model, solid modelling and direct generation. The triaxial specimen models were generated by solid modeling.

∴ The solution processor is used to apply loads and boundary conditions and then to determine the response of the model to them. In this part of an ANSYS analysis, the user can specify the analysis type, analysis options, load data, and load step options, and initiate the finite element solution. The analysis type for triaxial specimen models was a structural static nonlinear type. The analysis option for the triaxial specimen models the Newton-Raphson option.

In the ANSYS, the load data include degree of freedom-constrains, point load, surface loads, body loads, and inertia loads. Each configuration of a load is called a load step, and any analysis may consist of one or more load steps. Load step options are used to set output controls, convergence controls, and general load controls for each load step. For example, the user can define the number of substeps to be used for each load step or whether the values should be ramped over the load step.

Additional features of the solution phase allow the user to change material properties and some real constants, reactivate and deactivate elements.

The structural static analysis in the ANSYS program can also include nonlinearities such as plasticity, creep, swelling, large deflection, large strain and contact surface.

Nonlinear static analyses are performed by subdividing the load into a series of incremental load steps and, at each step, performing a succession of linear approximations to obtain equilibrium.

∴ With the ANSYS postprocessors, the user retrieves and examines the solution results to evaluate how the model performed, and to perform additional calculations of interest.

In the ANSYS, the nonlinearities were classified into three categories of material, geometric and element nonlinearities.

• A material nonlinearity exists when stress is not proportional to strain. Plasticity, multilinear elasticity, and hyperelasticity are characterised by a nonlinear stress-strain relationship. To fully account for plastic material behaviour in an analysis, three important concepts of the yield criterion, the flow rule, and the hardening law must be considered.

The ANSYS program can use one of three yield criteria to predict when yielding will begin: Von Mises, a modified Von Mises (Hill), and Drucker-Prager. For the clay material of the triaxial specimens, the Drucker-Prager with associative flow rule was used.

• Geometric nonlinearities occur when the displacements of a structure significantly change its stiffness. The ANSYS program can account for these types of geometric nonlinear effects: large strain, large deflection, stress stiffening and spin softening.

Large strain geometric nonlinearities account for the large localised deformations that may occur as a structure deflects. For the fully or partially fissured triaxial specimens, this aspect of nonlinearity has been considered because of the possibility of sliding along the fissure surfaces.

• Nonlinear elements are those elements which have their own nonlinear behaviour, independent of other elements. This behaviour is typically characterised by an abrupt change in stiffness due to a change in status such as a contact surface element changing from open to closed.

For the simulation of the fully or partially fissured specimens contact surface elements were used. Therefore, for the fully or partially fissured specimens, this aspect of nonlinearity must have been taken into consideration.

7.3 COMPUTER SIMULATION OF TRIAXIAL SPECIMENS

As discussed in Chapter 6, the time required for preparing and testing each specimen was about one month because of the very low permeability of clay materials.

Considering the number of tests required to study the effects of orientation of fissures in the fully and partially fissured specimens, as well as the effect of confining pressure on the strength and deformation behaviours of the fissured specimens, the study was founded on a numerical modelling as well.

Taking into account the financial and technical issues, the ANSYS version 5.2 was used to simulate three dimensional triaxial clay specimens. The availability of the Drucker-Prager model which is suitable for rock and soil materials and also different types of contact elements, especially the contact elements for the simulation of the three dimensional joints, cracks or fissures, as well as the capability of the user programming for yield criterion, element, and material properties, were the main technical reasons for the numerical simulation of the triaxial clay specimens with ANSYS.

Figures (7.1), (7.2) and (7.3) show the three models generated for the cylindrical specimens with a diameter of 50 mm and height of 100 mm for the simulation of the unfissured specimen, the fully fissured specimen with an inclination angle of 30°and the partially fissured specimen with an inclination angle of 30°. Each model consisted of 120 solid cubic elements (Solid 45).

For the fully or partially fissured specimen models, in addition to this element type used for material, contact surface elements (Contact 49) were assigned to the two separated surfaces of fissures in the fully or partially fissured specimens providing the possibility of sliding and opening of the fissure surfaces.

The nodes of the bottom of the cylindrical models were fixed in three dimensions X, Y and Z. Confining pressure was applied isotropically on the surfaces.

Axial displacement was applied on the nodes located at the top of the cylindrical models. Because the analysis type was static, the model response was time independent and the rate of axial strain did not affect the results significantly.

In order to define the material properties and real constants of the models, experimental results from triaxial and direct shear tests were applied. For example, for the triaxial specimens consolidated in the triaxial sample maker by $P'_c = 660$ kpa,

the Mohr Coulomb parameters for overconsolidated specimens were C'_p = 65 kpa and ϕ'_p = 10° and for normally consolidated specimens, C′ = 53 kpa, and ϕ' = 11.5°. From the unfissured triaxial specimen test, E (Young's Modulus) = 44 N/mm^2, ν (Poisson's ratio) = 0.395 and K_N (normal stiffness) = 146.6 N/mm^3. From the direct shear tests on the fully fissured specimen consolidated with P'_c = 660 kpa, K_T (shear stiffness) = 31.94 N/mm^3 and G (shear modulus) = 1.916667 × 10^7 pa were estimated for the coefficients required for the definition and generation of the contact elements.

In order to simulate the fully or partially fissured triaxial specimens, for example, for the specimens consolidated with P'_c = 660 kpa in the triaxial sample maker, the material properties obtained from the triaxial unfissured specimens were applied for the definition of the material properties required for the fully or partially fissured specimen models, and the fissure characteristics obtained from the direct shear tests, were applied for the definition of the coefficients required for the contact elements simulating the fissure surfaces. For different orientations of fissures, these coefficients were constant and only the orientation of fissures was variable. In order to avoid any accidental error and also to save the time required to run the models, the batch file of each model was prepared and run. The batch files for an unfissured and a fully fissured triaxial specimen models are reproduced in Appendices A(7.1) and A(7.2) respectively.

7.4 VERIFYING THE MODELS AND PREDICTIONS

After the definition and calibration of the coefficients required for the modelling of the unfissured and fully fissured specimens, the batch files of some specimens for which the experimental results were available, were prepared and run. The numerical results obtained from these cases were compared with the experimental results.

Table (7.1) displays the results obtained numerically for the same specimens tested experimentally in Chapter 6.

As it can be seen, the numerical results are verified by the same experimental results. For these two types of specimens, numerical models with fine mesh were also provided. For the fine mesh models, the total number of solid elements was increased

from 120 to 768 elements. The results show an increase of 8% of effective axial stress.

Therefore the fine mesh model results were very close to the experimental results and show a much better accordance with the experimental results.

For fine mesh models, the time required for the running the models was increased from 2 hours to 20. Taking into account the number of cases that should have been studied, subsequent models were run with the coarse mesh (120 elements).

The percentage of error because of this might be considered negligible and proportional, if the fully fissured or partially fissured models are run for the same confining pressures and axial deformation with the same material properties, but different inclination angles.

Strain softening behaviour, an intrinsic characteristic of the overconsolidated clay materials, could be simulated numerically in the ANSYS program by using the macro, MP CHAN command, if the relationships between axial deformation or volumetric deformation and c' or ϕ' are defined experimentally and properly.

The procedure that strain softening behaviour might be applied is to change the c' or ϕ' of the material by increasing the volumetric change or axial deformation.

Although the strain softening behaviour was effective on the mobilisation of strength and also on deformation behaviour of the fully and partially fissured specimens, the models were only run with a Mohr Coulomb perfect plastic behaviour to study the effect of orientation of fissures on the effective peak axial stress. The effect of strain softening behaviour was deliberately ignored from the numerical models generated and run subsequently.

The confining pressures applied commonly for all subsequent models were at two levels, 205 and 400 kpa. Additionally three more levels of 1000 kpa, 2000 kpa, and 3000 kpa were applied to some models to study of the effect of high confining pressures.

The inclination angles for low confining pressures in the both fully and partially fissured specimens, were 0.0°, 15°, 30°, 35°, 45°, 50°, 60°, and 90°, clockwise to the

direction of minimum principle stress. Additionally, for the partially fissured specimens, the models for inclination angles of -15°, -35°, and -50° (anti clockwise) to the direction of minimum principle stress were also generated. All these models were run with confining pressures of 205 kpa, and 400 kpa.

The fully and partially fissured specimens with inclination angles of 0.0°, 15°, 35°, 50°, 60° and 90° and the partially fissured specimens with inclination angles of 0.0°, 35°, 50°, 60° and 90° were run for the high confining pressures of 1000 kpa, 2000 kpa and 3000 kpa.

Two other fully fissured models, Figures (7.4a) and (7.4b) with double fissures with an inclination of 30° or -30° for two different arrangements, were generated in order to study the effect of the arrangement of fissures and also the effect of confining pressure on the strength and deformation behaviours of these models. In all models the material properties and real constants were defined for the fully fissured and unfissured specimens consolidated with $P'_c = 660$ kpa.

7.4.1 Numerical Models for the Study of Orientation of Fissures

Tables (7.2) and (7.3) display the models and results obtained for the effect of orientation of fissures in the fully and partially fissured specimens respectively. These models were run for the ratios of $\frac{\sigma'_3}{P'_c} = \frac{1}{OCR}$ of 0.31 and 0.60606. As indicated in Table (7.2), the fully fissured specimen models showed that the σ'_1, and $\Delta\sigma = \sigma'_1 - \sigma'_3$ and the ratios of $\frac{\Delta\sigma}{\sigma'_3}$, and $\frac{\sigma'_3}{\sigma'_1}$ were minimum at the inclination angle of 50°. The fully fissured specimen models with inclination angles of 0.0° and 90° showed a behaviour like the unfissured specimen models for low confining pressures.

But the partially fissured specimens with an inclination angle of 0.0° or 90° showed little difference. The partially fissured specimens did not show an obvious minimum of σ'_1 or $\Delta\sigma$ at a particular inclination angle of fissure within the range of angles modelled numerically. However, for the available range, the $\Delta\sigma = \sigma'_1 - \sigma'_3$ was

minimum at an inclination angle of 60°. The partially fissured specimen models showed a higher effective axial stress than the fully fissured specimens for the same inclination angles. As shown in Figures (7.5) and (7.6), the partially and fully fissured specimen models showed sliding along the fissure surfaces.

The relationships within OCR, σ'_1 - σ'_3, $\frac{\sigma'_1-\sigma'_3}{\sigma'_3}$, $\frac{\sigma'_3}{\sigma'_1}$ and i were evaluated statistically for the fully fissured specimens with low confining pressures in Equations (7.1), (7.4) and (7.7) and for the partially fissured specimens in Equations (7.10), (7.13), and (7.16)

$$\frac{1}{OCR} = b_0 + \frac{b_1}{\sigma'_1-\sigma'_3} \tag{7.1}$$

$$b_0 = 193.853 - 7.180\, i + 0.0754\, i^2 \tag{7.2}$$

$$b_1 = 199.678 \tag{7.3}$$

$$\frac{1}{OCR} = b_0 + b_1 \ln\frac{\sigma'_1-\sigma'_3}{\sigma'_3} \tag{7.4}$$

$$b_0 = 0.6813 - 0.0153\, i + 0.0002\, i^2 \tag{7.5}$$

$$b_1 = 0.4624 - 0.0177\, i + 0.0002\, i^2 \tag{7.6}$$

$$\frac{1}{OCR} = b_0\, e^{b_1 \frac{\sigma'_3}{\sigma'_1}} \tag{7.7}$$

$$b_0 = 0.7448 - 0.0007\, i + 1.8 \times 10^{-6}\, i^2 \tag{7.8}$$

$$b_1 = -0.1749 + 0.007\, i - 8 \times 10^{-5}\, i^2 \tag{7.9}$$

$$\frac{1}{OCR} = b_0 + \frac{b_1}{\sigma'_1-\sigma'_3} \tag{7.10}$$

$$b_0 = 157.076 - 2.5114\, i + 0.0263\, i^2 \tag{7.11}$$

$$b_1 = 187.198 - 1.3062\, i + 0.078\, i^2 \tag{7.12}$$

$$\frac{1}{OCR} = b_0 + b_1 \ln \frac{\sigma'_1 - \sigma'_3}{\sigma'_3} \tag{7.13}$$

$$b_0 = 0.5674 + 0.0005\, i + 4 \times 10^{-5}\, i^2 \tag{7.14}$$

$$b_1 = 0.3894 + 0.0004\, i - 6 \times 10^{-5}\, i^2 \tag{7.15}$$

$$\frac{1}{OCR} = b_0\, e^{b_1 \frac{\sigma'_3}{\sigma'_1}} \tag{7.16}$$

$$b_0 = 0.7587 - 3 \times 10^{-5}\, i + 4.8 \times 10^{-7}\, i^2 \tag{7.17}$$

$$b_1 = -0.1416 + 0.0006\, i - 7 \times 10^{-6}\, i^2 \tag{7.18}$$

As can be seen from the coefficients of the parameters i or i^2, the partially fissured specimen models showed less dependency to the inclination angles of fissures.

7.4.2 Numerical Models for the Study of the Effect of Confining Pressure

Experiments showed that the fully fissured specimens with inclination angles of 30° and 60° did not slide along the fissure surfaces when the confining pressure was 1500 kpa. But the fully fissured specimens with an inclination angle of 45° did show sliding when high confining pressure was applied. In other words, the fully fissured specimens with inclination angles of 30° and 60° showed plastic failure, but specimens with an inclination angle of 45° showed brittle failure or a behaviour between brittle and plastic failure.

The effect of confining pressure on the strength and deformation behaviours was investigated numerically for the high confining pressures of 1000, 2000 kpa and 3000 kpa on the unfissured, partially and fully fissured specimens.

Tables (7.4) and (7.5) display the models and the numerical results for the specimens with OCR's of, 0.66, 0.33 and 0.22 for the fully and partially fissured specimens.

In Table (7.4) it can be seen that the fully fissured specimen models showed a minimum effective axial strength or ($\sigma'_1 - \sigma'_3$), and $\frac{\sigma'_1 - \sigma'_3}{\sigma'_3}$, at angle of 50° and the

models of angles of 35°and 60° showed plastic failure like the experiments for angles of 30°and 60°. The fully fissured specimen models with inclination angles of 0.0°and 90° showed for the low confining pressure the same effective axial stress as the effective axial stress obtained for unfissured specimen models. But for the high confining pressures (2000 kpa and 3000 kpa) they showed less effective axial stress than the unfissured specimen models.

The fully fissured specimen models for the higher confining pressures showed less dependency on the inclination angles than the models for the low confining pressures, higher effective cohesion and less effective friction angle, than the fully fissured specimens models for the low confining pressures, and plastic failure rather than brittle failure. But for the low confining pressures, they showed brittle failure (sliding along the fissure surfaces) rather than plastic failure (no sliding along the fissure surfaces).

The relationships for the fully fissured specimen models within the $(\sigma'_1 - \sigma'_3)$, $\frac{\sigma'_1-\sigma'_3}{\sigma'_3}$, $\frac{\sigma'_3}{\sigma'_1}$, i, and OCR for the high confining pressures are regressed and depicted in Equations (7.19), (7.22) and (7.25).

$$\frac{1}{OCR} = b_0 + \frac{b_1}{\sigma'_1 - \sigma'_3} \tag{7.19}$$

$$b_0 = 270.042 - 8.8681\, i + 0.09\, i^2 \tag{7.20}$$

$$b_1 = 167.7655 \tag{7.21}$$

$$\frac{1}{OCR} = b_0 + b_1 \ln\frac{\sigma'_1 - \sigma'_3}{\sigma'_3} \tag{7.22}$$

$$b_0 = 0.5915 - 0.01182\, i + 0.0001\, i^2 \tag{7.123}$$

$$b_1 = 0.1733 - 0.0066\, i + 7.1 \times 10^{-5}\, i^2 \tag{7.24}$$

$$\frac{1}{OCR} = b_0\, e^{b_1 \frac{\sigma'_3}{\sigma'_1}} \tag{7.25}$$

$$b_0 = 0.7887666 \quad (7.26)$$

$$b_1 = -0.3028 + 0.01172\, i - 0.0001\, i^2 \quad (7.27)$$

According to the results indicated in Table (7.5), the partially fissured specimens for the high confining pressures did not show any fissure inclination dependency, because in the partially fissured models discontinuous fissures were not capable of propagating through the tips of fissures inside the specimens. Therefore, these models need more numerical research in order to simulate the real behaviour of the partially fissured specimens under amounts of high confining pressures.

The relationships between $(\sigma'_1 - \sigma'_3)$ and i or $\frac{\sigma'_1-\sigma'_3}{\sigma'_3}$, $\frac{\sigma'_3}{\sigma'_1}$, c' and ϕ' with i are also evaluated statistically. The general form of the equation is depicted in Equation (7.28) which is a quadratic equation.

$$i = a + bx + cx^2 \quad (7.28)$$

In this equation, i is the inclination angle, a, b, and c are the coefficients of the equation which for different types of variables (x), are listed in Tables (7.6) and (7.7). The coefficients for the parameter c, in Table (7.6), for variables of $\frac{\sigma'_1-\sigma'_3}{\sigma'_3}$ and $\frac{\sigma'_3}{\sigma'_1}$ showed less magnitudes for the confining pressures of 2000 kpa and 3000 kpa than the confining pressures of 205, 400 and 1000 kpa. In other words, the models with higher confining pressures showed less dependency on the inclination angles.

The coefficients for parameters b and c in Equation (7.28) showed less magnitude for the partially fissured specimens in comparison with the magnitudes for the fully fissured specimens for the same confining pressures. Thus, the partially fissured models showed less dependency on the inclination angles than the fully fissured models. Moreover it can be seen in Table (7.7), ϕ' showed less dependency on the changes of inclination angles than c'.

Figures (7.8) and (7.9) show the deformed shapes of the models run for the effects of the arrangement of fissures in the double fissured specimen models. For the low

amount of confining pressures, the models showed some sliding along both fissure surfaces. The results are listed in Table (7.8). It can be seen that the double fissured specimen showed less effective axial stress than the singled fissured specimens. For the low confining pressures, the double paralleled fissured models showed higher effective axial stress than the double transversed fissured models. But for the high confining pressures, the double transversed fissured specimens showed higher effective axial stress than the double paralleled fissured specimens.

7.5 CONCLUSION

The effective strength of the fully and partially fissured specimens was estimated with variations of OCR, and orientation of fissures numerically by using a three dimensional finite element analysis software, ANSYS. The relationships within the $\sigma'_1 - \sigma'_3$, $\frac{\sigma'_1-\sigma'_3}{\sigma'_3}$, $\frac{\sigma'_3}{\sigma'_1}$, OCR, c', ϕ', and i were evaluated statistically from the numerical results for both high and low levels of confining pressures, and also for fully and partially fissured specimen models.

The fully fissured models with inclination angles of 0.0° and 90° to the minimum principle stresses showed not only no effect of inclination fissures, but also no effect of fissures and they behaved like the unfissured specimens.

The fully fissured specimens showed a minimum effective axial stress at an inclination angle of 50° and the partially fissured specimens at 60°.

At high confining pressures, the fully fissured models showed no sliding along the fissure surfaces for inclination angles of 35° and 60° to the minimum principle stresses. Moreover, the fully fissured models under high confining pressures showed less dependency on the variation of fissure inclination angles. In other words, the specimens failed with plastic deformation of the material instead of a combination of plastic deformation of the material and sliding deformation along the fissure surfaces.

The partially fissured models showed less dependency to the inclination angles of fissures than the fully fissured models for the low confining pressures. The partially

fissured models with high confining pressures did not show any trend with variation of inclination angles of the fissures.

The double fissured models showed less strength than the singled fissured models for the same inclination angles of fissures. For the high confining pressures, the double transversed fissured models showed better strength than the double paralleled fissured models.

The partially fissured specimens need more numerical and experimental investigation. The available models were not satisfactory for the simulation of the real behaviour of the partially fissured specimens with a strain softening behaviour.

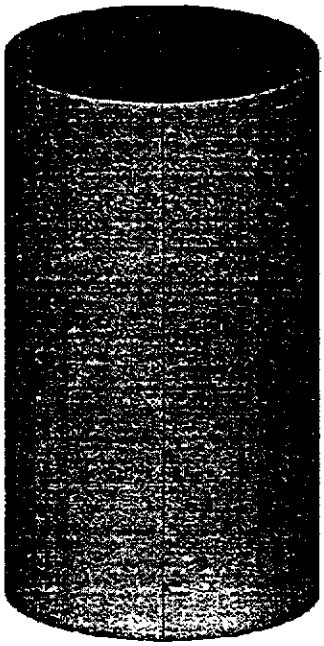

Figure (7.1): Generated triaxial model by ANSYS for the simulation of the unfissured specimens.

Figure (7.2): Generated triaxial model by ANSYS for the simulation of the fully fissured specimens with an inclination angle of 30°.

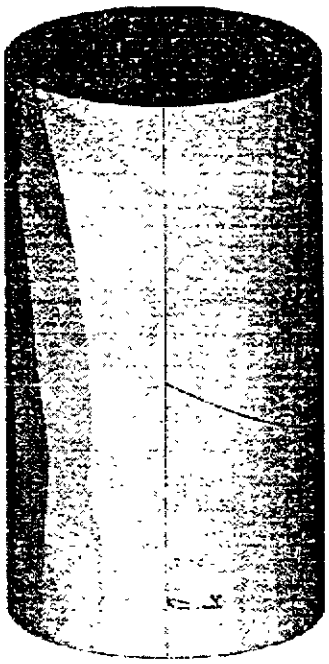

Figure (7.3): Generated triaxial model by ANSYS for the simulation of the partially fissured specimens with an inclination angle of 30°.

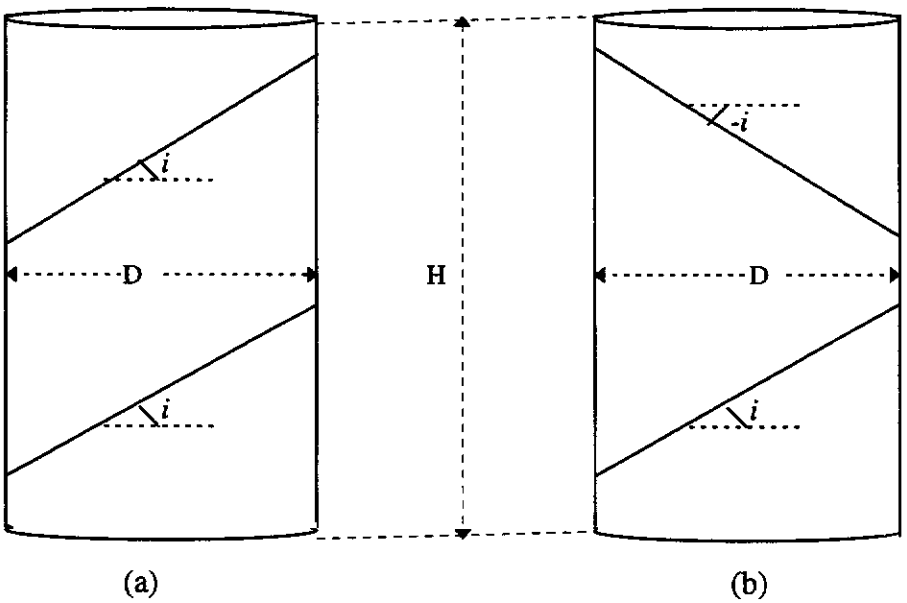

Figure (7.4): Double fissured specimen models for the inclination angle of ±30°, (a); double parallel fissure model for the inclination angle of +30°, (b); double transverse fissure model for the inclination angles of +30° and -30°.

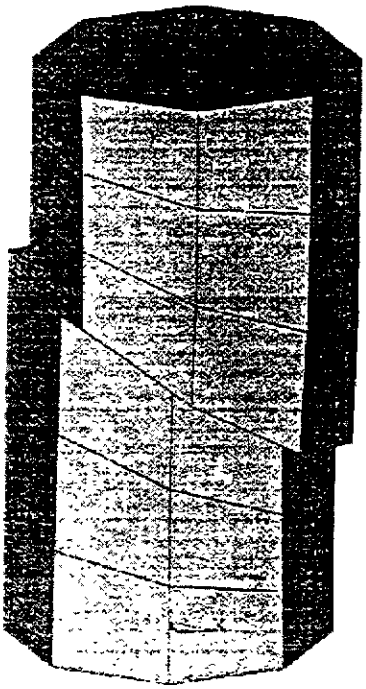

Figure (7.5): The deformed shape of the model generated for the fully fissured specimen with an inclination angle of 30°.

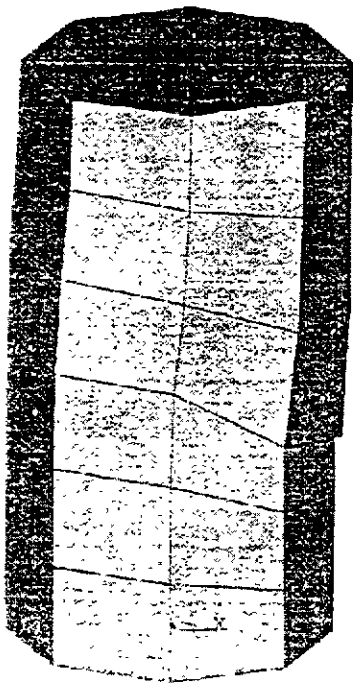

Figure (7.6): The deformed shape of the model generated for the partially fissured specimen with an inclination angle of 30°.

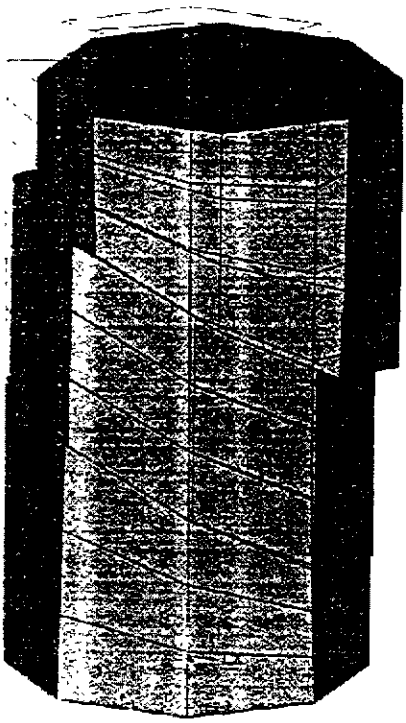

Figure (7.7): The deformed shape of the model generated for the double parallel fissure model.

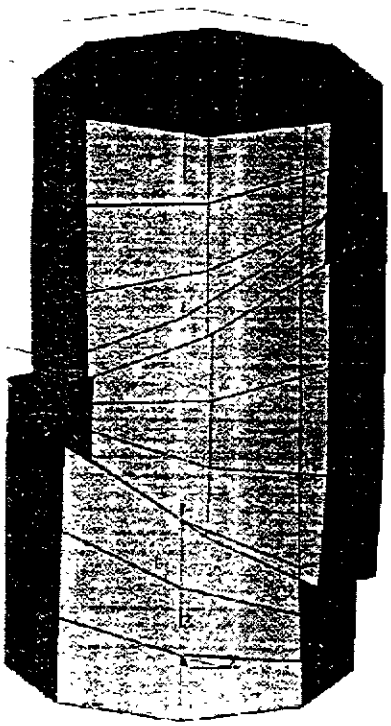

Figure (7.8): The deformed shape of the model generated for the double transverse fissure model.

Specimen Type: KB $P'_c = 660$ kpa		Test name	σ'_3	σ'_1
Experimental tests	unfissured	CUTT20	381.4	706.29
		CUTT28	246.9	502.945
	fully fissured i=30°	CUTT21	382.5	664.22
Numerical models	unfissured for coarse mesh	TTU660A1	381.4	642.87
		TTU660A2	257	481.6
	unfissured for fine mesh	TTUA1FM	381.4	695.85
		TTUA2FM	257	521.3
	fully fissured I=30° coarse mesh	TTF30A1	382.5	559
		TTF30A2	205	304.13
	fully fissured I=30° fine mesh	TTF30A1FM	382.5	658.047
		TTF30A2FM	205	347.309

Table (7.1): Comparison between experimental and numerical result from the study of the unfissured and fully fissured specimens.

Models name	Specimen type	i (deg.)	σ'_3	σ'_1	$\sigma'_1-\sigma'_3$	$\frac{\sigma'_1-\sigma'_3}{\sigma'_3}$	$\frac{\sigma'_3}{\sigma'_1}$	c′	ϕ′
TTU660AI	UFS	—	205	440.54	235.54	1.14897561	0.465338	71	8.5
TTU660A2I	UFS	—	400	702.828	302.8282	0.75707057	0.56912929		
TTF00AI	FFS	0.0	205	440.454	235.454	1.14855	0.4654288	71	8.4
TTF00A2I	FFS	0.0	400	702.52265	302.522	0.7563066	0.5693766		
TTF15AI	FFS	15	205	411.689	206.689	1.00824	0.497948	65	7.3
TTF15A2I	FFS	15	400	663.05222	263.0522	0.657630	0.603270		
TTF30A2	FFS	30	205	304.126	99.125	0.483541	0.67406274	-1	11.4
TTF30A2I	FFS	30	400	594.704727	194.7047	0.486767	0.6726027		
TTF35AI	FFS	35	205	285.550	82.5502	0.4046578	0.71191764	-7	11.3
TTF35A2I	FFS	35	400	576.2682	176.2682	0.44067	0.69412124		
TTF45AI	FFS	45	205	273.446	68.446	0.33388	0.548941	-3	9.0
TTF45A2I	FFS	45	400	540.464	140.464	0.351161	0.740104		
TTF50AI	FFS	50	205	267.51273	62.5127	0.30494	0.7663186	0	7.5
TTF50A2I	FFS	50	400	521.111	121.111	0.30277	0.76759		
TTF60AI	FFS	60	205	286.79975	81.79975	0.39902	0.7147844	15	6.2
TTF60A2I	FFS	60	400	528.69998	128.69998	0.32174997	0.756572754		
TTF90AI	FFS	90	205	440.7446	235.7446	1.1499736	0.465121977	71	8.5
TTF90A2I	FFS	90	400	703.694	303.694	0.759235	0.5684289		

Table (7.2): Numerical models for the effect of orientation of the fissures in the fully fissured specimens

Models name	Specimen type	i (deg.)	σ'_3	σ'_1	$\sigma'_1-\sigma'_3$	$\frac{\sigma'_1-\sigma'_3}{\sigma'_3}$	$\frac{\sigma'_3}{\sigma'_1}$	c′	ϕ′
TTU660AI	UFS	—	205	440.54	235.54	1.14897561	0.465338	71	8.5
TTU660A2I	UFS	—	400	702.828	302.8282	0.75707057	0.56912929		
TPF00AI	PFS	0.0	205	422.99	217.99	1.0634	0.4846	70	7.2
TPF00A2I	PFS	0.0	400	673.44	273.44	0.6836	0.5940		
TPF15AI	PFS	15	205	419.42	214.42	1.046	0.4888	68	7.3
TPF15A2I	PFS	15	400	671.25	271.25	0.6781	0.5959		
TPF30AI	PFS	30	205	412.90	207.9	1.0141	0.4973	69	6.5
TPF30A2I	PFS	30	400	658.06	258.06	0.6452	0.6078		
TPF35AI	PFS	35	205	412.21	207.21	1.0108	0.4973	70	6.4
TPF35A2I	PFS	35	400	656.07	256.07	0.6402	0.6097		
TTF45AI	PFS	45	205	418.48	213.48	1.0414	0.4899	71	6.0
TTF45A2I	PFS	45	400	650.68	250.68	0.6267	0.6147		
TTF50AI	PFS	50	205	412.92	207.92	1.0142	0.4965	76	5.3
TTF50A2I	PFS	50	400	647.37	247.37	0.6184	0.6179		
TTF60AI	PFS	60	205	404.11	199.11	0.9713	0.5073	74	4.9
TTF60A2I	PFS	60	400	635.19	235.19	0.588	0.6297		
TTF90AI	PFS	90	205	423.1	218.10	1.0639	0.4845	70	7.2
TTF90A2I	PFS	90	400	673.55	273.55	0.6839	0.5939		
TPF15AR	PFS	-15	205	420.68	215.58	1.0521	0.4873	70	7.0
TPF15A2R	PFS	15	400	669.93	269.93	0.6748	0.5971		
TPF30AR	PFS	-30	205	405.68	200.68	0.9789	0.5053	62	7.1
TPF30A2R	PFS	30	400	657.91	257.91	0.6448	0.6080		

Table (7.3): Numerical models for the effect of orientation of the fissures in the partially fissured.
I= inclination angle of fissure (+i clockwise -i anticlockwise)

Table (7.3) continued

TTF35AR	PFS	-35	205	403.50	198.50	0.9683	0.5081	61	7.3
TTF35A2R	PFS	-35	400	655.21	255.21	0.6380	0.6105		
TTF45AR	PFS	-45	205	398.38	193.38	0.9433	0.5146	59	7.2
TTF45A2R	PFS	-45	400	649.10	249.10	0.6228	0.6162		
TPF50AR	PFS	-50	205	394	189.0	0.9220	0.5203	57	7.3
TPF50A2R	PFS	-50	400	645.38	205.38	0.6135	0.6198		
TPF60AR	PFS	-60	205	384.69	179.69	0.8765	0.5329	53	7.3
TPF60A2R	PFS	-60	400	636.16	236.16	0.5904	0.6288		

Models name	Specimen type	i (deg.)	σ'_3	σ'_1	$\sigma'_1-\sigma'_3$	$\frac{\sigma'_1-\sigma'_3}{\sigma'_3}$	$\frac{\sigma'_3}{\sigma'_1}$	c'	ϕ'
TTU660A6	UFS	—	1000	1503.64	503.64	0.5036	0.6651	92	7.5
TTU660A7	UFS	—	2000	2817.07	817.07	0.4085	0.71		
TTU660A8	UFS	—	3000	4100.09	1100.09	0.3667	0.7317		
TTF00A4I	FFS	0.0	1000	1503.64	503.64	0.5036	0.6651	111	6.4
TTF00A5I	FFS	0.0	2000	2741.39	741.39	0.3707	0.7296		
TTF00A3I	FFS	0.0	3000	4003.93	1003.93	0.3346	0.7493		
TTF15A3I	FFS	15	1000	1435.2	435.20	0.4352	0.6968	86	6.4
TTF15A4I	FFS	15	2000	2701.15	701.15	0.3506	0.7404		
TTF15A5I	FFS	15	3000	3933.19	933.19	0.3111	0.7627		
TTF35A3I	FFS	35	1000	1347.29	347.29	0.3473	0.7422	38	7.1
TTF35A4I	FFS	35	2000	2671.77	671.77	0.3359	0.7486		
TTF35A5I	FFS	35	3000	389.41	890.41	0.2968	0.7711		

Table (7.4): Numerical models for the study of the effect of confining pressure on the fully fissured specimens

Table (7.4) continued:

TTF50A3I	FFS	50	1000	1248.33	248.33	0.2483	0.8011	2	6.8
TTF50A4I	FFS	50	2000	2594.20	594.20	0.2971	0.7710		
TTF50A5I	FFS	50	3000	3784.73	784.73	0.2616	0.7927		
TTF60A5I	FFS	60	1000	1820.6	320.69	0.3206	0.7572	48	6.1
TTF60A3I	FFS	60	2000	2631.84	631.84	0.3159	0.7599		
TTF60A4I	FFS	60	3000	3793.18	793.18	0.2644	0.7909		
TTF90A3I	FFS	90	1000	1502.6	502.6	0.5026	0.6655	111	6.4
TTF90A4I	FFS	90	2000	2740.1	740.1	0.3701	0.7299		
TTF90A5I	FFS	90	3000	4002.5	1002.5	0.3342	0.7495		

Models name	Specimen type	i (deg.)	σ'_3	σ'_1	$\sigma'_1-\sigma'_3$	$\frac{\sigma'_1-\sigma'_3}{\sigma'_3}$	$\frac{\sigma'_3}{\sigma'_1}$	c′	ϕ′
TTU660A6	UFS	—	1000	1503.64	503.64	0.5036	0.6651	92	7.5
TTU660A7	UFS	—	2000	2817.07	817.07	0.4085	0.71		
TTU660A8	UFS	—	3000	4100.09	1100.09	0.3667	0.7317		
TPF00A4I	PFS	0.0	1000	1434.58	434.58	0.4346	0.6971	89	6.2
TPF00A5I	PFS	0.0	2000	2695.40	695.4	0.3477	0.7420		
TPF00A3I	PFS	0.0	3000	3919.18	919.18	0.3064	0.7655		
TPF35A4I	PFS	35	1000	1441.77	441.77	0.4418	0.6939	88	6.4
TPF35A5I	PFS	35	2000	2705.63	705.63	0.3528	0.7392		
TPF35A6I	PFS	35	3000	3942.41	942.41	0.3141	0.7610		

Table(7.5): Numerical models for the study of the effect of confining pressure on the partially fissured specimens.

Table (7.5) continued:

TPF50A3I	PFS	50	1000	1441.82	441.82	0.4418	0.6936	86	6.5
TPF50A4I	PFS	50	2000	2705.68	705.68	0.3528	0.7392		
TPF50A5I	PFS	50	3000	3948.47	948.47	0.3162	0.7598		
TPF60A5I	PFS	60	1000	1444.92	449.02	0.4499	0.6921	93	6.3
TPF60A3I	PFS	60	2000	2725.24	725.24	0.3626	0.7339		
TPF60A4I	PFS	60	3000	3940.27	940.27	0.3134	0.7614		

Specimen type	variable (x)	σ'_3	a	b	c
fully fissured models	σ'_1-σ'_3	205	261.733	-7.9772	0.0846
		400	331.211	-7.7656	0.0810
		1000	527.392	-9.7456	0.1041
		2000	755.761	-5.3673	0.0567
		3000	1027.60	-8.8727	0.0933
	$\frac{\sigma'_1 - \sigma'_3}{\sigma'_3}$	205	1.2766	-0.0389	0.0004
		400	0.8280	-0.0194	0.0002
		1000	0.5274	-0.0097	0.0001
		2000	0.3779	-0.0027	2×10^{-5}
		3000	0.3425	-0.0030	3.1×10^{-5}
	$\frac{\sigma'_3}{\sigma'_1}$	205	0.4286	0.0109	-0.0001
		400	0.5335	0.0083	-9×10^{-5}

Table (7.6): Coeficients and different variables (σ'_1-σ'_3, $\frac{\sigma'_1 - \sigma'_3}{\sigma'_3}$, and $\frac{\sigma'_3}{\sigma'_1}$) for Equation (7.28).

Table (7.6) continued

		2000	0.7254	0.0015	2×10^{-5}
		3000	0.7444	0.0017	2×10^{-5}
Partially fissured model	$\sigma'_1 - \sigma'_3$	205	219.517	-0.5270	0.0055
		400	280.581	-1.2777	0.0127
	$\frac{\sigma'_1 - \sigma'_3}{\sigma'_3}$	205	1.0708	-0.0026	2.7×10^{-5}
		400	0.7014	-0.0032	3.2×10^{-5}
	$\frac{\sigma'_3}{\sigma'_1}$	205	0.4828	0.0006	-7×10^{-6}
		400	0.5873	0.0012	-1×10^{-5}

Mohr coulomb parameters		Coefficients for Equation (7.28)		
		a	b	c
Low confining pressure Max: 400 kpa	c'	81.6106	-3.5390	-0.0381
	ϕ'	8.6775	0.0225	-0.0004
Medium confining pressure Max: 1000 kpa	c'	82.6183	-2.9314	0.0309
	ϕ'	8.4321	-0.0785	0.0001
High confining pressure Min: 3000 kpa, Max: 3000 kpa	c'	120.541	-4.0321	0.0435
	ϕ'	6.4133	0.0129	-0.0002
Low confining pressure Max: 400 kpa, PFS	c'	67.9208	0.1443	-0.0012
	ϕ'	77.617	-0.0772	0.0007

Table (7.7): Coefficients and different types of variables (Mohr Coulomb parameters) for Equations(7.28)

Models name	σ'_3	σ'_1	$\sigma'_1-\sigma'_3$	$\frac{\sigma'_1-\sigma'_3}{\sigma'_3}$	$\frac{\sigma'_3}{\sigma'_1}$	c′	ϕ′
DPTF30AI	205	301.192	96.192	0.469229	0.680628	5	9.8
DPTF30AJ	400	576.573	176.573	0.44143	0.693754		
DPTF30AK	1000	1426.33	426.3	0.4263	0.70110		
DPTF30AL	2000	2680.57	680.57	0.340285	0.7461099	107	5.4
DPTF30AM	3000	3840.345	840.345	0.280115	0.781179		
DTTF30AI	205	295.829	90.829	0.443048	0.692977	1	10.2
DTTF30AJ	400	574.3838	174.3838	0.435959	0.6963984		
DTTF30AK	1000	1439.219	439.219	0.43922	0.694821		
DTTF30AL	2000	2719.486	719.486	0.359743	0.735433	95	6.2
DTTF30AM	3000	3921.425	921.425	0.307141	0.765028		
TTF30AI	205	304.12	99.12	0.483512	0.674076	-1	11.4
TTF30A2I	400	594.7	194.7	0.48675	0.6726080		
TTU660AI	205	440.54	235.54	1.148975	0.4653379	71	8.5
TTU660A2I	400	703.082	303.082	0.757705	0.5689236		

Table (7.8): The numerical model results for the effects of arrangement of fissures and confining pressures on the double fissured specimens.

Appendix A(7.1):

The ANSYS batch file for the modelling an unfissured triaxial specimen.

```
/batch,list
c*** define the geometry
/FILNAM,ttu660a1
/TITLE,simulation of triaxial unfissured clay sample (P'c=660kpa)
/PREP7
CYLIND,25,0,0,100,,0,360,
BLOCK,-10,10,-10,10,0,100,
FLST,2,2,6,ORDE,2
FITEM,2,1
FITEM,2,-2
VOVLAP,P51X
FLST,2,4,3
FITEM,2,7
FITEM,2,5
FITEM,2,2
FITEM,2,3
A,P51X
FLST,2,2,6,ORDE,2
FITEM,2,2
FITEM,2,-3
VSBA,P51X,     1
FLST,2,4,3
FITEM,2,6
FITEM,2,8
FITEM,2,1
FITEM,2,4
A,P51X
FLST,2,4,6,ORDE,3
FITEM,2,1
FITEM,2,4
FITEM,2,-6
VSBA,P51X,     1
ESHAPE,2,0
MOPT,QUAD,1
ET,1,SOLID45
FLST,2,4,4,ORDE,4
FITEM,2,44
FITEM,2,-45
FITEM,2,50
FITEM,2,55
LESIZE,P51X, , ,1,1,
FLST,2,4,4,ORDE,4
FITEM,2,38
FITEM,2,40
FITEM,2,59
FITEM,2,61
```

```
LESIZE,P51X, , ,2,1,
FLST,2,9,4,ORDE,9
FITEM,2,9
FITEM,2,-10
FITEM,2,13
FITEM,2,18
FITEM,2,20
FITEM,2,22
FITEM,2,31
FITEM,2,-32
FITEM,2,46
LESIZE,P51X, , ,6,1,
FLST,2,4,6,ORDE,4
FITEM,2,2
FITEM,2,-3
FITEM,2,7
FITEM,2,-8
VMESH,P51X
FLST,2,2,5,ORDE,2
FITEM,2,5
FITEM,2,14
ACCAT,P51X
FLST,2,2,5,ORDE,2
FITEM,2,20
FITEM,2,34
ACCAT,P51X
FLST,2,2,5,ORDE,2
FITEM,2,19
FITEM,2,30
ACCAT,P51X
FLST,2,2,5,ORDE,2
FITEM,2,12
FITEM,2,15
ACCAT,P51X
FLST,2,4,6,ORDE,2
FITEM,2,9
FITEM,2,-12
VMESH,P51X
TB,DP,1, , ,0
TBMODIF,1,1,0.065
TBMODIF,1,2,10,
UIMP,1,EX, , ,44,
UIMP,1,DENS, , , ,
UIMP,1,ALPX, , , ,
UIMP,1,REFT, , , ,
UIMP,1,NUXY, , ,0.395,
UIMP,1,GXY, , , ,
UIMP,1,MU, , , ,
UIMP,1,DAMP, , , ,
UIMP,1,KXX, , , ,
UIMP,1,C, , , ,
UIMP,1,ENTH, , , ,
UIMP,1,HF, , , ,
```

```
UIMP,1,EMIS, , ,1,
UIMP,1,QRATE, , , ,
UIMP,1,MURX, , , ,
UIMP,1,MGXX, , , ,
UIMP,1,RSVX, , , ,
UIMP,1,PERX, , , ,
UIMP,1,VISC, , , ,
UIMP,1,SONC, , , ,
FINISH
/SOLU
FLST,2,13,3,ORDE,9
FITEM,2,1
FITEM,2,-4
FITEM,2,9
FITEM,2,-12
FITEM,2,17
FITEM,2,-18
FITEM,2,21
FITEM,2,23
FITEM,2,25
DK,P51X, , , ,1,ALL
DTRAN
FLST,2,25,1,ORDE,23
FITEM,2,1
FITEM,2,-2
FITEM,2,15
FITEM,2,23
FITEM,2,29
FITEM,2,37
FITEM,2,43
FITEM,2,50
FITEM,2,57
FITEM,2,64
FITEM,2,-65
FITEM,2,78
FITEM,2,-79
FITEM,2,92
FITEM,2,-93
FITEM,2,106
FITEM,2,-109
FITEM,2,134
FITEM,2,-135
FITEM,2,149
FITEM,2,155
FITEM,2,162
FITEM,2,-163
D,P51X, ,-3, , , ,UZ
FLST,2,4,5,ORDE,4
FITEM,2,37
FITEM,2,41
FITEM,2,44
FITEM,2,48
SFA,P51X,1,PRES,0.381,
```

```
FLST,2,8,5,ORDE,8
FITEM,2,9
FITEM,2,28
FITEM,2,32
FITEM,2,36
FITEM,2,40
FITEM,2,43
FITEM,2,47
FITEM,2,50
SFA,P51X,1,PRES,0.381,
ANTYPE,0
NLGEOM,0
NROPT,AUTO, ,
LUMPM,0
EQSLV,FRONT,1e-008,0,
SSTIF
PSTRES
TOFFST,0,
TIME,10
AUTOTS,1
NSUBST,30,50,30,0
KBC,0
NEQIT,70,
LNSRCH,0
PRED,ON,,ON
NCNV,1,0,0,0,0,
OUTPR,ALL,ALL,
OUTRES,ALL,ALL,
LSWRITE,1,
SAVE,TTU660A1,db
/STAT,SOLU
SOLVE
SAVE,TTU660A1,db
FINISH
```

Appendix A(7.2):

The ANSYS batch file for the modelling a fully fissured triaxial specimen.

```
/batch,list
c*** define the geometry
/FILNAM,TTF30A2I
/TITLE,triaxial overconsolidated fissured clay sample(I=30 deg.)
/PREP7
CYLIND,25,0,0,100,,0,360,
BLOCK,-10,10,-10,10,0,100,
FLST,2,2,6,ORDE,2
FITEM,2,1
FITEM,2,-2
VOVLAP,P51X
FLST,2,4,3
FITEM,2,8
FITEM,2,6
FITEM,2,4
FITEM,2,1
A,P51X
FLST,2,2,6,ORDE,2
FITEM,2,2
FITEM,2,-3
VSBA,P51X,      1
FLST,2,4,3
FITEM,2,7
FITEM,2,5
FITEM,2,2
FITEM,2,3
A,P51X
FLST,2,4,6,ORDE,3
FITEM,2,1
FITEM,2,4
FITEM,2,-6
VSBA,P51X,      1
FLST,2,8,6,ORDE,4
FITEM,2,2
FITEM,2,-3
FITEM,2,7
FITEM,2,-12
VGLUE,P51X
FLST,2,2,3,ORDE,2
FITEM,2,23
FITEM,2,-24
KWPAVE,P51X
wpro,,,30.000000
RECTNG,-100,100,-100,100,
FLST,2,8,6,ORDE,4
FITEM,2,2
```

```
FITEM,2,-3
FITEM,2,7
FITEM,2,-12
VSBA,P51X,      1
FLST,3,8,5,ORDE,8
FITEM,3,16
FITEM,3,50
FITEM,3,57
FITEM,3,63
FITEM,3,69
FITEM,3,75
FITEM,3,80
FITEM,3,84
AGEN,2,P51X, , , , , , ,0
FLST,2,8,6,ORDE,8
FITEM,2,4
FITEM,2,6
FITEM,2,14
FITEM,2,16
FITEM,2,18
FITEM,2,20
FITEM,2,22
FITEM,2,24
VDELE,P51X
FLST,2,36,5,ORDE,26
FITEM,2,5
FITEM,2,12
FITEM,2,16
FITEM,2,-18
FITEM,2,25
FITEM,2,-26
FITEM,2,34
FITEM,2,38
FITEM,2,41
FITEM,2,43
FITEM,2,46
FITEM,2,48
FITEM,2,50
FITEM,2,-53
FITEM,2,57
FITEM,2,-60
FITEM,2,63
FITEM,2,-65
FITEM,2,69
FITEM,2,-72
FITEM,2,75
FITEM,2,-77
FITEM,2,80
FITEM,2,-82
FITEM,2,84
FITEM,2,-85
AGLUE,P51X
FLST,2,7,5,ORDE,6
```

```
FITEM,2,43
FITEM,2,51
FITEM,2,-52
FITEM,2,72
FITEM,2,75
FITEM,2,-77
VA,P51X
FLST,2,7,5,ORDE,7
FITEM,2,48
FITEM,2,64
FITEM,2,-65
FITEM,2,77
FITEM,2,82
FITEM,2,84
FITEM,2,-85
VA,P51X
FLST,2,7,5,ORDE,6
FITEM,2,46
FITEM,2,58
FITEM,2,-59
FITEM,2,71
FITEM,2,80
FITEM,2,-82
VA,P51X
FLST,2,7,5,ORDE,5
FITEM,2,17
FITEM,2,-18
FITEM,2,41
FITEM,2,69
FITEM,2,-72
VA,P51X
FLST,2,6,5,ORDE,4
FITEM,2,12
FITEM,2,26
FITEM,2,50
FITEM,2,-53
VA,P51X
FLST,2,6,5,ORDE,4
FITEM,2,25
FITEM,2,34
FITEM,2,57
FITEM,2,-60
VA,P51X
FLST,2,6,5,ORDE,5
FITEM,2,38
FITEM,2,53
FITEM,2,60
FITEM,2,63
FITEM,2,-65
VA,P51X
FLST,2,6,5,ORDE,5
FITEM,2,5
FITEM,2,16
```

```
FITEM,2,-18
FITEM,2,25
FITEM,2,-26
VA,P51X
FLST,2,8,6,ORDE,8
FITEM,2,1
FITEM,2,5
FITEM,2,13
FITEM,2,15
FITEM,2,17
FITEM,2,19
FITEM,2,21
FITEM,2,23
VDELE,P51X
FLST,2,36,5,ORDE,27
FITEM,2,1
FITEM,2,-4
FITEM,2,6
FITEM,2,-11
FITEM,2,13
FITEM,2,-15
FITEM,2,19
FITEM,2,29
FITEM,2,-30
FITEM,2,33
FITEM,2,37
FITEM,2,40
FITEM,2,42
FITEM,2,45
FITEM,2,47
FITEM,2,49
FITEM,2,54
FITEM,2,-56
FITEM,2,61
FITEM,2,-62
FITEM,2,66
FITEM,2,-68
FITEM,2,73
FITEM,2,-74
FITEM,2,78
FITEM,2,-79
FITEM,2,83
AGLUE,P51X
FLST,2,6,5,ORDE,6
FITEM,2,7
FITEM,2,32
FITEM,2,37
FITEM,2,39
FITEM,2,87
FITEM,2,-88
VA,P51X
FLST,2,6,5,ORDE,6
FITEM,2,6
```

```
FITEM,2,24
FITEM,2,33
FITEM,2,39
FITEM,2,44
FITEM,2,86
VA,P51X
FLST,2,6,5,ORDE,6
FITEM,2,3
FITEM,2,11
FITEM,2,27
FITEM,2,32
FITEM,2,35
FITEM,2,-36
VA,P51X
FLST,2,6,5,ORDE,6
FITEM,2,1
FITEM,2,4
FITEM,2,24
FITEM,2,27
FITEM,2,-28
FITEM,2,31
VA,P51X
FLST,2,7,5,ORDE,7
FITEM,2,15
FITEM,2,20
FITEM,2,44
FITEM,2,-45
FITEM,2,86
FITEM,2,90
FITEM,2,92
VA,P51X
FLST,2,7,5,ORDE,7
FITEM,2,14
FITEM,2,22
FITEM,2,35
FITEM,2,-36
FITEM,2,42
FITEM,2,89
FITEM,2,91
VA,P51X
FLST,2,7,5,ORDE,7
FITEM,2,8
FITEM,2,21
FITEM,2,28
FITEM,2,31
FITEM,2,40
FITEM,2,89
FITEM,2,-90
VA,P51X
FLST,2,7,5,ORDE,7
FITEM,2,19
FITEM,2,23
FITEM,2,47
```

```
FITEM,2,87
FITEM,2,-88
FITEM,2,91
FITEM,2,-92
VA,P51X
FLST,2,12,4,ORDE,4
FITEM,2,9
FITEM,2,-14
FITEM,2,19
FITEM,2,-24
LESIZE,P51X, , ,1,1,
FLST,2,4,4,ORDE,4
FITEM,2,26
FITEM,2,34
FITEM,2,46
FITEM,2,104
LESIZE,P51X, , ,2,1,
FLST,2,13,4,ORDE,2
FITEM,2,107
FITEM,2,-119
LESIZE,P51X, , ,3,1,
ET,1,SOLID45
ESHAPE,2,0
MOPT,QUAD,0
FLST,2,4,6,ORDE,4
FITEM,2,1
FITEM,2,5
FITEM,2,11
FITEM,2,-12
VMESH,P51X
FLST,2,2,5,ORDE,2
FITEM,2,35
FITEM,2,-36
ACCAT,P51X
FLST,2,2,5,ORDE,2
FITEM,2,87
FITEM,2,-88
ACCAT,P51X
FLST,2,2,5,ORDE,2
FITEM,2,44
FITEM,2,86
ACCAT,P51X
FLST,2,2,5,ORDE,2
FITEM,2,28
FITEM,2,31
ACCAT,P51X
FLST,2,4,6,ORDE,2
FITEM,2,13
FITEM,2,-16
VMESH,P51X
FLST,2,12,4,ORDE,12
FITEM,2,17
FITEM,2,30
```

```
FITEM,2,-31
FITEM,2,37
FITEM,2,-38
FITEM,2,44
FITEM,2,-45
FITEM,2,48
FITEM,2,50
FITEM,2,52
FITEM,2,55
FITEM,2,57
LESIZE,P51X, , ,1,1,
FLST,2,4,4,ORDE,4
FITEM,2,40
FITEM,2,42
FITEM,2,59
FITEM,2,61
LESIZE,P51X, , ,2,1,
FLST,2,13,4,ORDE,11
FITEM,2,66
FITEM,2,-69
FITEM,2,75
FITEM,2,-76
FITEM,2,82
FITEM,2,-83
FITEM,2,87
FITEM,2,93
FITEM,2,-94
FITEM,2,98
FITEM,2,102
LESIZE,P51X, , ,3,1,
FLST,2,4,6,ORDE,2
FITEM,2,7
FITEM,2,-10
VMESH,P51X
FLST,2,2,5,ORDE,2
FITEM,2,64
FITEM,2,-65
ACCAT,P51X
FLST,2,2,5,ORDE,2
FITEM,2,58
FITEM,2,-59
ACCAT,P51X
FLST,2,2,5,ORDE,2
FITEM,2,51
FITEM,2,-52
ACCAT,P51X
FLST,2,2,5,ORDE,2
FITEM,2,17
FITEM,2,-18
ACCAT,P51X
FLST,2,4,6,ORDE,3
FITEM,2,2
FITEM,2,-4
```

```
FITEM,2,6
VMESH,P51X
TB,DP,1, , ,0
TBMODIF,1,1,0.065
TBMODIF,1,2,10
FLST,5,8,5,ORDE,7
FITEM,5,1
FITEM,5,3
FITEM,5,6
FITEM,5,-8
FITEM,5,14
FITEM,5,-15
FITEM,5,19
ASEL,S, , ,P51X
APLOT
ALLSEL,BELOW,AREA
! THE FOLLOWING SELECT COMMANDS WERE GENERATED BY THE ALLSEL
COMMAND
LSLA
KSLL
NSLA,,1
ESLN,,1
CM,target,NODE
ALLSEL,ALL
! THE FOLLOWING SELECT COMMANDS WERE GENERATED BY THE ALLSEL
COMMAND
VSEL,ALL
ASEL,ALL
LSEL,ALL
KSEL,ALL
ESEL,ALL
NSEL,ALL

FLST,5,8,5,ORDE,8
FITEM,5,16
FITEM,5,50
FITEM,5,57
FITEM,5,63
FITEM,5,69
FITEM,5,75
FITEM,5,80
FITEM,5,84
ASEL,S, , ,P51X
APLOT
ALLSEL,BELOW,AREA
! THE FOLLOWING SELECT COMMANDS WERE GENERATED BY THE ALLSEL
COMMAND
LSLA
KSLL
NSLA,,1
ESLN,,1
CM,contact,NODE
ALLSEL,ALL
```

```
! THE FOLLOWING SELECT COMMANDS WERE GENERATED BY THE ALLSEL
COMMAND
VSEL,ALL
ASEL,ALL
LSEL,ALL
KSEL,ALL
ESEL,ALL
NSEL,ALL

ET,2,CONTAC49
KEYOPT,2,1,0
KEYOPT,2,2,0
KEYOPT,2,3,1
KEYOPT,2,7,1
R,1,146,31.9,1,1,5, ,
TYPE,2,
MAT,1,
REAL,1,
ESYS,0,
GCGEN,CONTACT,TARGET, , ,BOT,
UIMP,1,EX, , ,44,
UIMP,1,DENS, , , ,
UIMP,1,ALPX, , , ,
UIMP,1,REFT, , , ,
UIMP,1,NUXY, , ,0.395,
UIMP,1,GXY, , , ,
UIMP,1,MU, , ,0.176,
UIMP,1,DAMP, , , ,
UIMP,1,KXX, , , ,
UIMP,1,C, , , ,
UIMP,1,ENTH, , , ,
UIMP,1,HF, , , ,
UIMP,1,EMIS, , ,1,
UIMP,1,QRATE, , , ,
UIMP,1,MURX, , , ,
UIMP,1,MGXX, , , ,
UIMP,1,RSVX, , , ,
UIMP,1,PERX, , , ,
UIMP,1,VISC, , , ,
UIMP,1,SONC, , , ,
/SOLU
FLST,2,13,3,ORDE,9
FITEM,2,1
FITEM,2,-4
FITEM,2,9
FITEM,2,-12
FITEM,2,17
FITEM,2,-18
FITEM,2,21
FITEM,2,23
FITEM,2,25
DK,P51X, , , ,1,ALL
DTRAN
```

```
FLST,2,25,1,ORDE,15
FITEM,2,101
FITEM,2,-104
FITEM,2,117
FITEM,2,121
FITEM,2,-122
FITEM,2,129
FITEM,2,133
FITEM,2,137
FITEM,2,-142
FITEM,2,161
FITEM,2,-164
FITEM,2,177
FITEM,2,-180
FITEM,2,193
FITEM,2,-194
D,P51X, ,-3, , , ,UZ
FLST,2,8,5,ORDE,6
FITEM,2,20
FITEM,2,-23
FITEM,2,70
FITEM,2,76
FITEM,2,81
FITEM,2,85
SFA,P51X,1,PRES,0.400,
FLST,2,8,5,ORDE,8
FITEM,2,5
FITEM,2,12
FITEM,2,34
FITEM,2,38
FITEM,2,41
FITEM,2,43
FITEM,2,46
FITEM,2,48
SFA,P51X,1,PRES,0.400,
ANTYPE,0
NLGEOM,1
NROPT,AUTO, ,
LUMPM,0
EQSLV,FRONT,1e-008,0,
SSTIF
PSTRES
TOFFST,0,
TIME,10
AUTOTS,1
NSUBST,30,50,30,0
KBC,0
NEQIT,70,
LNSRCH,0
PRED,ON,,ON,
NCNV,1,0,0,0,0,
OUTRES,ALL,ALL,
OUTPR,ALL,ALL,
```

```
LSWRITE,1,
SAVE,TTF30A2I,DB
/STAT,SOLU
SOLVE
SAVE,TTF30A2I,DB
FINISH
```

CHAPTER 8

SUMMARY, CONCLUSION AND RECOMMENDATIONS

8.1 INTRODUCTION

In this chapter, research is summarised, conclusions made and, finally, recommendations or suggestions for further study are described.

The main purposes of this research were to prepare and test artificially overconsolidated fully, partially and unfissured clay specimens for both direct shear and triaxial tests, and also to simulate numerically the strain softening behaviour of the overconsolidated fissured and unfissured specimens subjected to direct shear tests and, finally, to evaluate experimentally or numerically, the effects of the parameters such as P'_c, OCR, rate of shearing, type of material, size of specimens, fissure parameters including width, spacing and orientation of fissures, confining pressure, and the effect of horizontal locked in stress on the effective peak and residual shear strengths of the unfissured specimens or intact overconsolidated clay materials.

To achieve these objectives a comprehensive series of tests has been carried out on the artificially prepared specimens for both direct shear and triaxial tests. They were simulated numerically for complementary studies by using FLAC for direct shear test specimens, and ANSYS for triaxial test specimens.

From the results obtained experimentally and numerically, relationships within different parameters have been established.

8.2 SUMMARY AND CONCLUSIONS

A comprehensive review of publications from experimental or analytical points of view concerning the formation, classification, and effect of fissures on shear strength, laboratory and in-situ tests on the natural and artificial specimens for determining the shear strength of intact, partially and fully fissured clay specimens and critical comments, have been presented.

Taking into account the continuous effect of weathering on the discontinuity surfaces, it seems that fully softened and residual shear strengths are not constant and change with time. In other words, the stability of slopes in fissured clays should be considered for a specific duration of time when the weathering has no influence on the effective shear strength parameters (c' and ϕ').

It was concluded from the literature that the overall shear strength or full-scale strength or fully softened shear strength depends on the form and shape of the failure surface. For example, if the failure surface is mostly formed of fissure surfaces, the amount of overall strength is near the amount of residual strength of the mass, whereas, if the failure surface is passed through the soil substances, the amount of overall strength is close to the peak strength of the soil material. For intermediate failure surfaces, the orientation and arrangement of fissures and the stress level of fissured clay elements located in the path of assumed failure surface and also the roughness of fissure surfaces located along failure surface, can affect the overall strength or fully softened strength of the fissured clay mass.

Strengths measured both in the laboratory and in field tests on the natural fissured clay mass or on specimens, indicated that the extent, spacing, inclination, shape and surface roughness of the fissures and fabric of soils are influencing parameters. For laboratory tests, in addition to these parameters, the strengths depend on the stress changes which occur during sampling, boring and testing and also on the length of time that the clay remains under particular stresses, the size of specimens and the magnitudes of stresses used for testing in laboratory apparatus, specially in triaxial

apparatus. However, the expensive costs of in-situ tests and also their specific and limited applications limit usage in-situ investigation.

The laboratory results obtained from the artificial brittle Kaolinite specimens subjected to the uniaxial compressive tests carried out by Vallejo (1986-89) indicated that a critical fissure inclination of the compressive strength reaches a minimum value, and also the longer the length of a crack or the larger the number of fissures in a sample, the lower was its unconfined compressive strength. Samples with fissures arranged in a left stepping manner were weaker in compression than samples containing right stepping fissures.

Noticeable problems with the laboratory and in-situ tests on the naturally fissured specimens or mass have been the lack of sufficient control of the effect of parameters, discussed previously, and the natural variability of the material properties on the effective shear strength of the natural fissured mass tested by in-situ tests or natural fissured specimens tested in the laboratory. Having taken into account these drawbacks, specimens were prepared artificially for this research.

Although the research carried out by Vallejo (1986-89) on the artificial specimens prepared from brittle Kaolinite clay gave an indication of the impact of orientation, length, and arrangement of fissures on the unconfined undrained compressive strength of the unsaturated and artificially fissured specimens, the need for more investigation for the study of these parameters on the effective shear strength of the artificially overconsolidated unfissured, partially and fully fissured specimens with considering the effect of strain softening, was noted.

To record the effect of spacing that fissures have in the development of the failure surface in stiff fissured clays for different arrangements and widths of fissures, a large direct shear box and for different orientations, a triaxial apparatus were required.

For experimental programs synthetic clay soil mixtures were designed to simulate the strain softening behaviour of over consolidated clays as well as to prepare the artificial fissured clay specimens. In order to create a fissure, a thin plastic sheet (used for transparency) was placed inside the artificial specimen before consolidating

and removed after completion. A thin wire was also used as another method to create a pre-cut.

The fissure surfaces created from the proposed methods of fissurising were flattened, non polished, or somewhat polished, but useful for this study.

The preparations of the materials and specimens were artificially investigated in the laboratory. K specimens showed less strain softening than KB specimens. Adding the bentonite in the KB specimens decreased the effective shear strength significantly and softened the specimens during shearing.

For this study it was necessary to have significant strain softening with large displacement. The type of clay material is considered very important in the strain softening behaviour.

The presence of fissures in the K specimens caused a significant strain softening. For the fissured K specimens, the strain softening occurred faster than in the unfissured K specimens. Moreover the KB specimens, even for the OCR of 1, showed a significant strain softening behaviour.

The pastes prepared for the K and KB specimens with water contents of 53 and 67 percent were wet enough to work, shape and avoid entrapping air bubbles while filling the moulds for the consolidation process and be fully saturated after consolidation.

The estimation of the amount of unconsolidated material needed for the preparation of each specimen was necessary particularly for the partially and fully fissured specimens. Passing the shearing surfaces in the direct shear tests through the fissures was important to investigate the effects of fissure parameters.

For the artificial consolidation of the specimens, both options of loading, one stage and multistage, were studied. The results of the direct shear test showed no difference for this feature.

Because the proposed water content of the pastes was adequate, the submergence of the specimens during the consolidation process did not influence the effective shear strength of the artificially consolidated specimens. Tests on both types of the

prepared specimens (submerged and unsubmerged) showed there was no difference from the effective shear strength point of view, even if the prepared specimens sheared without the presences of water (unflooded). However, for this research, the specimens were flooded during the shear process. The only possible effect of non submergence during the shearing of the specimens was dryness of the sheared surfaces specially when the rate was very slow.

For the unfissured locked specimens, the lateral stresses are not released. Therefore, during shearing, the clay particles are flattened and the sheared surfaces are smooth and even. But for the unlocked specimens, the lateral stresses ae released. Therefore, the clay particles are not flattened and the sheared surfaces are more bumpy and uneven. For this reason, the shear strength of unfissured unlocked specimens is greater than the unfissured locked specimens for the same initial conditions, such as water content, OCR, material type, size and rate of shearing. The magnitude of differences depends mainly on the type of mineral.

The effect of locked in horizontal stresses could be applied through the reduction functions or factors on the effective peak shear strength parameters of the unfissured unlocked specimens. Both K and KB materials showed that by increasing the shearing displacements, the differences between the unlocked and locked in horizontal stresses decreased. In other words at residual, this effect was negligible.

An increase in the rate of shearing increases the shear strength of the unfissured unlocked specimens, but it does not influence the peak shear strengths of the fully fissured unlocked specimens significantly.

In the fully fissured unlocked specimens, the increase in the rate of shearing does not have also any effect on the residual shear strengths of the specimens.

The rate of shearing applied for the drained tests was slow enough to dissipate extra pore pressure created during the shearing.

For the unfissured locked specimens, the rate of shearing has less influence on the shear strength than the unfissured unlocked specimens. Because of the bumpy surfaces created during shearing, there is a little suction in the quicker rates of shearing. Therefore, the shear strength is a little greater than the unfissured unlocked

specimens sheared by the slower rates of shearing . But for the unfissured locked specimens or the fully fissured specimens, the difference as a result of changing the rates of shearing is very little.

The effect of rate of the shearing could be applied as functions or factors on the effective peak shear strength parameters of the unfissured unlocked specimens.

For different OCR's, the swelling of the specimens as a result of unloading should be considered specially for the partially and fully fissured specimens to avoid passing the shearing surfaces through the material instead of predetermined fissure surfaces.

The results for different P'_c, either K or KB, showed that by increasing P'_c, effective peak shear strength increased because of increase of density or decrease of void ratio and porosity of the specimens.

In detail the increase of P'_C resulted in the increase of the both effective peak cohesion and friction (c'_p & ϕ'_p) mainly and the effective residual shear strength parameters (c'_r & ϕ'_r) somewhat for both the unfissured locked and unlocked KB specimens.

In the fully fissured unlocked KB specimens, the increase of P'_C increased the effective peak shear strength parameters and did not have any significant influence on the effective residual shear strength parameters of the fully fissured unlocked KB specimens.

In the unfissured locked or unlocked K specimens, the increase of P'_C increased c'_p and c'_r and decreased the ϕ'_p and ϕ'_r. In the fully fissured unlocked K specimens, the increase of P'_C increased the c'_p and decreased ϕ'_p, but had no significant impact on the c'_r & ϕ'_r of the fully fissured unlocked K specimens.

The extreme points of the changes of the c'_p & ϕ'_p by increasing the P'_C could be estimated from the trends of the graphs of c'_p & ϕ'_p with p'_c for each particular specimen size .

The results of the specimen size effect show that the peak shear strength mainly and the residual shear strengths somewhat are influenced by the size of the specimens for the same initial conditions.

The increase in size of specimens for each constant prescribed preconsolidation pressure decreases the effective peak and residual shear strengths of the specimens. The increase in size resulted in the decrease of c'_p & ϕ'_p of the unfissured locked or unlocked KB and K specimens mainly and the c'_r & ϕ'_r of the unfissured locked and unlocked KB and K specimens somewhat. But in the fully fissured unlocked KB and K specimens, the increase in size decreased the c'_p & ϕ'_p of the specimens and did not have any influence on the c'_r & ϕ'_r of the fully fissured unlocked KB and K specimens. The extreme reductions of the c'_p & ϕ'_p for the unfissured unlocked KB and K specimens have been estimated by the trends of results for the changes of c'_p & ϕ'_p with size for each prescribed preconsolidation pressure.

For any particular size in the partially fissured unlocked specimens, an increase in width of fissures decreases the effective peak shear strength of the specimens. On the contrary, the increase of spacing increases the effective peak shear strength for that particular size.

There are two limits of spacing for each size and width of fissure. Before the minimum limit of spacing, the partially fissured specimen behaves like a fully fissured specimen. After the maximum limit of spacing, it behaves like an unfissured specimen. These limits could be defined from the trends of the changes of peak shear strength with spacing experimentally on the very large specimens, or numerically, by modelling the partially fissured specimens. The effects of width and spacing of the fissures in the partially fissured specimens subjected to direct shear tests have been investigated by FLAC.

The inclined overconsolidated clay fissured specimens subjected to direct shear test do not show any impact of the inclination of fissure on the shear strength.

In the partially fissured specimens subjected to direct shear tests, the direction of shearing with respect to the length of fissures is important. Those sheared parallel to the length of fissure show an increase of effective peak shear strength rather than

those shear perpendicularly for the same initial conditions including material, size, and fissure specification.

The residual shear strength parameters (c'_r & ϕ'_r) of the fully fissured unlocked specimens do not show any impact with an increase in the P'_C, size and rate of shearing.

The type of the water used in this research for the preparation of the pastes and testing the specimens did not have any significant effect on the effective shear strength of the artificially overconsolidated clay specimens.

In order to simulate strain-softening behaviour of the specimen subjected to direct shear tests, FLAC programming (FISH) was used. Two programs were written for the simulation of the strain softening behaviours observed experimentally for the unfissured and fully fissured specimens. The fissured parameters were studied numerically by considering the strain softening behaviour. The results from the study of the fissure parameters and the experimental results from the different parameters discussed in Chapters 3 and 4 were formulated and used in another FLAC model called, HSSM. This was used to estimate or predict the effective shear strength of the specimens by homogenising the effects of the parameters discussed previously and applying the strain softening model written for the unfissured unlocked specimens.

In the FLAC program, shear strength softening can simulated by making Mohr Coulomb properties (cohesion and friction) functions of plastic strain and these functions are specified as linear piecewises by using the TABLE command. Tabulation of the c' and ϕ', instead of introducing the functions for them and only relating these parameters to the plastic deformation and ignoring to provide the conditions for the possibility of sliding or separation of the upper half of the specimen in the direct shear box models, could influence the prediction of the behaviour of the models in comparison with the real behaviour observed in the laboratory tests.

In a direct shear box, sliding and plastic deformation occur along the shear band or shearing surfaces. Therefore, in this study, the reductions of c' and ϕ' due to strain

can be related to the horizontal strain or shear deformation which is a combination of sliding and plastic deformation.

In the numerical simulation of the direct shear box specimens, an interface was assigned along the shearing surfaces. The interface could simulate properly the behaviour of the material along the sheared zone or shearing surfaces by providing conditions for the sliding of the material, as well as the plastic deformation along the sheared zone or shearing surfaces.

Applying strain-softening behaviour to the main interface in the direct shear box simulation by the FLAC showed much less mesh dependency in comparison with finite element modelling of the direct shear box.

The reduction of effective shear strength because of the presence of oriented fissures in the direct shear box modelling is negligible.

The simulation of the effect of locked-in horizontal stress by the possible numerical approach proposed in this research is not satisfactory. However, the effects could be applied through the coefficients obtained by the results of vast experimental tests.

In direct shear box numerical modelling, because the shearing surfaces coincide with the plane surfaces of the two halves of the box, an interface could be assigned along the shearing surfaces to provide the possibility of sliding which takes place during shearing. This procedure is not applicable where the direction of the shear band or shearing zone, as well as the direction of the propagation of a pre-existing fissure, eg. (in a triaxial specimen), is not predictable. The propagation of discontinuous fissures in the partially fissured specimens subjected to triaxial tests needs more numerical and experimental investigation.

The partially or fully fissured triaxial specimens were prepared artificially for three angles of inclinations. The results showed that by increasing P'_C in the triaxial KB clay specimens, the ϕ' mainly increased.

The ratio of deviator stress to effective confining pressure, $\frac{\sigma'_1 - \sigma'_3}{\sigma'_3}$, is increased by increasing the P'_C, but the ratio of effective confining pressure to effective axial stress is decreased by increasing the P'_C.

In the fully fissured KB triaxial specimens, the effective axial stress for the specimens consolidated with the same pressure showed some changes with the variation of the angle of fissure. An inclination of 45° was coincident with the minimum effective axial stress within the test results obtained from angles of 30°, 45° and 60°.

Moreover, by applying high confining pressure (σ_3), the fully fissured KB specimens with inclinations of 30° and 60° showed less sliding along the fissure surfaces than the fully fissured specimens with an angle of 45°.

The partially fissured KB specimens with an inclination angle of 30° did not show any obvious effect of discontinuous fissure on the deformation behaviour and effective Mohr Coulomb parameters. The study of the effect of other inclination angles of discontinuous fissures needs more experimental investigation which is beyond of the scope of this research.

In the fully fissured KB triaxial specimens, the ratio of $\frac{\sigma'_1 - \sigma'_3}{\sigma'_3}$ decreased by increasing the inclination angle of fissure (i). But the ratio of $\frac{\sigma'_3}{\sigma'_1}$ increased by increasing the inclination angle of fissure (i). This behaviour was similar to that observed for the decrease of P'_C on the unfissured triaxial KB specimens. Taking into account the huge amount of time required for preparing and testing the fully or partially fissured triaxial KB specimens for the study of the other angles of inclination, as well as for the study of the effect of confining pressure on the effective axial stress, the numerical modelling of triaxial specimens was applied. The effect of fissure inclination or orientation of the fissures and also the effect of confining pressure on the effective shear strength of the triaxial fully or partially fissured clay specimens were studied numerically.

The effective strength of the fully and partially fissured specimens was estimated numerically with the variation of OCR, orientation of fissures by using the three dimensional finite element analysis software, ANSYS. The relationships within the

$\sigma'_1 - \sigma'_3$, $\frac{\sigma'_1-\sigma'_3}{\sigma'_3}$, $\frac{\sigma'_3}{\sigma'_1}$, OCR, c', ϕ', and i were evaluated statistically from the numerical results obtained for both high and low levels of confining pressures, and also for the fully and partially fissured specimen models.

The fully fissured models with inclination angles of 0.0° and 90° to the minimum principle stresses show no effect of fissures or fissure orientations and behave like the unfissured specimens.

The fully fissured KB specimens showed a minimum effective axial stress at an inclination angle of 50° and the partially fissured KB specimens showed at 60°.

At high confining pressures, the fully fissured models showed no sliding along the fissure surfaces for the inclination angles of 35° and 60° to the minimum principle stresses. Moreover, the fully fissured models under high confining pressures showed less dependency on the variation of fissure inclination angles. In other words, the specimens failed with plastic deformation of the material instead of a combination of plastic deformation in the material and sliding deformation along the fissure surfaces.

The partially fissured models showed less dependency to the inclination angles of fissures than the fully fissured models for low confining pressures. The partially fissured models with high confining pressures did not show any particular trend with variation of inclination angles of the fissures.

The double fissured models showed less strength than the singled fissured models for the same inclination angles of fissures. For high confining pressures, the double transverse fissured models showed better strength than the double paralleled fissured models.

The partially fissured specimens need more numerical and experimental investigation. Taking into account the strain softening behaviour and propagation of discontinuous fissures in the partially fissured specimen, as well as providing the possibility of sliding along the fissure surfaces, the available ANSYS models were not satisfactory for the simulation of the real behaviour of the partially fissured specimens.

The specially designed and constructed sample makers and the commissioning of the tools either for the direct shear box tests or triaxial tests were positive steps to study the effects of these parameters in the laboratory.

These sample makers were used for the size and specification of the specimens proposed and defined in this study. The procedures used to make the artificially over-consolidated unfissured, partially or fully fissured specimens, could be useful for further studies in this area.

8.3 SUGGESTION FOR FURTHER STUDIES

The development of secondary fissures in the partially fissured overconsolidated clay triaxial specimens needs more experimental and numerical investigation particularly to consider the strain softening behaviours of the intact material and fissure.

In the analysis of the overconsolidated fissured clay slopes with a strain softening behaviour of the material, providing the conditions for the possibilities of sliding along the fissures, opening the fissures or propagating the secondary fissures from the tips of the pre existing fissures are necessary and need more experimental and numerical research.

The effect of P'_c, OCR, fissure parameters, material type on the K_0, and plasticity parameters in order to modify the available clay yield criteria for the application in the overconsolidated fissured clay mass or stiff fissured clay mass also needs more experimental investigation.

REFERENCES

Aitchison, G. D. (1953). The mechanics of gilgai formation. Proc. of Conf. on Soil Science, Adelaide, 2(6.25), pp. 1-3.

Agarwal, K. B. (1967). The influence of size and orientation of samples on the strength of London clay. PhD thesis, Imperial College, University of London.

ANSYS, Inc (1996). The ANSYS finite element program, version 5.2.

Apted, J. P. (1977). Effect of Weathering of some geotechnical properties of London clay. Ph.D thesis, Imperial College, University of London.

Ashby, M. F., and Verral, R. A. (1977). Micromechanisms of flow and fracture and their relevance to the rheology of the upper mantle. Philos. Trans. Royal Soc. of London, 288A, pp. 59-95.

Bates R. L. and Jackson J. A., Dictionary of geological terms, 3d ed., Anchor Press/Doubleday, Garden City, New York, 1984.

Baker, R. 1981. Tensile strength, tension cracks, and stability of slopes. Soil and Foundations, 21: pp. 1-17.

Bishop, A. W.; Webb, D. C. and Lewis, P. I, (1965). Undisturbed sample of London clay from Ashford Common Shaft: strength-effective stress relationship. Geotechnique, 150, pp. 1-31.

Bishop, A.W. (1967). Discussion on progressive failure with special reference to the mechanism causing it. Proc. Geotech. Conf., Oslo 2, pp. 142-150.

Bishop, A. W. and V. K. Garga (1969). Drained tensile tests in London clay. Geotechnique, Vol. 19, pp. 309-313.

Bishop, A. W., N. K. Kumapley, and A. El-Ruwagth (1975). The influence of pore water tension on the strength of clay. transactions of the Royal Soc. of London, Vol. 278, Series A, pp. 511-554.

Bishop, A. W. and Weley, L. D. (1975a). A hydraulic triaxial apparatus for controlled stress path testing. Geotechnique 25, No. 4, pp. 657-670.

Bjerrum, L. & Simons, N. E. (1960). Comparison of shear strength characteristics of normally consolidated clays. Proc. Am. Soc. Civ. Engrs Res. Conf. on shear strength of cohesive soils, pp. 711-726.

Bjerrum,L. (1967). Progressive failure in slopes of over-consolidated plastic clay and shales. J. Soil Mech. Fnds Div. Am. Soc. Civ. Engrs 93, SM5, pp. 3-49.

Blight, G. E. and Williams, A.A.B. (1971) The formation of cracks and fissures by shrinkage and swelling. Proc. 5th Reg. Conf. for Africa on Soil Mech. and Found. Engng, Luanda, vol. 1, pp. 15-21.

Bowles, J. E. (1978). Engineering properties of soils and their measurement. New York: McGraw Hill.

Brown, E. T., Richards, L. R. and Barr, M.V. (1977)."Shear strength characteristics of the Delabole Srares" Proc. Conf. Rock Eng., Newcastle upon Tyne, pp. 33-51.

Burford, A. E., and Dixon, J. M. (1978). Systematic fracturing in ypung clay of the Guyahoga River Valley, Ohio and its relation to bedrock jointing and drainage segments. Geotechnique, 28. pp. 201-6.

Calabresi, G. & Manfredini, G.(1973). Shear strength characteristics of the jointed clay of S. Barbara. Geotechnique 23, No.2, pp. 233-244.

Casagrade, A. (1949) Notes on swelling characteristic of clay-shales. Harvard university (Gordon McKay library).

Chandler, R. J. (1973). A study of structural discontinuities in stiff clays using a polarising microscope. Proc. Int. Symp. on Soil Structure, Gothenburg, pp. 78-85.

Chandler, R.J. and Skempton, A,W. (1974). The design of permanent cutting slopes in stiff fissured clays. Geotechnique 24, No. 4, pp. 457-466.

Chandler, R.J. (1984). Recent European experience of landslides in overconsolidated clays and soft rocks. Proc. Fourth International Symposium on Landslides. Toronto. Vol. 1 pp. 61-81.

Chen Y. J. (1991). A disscussion on fissure parameters in stiff clays under compression. Geotechnical Engineering. J. volume 117 No. 5 1991 pp. 845- 849.

Chowdhury, R. N. (1978). Propagation of failure surfaces in natural slopes. J. Geophys. Res. 83, B12, pp. 5983-5988.

Chu, J; Lo, S.-C. R. and Lee, I. K. (1992). Strain softening behaviour of granular soil in strain path testing. J. Geotech. Engng Div. Am. Soc. Civ. Engrs, 118, No. 2, pp. 191-208.

Chu, J; Lo, S.-C. R. and Lee, I. K. (1996). Strain softening and shear band formation of sand in multi-axial testing. Geotechnique, 46, Nol, pp. 63-82.

Costa-Filho, L.M. (1980). A Laboratory investigation of the small strain behaviour of London clay. PhD thesis, Imperial College, University of London.

Costa-Filho, L.M. (1984). A note on the influence of fissures on the deformation characteristic of London clay. Geotechnique 34, No. 2, pp. 268-272.

Covarrubias, S. W. (1969). Cracking of earth and rockfill dams. Harvard Soil Mech. Series, pp. 82.

Deere, D.U. & Patton, F.D. (1971). Slope stability in residual soils. Proceedings of the Fourth Pan-American Conference on Soil Mechanics and Foundation Engineering, Puerto Rico, vol. 1, pp. 87-170.

Devendra, N. T. (1968). Some aspects of rock pressure modelling on equivalent materials. Int. J. Rock Mech. Min. Sci & Geomech. Abstr. Vol. 5, pp. 355-369.

Dounias, G. T; Potts, D. M. and Vaughan, P. R.(1988)."The shear strength of soils containing undulating shear zones- a numerical study" Can. Geotech. J. Vol. 25, pp. 550-558.

Duan, Shu-jin; Nakagawa, K and Sakaida, T, (1991). A mathematical model to approach the fracture process of overconsolidated clay Engineering fracture mechanics, vol. 38, No. 6, pp. 361-369.

Duncan, J. M. & Dunlop, P. (1969). Slopes in stiff fissured clays and shales. J. Soil Mech. Fdns. Div. Am. Soc. Civ. Engrs 95 SM2, pp. 467-491.

Eide, O. (1967) Discussion on shear strength of soft clay. Proc. of Geotech. Conf. Oslo, Norwegian Geotech, Inst., vol. 2, pp. 133-135.

Einstein, H. H., Nelson, R. A., Bruhn, R. W., Hirsch Feld, R. C., (1970). Model studies of jointed rock behaviour. Proc. 11th Us Symp. Rock Mech. Berkeley. Calif. pp. 83-103.

Erdogan, R. & Sih, G. C. (1963). On the crack extension in plates under plain loading and transverse shear. J. Bas. Engng 85, 519-527.

Esu, F. (1966). Short term stability of slopes in unweatered jointed clays. Geotechniqe 16, No. 4, pp. 321-328.

Esu, F. & Calabresi, G. (1969). Slope stability in an overconsolidated clay. Proc. 7th Int. Conf. Soil Mech., Mexico 2, pp. 555-563.

Fookes, P. G. (1965). Orientation of fissures in stiff overconsolidated clay of the Siwalik System. Gotechnique, vol. 15, no. 2, pp. 195-206.

Fookes, P. G. and Denness, B. (1969). Observational studies on fissure patterns in cretaceous sediments of South-East England. Geotechnique 19, No. 4, pp. 453-477.

Fookes, P. G. & Parrish, D. (1968). Observations on small-scale structural discontinuities in the London clay and their relationships to regional geology. Q. J. Energy Geol 1, No. 4, pp. 217-240.

Fortin, M. Gill, D. E. & Ladanyi, B; Aubertin, M; Archambault, G, (1990). Simulation the effect of a variable normal stiffness on shear behaviour of discontinuities Mechanics of Jointed and Faulted Rock, Rossmanith (ed). pp. 381-388.

Gamon, T. I., and Finn, R. P. (1984). The structure of the Hong Kong Granite-a preliminary appraisal. Geol. Soc. Hong Kong Newsletter, 2(2), pp. 5-10.

Garga, V. K. (1970). Residual shear strength under large strains and the effect of sample size on the consolidation of fissured clay. Ph.D thesis, Imperial College, University of London.

Garga, V. K., (1988). Effect of sample size on consolidation of a fissured clay. Can. Geotech. J. 25, pp 76-84.

Gdoutos, E. E. (1984). Problems of mixed mode crack propagation. Martinus Nijhoff Publishers, The Hague, Holland, pp. 11-21.

Giani, G. P. (1988). Rock slope stability analysis. Rotterdam Balkema.

Goodman, R. (1976). Methods of geological engineering in discontinuous rock. West Publ. Co.

Head K. (1985). Soil laboratory testing 3 Volums, Pentech Press, London.

Hencher, S. R. (1987). The implications of joints and structures for slope stability. Slope stability,(eds. M. G. Anderson and K. S. Richards)., pp. 145-186.

Herget, G. (1977). Pit Slope Manual Chapter 2-Structural Geology, CANMET (Canada Centre for Mineral and Energy Technology), CANMET Report 77-41, 123.

Hudson, J.A. and Priest, S. (1975) Instrumentation and monitoring of tunnels. Tunnels and tunnelling, vol. 7 no. 5, pp. 64-70.

Hudson, J. A., and Priest, S. D. (1983). Discontinuity frequency in rock masses. Int. J. Rock Mech. Mining Sci. Geomech. Abstr. 20, pp. 73-89.

Hvorslev, M. J. (1960). Physical components of the shear strength of saturated clays. Proc. Research conf. shear strength of cohesive soils, Boulder, New York: American Society of Civil Engineers, pp. 437-501.

Ingraffea, A. R., and Heuze, F. E. (1980). Finite element models for rock fracture mechanics. Int. j. Numer. Anal. Methods Geomech., 4(1), pp. 25-43.

Irfan, T.Y., Koirala, N.P. & Tang, K.Y. (1987). A complex slope failure in a highly weathered rock mass. Proceedings of the Sixth International Congress on Rock Mechanics, Montreal. pp. 397-402.

Irfan, T. Y. (1988). The influence of relict discontinuities on slope stability in Saprolitic Soils. Proc. 2nd Int. Conf. on Geomechanics of Tropical Soils, pp. 267-276.

Irwin, G. R. (1957). Analysis of stresses and strains near the end of a crack. Journal of Applied Mechanics, Vol. 24, pp. 361-364.

Itasca consulting Group, Inc. FLAC (Fast Lagrangian Analysis of Continua), Version 3.2, (1993).Volume III: Appendices, pp. E15-E18.

ISRM (1978). Suggested methods for the quantitative description of discontinuities in rock masses. International Society for Rock mechanics Committee on Laboratory Tests. International Journal of Rock Mechanics and Mining Sciences and Geomechanics Abstracts, vol. 15, pp. 319-368.

James, P. M. (1971). The role of progressive failure in clay slopes. Proc. of the 1st. Australian-Newzealand Conf. on Geomechanics, Vol. 1, pp. 344-348.

Jenninigs, J.E. (1970). A mathematical theory for the calculation of the stability of slopes in open cast mines. Proc. Symp. on planning open pit mines, S.A. Inst. Min. and Met. pp. 87-102.

Kallstenius, T. (1963). Studies on clay samples taken with standard piston sampler. Proc. no. 21, Swedish Geotech. Inst., Stockholm.

Kanji, M. A. (1974). The relationship between drained friction angles and Atterberg Limits of natural soils. Geotechnique 24, No. 4, pp. 671-674.

Koo, Y.C (1982). The mass strength of jointed residual soils. Canadian Geotechnical Journal, Vol. 19.

Langharr, H. L., (1951). Dimensional analysis and theory of models. Wesley, New York.

Lawn, B. R. and T. R. Wilshaw (1975). Fracture of Brittle Solids. Cambridge Univ. press, pp. 232 .

Lo, K. Y. (1970). The operational strength of fissured clays. Geotechnique 20, No. 1, 57-74.

Lo, K. Y. & Valee, J. (1970). Strength anisotropy due to parallel planes of discontinuities in clays, Proc. 2nd S. E. Asian Conf. on Soil Engng, Singapore, pp. 1-20.

Lumb, P. (1970). Safety factors and the probability distribution of soil strength. Canadian Geotechnical Journal ,Vol. 7, pp. 225-242.

Lupini, J.F., Skinner, A.E. and Vaughan, P.R. (1981). The drained residual strength of cohesive soils. Geotechnique 31, No. 2, pp. 181-213.

MacGregor, J.P., Olds R. and Fell R. (1990). Landsliding in extremely weathered basalt, Plantes Hill, Victoria. In Engineering Geology of Weak Rocks. Proc. Twenty Sixth Annual Conference of the Geological Society, edited by Cripps, J.C. and Moon, C.F., University of Leeds.

Maguire, W. M. (1975). The undrained strength and stress-strain behaviour of brecciated Upper Lias clay. Ph.D thesis, Imperial College, University of London.

Marsal, R. J. (1979). Stability investigations relatedto clay shell. Proc. Int. Symp. Soil Mech., Doxoca 1, pp. 51-74.

Marsland A, 1971. Laboratory and in-situ measurements of the deformation moduli on London Clay. Proceeding, Symposium on the Interaction of Structure and Foundation. Midland Soil Mechanics & Foundation Engineering Society, Birmingham. July 1971.

Marsland, A. (1971a). Large in situ tests to measure the properties of stiff fissured clays. Proc. 1st Aust. N.Z. conf. Geomechanics, Melbourne, vol. 1, pp. 180-189.

Marsland, A. (1971b). Clays subjected to in situ plate tests. Ground Enngng, vol. 5, no. 7, pp. 24-31.

Marsland, A. (1972). The shear strength of stiff fissured clays. In: Stress Strain Behaviour of Soils Edited by R. H. G. Parry, G. T. Foulis and Co., England, pp. 59-68.

Masland, A. & Butler, Muriel E. (1967). Strength measurements on stiff fissured Barton Clay from Fawley, Hampshire. Proc. Geotechnical Conference, Oslo, 1967, vol 1, pp. 139-146.

Massad, F. & Teixeira, H.R. (1985). Deep cut on saprolitic soils conditioned by relict structures. Proceedings of the First International Conference on Tropical Lateritic and Saprolitic Soils, Brasilia, vol. 2, pp. 381-391.

McGown, A., Sali, A. & Radwan, A. M. (1974). Fissure patterns and slope failures in boulder clay at Hurlford, Ayrshire. Q. J. Engng. Geol. 7, pp. 1-26.

McGown, A., Radwan, A. M. & Gabr, A. W. A. (1977). Laboratory testing of fissured and laminated soils. Proc. 9th Int. Conf. Soil Mech. Fdn Engng Tokyo 1, pp. 205-210.

McGown, A., Marsland, A., Radwan, A. M., & Gabbr, A. W. A. (1980). Recording and interpreting soil macrofabric data. Geotechnique 30 ,No. 4, pp. 417-447.

Menzies, B. K; Sutton, H., and Davies, R. E, (1977). A new system for automatically simulating K_0 consolidation and K_0 swelling in conventional triaxial cell. Geotechnique, Vol. 27, No. 4, pp. 593-596.

Menzies, B. K. (1988). A computer controlled Hydraulic Triaxial Testing System, Advances Triaxial Testing of Soil and Rock , ASTM STP977, Robert T. Donaghe, Ronald C. Chaney, and Marshal L. Silver, Eds., American Society for Testing and Materials, Philadelphia, 1988, pp. 82-94.

Moon, A.T. (1983). Residual shearing mechanisms in natural soils. Australian Geomechanics News, Special Edition for 5th ISRM Congress.

Moon, A. T. (1984). Effective shear strength parameters for stiff fissured clays. Proc. Fourth Australia New Zealand Conference on Geomechanics, perth. Vol. I pp. 107-111.

Morgenstern, N. R. & Tchalenko, J. S. (1967). Microscopic structures in kaoline subjected to direct shear. Geotechnique 17, pp. 309-328.

Morgenstern, N. (1977). Slopes and excavation in heavily over-consolidated clays. Proc., Ninth Int. Conference on Soil Mech. and Found. Engrg., State of The Art Report, 2, Tokyo, Japan, pp. 567-581.

Morris, P. H., Graham, J., and Williams, D. J. (1992). Cracking in drying soils. Canadian Geotechnical Journal Vol. 29, pp. 263-277.

Nikraz, H. R., (1990). Laboratory evaluation of the geotechnical design characteristics of the sandstone aquifers in the Collie Basin, Ph.D Thesis, Curtin University of Technology, pp. 133-136

Nikraz, H. R., (1985) Instrumentation for laboratory and insitu determination of lateral earth pressure, swelling pressure and heave prediction, Msc Thesis, Curtin University of Technology, pp. 158.

Noonan, D. K. & Nixon, J. F. (1972). The determination of Young Modulus from the direct shear test. Can. Geotech. J. 9, pp. 504-507.

Palladino, R.B. and R. B. Peck (1972). Slope failures in an overconsolidated clay, Seattle, Wash., Geotechnique, Vol. 22, pp. 563-595.

Palmer, A. C. and Rice, J. R. (1973). The growth of slip surfaces in the progressive failure of over-consolidated clay. Proc. Roy. Soc. Lond. A. 332, pp. 527-548.

Peck, R. B. (1967). Stability of natural slopes. J. of the Soil Mech. and Found. Div., ASCE, VOL. 93, pp. 403-417.

Phillips, F. C. (1971). The use of stereographic projection in structural geology, 3rd edition. London: Arnold.

Pitts, J. (1985). Structural control of landslides in solis in Singapore. Proc. 4th, Int. Conf. and Field Workshop on Landslides, Tokyo, pp. 251-256.

Potts, D. M; Dounias, G. T; Vaughan, P. R (1987). Finite element analysis of the direct shear box test. Geotechnique, 37(1), pp. 11-23.

Price, N. J. (1966). Fault and Joint Development in Brittle and Semi-brittle Rock. Pergamon Press, pp. 176.

Radwan, A. M. (1974). The presence and influence of fissures in the boulder clays of West Centeral Scotland. Ph.D thesis, University of Strathclyde.

Rivard, P.J., and Lu, Y. (1978). Shear strength of soft fissured clays. Canadian Geotechnical Journal, Vol. 15, pp. 382-390.

Rizkallah, V. (1977). Stress strain behavior of fissured stiff clays. Proc. 9th Int. Conf. Soil Mech. Fnd Engng, Tokyo 1, pp. 267-270.

Rowe, P. W. (1968). Failure of foundations and slopes on layered deposits in relation to site investigation practice. Proc. Instn Civ. Engrs, London. Suppl., pp. 73-131.

Rowe, P. W. (1972). The relevance of soil fabric to site investigation practice. Geotechnique 22, pp. 195-300.

Saada, A. S; Bianchini, G. F. and Liqun, Liang (1994). "Cracks, bifurcation and shear bands propagation in saturated clays." Geotechnique, 44(1), pp. 35-64.

Sherard, J. L., Woodward, R. J., Gizienski, S. F. & Clevenger, W. A. (1963) Earth and earth-rock dams. New-york: Wiley

Sherard, J. L. (1973). Embankment dam cracking. Embankment dam engineering, Casagrande Volume, R. C. Hirschfeld and S. J. Poulos, eds., Wiley-Interscience, New York, N.Y., pp. 271-353.

Sih, G. C., and Liebowitz, H. (1968). Mathematical theories of brittle fracture. Fracture, H. Liebowitz, ed., Vol. II, Academic Press, New York, N.Y., pp. 67-190.

Skempton, A. W (1948).The rate of softening in stiff fissured clays, with special reference to London Clay. Proc. 2nd Int. Conf. Soil Mech. Rotterdam, 2, pp. 50-53.

Skempton, A. W. (1964). Long term stability of clay slopes. Geotechnique 14, No. 2, pp. 77-101.

Skempton, A. W., and LaRochelle, P. (1965). The Bradwell slip: A short-term failure in London clay. Geotechnique, 15(3), pp. 221-242.

Skempton, A. W. (1966) Some observation on tectonic shear zones. Proc. 1st Congr. Inst. Soc. of rock Mech., Lisbon, vol. 1, pp. 329-335.

Skempton, A.W. & Petley, D. J. (1967). The strength along structural discontinuities in stiff clays. Proc. Geotech. Conf. Oslo 2, pp. 29-46.

Skempton, A. W., Schuster, R. L., and Petley, D. J. (1969). Joints and fissures in the London Clay at Wraysbury and Edgware. Geotechnique, 19, No. 2, pp. 205-217.

Skempton, A. W. (1970). First-Time slides in over-consolidated clays. Geotechnique Vol. 20, No. 3, pp. 320-324.

Skempton, A. W. (1977). Slope stability of cuttings in Brown London Clay. Special Lectures Section, Proc. of the 9th Int. Conf. on Soil Mech. and Found. Eng., Tokyo, Vol. 3, pp. 261-270.

Skempton, A. W. (1985). Residual strength of clays in landslides, folded strata, and laboratory. Geotechnique 35,1 pp. 3-18.

Sowers, G.F. (1985). Residual soils in the United States. In Sampling and Resting of Residual Soils: A Review of International Practical (ed. E.W. Brand and H.B. Phillipson), Scorpion Press, Hong Kong, pp. 183-191.

Stapledon, D. H. (1970). Changes and structural effects developed in some South Australian clays, and their engineering consequences. Proceedings of a Symposium on Soils and Earth Structures in Arid Climates, Adelaide, pp. 62-71.

St. John, B. J., Sowers, G. F. & Weavers, C. H. E. (1969). Slickensides in redual soils and their engineering significance. Proceedings of the Seventh International Conference of Soil Mechanics and Foundation Engineering, Mexico, Vol. II, pp. 591-597.

Terzaghi, K. (1936). Stability of slopes in natural clay. Proc. of the 1st. Int. Conf. on Soil Mech. and Found. Eng., Vol. 1, pp. 161-165.

Terzaght, K. (1961). Discussion on horizontal stresses in an overconsolidated eocene clay. Proc. Paris, vol. 3, pp. 144-145.

Thorne, C. P. (1984). Strength assessment and stability analysis for fissured clay. Geotechnique. Vol. 34 No. 3 pp. 305-322.

Vallejo, L. E. (1985). Fissure interaction and progressive failure of slopes. Proc. 11th Int. Conf. Soil Mech. Fdn Engng, San Francisco 4, pp. 2353-2356.

Vallejo, L. E. (1986). Mechanics of crack propagation in stiff clays. Geotechnical aspects of stiff and hard clays (eds. R. P. Khera and C. W. Lowell), pp. 14-27. New York : American Society of Civil Engineers.

Vallejo, L. E. (1987). The influence of fissures in a stiff clay subjected to direct shear. Geotechnique 37, No. 1, pp. 69-82.

Vallejo, L. E. (1989). Fissure parameters in stiff clays under compression. J. of Geotech. Engng Vol. 115, No. 9, pp. 1303-1321.

Walsh, J. B. (1965). The effect of cracks on the uniaxial elastic compression of rocks. J. Geophys. Res. 70, pp. 5249-5257.

Ward, W H, Marsland, A and Samuels, S G and Butler, M E (1959). Further studies of the properties of London clay. Geotechnique, Vol 14, 1959, No 2, pp. 33-38.

Ward, W H, Marsland, A and Samuels, S G. (1965). Properties of London Clay at the Ashford Common shaft: In-situ and undrained strength tests. Geotechnique, vol 15, pp. 321-344.

Ward, W. H. (1967). Discussion. Proc. Geotech. Conf., Oslo 2, pp. 140-141.

Ward, W. H. (1972). Some field techniques for improving site investigation and engineering design. Proc. Symp. Stress-strain Behaviour of Soils, pp. 676-682, Cambridge.

Webb, D. L. (1966). The mechanical properties of undisturbed London clay and pierre shale. PhD thesis, Imperial College, University of London.

Williams, A.A.B. (1958). Discussion on the prediction of total heave from the double oedometer test. by J. E. Jennings and K. Knight. Trans. S. Afr. Instn Civ. Engrs, Vol. 8, no. 6, pp. 123-124.

Williams, A. A. B. & Jennings, J. E. (1977). The in situ shear behaviour of fissured soils. Proc. Ninth International Conference on Soil Mechanics and Foundation Engineering, Tokyo Vol. 2, pp. 169-176.

Wolle C.M. (1985). Slope stability Peculiarities of geotechnical behaviour of tropical lateritic and saprolitic soils. Progress Report, Theme 3.2, Brazilian Society for Soil Mechanics, Sao Paulo, pp. 164-214.

Wroth, C. P. and Hughes, J. M. O. (1973). An instrument for the in situ measurements of the properties of soft clays. Proc. 8th Int. Conf. Soil Mech., Moscow, 1.2, pp. 487-494.